VOLUME 119 NUMBER 1

THE ASTROPHYSICAL JOURNAL

AN INTERNATIONAL REVIEW OF SPECTROSCOPY AND ASTRONOMICAL PHYSICS

JANUARY 1954

GALACTIC MAGNETIC FIELDS AND THE ORIGIN OF COSMIC RADIATION . . . *E. Fermi* 1

THE GRAVITATIONAL INSTABILITY OF AN INFINITE HOMOGENEOUS MEDIUM WHEN CORIOLIS FORCE IS ACTING AND A MAGNETIC FIELD IS PRESENT . . . *S. Chandrasekhar* 7

ON THE PULSATION OF A STAR IN WHICH THERE IS A PREVALENT MAGNETIC FIELD . . . . . *S. Chandrasekhar and D. Nelson Limber* 10

ON EQUILIBRIUM CONFIGURATIONS OF OBLATE FLUID SPHEROIDS WITH A MAGNETIC FIELD . . . . . *Guro Gjellestad* 14

WAVES OF FINITE AMPLITUDE IN AN INFINITE HOMOGENEOUS MEDIUM . . . *H. Lawrence Helfer* 34

THE TRANSFER OF RADIATION BY AN EMITTING ATMOSPHERE. II . . . *Henry G. Horak and Charles A. Lundquist* 42

EXACT CURVES OF GROWTH. III. THE SCHUSTER-SCHWARZSCHILD MODEL . . . *M. H. Wrubel* 51

COMPTON SCATTERING BY ELECTRON ATMOSPHERES. I. THE SCHUSTER PROBLEM . . . . . *Frank N. Edmonds, Jr.* 58

OPACITY OF A HIGHLY COMPRESSED HYDROGEN GAS . . . . *H. T. Hsieh Tsao* 70

ON THE SOLUTION OF AN INTEGRAL EQUATION OF CHANDRASEKHAR AND MÜNCH . . . . . *Alladi Ramakrishnan and P. M. Mathews* 81

COMPARISON OF THE SYNTHETIC AND ACTUAL DISTRIBUTION OF GALAXIES ON A PHOTOGRAPHIC PLATE . . . . *E. L. Scott, C. D. Shane, and M. D. Swanson* 91

THE ABUNDANCE OF BERYLLIUM IN THE SUN . . . *Jesse L. Greenstein and Einar Tandberg-Hanssen* 113

SOLAR FLARES AND THE YELLOW CORONAL LINE . . . *Frederick P. Dolder, Walter Orr Roberts, and Donald E. Billings* 120

(Continued on inside page)

THE UNIVERSITY OF CHICAGO PRESS
CHICAGO, ILLINOIS, U.S.A.

January 1954 Vol. 119, No. 1

THE ASTROPHYSICAL JOURNAL

AN INTERNATIONAL REVIEW OF SPECTROSCOPY AND ASTRONOMICAL PHYSICS

Founded in 1895 by George E. Hale and James E. Keeler

Published in Collaboration with the American Astronomical Society

S. CHANDRASEKHAR
Managing Editor

GERARD P. KUIPER
Associate Editor

Yerkes Observatory of the University of Chicago

EDITORIAL BOARD

MARTIN SCHWARZSCHILD, JR. (1954-58)
Princeton University Observatory

O. HERZBERG (1952-56)
National Research Council, Ottawa

H. W. BABCOCK (1953-57)
Mount Wilson Observatory of the Carnegie Institution of Washington

FRED L. WHIPPLE (1952-54)
Harvard College Observatory

C. D. SHANE (1952-55)
Lick Observatory, University of California

The Astrophysical Journal is published bimonthly by the University of Chicago at the University of Chicago Press, 5750 Ellis Avenue, Chicago 37, Illinois, during January, March, May, July, September, and November. ¶Two volumes are published per year, one beginning with the January issue and the other beginning with the July issue. The subscription price is $6.00 per volume or $12.00 per year; the price of single copies is $3.00. (Orders for service of less than a volume will be charged at the single copy rate.) ¶Postage is prepaid by the publishers on all orders from the United States and its possessions. No extra charge is made for postage to countries in the Pan American Postal Union. ¶Postage is charged extra as follows: for Canada, 20 cents per volume, 40 cents per year (total $6.20 per volume, $12.40 per year); on single copies 5 cents (total $3.05); for all other countries in the Postal Union, 40 cents per volume, 75 cents per year (total $6.40 per volume, $12.75 per year), on single copies 10 cents (total $3.10). ¶Subscriptions are payable in advance. Please make all remittances payable to The University of Chicago Press, in United States currency or its equivalent by postal or express money orders or bank drafts.

The following is an authorised agent:

For the British Empire, except North America and Australasia: The Cambridge University Press, Bentley House, 200 Euston Road, London, N.W. 1, England. Prices of yearly subscriptions and of single copies may be had on application.

Claims for missing numbers should be made within the month following the regular month of publication. The publishers expect to supply missing numbers free only when losses have been sustained in transit, and when the reserve stock will permit.

Business correspondence should be addressed to The University of Chicago Press, Chicago 37, Illinois.

Communications for the editors and manuscripts should be addressed to: S. Chandrasekhar, Editor of THE ASTROPHYSICAL JOURNAL, Yerkes Observatory, Williams Bay, Wisconsin.

Line drawings and photographs should be made by the author, and all marginal notes such as co-ordinates, wave lengths, etc., should be included in the cuts. It will not be possible to set up such material in type.

One copy of the corrected galley proof should be returned as soon as possible to the editor, Yerkes Observatory, Williams Bay, Wisconsin. Authors should take notice that the manuscript will not be sent to them with the proof.

The cable address is "Observatory, Williamsbay, Wisconsin."

The articles in this journal are indexed in the *International Index to Periodicals*, New York, N.Y.

Applications for permission to quote from this journal should be addressed to The University of Chicago Press, and will be freely granted.

Microfilms of complete journal volumes are available to regular subscribers only and may be obtained at the end of the year. Orders and inquiries should be addressed to University Microfilms, 313 North First Street, Ann Arbor, Michigan.

Notice to subscribers: If you change your address, please notify us and your local postmaster immediately.

Entered as second-class matter, July 22, 1940, at the Post-Office at Chicago, Ill., under the Act of March 3, 1879.
Acceptance for mailing at special rate of postage provided for in United States Postal Act of October 3, 1917, Section 1103, Amended February 28, 1925.
Copyright 1954 by the University of Chicago.

[PRINTED IN U.S.A.]

(*Continued from front cover*)

THE ABSORPTION SPECTRA OF NOVA HERCULIS: A NEW INTERPRETATION
Dean B. McLaughlin 124

ON THE SPECTRUM OF CHI CYGNI NEAR THE TIME OF LIGHT-MAXIMUM
Yoshio Fujita 141

THE SPECTRA AND ROTATIONAL VELOCITIES OF THE BRIGHT STARS OF DRAPER TYPES B8–A2 . . . . . *Arne Slettebak* 146

THE VELOCITY-CURVE OF BETA CANIS MAJORIS
O. Struve, D. H. McNamara, S. M. Kung, A. van Hoof, and R. Deurinck 168

OBJECTIVE-PRISM SPECTRA OF LONG-PERIOD VARIABLES IN THE NEAR INFRA-RED . . . . . *Jason J. Nassau and Donald M. Cameron* 175

THE STANDARD REGION NEAR IC 4665 . . . . . *Harold L. Johnson* 181

MAGNITUDES AND COLORS IN M34 . . . . . *Harold L. Johnson* 185

A STUDY OF THE GALACTIC CLUSTER NGC 2287 . . . . . *Arthur N. Cox* 188

THE MASS OF THE GLOBULAR CLUSTER M92 . . *O. C. Wilson and Mary F. Coffeen* 197

A STUDY OF THE ORION AGGREGATE OF EARLY-TYPE STARS. II *Stewart Sharpless* 200

IDENTIFICATION OF THE RADIO SOURCES IN CASSIOPEIA, CYGNUS A, AND PUPPIS A . . . . . *W. Baade and R. Minkowski* 206

ON THE IDENTIFICATION OF RADIO SOURCES . . . *W. Baade and R. Minkowski* 215

THE SPECTRUM OF THE RADIO SOURCE IN CASSIOPEIA
R. Minkowski and Lawrence H. Aller 232

THE POWER RADIATED BY SOME DISCRETE SOURCES OF RADIO NOISE
Rudolph Minkowski and Jesse L. Greenstein 238

SPECTROPHOTOMETRY OF THE CENTRAL STARS OF FOUR PLANETARY NEBULAE . . . . . *L. H. Aller and O. C. Wilson* 243

OBSERVATIONS OF THE ZODIACAL LIGHT
F. E. Roach, Helen B. Pettit, E. Tandberg-Hanssen, and Dorothy N. Davis 253

THE LABORATORY DETERMINATION OF RELATIVE TRANSITION PROBABILITIES OF DIATOMIC MOLECULES. I. THE a-SYSTEM OF *TiO* . . *John G. Phillips* 274

VIBRATIONAL TRANSITION PROBABILITIES OF DIATOMIC MOLECULES; COLLECTED RESULTS II, N_2^+, *CN*, C_2, O_2, *TiO* *P. A. Fraser, W. R. Jarmain, and R. W. Nicholls* 286

SOME REMARKS ON THE LIFE-HISTORY OF METEORITES . . . *S. F. Singer* 291

NOTES

THE POSSIBLE ROLE OF ACCELERATED SECONDARY ELECTRONS IN THE AURORA . . *C. Y. Fan* 294

ABUNDANCES OF METALS IN THE SOLAR CHROMOSPHERE . . . . . *Sandra Schwartz* 296

ON THE SPACE REDDENING OF ETA AQUILAE . . . . . *Daniel L. Harris III* 297

A NEW SPECTROGRAPHIC ORBIT OF 30 TAU CANIS MAJORIS . . . *O. Struve and R. P. Kraft* 299

A WOLF-RAYET STAR OF TENTH MAGNITUDE: CORRECTION TO *HDC* . . *A. N. Vyssotsky* 300

ABSTRACTS OF ASTROPHYSICAL JOURNAL: SUPPLEMENT SERIES

CHROMOSPHERIC STRUCTURE OF THE K-TYPE COMPONENT OF ZETA AURIGAE
O. C. Wilson and Helmut A. Abt 301

THE ASTROPHYSICAL JOURNAL

AN INTERNATIONAL REVIEW OF SPECTROSCOPY AND ASTRONOMICAL PHYSICS

VOLUME 119 JANUARY 1954 NUMBER 1

GALACTIC MAGNETIC FIELDS AND THE ORIGIN OF COSMIC RADIATION*

E. FERMI

Institute for Nuclear Studies, University of Chicago

Received September 11, 1953

I became interested in the possible existence of magnetic fields extending through the volume of the galaxy in connection with a discussion on the origin of the cosmic radiation a few years ago.[1] The hypothesis was discussed then that the acceleration of cosmic-ray particles to extremely high energies was due to their interaction with a galactic magnetic field that was postulated to pervade the galactic space. According to Alfvén's ideas on magnetohydrodynamics, this field would be strongly influenced by the turbulent motions of the diffuse matter within the galaxy. Indeed, the electric conductivity of this matter is so large that any lateral shift of the magnetic lines of force with respect to the matter is effectively prevented. A strong magnetic field quenches the transverse components of the displacement due to the turbulent motion. A weak field yields to the material motions, so that its lines of force are soon bent into a very crooked pattern.

The observation by Hiltner and Hall of an appreciable polarization of the light coming to us from distant stars has been interpreted[2] as due to the orientation of nonspherical dust grains by a magnetic field. If this general type of interpretation is correct, the polarization gives us some information on the strength and the direction of the magnetic field. Hiltner's measurements[3] indicate that in the vicinity of the earth the magnetic field is approximately parallel to the direction of the spiral arm. This fact suggests that we may perhaps think that the spiral arms are magnetic tubes of force. In the following discussion we will assume that this is the case.

The direction of polarization of the stellarlight indicates further that in our vicinity the magnetic lines of force show irregular deviations from parallelism of the order of 10°. This fact excludes the hypothesis that the lines of force yield completely to the turbulent motions of interstellar matter, because then they would be rapidly bent into shapes much more irregular than those observed. One is rather led to the conclusion that the field is

* Sixth Henry Norris Russell Lecture of the American Astronomical Society delivered at Boulder, Colorado, on August 28, 1953.

[1] E. Fermi, *Phys. Rev.*, **75**, 1169, 1949; cited hereafter as "R."

[2] Davis and Greenstein, *Ap. J.*, **114**, 206, 1951; Spitzer and Tukey, *Ap. J.*, **114**, 187, 1951.

[3] *Ap. J.*, **114**, 241, 1951.

sufficiently strong to yield only a little to the transverse component of the turbulent motion. Indeed, as was pointed out by Davis, the small deviations from parallelism of the field enable one to estimate that the intensity of the magnetic field must be of the order of 10^{-5} gauss. Recently Chandrasekhar and I[4] have re-examined this problem, considering, in particular, the balance between magnetic and gravitational effects in the spiral arm. Our conclusion is that the field intensity is about 6×10^{-6} gauss. Owing to the turbulence, the lines of force are irregularly pushed sidewise until the magnetic stress increases to the point of forcing a reversal of the material motion and of pushing back the diffuse matter, impressing on it some kind of very irregular oscillatory motion. One expects, therefore, that the lines of force sway back and forth and also that the field intensity will fluctuate along the same line of force.

A cosmic-ray particle spiraling around these moving lines of force is gradually accelerated. The acceleration mechanism was discussed in R, although the shape of the lines of force assumed then was quite different from what we now believe it to be. A cosmic-ray proton of 10 bev energy is bent in a magnetic field of 6×10^{-6} gauss in a spiral having a radius of the order of one-third the radius of the earth's orbit. This is very small on the galactic scale. The motion of a proton with this energy and also of one with much greater energy is, therefore, properly described as a very small radius spiral around a line of force. Apart from the very rapid changes due to the spiraling, the general direction of motion may change for two reasons. One is that the line of force around which the particle spirals may be curved. In R a change of direction of this kind was called a "collision of type *b*." A second type of event, called a "collision of type *a*," takes place when the particle in its spiraling encounters a region of high field strength.

Let ϑ be the angle between the direction of the line of force and the direction of motion of the spiraling particle. The angle ϑ will be called the "angle of pitch." One can prove that, in a static magnetic field, the quantity

$$q = \frac{\sin^2 \vartheta}{H} \tag{1}$$

is approximately constant with time. For this reason, in a static field, the particle cannot enter a region where

$$H > \frac{1}{q}. \tag{2}$$

When the particle approaches such a region, its pitch decreases until $\vartheta = 90°$, at which moment the particle is reflected and spirals backward in the direction whence it came.

In a variable magnetic field both *a*- and *b*-type collisions may cause changes in energy. As a rule, the energy will increase or decrease according to whether the irregularity of the field that causes the collision moves toward the particle (head-on collision) or away from it (overtaking collision). It was shown in R that, on the average, the energy tends to increase primarily because the head-on collisions are more probable than the overtaking collisions. In the present discussion the same general acceleration mechanism will be assumed. The details, however, will be quite different from those previously assumed.

It was shown in R that through this mechanism the energy of the particle increases at a rate that, for extreme relativistic particles, is proportional to their energy. The energy E, therefore, increases exponentially with time:

$$E(t) = E_0 e^{t/A}. \tag{3}$$

According to this law, the oldest particles should have the highest energy.

The time A needed for an energy increase by a factor e was estimated in R to be about 100 million years. If this estimate was correct, A would be comparable to the time B for

[4] *Ap. J.*, **118**, 113, 1953.

nuclear collisions of the particle. Assuming that a nuclear collision effectively destroys the particle, the probability that a particle has the age t should be

$$e^{-t/B}\frac{dt}{B}. \tag{4}$$

Combining conditions (3) and (4), one readily finds that the probability that a particle observed now has energy E should be proportional to

$$\frac{dE}{E^n}, \tag{5}$$

with

$$n = 1 + \frac{A}{B}. \tag{6}$$

An exponent law like (5), with n of the order of 2 or 3, seems to fit fairly well the observed energy spectrum of the cosmic radiation.

Two main objections can be raised against the theory proposed in R. One is that, according to present evidence, the structure of the galactic magnetic field is much more regular than was assumed in R. We shall try to make plausible the conclusion that, in spite of this fact, the acceleration may still take place at an adequate rate. Indeed, as will be discussed below, it will be necessary to provide an acceleration process five to ten times more efficient than was previously supposed. The second difficulty arises from the fact that the protonic and the nuclear components of the cosmic radiation have very much the same energy spectrum. Heavy nuclei have a larger nuclear collision cross-section than protons. Their mean life B, therefore, should be shorter, and the exponent n given by equation (6) should be larger.

This difficulty would be removed if the process that eliminates the particles were equally effective against protons and against larger nuclei, because B would then be the same for both kinds of particle. For example, collisions against stars or planets do not differentiate between protons and nuclei. On the other hand, a simple estimate shows that the probability of collisions against such massive objects is quite negligible, even in a time equal to the age of the universe. Another means of removing cosmic-ray particles that is equally effective for protons and nuclei is diffusion outside the galaxy. Assume, for example, that the lines of force follow the spiral arms. The stretched-out length of the galactic spiral is about a million light-years, and the particles travel with a velocity very close to that of light. They could, therefore, escape in a time of the order of a million years. The escape time, of course, would be longer if the particle occasionally reversed its direction, owing, for example, to collisions of type *a*.

In a theory that yields essentially the same energy spectrum for cosmic-radiation protons and nuclei it will be necessary to assume that the escape time for diffusion outside the galaxy is appreciably shorter than the nuclear collision time. Then escape will be dominant with respect to nuclear collisions. We will assume that this is the case, and we will take, somewhat arbitrarily, in the numerical examples the escape time,

$$B = 10 \text{ million years}. \tag{7}$$

The excape time is then about ten times shorter than the nuclear collision time.

Assuming 2.5 as an average value of the exponent n in quantity (5), we have, from equation (6),

$$A = 1.5B = 15 \text{ million years}, \tag{8}$$

in which A is the time through which the energy of the particle increases, on the average, by the factor e. This time, 15 million years, is appreciably shorter than was estimated in R.

It therefore appears necessary to modify the acceleration mechanism of R in two ways. The mean free path must be much longer, in order to allow the escape of the particles from the galaxy in a relatively short time. And the process of acceleration must be much faster. At first sight, these two requirements seem to be contradictory, and perhaps they are. On the other hand, there is an acceleration mechanism that is potentially much more efficient than the others. This process was discussed in R and was then dismissed as of little importance for certain reasons to be mentioned shortly. I propose to criticize those reasons and to make a case in favor of this acceleration mechanism.

First of all, we observe that the knowledge that we now have of the general shape of the magnetic field makes the collisions of type *b* rather unimportant. We shall therefore concentrate our attention on type-*a* collisions. They take place, as will be remembered, when the particle encounters a region of large field strength, where condition (2) is fulfilled. A particle that finds itself between two such regions will be trapped on the stretch of line of force comprised between them. When this happens, the energy of the particle will change with time at a rate much faster than usual. It will decrease or increase according to whether the jaws of the trap move away from or toward each other.

Let H be the average value of the magnetic field and $H_{\max}$ the maximum field along the line of force that may be likely to cause a type-*a* reflection. If ϑ is the angle of pitch of the spiral where the field is average, reflections will occur only for particles having

$$\vartheta > \chi, \tag{9}$$

where

$$\sin \chi = \sqrt{\frac{H}{H_{\max}}}. \tag{10}$$

A simple calculation shows that when a particle with $\vartheta > \chi$ is caught in a trap, both its energy and its angle of pitch will change with time, but the product,

$$E \sin \vartheta, \tag{11}$$

remains approximately constant. The particle can escape the trap only when ϑ has decreased to the point that condition (9) is no longer fulfilled. In this process the energy must increase by a factor

$$\frac{\sin \vartheta}{\sin \chi}. \tag{12}$$

This process may lead to a sizable energy gain in a relatively short time. For example, if the jaws of the trap are 10 light-years apart and move toward each other at 10 km/sec, the time needed for a 10 per cent energy increase is only a few tens of thousands of years.

To be sure, the jaws will occasionally move away from each other, causing a loss instead of a gain of energy. But in this case ϑ will increase, making the particle more easily caught in similar traps. The process ends only when the energy has increased to the point that ϑ has become less than χ, because only then will the particle be capable of passing without reflection through occasional maxima of the field intensity that it may encounter along its path.

When this condition is reached, the process of acceleration becomes exceedingly slow. Indeed, if q in equation (1) were exactly a constant of motion, the particle would always keep on spiraling in the same direction and would eventually escape from the galaxy. It is for this reason that the process of acceleration in a trap was not considered of major importance in R. The process may become important only if there is machinery whereby the angle of pitch, after having been reduced to a small value in the process of acceleration in a trap, can be increased. If this is the case, the trap mechanism again becomes operative, and the energy may be increased by a further factor.

Now one finds that q is almost exactly a constant as long as the particle is not caught in a trap and there are no sharp variations in the magnetic field either in time or in space. When I first discussed the acceleration of cosmic rays by magnetic fields, I was not aware of the possibility of sharp discontinuities of the field and for this reason did not think that the traps could be the dominant factor. I propose now to show that discontinuities in the direction of the magnetic field should not be too exceptional in the galaxy.

Recently de Hoffmann and Teller[5] have discussed the features of magnetohydrodynamic shocks. They show, in particular, that at a shock front sudden variations in direction and intensity of the field are likely to occur. One is tempted to identify the boundaries of many clouds of the galactic diffuse matter with shock fronts. If this is correct, we have a source of magnetic discontinuities. Probably many of these discontinuities will be rather small. However, either their cumulative effect or the effect of some occasional major discontinuity will tend to convert the angle of pitch that a previous trap acceleration has reduced to a small value back to a statistical distribution corresponding to isotropy of direction. At this moment the particle is ready for a new trap acceleration.

Probably our knowledge of the galactic magnetic field is still inadequate for a realistic discussion of the process here proposed. I would like, nevertheless, to list here in a purely hypothetical way a set of parameters that may be compatible with our present knowledge. We assume that a particle for part of the time has $\vartheta < \chi$ and that it spirals in the same direction along the line of force without being caught in traps. Let λ be the average distance of travel while the particle is in this state, measured along the line of force. After the mean path λ, the particle will change ϑ back to a high value and for a period of time will be frequently caught in traps, until its energy increases by a factor f and ϑ decreases again to $\vartheta < \chi$. After this the process repeats itself. Let T be the average duration of one such cycle. The time A for acceleration by a factor e, then, is

$$A = \frac{T}{\ln f}. \tag{13}$$

The escape time B can be estimated as follows. Let L be the stretched-out length of the galaxy. The motion of the particle along L can be described as a random walk, with steps of duration T. The mean displacement in a step is given in first approximation by λ, because the particle, during the acceleration phase, changes its direction very frequently and does not move far. Estimating B with the diffusion theory, one finds

$$B = \frac{T\,(L/\lambda)^2}{\pi^2}. \tag{14}$$

A set of parameters that yields $A = 15$ million years and $B = 10$ million years is the following.

$$L = 1.3 \times 10^{24}\ \text{cm}, \qquad \lambda = 2 \times 10^{23}\ \text{cm};$$

$$T = 2.3 \times 10^{6}\ \text{years}, \qquad f = 1.17.$$

Naturally, these values are given here merely as an indication of possible orders of magnitude. Only a much more thorough discussion of the actual conditions in the galaxy may enable one to find reliable values of these quantities.

Two important questions should be discussed further. One is the injection mechanism that should feed into interstellar space an adequate number of particles of energy large enough for the present acceleration mechanism to take over. This problem was discussed in R, but no definite conclusion was reached there. The fact that the acceleration by the galactic magnetic field discussed here is appreciably faster than in R makes the requirements of the injection somewhat less stringent. Nevertheless, one still needs a very

[5] *Phys. Rev.*, **80**, 692, 1950.

powerful injection mechanism. Recent evidence that cosmic-ray-like particles are emitted by the sun indicates the stars, or perhaps stars of special types, as the most likely injectors.

A second question has to do with the energy balance of the turbulence of the interstellar gas. If it is true that the cosmic radiation leaks out of the galaxy in a time of the order of 10 million years, it is necessary that its energy be replenished a few hundred times during a time equal to the age of the universe. A simple estimate shows that the energy present in the galaxy in the form of cosmic rays is comparable to the kinetic energy due to the turbulence of the intergalactic gas. According to the present theory, the cosmic rays are accelerated at the expense of the turbulent energy. This last, therefore, must be continuously renewed by some very abundant source, perhaps like a small fraction of the radiation energy of the stars.

In conclusion, I should like to stress the fact that, regardless of the details of the acceleration mechanism, cosmic radiation and magnetic fields in the galaxy must be counted as very important factors in the equilibrium of interstellar gas.

THE GRAVITATIONAL INSTABILITY OF AN INFINITE HOMOGENEOUS MEDIUM WHEN CORIOLIS FORCE IS ACTING AND A MAGNETIC FIELD IS PRESENT*

S. CHANDRASEKHAR
Yerkes Observatory
Received August 24, 1953

ABSTRACT

It is shown that Jeans's criterion for the gravitational instability of an infinite homogeneous medium is unaffected by the presence of a magnetic field, even if the system is partaking in rotation and Coriolis force is operative.

1. *Introduction.*—It has recently been shown that Jeans's criterion for the gravitational instability of an infinite homogeneous medium remains unaffected both when Coriolis force is acting[1] and when a magnetic field is present.[2] Generalizing these results, we shall show in this paper that Jeans's criterion remains valid also when both the agencies, Coriolis force and magnetic field, are simultaneously acting.

2. *The three modes of wave propagation and the condition for gravitational instability.*—Consider an extended homogeneous medium of infinite electrical conductivity partaking in rotation with an angular velocity $\boldsymbol{\Omega}$; and let there be present also a uniform magnetic field of intensity $\boldsymbol{H}$. Then the fluctuations in the density ($\delta\rho$), pressure (δp), magnetic field ($\boldsymbol{h}$), and gravitational potential (δV) are governed by the equations

$$\rho\frac{\partial \boldsymbol{u}}{\partial t}=\frac{1}{4\pi}\operatorname{curl}\boldsymbol{h}\times\boldsymbol{H}+2\rho\boldsymbol{u}\times\boldsymbol{\Omega}-\operatorname{grad}\delta p+\rho\operatorname{grad}\delta V\,,$$

$$\frac{\partial \boldsymbol{h}}{\partial t}=\operatorname{curl}(\boldsymbol{u}\times\boldsymbol{H})\,;\qquad \operatorname{div}\boldsymbol{h}=0\,, \tag{1}$$

$$\frac{\partial}{\partial t}\delta\rho=-\rho\operatorname{div}\boldsymbol{u}\qquad\text{and}\qquad\nabla^2\delta V=-4\pi G\delta\rho\,.$$

If the changes in pressure and density are assumed to take place adiabatically, then

$$\delta p=c^2\delta\rho \tag{2}$$

where $c=\sqrt{(\gamma p/\rho)}$ denotes the conventional velocity of sound.

In the further discussion of equations (1) we shall suppose that the orientation of the co-ordinate axes is so chosen that

$$\boldsymbol{H}=(0,\,H_y,\,H_z)\,,\qquad\text{while}\qquad\boldsymbol{\Omega}=(\Omega_x,\,\Omega_y,\,\Omega_z)\,. \tag{3}$$

We shall seek solutions of equations (1) which correspond to the propagation of waves in the z-direction. Then $\partial/\partial z$ is the only nonvanishing component of the gradient; and it follows at once from the divergence condition, div $\boldsymbol{h}=0$, that $h_z=0$. Equations (1)

* The research reported in this paper has been supported in part by the Geophysics Research Directorate of the Air Force Cambridge Research Center, Air Research and Development Command, under Contract AF 19(604)-299 with the University of Chicago.

[1] S. Chandrasekhar, *Vistas in Astronomy* (London: Pergamon, 1954).

[2] S. Chandrasekhar and E. Fermi, *Ap. J.*, **118**, 116, 1953.

then take the forms

$$\begin{aligned}
&\frac{\partial h_x}{\partial t} - H_x \frac{\partial u_x}{\partial z} = 0\,,\\
&\frac{\partial h_y}{\partial t} + H_y \frac{\partial u_x}{\partial z} - H_z \frac{\partial u_y}{\partial z} = 0\,,\\
&\frac{\partial u_x}{\partial t} - \frac{H_z}{4\pi\rho}\frac{\partial h_x}{\partial z} + 2\,(u_z\Omega_y - u_y\Omega_z) = 0\,,\\
&\frac{\partial u_y}{\partial t} - \frac{H_z}{4\pi\rho}\frac{\partial h_y}{\partial z} + 2\,(u_z\Omega_z - u_z\Omega_x) = 0\,,\\
&\frac{\partial u_z}{\partial t} + \frac{H_y}{4\pi\rho}\frac{\partial h_y}{\partial z} + \frac{c^2}{\rho}\frac{\partial}{\partial z}\,\delta\rho - \frac{\partial}{\partial z}\,\delta V + 2\,(u_y\Omega_z - u_x\Omega_y) = 0\,,\\
&\frac{\partial}{\partial t}\,\delta\rho + \rho\frac{\partial u_z}{\partial z} = 0\,,
\end{aligned} \tag{4}$$

and

$$\frac{\partial^2}{\partial z^2}\,\delta V + 4\pi G\,\delta\rho = 0\,.$$

For a solution which represents the propagation of a wave in the z-direction

$$\frac{\partial}{\partial t} = i\omega \quad \text{and} \quad \frac{\partial}{\partial z} = -ik\,, \tag{5}$$

where ω denotes the frequency and k the wave number. Making substitutions (5) in equations (4), we obtain a system of linear homogeneous equations for the amplitudes of the various quantities which can be written in matrix notation in the following form:

$$\begin{vmatrix}
\omega & 0 & kH_z & 0 & 0 & 0 & 0 \\
0 & \omega & 0 & kH_z & -kH_y & 0 & 0 \\
\dfrac{kH_z}{4\pi\rho} & 0 & \omega & +2i\Omega_z & -2i\Omega_y & 0 & 0 \\
0 & \dfrac{kH_z}{4\pi\rho} & -2i\Omega_z & \omega & +2i\Omega_x & 0 & 0 \\
0 & -\dfrac{kH_y}{4\pi\rho} & +2i\Omega_y & -2i\Omega_x & \omega & -\dfrac{c^2k}{\rho} & k \\
0 & 0 & 0 & 0 & -\rho k & \omega & 0 \\
0 & 0 & 0 & 0 & 0 & 4\pi G & -k^2
\end{vmatrix}
\begin{vmatrix}
h_x \\ h_y \\ u_x \\ u_y \\ u_z \\ \delta\rho \\ \delta V
\end{vmatrix} = 0\,. \tag{6}$$

The condition that equation (6) has a nontrivial solution is that the determinant of the matrix on the left-hand side should vanish. On expanding the determinant, we find that it can be reduced to the form

$$\begin{aligned}
&\omega^6 - \omega^4\{\,(4\Omega^2 + \Omega_A^2) + (\Omega_A^2 + \Omega_B^2 + \Omega_J^2)\,\}\\
&\qquad + \omega^2\{\Omega_J^2\,(4\Omega_z^2 + \Omega_A^2) + \Omega_A^2\,(4\Omega_z^2 + \Omega_A^2 + \Omega_B^2 + \Omega_J^2) + 4\,(\Omega_y\Omega_A - \Omega_z\Omega_B)^2\}\\
&\qquad - \Omega_A^4\Omega_J^2 = 0\,,
\end{aligned} \tag{7}$$

where

$$\Omega_A^2 = \frac{k^2 H_z^2}{4\pi\rho}, \qquad \Omega_B^2 = \frac{k^2 H_y^2}{4\pi\rho}, \tag{8}$$[3]

$$\Omega_J^2 = c^2k^2 - 4\pi G\rho\,, \qquad \text{and} \qquad \Omega^2 = |\,\mathbf{\Omega}\,|^2\,.$$

From equation (7) it follows that there are, in general, three modes in which a wave can be propagated through the medium; and that if ω_1, ω_2, and ω_3 denote the frequencies of these three modes, then

$$\omega_1^2 + \omega_2^2 + \omega_3^2 = 4\Omega^2 + 2\Omega_A^2 + \Omega_B^2 + \Omega_J^2\,, \tag{9}$$

and

$$\omega_1\omega_2\omega_3 = \Omega_A^2\Omega_J\,. \tag{10}$$

Hence *if Ω_J is imaginary, then either ω_1, ω_2, or ω_3 must be imaginary.* In all cases, there will therefore be a mode of wave propagation which will become unstable when Ω_J becomes imaginary. Now the condition for Ω_J to become imaginary is

$$c^2k^2 < 4\pi G\rho\,; \tag{11}$$

but this is precisely Jeans's condition. The condition for gravitational instability is therefore unaffected by Coriolis and magnetic forces acting jointly or separately.

[3] It can be readily verified that, when $\boldsymbol{H} = 0$, this equation reduces to eq. (14), given in reference 1, while, when $\mathbf{\Omega} = 0$, it reduces to eq. (169), given in reference 2.

ON THE PULSATION OF A STAR IN WHICH THERE IS A PREVALENT MAGNETIC FIELD*

S. CHANDRASEKHAR AND D. NELSON LIMBER
Yerkes Observatory
Received August 24, 1953

ABSTRACT

In this paper a simple approximate formula is obtained for the frequency (σ) of radial pulsation of a gaseous star in which there is a prevalent magnetic field. The formula is

$$\sigma^2 I = -(3\gamma - 4)(\Omega + \mathfrak{M}),$$

where γ is the ratio of the specific heats,

$$I = \int_0^M r^2 dm\,(r),$$

and Ω and $\mathfrak{M}$ denote the gravitational potential energy and the magnetic energy of the star, respectively. The formula is derived from the virial theorem in the form recently established by Chandrasekhar and Fermi; and it supports their conclusion that the period of pulsation can be made as long as one may desire by letting the magnetic energy approach the upper limit (namely, $|\Omega|$) set by the virial theorem.

1. *Introduction.*—The pulsation of a star in which there is a prevalent magnetic field has been the subject of several investigations.[1] But so far no simple formula has been derived in terms of which one may easily visualize the effect of the magnetic field on the period. In this paper we shall show how such a formula can be derived by making use of the virial theorem in the form recently established by Chandrasekhar and Fermi.[2]

2. *An integral formula for the frequency of oscillation.*—We start with the statement of the virial theorem in the form (Paper I, eq. [11])

$$\frac{1}{2}\frac{d^2 I}{dt^2} = 2T + 3(\gamma - 1)\mathfrak{U} + \Omega + \mathfrak{M}, \tag{1}$$

where Ω denotes the gravitational potential energy,

$$I = \int_0^M r^2 dm, \qquad T = \frac{1}{2}\int_0^M |\boldsymbol{u}|^2 dm, \tag{2}$$

$$(\gamma - 1)\mathfrak{U} = \int_0^M \frac{p}{\rho}\, dm, \qquad \text{and} \qquad \mathfrak{M} = \int_0^M \frac{|\boldsymbol{H}|^2}{8\pi\rho}\, dm. \tag{2a}$$

In equations (2),

$$dm = \rho dx_1 dx_2 dx_3 \tag{3}$$

denotes the element of mass, and the integrations are effected over the entire mass, M,

* The research reported in this paper has been supported in part by the Geophysics Research Directorate of the Air Force Cambridge Research Center, Air Research and Development Command, under Contract AF 19(604)-299 with the University of Chicago.

[1] M. Schwarzschild, *Ann. d'ap.*, **12**, 148, 1949; G. Gjellestad, *Rep. No. 1. Inst. Theor. Ap.* (Oslo, 1950) and *Ann. d'ap.*, **15**, 276, 1952; V. C. A. Ferraro and D. J. Memory, *M.N.*, **112**, 361, 1952; T. G. Cowling, *M.N.*, **112**, 527, 1952.

[2] S. Chandrasekhar and E. Fermi, *Ap. J.*, **118**, 116, 1952. This paper will be referred to hereafter as "Paper I."

of the configuration. The remaining symbols have their usual meanings (they are all defined in Paper I).

We shall apply equation (1) to the adiabatic pulsation of a gaseous star in which there is a prevalent magnetic field. In analyzing this problem, we shall adopt the Lagrangian mode of description and follow each element of mass, dm, as it moves. The advantage of the Lagrangian over the Eulerian mode in our present context arises from the fact that dm remains constant during the motion; this is required by the conservation of mass.

Considering periodic oscillations with a frequency σ, we shall let $\boldsymbol{\xi} e^{i\sigma t}$ denote the displacement of an element of mass, dm, from its equilibrium position, $\boldsymbol{r}$. Similarly, we shall let $\delta p e^{i\sigma t}$, $\delta\rho e^{i\sigma t}$, and $\delta \boldsymbol{H} e^{i\sigma t}$ denote the corresponding changes in the other physical variables as we follow the element during its motion. The assumption that the oscillation takes place adiabatically requires that the changes in pressure and density, as we follow the motion, are related by

$$\frac{\delta p}{p} = \gamma \frac{\delta \rho}{\rho}, \tag{4}$$

while the equation of continuity requires that

$$\frac{\delta \rho}{\rho} = -\frac{\partial \xi_i}{\partial x_i} \tag{5}$$

(as in Paper I, we are adopting the summation convention).

Returning to equation (1) and letting $\delta I e^{i\sigma t}$, $\delta \mathfrak{U} e^{i\sigma t}$, $\delta\Omega e^{i\sigma t}$, and $\delta \mathfrak{M} e^{i\sigma t}$ denote the changes in I, $\mathfrak{U}$, Ω, and $\mathfrak{M}$, we can write

$$-\sigma^2 \int_0^M \xi_i x_i \, dm = 3(\gamma - 1)\,\delta\mathfrak{U} + \delta\Omega + \delta\mathfrak{M}, \tag{6}$$

since, to the first order in the displacement, the term in T will not make any contribution.

Considering the first of the three terms on the right-hand side of equation (6), we have (cf. eqs. [2], [4], and [5])

$$\begin{aligned} 3(\gamma-1)\,\delta\mathfrak{U} &= 3\int_0^M \delta\left(\frac{p}{\rho}\right) dm = 3(\gamma-1)\int_0^M \frac{p}{\rho}\frac{\delta\rho}{\rho}\, dm \\ &= -3(\gamma-1)\iiint p\,\frac{\partial \xi_i}{\partial x_i}\, dx_1 dx_2 dx_3, \end{aligned} \tag{7}$$

where the integration over x_1, x_2, and x_3 is over the entire volume[3] of the configuration. Letting

$$P = p + \frac{|\boldsymbol{H}|^2}{8\pi} \tag{8}$$

denote the total pressure, we shall rewrite equation (7) in the form

$$\begin{aligned} 3(\gamma-1)\,\delta\mathfrak{U} = &-3(\gamma-1)\iiint P\,\frac{\partial \xi_i}{\partial x_i}\, dx_1 dx_2 dx_3 \\ &+3(\gamma-1)\iiint \frac{|\boldsymbol{H}|^2}{8\pi}\,\frac{\partial \xi_i}{\partial x_i}\, dx_1 dx_2 dx_3. \end{aligned} \tag{9}$$

Integrating by parts the first of the two integrals on the right-hand side of equation (9) and making use of the equation (cf. Paper I, eq. [4])

$$\frac{\partial P}{\partial x_i} = \rho\frac{\partial V}{\partial x_i} + \frac{1}{4\pi}\frac{\partial}{\partial x_j} H_i H_j \tag{10}$$

[3] For a star with a prevailing magnetic field, the effective boundary may have to be placed quite outside the conventional photospheric surface. We return to this question presently.

(where V denotes the gravitational potential), which obtains in the equilibrium state, we find

$$\iiint P \frac{\partial \xi_i}{\partial x_i}\, dx_1 dx_2 dx_3 = \int_{\text{surface}} P\boldsymbol{\xi}\cdot d\boldsymbol{S} - \iiint \xi_i \left(\rho \frac{\partial V}{\partial x_i} + \frac{1}{4\pi}\frac{\partial}{\partial x_j} H_i H_j\right) dx_1 dx_2 dx_3 . \tag{11}$$

In equation (11) the surface integral is over the bounding surface ($\boldsymbol{S}$) of the configuration. We shall now assume that P vanishes on $\boldsymbol{S}$. This assumption requires that not only p but also $\boldsymbol{H}$ vanish on the bounding surface. Accordingly, we must suppose that the bounding surface, $\boldsymbol{S}$, is placed at a sufficient distance from the photospheric surface that $\boldsymbol{H}$ may indeed be considered negligible here. It would appear that in most astrophysical contexts we can accomplish this without violating the assumption of the infinite electrical conductivity of the stellar material which underlies this whole development.

Assuming, then, that P vanishes on the bounding surface, we have (cf. eq. [11])

$$\iiint P \frac{\partial \xi_i}{\partial x_i}\, dx_1 dx_2 dx_3 = -\iiint \rho \xi_i \frac{\partial V}{\partial x_i}\, dx_1 dx_2 dx_3 - \frac{1}{4\pi}\iiint \xi_i \frac{\partial}{\partial x_j} H_i H_j\, dx_1 dx_2 dx_3 . \tag{12}$$

After a further integration by parts (of the second integral on the right-hand side), we obtain

$$\iiint P \frac{\partial \xi_i}{\partial x_i}\, dx_1 dx_2 dx_3 = -\iiint \rho \xi_i \frac{\partial V}{\partial x_i}\, dx_1 dx_2 dx_3 + \frac{1}{4\pi}\iiint H_i H_j \frac{\partial \xi_i}{\partial x_j}\, dx_1 dx_2 dx_3 , \tag{13}$$

the integrated part again making no contribution, since $\boldsymbol{H}$ has been assumed to vanish on the bounding surface.

Now, combining equations (9), (11), (12), and (13), we have

$$3(\gamma-1)\,\delta\mathfrak{U} = 3(\gamma-1)\left\{\int_0^M \xi_i \frac{\partial V}{\partial x_i}\, dm + \frac{1}{8\pi}\iiint |\boldsymbol{H}|^2 \frac{\partial \xi_i}{\partial x_i}\, dx_1 dx_2 dx_3 - \frac{1}{4\pi}\iiint H_i H_j \frac{\partial \xi_i}{\partial x_j}\, dx_1 dx_2 dx_3\right\} . \tag{14}$$

Turning next to the terms $\delta\Omega$ and $\delta\mathfrak{M}$ in equation (6), we first observe that

$$\delta\Omega = -\int^M \xi_i \frac{\partial V}{\partial x_i}\, dm . \tag{15}$$

This follows from entirely elementary considerations. It remains only to evaluate $\delta\mathfrak{M}$. We have (cf. eq. [2a])

$$\delta\mathfrak{M} = \frac{1}{4\pi}\iiint H_i\, \delta H_i\, dx_1 dx_2 dx_3 - \frac{1}{8\pi}\iiint |\boldsymbol{H}|^2 \frac{\delta\rho}{\rho}\, dx_1 dx_2 dx_3 ; \tag{16}$$

or, using equation (5), we have

$$\delta\mathfrak{M} = \frac{1}{4\pi}\iiint H_i\, \delta H_i\, dx_1 dx_2 dx_3 + \frac{1}{8\pi}\iiint |\boldsymbol{H}|^2 \frac{\partial \xi_i}{\partial x_i}\, dx_1 dx_2 dx_3 . \tag{17}$$

Now the change in the magnetic field $\delta \boldsymbol{H}$ as we follow the motion of an element of gas of infinite electrical conductivity is given by (cf. Paper I, eq. [36])

$$\delta \boldsymbol{H} = \operatorname{curl} (\boldsymbol{\xi} \times \boldsymbol{H}) + (\boldsymbol{\xi} \cdot \operatorname{grad}) \boldsymbol{H} , \tag{18}$$

or, alternatively,

$$\delta H_i = H_j \frac{\partial \xi_i}{\partial x_j} - H_i \frac{\partial \xi_j}{\partial x_j} . \tag{19}$$

Substituting this last expression for δH_i in equation (17), we obtain

$$\delta \mathfrak{M} = \frac{1}{4\pi} \iiint H_i H_j \frac{\partial \xi_i}{\partial x_j} - \frac{1}{8\pi} \iiint |\boldsymbol{H}|^2 \frac{\partial \xi_i}{\partial x_i} \, dx_1 dx_2 dx_3 . \tag{20}$$

Finally, inserting the expressions (14), (15), and (20) for $3(\gamma - 1)\delta \mathfrak{U}$, $\delta \Omega$, and $\delta \mathfrak{M}$ in equation (6), we obtain

$$\begin{aligned} \sigma^2 \int_0^M \xi_i x_i \, dm = & - (3\gamma - 4) \left\{ \int_0^M \xi_i \frac{\partial V}{\partial x_i} \, dm \right. \\ & \left. + \frac{1}{8\pi} \iiint |\boldsymbol{H}|^2 \frac{\partial \xi_i}{\partial x_i} \, dx_1 dx_2 dx_3 - \frac{1}{4\pi} \iiint H_i H_j \frac{\partial \xi_i}{\partial x_j} \, dx_1 dx_2 dx_3 \right\} . \end{aligned} \tag{21}$$

This is the required integral formula for σ^2.

3. *An approximate formula for the frequency of radial pulsation.*—It is known from an analysis by Ledoux[4] similar to the foregoing but relating to the radial pulsation of ordinary stars that a reliable estimate of the period of pulsation of such stars can be obtained by writing

$$\xi_i = \text{Constant } x_i , \tag{22}$$

in a formula for σ^2 analogous to equation (21); indeed, Ledoux's formula for σ^2 can be obtained by setting $\boldsymbol{H} = 0$ in equation (21). We shall assume that this will continue to be the case in our present problem. Therefore, making the substitution (22) in equation (21), we obtain

$$\sigma^2 \int_0^M r^2 dm = - (3\gamma - 4) \left\{ \int_0^M x_i \frac{\partial V}{\partial x_i} \, dm + \frac{1}{8\pi} \iiint |\boldsymbol{H}|^2 dx_1 dx_2 dx_3 \right\} , \tag{23}$$

or (cf. eqs. [2])

$$\sigma^2 = - (3\gamma - 4) \frac{(\Omega + \mathfrak{M})}{I} . \tag{24}$$

This formula for σ^2 confirms the conclusion reached by Chandrasekhar and Fermi (Paper I, p. 119) on general grounds that σ^2 must tend to zero as the total magnetic energy ($\mathfrak{M}$) of the star tends to the upper limit (namely, $|\Omega|$) set by the virial theorem.

[4] P. Ledoux, *Ap. J.*, **102**, 143, 1945.

ON EQUILIBRIUM CONFIGURATIONS OF OBLATE FLUID SPHEROIDS WITH A MAGNETIC FIELD*

GURO GJELLESTAD†
Yerkes Observatory, University of Chicago
Received April 13, 1953; revised August 10, 1953

ABSTRACT

It is shown that a homogeneous incompressible oblate fluid spheroid of infinite electrical conductivity can be an equilibrium configuration if it has a uniform internal magnetic field and an external dipole field. The condition for stability is established, and the equilibrium spheroids are discussed briefly. It is shown that an oblate spheroidal cloud in an interstellar magnetic field in a spiral arm, as estimated by Chandrasekhar and Fermi, will be stable if the density is at least 14 times larger than the average density of the surrounding interstellar matter, while it will be unstable and contract to a disklike shape or disintegrate if the density is less than 14 times the average density.

I. INTRODUCTION

Chandrasekhar and Fermi have recently shown[1] that a gravitating incompressible fluid sphere of infinite electrical conductivity with an initially uniform magnetic field inside and a dipole field outside is not a configuration of equilibrium and that the sphere will tend to contract in the direction of the axis of symmetry. In this paper we shall show, following the method developed by Chandrasekhar and Fermi, that there exists a sequence of oblate spheroids of equilibrium in a magnetic field of the same characteristics as that for a sphere (uniform field inside, dipole field outside), though in the absence of such a magnetic field an oblate spheroid cannot be in equilibrium under its own gravity.

II. FORMULATION OF THE PROBLEM

The system of spheroids to be studied is assumed to be incompressible, homogeneous and nonrotating, and in infinite empty space. It is further assumed that there is a uniform magnetic field, $\boldsymbol{H}$, inside the spheroid. The corresponding external field is taken to be one which can be described by a central dipole, the axis of symmetry being parallel to the uniform field and along the minor axis of the spheroid. The electrical conductivity is considered infinite.

It is convenient to discuss the problem in spheroidal co-ordinates defined in terms of the triple infinity of orthogonal surfaces provided by the confocal spheroids,

$$\frac{x^2+y^2}{1+\zeta^2}+\frac{z^2}{\zeta^2}=c^2 \qquad (0 \leqslant \zeta < \infty), \quad (1)$$

the confocal hyperboloids,

$$\frac{x^2+y^2}{1-\mu^2}-\frac{z^2}{\mu^2}=c^2 \qquad (-1 \leqslant \mu \leqslant +1), \quad (2)$$

and the planes,

$$\varphi = \text{Constant} \qquad (0 \leqslant \varphi \leqslant 2\pi) \quad (3)$$

through the z-axis. In equations (1) and (2), c is a constant equal to half the distance between the foci.

* The research reported in this paper has been supported in part by the Geophysics Research Directorate of the Air Force Cambridge Research Center, Air Research and Development Command, under Contract AF 19(604)-299 with the University of Chicago.

† Research and tutorial fellow of University of Oslo (Institute of Theoretical Astrophysics, Blindern-Oslo, Norway); I.F.U.W. fellow, 1952–53.

[1] *Ap. J.*, **118**, 116, 1953.

According to equations (1), (2), and (3),

$$x = c\,[(1+\zeta^2)(1-\mu^2)]^{1/2}\cos\varphi\,, \qquad y = c\,[(1+\zeta^2)(1-\mu^2)]^{1/2}\sin\varphi\,, \tag{4}$$
$$z = c\,\zeta\mu\,.$$

Now, considering an oblate spheroid whose boundary is given by

$$\zeta = E\,, \tag{5}$$

we shall investigate its stability to a deformation which changes the boundary (5) into one given by

$$\zeta = E + \epsilon\,\frac{1+E^2}{E^2+\mu^2}P_n(\mu) \qquad (n>0)\,, \tag{6}$$

where ϵ is a nondimensional constant. The reason for choosing a deformation of this form will become apparent in Section III. We shall call this deformation a "P_n-deformation."

We shall see that for a P_2-deformation the change in the magnetic energy, $\Delta\mathfrak{M}$, and the change in the gravitational potential energy, $\Delta\Omega$, are both of the first order in ϵ and of opposite signs. The condition $\Delta\mathfrak{M} + \Delta\Omega = 0$ (for a P_2-deformation) is used to define the equilibrium spheroids.

III. THE DISPLACEMENT $\boldsymbol{\xi}$

Following Chandrasekhar and Fermi, we shall consider the deformation (6) as the result of applying a (small) displacement $\boldsymbol{\xi}$ to each point of the spheroid.

Expressing the displacement in the form

$$\boldsymbol{\xi} = \operatorname{grad}\psi\,, \tag{7}$$

we can determine ψ as the solution of Laplace's equation,

$$\nabla^2\psi = 0\,. \tag{8}$$

In solving this and other equations we shall consider only solutions which have axial symmetry. In the system of co-ordinates chosen, equation (8) takes the form

$$\left\{\frac{\partial}{\partial\zeta}\left[(1+\zeta^2)\frac{\partial}{\partial\zeta}\right] + \frac{\partial}{\partial\mu}\left[(1-\mu^2)\frac{\partial}{\partial\mu}\right]\right\}\psi = 0\,. \tag{9}$$

A particular solution of this equation which has no singularities within a finite spheroid is known to be[2]

$$\psi_n = B_n P_n(i\zeta)P_n(\mu)\,, \tag{10}$$

where B_n is an arbitrary constant. The functions $P_n(i\zeta)$ and $P_n(\mu)$ are Legendre functions of the first kind.

The particular forms of the functions $P_n(i\zeta)$ for $n = 1$, 2, and 4, which we shall need, may be noted here:

$$P_0(i\zeta) = 1\,, \quad P_1(i\zeta) = i\zeta\,, \quad P_2(i\zeta) = -\tfrac{1}{2}(3\zeta^2+1)\,;$$
$$P_n^1(i\zeta) = (1+\zeta^2)^{1/2}\frac{dP_n(i\zeta)}{d\zeta}\,, \quad P_1^1(i\zeta) = i(1+\zeta^2)^{1/2}\,; \tag{11}$$
$$P_2^1(i\zeta) = -3\zeta(1+\zeta^2)^{1/2}\,, \quad P_4^1(i\zeta) = \tfrac{5}{2}\zeta(7\zeta^2+3)(1+\zeta^2)^{1/2}\,.$$

[2] A convenient reference for the functions $P_n(i\zeta)$ and functions $Q_n(i\zeta)$ introduced later in the discussion is W. R. Smythe, *Static and Dynamic Electricity* (New York and London: McGraw-Hill Book Co., Inc., 1939), chap. v.

Combining equations (7), (10), and (11), we have

$$\xi_\zeta = \frac{1}{c}\left(\frac{1+\zeta^2}{\zeta^2+\mu^2}\right)^{1/2}\frac{\partial \psi_n}{\partial \zeta} = \frac{B_n}{c\,(\zeta^2+\mu^2)^{1/2}}P_n^1(i\zeta)P_n(\mu) \tag{12}$$

and

$$\xi_\theta = -\frac{1}{c}\left(\frac{1-\mu^2}{\zeta^2+\mu^2}\right)^{1/2}\frac{\partial \psi_n}{\partial \mu} = -\frac{B_n}{c\,(\zeta^2+\mu^2)^{1/2}}P_n(i\zeta)P_n^1(\mu) \tag{13}$$

(the subscript θ will be used for convenience instead of μ).

At the boundary ($\zeta = E$), we have

$$\xi_\zeta = \frac{B_n}{c\,(E^2+\mu^2)^{1/2}}P_n^1(iE)P_n(\mu) \qquad (\zeta = E)\,. \tag{14}$$

This linear displacement along the hyperbolic arc, μ = Constant, corresponds to a change in the ζ-co-ordinate at the boundary, given by

$$d\zeta = \frac{\xi_\zeta}{\partial s/\partial \zeta} = \xi_\zeta\,\frac{1}{c}\left(\frac{1+E^2}{E^2+\mu^2}\right)^{1/2} = \frac{B_n}{c^2}\,\frac{(1+E^2)^{1/2}P_n^1(iE)}{E^2+\mu^2}P_n(\mu)\,. \tag{15}$$

On the other hand, by equation (6), we have

$$d\zeta = \epsilon\,\frac{1+E^2}{E^2+\mu^2}P_n(\mu)\,. \tag{16}$$

Hence

$$\epsilon = \frac{B_n}{c^2\,(1+E^2)^{1/2}}P_n^1(iE) \qquad \text{or} \qquad B_n = \frac{c^2\,(1+E^2)^{1/2}}{P_n^1(iE)}\,\epsilon\,; \tag{17}$$

and we have

$$\xi_\zeta = \epsilon\,\frac{c\,(1+E^2)^{1/2}}{P_n^1(iE)\,(\zeta^2+\mu^2)^{1/2}}P_n^1(i\zeta)P_n(\mu) \tag{18}$$

and

$$\xi_\theta = -\epsilon\,\frac{c\,(1+E^2)^{1/2}}{P_n^1(iE)\,(\zeta^2+\mu^2)^{1/2}}P_n(i\zeta)P_n^1(\mu)\,. \tag{19}$$

At the poles,

$$\xi_\zeta = c\epsilon P_n(\pm 1) = \begin{cases} c\epsilon & \text{when } \mu = +1 \\ (-1)^n c\epsilon & \text{when } \mu = -1 \end{cases} \tag{20}$$

and, at the equator,

$$\xi_\zeta = \frac{c\epsilon}{E}\,(1+E^2)^{1/2}P_n(0)\,. \tag{21}$$

Using the expression for $\boldsymbol{\xi}$ we have derived, we shall now proceed to calculate the changes in the magnetic and gravitational energies.

IV. THE CHANGE IN THE INTERNAL MAGNETIC FIELD AND IN THE INTERNAL MAGNETIC ENERGY

Since infinite electrical conductivity is assumed, the change, $\delta \boldsymbol{H}^{(i)}$, in the internal magnetic field is given by

$$\delta \boldsymbol{H}^{(i)} = \operatorname{curl}(\boldsymbol{\xi} \times \boldsymbol{H})\,. \tag{22}$$

When $\boldsymbol{H}$ is constant and div $\boldsymbol{\xi} = 0$ and $\boldsymbol{\xi} = \operatorname{grad}\psi$, equation (22) reduces to (cf. Chan-

drasekhar and Fermi, *op. cit.*, eq. [132])

$$\delta \boldsymbol{H}^{(i)} = (\boldsymbol{H} \cdot \operatorname{grad})\, \boldsymbol{\xi} = H \frac{\partial}{\partial z} \boldsymbol{\xi} = H \frac{\partial}{\partial z} \operatorname{grad} \psi = \operatorname{grad} \left(H \frac{\partial \psi}{\partial z} \right) \tag{23}$$

or

$$\delta \boldsymbol{H}^{(i)} = \operatorname{grad} (\boldsymbol{H} \cdot \operatorname{grad} \psi) . \tag{24}$$

This shows that $\delta \boldsymbol{H}^{(i)}$ is derivable from a scalar potential,

$$\delta \phi^{(i)} = \boldsymbol{H} \cdot \operatorname{grad} \psi . \tag{25}$$

The components H_ζ and H_θ of the uniform field $\boldsymbol{H}$ in the z-direction inside the spheroid are (cf. eqs. [12] and [13])

$$H_\zeta = H \left(\frac{1+\zeta^2}{\zeta^2+\mu^2} \right)^{1/2} \mu \qquad \text{and} \qquad H_\theta = -H \left(\frac{1-\mu^2}{\zeta^2+\mu^2} \right)^{1/2} \zeta . \tag{26}$$

Introducing equations (10) and (26) into equation (25), we obtain

$$\delta \phi^{(i)} = H_\zeta \frac{1}{c} \left(\frac{1+\zeta^2}{\zeta^2+\mu^2} \right)^{1/2} \frac{\partial \psi}{\partial \zeta} - H_\theta \frac{1}{c} \left(\frac{1-\mu^2}{\zeta^2+\mu^2} \right)^{1/2} \frac{\partial \psi}{\partial \mu}$$

or

$$\delta \phi^{(i)} = \frac{HB_n}{c\,(\zeta^2+\mu^2)} \left[\mu\,(1+\zeta^2)^{1/2} P_n^1(i\zeta) P_n(\mu) - \zeta\,(1-\mu^2)^{1/2} P_n(i\zeta) P_n^1(\mu) \right] . \tag{27}$$

Using the standard recurrence relations satisfied by the Legendre functions, we find that the expression for $\delta \phi^{(i)}$ can be reduced to the form

$$\delta \phi^{(i)} = \frac{B_n H n\,(n+1)}{i c\,(2n+1)} \frac{1}{\zeta^2+\mu^2} \left[P_{n+1}(i\zeta) P_{n-1}(\mu) - P_{n-1}(i\zeta) P_{n+1}(\mu) \right] . \tag{28}$$

This equation can be reduced further in the following way. Using the recurrence relation

$$(2n+1)\, x P_n = n P_{n-1} + (n+1) P_{n+1} \tag{29}$$

twice, we obtain

$$(2n+1)\, x^2 P_n(x) = \frac{(n+1)(n+2)}{2n+3} P_{n+2}(x) + \left[\frac{(n+1)^2}{2n+3} + \frac{n^2}{2n-1} \right] P_n(x) + \frac{n(n-1)}{2n-1} P_{n-2}(x)$$

and

$$(2n+1)\, x'^2 P_n(x') = \frac{(n+1)(n+2)}{2n+3} P_{n+2}(x') + \left[\frac{(n+1)^2}{2n+3} + \frac{n^2}{2n-1} \right] \times P_n(x') + \frac{n(n-1)}{2n-1} P_{n-2}(x') . \tag{30}$$

Multiplying the above identities by $P_n(x')$ and $P_n(x)$, respectively, and subtracting,[3] we obtain

$$(2n+1)(x^2-x'^2) P_n(x) P_n(x') = \frac{(n+1)(n+2)}{2n+3} [P_{n+2}(x) P_n(x') - P_{n+2}(x') P_n(x)] - \frac{n(n-1)}{2n-1} [P_n(x) P_{n-2}(x') - P_n(x') P_{n-2}(x)] . \tag{31}$$

[3] The method used here is similar to one used in establishing the Christoffel identity (cf. E. W. Hobson, *Spherical and Ellipsoidal Harmonics* [Cambridge: At the University Press, 1931], p. 318).

By repeated use of this last recurrence formula, we obtain

$$\sum_{l}^{n}{}'(2l+1)(x^2-x'^2)P_l(x)P_l(x') = \frac{(n+2)(n+1)}{2n+3}[P_{n+2}(x)P_n(x')-P_{n+2}(x')P_n(x)], \tag{32}$$

where $\sum_{l}^{n}{}'$ stands for the summation over l starting from $l = n$ and running through the values $(l-2)$, $(l-4)$, etc., and ending with $l = 0$ or 1, depending upon whether l is even or odd. Lowering n by one unit and putting $x = i\zeta$ and $x' = \mu$, we can rewrite equation (32) in the form

$$\frac{n(n+1)}{2n+1}\frac{1}{\zeta^2+\mu^2}[P_{n+1}(i\zeta)P_{n-1}(\mu)-P_{n-1}(i\zeta)P_{n+1}(\mu)] = -\sum_{l}^{n-1}{}'(2l+1)P_l(i\zeta)P_l(\mu). \tag{33}$$

Using this relation in equation (28), we obtain

$$\delta\phi^{(i)} = \frac{i}{c}B_nH\sum_{l}^{n-1}{}'(2l+1)P_l(i\zeta)P_l(\mu). \tag{34}$$

Hence

$$\delta H_\zeta^{(i)} = \frac{iB_nH}{c^2(\zeta^2+\mu^2)^{1/2}}\sum_{l}^{n-1}{}'(2l+1)P_l^1(i\zeta)P_l(\mu),$$

and

$$\delta H_\theta^{(i)} = -\frac{iB_nH}{c^2(\zeta^2+\mu^2)^{1/2}}\sum_{l}^{n-1}{}'(2l+1)P_l(i\zeta)P_l^1(\mu). \tag{35}$$

According to equations (26) and (35), the change in the internal magnetic energy per unit volume is given by

$$\delta^{(i)}\left(\frac{H^2}{8\pi}\right) = \frac{1}{4\pi}\boldsymbol{H}\cdot\delta\boldsymbol{H}^{(i)} = \frac{iB_nH^2}{4\pi c^2}\left[\mu\frac{(1+\zeta^2)^{1/2}}{\zeta^2+\mu^2}\sum_{l}^{n-1}{}'(2l+1)P_l^1(i\zeta)P_l(\mu) + \zeta\frac{(1-\mu^2)^{1/2}}{\zeta^2+\mu^2}\sum_{l}^{n-1}{}'(2l+1)P_l(i\zeta)P_l^1(\mu)\right]. \tag{36}$$

Because of the orthogonality of the functions $P_l(\mu)$ in the interval -1 to $+1$, the foregoing expression, when integrated over the volume of the spheroid, vanishes for all values of l except for $l = 1$. Hence the total change in the internal magnetic energy, $\delta\mathfrak{M}^{(i)}$, is

$$\delta\mathfrak{M}^{(i)} = 0 \qquad (n \text{ odd}),$$

$$\delta\mathfrak{M}^{(i)} = \frac{3B_nH^2}{4\pi c^2}\int_0^R\int_{-1}^{+1}\int_0^{2\pi}(\zeta^2+\mu^2)^{-1}\{[P_1^1(i\zeta)]^2[P_1(\mu)]^2 + [P_1(i\zeta)]^2[P_1^1(\mu)]^2\}c^3(\zeta^2+\mu^2)\,d\zeta d\mu d\varphi \qquad (n \text{ even}). \tag{37}$$

Evaluating the integrals over μ and ζ (cf. eqs. [11]), equation (37) reduces to

$$\delta \mathfrak{M}^{(i)} = \frac{3\, cB_n H^2}{4\pi}\left[-\frac{2}{3}\left(E+\frac{E^3}{3}\right)-\frac{4}{3}\frac{E^3}{3}\right] 2\pi \tag{38}$$

$$= -H^2 cB_n E\,(1+E^2) \qquad (n \text{ even}).$$

On introducing for B_n from equation (17) into equation (38), we have

$$\delta \mathfrak{M}^{(i)} = 0 \qquad (n \text{ odd}) \tag{39}$$

and

$$\delta \mathfrak{M}^{(i)}_{2n} = -H^2 c^3 E\,(1+E^2)^{3/2}\,[P^1_{2n}(iE)]^{-1}\epsilon_{2n}$$

$$= \frac{H^2 c^3 (1+E^2)\, P^1_2(iE)}{3P^1_{2n}(iE)}\,\epsilon_{2n} \qquad (n \text{ even}),$$

where we have inserted subscripts $2n$ for $\delta\mathfrak{M}^{(i)}$ and ϵ to emphasize that we are dealing with a general P_{2n}-deformation.

V. THE CHANGE IN THE EXTERNAL MAGNETIC FIELD AND IN THE EXTERNAL MAGNETIC ENERGY

The external magnetic field, $\boldsymbol{H}^{(e)}$, corresponding to equations (26), must satisfy the equations

$$\operatorname{curl} \boldsymbol{H}^{(e)} = 0 \qquad \text{and} \qquad \operatorname{div} \boldsymbol{H}^{(e)} = 0\,, \tag{40}$$

and the boundary condition

$$H^{(e)}_\zeta = H^{(i)}_\zeta \qquad \text{at} \qquad \zeta = E\,. \tag{41}$$

The components $H^{(e)}_\zeta$ and $H^{(e)}_\theta$ of $\boldsymbol{H}^{(e)}$ which satisfy equations (40) and (41) are

$${}^0H^{(e)}_\zeta = H\,\frac{(1+E^2)^{1/2}}{Q^1_1(iE)}\,\frac{1}{(\zeta^2+\mu^2)^{1/2}}\,Q^1_1(i\zeta)\,P_1(\mu)$$

and (42)

$${}^0H^{(e)}_\theta = -H\,\frac{(1+E^2)^{1/2}}{Q^1_1(iE)}\,\frac{1}{(\zeta^2+\mu^2)^{1/2}}\,Q_1(i\zeta)\,P^1_1(\mu)\,.$$

The functions $Q_l(i\zeta)$ denote the Legendre functions of the second kind and represent the other set of solutions of Legendre's equation for $(i\zeta)$. The functions can be defined in various ways, essentially depending upon the range of the variable. It is convenient for the problem studied here to define $Q_l(i\zeta)$ by the following series:

$$Q_l(i\zeta) = -i\cot^{-1}\zeta P_l(i\zeta) - \frac{2l-1}{1\cdot l}\,P_{l-1}(i\zeta) - \frac{2l-5}{3\,(l-1)}\,P_{l-3}(i\zeta) - \ldots, \tag{43}$$

which is valid not only for the range of ζ defined in equation (1) but also for corresponding negative values of ζ. By the series (43) and with the help of equations (11), the following functions are derived:

$$Q_0(i\zeta) = -i\cot^{-1}\zeta\,, \qquad Q_1(i\zeta) = \zeta\cot^{-1}\zeta - 1$$

and (44)

$$Q_2(i\zeta) = \tfrac{1}{2}i\,[(3\zeta^2+1)\cot^{-1}\zeta - 3\zeta]\,,$$

$$Q^1_1(i\zeta) = (1+\zeta^2)^{1/2}\left[\cot^{-1}\zeta - \frac{1\zeta}{1+\zeta^2}\right].$$

The function $\cot^{-1}\zeta$ is defined in the range $0 \le \cot^{-1}\zeta \le \pi$.

The components of the external magnetic field after the deformation can be written in the following way:

$$H_\zeta^{(\epsilon)} = {}^0H_\zeta^{(\epsilon)} + \delta H_\zeta = H\,\frac{(1+E^2)^{1/2}}{Q_1^1(iE)}\,\frac{1}{(\zeta^2+\mu^2)^{1/2}}\,Q_1^1(i\zeta)\,P_1(\mu) + \delta H_\zeta^{(\epsilon)}$$

and (45)

$$H_\theta^{(\epsilon)} = {}^0H_\theta^{(\epsilon)} + \delta H_\theta = -H\,\frac{(1+E^2)^{1/2}}{Q_1^1(iE)}\,\frac{1}{(\zeta^2+\mu^2)^{1/2}}\,Q_1(i\zeta)\,P_1^1(\mu) + \delta H_\theta^{(\epsilon)}\,.$$

Here $\delta H_\zeta^{(\epsilon)}$ and $\delta H_\theta^{(\epsilon)}$ represent the change in the external magnetic field. Since $\delta \boldsymbol{H}^{(\epsilon)}$ must satisfy the equations

$$\operatorname{curl} \delta \boldsymbol{H}^{(\epsilon)} = 0 \qquad \text{and} \qquad \operatorname{div} \delta \boldsymbol{H}^{(\epsilon)} = 0\,, \tag{46}$$

we must have

$$\delta H_\zeta^{(\epsilon)} = \frac{\epsilon H}{(\zeta^2+\mu^2)^{1/2}} \sum_{l=1}^{\infty} D_l Q_l^1(i\zeta)\,P_l(\mu)$$

and (47)

$$\delta H_\theta^{(\epsilon)} = -\frac{\epsilon H}{(\zeta^2+\mu^2)^{1/2}} \sum_{l=1}^{\infty} D_l Q_l(i\zeta)\,P_l^1(\mu)\,.$$

The constants D_l are determined by the requirement that, to the first order in ϵ, the normal component of the magnetic field be continuous at the boundary (6). The tangential component of the magnetic field is not continuous at the boundary, and a surface current, proportional to ϵ, will therefore be established. The effect of the surface current is, however, in other respects of no significance for the problem studied here. (This also applies to the undisturbed case, in which there must also be a surface current because of the discontinuity in the tangential component of the magnetic field.)

The normal component, A_N, of a vector $\boldsymbol{A}$ at the boundary (6) in the meridian plane is given by

$$A_N = A_\zeta + A_\theta \left(\frac{1-\mu^2}{1+E^2}\right)^{1/2} \frac{\partial}{\partial \mu}\left[\frac{1+E^2}{E^2+\mu^2}\,\epsilon P_n(\mu)\right]. \tag{48}$$

Correct to the first order of ϵ, the boundary condition for the normal component of the magnetic field therefore gives

$$[H_\zeta^{(i)} - H_\zeta^{(\epsilon)}]_{\zeta'} + [H_\theta^{(i)} - H_\theta^{(\epsilon)}]_E \left(\frac{1-\mu^2}{1+E^2}\right)^{1/2} \frac{\partial}{\partial \mu}\left[\frac{1+E^2}{E^2+\mu^2}\,\epsilon P_n(\mu)\right] + [\delta H_\zeta^{(i)} - \delta H_\zeta^{(\epsilon)}]_E = 0\,, \tag{49}$$

where ζ' is used as an abbreviation for $[E + (1 + E^2)\epsilon P_n(\mu)/(E^2 + \mu^2)]$. On introducing equations (26), (35), (42), (47), and (17) into equation (49), we obtain

$$\begin{aligned}\left[H\left(\frac{1+\zeta'^2}{\zeta'^2+\mu^2}\right)^{1/2}\mu - H\,\frac{(1+E^2)^{1/2}}{Q_1^1(iE)}\,\frac{Q_1^1(i\zeta')}{(\zeta'^2+\mu^2)^{1/2}}\,\mu\right] - \Bigg[H\left(\frac{1-\mu^2}{E^2+\mu^2}\right)^{1/2} E \\ - H\,\frac{(1+E^2)^{1/2}}{Q_1^1(iE)}\,\frac{Q_1(iE)}{(E^2+\mu^2)^{1/2}}\,(1-\mu^2)^{1/2}\Bigg]\left(\frac{1-\mu^2}{1+E^2}\right)^{1/2}\frac{\partial}{\partial\mu}\left[\frac{1+E^2}{E^2+\mu^2}\,\epsilon P_n(\mu)\right] \\ + \frac{i\,(1+E^2)^{1/2} H\epsilon}{(E^2+\mu^2)^{1/2} P_n^1(iE)} \sum_{l}^{n-1}{}' (2l+1)\,P_l^1(iE)\,P_l(\mu) \\ - \frac{\epsilon H}{(E^2+\mu^2)^{1/2}} \sum_{l=1}^{\infty} D_l Q_l^1(iE)\,P_l(\mu) = 0\,.\end{aligned} \tag{50}$$

To the first order in ϵ, we have

$$\left(\frac{1+\zeta'^2}{\zeta'^2+\mu^2}\right)^{1/2}=\left(\frac{1+E^2}{E^2+\mu^2}\right)^{1/2}+\left[\frac{E\,(1+E^2)^{1/2}}{(E^2+\mu^2)^{3/2}}-\frac{E\,(1+E^2)^{3/2}}{(E^2+\mu^2)^{5/2}}\right]\epsilon P_n(\mu)$$

and (51)

$$\frac{Q_1^1(i\zeta)}{(\zeta'^2+\mu^2)^{1/2}}=\frac{Q_1^1(iE)}{(E^2+\mu^2)^{1/2}}+\left[\frac{(1+E^2)\,\partial Q_1^1(iE)/\partial E}{(E^2+\mu^2)^{3/2}}-\frac{E\,(1+E^2)\,Q_1^1(iE)}{(E^2+\mu^2)^{5/2}}\right]\epsilon P_n(\mu).$$

From equations (44) it follows that

$$\begin{aligned}\frac{\partial Q_1^1(iE)}{\partial E}&=E\,(1+E^2)^{-1/2}\left[\cot^{-1}E-\frac{E}{1+E^2}\right]+(1+E^2)^{1/2}\left[-\frac{1}{1+E^2}-\frac{1-E^2}{(1+E^2)^2}\right]\\&=(1+E^2)^{-1/2}\,[E\cot^{-1}E-1]\;-\;(1+E^2)^{-3/2}\\&=(1+E^2)^{-1/2}Q_1(iE)\;-\;(1+E^2)^{-3/2}.\end{aligned}\tag{52}$$

On introducing equations (51) and (52) into equation (50), we obtain

$$\begin{aligned}&H\left(\frac{1+E^2}{E^2+\mu^2}\right)^{1/2}\mu+H\left[\frac{E\,(1+E^2)^{1/2}}{(E^2+\mu^2)^{3/2}}-\frac{E\,(1+E^2)^{3/2}}{(E^2+\mu^2)^{5/2}}\right]\epsilon\mu P_n(\mu)\;-\;H\,\frac{(1+E^2)^{1/2}}{Q_1^1(iE)}\\&\times\frac{Q_1^1(iE)}{(E^2+\mu^2)^{1/2}}\,\mu-H\,\frac{(1+E^2)^{1/2}}{Q_1^1(iE)}\left[\frac{(1+E^2)\,[(1+E^2)^{-1/2}Q_1(iE)-(1+E^2)^{-3/2}]}{(E^2+\mu^2)^{3/2}}\right.\\&\left.-\frac{E\,(1+E^2)\,Q_1^1(iE)}{(E^2+\mu^2)^{5/2}}\right]\epsilon\mu P_n(\mu)\;-\;H\,\frac{1-\mu^2}{(E^2+\mu^2)^{1/2}}\left[E-\frac{(1+E^2)^{1/2}Q_1(iE)}{Q_1^1(iE)}\right]\\&\times(1+E^2)^{1/2}\,\frac{\partial}{\partial\mu}\left[\frac{\epsilon P_n(\mu)}{E^2+\mu^2}\right]+\frac{i\,(1+E^2)^{1/2}H\epsilon}{(E^2+\mu^2)^{1/2}P_n^1(iE)}\sum_l{}'^{n-1}(2l+1)\,P_l^1(iE)\,P_l(\mu)\\&-\frac{H\epsilon}{(E^2+\mu^2)^{1/2}}\sum_{l=1}^{\infty}D_lQ_l^1(iE)\,P_l(\mu)=0.\end{aligned}\tag{53}$$

The two zero-order terms cancel out, as well as two other terms. On dropping the canceling terms and dividing by the common factor ϵH, equation (53) reduces to

$$\begin{aligned}&\frac{(1+E^2)^{1/2}}{(E^2+\mu^2)^{3/2}}\left[\frac{EQ_1^1(iE)\;-\;(1+E^2)^{1/2}Q_1(iE)}{Q_1^1(iE)}\right]\mu P_n(\mu)+\frac{\mu P_n(\mu)}{(E^2+\mu^2)^{3/2}Q_1^1(iE)}\\&-\frac{(1+E^2)^{1/2}}{(E^2+\mu^2)^{1/2}}(1-\mu^2)\left[\frac{EQ_1^1(iE)\;-\;(1+E^2)^{1/2}Q_1(iE)}{Q_1^1(iE)}\right]\frac{\partial}{\partial\mu}\left[\frac{P_n(\mu)}{E^2+\mu^2}\right]\\&+\frac{i\,(1+E^2)^{1/2}}{(E^2+\mu^2)^{1/2}P_n^1(iE)}\sum_l{}'^{n-1}(2l+1)\,P_l^1(iE)\,P_l(\mu)\\&-\frac{1}{(E^2+\mu^2)^{1/2}}\sum_{l=1}^{\infty}D_lQ_l^1(iE)\,P_l(\mu)=0.\end{aligned}\tag{54}$$

From equations (44) we obtain

$$EQ_1^1(iE) - (1+E^2)^{1/2}Q_1(iE) = E(1+E^2)^{1/2}\left[\cot^{-1}E - \frac{E}{1+E^2}\right] - (1+E^2)^{1/2}[E\cot^{-1}E - 1] = (1+E^2)^{-1/2}. \tag{55}$$

Introducing equation (55) into equation (54), we obtain

$$\frac{\mu P_n(\mu)}{Q_1^1(iE)(E^2+\mu^2)^{3/2}} + \frac{\mu P_n(\mu)}{Q_1^1(iE)(E^2+\mu^2)^{3/2}} - \frac{1-\mu^2}{Q_1^1(iE)(E^2+\mu^2)^{1/2}}\frac{\partial}{\partial\mu}\left[\frac{P_n(\mu)}{E^2+\mu^2}\right] + \frac{i(1+E^2)^{1/2}}{P_n^1(iE)(E^2+\mu^2)^{1/2}}\sum_l{}'^{n-1}(2l+1)P_l^1(iE)P_l(\mu) - \frac{1}{(E^2+\mu^2)^{1/2}}\sum_{l=1}^{\infty} D_l Q_l^1(iE)P_l(\mu) = 0 \tag{56}$$

or

$$\frac{2\mu P_n(\mu)}{Q_1^1(iE)(E^2+\mu^2)^{3/2}} - \frac{1-\mu^2}{Q_1^1(iE)(E^2+\mu^2)^{1/2}}\frac{\partial}{\partial\mu}\left[\frac{P_n(\mu)}{E^2+\mu^2}\right] + \frac{i(1+E^2)^{1/2}}{P_n^1(iE)(E^2+\mu^2)^{1/2}} \times \sum_l{}'^{n-1}(2l+1)P_l^1(iE)P_l(\mu) = \frac{1}{(E^2+\mu^2)^{1/2}}\sum_{l=1}^{\infty} D_l Q_l^1(iE)P_l(\mu). \tag{57}$$

In order to find the expansion coefficients D_l, one can multiply equation (57) by, say, $(E^2+\mu^2)^{1/2}P_m(\mu)$ and integrate over μ from -1 to $+1$. Because of the orthogonality of the Legendre functions in this interval, we obtain

$$D_m(n) = \frac{2m+1}{2Q_1^1(iE)Q_m^1(iE)}\left\{\int_{-1}^{+1}\left[\frac{2\mu P_n(\mu)}{E^2+\mu^2} - (1-\mu^2)\frac{\partial}{\partial\mu}\left\{\frac{P_n(\mu)}{E^2+\mu^2}\right\}\right]P_m(\mu)\,d\mu + \frac{i(1+E^2)^{1/2}Q_1^1(iE)}{P_n^1(iE)}\sum_l{}'^{n-1}(2l+1)P_l^1(iE)\int_{-1}^{+1}P_l(\mu)P_m(\mu)\,d\mu\right\}. \tag{58}$$

Integrating the first term by parts and contracting, we obtain

$$\int_{-1}^{+1}\left\{\frac{2\mu P_n(\mu)P_m(\mu)}{E^2+\mu^2} - (1-\mu^2)P_m(\mu)\frac{\partial}{\partial\mu}\left[\frac{P_n(\mu)}{E^2+\mu^2}\right]\right\}d\mu = \int_{-1}^{+1}\frac{2\mu P_n(\mu)P_m(\mu)}{E^2+\mu^2}\,d\mu - \frac{(1-\mu^2)P_m(\mu)P_n(\mu)}{E^2+\mu^2}\Big|_{-1}^{+1} + \int_{-1}^{+1}\frac{P_n(\mu)}{E^2+\mu^2}[-2\mu P_m(\mu) + (1-\mu^2)^{1/2}P_m^1(\mu)]\,d\mu = \frac{m(m+1)}{2m+1}\int_{-1}^{+1}\frac{P_{m-1}(\mu) - P_{m+1}(\mu)}{E^2+\mu^2}P_n(\mu)\,d\mu. \tag{59}$$

Introducing equation (59) into equation (58), we obtain

$$D_m(n) = \frac{1}{Q_1^1(iE)Q_m^1(iE)}\left\{\frac{m(m+1)}{2}\int_{-1}^{+1}\frac{P_{m-1}(\mu) - P_{m+1}(\mu)}{E^2+\mu^2}P_n(\mu)\,d\mu + \frac{i(1+E^2)^{1/2}Q_1^1(iE)}{P_n^1(iE)}\frac{2m+1}{2}\sum_l{}'^{n-1}(2l+1)P_l^1(iE)\int_{-1}^{+1}P_l(\mu)P_m(\mu)\,d\mu\right\}. \tag{60}$$

Since the Legendre functions are power series in μ, we can write expressions of the form

$$\frac{P_{m\pm1}(\mu)\,P_n(\mu)}{E^2+\mu^2}$$

in the following way:

$$\frac{P_{m\pm1}(\mu)\,P_n(\mu)}{E^2+\mu^2} \tag{61}$$
$$= A_{(m\pm1+n)-2}(E^2,\ m,\ n)\,\mu^{(m\pm1+n)-2} + A_{(m\pm1+n)-4}(E^2,\ m,\ n)\,\mu^{(m\pm1+n)-4} + \ldots,$$

where the A's are power series in E^2 (and functions of m and n). The last terms of the series (61) are

$$A_1(E^2,\ m,\ n)\,\mu + \frac{A'(E^2,\ m,\ n)\,\mu}{E^2+\mu^2} \qquad \text{if} \quad (m+n) \text{ is even}$$

and (62)

$$A_0(E^2,\ m,\ n) + \frac{A''(E^2,\ m,\ n)}{E^2+\mu^2} \qquad \text{if} \quad (m+n) \text{ is odd}.$$

Thus the integral (59) *vanishes if* $(m+n)$ *is even*. If $(m+n)$ is *odd*, the integral (59) can be evaluated as indicated above and will give expressions of the following form:

$$\int_{-1}^{+1} \frac{P_{m\pm1}(\mu)\,P_n(\mu)}{E^2+\mu^2}\,d\mu = \begin{cases} (1) \text{ a power series in } E^2 \text{ plus} \\ (2) \text{ a term proportional to the product of another} \\ \quad \text{power series in } E^2 \text{ and } (2/E\,\cot^{-1}E). \end{cases} \tag{63}$$

According to equations (45) and (47), we have, to the first order in ϵ,

$$[H_\zeta^{(e)}]^2 + [H_\theta^{(e)}]^2 = \frac{H^2(1+E^2)}{[Q_1^1(iE)]^2}\,\frac{1}{\zeta^2+\mu^2}\{[Q_1^1(i\zeta)]^2\mu^2 + [Q_1(i\zeta)]^2(1-\mu^2)\}$$
$$+ \frac{2\epsilon H^2(1+E^2)^{1/2}}{Q_1^1(iE)}\,\frac{1}{\zeta^2+\mu^2}\Big\{Q_1^1(i\zeta)\,P_1(\mu)\sum_{l=1}^{\infty} D_l Q_l^1(i\zeta)\,P_l(\mu) \tag{64}$$
$$+ Q_1(i\zeta)\,P_1^1(\mu)\sum_{l=1}^{\infty} D_l Q_l(i\zeta)\,P_l^1(\mu)\Big\}.$$

The change, $\delta\mathfrak{M}^{(e)}$, in the external magnetic energy is therefore, to the first order in ϵ,

$$\delta\mathfrak{M}^{(e)} = \frac{H^2(1+E^2)}{8\pi\,[Q_1^1(iE)]^2}\int_E^{\zeta'}\int_{-1}^{+1}\int_0^{2\pi}\left(\frac{1}{\zeta^2+\mu^2}\right)_E$$
$$\times\{[Q_1^1(i\zeta)]^2\mu^2 + [Q_1(i\zeta)]^2(1-\mu^2)\}_E\,c^3(\zeta^2+\mu^2)_E\,d\zeta\,d\mu\,d\varphi$$
$$+ \frac{2\epsilon H^2(1+E^2)^{1/2}}{8\pi Q_1^1(iE)}\int_E^{\infty}\int_{-1}^{+1}\int_0^{2\pi}\frac{1}{\zeta^2+\mu^2}\Big\{Q_1^1(i\zeta)\,P_1(\mu)\sum_{l=1}^{\infty} D_l Q_l^1(i\zeta)\,P_l(\mu) \tag{65}$$
$$+ Q_1(i\zeta)\,P_1^1(\mu)\sum_{l=1}^{\infty} D_l Q_l(i\zeta)\,P_l^1(\mu)\Big\}\,c^3(\zeta^2+\mu^2)\,d\zeta\,d\mu\,d\varphi.$$

Here

$$\zeta' = E + \frac{1+E^2}{E^2+\mu^2}\,\epsilon P_n(\mu) \tag{66}$$

is introduced as an abbreviation. The first term reduces to (cf. eq. [6])

$$\frac{H^2(1+E^2)\epsilon}{8\pi[Q_1^1(iE)]^2}\,2\pi c^3\int_{-1}^{+1}\{[Q_1^1(iE)]^2\mu^2+[Q_1(iE)]^2(1-\mu^2)\}\frac{1+E^2}{E^2+\mu^2}P_n(\mu)\,d\mu$$

$$=\frac{H^2(1+E^2)^2\epsilon c^3}{4[Q_1^1(iE)]^2}\Big\{[Q_1^1(iE)]^2\int_{-1}^{+1}\frac{\mu^2}{E^2+\mu^2}P_n(\mu)\,d\mu+[Q_1(iE)]^2$$

$$\times\int_{-1}^{+1}\frac{1-\mu^2}{E^2+\mu^2}P_n(\mu)\,d\mu\Big\}$$

$$=\frac{H^2(1+E^2)^2\epsilon c^3}{4[Q_1^1(iE)]^2}\Big\{[Q_1^1(iE)]^2\int_{-1}^{+1}\left(1-\frac{E^2}{E^2+\mu^2}\right)P_n(\mu)\,d\mu-[Q_1(iE)]^2 \tag{67}$$

$$\times\int_{-1}^{+1}\left(1-\frac{1+E^2}{E^2+\mu^2}\right)P_n(\mu)\,d\mu\Big\}$$

$$=\frac{H^2(1+E^2)^2\epsilon c^3}{4[Q_1^1(iE)]^2}\{-E^2[Q_1^1(iE)]^2+(1+E^2)[Q_1(iE)]^2\}\int_{-1}^{+1}\frac{P_n(\mu)}{E^2+\mu^2}\,d\mu\,.$$

Referring to equations (61) and (63) and to the arguments concerning them, we find that the integral on the extreme right-hand side of equation (67) vanishes if *n is odd*, and, if *n is even*, is equal to (1) a power series in E^2 plus (2) a term proportional to the product of another power series in E^2 times $(2/E\cot^{-1}E)$. Because of the orthogonality of the Legendre functions in the interval -1 to $+1$, the second integral in equation (65) vanishes for all values of l except for $l=1$. The second integral therefore reduces to

$$\frac{2H^2\epsilon(1+E^2)^{1/2}c^3}{8\pi Q_1^1(iE)}\,2\pi D_1(n)\int_E^\infty\int_{-1}^{+1}\{[Q_1^1(i\zeta)]^2[P_1(\mu)]^2$$

$$+[Q_1(i\zeta)]^2[P_1^1(\mu)]^2\}\,d\zeta\,d\mu$$

$$=\frac{H^2\epsilon c^3(1+E^2)^{1/2}}{2Q_1^1(iE)}D_1(n)\int_E^\infty\{\tfrac{2}{3}[Q_1^1(i\zeta)]^2+\tfrac{4}{3}[Q_1(i\zeta)]^2\}\,d\zeta \tag{68}$$

$$=\frac{H^2\epsilon c^3(1+E^2)^{1/2}}{3Q_1^1(iE)}D_1(n)\int_E^\infty\{[Q_1^1(i\zeta)]^2+2[Q_1(i\zeta)]^2\}\,d\zeta\,.$$

The integral over ζ can be evaluated by integrating by parts in the following way:

$$\int_E^\infty\{[Q_1^1(i\zeta)]^2+2[Q_1(i\zeta)]^2\}\,d\zeta=\int_E^\infty(1+\zeta^2)\,\frac{\partial Q_1(i\zeta)}{\partial\zeta}\,\frac{\partial Q_1(i\zeta)}{\partial\zeta}\,d\zeta$$

$$+2\int_E^\infty[Q_1(i\zeta)]^2d\zeta=(1+\zeta^2)\frac{\partial Q_1(i\zeta)}{\partial\zeta}Q_1(i\zeta)\Big|_E^\infty-\int_E^\infty\Big\{2\zeta\frac{\partial Q_1(i\zeta)}{\partial\zeta} \tag{69}$$

$$+(1+\zeta^2)\frac{\partial^2Q_1(i\zeta)}{\partial\zeta^2}\Big\}Q_1(i\zeta)\,d\zeta+2\int_E^\infty[Q_1(i\zeta)]^2d\zeta\,.$$

The last two integrals cancel out according to the definition of the function $Q_1(i\zeta)$ by Legendre's equation.

Using the asymptotic value

$$Q_1(i\zeta)\xrightarrow[\zeta\to\infty]{}-\frac{1}{3\zeta^2} \tag{70}$$

and the expansion

$$\cot^{-1}x=\frac{1}{x}-\frac{1}{3x^3}+\frac{1}{5x^5}-\ldots, \tag{71}$$

we find, by equations (44),

$$(1+\zeta^2)\,Q_1(i\zeta)\,\frac{\partial Q_1(i\zeta)}{\partial\zeta}\xrightarrow[\zeta\to\infty]{}-\frac{1+\zeta^2}{3\zeta^2}\Big[\cot^{-1}\zeta-\frac{\zeta}{1+\zeta^2}\Big]\xrightarrow[\zeta\to\infty]{}-\frac{1}{3\zeta^2}\,[\zeta^2\cot^{-1}\zeta$$

$$-\cot^{-1}\zeta-\zeta]\xrightarrow[\zeta\to\infty]{}-\frac{1}{3\zeta^2}\Big[\Big(\zeta-\frac{1}{3\zeta}+\dots\Big)+\Big(\frac{1}{\zeta}-\frac{1}{3\zeta^3}+\dots\Big)-\zeta\Big] \tag{72}$$

$$\xrightarrow[\zeta\to\infty]{}-\frac{2}{9\zeta^2}.$$

The integral (69) thus reduces to

$$\int_E^\infty\{\,[Q_1^1(i\zeta)\,]^2+2\,[Q_1(i\zeta)\,]^2\}\,d\zeta=-\,(1+E^2)\,\frac{\partial Q_1(iE)}{\partial E}\,Q_1(iE)$$

$$=-\,(1+E^2)^{1/2}Q_1(iE)\,Q_1^1(iE)\,. \tag{73}$$

Introducing equations (67), (68), and (73) into equation (65), we obtain

$$\delta\mathfrak{M}^{(e)}=-\frac{H^2\epsilon\,c^3\,(1+E^2)^{1/2}}{3Q_1^1(iE)}\,D_1(n)\,(1+E^2)^{1/2}Q_1(iE)\,Q_1^1(iE)=0\qquad(n\text{ odd})$$

and

$$\delta\mathfrak{M}_{2n}^{(e)}=\frac{H^2\,(1+E^2)^2\,c^3\epsilon_{2n}}{4\,[Q_1^1(iE)\,]^2}\,\{-E^2\,[Q_1^1(iE)\,]^2+(1+E^2)\,[Q_1(iE)\,]^2\}$$

$$\times\int_{-1}^{+1}\frac{P_{2n}(\mu)}{E^2+\mu^2}\,d\mu-\frac{H^2\,(1+E^2)\,c^3\epsilon_{2n}Q_1(iE)}{3}\,D_1(2n) \tag{74}$$

(cf. eqs. [61]–[63]). Again subscripts $2n$ have been inserted to emphasize that we are dealing with a general P_{2n}-deformation.

By putting $m=1$ in equation (60), we find, for a general P_{2n}-deformation (cf. eqs. [61]–[63], [11], and [6]),

$$D_1(2n)=\frac{1}{[Q_1^1(iE)\,]^2}\Big\{\frac{1\cdot2}{2}\int_{-1}^{+1}\frac{P_0(\mu)-P_2(\mu)}{E^2+\mu^2}\,P_{2n}(\mu)\,d\mu$$

$$+\frac{i\,(1+E^2)^{1/2}Q_1^1(iE)}{P_{2n}^1(iE)}\cdot\frac{3}{2}\cdot3P_1^1(iE)\int_{-1}^{+1}[P_1(\mu)\,]^2d\mu\Big\}$$

$$=\frac{1}{[Q_1^1(iE)\,]^2}\Big\{\int_{-1}^{+1}\frac{1-\frac{1}{2}\,(3\mu^2-1)}{E^2+\mu^2}\,P_{2n}(\mu)\,d\mu$$

$$+\frac{i\,(1+E^2)^{1/2}Q_1^1(iE)}{P_{2n}^1(iE)}\cdot\frac{3}{2}\cdot3i\,(1+E^2)^{1/2}\cdot\frac{2}{3}\Big\} \tag{75}$$

$$=\frac{1}{[Q_1^1(iE)\,]^2}\Big\{\frac{3}{2}\int_{-1}^{+1}\Big[-1+\frac{1+E^2}{E^2+\mu^2}\Big]P_{2n}(\mu)\,d\mu-\frac{3\,(1+E^2)\,Q_1^1(iE)}{P_{2n}^1(iE)}\Big\}$$

$$=\frac{1+E^2}{[Q_1^1(iE)\,]^2}\Big\{\frac{3}{2}\int_{-1}^{+1}\frac{P_{2n}(\mu)}{E^2+\mu^2}\,d\mu-\frac{3Q_1^1(iE)}{P_{2n}^1(iE)}\Big\}.$$

Introducing equation (75) into equation (74), we obtain

$$\delta \mathfrak{M}^{(e)} = 0 \qquad (n \text{ odd})$$

and

$$\delta \mathfrak{M}_{2n}^{(e)} = \frac{H^2 (1+E^2)^2 c^3 \epsilon_{2n}}{4 [Q_1^1 (iE)]^2} \{ -E^2 [Q_1^1 (iE)]^2 + (1+E^2) [Q_1 (iE)]^2 \}$$
$$\times \int_{-1}^{+1} \frac{P_{2n}(\mu)}{E^2+\mu^2} d\mu - \frac{H^2 (1+E^2)\, c^3 \epsilon_{2n} Q_1 (iE)}{3} \cdot \frac{1+E^2}{[Q_1^1 (iE)]^2}$$
$$\times \left\{ \frac{3}{2} \int_{-1}^{+1} \frac{P_{2n}(\mu)}{E^2+\mu^2} d\mu - \frac{3 Q_1^1 (iE)}{P_{2n}^1 (iE)} \right\} \qquad (76)$$
$$= \frac{H^2 (1+E^2)^2 c^3 \epsilon_{2n}}{4 [Q_1^1 (iE)]^2} \left\{ [-E^2 \{Q_1^1 (iE)\}^2 + (1+E^2) \{Q_1 (iE)\}^2 - 2 Q_1 (iE)] \right.$$
$$\left. \times \int_{-1}^{+1} \frac{P_{2n}(\mu)}{E^2+\mu^2} d\mu + \frac{4 Q_1 (iE) Q_1^1 (iE)}{P_{2n}^1 (iE)} \right\}.$$

By means of equation (55) we find

$$-[E Q_1^1 (iE)]^2 = -\{(1+E^2)^{1/2} Q_1 (iE) + (1+E^2)^{-1/2}\}^2$$
$$= -(1+E^2)[Q_1 (iE)]^2 - 2 Q_1 (iE) - (1+E^2)^{-1}. \qquad (77)$$

Introducing equation (77) into equation (76), finally we obtain, for the change in external magnetic energy for a general P_n-deformation,

$$\delta \mathfrak{M}^{(e)} = 0 \qquad (n \text{ odd})$$

and

$$\delta \mathfrak{M}_{2n}^{(e)} = \frac{H^2 (1+E^2)^2 c^3 \epsilon_{2n}}{4 [Q_1^1 (iE)]^2} \left\{ \left[-4 Q_1 (iE) - \frac{1}{1+E^2} \right] \int_{-1}^{+1} \frac{P_{2n}(\mu)}{E^2+\mu^2} d\mu \right.$$
$$\left. + \frac{4 Q_1 (iE) Q_1^1 (iE)}{P_{2n}^1 (iE)} \right\}$$
$$= \frac{H^2 (1+E^2)^2 c^3 \epsilon_{2n}}{[Q_1^1 (iE)]^2} \left\{ -\left[Q_1 (iE) + \frac{1}{4 (1+E^2)} \right] \int_{-1}^{+1} \frac{P_{2n}(\mu)}{E^2+\mu^2} d\mu \right. \qquad (78)$$
$$\left. + \frac{Q_1 (iE) Q_1^1 (iE)}{P_{2n}^1 (iE)} \right\}.$$

VI. THE TOTAL CHANGE IN MAGNETIC ENERGY DUE TO A GENERAL P_n-DEFORMATION

The total change, $\Delta \mathfrak{M}$, in magnetic energy is, by equations (39), (78), (11), and (55),

$$\Delta \mathfrak{M} = 0 \qquad (n \text{ odd})$$

and

$$\Delta\mathfrak{M}_{2n} = -\frac{H^2 c^3 (1+E^2)^{3/2} E\epsilon_{2n}}{P^1_{2n}(iE)} + \frac{H^2 (1+E^2)^2 c^3 \epsilon_{2n}}{[Q^1_1(iE)]^2}\left\{ -\left[Q_1(iE) + \frac{1}{4(1+E^2)}\right] \times \int_1^{+1} \frac{P_{2n}(\mu)}{E^2+\mu^2}\, d\mu + \frac{Q_1(iE)\, Q^1_1(iE)}{P^1_{2n}(iE)}\right\}$$

$$= \frac{H^2 (1+E^2)\, c^3 \epsilon_{2n}}{Q^1_1(iE)}\left\{ -\frac{E(1+E^2)^{1/2} Q^1_1(iE) + (1+E^2) Q_1(iE)}{P^1_{2n}(iE)} - \frac{(1+E^2) Q_1(iE) + \frac{1}{4}}{Q^1_1(iE)} \int_{-1}^{+1} \frac{P_{2n}(\mu)}{E^2+\mu^2}\, d\mu \right\} \tag{79}$$

$$= -\frac{H^2 (1+E^2)\, c^3 \epsilon_{2n}}{Q^1_1(iE)}\left\{ \frac{1}{P^1_{2n}(iE)} + \frac{(1+E^2) Q_1(iE) + \frac{1}{4}}{Q^1_1(iE)} \int_{-1}^{+1} \frac{P_{2n}(\mu)}{E^2+\mu^2}\, d\mu \right\}.$$

VII. THE GRAVITATIONAL POTENTIAL; CHANGE IN THE GRAVITATIONAL POTENTIAL ENERGY

The work done against the gravitational force during the deformation $\boldsymbol{\xi}$ is

$$\rho \iiint_\tau \boldsymbol{\xi} \cdot \operatorname{grad} V^{(i)}\, d\tau\,, \tag{80}$$

where ρ is the density of the spheroid. The change in the potential energy, which is the negative of the above expression, will be correct to the first order in ϵ if the volume integral is taken over the undisturbed body and $V^{(i)}$ is the internal gravitational potential for the undisturbed spheroid.

The internal potential, $V^{(i)}$, and the external potential, $V^{(e)}$, must satisfy Poisson's equation,

$$\nabla^2 V^{(i)} = -4\pi G\rho\,, \tag{81}$$

and Laplace's equation,

$$\nabla^2 V^{(e)} = 0\,, \tag{82}$$

respectively, and the boundary conditions at the undisturbed surface of the spheroid.

With the help of the operator

$$\nabla^2 = \frac{1}{c^2(\zeta^2+\mu^2)}\left\{ \frac{\partial}{\partial\zeta}\left[(1+\zeta^2)\frac{\partial}{\partial\zeta}\right] + \frac{\partial}{\partial\mu}\left[(1-\mu^2)\frac{\partial}{\partial\mu}\right]\right\},$$

it is easily verified that

$$V^{(i)}_1 = -\tfrac{2}{3}\pi G\rho\, c^2(\zeta^2-\mu^2) \tag{83}$$

is a particular integral of equation (81). The general solution of equation (81) is the sum of the particular integral (83) and the general solution of Laplace's equation. By equations (83) and (10) we therefore find, as the general solution of equation (81),

$$V^{(i)} = -\tfrac{2}{3}\pi G\rho\, c^2(\zeta^2-\mu^2) + \sum_{n=0}^{\infty} A_n P_n(i\zeta) P_n(\mu)\,. \tag{84}$$

The general solution of equation (82) is, correspondingly,

$$V^{(e)} = C' + \sum_{n=0}^{\infty} B'_n Q_n(i\zeta) P_n(\mu)\,. \tag{85}$$

On applying the boundary conditions that V, $\partial V/\partial\zeta$, and $\partial V/\partial\mu$ are continuous at the undisturbed boundary, we find

$$V^{(i)} = g\,(\zeta^2-\mu^2) + A_0 + A_2 P_2(i\zeta)\,P_2(\mu)\,, \tag{86}$$

where

$$\begin{aligned} g &= -\tfrac{2}{3}\pi G\rho\,c^2\,, \\ A_0 &= \tfrac{2}{3}\pi G\rho\,c^2\,(E^2-\tfrac{1}{3}) + \tfrac{4}{3}\pi G\rho\,c^2 E\,(1+E^2)\cot^{-1}E\,, \end{aligned} \tag{87}$$

and

$$A_2 = -\tfrac{4}{9}\pi G\rho\,c^2\,(1+E^2)\left[3E\cot^{-1}E - \frac{3E^2+2}{1+E^2}\right];$$

and the components of the force are given by

$$\begin{aligned} [\text{grad } V^{(i)}]_\zeta &= \frac{1}{c}\left(\frac{1+\zeta^2}{\zeta^2+\mu^2}\right)^{1/2}\frac{\partial V^{(i)}}{\partial\zeta} \\ &= \frac{1}{c\,(\zeta^2+\mu^2)^{1/2}}\left[-\tfrac{2}{3}gP_2^1(i\zeta) + A_2P_2^1(i\zeta)\,P_2(\mu)\right] \end{aligned} \tag{88}$$

and

$$\begin{aligned} [\text{grad } V^{(i)}]_\theta &= -\frac{1}{c}\left(\frac{1-\mu^2}{\zeta^2+\mu^2}\right)^{1/2}\frac{\partial V^{(i)}}{\partial\mu} \\ &= -\frac{1}{c\,(\zeta^2+\mu^2)^{1/2}}\left[-\tfrac{2}{3}gP_2^1(\mu) + A_2P_2(i\zeta)\,P_2^1(\mu)\right]. \end{aligned}$$

We can evaluate the change in the potential energy in terms of $\boldsymbol{\xi}$ and grad $V^{(i)}$ given by equations (12), (13), and (88). Because of the orthogonality of the functions $P_n(\mu)$ in the interval, the integration, when effected over the volume, will give a nonvanishing result only for $n = 2$. And in this case the change in the gravitational potential energy, $\Delta\Omega$, is determined by

$$\begin{aligned} -\Delta\Omega = \rho\frac{B_2}{c^2}\int_0^E\int_{-1}^{+1}\int_0^{2\pi} &\{\,[\,(\zeta^2+\mu^2)^{-1/2}P_2^1(i\zeta)\,P_2(\mu)\,]\,(\zeta^2+\mu^2)^{-1/2} \\ &\times[-\tfrac{2}{3}gP_2^1(i\zeta) + A_2P_2^1(i\zeta)\,P_2(\mu)\,] + [\,(\zeta^2+\mu^2)^{-1/2}P_2(i\zeta)\,P_2^1(\mu)\,] \\ &\times(\zeta^2+\mu^2)^{-1/2}[-\tfrac{2}{3}gP_2^1(\mu) + A_2P_2(i\zeta)\,P_2^1(\mu)\,]\,\}\,c^3\,(\zeta^2+\mu^2)\,d\zeta\,d\mu\,d\varphi \end{aligned} \tag{89}$$

$$\begin{aligned} &= -2\pi\rho\,cB_2\int_0^E\int_{-1}^{+1}\{\tfrac{2}{3}g\,[\{P_2^1(i\zeta)\}^2P_2(\mu) + P_2(i\zeta)\,\{P_2^1(\mu)\}^2] \\ &\qquad + A_2\,[-\{P_2^1(i\zeta)\}^2\{P_2(\mu)\}^2 - \{P_2(i\zeta)\}^2\{P_2^1(\mu)\}^2]\,\}\,d\zeta\,d\mu\,. \end{aligned}$$

Carrying out the integration over μ, we obtain

$$\Delta\Omega = 2\pi\rho\,cB_2\int_0^E\{\tfrac{2}{3}\cdot\tfrac{12}{5}gP_2(i\zeta) - A_2\,[\tfrac{2}{5}\{P_2^1(i\zeta)\}^2 + \tfrac{12}{5}\{P_2(i\zeta)\}^2]\}\,d\zeta\,. \tag{90}$$

Substituting for $P_2(i\zeta)$ and $P_2^1(i\zeta)$ according to equations (11), we can carry out the integration over ζ. In this manner we obtain

$$\begin{aligned} \Delta\Omega &= 2\pi\rho\,cB_2\{-\tfrac{6}{5}\cdot g\cdot\tfrac{1}{2}E\,(1+E^2) - A_2\,[\tfrac{2}{5}\cdot\tfrac{3}{5}E^3\,(3E^2+5) \\ &\qquad + \tfrac{12}{5}\cdot\tfrac{1}{20}E\,(9E^4+10E^2+5)\,]\,\} \\ &= -\tfrac{2}{5}\pi\rho\,cB_2E\,(1+E^2)\,[4g+3A_2\,(3E^2+1)\,]\,, \end{aligned} \tag{91}$$

or, substituting for g and A_2 from equations (87) in equation (91), we obtain, after some further reduction,

$$\Delta\Omega = -\tfrac{2}{5}\pi\rho\, cB_2E\,(1+E^2)\,[12\pi G\rho\, c^2E^2\,(1+E^2) - 4\pi G\rho\, c^2E\,(1+E^2)\,(3E^2+1)\cot^{-1}E]\,, \tag{92}$$

or, substituting for B_2 in accordance with equation (17), we have

$$\Delta\Omega = \tfrac{2}{15}\pi\rho\, c^3\epsilon_2\,(1+E^2)\,[12\pi G\rho\, c^2E^2\,(1+E^2) - 4\pi G\rho\, c^2E\,(1+E^2)\,(3E^2+1)\cot^{-1}E]\,. \tag{93}$$

It is convenient to introduce into this expression the mass of the spheroid,

$$M = \tfrac{4}{3}\pi\rho\, c^3E\,(1+E^2)\,. \tag{94}$$

Thus we finally obtain, for the change in the gravitational potential energy of the spheroid, the expression

$$\Delta\Omega = -\frac{3}{10}\frac{M^2G}{c}\,\epsilon_2\left[\frac{3E^2+1}{E}\cot^{-1}E - 3\right] \qquad \text{for } n=2 \tag{95}$$

and

$$\Delta\Omega = 0 \qquad \text{for } n\neq 2\,.$$

VIII. CONDITION FOR STABILITY

We have seen that while the change in the gravitational potential energy, $\Delta\Omega$, of the spheroid is of the first order in ϵ only for a P_2-deformation and of higher order for all higher-order deformations, the change in the magnetic energy, $\Delta\mathfrak{M}$, is of the order ϵ for all *even* P_n-deformations. Therefore, we shall suppose that the original deformation of the boundary is given by (cf. eq. [6])

$$\zeta = E + \sum_m \epsilon_m \frac{1+E^2}{E^2+\mu^2}\,P_m(\mu)\,. \tag{96}$$

For this deformation (cf. eqs. [79] and [95])

$$\Delta\mathfrak{M} = -\frac{H^2\,(1+E^2)\,c^3}{Q_1^1(iE)}\sum_{n=1}\left\{\frac{1}{P_{2n}^1(iE)} + \frac{(1+E^2)\,Q_1(iE) + \tfrac{1}{4}}{Q_1^1(iE)}\int_{-1}^{+1}\frac{P_{2n}(\mu)}{E^2+\mu^2}\,d\mu\right\}\epsilon_{2n} \tag{97}$$

and

$$\Delta\Omega = -\frac{3}{10}\frac{M^2G}{c}\,\epsilon_2\left[\frac{3E^2+1}{E}\cot^{-1}E - 3\right]. \tag{98}$$

For equilibrium, the total change in energy, $\Delta\mathfrak{E}$, must satisfy the equation

$$\Delta\mathfrak{E} = \Delta\mathfrak{M} + \Delta\Omega = 0\,. \tag{99}$$

On introducing equations (97) and (98) into equation (99) and then introducing the eccentricity of the spheroid

$$e = (1+E^2)^{-1/2} \tag{100}$$

and

$$H_{eq} = \sqrt{\left(\frac{3}{10}\right)}\frac{M\sqrt{G}}{a^2}\,, \tag{101}$$

where a is the major half-axis of the spheroid, we obtain

$$\Delta \mathfrak{E} = \frac{3}{10}\frac{M^2G}{c}\left\{\left(\frac{H}{H_{eq}}\right)^2 \sum_{n=1} e^2 F_{2n}(e)\,\epsilon_{2n} - f(e)\,\epsilon_2\right\} \tag{102}$$

$$= 0 \qquad \text{(condition for equilibrium)}.$$

Here

$$f(e) = \frac{3-2e^2}{e(1-e^2)^{1/2}}\cot^{-1}\left(\frac{1-e^2}{e^2}\right)^{1/2} - 3, \tag{103}$$

while

$$F_{2n}(e) = -\left\{\frac{1}{Q_1^1(iE)\,P_{2n}^1(iE)} + \frac{4Q_1(iE)+e^2}{[2eQ_1^1(ie)]^2}\int_{-1}^{+1}\frac{P_{2n}(\mu)}{E^2+\mu^2}\,d\mu\right\}. \tag{104}$$

Here, as occasionally in the following, E is used as an abbreviation for $(1-e^2)^{1/2}/e$ (cf. eq. [100]).

IX. EQUILIBRIUM SPHEROIDS

Chandrasekhar and Fermi have shown that a sphere with a uniform internal magnetic field and an external dipole field is not stable to a P_2-deformation, i.e., it is unstable for all modes of pulsation. In the following we shall therefore restrict the discussion to cases in which the eccentricity is in the range

$$0 < e \leqslant 1. \tag{105}$$

It follows, then, from equation (102) that the total increase, $\Delta\mathfrak{E}_2$, in the energy due to a P_2-deformation is

$$\Delta \mathfrak{E}_2 = \frac{3}{10}\frac{M^2G}{c}\,\epsilon_2\left[\left(\frac{H}{H_{eq}}\right)^2 e^2F_2(e) - f(e)\right]. \tag{106}$$

Putting $2n = 2$ in equation (104) and using equations (11), we find

$$\begin{aligned} F_2(e) &= -\left\{\frac{1}{Q_1^1(iE)\,P_2^1(iE)} + \frac{4Q_1(iE)+e^2}{[2eQ_1^1(iE)]^2}\int_{-1}^{+1}\frac{P_2(\mu)}{E^2+\mu^2}\,d\mu\right\} \\ &= -\left\{\frac{1}{Q_1^1(iE)\,P_2^1(iE)} + \frac{4Q_1(iE)+e^2}{[2eQ_1^1(iE)]^2}\cdot\frac{1}{2}\int_{-1}^{+1}\frac{3\mu^2-1}{E^2+\mu^2}\,d\mu\right\} \\ &= -\left\{\frac{1}{Q_1^1(iE)\,P_2^1(iE)} + \frac{4Q_1(iE)+e^2}{[2eQ_1^1(iE)]^2}\left[3 - \frac{3-2e^2}{e(1-e^2)^{1/2}}\cot^{-1}E\right]\right\} \\ &= \frac{e^2}{3(1-e^2)^{1/2}Q_1^1(iE)} + \frac{4Q_1(iE)+e^2}{[2eQ_1^1(iE)]^2}\,f(e) \end{aligned} \tag{107}$$

(cf. eqs. [103] and [44]). For a negative ϵ_2 (which makes the spheroid more oblate), the change in magnetic energy is negative, while the corresponding change in the gravitational energy is positive. It follows from equation (106) that a configuration stable for a P_2-deformation is obtained if

$$\left(\frac{H}{H_{eq}}\right)^2 = \frac{f(e)}{e^2F_2(e)} \tag{108}$$

or

$$H = H_{eq}\left[\frac{f(e)}{e^2F_2(e)}\right]^{1/2}. \tag{109}$$

The function H/H_{eq} is plotted against e in Figure 1.

Equations (94) and (109) show that, if three of the five parameters, H, M, a, e, and ρ are given, the two others are determined. There therefore exists a *unique configuration for a spheroid with a uniform internal magnetic field and an external dipole field which is stable to a P_2-deformation.*

The equilibrium spheroids defined by equations (94) and (109) will, in general, not be stable to any other *single* P_{2n}-deformation. The reason for this is to be found in the condition for stability set forth by equation (99), that the total change in energy due to

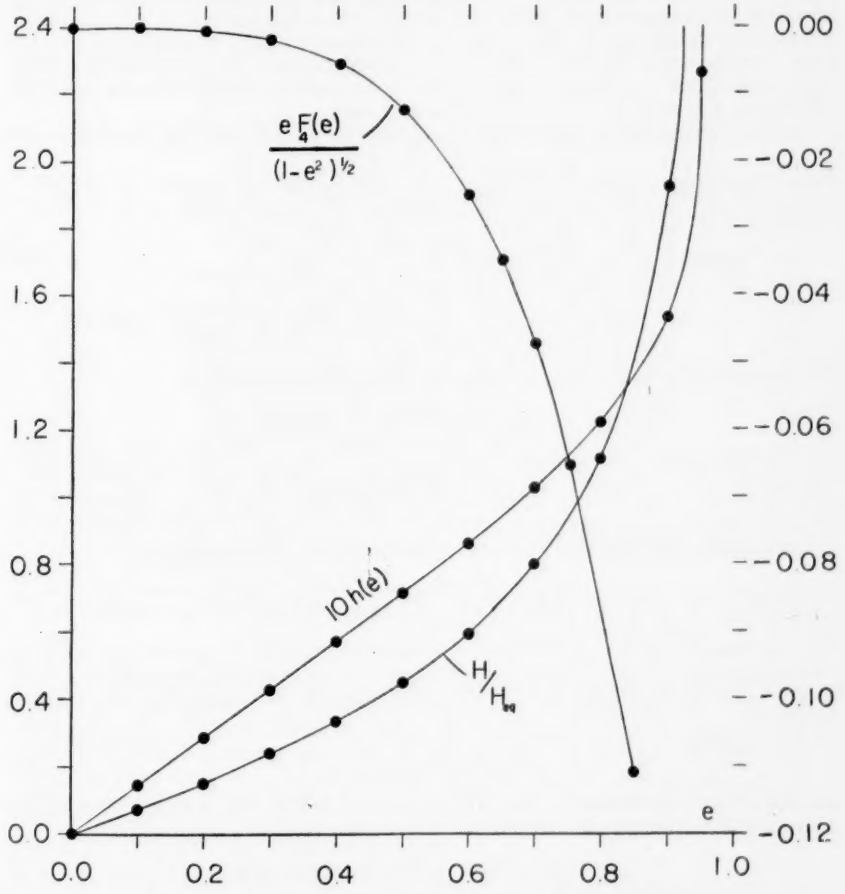

FIG. 1.—The function $H/H_{eq} = [f(e)/\{e^2F_2(e)\}]^{1/2}$ (eq. [109]) is plotted against the eccentricity e. The functions $f(e)$ and $F_2(e)$ are defined in equations (103) and (107), respectively. The slope at the origin is given by $H/H_{eq} = 0.77e$ and thus corresponds to the equilibrium value of e (for $e \to 0$) given by Chandrasekhar and Fermi (*Ap. J.*, **118**, 116, 1953, eq. [155]). The second curve is of the function $10h(e)$, defined by equation (117), plotted against the eccentricity. The remaining curve is of the function $eF_4(e)/(1 - e^2)^{1/2}$, plotted against the eccentricity. The function $F_4(e)$ is defined by equation (110). The scale on the left-hand side is for the functions H/H_{eq} and $10h(e)$, while the scale on the right-hand side is for the function $eF_4(e)/(1 - e^2)^{1/2}$.

the deformation must vanish. For a single higher-order deformation ($2n > 2$) there is (to the first order in ϵ) no gravitational term to balance the magnetic term in $\Delta\mathfrak{E}$. The change in the magnetic energy comes about by magnetic lines of force being brought together in some regions and separated in other regions; and, depending upon the sizes of these regions, the change in magnetic energy will, in general, be positive or negative. We shall shortly study a P_4-deformation, and shall see that for this deformation the change in the magnetic energy will be either positive or negative, depending upon the sign of ϵ_4, for the whole range of the eccentricity ($e > 0$). Higher-order deformations have not been calculated in detail. But if it should so happen that any higher-order deformation should give vanishing $\Delta\mathfrak{M}$ for one or more values of e, we shall still not know whether this means that the spheroid is really stable to that kind of deformation; only a calculation to a higher order of ϵ can decide whether this is so or not, and such calculation is beyond the scope of the present paper.

For a P_4-deformation it follows from equation (104) (cf. eqs. [11], [44], and [100]) that

$$F_4(e) = \frac{-1}{Q_1^1(iE)\,P_4^1(iE)} - \frac{4Q_1(iE) + e^2}{[2eQ_1^1(iE)]^2}\int_{-1}^{+1}\frac{P_4(\mu)}{E^2+\mu^2}\,d\mu$$

$$= \frac{-1}{Q_1^1(iE)\,P_4^1(iE)} - \frac{4Q_1(iE) + e^2}{[2eQ_1^1(iE)]^2}\cdot\frac{1}{4}\left\{\frac{35}{3} - \frac{5(7-e^2)}{e^2}\right. \tag{110}$$

$$\left. + \frac{8e^4 - 40e^2 + 35}{e^3(1-e^2)^{1/2}}\cot^{-1}E\right\}.$$

The change in the energy, according to equations (102) and (101), is

$$\Delta\mathfrak{E}_4 = \Delta\mathfrak{M}_4 = \frac{3}{10}\frac{M^2G}{c}\left(\frac{H}{H_{eq}}\right)^2 e^2F_4(e)\,\epsilon_4$$

$$= H^2\frac{a^4e^2}{c}F_4(e)\,\epsilon_4. \tag{111}$$

On introducing the volume, V, of the spheroid, equation (111) reduces to

$$\Delta\mathfrak{E}_4 = \frac{3}{4\pi}H^2V\epsilon_4\frac{eF_4(e)}{(1-e^2)^{1/2}}. \tag{112}$$

The function $eF_4(e)/(1-e^2)^{1/2}$ is plotted against e in Figure 1. It appears that this function is negative for the whole range of the argument e ($e > 0$); and, since $\Delta\mathfrak{E}_4$ is proportional to the product $\epsilon_4 eF_4(e)/(1-e^2)^{1/2}$, we have $\Delta\mathfrak{E}_4 \gtrless 0$, depending upon whether $\epsilon_4 \lesseqgtr 0$.

By requiring

$$\Delta\mathfrak{M}_2 + \Delta\mathfrak{M}_4 + \Delta\Omega_2 = 0\,, \tag{113}$$

we can obtain a configuration of equilibrium which will be stable to a *superposed* P_2- and P_4-deformation but, in general, not to any other *single* P_{2n}-deformation.

X. INTERSTELLAR CLOUDS IN SPIRAL ARMS

We shall now be interested in considering the spheroid as a cloud imbedded in a less dense medium, for instance, a cloud in a spiral arm. The mathematical simplification made in Section II, that the spheroid was in empty space, should not seriously affect the following discussion.

Let $\bar{\rho}$ be the average density of the medium in which the spheroid is situated and ρ the density of the spheroidal cloud itself. On introducing the normal field strength,

$$H_S = 4\pi\bar{\rho}R\sqrt{G}\,, \tag{114}$$

defined by Chandrasekhar and Fermi[1] (eq. [93]) and putting $R = a$, we find that, for a P_2-deformation,

$$H_{eq} = H_S \frac{\rho}{\bar{\rho}} \left(\frac{1 - e^2}{30}\right)^{1/2}, \tag{115}$$

and thus

$$\frac{H}{H_S} = \frac{\rho}{\bar{\rho}} \left[\frac{(1 - e^2) f(e)}{30 e^2 F_2(e)}\right]^{1/2} = \frac{\rho}{\bar{\rho}} h(e) \tag{116}$$

where

$$h(e) = \left[\frac{(1 - e^2) f(e)}{30 e^2 F_2(e)}\right]^{1/2} = \left(\frac{1 - e^2}{30 e^2}\left[\frac{3 - 2e^2}{e(1 - e^2)^{1/2}} \cot^{-1} E - 3\right]\right.$$
$$\left. \times \left\{\frac{e^2}{3(1 - e^2)^{1/2} Q_1^1(iE)} + \frac{4Q_1(iE) + e^2\left[\frac{3 - 2e^2}{e(1 - e^2)^{1/2}} \cot^{-1} E - 3\right]}{[2eQ_1^1(iE)]^2}\right\}^{-1}\right)^{1/2}. \tag{117}$$

The function $10h(e)$ is plotted against e in Figure 1. Using these values of $h(e)$, we can derive Table 1, which gives $\rho/\bar{\rho}$ as a function of e for $H = H_S$. From an examination of

TABLE 1

e	$\rho/\bar{\rho}$	e	$\rho/\bar{\rho}$
0.10	≈75	0.70	≈10
.30	≈24	.80	≈ 8
0.50	≈14	0.90	≈ 7

this table we conclude that *very dense* clouds will be stable to the fundamental P_2-deformation, if a magnetic field of the strength one would expect to find, according to Chandrasekhar and Fermi, in the spiral arms is present. If the density of the cloud approaches eight times the average density or less, the configuration will become unstable, either by contracting to disklike shapes,[4] as stated by Chandrasekhar and Fermi, or by breaking up if higher modes are excited.

The arguments given here hold, of course, only if the spheroid is under conditions which compare to the average values of the density and the magnetic field in spiral arms.

I am indebted to Professors S. Chandrasekhar and E. Fermi, of the University of Chicago, for informing me about their work before it was published, and I am particularly grateful to Professor Chandrasekhar for suggesting this problem to me and for many valuable discussions of its various aspects. I wish to express my deep-felt gratitude to both of them. I also wish, in conclusion, to express my most sincere thanks to the International Federation of University Women for the Virginia C. Gildersleeve International Fellowship for 1952–1953 and to the Yerkes Observatory, University of Chicago, for hospitality during the current academic year.

[4] "Interstellar magnetic pancake fields" suggests itself as a description of the phenomena.

WAVES OF FINITE AMPLITUDE IN AN INFINITE HOMOGENEOUS MEDIUM

H. Lawrence Helfer*
Yerkes Observatory
Received June 10, 1953; revised September 21, 1953

ABSTRACT

The existence of a particular class of finite waves in an infinite homogeneous medium when the gravitational effect of the fluctuation is included is demonstrated. Stationary, progressive, and solitary waves are all permitted solutions. It is shown that the Jeans critical length, valid for determining the maximum wave length of stable infinitesimal density fluctuations, adequately represents the effective lengths of these disturbances, provided that the development of the density fluctuations is always along the same adiabatic. Departure from this requirement, as, for example, in the occurrence of shock waves, may result in stable fluctuations of dimensions considerably in excess of the Jeans criterion.

I. INTRODUCTION

The problem of the gravitational stability of an infinite homogeneous inviscid medium was first considered by Jeans,[1] and the criterion for instability which he derived has been generalized by Chandrasekhar[2] to include the effects of turbulence. In this paper some of the simpler types of density fluctuations of finite amplitude will be investigated, in order to estimate the range of applicability of the above criteria. It is to be noted that this problem is of considerable interest, in that the results may be utilized in discussions of such problems as the formation and possible evolution of discrete interstellar clouds.

In general, a density fluctuation in a medium results in a local increase in the compressional energy and a decrease in the gravitational energy, the amount of each depending upon the linear dimensions of the fluctuation. If the former exceeds the latter, the situation is stable in the sense that the fluctuation will be eventually damped out, the surplus energy going into kinetic energy of a wave motion and being gradually dissipated by viscosity. If, however, the reverse case is true, the total energy change is negative, and the situation is clearly unstable. By analyzing an arbitrary infinitesimal fluctuation in density in a Fourier analysis, Jeans showed that the Fourier component waves having wave lengths exceeding the value

$$\lambda_c = \frac{2\pi c}{\sqrt{(4\pi G\rho)}}, \tag{1}$$

where $c = (\gamma p/\rho)^{1/2}$ denotes the velocity of sound and G denotes the constant of gravitation, are unstable. The work of Chandrasekhar indicated that this critical wave length may be increased considerably if turbulence plays an important role in the medium.

Jeans's original physical argument, applied to the case of finite density fluctuations, could be expected to yield a stability expression similar to equation (1), provided that the density fluctuation follows an adiabatic. If, however, a nonadiabatic disturbance, such as, e.g., a shock wave, develops, departures from equation (1) may be expected; for in this case there will be dissipation of energy at the shock front and entropy will no longer be invariant as we follow the motion of the material across the shock front. Equation (1) then may well be an underestimate of the critical wave length. The following

* National Science Foundation predoctoral fellow, 1952–1953.

[1] *Phil. Trans. A*, **199**, 1. 1902; *Astronomy and Cosmogony* (Cambridge: At the University Press, 1928), pp. 337–341.

[2] *Proc. R. Soc. London, A*, **210**, 26, 1951.

analysis is in conformity with these conclusions. We shall proceed by demonstrating the existence of a class of progressive waves of finite amplitude which owe their existence to the presence of the gravitational field.

II. THE HYDRODYNAMIC EQUATIONS OF MOTION

Let us consider only those density fluctuations which are stable and hence result in wave motion. In general, the wave form of such a fluctuation will change with time. Let us assume that, during the passage of time, the wave form eventually becomes independent of time. In particular, we shall assume that the density fluctuation is of the form

$$\delta\rho = \delta\rho(x'); \qquad x' = x - vt \qquad (v = \text{Const.}), \tag{2}$$

so that we have a progressive wave of finite amplitude. We shall show that the hydrodynamic equations admit a class of such solutions. If the original density fluctuations are such that shock waves develop, a solution of the form considered here will satisfactorily represent the density distribution behind a shock front.

We shall choose a co-ordinate system moving with constant velocity v in the direction of the $+x$-axis. Then, by the assumption stated in equation (2), the hydrodynamic equations become

$$\frac{\partial}{\partial x}(\rho u) = 0 \tag{3}$$

and

$$\frac{\partial}{\partial x}(\rho u^2 + p) = \rho \frac{\partial V}{\partial x}, \tag{4}$$

where ρ represents the density, u the velocity of the fluid (with respect to the moving co-ordinate system), and V the gravitational potential, given by the Poisson equation,

$$\frac{\partial^2 V}{\partial x^2} = -4\pi G(\rho - \rho_0); \tag{5}$$

here ρ_0 represents the density of the undisturbed medium.

If the substitution suggested by equation (3),

$$\rho u = m \qquad (m = \text{Const.}), \tag{6}$$

is made, the system of equations (3)–(5) may be combined in the form

$$\frac{d}{dx}\left[\frac{1}{\rho}\frac{d}{dx}\left(\frac{m^2}{\rho} + p\right)\right] = -4\pi G(\rho - \rho_0). \tag{7}$$

Introducing the variable y by

$$\frac{d}{dx} = y\frac{d}{d\rho}, \qquad y \equiv \frac{d\rho}{dx}, \tag{8}$$

we find that equation (7) reduces to the form

$$\tfrac{1}{2}F\frac{dy^2}{d\rho} + y^2\frac{dF}{d\rho} = -4\pi G(\rho - \rho_0), \tag{9}$$

where

$$F \equiv \frac{1}{\rho}\frac{d}{d\rho}\left[\frac{m^2}{\rho} + a\rho^\gamma\right]. \tag{10}$$

In expression (10) we have assumed the validity of the adiabatic relation,

$$p = a\rho^\gamma. \tag{11}$$

Equation (9) may be rewritten as

$$\frac{d}{d\rho}(F^2y^2) = -8\pi G(\rho-\rho_0)F; \tag{12}$$

on integrating this equation, we obtain

$$y^2 = \frac{A' - 8\pi G(a\rho^\gamma + m^2/\rho) + 8\pi G\rho_0[\gamma a\rho^{\gamma-1}/(\gamma-1) + m^2/2\rho^2]}{(\gamma a\rho^{\gamma-2} - m^2/\rho^3)^2}, \tag{13}$$

where we have substituted for F in accordance with equation (10). In equation (13) the quantity A' is a constant of integration so chosen as to insure that the right-hand side of equation (13) is positive in the range of ρ of interest.

Equation (13) may be brought into the more convenient form,

$$\left(\frac{dq}{dx}\right)^2 = C^2q^4\frac{Aq^2 + q^{\gamma+1}[1/(\gamma-1) - q/\gamma] - B(q-\frac{1}{2})}{(q^{\gamma+1}-B)^2}, \tag{14}$$

by writing

$$q \equiv \frac{\rho}{\rho_0}, \qquad C^2 \equiv \frac{8\pi G\rho_0^{2-\gamma}}{\gamma a}, \qquad B \equiv \frac{m^2}{\gamma a\rho_0^{\gamma+1}}, \tag{15}$$

where A is the constant of integration.

In particular, if we denote by a subscript 1 the values of the physical quantities when $\rho = \rho_1$, then

$$C^2 = \frac{2}{\eta^{2-\gamma}}\left(\frac{2\pi}{\lambda_1}\right)^2; \qquad B = \left(\frac{u_1}{c_1}\right)^2\eta^{\gamma+1}, \tag{16}$$

where

$$\eta \equiv \frac{\rho_1}{\rho_0}; \qquad c_1^2 = \frac{\gamma p_1}{\rho_1}, \tag{17}$$

and λ_1 is given by the corresponding modification of equation (1).

Equation (14) may be integrated to

$$\pm Cx = \int_\eta^q \frac{|q^{\gamma+1} - B|\,dq}{q^2\{Aq^2 + q^{\gamma+1}[1/(\gamma-1) - q/\gamma] - B(q-\frac{1}{2})\}^{1/2}}. \tag{18}$$

If the development of the wave is such that the pressure and density of the undisturbed medium lie along the same adiabatic that the fluctuation follows, then equations (16) may be rewritten as follows:

$$C^2 = 2\left(\frac{2\pi}{\lambda_0}\right)^2; \qquad B = \left(\frac{u_1}{c_0}\right)^2\eta^2. \tag{19}$$

This form suggests that we introduce the quantity

$$U \equiv \left(\frac{u_1}{c_1}\right)^2\eta^{\gamma-1}; \qquad B = U\eta^2. \tag{20}$$

The actual form of the solution of equation (18) has been investigated numerically. If we let $q = \eta$ denote the maximum value of q permissible, so that the right-hand side of equation (14) vanishes for $q = \eta$, the constant A is easily determined to be

$$A = U(\eta - \tfrac{1}{2}) + \frac{1}{\gamma}\eta^{\gamma-1}\left(\eta - \frac{\gamma}{\gamma-1}\right). \tag{21}$$

The nature of the solution depends upon the behavior of the quantity under the radical sign in the denominator of expression (18),

$$D^2 \equiv A\,q^2 + q^{\gamma+1}\left[\frac{1}{\gamma-1} - \frac{q}{\gamma}\right] - B\,(q - \tfrac{1}{2})\,, \tag{22}$$

which may be brought, by substitution of equations (20) and (21), into the form

$$D^2 = S_1 + S_2 U\,, \tag{23}$$

where

$$S_1 = \frac{1}{\gamma}\,q^2\left[\eta^{\gamma-1}\left(\eta - \frac{\gamma}{\gamma-1}\right) - q^{\gamma-1}\left(q - \frac{\gamma}{\gamma-1}\right)\right], \tag{24}$$

$$S_2 = [\,q^2(\eta - \tfrac{1}{2}) - \eta^2(q - \tfrac{1}{2})\,]\,.$$

If D^2 has another root q_0, $0 < q_0 < \eta$; and if D^2 is positive in the region (q_0, η), then the solution described by equation (18) is periodic; the function is bounded, and any solution is symmetric with respect to its normal whenever it assumes a boundary value.[3] If, however, the root q_0 is a multiple root, the solution is no longer periodic, and q approaches the value $q = q_0$ asymptotically.

That, in general, three different classes of solutions are described by equation (18) may be seen if reference is made to Figure 1. In this diagram, the quantities S_1 and $-S_2$ (cf. eq. [24]) are plotted as a function of q for the particular case $\eta = 2$ and $\gamma = \frac{5}{3}$. This graph represents the behavior of D^2 for $U = 1$; in order to obtain a representation for the case $U = U_1$, one need only multiply the ordinate of the $-S_2$-curve uniformly by U_1. An intersection of the two curves corresponds to $D^2 = 0$ for that particular q-value; $D^2 \gtrless 0$ occurs whenever the S_1-curve lies above the $-US_2$-curve. The amplitude of the negative portion of the S_1-curve has been exaggerated; actually, for example, $S_1(q = 0.1) = -0.0014$. Indeed, the negative portion of the S_1-curve exists only for $\eta < 2.5$ (in general, $\eta \leqslant \gamma/[\gamma - 1]$).

The case $U = 0$ represents a periodic *stationary-wave* solution. The minimum values of q permitted, found by solving the equation $S_1 = 0$, are listed for a few representative η values in Table 1. The physical interpretation of these waves is clear; they result from

TABLE 1

VALUES OF $q_{\min}$ FOR THE CASE $U = 0$, $\gamma = \frac{5}{3}$

η	$q_{\min}$	η	$q_{\min}$	η	$q_{\min}$
1.25	0.70	1.75	0.35	2.25	0.08
1.50	0.55	2.00	0.20	2.50	0.00

simply setting the pressure gradient equal to the gravitational force. This type of solution exists for all values of $\eta \gtrsim 1$.

The second class of solutions is obtained by choosing U such that the $-US_2$-curve is just tangent to the S_1-curve. This occurs at $q = 1$, as the following argument shows:

Let $q = 1 + \epsilon$, where $0 < \epsilon \ll 1$; then equation (23) becomes

$$D^2 = \frac{1}{\gamma}(1 + 2\epsilon)\left[\eta^{\gamma-1}\left(\eta - \frac{\gamma}{\gamma-1}\right) + \frac{1}{\gamma-1} - \frac{\gamma}{2}\,(\eta-1)^2 U\right] + O(\epsilon^2)\,. \tag{25}$$

[3] Cf., e.g., J. L. Synge and B. A. Griffith, *Principles of Mechanics* (New York: McGraw-Hill Book Co., 1942), pp. 358–361.

Let us choose $U = U_0$ such that

$$U_0 = \frac{2}{\gamma(\eta-1)^2}\left[\frac{1}{\gamma-1} + \eta^{\gamma-1}\left(\eta - \frac{\gamma}{\gamma-1}\right)\right]; \tag{26}$$

we see, then, that D^2 vanishes except for terms of the order of ϵ^2 or higher. This implies that, for this particular choice of U, the two possible intersections of the S_1- and $-US_2$-curves coincide at the value $q = 1$. Since only two roots are permissible here, it follows that the integrand in expression (18) must behave like $(q-1)^{-1}$ when $q \to 1$. This type of solution represents a single condensation, traveling with a finite subsonic velocity. We may call such disturbances "solitary waves." In Table 2, values of U_0 are listed as a function of η; it is seen that all values of $\eta \geqslant 1$ are permitted.

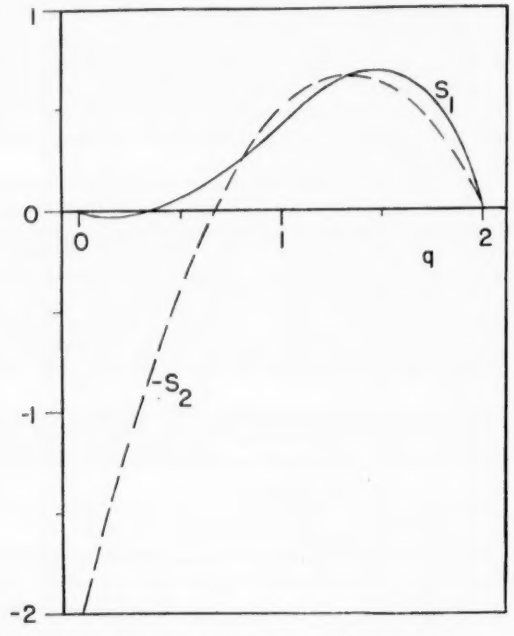

FIG. 1.—Graph of the behavior of the partial sums S_1 and S_2 for the case $\eta = 2$, $\gamma = \frac{5}{3}$

TABLE 2

VALUES OF U_0 FOR $\gamma = \frac{5}{3}$

η	U_0	η	U_0
1.0	1.0000	5	0.6608
1.5	0.9102	10	0.5380
2.0	0.8476	20	0.4336
2.5	0.8000	50	0.3230
3.0	0.7620	100	0.2574

The third class of solutions differs from the preceding two classes in existing only for cases in which $\eta \leqslant \gamma/(\gamma - 1)$. If reference is made to Figure 1, it will be noted that if U is chosen sufficiently small, the $-US_2$-curve may be made to intersect the negative part of the S_1-curve. Such waves, possessing $U \neq 0$, are true *progressive waves*. However, as may be judged from the diagram, such waves move with extremely small velocities. For the particular case considered, $\eta = 2$, $\gamma = \frac{5}{3}$, the fastest wave possesses $U = 0.001227$,

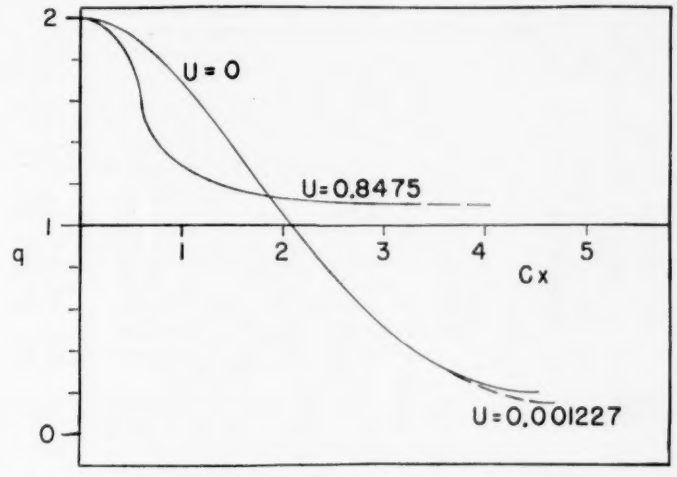

FIG. 2.—The wave solutions for the case $\eta = 2$, $\gamma = \frac{5}{3}$. Only half the curves are shown, since reflection in the q-axis is permitted. The progressive and the standing waves repeat themselves, being periodic.

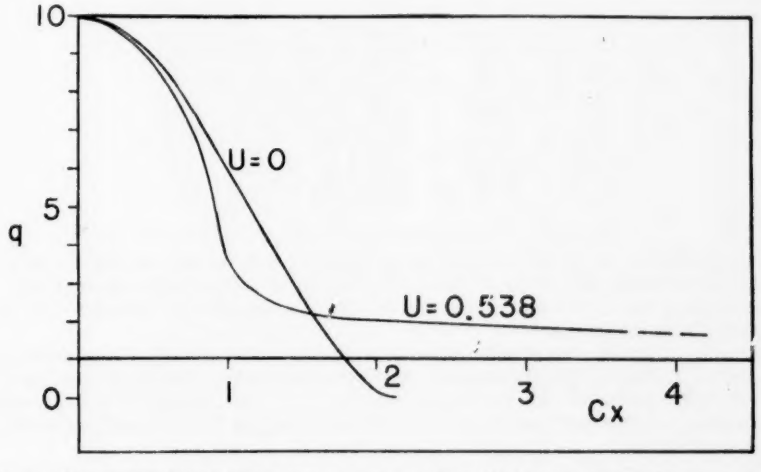

FIG. 3.—The wave solutions for the case $\eta = 10$, $\gamma = \frac{5}{3}$. In this case the progressive waves are no longer permitted.

corresponding to $(u_1/c_0) = 0.035$. This particular wave oscillates between the values $q = 2$ and $q = 0.15$; all other possible progressive waves traveling more slowly than this have their minima in the region $0.15 \leqslant q_{\min} \leqslant 0.2$.

To illustrate the general features of these three types of disturbances, the results of the actual numerical integrations are shown in Figures 2 and 3 and are tabulated in Table 3 for a few representative cases. Owing to the symmetry of the solutions, only half the

TABLE 3

WAVE SOLUTIONS FOR THE CASE $\gamma = \frac{5}{3}$, $\eta = 2$

q	Cx			q	Cx	
	$U=0$	$U=0.001227$	$U=0.8745$		$U=0$	$U=0.001227$
2.0	0.000	0.000	0.000	1.0	2.103	2.101
1.9	0.571	0.571	0.373	0.9	2.260	2.257
1.8	0.818	0.817	0.506	0.8	2.424	2.420
1.7	1.016	1.015	0.584	0.7	2.601	2.595
1.6	1.190	1.190	0.617	0.6	2.794	2.785
1.5	1.352	1.351	0.632	0.5	3.015	3.000
1.4	1.506	1.505	0.729	0.4	3.279	3.251
1.3	1.655	1.654	0.922	0.3	3.635	3.569
1.2	1.803	1.802	1.359	0.2031	4.523	.....
1.15	.....	.....	1.739	0.2	.....	4.026
1.1	1.952	1.950	2.370	0.1500	.....	4.471
1.05	.....	.....	3.63			

WAVE SOLUTIONS FOR THE CASE $\gamma = \frac{5}{3}$, $\eta = 10$

q	Cx		q	Cx
	$U=0$	$U=0.538$		$U=0$
10	0.000	0.000	1.0	1.777
9	0.463	0.431	0.8	1.822
8	0.667	0.612	0.6	1.870
7	0.835	0.750	0.4	1.924
6	0.986	0.857	0.2	1.989
5	1.131	0.928	0.0	2.102
4	1.276	0.968		
3	1.425	1.161		
2	1.587	2.314		
1.5	.....	5.13		

curves are shown. As an aid for future calculations, it is to be noticed that the effective dimensions of those parts of the disturbance satisfying $q \geqslant 1$ are well represented by the dimensions of the $U = 0$ curve, and the numerical integration of equation (18) is extremely simple for this case.

Actually, a fourth class of solutions may be considered as existent, if one permits the occurrence of density disturbances with discontinuous density gradients; then any solution of the integral expression (18) may be used for $q \geqslant 1$; and when the solution assumes the value $q = 1$, we may join on the constant solution $q \equiv 1$ for the region outside the disturbance proper.

The dimensions of the density condensations in the case of the progressive and stationary waves may be taken to be $L \sim 2x_0$, where $x = x_0$ when $q = 1$. This length will

also represent roughly the effective dimensions of the solitary wave (cf. Figs. 2 and 3). Denoting the Jeans length of a density condensation by $l \sim \lambda_0/2$, we find that the ratio

$$\frac{L}{l} = \frac{\sqrt{(2)}}{\pi} [Cx_0] = 0.45\ [Cx_0]$$

has a value $L/l \sim 0.95$ for the case $\eta = 2$, $\gamma = \frac{5}{3}$; and a value $L/l \sim 0.80$ for $\eta = 10$, $\gamma = \frac{5}{3}$. It appears, then, that in the simple case in which the density fluctuation develops continuously along the same adiabatic, the length of the disturbance is closely given by the Jeans critical length. It is to be noted, however, that a Fourier analysis of the stable solitary wave would result in components of wave length considerably in excess of the Jeans critical wave length, which are, nevertheless, stable.

It is to be emphasized that no proof has been offered which insures that all stable density fluctuations do develop into progressive waves of the form considered here; and the possibility exists that other paths of evolution are permissible for a developing density fluctuation. If, for example, shock waves develop, the material distribution behind the shock front may be described by a solution of the form of equation (18), and, while the adiabatic relation may hold for this region, the pressure and density of the medium in front of the shock front will not lie upon the same adiabatic, and the reduction of equation (16) to equation (19) would no longer be permissible. Judging from the behavior of ordinary shock waves in the absence of a gravitational field, the temperature rise behind the shock front may be much in excess of the corresponding density rise, and hence it may well be possible to obtain cases in which $\lambda_1 \gg \lambda_0$.

In conclusion, I wish to express my thanks to Dr. Chandrasekhar for suggesting this problem and for holding many invaluable discussions with me concerning stability problems in general.

THE TRANSFER OF RADIATION BY AN EMITTING ATMOSPHERE. II

HENRY G. HORAK AND CHARLES A. LUNDQUIST
University of Kansas
Received August 25, 1953

ABSTRACT

The transfer of radiation by a plane-parallel atmosphere containing a linear distribution of emission sources is considered for the isotropic case. The exact expressions for the emergent intensity are derived for both finite and semi-infinite atmospheres. It is shown how the exact field at any depth can be obtained.

I. INTRODUCTION

We shall continue the discussion, begun in a previous paper,[1] of radiative transfer by an emitting atmosphere. The problem which will be considered here is that in which the source function for the emitters varies linearly with optical depth. Only isotropic scattering will be treated, but the extension to other phase functions is quite straightforward.

II. SYMMETRIES AND INVARIANCES

Consider a plane-parallel atmosphere of finite optical thickness τ_1, in which the source function, ϵ, for the emission sources varies linearly with optical depth, i.e.,

$$\epsilon = \epsilon_1 \tau \,, \tag{1}$$

where ϵ_1 is a constant. For the case of isotropic scattering with an albedo ϖ_0 the equation of transfer has the form

$$\mu \frac{dI(\tau, \mu)}{d\tau} = I(\tau, \mu) - \varpi_0 J(\tau) - \epsilon_1 \tau \,, \tag{2}$$

where

$$J(\tau) = \frac{1}{2} \int_{-1}^{+1} I(\tau, \mu)\, d\mu \,. \tag{3}$$

We shall now derive an important relation connecting the emergent field in the linear case with that of the uniform case. Suppose that we have two finite atmospheres of thickness $\tau_1 - \tau$ (Fig. 1), but with linear distributions exactly reversed. Let $\mathfrak{I}(l, \mu)$ represent the radiation field for the case $\epsilon = \epsilon_1 l$, and $\mathfrak{I}^*(l, \mu)$ the radiation field for the case $\epsilon = \epsilon_1(\tau_1 + \tau - l)$. It is apparent from symmetry that

$$\mathfrak{I}(l, +\mu) = \mathfrak{I}^*(\tau_1 + \tau - l, -\mu)$$

and

$$\mathfrak{I}(\tau, +\mu) = \mathfrak{I}^*(\tau_1, -\mu) \qquad (0 \leqslant \mu \leqslant 1) \,. \tag{4}$$

The superposition of these two atmospheres gives a uniform source atmosphere in which $\epsilon = \epsilon_1(\tau_1 + \tau)$. Let $\mathfrak{I}^{(u)}(\tau, \mu)$ represent the emergent field for this uniform case. Adding the respective equations of transfer, using equation (4) and the known solution for the

[1] Horak, *Ap. J.*, **116**, 477, 1952, hereafter referred to as "*E.A. I.*" This paper is a necessary preliminary to the present one.

uniform case (*E.A. I*, eq. [20]), we obtain

$$
\begin{aligned}
{}^{(u)}\mathfrak{J}(\tau, +\mu) &= \mathfrak{J}(\tau, +\mu) + \mathfrak{J}^*(\tau, +\mu) \\
&= \mathfrak{J}(\tau, +\mu) + \mathfrak{J}(\tau_1, -\mu) \\
&= \frac{2\epsilon_1(\tau_1 - \tau)}{2 - \varpi_0[a_0(\tau_1 - \tau) - \beta_0(\tau_1 - \tau)]}\,[X(\tau_1 - \tau; \mu) - Y(\tau_1 - \tau; \mu)]\,,
\end{aligned}
\tag{5}
$$

where the X- and Y-functions are defined with respect to the characteristic function $\Psi = \varpi_0/2$ and a_0 and β_0 are, respectively, their zero moments. It will be seen later that this relation combined with the invariance principles suffices to solve our problem.

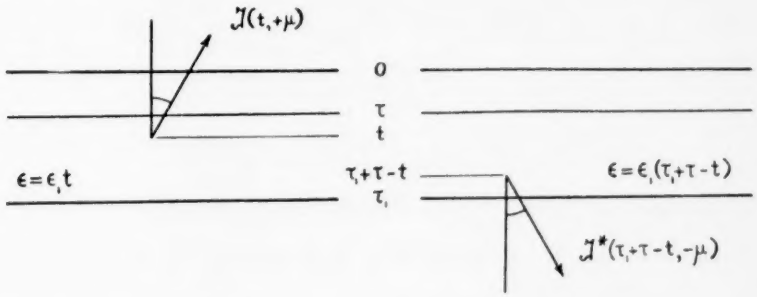

FIG. 1.—The superposition of the two atmospheres of thickness $\tau_1 - \tau$, gives a uniform source atmosphere in which $\epsilon = \epsilon_1(\tau_1 + \tau)$.

There are four invariance principles applicable to the emitting atmoshere. The mathematical formulation of these is the following (refer to *E.A. I*, eqs. [2] and [3]):

$$
I(\tau, +\mu) = \mathfrak{J}_{\tau_1 - \tau}(\tau, +\mu) + \frac{1}{2\mu}\int_0^1 S(\tau_1 - \tau; \mu, \mu')\, I(\tau, -\mu')\, d\mu'\,, \tag{6}
$$

$$
I(\tau, -\mu) = \mathfrak{J}_{\tau}(\tau, -\mu) + \frac{1}{2\mu}\int_0^1 S(\tau; \mu, \mu')\, I(\tau, +\mu')\, d\mu'\,, \tag{7}
$$

$$
\begin{aligned}
I(0, +\mu) = \mathfrak{J}_{\tau}(0, +\mu) &+ e^{-\tau/\mu} I(\tau, +\mu) \\
&+ \frac{1}{2\mu}\int_0^1 T(\tau; \mu, \mu')\, I(\tau, +\mu')\, d\mu'\,,
\end{aligned}
\tag{8}
$$

$$
\begin{aligned}
I(\tau_1, -\mu) = \mathfrak{J}_{\tau_1 - \tau}(\tau_1, -\mu) &+ e^{-(\tau_1 - \tau)/\mu} I(\tau, -\mu) \\
&+ \frac{1}{2\mu}\int_0^1 T(\tau_1 - \tau; \mu, \mu')\, I(\tau, -\mu')\, d\mu'\,.
\end{aligned}
\tag{9}
$$

The intensity $\mathfrak{J}_\tau$ refers to the field which would exist if there were no layer from τ to τ_1; $\mathfrak{J}_{\tau_1 - \tau}$ refers to the field if there were no layer from 0 to τ; and S and T are, respectively, the scattering and transmission functions.

III. THE SOLUTION FOR ISOTROPIC SCATTERING WITH $\varpi_0 < 1$

Differentiating the four invariances with respect to τ, letting $\tau \to 0$ or τ_1, and using equation (2), we obtain

$$I(0, +\mu) = \mu \left[\frac{\partial \mathfrak{I}_{\tau_1-\tau}(\tau, +\mu)}{\partial \tau}\right]_0 + \varpi_0 J(0)\, X(\mu), \tag{10}$$

$$I(\tau_1, -\mu) = -\mu \left[\frac{\partial \mathfrak{I}_{\tau}(\tau, -\mu)}{\partial \tau}\right]_{\tau_1} + [\varpi_0 J(\tau_1) + \epsilon_1 \tau_1]\, X(\mu), \tag{11}$$

$$\mu \left[\frac{\partial \mathfrak{I}_{\tau}(0, +\mu)}{\partial \tau}\right]_{\tau_1} = [\varpi_0 J(\tau_1) + \epsilon_1 \tau_1]\, Y(\mu), \tag{12}$$

$$-\mu \left[\frac{\partial \mathfrak{I}_{\tau_1-\tau}(\tau_1, -\mu)}{\partial \tau}\right]_0 = \varpi_0 J(0)\, Y(\mu), \tag{13}$$

where

$$X(\mu) = 1 + \frac{1}{2}\int_0^1 S(\tau_1; \mu, \mu')\frac{d\mu'}{\mu'}$$

and (14)

$$Y(\mu) = e^{-\tau_1/\mu} + \frac{1}{2}\int_0^1 T(\tau_1; \mu, \mu')\frac{d\mu'}{\mu'}.$$

Adding equations (10) and (13) and using equation (5), we obtain

$$\begin{aligned} I(0, +\mu) &= \mu \left\{\frac{\partial}{\partial \tau}[\mathfrak{I}_{\tau_1-\tau}(\tau, +\mu) + \mathfrak{I}_{\tau_1-\tau}(\tau_1, -\mu)]\right\}_0 \\ &\quad + \varpi_0 J(0)[X(\mu) + Y(\mu)] \\ &= \mu \left\{\frac{\partial}{\partial \tau}\, \mathfrak{I}^{(\omega)}_{\tau_1-\tau}(\tau, +\mu)\right\}_0 + \varpi_0 J(0)[X(\mu) + Y(\mu)]. \end{aligned} \tag{15}$$

Differentiating equation (5) and letting $\tau \to 0$, we have

$$\begin{aligned} \left\{\frac{\partial}{\partial \tau}\, \mathfrak{I}^{(\omega)}_{\tau_1-\tau}(\tau\ \ +\mu)\right\}_0 &= \frac{2\epsilon_1\tau_1}{2-\varpi_0(a_0-\beta_0)}\left[\frac{\partial Y(\tau_1;\mu)}{\partial \tau_1} - \frac{\partial X(\tau_1;\mu)}{\partial \tau_1}\right] \\ &\quad + \left\{\frac{2\epsilon_1}{2-\varpi_0(a_0-\beta_0)} + \frac{2\epsilon_1\tau_1\varpi_0}{[2-\varpi_0(a_0-\beta_0)]^2}\frac{\partial}{\partial \tau_1}(\beta_0 - a_0)\right\} \\ &\quad \times [X(\tau_1;\mu) - Y(\tau_1;\mu)]. \end{aligned} \tag{16}$$

The following relations may be used:[2]

$$\frac{\partial X}{\partial \tau_1} = \frac{\varpi_0}{2}\beta_{-1}Y; \qquad \frac{\partial Y}{\partial \tau_1} = \frac{\varpi_0}{2}\beta_{-1}X - \frac{1}{\mu}Y; \tag{17}$$

whence

$$\frac{\partial a_0}{\partial \tau_1} = \frac{\varpi_0}{2}\beta_{-1}\beta_0; \qquad \frac{\partial \beta_0}{\partial \tau_1} = -\frac{\beta_{-1}}{2}(2 - \varpi_0 a_0). \tag{18}$$

It follows that

$$\begin{aligned} \left\{\frac{\partial}{\partial \tau}\, \mathfrak{I}^{(\omega)}_{\tau_1-\tau}(\tau, +\mu)\right\}_0 &= \frac{2\epsilon_1}{2-\varpi_0(a_0-\beta_0)}[X(\mu) - Y(\mu)] \\ &\quad - \frac{2\epsilon_1\tau_1}{2-\varpi_0(a_0-\beta_0)} \cdot \frac{1}{\mu}\, Y(\mu). \end{aligned} \tag{19}$$

[2] S. Chandrasekhar, *Radiative Transfer* (Oxford: Clarendon Press, 1950), p. 210, eqs. (13) and (15); hereafter cited as "*R.T.*"

Substituting this result in equation (15) gives

$$I(0, +\mu) = \frac{2\epsilon_1\mu}{2-\varpi_0(a_0-\beta_0)}[X(\mu) - Y(\mu)] - \frac{2\epsilon_1\tau_1}{2-\varpi_0(a_0-\beta_0)} Y(\mu) + \varpi_0 J(0)[X(\mu) + Y(\mu)]. \tag{20}$$

In similar fashion, beginning with equations (11) and (12), it can be shown that

$$I(\tau_1, -\mu) = -\frac{2\epsilon_1\mu}{2-\varpi_0(a_0-\beta_0)}[X(\mu) - Y(\mu)] - \frac{2\epsilon_1\tau_1}{2-\varpi_0(a_0-\beta_0)} Y(\mu) + [\varpi_0 J(\tau_1) + \epsilon_1\tau_1][X(\mu) + Y(\mu)]. \tag{21}$$

Next we must evaluate $J(0)$ and $J(\tau_1)$. Multiplying through equations (20) and (21) by $\frac{1}{2}$ and integrating over the range of μ gives the following:

$$J(0) = \frac{\epsilon_1(a_1-\beta_1-\beta_0\tau_1)}{2(1-\varpi_0)}; \tag{22}$$

$$J(\tau_1) = \frac{\epsilon_1[(2-a_0)\tau_1 - (a_1-\beta_1)]}{2(1-\varpi_0)}. \tag{23}$$

The final and exact solution for the emergent fields is, therefore,

$$\frac{I(0, +\mu)}{\epsilon_1} = \frac{2\mu}{2-\varpi_0(a_0-\beta_0)}[X(\mu) - Y(\mu)] - \frac{2\tau_1}{2-\varpi_0(a_0-\beta_0)} Y(\mu) + \frac{\varpi_0(a_1-\beta_1-\beta_0\tau_1)}{2(1-\varpi_0)}[X(\mu) + Y(\mu)], \tag{24}$$

and

$$\frac{I(\tau_1, -\mu)}{\epsilon_1} = \frac{-2\mu}{2-\varpi_0(a_0-\beta_0)}[X(\mu) - Y(\mu)] - \frac{2\tau_1}{2-\varpi_0(a_0-\beta_0)} Y(\mu) - \frac{\varpi_0}{2(1-\varpi_0)}\left[a_1-\beta_1-\left(\frac{2}{\varpi_0}-a_0\right)\tau_1\right][X(\mu) + Y(\mu)]. \tag{25}$$

Actually, it is unnecessary to use equation (25), since we have the relation (eq. [5])

$$\frac{I(\tau_1, -\mu)}{\epsilon_1} = \frac{2\tau_1}{2-\varpi_0(a_0-\beta_0)}[X(\mu) - Y(\mu)] - \frac{I(0, +\mu)}{\epsilon_1}. \tag{26}$$

When $\varpi_0 = 0$, we obtain the direct field, i.e., there is no scattering of light. We have simply $X(\mu) = 1$ and $Y(\mu) = e^{-\tau_1/\mu}$, and it follows at once that

$$\frac{I(0, +\mu)}{\epsilon_1} = \mu(1 - e^{-\tau_1/\mu}) - \tau_1 e^{-\tau_1/\mu} \tag{27}$$

and

$$\frac{I(\tau_1, -\mu)}{\epsilon_1} = -\mu(1 - e^{-\tau_1/\mu}) + \tau_1. \tag{28}$$

These results can be verified by directly integrating the equation of transfer.

The solution for the semi-infinite case can be readily obtained, beginning with the equation analogous to (10), viz.:

$$I(0, +\mu) = \mu\left[\frac{\partial \mathfrak{J}_{\infty-\tau}(\tau, +\mu)}{\partial\tau}\right]_0 + \varpi_0 J(0) H(\mu). \tag{29}$$

Now

$$\mathfrak{I}_{\infty-\tau}(\tau, +\mu) = \mathfrak{I}^{(u)}_{\infty-\tau}(\tau, +\mu) + I(0, +\mu), \tag{30}$$

where (*E.A. I*, eq. [23])

$$\mathfrak{I}^{(u)}_{\infty-\tau}(\tau, +\mu) = \epsilon_1 \tau (1-\varpi_0)^{-1/2} H(\mu). \tag{31}$$

Evaluating the derivative, we obtain

$$\left[\frac{\partial}{\partial \tau}\, \mathfrak{I}_{\infty-\tau}(\tau, +\mu)\right] = \epsilon_1 (1-\varpi_0)^{-1/2} H(\mu). \tag{32}$$

Hence

$$I(0, +\mu) = \mu\epsilon_1 (1-\varpi_0)^{-1/2} H(\mu) + \varpi_0 J(0) H(\mu). \tag{33}$$

It follows that

$$J(0) = \frac{\epsilon_1 a_1}{2(1-\varpi_0)}, \tag{34}$$

and, finally,

$$\frac{I(0, +\mu)}{\epsilon_1} = \mu (1-\varpi_0)^{-1/2} H(\mu) + \frac{\varpi_0 a_1}{2(1-\varpi_0)} H(\mu). \tag{35}$$

This result was first obtained by Chandrasekhar by a different method.[3] Also this equation follows from equation (24) if we assume that, as $\tau_1 \to \infty$, $X(\mu) \to H(\mu)$, $Y(\mu) \to 0$, and $\beta_0 \tau_1 \to 0$.

IV. CONSERVATIVE SCATTERING

When the albedo ϖ_0 is unity, we have the case of conservative scattering. A certain nonuniqueness exists,[4] and in terms of the so-called "standard solutions," $X_s(\mu)$ and $Y_s(\mu)$, we have

$$\begin{aligned} X(\mu) &= X_s(\mu) + Q\mu [X_s(\mu) + Y_s(\mu)], \\ Y(\mu) &= Y_s(\mu) - Q\mu [X_s(\mu) + Y_s(\mu)], \end{aligned} \tag{36}$$

and

$$\begin{aligned} a_n &= a^s_n + Q(a_{n+1} + \beta_{n+1}), \\ \beta_n &= \beta^s_n - Q(a_{n+1} + \beta_{n+1}), \\ a^s_0 &= 2, \qquad \beta^s_0 = 0, \qquad a_0 + \beta_0 = 2. \end{aligned} \tag{37}$$

Beginning with the invariance principles, our derivation proceeds exactly as in the nonconservative case, but, instead of equations (20) and (21), we obtain

$$I(0, +\mu) = \frac{\epsilon_1 \mu}{\beta_0} [X(\mu) - Y(\mu)] - \frac{\epsilon_1 \tau_1}{\beta_0} Y(\mu) + J(0) [X(\mu) + Y(\mu)], \tag{38}$$

$$I(\tau_1, -\mu) = -\frac{\epsilon_1 \mu}{\beta_0} [X(\mu) - Y(\mu)] + \frac{\epsilon_1 \tau_1}{\beta_0} X(\mu) - J(0) [X(\mu) + Y(\mu)]. \tag{39}$$

The quantities Q and $J(0)$ can be determined as follows: Let us multiply through equation (38) by $\frac{1}{2}$ and integrate over the range of μ. We obtain the relation

$$a_1 - \beta_1 - \beta_0 \tau_1 = 0. \tag{40}$$

[3] *Ap. J.*, **106**, 145, 1945; and *R.T.*, p. 321.

[4] *R.T.*, pp. 190 ff.

Q can be found from this equation thus:

$$Q = \frac{-(\alpha_1^s - \beta_1^s)}{(\alpha_1 + \beta_1)\tau_1 + 2(\alpha_2 + \beta_2)}. \tag{41}$$

From the equation of transfer (eq. [2]) it follows that

$$F(\tau) = -2\epsilon_1\tau^2 + F(0) \tag{42}$$

and

$$K(\tau) = -\frac{\epsilon_1}{6}\tau^3 + \tfrac{1}{4}F(0)\tau + K(0). \tag{43}$$

The quantities $F(0)$, $K(0)$, $F(\tau_1)$, and $K(\tau_1)$ can be found in two ways, viz., from equations (38) and (39) and from equations (42) and (43). We obtain the following:

$$F(0) = \frac{2\epsilon_1}{\beta_0}(\alpha_2 - \beta_2) - \frac{2\epsilon_1\tau_1}{\beta_0}\beta_1 + J(0)\,2(\alpha_1 + \beta_1), \tag{44}$$

$$-F(\tau_1) = -\frac{2\epsilon_1}{\beta_0}(\alpha_2 - \beta_2) + \frac{2\epsilon_1\tau_1}{\beta_0}\alpha_1 - J(0)\,2(\alpha_1 + \beta_1) = 2\epsilon_1\tau_1^2 - F(0), \tag{45}$$

$$K(0) = \frac{1}{2}\frac{\epsilon_1}{\beta_0}(\alpha_3 - \beta_3) - \frac{1}{2}\frac{\epsilon_1\tau_1}{\beta_0}\beta_2 + J(0)\,\tfrac{1}{2}(\alpha_2 + \beta_2), \tag{46}$$

$$K(\tau_1) = -\frac{1}{2}\frac{\epsilon_1}{\beta_0}(\alpha_3 - \beta_3) + \frac{1}{2}\frac{\epsilon_1\tau_1}{\beta_0}\alpha_2 - J(0)\,\tfrac{1}{2}(\alpha_2 + \beta_2) = -\frac{\epsilon_1}{6}\tau_1^3 + \tfrac{1}{4}F(0)\tau_1 + K(0). \tag{47}$$

Eliminating $F(0)$ and $K(0)$ and solving for $J(0)$ yields the result

$$\frac{J(0)}{\epsilon_1} = [(\alpha_1 + \beta_1)\tau_1 + 2(\alpha_2 + \beta_2)]^{-1}\left[-\tfrac{1}{6}\tau_1^3 + \frac{\alpha_1 + \beta_1}{2\beta_0}\tau_1^2 + \frac{2\beta_2}{\beta_0}\tau_1 - \frac{2(\alpha_3 - \beta_3)}{\beta_0}\right]. \tag{48}$$

Also, from equation (26), we have

$$\frac{J(\tau_1)}{\epsilon_1} = \frac{\tau_1(1 - \beta_0)}{\beta_0} - \frac{J(0)}{\epsilon_1}. \tag{49}$$

The final solution for the emergent radiation is then given by

$$\frac{I(0, +\mu)}{\epsilon_1} = \frac{-\mu}{Q(\alpha_1 + \beta_1)}[X^*(\mu) - Y^*(\mu)] + \frac{\tau_1}{Q(\alpha_1 + \beta_1)}Y^*(\mu) + \frac{J(0)}{\epsilon_1}[X^*(\mu) + Y^*(\mu)] \tag{50}$$

and

$$\frac{I(\tau_1, -\mu)}{\epsilon_1} = \frac{-\tau_1}{Q(\alpha_1 + \beta_1)}[X^*(\mu) - Y^*(\mu)] - \frac{I(0, +\mu)}{\epsilon_1}, \tag{51}$$

where

$$\frac{J(0)}{\epsilon_1} = \frac{Q}{6(\alpha_1^s - \beta_1^s)}\tau_1^3 + \frac{1}{2(\alpha_1^s - \beta_1^s)}\tau_1^2 + \frac{2}{(\alpha_1^s - \beta_1^s)(\alpha_1 + \beta_1)} \times [\beta_2^s - Q(\alpha_2 + \beta_3)]\tau_1 - \frac{2}{(\alpha_1^s - \beta_1^s)(\alpha_1 + \beta_1)}[(\alpha_3^s - \beta_3^s) + 2Q(\alpha_4 + \beta_4)], \tag{52}$$

and $X^*(\mu)$ and $Y^*(\mu)$ are the X- and Y-functions defined by equations (36) when Q has the value given by equation (41).

V. THE FINITE APPROXIMATION SOLUTION

The equation of transfer, equation (2), can be solved in the nth approximation by the method of Chandrasekhar. The integral $J(\tau)$ is replaced by a sum, using the Gaussian quadrature formula, and the integrodifferential equation is replaced by a simultaneous system of ordinary differential equations, thus:

$$\mu \frac{dI(\tau, \mu_i)}{d\tau} = I(\tau, \mu_i) - \frac{\varpi_0}{2} \sum_j a_j I(\tau, \mu_j) - \epsilon_1 \tau \qquad (i, j = \pm 1, \ldots, \pm n), \tag{53}$$

where a_j and μ_j are, respectively, the Gaussian weights and divisions.

The solution of the homogeneous part is known to be[5]

$$I(\tau, \mu_i) = \sum_{a=-n}^{+n} \frac{L_a e^{-k_a \tau}}{1 + \mu_i k_a} \qquad (i = \pm 1, \ldots, \pm n), \tag{54}$$

where the L_a's are $2n$ integration constants and the k_a's are the roots of the characteristic equation

$$1 = \varpi_0 \sum_{j=1}^{n} \frac{a_j}{1 - \mu_j^2 k^2}. \tag{55}$$

The particular integral is given by[6]

$$I(\tau, \mu_i) = \frac{\epsilon_1}{1 - \varpi_0} (\tau + \mu_i) \qquad (\varpi_0 < 1). \tag{56}$$

The complete solution at the points of Gaussian division is, therefore,

$$I(\tau, \mu_i) = \sum_{a=-n}^{+n} \frac{L_a e^{-k_a \tau}}{1 + \mu_i k_a} + \frac{\epsilon_1}{1 - \varpi_0} (\tau + \mu_i) \qquad (i = \pm 1, \ldots, \pm n; \varpi_0 < 1). \tag{57}$$

Let

$$T(\tau, \mu) = \sum_{a=-n}^{+n} \frac{L_a e^{-k_a \tau}}{1 + \mu k_a} + \frac{\epsilon_1}{1 - \varpi_0} (\tau + \mu). \tag{58}$$

The boundary conditions which determine the constants L_a are expressed by

$$T(0, -\mu_i) = T(\tau_1, +\mu_i) = 0 \qquad (i = 1, \ldots, n). \tag{59}$$

The source function $\mathfrak{J}(\tau) = \varpi J(\tau) + \epsilon_1 \tau$ is given by

$$\begin{aligned} \mathfrak{J}(\tau) &= \frac{\varpi_0}{2} \sum_j a_j I(\tau, \mu_j) + \epsilon_1 \tau \\ &= \sum_{a=-n}^{+n} L_a e^{-k_a \tau} + \frac{\epsilon_1}{1 - \varpi_0} \tau. \end{aligned} \tag{60}$$

[5] *Ibid.*, p. 81, eqs. (86) and (84).

[6] *Ibid.*, p. 323, eq. (26).

The solution for the radiation field is then found from the formal solution of the equation of transfer, viz.,

$$I(\tau, +\mu) \int_{\tau}^{\tau_1} e^{-(t-\tau)/\mu} \mathfrak{J}(t) \frac{dt}{\mu}. \tag{61}$$

We obtain

$$I(\tau, +\mu) = T(\tau, \mu) - e^{-(\tau_1-\tau)/\mu} T(\tau_1, \mu) \tag{62}$$

and

$$I(\tau, -\mu) = T(\tau, -\mu) - e^{-\tau/\mu} T(0, -\mu). \tag{63}$$

In the conservative case the particular integral which replaces equation (56) is the following:

$$I(\tau, \mu_i) = -3\epsilon_1\mu_i^3 - 3\epsilon_1\tau\mu_i^2 - \tfrac{3}{2}\epsilon_1\tau^2\mu_i - \tfrac{1}{2}\epsilon_1\tau^3. \tag{64}$$

VI. CALCULATIONS AND FINAL REMARKS

Some calculations have been made illustrating the form of the emergent fields for an atmosphere of optical thickness $\tau_1 = 0.20$. The results are given in Table 1 and are illus-

TABLE 1

THE EMERGENT RADIATION FIELD, $\tau_1 = 0.20$

μ	$\varpi_0 = 0.50$		$\varpi_0 = 0.90$		$\varpi_0 = 1.00$	
	$I(0, \mu)/\epsilon_1$	$I(\tau_1, -\mu)/\epsilon_1$	$I(0, \mu)/\epsilon_1$	$I(\tau_1, -\mu)/\epsilon_1$	$I(0, \mu)/\epsilon_1$	$I(\tau_1, -\mu)/\epsilon_1$
0.00	0.010	0.215	0.021	0.229	0.024	0.234
0.02	.031	.196	.043	.213	.047	.218
0.05	.058	.167	.071	.183	.075	.188
0.10	.071	.127	.084	.141	.088	.146
0.15	.068	.101	.079	.113	.082	.116
0.20	.062	.083	.072	.093	.074	.096
0.30	.050	.061	.058	.069	.060	.071
0.40	.042	.049	.048	.054	.050	.056
0.50	.036	.040	.041	.045	.042	.047
0.60	.031	.034	.036	.038	.037	.040
0.70	.027	.030	.032	.033	.033	.035
0.80	.025	.026	.029	.029	.029	.031
0.90	.022	.024	.026	.026	.026	.028
1.00	0.020	0.021	0.024	0.024	0.024	0.025

trated graphically in polar form for the case $\varpi_0 = 0.90$ (Fig. 2). The exact X- and Y-functions and moments were used.[7] In the conservative case it is necessary to compute some of the higher moments.

The exact radiation field at any depth τ can be found by iteration, using two of the invariance principles, viz., equations (6) and (7). It is necessary to have starting values for $I(\tau, +\mu)$ and $I(\tau, -\mu)$. These can be obtained from the finite approximation solution, equations (64) and (65). Usually it is sufficient to take $n = 2$. The integrations can be performed by some convenient quadrature formula, using, say, ten equal intervals.

The Milne-Eddington model for the formation of spectral lines, with η_ν assumed constant with depth and $B_\nu = a + b\tau_\nu$, leads to an equation of transfer which mathematically represents the superposition of two semi-infinite emitting atmospheres, one with a uniform distribution of sources and the other with a linear distribution. It is now pos-

[7] Chandrasekhar, Elbert, and Franklin, *Ap. J.*, **115**, 244, 1952.

sible to find the *exact* radiation field at any depth, since the solution for the finite atmosphere is known. It is intended in a later paper to consider this problem and to perform some calculations for the case in which the variation of η_ν with depth is taken into ac-

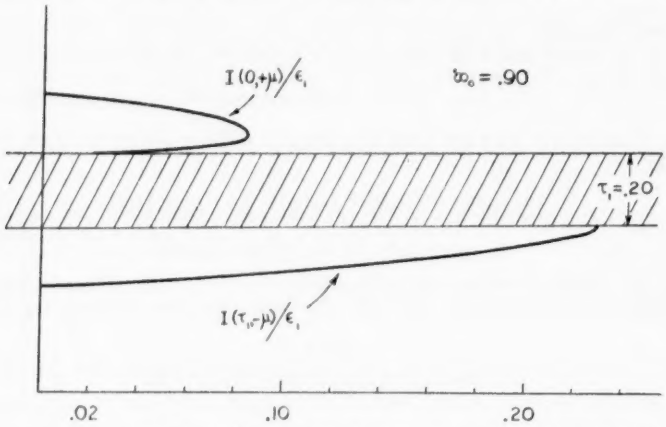

FIG. 2.—The emergent radiation fields are shown here for an atmosphere of optical thickness $\tau_1 = 0.20$, which contains a linear distribution of sources. This is a polar diagram in which the vertical line represents $\mu = 1$.

count. Other source distributions will also be considered in a later paper. At the present time the polynomial distribution, $\epsilon = \Sigma \epsilon_j \tau^j$, has been worked out by one of us (Lundquist).

We wish to thank Dr. Chandrasekhar for encouragement and advice. Dr. Horak wishes to thank the University of Kansas for a research grant.

EXACT CURVES OF GROWTH. III. THE SCHUSTER-SCHWARZSCHILD MODEL*

M. H. WRUBEL
Goethe Link Observatory, Indiana University
Received August 13, 1953

ABSTRACT

Curves of growth have been computed for six values of the damping from $\log a = -3.0$ to $\log a = -1.0$ and four values of $I^{(0)}/I^{(1)}$ from $\frac{1}{4}$ to 2, using Chandrasekhar's exact solution of the equation of transfer for the Schuster-Schwarzschild model and Harris' expansion of the line-scattering coefficient.

NOTATION

The symbols used in this paper are essentially the same as in Paper I of this series,[1] with the following additions and modifications:

$I^{(0)} + I^{(1)}\mu$: Law of darkening of the photosphere in the neighborhood of a line;

τ_1: Optical depth of the "reversing layer" at a point in the line;

τ_0: "Fictitious" optical depth at the center of the line;

$H(a, v)$: Harris' expansion of the line-scattering coefficient;[2]

$a_1, a_2, \beta_1, \beta_2$: Moments of Chandrasekhar's X- and Y-functions.

INTRODUCTION

The Schuster-Schwarzschild (S-S) and Milne-Eddington (M-E) models represent opposite physical approximations to the conditions under which stellar absorption lines are formed. The principal difference lies in the role played by the continuous absorption. In the S-S model it is assumed that the line is formed above the continuum and that continuous opacity plays only an indirect role; in the M-E model, line and continuum are formed simultaneously, and radiation within the line is subject to continuous absorption along the path between individual scatterings. (In the latter case it is further assumed that the ratio of the line-scattering coefficient to the continuous-absorption coefficient is constant with depth.) The circumstances of the formation of an observed line probably lie between the extremes represented by these models.

Although the equations of radiative transfer appropriate to these models have been known for a long time, it was not until the recent work of Chandrasekhar that the exact mathematical solutions of these equations were found. Effects due to physical differences between these models now stand apart from mathematical approximations. A calculation of these curves of growth was undertaken, to make use of the new solutions for the S-S model and to present a set complementary to the M-E curves published previously.[1]

STATEMENT OF THE PROBLEM

The theoretical calculation of absorption-line profiles and equivalent widths requires knowledge of the atomic absorption coefficient, a model structure of the atmosphere, and

* *Publications of the Goethe Link Observatory, Indiana University*, No. 13.

[1] M. H. Wrubel, *Ap. J.*, **109**, 66, 1949.

[2] D. L. Harris III, *Ap. J.*, **108**, 112, 1948.

the solution of the problem of energy transport. The absorption coefficient involves properties of the individual atom, interactions between atoms, and the effect of thermal and convective or turbulent motions. The model in the simplest case describes the relative importance of line absorption to continuous absorption; the relative importance of scattering to absorption in the line; and the limb darkening. The mode of energy transport can be radiation or convection in varying proportions. The calculations of this paper are based upon a line coefficient valid only for a Maxwellian velocity distribution; pure scattering is assumed in the reversing layer of the S-S model; and radiation is the only means of energy transport considered.

Since the S-S model is described in detail elsewhere,[3] it suffices to say that the law of darkening of the continuously radiating photosphere is taken in this paper to be

$$I(0, \mu) = I^{(0)} + I^{(1)}\mu . \tag{1}$$

The optical depth of the reversing layer at a point in the line is denoted by τ_1 and can be calculated from the expression

$$\tau_1 = \tau_0 H(a, v) , \tag{2}$$

where τ_0 is the "fictitious" optical depth at the center of the line and $H(a, v)$ is Harris' expansion of the line-scattering coefficient.[2] The dimensionless quantities a and v have their usual definitions (see Paper I). The solution of the transfer problem as given by Chandrasekhar[4] can be written in the form

$$R = \frac{\frac{4}{3} + Ky}{\frac{4}{3} + \tau_1 + 2y} , \tag{3}$$

where R is the residual intensity,

$$K = \frac{4}{3\,[I^{(0)}/\,I^{(1)}] + 2} , \tag{4}$$

$$y = \frac{\alpha_2 + \beta_2}{\alpha_1 + \beta_1} - \frac{2}{3} , \tag{5}$$

and the α's and β's refer to moments of Chandrasekhar's X- and Y-functions and y has been tabulated as a function of τ_1.[5]

The equivalent width is calculated from the residual intensity by means of the integral

$$\frac{W}{v} = \int_{-\infty}^{+\infty} (1 - R)\, dv . \tag{6}$$

Curves have been computed for six values of the damping, running from $\log a = -3.0$ to $\log a = -1.0$ in intervals of 0.4 and for $I^{(0)}/I^{(1)}$ equal to $\frac{1}{4}$, $\frac{1}{2}$, 1, and 2. The results are given in Table 1. Two sets of curves are illustrated in Figures 1 and 2. All curves refer to the integrated flux.

CONSTRUCTION OF TABLES

[Most of the calculations were done on I.B.M. punch-card equipment. Time on the machines was kindly provided by Indiana University without charge, and all coding was done by the author. For each assigned value of a and τ_0, τ_1 was calculated as a function of v, using Harris' tables. A critical table of y as a function of τ_1 was constructed by La-

[3] E.g., B. Strömgren, *Astrophysics*, ed. J. A. Hynek (New York: McGraw-Hill Book Co., 1951), chap. v; L. Aller, *Astrophysics* (New York: Ronald Press Co., 1953); or R. Woolley and D. Stibbs, *The Outer Layers of a Star* (Oxford: Clarendon Press, 1953).

[4] *Radiative Transfer* (Oxford: Oxford University Press, 1950), p. 320.

[5] S. Chandrasekhar and Donna Elbert, *Ap. J.*, **115**, 269, 1952. The authors generously provided these tables in advance of publication.

TABLE 1

LOG τ_0	LOG a					
	−1.0	−1.4	−1.8	−2.2	−2.6	−3.0
	log W/b for $I^{(0)}/I^{(1)}=\frac{1}{4}$					
−2.8	−2.640	−2.640	−2.640	−2.640	−2.641	−2.641
−2.4	−2.242	−2.242	−2.242	−2.242	−2.243	−2.243
−2.0	−1.845	−1.845	−1.845	−1.845	−1.845	−1.846
−1.6	−1.449	−1.450	−1.451	−1.451	−1.451	−1.451
−1.2	−1.061	−1.062	−1.063	−1.063	−1.064	−1.064
−0.8	−0.685	−0.689	−0.691	−0.692	−0.692	−0.692
−0.4	−0.335	−0.343	−0.346	−0.348	−0.348	−0.348
0.0	−0.027	−0.041	−0.047	−0.050	−0.051	−0.051
+0.4	+0.226	+0.201	+0.190	+0.186	+0.184	+0.183
+0.8	*+0.421*	+0.381	+0.363	+0.356	+0.352	+0.351
+1.2	+0.577	*+0.517*	+0.487	+0.474	+0.469	+0.467
+1.6	+0.722	+0.632	*+0.584*	+0.562	+0.553	+0.549
+2.0	+0.874	+0.750	+0.674	*+0.635*	+0.618	+0.611
+2.4	+1.043	+0.887	+0.774	+0.708	*+0.676*	+0.662
+2.8	+1.227	+1.048	+0.899	+0.796	+0.738	*+0.710*
+3.2	+1.420	+1.229	+1.053	+0.910	+0.815	+0.763
+3.6	+1.617	+1.420	+1.230	+1.058	+0.921	+0.833
+4.0	+1.816	+1.617	+1.421	+1.232	+1.063	+0.932
+4.4	+2.015	+1.816	+1.617	+1.421	+1.234	+1.068
+4.8	+2.215	+2.015	+1.816	+1.617	+1.422	+1.236
+5.2	+2.415	+2.215	+2.015	+1.816	+1.618	+1.423
+5.6	+2.615	+2.415	+2.215	+2.015	+1.816	+1.618
+6.0	+2.815	+2.615	+2.415	+2.215	+2.015	+1.816
	log W/b for $I^{(0)}/I^{(1)}=\frac{1}{3}$					
−2.8	−2.621	−2.621	−2.621	−2.621	−2.621	−2.621
−2.4	−2.223	−2.223	−2.224	−2.224	−2.224	−2.224
−2.0	−1.826	−1.827	−1.827	−1.827	−1.827	−1.827
−1.6	−1.431	−1.432	−1.433	−1.433	−1.433	−1.433
−1.2	−1.044	−1.046	−1.047	−1.047	−1.047	−1.047
−0.8	−0.671	−0.675	−0.677	−0.677	−0.678	−0.678
−0.4	−0.324	−0.332	−0.335	−0.337	−0.337	−0.338
0.0	−0.018	−0.033	−0.040	−0.042	−0.043	−0.044
+0.4	+0.231	+0.206	+0.195	+0.190	+0.188	+0.188
+0.8	*+0.425*	+0.385	+0.366	+0.359	+0.355	+0.354
+1.2	+0.582	*+0.520*	+0.490	+0.477	+0.471	+0.469
+1.6	+0.726	+0.636	*+0.587*	+0.564	+0.554	+0.550
+2.0	+0.879	+0.755	+0.677	*+0.637*	+0.619	+0.612
+2.4	+1.049	+0.892	+0.778	+0.711	*+0.678*	+0.663
+2.8	+1.233	+1.054	+0.904	+0.799	+0.740	*+0.711*
+3.2	+1.426	+1.235	+1.059	+0.915	+0.818	+0.765
+3.6	+1.523	+1.427	+1.237	+1.063	+0.926	+0.836
+4.0	+1.822	+1.624	+1.427	+1.238	+1.068	+0.936
+4.4	+2.022	+1.822	+1.624	+1.428	+1.240	+1.073
+4.8	+2.222	+2.022	+1.822	+1.624	+1.428	+1.242
+5.2	+2.422	+2.222	+2.022	+1.822	+1.624	+1.429
+5.6	+2.621	+2.422	+2.222	+2.022	+1.822	+1.624
+6.0	+2.821	+2.621	+2.422	+2.222	+2.022	+1.822

TABLE 1—*Continued*

LOG τ_0	LOG a					
	−1.0	−1.4	−1.8	−2.2	−2.6	−3.0
	log W/b for $I^{(0)}/I^{(1)}=1$					
−2.8	−2.600	−2.600	−2.600	−2.600	−2.601	−2.601
−2.4	−2.203	−2.204	−2.204	−2.204	−2.204	−2.204
−2.0	−1.807	−1.808	−1.808	−1.808	−1.808	−1.808
−1.6	−1.413	−1.414	−1.414	−1.414	−1.414	−1.414
−1.2	−1.026	−1.028	−1.029	−1.029	−1.030	−1.030
−0.8	−0.655	−0.659	−0.662	−0.662	−0.663	−0.663
−0.4	−0.311	−0.320	−0.323	−0.325	−0.326	−0.326
0.0	−0.009	−0.024	−0.031	−0.034	−0.035	−0.036
+0.4	+0.238	+0.212	+0.200	+0.195	+0.193	+0.193
+0.8	*+0.430*	+0.389	+0.370	+0.362	+0.359	+0.357
+1.2	+0.586	*+0.524*	+0.493	+0.479	+0.473	+0.471
+1.6	+0.732	+0.640	*+0.590*	+0.566	+0.556	+0.552
+2.0	+0.885	+0.759	+0.680	*+0.639*	+0.621	+0.613
+2.4	+1.056	+0.898	+0.782	+0.714	*+0.680*	+0.664
+2.8	+1.240	+1.060	+0.909	+0.803	+0.742	*+0.713*
+3.2	+1.433	+1.242	+1.065	+0.920	+0.822	+0.767
+3.6	+1.630	+1.434	+1.243	+1.070	+0.931	+0.839
+4.0	+1.829	+1.631	+1.434	+1.245	+1.074	+0.941
+4.4	+2.029	+1.829	+1.631	+1.435	+1.247	+1.079
+4.8	+2.229	+2.029	+1.829	+1.631	+1.435	+1.248
+5.2	+2.429	+2.229	+2.029	+1.829	+1.631	+1.436
+5.6	+2.629	+2.429	+2.229	+2.029	+1.830	+1.631
+6.0	+2.829	+2.629	+2.429	+2.229	+2.029	+1.830
	log W/b for $I^{(0)}/I^{(1)}=2$					
−2.8	−2.583	−2.584	−2.584	−2.584	−2.584	−2.584
−2.4	−2.186	−2.187	−2.187	−2.187	−2.187	−2.187
−2.0	−1.791	−1.791	−1.792	−1.792	−1.792	−1.792
−1.6	−1.397	−1.398	−1.398	−1.398	−1.398	−1.398
−1.2	−1.011	−1.013	−1.014	−1.015	−1.015	−1.015
−0.8	−0.642	−0.646	−0.649	−0.650	−0.650	−0.650
−0.4	−0.301	−0.309	−0.313	−0.315	−0.316	−0.316
0.0	−0.001	−0.017	−0.024	−0.027	−0.028	−0.029
+0.4	+0.243	+0.217	+0.205	+0.200	+0.198	+0.197
+0.8	*+0.435*	+0.392	+0.373	+0.365	+0.361	+0.360
+1.2	+0.590	*+0.527*	+0.495	+0.481	+0.475	+0.473
+1.6	+0.736	+0.643	*+0.592*	+0.568	+0.557	+0.553
+2.0	+0.890	+0.763	+0.683	*+0.641*	+0.622	+0.614
+2.4	+1.061	+0.903	+0.786	+0.716	*+0.681*	+0.665
+2.8	+1.246	+1.066	+0.914	+0.806	+0.744	*+0.714*
+3.2	+1.439	+1.248	+1.070	+0.924	+0.825	+0.769
+3.6	+1.636	+1.440	+1.249	+1.075	+0.935	+0.842
+4.0	+1.835	+1.637	+1.440	+1.251	+1.079	+0.945
+4.4	+2.035	+1.835	+1.637	+1.441	+1.252	+1.084
+4.8	+2.235	+2.035	+1.836	+1.637	+1.441	+1.254
+5.2	+2.435	+2.235	+2.035	+1.836	+1.637	+1.442
+5.6	+2.635	+2.435	+2.235	+2.035	+1.836	+1.637
+6.0	+2.835	+2.635	+2.435	+2.235	+2.035	+1.836

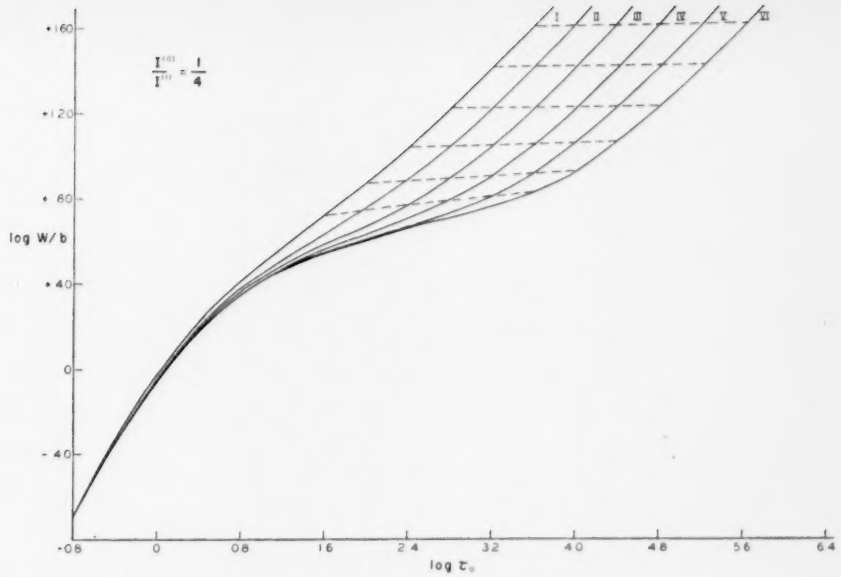

FIG. 1.—Theoretical curves of growth for $I^{(0)}/I^{(1)} = \frac{1}{4}$: curve *I*, $\log a = -1.0$; curve *II*, $\log a = -1.4$; curve *III*, $\log a = -1.8$; curve *IV*, $\log a = -2.2$; curve *V*, $\log a = -2.6$; curve *VI*, $\log a = -3.0$.

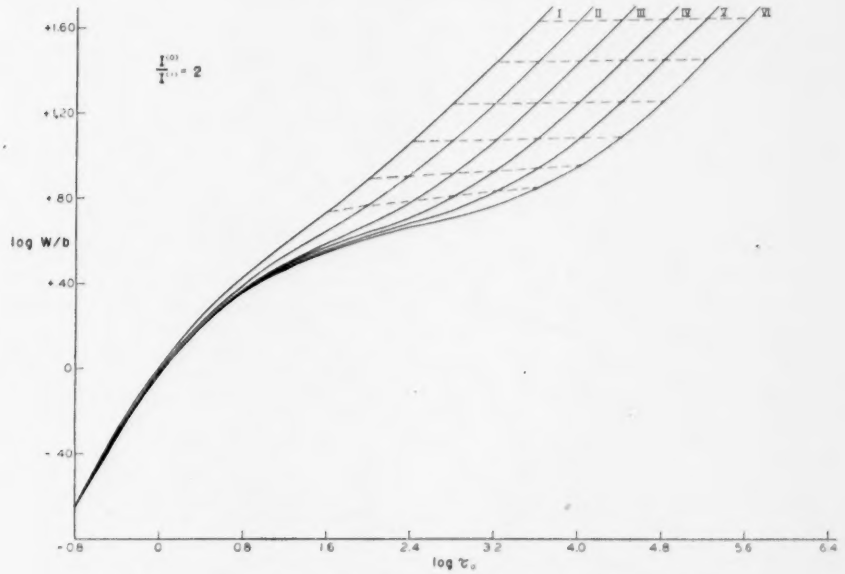

FIG. 2.—Theoretical curves of growth for $I^{(0)}/I^{(1)} = 2$: same notation as in Fig. 1

grangian interpolation, regarding y initially as a function of $e^{-\tau_1}$. The residual intensity was then calculated simultaneously for the four values of K corresponding to the four values of limb darkening.

The equivalent width was calculated by numerical integration far into the wings. When the residual intensity became sufficiently small and v sufficiently large, the integration was continued analytically, by using the asymptotic expression for $H(a, v)$. For the weakest lines, an expansion of y valid for small values of τ_1 was used.

USE OF TABLES

Interpolation in log a for constant $I^{(0)}/I^{(1)}$.—For moderate values of τ_0, interpolation for different values of the damping may easily be done directly across Table 1. For values of W/b lying below the values in italics, it is more convenient to interpolate along lines of constant $a\tau_0$. In Figures 1 and 2, which accompany the tables, the dotted lines are lines of constant $a\tau_0$.

Interpolation in $I^{(0)}/I^{(1)}$, *with log a and log* τ_0 *constant.*—It follows directly from the form of R that there is a constant difference between numerical values of W/b (not the logarithms) for the four values of $I^{(0)}/I^{(1)}$ tabulated, provided that log a and log τ_0 are constant. In order to find W/b for intermediate values of $I^{(0)}/I^{(1)}$, it is necessary only to multiply this difference by a numerical factor m and add it to the initial value. Table 2 gives the value of W/b for $I^{(0)}/I^{(1)} = 1$, as well as the difference D; further,

$$\left(\frac{W}{b}\right)_{I^{(0)}/I^{(1)}} = \left(\frac{W}{b}\right)_1 + m\,D \tag{7}$$

and

$$m = \frac{7\,[I^{(0)}/I^{(1)}] - 7}{2 + 3\,[I^{(0)}/I^{(1)}]}\,. \tag{8}$$

Reduction to a single curve of growth.—If log W/b and log a are kept constant, the curves for varying $I^{(0)}/I^{(1)}$ can be brought into approximate coincidence with the curve for $I^{(0)}/I^{(1)} = \frac{2}{3}$ (computed according to the foregoing paragraph) by the following average shifts in τ_0: for $I^{(0)}/I^{(1)} = 2$, 1, $\frac{1}{2}$, and $\frac{1}{4}$, the shifts are $+0.02$, $+0.01$, -0.01 and -0.02, respectively. This is not meant to imply that the curves can be brought into exact coincidence by lateral shifts. The shift is actually slightly larger (absolutely) for weak lines than for strong and is at a minimum near log $W/b = +0.2$. However, the total variation is relatively small.

COMPARISON OF S-S AND M-E CURVES

Since the general shape of a curve of growth is determined by the absorption coefficient and is independent of the model, the S-S and M-E curves are generally similar. However, two points of difference are apparent on further examination: the effect of limb darkening is smaller in the S-S model, and the curves for different values of limb darkening are shifted in opposite directions in the two models.

Limb darkening is a direct result of the continuous opacity. Since line scattering and continuous absorption are intertwined in the M-E model, it is clear that variation in limb darkening should be more effective in the M-E than in the S-S model, where it occurs only as a boundary condition.

Furthermore, in the S-S model, radiation leaving the photosphere at a large angle to the normal traverses more scattering material in the reversing layer and is therefore attenuated more than the radiation at smaller angles. If the limb darkening is decreased (or $I^{(0)}/I^{(1)}$ increased), more energy leaves the photosphere at large angles, and hence a larger fraction of the total energy leaving the photosphere is lost. Thus the energy in the line decreases, relative to the continuum, and the equivalent width increases.

In the M-E model, a decrease in limb darkening implies an increase in the continuous opacity of the atmosphere. Although the energy decreases in both the continuum and the line, the ratio of the energy in the line to that in the continuum increases. Thus the line

TABLE 2

log τ_0	log $a = -3.0$		log $a = -2.6$		log $a = -2.2$	
	$(W/b)_1$	D	$(W/b)_1$	D	$(W/b)_1$	D
−0.8	0.2174	0.0074	0.2174	0.0074	0.2176	0.0074
−0.4	0.4722	0.0125	0.4724	.0126	0.4732	.0126
0.0	0.9210	0.0170	0.9220	.0170	0.9245	.0172
+0.4	1.5583	0.0180	1.5612	.0182	1.5683	.0184
+0.8	2.276	0.016	2.283	.017	2.301	.017
+1.2	2.958	0.014	2.974	.015	3.013	.016
+1.6	3.563	0.013	3.597	.014	3.681	.017
+2.0	4.103	0.012	4.178	.015	4.360	.022
+2.4	4.616	0.014	4.781	.020	5.172	.033
+2.8	5.163	0.018	5.525	.031	6.354	.055
+3.2	5.855	0.029	6.636	.053	8.320	.096
+3.6	6.907	0.052	8.525	.095	11.737	.163
+4.0	8.729	0.093	11.866	.162	17.57	0.27
+4.4	11.999	0.161	17.64	0.27	.....	.....
+4.8	17.72	0.27	.....	.....	.....	.....
+5.2	27.28	0.43	.....	.....	.....	.....
+5.6	42.77	0.68	.....	.....	.....	.....
+6.0	67.54	1.09	.....	.....	.....	.....

log τ_0	log $a = -1.8$		log $a = -1.4$		log $a = -1.0$	
	$(W/b)_1$	D	$(W/b)_1$	D	$(W/b)_1$	D
−0.8	0.2180	0.0075	0.2190	0.0076	0.2213	0.0078
−0.4	0.4749	.0128	0.4790	.0131	0.4884	0.0139
0.0	0.9305	.0175	0.9452	.0184	0.9792	0.0204
+0.4	1.5860	.0192	1.6290	.0210	1.7292	0.025
+0.8	2.344	.019	2.449	.022	2.693	0.030
+1.2	3.109	.020	3.339	.027	3.858	0.041
+1.6	3.886	.024	4.362	.038	5.389	0.063
+2.0	4.789	.035	5.744	.060	7.679	0.102
+2.4	6.058	.057	7.903	.100	11.366	0.167
+2.8	8.112	.098	11.490	.166	17.39	0.27
+3.2	11.612	.165	17.45	0.27	27.12	0.43
+3.6	17.51	0.27	.....	.....	42.70	0.68
+4.0	.....	.....	.....	.....	67.50	1.09
+4.4	.....	.....	.....	.....	106.87	1.72
+4.8	.....	.....	.....	.....	169.3	2.7
+5.2	.....	.....	.....	.....	268.3	4.3
+5.6	.....	.....	.....	.....	425.2	6.9
+6.0	.....	.....	.....	.....	673.8	10.9

becomes weaker and weaker and ultimately vanishes when the atmosphere becomes impenetrable.

A more detailed comparison between the models is now being made in connection with the analysis of high-dispersion spectra of Procyon.

These calculations were supported by a contract with the Office of Naval Research and several grants from the Graduate School of Indiana University. The author wishes to thank Thomas L. Swihart and John P. Cox for their very competent assistance in the course of these computations.

COMPTON SCATTERING BY ELECTRON ATMOSPHERES
I. THE SCHUSTER PROBLEM

FRANK N. EDMONDS, JR.
Department of Mathematics and Astronomy, University of Texas, Austin, Texas
Received June 22, 1953

ABSTRACT

The problem of the transfer of radiation in an atmosphere of free electrons is solved in the first approximation under the conditions of the standard Schuster problem of line formation. In the solution, account is taken of the noncoherent character of the electron scattering due to the Doppler shifts arising from a Maxwellian distribution of thermal velocities, the red shift of the Compton effect, and a non-Doppler blue shift arising from thermal motions and first pointed out by Dirac. The latter two effects, designated as "Compton scattering," are shown to produce asymmetries in spectral lines which would be very difficult to detect for stellar temperatures, as they are much smaller than the thermal broadening.

I. INTRODUCTION

Scattering of radiation by free electrons not only contributes to the continuous opacity of high-temperature stellar atmospheres but also produces broadening and asymmetries in the spectral lines of such stars. These changes in line profiles are effects of noncoherent scattering, i.e., scattering which redistributes the radiation in frequency. This noncoherency in scattering is produced by the Doppler effects due to mass and thermal motions of the electrons and by the Compton effect in the scattering process. Münch[1] has investigated the broadening of spectral lines due to thermal motions and has found this effect in a Wolf-Rayet atmosphere. Asymmetric broadening due to mass motions of an expanding electron atmosphere in combination with thermal motions has also been analyzed.[2] In both these investigations the effects of Compton shifts have been neglected. Chandrasekhar[3] and O'Rourke[4] have determined the shifts effected by Compton scattering, but they neglected Doppler shifts and used a Taylor series expansion (to the first derivative) within the source function of the equation of transfer.

Compton scattering by electrons in thermal motion was first studied by Dirac,[5] who obtained the interesting result that thermal motions produced a non-Doppler blue shift which, for sufficiently high temperatures and low frequencies, would be greater than the red Compton shift. The spectral distribution function for radiation scattered by electrons in thermal motion as determined in the second approximation[6] accounts for these two opposing shifts, as well as for the Doppler shifts.

In this paper the transfer of monochromatic radiation through a plane-parallel atmosphere of free electrons is analyzed, by means of the approximate methods of radiative-transfer theory developed by Chandrasekhar.[7] The noncoherent Compton scattering by these electrons in thermal motion is accounted for by using the second-approximation

[1] *Ap. J.*, **108**, 116, 1948, and **112**, 266, 1950.

[2] F. N. Edmonds, Jr., *Ap. J.*, **112**, 307 and 324, 1950. The first paper will be referred to as "Moving Atmosphere I," and equations in that paper will be designated by prefixing "MAI," e.g., "equation MAI (46)."

[3] *Proc. R. Soc. London, A*, **192**, 508, 1948.

[4] *Phys. Rev.*, **85**, 881, 1952.

[5] *M.N.*, **85**, 825, 1925.

[6] F. N. Edmonds, Jr., *Ap. J.*, **117**, 298, 1953. This paper will be referred to as "Compton Scattering," and equations in this paper will be designated by prefixing "CS," e.g., "equation CS (26)."

[7] *Radiative Transfer* (Oxford: Clarendon Press, 1950), chap. ii.

spectral distribution function. The appropriate equation of radiative transfer is solved in the first approximation, subject to the boundary conditions of the Schuster problem. This solution is then used to determine the asymmetry produced in the broadening of spectral lines by an electron atmosphere whose temperature and optical depth (corresponding to those expected for a Wolf-Rayet star) should provide favorable conditions for detection of the asymmetry. For the temperature of this atmosphere (80,000° K), the non-Doppler blue shift due to thermal motions should be about eight times the Compton red shift, as shown in Figure 2 of the Compton Scattering paper. As may be expected, therefore, this asymmetry is to the blue, but it is of the order of 10^{-3} the thermal broadening and produces a shift of the center of the line of approximately one Compton wave length (0.024 A). Hence detection of the asymmetric effects of Compton scattering would be a very difficult matter.

II. EMISSION COEFFICIENT AND TRANSFORMATION OF THE EQUATION OF TRANSFER

As in the standard Schuster problem, it will be supposed that an atmosphere consisting only of free electrons in thermal motion is a layer of finite optical thickness lying outside an infinite plane surface radiating outward into the atmosphere. The radiation from this surface has a known intensity distribution in frequency and in direction and is symmetric with respect to the outward normal. The thermal motions of the electrons will be described by a Maxwellian distribution of velocities associated with a kinetic temperature T, which is constant throughout the atmosphere. Optical depth within the atmosphere, is defined by

$$d\tau = -N_e \sigma_e dn\,, \tag{1}$$

where N_e is the number of free electrons per cubic centimeter, dn is measured along the outward normal, and

$$\sigma_e = \frac{8\pi}{3}\frac{e^4}{m^2 c^4}. \tag{2}$$

In equation (2), e is the electron's charge, m its rest mass, and c the velocity of light. The direction of radiation is designated by

$$\mu = \cos\theta\,, \tag{3}$$

where θ is the polar angle with respect to the outward normal, and by the azimuthal angle φ.

The emission coefficient for Compton scattering by electrons in thermal motion is given by equation CS (16) as

$$j(\nu, \tau, \mu) = N_e \sigma_e \int d\omega' \tfrac{3}{4}(1+\cos^2\Theta) \int_0^\infty d\nu' I(\nu', \tau, \mu') \psi(\nu, \Theta, \nu')\,, \tag{4}$$

where primed quantities refer to the incident radiation, unprimed to the scattered radiation. In equation (4) ν is the frequency of radiation, $d\omega'$ is the increment of solid angle about the direction of the incident radiation whose intensity is $I(\nu', \tau, \mu')$, and Θ, the angle of scattering, is given by

$$\cos\Theta = \mu\mu' + [(1-\mu^2)(1-\mu'^2)]^{1/2}\cos(\varphi - \varphi')\,. \tag{5}$$

The spectral distribution function for scattered radiation is given, to the second approximation, by equation CS (26) as

$$\psi(\nu, \Theta, \nu') = \frac{mc}{4\pi}[4\pi mkT(1-\cos\Theta)]^{-1/2}\frac{1}{\nu'}\left[1-\frac{3}{2}\left(\frac{\nu'-\nu}{\nu}\right)\right] \times \exp\left\{\frac{-mc^2}{4kT(1-\cos\Theta)}\left[\frac{\nu'-\nu}{\nu} - \frac{h\nu'}{mc^2}(1-\cos\Theta)\right]^2\left[1+\frac{\nu'-\nu}{\nu}\right]^{-1}\right\}, \tag{6}$$

where k is Boltzmann's constant and h is Planck's constant. The system of successive approximations involved in determining $\psi(\nu, \Theta, \nu')$ is discussed in Section IV of the Compton Scattering paper. The second-approximation expression, equation (6), involves neglecting terms containing the fourth and higher powers in the exponential factor and the second and higher powers elsewhere of

$$\left[\frac{4kT}{mc^2}\right]^{1/2} \simeq \left[\frac{h\nu}{mc^2}\right]^{1/2} \simeq \frac{\nu' - \nu}{\nu}. \tag{7}$$

In further work it is convenient to express frequency in velocity units of approximately $\sqrt{2}$ Doppler half-widths by the transformations

$$\begin{aligned} a &= \left[\frac{mc^2}{4kT}\right]^{1/2} \left(\frac{\nu - \nu_0}{\nu_0}\right) \left[1 + \frac{\nu - \nu_0}{\nu_0}\right]^{1/2} \\ &= -\left[\frac{mc^2}{4kT}\right]^{1/2} \left(\frac{\lambda - \lambda_0}{\lambda_0}\right) \left[1 - \frac{1}{2}\left(\frac{\lambda - \lambda_0}{\lambda_0}\right)\right] \end{aligned} \tag{8}$$

and

$$a' = \left[\frac{mc^2}{4kT}\right]^{1/2} \left(\frac{\nu' - \nu_0}{\nu_0}\right) \left[1 + \frac{\nu' - \nu_0}{\nu_0}\right]^{1/2}, \tag{9}$$

where λ and λ_0 are the wave lengths corresponding to ν and ν_0 and ν_0 is a fixed frequency. In terms of these new variables, the following second-approximation expression for the emission coefficient can be obtained from equations (4) and (6):

$$\begin{aligned} j(a, \tau, \mu) &= N_e \sigma_e \int \frac{d\omega'}{4\pi} \frac{\frac{3}{4}(1 + \cos^2\Theta)}{[\pi(1 - \cos\Theta)]^{1/2}} \int_{-\infty}^{\infty} da' I(a', \tau, \mu') \\ &\times \left[1 - \frac{3}{2}\left(\frac{4kT}{mc^2}\right)^{1/2} (a' - a)\right] \exp\left\{-\frac{(a' - a)^2}{1 - \cos\Theta} + 2\left(\frac{mc^2}{4kT}\right)^{1/2} \frac{h\nu_0}{mc^2}(a' - a)\right\}. \end{aligned} \tag{10}$$

As stated in Section IV of the Compton Scattering paper, to the second approximation the electron-scattering coefficient can be replaced by σ_e, and so the equation of radiative transfer for the electron atmosphere is

$$\mu \frac{\partial I(a, \tau, \mu,)}{\partial \tau} = I(a, \tau, \mu) - \frac{j(a, \tau, \mu)}{N_e \sigma_e}. \tag{11}$$

Under the conditions of the Schuster problem, solutions of this equation are required to satisfy the boundary conditions

$$\left.\begin{aligned} I(a, \tau_1, \mu) &= \Im(a, \mu) \\ I(a, 0, -\mu) &\equiv 0 \end{aligned}\right\} (\mu \geq 0), \tag{12}$$

where τ_1 is the total optical thickness of the atmosphere, and $\Im(a, \mu)$ represents the radiation field incident on the inner surface of the atmosphere. Normal methods for solving equation (11) cannot be employed because of the mixing of frequencies represented by the integration over a' in the expression for $j(a, \tau, \mu)$ given by equation (10). The removal of this integration and the difficulty it presents is possible by applying a transformation to equation (11) first suggested by Münch.[1] Multiplication by $e^{i\xi a}/\sqrt{(2\pi)}$ and integration over a transform equation (11) to the following form:

$$\begin{aligned} \mu \frac{\partial \chi(\xi, \tau, \mu)}{\partial \tau} &= \chi(\xi, \tau, \mu) - \int \frac{d\omega'}{4\pi} \chi(\xi, \tau, \mu') \tfrac{3}{4}(1 + \cos^2\Theta) \\ &\times \left[1 + i\frac{3}{4}\left(\frac{4kT}{mc^2}\right)^{1/2} (1 - \cos\Theta)\xi\right] \exp\left\{-(1 - \cos\Theta)\left[\frac{\xi^2}{4} + i\left(\frac{4kT}{mc^2}\right)^{1/2} \frac{h\nu_0}{4kT}\xi\right]\right\}, \end{aligned} \tag{13}$$

where

$$\chi(\xi, \tau, \mu) = \frac{1}{\sqrt{(2\pi)}} \int_{-\infty}^{\infty} e^{i\xi a} I(a, \tau, \mu)\, da \tag{14}$$

is the Fourier transform of intensity.

Substitution of equation (5) in equation (13) and integration over the azimuthal angle $\varphi - \varphi'$ give

$$\mu \frac{\partial \chi(\xi, \tau, \mu)}{\partial \tau} = \chi(\xi, \tau, \mu) - \frac{3}{8} \int_{-1}^{+1} \chi(\xi, \tau, \mu') [p_r(\xi, \mu, \mu') + i p_i(\xi, \mu, \mu')]\, d\mu', \tag{15}$$

where the phase functions $p_r(\xi, \mu, \mu')$ and $p_i(\xi, \mu, \mu')$ are given by

$$\begin{aligned} p_r(\xi, \mu, \mu')\, e^{(1-\mu\mu')\xi^2/4} = {} & [p_1 U_0(z) - p_2 V_1(z) - p_3 U_2(z)] \cos \tfrac{3}{2}\beta(1-\mu\mu')\xi \\ & + [p_1 V_0(z) + p_2 U_1(z) - p_3 V_2(z)] \sin \tfrac{3}{2}\beta(1-\mu\mu')\xi \\ & + \tfrac{3}{2}\beta\gamma [p_4 V_0(z) + p_5 U_1(z) - p_6 V_2(z) - p_7 U_3(z)]\, \xi \cos \tfrac{3}{2}\beta(1-\mu\mu')\xi \\ & - \tfrac{3}{2}\beta\gamma [p_4 U_0(z) - p_5 V_1(z) - p_6 U_2(z) + p_7 V_3(z)]\, \xi \sin \tfrac{3}{2}\beta(1-\mu\mu')\xi, \end{aligned} \tag{16}$$

$$\begin{aligned} p_i(\xi, \mu, \mu')\, e^{(1-\mu\mu')\xi^2/4} = {} & [p_1 V_0(z) + p_2 U_1(z) - p_3 V_2(z)] \cos \tfrac{3}{2}\beta(1-\mu\mu')\xi \\ & - [p_1 U_0(z) - p_2 V_1(z) - p_3 U_2(z)] \sin \tfrac{3}{2}\beta(1-\mu\mu')\xi \\ & - \tfrac{3}{2}\beta\gamma [p_4 U_0(z) - p_5 V_1(z) - p_6 U_2(z) + p_7 V_3(z)]\, \xi \cos \tfrac{3}{2}\beta(1-\mu\mu')\xi \\ & - \tfrac{3}{2}\beta\gamma [p_4 V_0(z) + p_5 U_1(z) - p_6 V_2(z) - p_7 U_3(z)]\, \xi \sin \tfrac{3}{2}\beta(1-\mu\mu')\xi, \end{aligned} \tag{17}$$

$$p_1(\mu, \mu') = 1 + (\mu\mu')^2 + \tfrac{1}{2}(1-\mu^2)(1-\mu'^2), \tag{18}$$

$$p_2(\mu, \mu') = 2\mu\mu' [(1-\mu^2)(1-\mu'^2)]^{1/2}, \tag{19}$$

$$p_3(\mu, \mu') = \tfrac{1}{2}(1-\mu^2)(1-\mu'^2), \tag{20}$$

$$p_4(\mu, \mu') = \mu\mu'(1-\mu^2)(1-\mu'^2) - (1-\mu\mu')[1 + (\mu\mu')^2 + \tfrac{1}{2}(1-\mu^2)(1-\mu'^2)], \tag{21}$$

$$p_5(\mu, \mu') = [1 + 3(\mu\mu')^2 - 2\mu\mu' + \tfrac{3}{4}(1-\mu^2)(1-\mu'^2)] [(1-\mu^2)(1-\mu'^2)]^{1/2}, \tag{22}$$

$$p_6(\mu, \mu') = \tfrac{1}{2}(3\mu\mu' - 1)(1-\mu^2)(1-\mu'^2), \tag{23}$$

$$p_7(\mu, \mu') = \tfrac{1}{4}[(1-\mu^2)(1-\mu'^2)]^{3/2}. \tag{24}$$

Also, as indicated by equation CS (28),

$$\gamma = \frac{3kT}{h\nu_0} \tag{25}$$

is the ratio of the non-Doppler blue shift to the red Compton shift, while

$$\beta = \frac{1}{6}\left[\frac{4kT}{mc^2}\right]^{1/2} \frac{h\nu_0}{kT} \tag{26}$$

is a parameter that is important in classifying the mathematical properties of the solution to the transformed equation of transfer, as obtained in the next section. In equations (16) and (17) $U_n(z)$ and $V_n(z)$ are real and imaginary parts, respectively, of Bessel functions of the first kind with the complex argument,

$$z = [(1-\mu^2)(1-\mu'^2)]^{1/2}(\tfrac{3}{2}\beta\xi - \tfrac{1}{4}i\xi^2). \tag{27}$$

These Bessel functions appear in the phase functions because integration over azimuthal angle involves integrals of the type[8]

$$\frac{1}{2\pi}\int_0^{2\pi} e^{iz\cos\varphi}\cos n\varphi\, d\varphi = i^n[U_n(z) + iV_n(z)]. \tag{28}$$

For values of ν_0 and T of astrophysical interest,

$$5\times 10^{-5} < \beta < 10^{-2}, \qquad 500 > \gamma > 0.05. \tag{29}$$

Equation (15) can be separated into real and imaginary parts by letting

$$\chi(\xi,\tau,\mu) = \chi^{(r)}(\xi,\tau,\mu) + i\chi^{(i)}(\xi,\tau,\mu), \tag{30}$$

which gives, for the transformed equation of transfer,

$$\mu\frac{\partial\chi^{(r)}(\xi,\tau,\mu)}{\partial\tau} = \chi^{(r)}(\xi,\tau,\mu) - \frac{3}{8}\int_{-1}^{+1}[\chi^{(r)}(\xi,\tau,\mu')\,p_r(\xi,\mu,\mu') - \chi^{(i)}(\xi,\tau,\mu')\,p_i(\xi,\mu,\mu')]\,d\mu' \tag{31}$$

and

$$\mu\frac{\partial\chi^{(i)}(\xi,\tau,\mu)}{\partial\tau} = \chi^{(i)}(\xi,\tau,\mu) - \frac{3}{8}\int_{-1}^{+1}[\chi^{(i)}(\xi,\tau,\mu')\,p_r(\xi,\mu,\mu') + \chi^{(r)}(\xi,\tau,\mu')\,p_i(\xi,\mu,\mu')]\,d\mu'. \tag{32}$$

The boundary conditions (12), when transformed and separated in the same manner, become

$$\left.\begin{aligned}\chi^{(r)}(\xi,\tau_1,\mu) &= X^{(r)}(\xi,\mu), \qquad \chi^{(i)}(\xi,\tau,\mu) = X^{(i)}(\xi,\mu)\\ \chi^{(r)}(\xi,0,-\mu) &\equiv \chi^{(i)}(\xi,0,-\mu) \equiv 0\end{aligned}\right\} \qquad (\mu\geq 0), \tag{33}$$

where $X^{(r)}(\xi,\mu)$ and $X^{(i)}(\xi,\mu)$ are the real and imaginary parts of the Fourier transform of $\mathfrak{I}(a,\mu)$.

III. SOLUTION OF THE TRANSFORMED EQUATION OF TRANSFER IN THE FIRST APPROXIMATION

Equations (31) and (32) can now be solved by standard approximate methods of radiative-transfer theory,[7] in which they are replaced by a system of linear differential equations. The forms of $p_r(\xi,\mu,\mu')$ and $p_i(\xi,\mu,\mu')$ prevent a general method of obtaining a solution in the nth approximation and make the solution for approximations higher than the first quite laborious. Further, since the electron atmosphere under consideration is, at best, a first approximation of a high-temperature stellar atmosphere, such labor would be unwarranted. Therefore, these equations will be solved in the first approximation, and

[8] Cf. E. Jahnke and F. Emde, *Tables of Functions* (New York: Dover Publications, 1945), p. 149.

the corresponding system of differential equations is

$$\frac{1}{\sqrt{3}}\frac{\partial \chi_{+1}^{(r)}(\xi,\tau)}{\partial \tau}=\chi_{+1}^{(r)}(\xi,\tau)-M(\xi)\chi_{+1}^{(r)}(\xi,\tau)-N(\xi)\chi_{-1}^{(r)}(\xi,\tau)+L(\xi)\chi_{+1}^{(i)}(\xi,\tau)+K(\xi)\chi_{-1}^{(i)}(\xi,\tau), \tag{34}$$

$$-\frac{1}{\sqrt{3}}\frac{\partial \chi_{-1}^{(r)}(\xi,\tau)}{\partial \tau}=\chi_{-1}^{(r)}(\xi,\tau)-M(\xi)\chi_{-1}^{(r)}(\xi,\tau)-N(\xi)\chi_{+1}^{(r)}(\xi,\tau)+L(\xi)\chi_{-1}^{(i)}(\xi,\tau)+K(\xi)\chi_{+1}^{(i)}(\xi,\tau), \tag{35}$$

$$\frac{1}{\sqrt{3}}\frac{\partial \chi_{+1}^{(i)}(\xi,\tau)}{\partial \tau}=\chi_{+1}^{(i)}(\xi,\tau)-M(\xi)\chi_{+1}^{(i)}(\xi,\tau)-N(\xi)\chi_{-1}^{(i)}(\xi,\tau)-L(\xi)\chi_{+1}^{(r)}(\xi,\tau)-K(\xi)\chi_{-1}^{(r)}(\xi,\tau), \tag{36}$$

and

$$\frac{-1}{\sqrt{3}}\frac{\partial \chi_{-1}^{(i)}(\xi,\tau)}{\partial \tau}=\chi_{-1}^{(i)}(\xi,\tau)-M(\xi)\chi_{-1}^{(i)}(\xi,\tau)-N(\xi)\chi_{+1}^{(i)}(\xi,\tau)-L(\xi)\chi_{-1}^{(r)}(\xi,\tau)-K(\xi)\chi_{+1}^{(r)}(\xi,\tau), \tag{37}$$

where

$$\begin{aligned}2M(\xi)\,e^{\xi^3/6}=&\,[U_0(z)-\tfrac{1}{3}V_1(z)-\tfrac{1}{6}U_2(z)]\cos\beta\xi\\&+[V_0(z)+\tfrac{1}{3}U_1(z)-\tfrac{1}{6}V_2(z)]\sin\beta\xi\\&-\tfrac{1}{12}\beta\gamma[10V_0(z)-9U_1(z)+U_3(z)]\,\xi\cos\beta\xi\\&+\tfrac{1}{12}\beta\gamma[10U_0(z)+9V_1(z)-V_3(z)]\,\xi\sin\beta\xi,\end{aligned} \tag{38}$$

$$\begin{aligned}2N(\xi)\,e^{\xi^3/3}=&\,[U_0(z)+\tfrac{1}{3}V_1(z)-\tfrac{1}{6}U_2(z)]\cos 2\beta\xi\\&+[V_0(z)-\tfrac{1}{3}U_1(z)-\tfrac{1}{6}V_2(z)]\sin 2\beta\xi\\&-\tfrac{1}{12}\beta\gamma[26V_0(z)-21U_1(z)-6V_2(z)+U_3(z)]\,\xi\cos 2\beta\xi\\&+\tfrac{1}{12}\beta\gamma[26U_0(z)+21V_1(z)-6U_2(z)-V_3(z)]\,\xi\sin 2\beta\xi,\end{aligned} \tag{39}$$

$$\begin{aligned}2L(\xi)\,e^{\xi^3/6}=&\,[V_0(z)+\tfrac{1}{3}U_1(z)-\tfrac{1}{6}V_2(z)]\cos\beta\xi\\&-[U_0(z)-\tfrac{1}{3}V_1(z)-\tfrac{1}{6}U_2(z)]\sin\beta\xi\\&+\tfrac{1}{12}\beta\gamma[10U_0(z)+9V_1(z)-V_3(z)]\,\xi\cos\beta\xi\\&+\tfrac{1}{12}\beta\gamma[10V_0(z)-9U_1(z)+U_3(z)]\,\xi\sin\beta\xi,\end{aligned} \tag{40}$$

and

$$\begin{aligned}2K(\xi)\,e^{\xi^3/3}=&\,[V_0(z)-\tfrac{1}{3}U_1(z)-\tfrac{1}{6}V_2(z)]\cos 2\beta\xi\\&-[U_0(z)+\tfrac{1}{3}V_1(z)-\tfrac{1}{6}U_2(z)]\sin 2\beta\xi\\&+\tfrac{1}{12}\beta\gamma[26U_0(z)+21V_1(z)-6U_2(z)-V_3(z)]\,\xi\cos 2\beta\xi\\&+\tfrac{1}{12}\beta\gamma[26V_0(z)-21U_1(z)-6V_2(z)+U_3(z)]\,\xi\sin 2\beta\xi\end{aligned} \tag{41}$$

are the phase functions and

$$z = \beta\xi - \tfrac{1}{6} i\xi^2 . \tag{42}$$

Equations (34)–(37) constitute a fourth-order system of linear, homogeneous, differential equations, and, since ξ may be considered as a parameter, they have constant coefficients. Standard methods for solving such systems give a general solution identical to that given by equations MAI (46)–(49). In these equations the characteristic roots $k'(\xi)$ and $k''(\xi)$ are defined by the relations

$$\tfrac{1}{3}(k'^2 - k''^2) = (M-1)^2 - N^2 - L^2 + K^2 \tag{43}$$

and

$$\tfrac{1}{3} k'k'' = L(M-1) - NK , \tag{44}$$

while

$$(K^2+N^2) E_1(\xi) = K\left(L + \frac{k''}{\sqrt{3}}\right) + N\left(M - 1 + \frac{k'}{\sqrt{3}}\right), \tag{45}$$

$$(K^2+N^2) E_2(\xi) = N\left(L + \frac{k''}{\sqrt{3}}\right) - K\left(M - 1 + \frac{k'}{\sqrt{3}}\right), \tag{46}$$

$$(K^2+N^2) E_3(\xi) = K\left(L - \frac{k''}{\sqrt{3}}\right) + N\left(M - 1 - \frac{k'}{\sqrt{3}}\right), \tag{47}$$

and

$$(K^2+N^2) E_4(\xi) = N\left(L - \frac{k''}{\sqrt{3}}\right) - K\left(M - 1 - \frac{k'}{\sqrt{3}}\right). \tag{48}$$

Furthermore, equations (43)–(48) give

$$E_3^2 + E_4^2 = (E_1^2 + E_2^2)^{-1} = \frac{E_3}{E_1} = -\frac{E_4}{E_2} , \tag{49}$$

which is identical with equations MAI (52). Therefore, the determination from the boundary conditions of D_1, D_2, D_3, and D_4, the arbitrary functions of ξ appearing in the general solution, will be identical with that given in the Moving Atmosphere I paper, and equations MAI (53)–(63) apply. Finally, the solution for radiation emerging from the electron atmosphere at the outer surface $\tau = 0$ is given by equations MAI (64)–(68), with the exception that N^2 is replaced by $N^2 + K^2$ on the left-hand side of equations MAI (66)–(68).

The solution obtained has the required symmetry in ξ, to insure that its inverse Fourier transform will give a real function. Also, the validity of the application of the Fourier transform (14) can be established within the scheme of the first approximation by placing the integrable-square requirement on $X_{+1}^{(r)}(\xi)$ and $X_{+1}^{(s)}(\xi)$, since their coefficients remain bounded for all ξ.[9]

Application of the solution for emergent radiation requires knowledge of $\Gamma_1(\xi)$ and $\Gamma_2(\xi)$ as given by equations MAI (66) and (67) for $\xi = 0$, where they become indeterminate, and for large values of ξ, where they can be represented by asymptotic expansions. Their indeterminate form can be evaluated[9] with the following results:

$$\Gamma_1 \to (1 + \tfrac{1}{2}\tau_1\sqrt{3})^{-1} , \qquad \Gamma_2 \to 0 , \qquad \text{as} \qquad \xi \to 0 . \tag{50}$$

For large values of ξ, N^2, K^2, and NK become very small and may be neglected in comparison to $(M-1)^2$, L^2, or $L(M-1)$, since they differ by a factor of $e^{-\xi^2/3}$. There-

[9] The solutions given by equations MAI (53)–(68) become indeterminate for $\xi = 0$, but they can be evaluated by the standard technique of expanding them as a power series in ξ and passing to the limit $\xi = 0$.

fore, it follows from equations (43) and (44) that, for $|\xi|$ sufficiently large,

$$\frac{k'}{\sqrt{3}} \simeq -(M-1), \qquad \frac{k''}{\sqrt{3}} \simeq -L, \tag{51}$$

which, in combination with equations MAI (66)–(68), give

$$\begin{aligned} \Gamma_1 &\simeq e^{(M-1)\tau_1\sqrt{3}} \cos(L\tau_1\sqrt{3}), \\ \Gamma_2 &\simeq e^{(M-1)\tau_1\sqrt{3}} \sin(L\tau_1\sqrt{3}). \end{aligned} \tag{52}$$

The approximate representations (52) involve neglecting terms of the order of $e^{-\xi^3/3}$, thereby providing a reliable criterion for determining the value $\xi = a$, at which they can be used. The functions $M - 1$ and L can be expressed in terms of asymptotic expansions of the Bessel functions[10] which they contain. These expansions produce usable expressions only when $\xi > \beta$, and they yield the result

$$\Gamma_1 \to e^{-\tau_1\sqrt{3}}, \qquad \Gamma_2 \to 0, \qquad \text{as} \qquad \xi \to \pm\infty. \tag{53}$$

The difference between the approximate representations (52) and the limiting representations (53) can also be determined from these asymptotic expansions, where for astrophysical applications terms involving the second and higher powers of β can be neglected, as indicated by equation (29). These differences are

$$\Gamma_1 - e^{-\tau_1\sqrt{3}} = \tfrac{1}{2} g e^{-\tau_1\sqrt{3}} \{ 2\xi^{-1} + g\xi^{-2} + (\tfrac{1}{3}g^2 - \tfrac{5}{2})\xi^{-3} + (\tfrac{1}{12}g^2 - \tfrac{5}{2}) g\xi^{-4} + \ldots \} \tag{54}$$

and

$$\Gamma_2 = 3\beta(\quad -1)\, g e^{-\tau_1\sqrt{3}} \{ \xi^{-2} + g\xi^{-3} + \tfrac{1}{4}[2g^2 + 15(\gamma-1)^{-1}]\xi^{-4} + \ldots \}, \tag{55}$$

where

$$g(\tau_1) = \frac{9\tau_1}{4\sqrt{\pi}}. \tag{56}$$

The expressions for Γ_1 and Γ_2 can be simplified considerably for the moderate values of $\xi \leq a$ if terms of the order of magnitude of the second and higher powers of β are neglected. Examination of the power-series representation of the Bessel functions appearing in equations (38)–(42) shows that, when terms containing the second and higher powers of β are neglected,

$$\begin{aligned} V_0(z) &< 4a\beta U_0(z), & U_0(z) &= I_0\left(\frac{\xi^2}{6}\right); \\ U_1(z) &< 5a\beta V_1(z), & V_1(z) &= -I_1\left(\frac{\xi^2}{6}\right); \\ V_2(z) &< 6a\beta U_2(z), & U_2(z) &= -I_2\left(\frac{\xi^2}{6}\right); \\ U_3(z) &< 7a\beta V_3(z), & V_3(z) &= I_3\left(\frac{\xi^2}{6}\right). \end{aligned} \tag{57}$$

In equations (57), $I_n(\xi^2/6)$ is a Bessel function of the first kind, of order n and of imaginary argument. These equations, in turn, produce the following simplifications of equations (38)–(40), (43), (44), and MAI (66)–(68):

$$2M(\xi)\, e^{\xi^3/6} = I_0\left(\frac{\xi^2}{6}\right) + \tfrac{1}{3} I_1\left(\frac{\xi^2}{6}\right) + \tfrac{1}{6} I_2\left(\frac{\xi^2}{6}\right), \tag{58}$$

[10] G. N. Watson, *Treatise on the Theory of Bessel Functions* (New York: Macmillan Co., 1945), p. 202.

$$2N(\xi)\, e^{\xi^3/3} = I_0\left(\frac{\xi^2}{6}\right) - \tfrac{1}{3} I_1\left(\frac{\xi^2}{6}\right) + \tfrac{1}{6} I_2\left(\frac{\xi^2}{6}\right), \tag{59}$$

$$\begin{aligned} 2L(\xi)\, e^{\xi^3/6} &= V_0(z) + \tfrac{1}{3} U_1(z) - \tfrac{1}{6} V_2(z) \\ &+ \tfrac{1}{12}\beta\xi\left[(10\gamma - 12)\, I_0\left(\frac{\xi^2}{6}\right) - (9\gamma + 4)\, I_1\left(\frac{\xi^2}{6}\right) - 2 I_2\left(\frac{\xi^2}{6}\right) - \gamma I_3\left(\frac{\xi^2}{6}\right)\right], \end{aligned} \tag{60}$$

$$\frac{k'}{\sqrt{3}} = [(M-1)^2 - N^2]^{1/2}, \qquad \frac{k''}{\sqrt{3}} = 0, \tag{61}$$

$$\Gamma_1 = [\cosh k'\tau_1 - (\sqrt{3})(M-1)\, k'^{-1} \sinh k'\tau_1]^{-1}, \tag{62}$$

and

$$\Gamma_2 = (\sqrt{3})\, k' L \sinh k'\tau_1 [k' \cosh k'\tau_1 - (\sqrt{3})(M-1) \sinh k'\tau_1]^{-2}. \tag{63}$$

Equations (61)–(63) follow from the fact that L and K are of the order of β. Equations (62) and (54) show that Γ_1 is identical for $\xi \leq a$ and $\xi \geq a$, respectively, to Münch's solution[11] for the Schuster problem, in which the effects of Compton scattering have been neglected. This means that Γ_1, to the approximation in which second and higher powers of β have been neglected, represents only the effects of the Doppler shifts in scattering due to thermal motions of the electrons. Hence the effects of Compton scattering, the red Compton shift, and the non-Doppler blue shift are represented by Γ_2 as given by equations (63) and (55).

IV. THE INVERSE TRANSFORM OF THE SOLUTION FOR EMERGENT RADIATION

The inverse Fourier transform of the solution for emergent radiation given by equations MAI (64) and (65) is

$$I_{+1}(a, 0) = \frac{1}{\sqrt{(2\pi)}} \int_{-\infty}^{\infty} e^{-ia\xi} (\Gamma_1 + i\Gamma_2) [X_{+1}^{(r)} + i X_{+1}^{(i)}]\, d\xi. \tag{64}$$

Adding and subtracting in the integrand of equation (64) of the limiting representations for Γ_1 and Γ_2 as given by equations (53) allows a mathematical simplification of this inverse transform, the physical interpretation of which is the separation of scattered from unscattered radiation. This gives

$$\begin{aligned} I_{+1}(a, 0) &= \frac{e^{-\tau_1\sqrt{3}}}{\sqrt{(2\pi)}} \int_{-\infty}^{\infty} e^{-ia\xi} [X_{+1}^{(r)} + i X_{+1}^{(i)}]\, d\xi \\ &\quad + \frac{1}{\sqrt{(2\pi)}} \int_{-\infty}^{\infty} e^{-ia\xi} (\Gamma_1 - e^{-\tau_1\sqrt{3}} + i\Gamma_2) [X_{+1}^{(r)} + i X_{+1}^{(i)}]\, d\xi \\ &= \Im_{+1}(a)\, e^{-\tau_1\sqrt{3}} + \int_{-\infty}^{\infty} \Im_{+1}(\epsilon) [\Delta_{TB}(\tau_1;\, a - \epsilon) \\ &\quad + \Delta_{CS}(\tau_1, T, \nu_0;\, a - \epsilon)]\, d\epsilon, \end{aligned} \tag{65}$$

where

$$\Delta_{TB}(\tau_1;\, x) = \frac{1}{\pi} \int_0^{\infty} (\Gamma_1 - e^{-\tau_1\sqrt{3}}) \cos x\xi\, d\xi \tag{66}$$

and

$$\Delta_{CS}(\tau_1, T, \nu_0;\, x) = \frac{1}{\pi} \int_0^{\infty} \Gamma_2 \sin x\xi\, d\xi. \tag{67}$$

The final form of equation (65) follows from the use of the inverse Fourier transform for

[11] *Ap. J.*, **108**, 116, eqs. (43) and (48), 1948.

the incident intensity and Parseval's formula,[12]

$$\int_{-\infty}^{\infty} F_1(t)\, F_2(t)\, e^{-ixt} dt = \int_{-\infty}^{\infty} f_1(u)\, f_2(x-u)\, du\,, \tag{68}$$

where $F_1(t)$ and $F_2(t)$ are Fourier transforms of $f_1(x)$ and $f_2(x)$, respectively. The application of this formula to equation (65) is valid, provided that $\Delta_{TB}+\Delta_{CS}$ and $X_{+1}^{(r)}+iX_{+1}^{(i)}$ are integrable with respect to their arguments. The latter condition is satisfied, since $X_{+1}^{(r)}$ and $X_{+1}^{(i)}$ are assumed to be integrable square; the former condition is shown to be satisfied below. The fact that Γ_1 is an even function in ξ and Γ_2 is an odd function in ξ has also been used in obtaining equations (66) and (67).

The physical interpretation of equations (65)–(67) is straightforward. The first term on the right-hand side of equation (65) represents the contribution to the emergent radiation of the incident radiation which passes through the electron atmosphere without having suffered a single scattering process. The second term on the right-hand side of equation (65) represents the contribution from incident radiation which has suffered one or more scattering processes, the noncoherent nature of this scattering being indicated by the integration over ϵ. Hence, the function $\Delta_{TB}+\Delta_{CS}$ represents the spectral distribution of emergent radiation arising from incident monochromatic radiation at a frequency ϵ and of unit intensity. The function $\Delta_{TB}(\tau_1; x)$ expresses the noncoherency resulting from Doppler shifts due to thermal motions and, therefore, will depend parametrically on τ_1. This function has been evaluated by Münch,[13] who also shows that it is integrable with respect to its argument. The function $\Delta_{CS}(\tau_1, T, \nu_0; x)$ expresses the noncoherency resulting from the effects of Compton scattering, i.e., the red Compton shift, which accounts for the parametric dependence on ν_0, and the non-Doppler blue shift due to thermal motions, which accounts for the dependence on T. It is seen from equation (67) that Δ_{CS} is an odd function in x and hence is integrable with respect to this argument.

In equations (66) and (67) the integration over ξ represents the taking of the inverse Fourier transform of the solution for emergent radiation. For Δ_{CS} this integration presents difficulties because of the complicated dependence of Γ_2 on ξ. For $\xi \leq a$, numerical integration is necessary, the values of the integrand being given by equations (50) and (63). However, for $\xi \geq a$, analytic integration is possible with the use of equation (55), and such integration gives the result

$$\begin{aligned}\Delta_{CS}(\tau_1, T, \nu_0; x) = {} & \frac{\sqrt{3}}{\pi}\int_0^a \frac{k'L \sinh k'\tau_1 \sin x\xi\, d\xi}{[k' \cosh k'\tau_1 - (\sqrt{3})(M-1)\sinh k'\tau_1]^2} \\ & + \frac{3}{\pi}\beta(\gamma-1)\, g\, e^{-\tau_1\sqrt{3}}\left\{ x\left[\frac{\sin ax}{ax} - Ci(ax)\right]\right. \\ & + \frac{x^2}{2}\, g\left[\frac{\sin ax}{(ax)^2} + \frac{\cos ax}{ax} - \frac{\pi}{2} + Si(ax)\right] \\ & \left. + \frac{x^3}{24}\left[2g^2 + \frac{15}{\gamma-1}\right]\left[\frac{2\sin ax}{(ax)^3} + \frac{\cos ax}{(ax)^2} - \frac{\sin ax}{ax} + Ci(ax)\right] + \ldots\right\},\end{aligned} \tag{69}$$

where

$$Si(ax) = \int_0^{ax} \frac{\sin t}{t}\, dt\,, \qquad Ci(ax) = -\int_{ax}^{\infty} \frac{\cos t}{t}\, dt \tag{70}$$

are the sine and cosine exponential integrals.

The function $\Delta_{CS}(\tau_1, T, \nu_0; x)$ has been computed for $\tau_1 = 0.8$, $T = 80{,}000°$ K, and

[12] Cf. E. C. Titchmarsh, *Introduction to the Theory of Fourier Integrals* (Oxford: Clarendon Press, 1937), eq. (2.1.8), p. 51.

[13] *Ap. J.*, **108**, 116, eqs. (56), (62), and (66) and Table 1, 1948.

$\lambda_0 = 4400$ A, for which $\beta = 5 \times 10^{-4}$ and $\gamma = 7.347$; the results are given in Table 1. Comparison with $\Delta_{TB}(\tau_1; x)$ as tabulated by Münch[13] shows that $\Delta_{CS}(\tau_1, T, \nu_0; x)$ is more than one hundred times smaller for these values of the parameters. It decreases rather slowly to zero for $x > 1$. A problem of physical rather than astrophysical interest is the multiple Compton scattering of low-energy gamma radiation, which has been discussed by O'Rourke[4] and which involves values of β of the order of 100. The problems of evaluating $\Delta_{TB} + \Delta_{CS}$ for $\beta > 1$ are discussed in the appendix of the second paper[14] of the series.

TABLE 1

THE FUNCTION $\Delta_{CS}(\tau_1, T, \nu_0; x)$ FOR $\tau_1 = 0.8$, $T = 80{,}000°$ K, AND $\lambda_0 = 4400$ A

	x								
	0	0.25	0.50	0.75	1.00	1.50	2.00	3.00	4.00
$\Delta_{CS}(\tau_1, T, \nu_0; x) \times 10^{4*}$	0	1.51	1.87	1.85	1.67	0.958	0.488	0.11	0.02

* $\Delta_{CS}(\tau_1, T, \nu_0; x) = -\Delta_{CS}(\tau_1, T, \nu_0; -x)$.

V. CHANGES PRODUCED IN PROFILES OF SPECTRAL LINES

An important application of the solution for emergent radiation as given by equations (65) and (69) occurs when the incident intensity is the residual intensity of a spectral line

$$\mathfrak{r}_{+1}(a) = \frac{\mathfrak{I}_{+1}(a)}{\mathfrak{I}^c_{+1}}, \tag{71}$$

where $\mathfrak{I}^c_{+1}$ is the intensity of the incident continuum. As discussed in Section VII of the Moving Atmosphere I paper, the assumption of constancy of $\mathfrak{I}^c_{+1}$ over the limited frequency range of the spectral line transforms equation (65) to the following expression for the emergent residual intensity $r_{+1}1(a)$:

$$(1 + \tfrac{1}{2}\tau_1\sqrt{3})^{-1} r_{+1}(a) = \mathfrak{r}_{+1}(a)\, e^{-\tau_1\sqrt{3}} + \int_{-\infty}^{\infty} \mathfrak{r}_{+1}(\epsilon)\, \Delta_{TB}(\tau_1; a - \epsilon)\, d\epsilon + \int_{-\infty}^{\infty} \mathfrak{r}_{+1}(\epsilon)\, \Delta_{CS}(\tau_1, T, \nu_0; a - \epsilon)\, d\epsilon. \tag{72}$$

The first term on the right-hand side of equation (72) represents the contribution of unscattered radiation to the profile of the emergent radiation; the second term represents the contribution of the thermal-broadening effect of electron scattering; the third term represents the asymmetric contribution of the effects of Compton scattering—the red Compton shift and the non-Doppler blue shift. Integration of equation (72) over a shows that the equivalent width of the spectral line is unchanged by Compton scattering.

The effects of Compton scattering on a profile which may be considered typical of certain lines in high-temperature stellar atmospheres have been computed for an atmosphere characterized by the parameters $\tau_1 = 0.8$, $T = 80{,}000°$ K, and $\lambda_0 = 4400$ A. For these values equation (8) becomes

$$a = \frac{\lambda_0 - \lambda}{32.4}, \tag{73}$$

neglecting the nonlinear term. The line profile is given by

$$\mathfrak{r}_{+1}(a) = 1 - (4 + 256a^2)^{-1}, \tag{74}$$

[14] To be published in the *Astrophysical Journal*.

corresponding to a half-width of 3.5 A and an equivalent width of 2.75 A, and is tabulated in Table 2. In an analysis of the spectrum of the Wolf-Rayet star V444 Cygni, Münch[15] computed for this profile the thermal broadening produced by electron scattering, i.e., the profile resulting from the first two terms on the right-hand side of equation (72). The results of these calculations are given in Table 2 as a symmetric correction to the original profile. Using $\Delta_{CS}(\tau_1, T, \nu_0; x)$ tabulated in Table 1, the asymmetry produced by Compton scattering (the third term on the right-hand side of equation [72]) has been determined and is given in Table 2 as an additional asymmetric correction to the original profile. This asymmetry is to the blue, i.e., a negative correction for positive α, or the blue side of the profile, and a positive correction for negative α, or the red side of the profile.

TABLE 2

THERMAL-BROADENING AND COMPTON-SCATTERING CORRECTIONS TO $r_{+1}(\alpha)$ FOR $\tau_1 = 0.8$, $T = 80{,}000°$ K, AND $\lambda_0 = 4400$ A

α	$\lambda - \lambda_0$ (A)	$r_{+1}(\alpha)$ from Eq. (74)	Correction for Thermal Broadening	Additional Correction for Compton Scattering
0	0	0.750	+0.094	0
±0.25	∓ 8.10	.950	− .013	∓0.000019
±0.50	∓16.2	.985	− .017	∓ .000027
±0.75	∓24.3	.993	− .012	∓ .000046
±1.00	∓32.4	.996	− .008	∓ .000025
±1.25	∓40.5	0.998	−0.006	∓0.000021

The asymmetry to the blue produced by Compton scattering results from the fact that the non-Doppler blue shift is $\gamma = 7.35$ times the Compton red shift for values of the parameters T and λ_0 used in the calculation, as shown in Figure 2 of the Compton Scattering paper. Determination of the shift of the center of the line profile would require extensive calculations of the corrections for thermal broadening and Compton scattering for very small values of α. A crude calculation based on the corrections given in Table 2 indicates that the center is shifted to the blue about one Compton wave length (0.024 A). This shift is nearly equal to that associated with the asymmetry of the spectral distribution function for scattered radiation $\psi(\nu, \Theta, \nu')$ given by equation (6). The latter shift is determined from equation CS (28), using equation (5) and averaging over the azimuthal angle φ. It appears, therefore, that such shifts determined from equation CS (28) will give a rough indication of the expected shifts of the centers of spectral lines for moderate values of τ_1.

The detection of the changes in a line profile produced by Compton scattering would be a very difficult matter. The small shift of the center of the line would be effectively masked by the thermal broadening of the center. Even greater difficulties would be encountered in detecting the asymmetry, as the Compton-scattering corrections are of the order of 10^{-3} of the thermal-broadening corrections. Furthermore, they seem to reach a maximum out in the wings of the profile, where problems of detection are more serious. This results from the fact that $\Delta_{CS}(\tau_1, T, \nu_0; x)$ is an odd function in x and does not go to zero rapidly for $x > 1$.

I wish to thank the University Research Institute of the University of Texas for support of the computations, Mrs. LaNelle Janca Kahlbau for performing the computations, and Dr. Guido Münch, who kindly furnished his tabulations of $I_n(\xi^2/6)$, $k'(\xi)$, and $\Gamma_1(\xi)$ used in the computations.

[15] *Ap. J.*, **112**, 266, eqs. (6) and (9) and Fig. 12, 1950. These calculations account for blending of the wings of adjacent lines and for a continuum emitted by the electron atmosphere, effects which do not appear in the thermal-broadening corrections given in Table 2.

OPACITY OF A HIGHLY COMPRESSED HYDROGEN GAS*

H. T. HSIEH TSAO
Massachusetts Institute of Technology, Cambridge, Massachusetts
Received March 27, 1953; revised, September 11, 1953

ABSTRACT

The opacity of a highly compressed hydrogen gas is calculated by considering both the free-free and the bound-free transitions. The electrons are assumed to move in an average potential field of spherical symmetry. For a very dense case such that all the hydrogen atoms lose their electrons by pressure ionization, the problem is solved by assuming that the medium consists of ions imbedded in a highly degenerate Fermi-Dirac electron gas. The wave functions are determined by a simplified self-consistent field calculation. For density such that only one bound level exists, the broadening of the level due to the presence of the neighboring atoms is obtained by a method similar to that used in the theory of solids. The wave functions obtained from the self-consistent field calculation are then used for determining the opacity.

I. INTRODUCTION

A calculation of the opacity of stellar matter has been made by Eddington,[1] using Kramers'[2] absorption coefficients obtained from a semiclassical approach to the problem. The results have been further improved by Strömgren[3] and many others on the basis of the quantum-mechanical treatment of the absorption of radiation. However, the results so far obtained are based on wave functions of the hydrogen type belonging to single atoms. This simple picture is no longer valid when the interatomic distances become so close that the presence of the neighboring atoms cannot be overlooked.

The quantum theory of metals shows that, as the atoms are brought closer, the originally discrete energy levels of the individual atoms are broadened into energy bands. The band widths are greater for the higher levels. As the density becomes very high, the bands are broadened to such an extent that they overlap and eventually merge into a continuum, with the electrons becoming essentially free. The density may be so high that even the lowest level may be broadened into the continuum and the gas medium consists only of the free electrons and the bare nuclei. In other words, the gas is pressure-ionized. It is the purpose of the present study to calculate the opacity of hydrogen gas for the case in which it is pressure-ionized, as well as for the situation in which electrons remain bound with lowered ionization potential. The wave functions will be determined by the method of the self-consistent field.

II. WAVE FUNCTIONS OF ELECTRONS IN A HIGHLY COMPRESSED HYDROGEN GAS

The problem to be considered is a many-body problem: the electrons moving in the field of the closest nucleus, the neighboring nuclei, and the other electrons. As the gas atoms are distributed at random, the problem can be treated by assuming that the electrons move in a potential field of spherical symmetry. The Schrödinger equation can then be solved by using an average potential field. The calculation is to be made so that the assumed potential and the charge density fulfil the condition of self-consistency. The method of self-consistent field, originated by Hartree[4] and extended later by Fock[5] and

* Part of a thesis submitted in partial fulfilment of the requirements for the degree of Doctor of Philosophy in Physics in Massachusetts Institute of Technology. This work was supported by the Office of Naval Research.

[1] *The Internal Constitution of the Stars* (Cambridge: At the University Press, 1926).
[2] *Phil. Mag.* **46**, 836, 1923.
[3] *Zs. f. Ap.*, **4**, 118, 1932.
[4] *Proc. Cambridge Phil. Soc.*, **24**, 89, 1928.
[5] *Zs. f. Phys.* **61**, 126, 1930.

Slater,[6] has been widely applied in finding wave functions of electrons in complex atoms. The method to be described here is simpler than that frequently employed for atoms. The discussion will be carried out separately for the pressure-ionized gas and for the high-density hydrogen gas.

A. WAVE FUNCTION FOR A PRESSURE-IONIZED GAS

Since the electrons which are squeezed out of the bound levels remain in the gas, the medium is electrically neutral. The free-electron gas can be considered as strongly degenerate, with all the energy states completely filled up to the top of the Fermi energy band. The Fermi energy at absolute zero is a function only of density, and therefore the condition of strong degeneracy is best satisfied for a gas of high density. To describe the medium which consists of bare nuclei imbedded in a degenerate gas, each electron is first assumed to move in an average potential of this type:

$$V = -\left(\frac{e}{r} - \frac{e}{a}\right) \qquad (r \leqq a) \,, \qquad V = 0 \qquad (r \geqq a) \,. \tag{1}$$

The assumed potential is cut off at a radius a. Physically, such a field is due to the presence of a nucleus and a spherical shell of electrons with radius a carrying the same amount of charge as that of the nucleus. This kind of potential has been used by Guth and Sexl[7] to study the emission of alpha particles by radioactive nuclei and by Allis and Morse[8] in determining the scattering cross-section of electrons in monatomic gases.

The Schrödinger equation is then solved exactly, using the assumed potential. It can be shown that bound levels can exist only when the cutoff radius a is greater than a certain value, which for hydrogen is $1.75a_0$, where a_0 is the Bohr orbit radius. For the pressure-ionized gas, calculations are made for cutoff radii less than this limiting value. The wave functions are normalized, so that the radial wave function has the asymptotic form

$$R(r) \underset{r\to 0}{\rightarrow} \frac{\sin(kr - \frac{1}{2}l\pi + \eta_l)}{kr} \,, \tag{2}$$

where η_l is the phase shift for the lth partial wave.

The density of electrons with energy ϵ at any position is given by $|\psi_\epsilon(\gamma, \theta, \varphi)|^2$, where $\psi_\epsilon(\gamma, \theta, \varphi)$ is the solution of the Schrödinger equation. To obtain the total electron density, the value of $|\psi_\epsilon(\gamma, \theta, \varphi)|^2$ is to be summed over all the possible states in the Fermi band. Owing to the spherical symmetry, the electron density at the radius r is

$$n(r) = \sum_l \frac{(2l+1)}{2\pi^2} \int_0^{\epsilon_{F_0}} |R_{\epsilon,l}(r)|^2 \epsilon^{1/2} d\epsilon \,, \tag{3}$$

where ϵ_{F_0} is the Fermi energy for electrons at the absolute zero of temperature.

When the charge density is known, the exact potential in which the electron is moving can be determined. The wave function that describes the entire medium is an antisymmetric combination of all the one-electron wave functions. It has been shown by many authors[9] that the Hartree-Fock equation can be obtained by varying the one-electron

[6] *Phys. Rev.*, **81**, 385, 1951.

[7] *Zs. f. Phys.*, **66**, 577, 1930.

[8] *Zs. f. Phys.*, **70**, 567, 1931. The exact solutions are confluent hypergeometric functions for $r < a$ and Bessel functions for $r > a$.

[9] See, among others, F. Seitz, *Modern Theory of Solids* (2d ed.; New York: McGraw-Hill Book Co., 1940).

wave function so as to make the energy an extreme. The equation is of the following type:

$$Hu_i(x_1) + \left[\sum_{k=1}^{N} \int u_k^*(x_2)\, u_k(x_2) \frac{2}{r_{12}}\, dx_2\right] u_i(x_1) - \sum_{k=1}^{N} \left[\int u_k^*(x_2)\, u_i(x_2) \frac{2}{r_{12}}\, dx_2\right] u_k(x_1) = \epsilon_i u_i(x_1)\ , \tag{4}$$

where $u_i(x_i)$ is the one-electron wave function of both co-ordinates x_i and spin for the kth electron and the integration dx_2 also includes the summation of the spin and the summation is over all electrons. It follows from equation (4) that the electron moves in the field of all nuclei and $N-1$ electrons, the removed electron being localized at the position x_i of the ith electron. Although equation (4) gives a good description of the field in which the electron is moving, it is of little practical applicability, since the exchange integral is usually difficult to evaluate. It can be evaluated for electrons that are completely free and the result is given by [6, 10]

$$eV(r)_{\text{exchange}} = -6\left[\frac{3n(r)}{8\pi}\right]^{1/3}. \tag{5}$$

Equation (5) can be used in the present case, since the electrons considered do not differ too much from completely free electrons.

If the average density of the medium is expressed as $n_0 = 3/4\pi\beta^3$, then the parameter β determines the Fermi energy, ϵ_{F_0}. Equation (3) shows that the total charge density at a given radius depends on the value of ϵ_{F_0} and therefore on the choice of β.

As the ions are imbedded in a highly degenerate electron gas, one can simplify the problem by considering a box with the ion at the center surrounded by enough electrons to make the whole medium electrically neutral. The self-consistent calculation need be carried out only about one ion. The calculated potential energy of an electron at the radius r can be written as follows:

Potential energy =

$$-\frac{2}{r} + \frac{2}{r}\int_0^r 4\pi r'^2 n(r')\, dr' - 2\int_0^{\delta} 4\pi r' n(r')\, dr' - 6\left[\frac{3n(r)}{8\pi}\right]^{1/3}, \tag{6}$$

where the parameter δ is determined by the following condition:

$$\int_0^{\delta} 4\pi r^2 n(r)\, dr = 1\ . \tag{7}$$

The self-consistent calculation is made by adjusting the parameter β so that the following criteria are satisfied:

$$(i) \quad V_{\text{calculated}}(r = \delta) = 0\ ,$$

$$(ii) \quad V_{\text{assumed}}(r = 0) = V_{\text{calculated}} \quad (r = 0)\ .$$

It is found that these two conditions can be best satisfied if an extra constant, $\bar{V}'$, which may be considered as representing an average potential in the medium, is added to equation (6). The parameters a, β, and δ bear the following relation in the order of magnitude, $a < \delta < \beta$. From the definition of δ given by equation (7), it is known that the distance between each electron and the nucleus ranges from 0 to δ; since a is the radius of a spherical shell of unit charge, which represents the average effect of all the electrons, a must be smaller than δ. The discrepancy between δ and β is, however, difficult to explain;

[10] Atomic units are used in calculating the potential energy.

as it is impossible to divide the entire space into equal-volume spheres, β may represent an effective radius of a volume which includes a sphere of radius δ and the space between the spheres. The charge density and the values of β, δ, and $\tilde{V}'$ as functions of the cutoff radius a are shown in Figures 1 and 2.

B. WAVE FUNCTIONS FOR A HIGHLY COMPRESSED ATOMIC HYDROGEN GAS

Calculations have also been made for densities such that only the K state exists. The electrons, instead of forming a free, degenerate Fermi gas, are loosely bound by the respective nuclei. If the interatomic distances are not too much greater than the magnitude of the electron orbits of an individual atom, the loosely bound electron, instead of re-

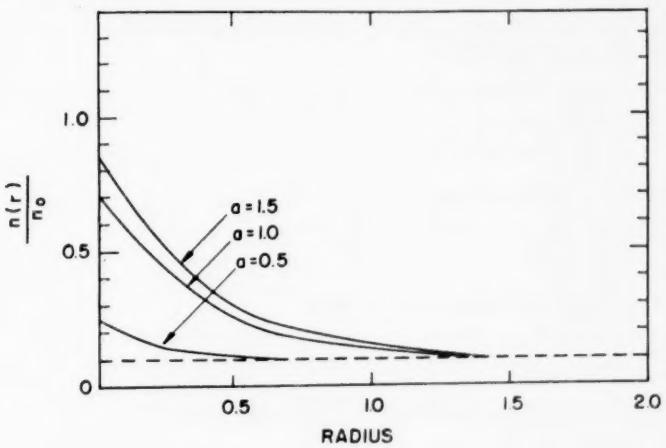

FIG. 1.—Charge distribution for various cutoff radii a; $n_0(r) = \frac{3}{4}\pi\beta^3$

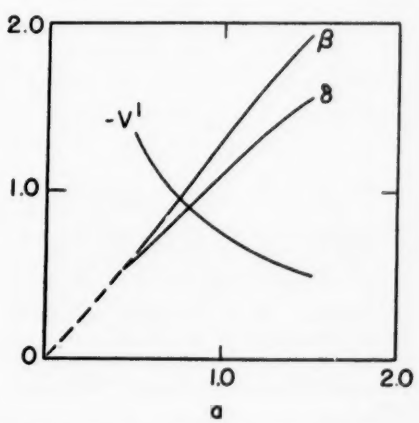

FIG. 2.—Values of $\tilde{V}'$, β, and δ as functions of cutoff radii

maining around one atom, can be considered as traveling from one atom to the other. This suggests the possibility of using wave functions of the Bloch type as a single electron-wave function. The modulated electron wave may have various possible energies, and the discrete energy levels are spread into bands. Bloch[11] has shown that the wave function of an electron in a periodic potential can be written as

$$\psi(\mathbf{r}) = \frac{1}{(N)^{1/2}} \sum_j \phi(|\mathbf{r}-\mathbf{r}_j|)\, e^{i\mathbf{k}\cdot\mathbf{r}_j}, \tag{8}$$

where $\phi(|\mathbf{r}-\mathbf{r}_j|)$ is the wave function of an electron surrounding the jth nucleus, $\mathbf{r}_j$ is the radius vector of the jth nucleus, and N is the normalizing factor. For cases in which overlapping of wave functions is negligible, N is just equal to the number of electrons in the medium. The wave function $\phi(|\mathbf{r}-\mathbf{r}_j|)$ is determined by solving the Schrödinger equation with the potential given by

$$U(|\mathbf{r}-\mathbf{r}_j|) = \left(\frac{e}{|\mathbf{r}-\mathbf{r}_j|} - \frac{e}{a}\right) \qquad (|\mathbf{r}-\mathbf{r}_j| \leqq a), \tag{9}$$

$$U(|\mathbf{r}-\mathbf{r}_j|) = 0 \qquad (|\mathbf{r}-\mathbf{r}_j| \geqq a).$$

The potential of the entire medium is

$$V(\mathbf{r}) = \sum_j U(|\mathbf{r}-\mathbf{r}_j|). \tag{10}$$

The Bloch wave function ψ satisfies the equation

$$\nabla^2\psi + (E - 2V)\psi = 0. \tag{11}$$

It follows that the energy is

$$E = \frac{\int \psi^* [-\nabla^2 + 2V]\psi d\tau}{\int |\psi|^2 d\tau}. \tag{12}$$

Equation (12) can be evaluated with the known values of $\phi(|\mathbf{r}-\mathbf{r}_j|)$ and the potential V. It can be shown that equation (12) has the form

$$E = E_0 + \frac{A+C}{1+D}, \tag{13}$$

where A, C, and D are given by

$$A = \sum_{\boldsymbol{\rho}_i} e^{-i\mathbf{k}\cdot\boldsymbol{\rho}_i} \int \phi(|\mathbf{r}-\boldsymbol{\rho}_i|)\, [V(\mathbf{r}) - U(\mathbf{r})]\, \phi(\mathbf{r})\, d\tau, \tag{14a}$$

$$C = \int \phi^*(|\mathbf{r}-\mathbf{r}_j|)\, [V(\mathbf{r}) - U(|\mathbf{r}-\mathbf{r}_j|)]\, \phi(|\mathbf{r}-\mathbf{r}_j|)\, d\tau, \tag{14b}$$

$$D = \sum_{\boldsymbol{\rho}_i \neq 0} e^{-i\mathbf{k}\cdot\boldsymbol{\rho}_i} \int \phi^*(|\mathbf{r}-\boldsymbol{\rho}_i|)\, \phi(\mathbf{r})\, d\tau, \tag{14c}$$

where ρ_i is the interatomic distance. When ρ_i is great, so that the overlapping between the wave functions of the neighboring atoms is negligible, the energy differs only slightly from that of the discrete level. It is found that the lowest energy in the band is lower than that of a discrete level, because of the increase of the Coulombian energy of the electron when the atoms are nearer.

The determination of the energy band involves the integrals (14a) to (14c), which con-

[11] *Zs. f. Phys.*, **52**, 555, 1928.

tain wave functions belonging to various centers. The integrals are evaluated by the method given by Coulson.[12] The present problem differs from that of a metal, in that the gas atoms do not form a periodic array. The relative directions of the propagation vector $\boldsymbol{k}$ and the radius vector $\boldsymbol{r}_{ij}$ are random. Consequently, the energy band is determined by averaging out all the possible relative positions in direction of the atoms. The energy as a function of the propagation vector $\boldsymbol{k}$ is shown in Figure 3 for various cutoff radii.

The wave functions of all the electrons is an antisymmetric combination of all the

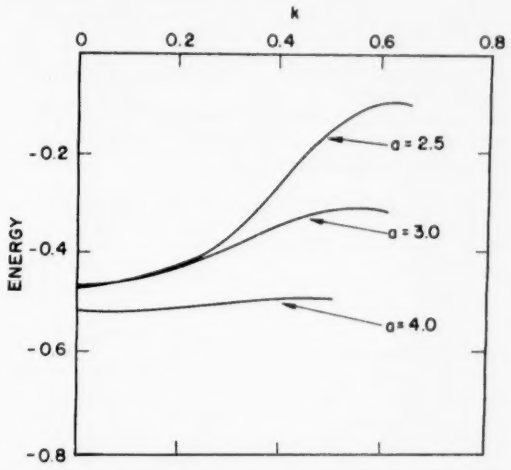

FIG. 3.—Energy bands as functions of $\boldsymbol{k}$ for various cutoff radii

single electron-wave functions of the Bloch type. The wave function of an electron with co-ordinate $\boldsymbol{r}_m$ having a propagation vector $\boldsymbol{k}_n$ can be written as

$$\psi_n(\boldsymbol{r}_m) = \frac{1}{(N)^{1/2}} \sum_j e^{i\boldsymbol{k}_n \cdot \boldsymbol{r}_j} \phi(|\boldsymbol{r}_m - \boldsymbol{r}_j|)\, \chi(\sigma_1)\,, \tag{15}$$

where $\chi(\sigma_1)$ is the spin function. The charge density at $\boldsymbol{r}_1$ due to all the electrons is given by

$$n(\boldsymbol{r}_1) = \sum_{k_n} |\chi_n(\boldsymbol{r}_1)|^2, \tag{16}$$

where the summation is over electrons of all energies.

The integral for the exchange potential is not simple, but it has been worked out when the band is narrow.[13] Self-consistent calculations are made for cutoff radii of $3a_0$ and $4a_0$. Satisfactory agreement between the assumed and the calculated potential can be achieved by adjusting the potential thus:

$$U(|\boldsymbol{r} - \boldsymbol{r}_j|) = \left(\frac{e}{\boldsymbol{r} - \boldsymbol{r}_j} - \frac{e}{a}\right) \qquad (|\boldsymbol{r} - \boldsymbol{r}_j| \leqq \tfrac{2}{3}a)\,,$$

$$U(|\boldsymbol{r} - \boldsymbol{r}_j|) = -\frac{e}{2a} \qquad (|\boldsymbol{r} - \boldsymbol{r}_j| \geqq \tfrac{2}{3}a)\,, \tag{17}$$

[12] *Proc. Cambridge Phil. Soc.*, **33**, 104, 1937. [13] Seitz, *op. cit.*, p. 336.

where $-e/2a$ represents an average potential determined by

$$-\bar{V}=\frac{3}{4\pi a^3}\int_0^a-\left(\frac{e}{r}-\frac{e}{a}\right)4\pi r^2 dr\,. \tag{18}$$

III. CALCULATION OF THE OPACITY

It is known that the opacity of a gas is due to the absorption of radiation by free electrons in the presence of the atomic field and absorption by the process of photoionization of the bound electrons, as well as that caused by scattering. In the temperature region to be covered by the present study, the opacity due to scattering will not be considered. An absorption coefficient[14] per electron a_ω for a given frequency ω is defined so that radiation of frequency ω is reduced by a factor e^{-Na_ω} in passing through 1 cm of gas containing N electrons per cubic centimeter.

For the pressure-ionized gas, the free-free transition is the only mechanism in the process of absorption. The absorption coefficient is evaluated for an electron of a given energy ϵ_i and is given from the quantum theory by

$$a_\omega(\epsilon_i)=\frac{256\pi^2}{3}\left(\frac{e^2}{\hbar c}\right)(a_0)^5\frac{(\epsilon_f)^{1/2}}{\omega^3}\sum_{l=1}^{\infty}l\left\{\left|\left(l-1,\epsilon_i\left|\frac{1}{r^2}\right|l,\epsilon_f\right)\right|^2+\left|\left(l,\epsilon_i\left|\frac{1}{r^2}\right|l-1,\epsilon_f\right)\right|^2\right\}, \tag{19}$$

where the matrix element corresponding to the acceleration has been selected in preference to that of the dipole moment on account of the better convergence. The quantities ϵ_i and ϵ_f are the energies of the initial and final states; a_0 is the Bohr radius; ω is the frequency of the absorbed radiation; and l is the orbital angular-momentum quantum number of the final state. The matrix element is evaluated by using the wave function determined by the self-consistent calculation. The absorption coefficient is usually expressed in terms of Kramers' formula multiplied by the Gaunt factor $g(\omega, \epsilon_i)$:

$$a_\omega=\frac{4}{(3)^{3/2}}\left(\frac{\hbar c}{e^2}\right)^4\left(\frac{h}{mc}\right)^5\frac{1}{\epsilon_i^{1/2}\omega^3}\,g(\omega,\epsilon_i)\,. \tag{20}$$

To obtain the absorption coefficient as a function of frequency, one has to sum over all the electrons in the initial states; moreover, the transition can take place only when the upper state is vacant. In the pressure-ionized case the electron gas is considered to be strongly degenerate, and, as all the states in the Fermi band are occupied, the only transitions that can take place are between states in the band and ones above it. Taking into account the energy distribution of electrons in the Fermi band and the probability that the states above it are vacant, the absorption coefficient per gram of gas k is

$$k_\omega=\frac{4.87\times10^6}{\omega^3}\int_{\epsilon_F-\omega}^{\epsilon_F}(g\omega,\epsilon_i)\,d\epsilon_i\ \text{cm}^2/\text{gm}\,. \tag{21}$$

The opacity is then calculated by evaluating the Rosseland mean, obtained by[15] averaging $(1/k_\omega)$ over the distribution of the intensity of radiation given by Planck's law; thus,

$$\frac{1}{K}=\frac{15}{4\pi^4}\int_0^\infty\frac{1}{k_\omega}u^4e^2u\,(e^u-1)^3du\,;\qquad u=\frac{\omega}{T_a}\,. \tag{22}$$

[14] The absorption coefficient is expressed in units of square centimeters; ω is given in terms of the atomic unit 3.29×10^{15} sec^{-1}.

[15] T_a is measured by the atomic unit $e^2/2a_0k = 157{,}000°$ C, where k is the Boltzmann constant.

For the high-density atomic hydrogen gas, both the bound-free and the free-free absorptions give contribution. In the present problem, only the absorption due to the K electron has to be considered. The absorption coefficient can be written as

$$a_\omega = \frac{4\pi e^2}{3\hbar c}(a_0)^2 \omega \epsilon_f^{1/2} |(l=0, \epsilon_i | r | l=1, \epsilon_f)|^2 \text{ cm}^2 . \tag{23}$$

In terms of Kramers' formula, equation (23) becomes

$$k_\omega = \frac{16 e^2}{M_H^{3/2} m c R y (\omega)^3} g(\omega) \text{ cm}^2/\text{gm} , \tag{24}$$

where Ry is the Rydberg constant and M_H is the mass of the hydrogen atom. The number of electrons having a negative energy $-I$ is

$$\frac{2}{1-(1/A)\, e^{-I/T_a}} , \tag{25}$$

where A is related to the number of free electrons N through the relation

$$N = \frac{T_a^{3/2}}{2\pi^2} \int_0^\infty \frac{x^{1/2} dx}{1+(1/A)\, e^x} \left(\frac{1}{a_0^3}\right) \qquad \left(x = \frac{\omega}{T_a}\right). \tag{26}$$

The probability that the upper state is vacant is

$$\frac{(1/A)\, e^{-(I+\omega)/T_a}}{(1/A)\, e^{-(I+\omega)/T_a} + 1} . \tag{27}$$

The absorption coefficient for the bound-free transition is then obtained by multiplying equation (24) by quantities (25) and (27).

To calculate the opacity, the total absorption coefficient due to both the bound-free and the free-free transition must be considered. In the temperature region when $e^{-\epsilon_F/T_a} \ll 1$, the electron gas is nondegenerate, and the absorption is given by

$$\begin{aligned} k_\omega &= \frac{9.48 \times 10^6 n}{u^3 (T_a)^{3.5}} g'(\omega) \text{ cm}^2/\text{gm} && (\omega < I) , \\ k_\omega &= \frac{9.48 \times 10^6 n}{u^3 (T_a)^{3.5}} \left[1 + \frac{1.99\, e^{I/T_a}}{T_a} g(\omega) \right] && (\omega > I) , \end{aligned} \tag{28}$$

where n is the density of the gas and $g'(\omega)$ and $g(\omega)$ are the Gaunt factors for the free-free and bound-free transitions. For temperature such that the Maxwellian distribution is no longer valid, the absorption coefficient is

$$k_\omega = \frac{4.87 \times 10^6}{u^3 T_a^2} \left(\frac{e^u}{e^u - 1}\right) g'(\omega) \ln \left[\frac{e^u (A+1)}{e^u + A} \right] \text{cm}^2/\text{gm} \qquad (\omega < I) ,$$

$$k_\omega = \frac{1}{u^3 - T_a^3} \left\{ 4.87 \times 10^6 \frac{T_a g'(\omega)\, e^u}{e^u - 1} \ln \left[\frac{e^u (A+1)}{e^u + A} \right] + 4.76 \times 10^6 \frac{2}{(1+e^{-I/T_a})/A} \left[\frac{(1/A)\, e^{-(I/T_a)+u}}{(1/A)\, e^{-(I/T_a)+u} + 1} \right] \right\} . \tag{29}$$

The absorption coefficients are determined by using the wave functions obtained from the self-consistent calculations. The Gaunt factors for the free-free transition are shown

in Figure 4. It can be seen that for a pressure-ionized gas the electrons near the top of the Fermi band give the major contribution in determining the opacity. Absorption coefficients for the bound-free transitions corresponding to various cutoff radii are given in Figures 5 and 6. They are compared with the absorption coefficients of the K electron for a normal hydrogen atom. The essential difference lies in the shift of the absorption edges. Opacities as functions of temperature for various densities are given in Figure 7.

For the pressure-ionized gas, the opacity varies as T^{-2}. As the distribution of electrons in the Fermi band is temperature-independent for a highly degenerate electron gas, it is

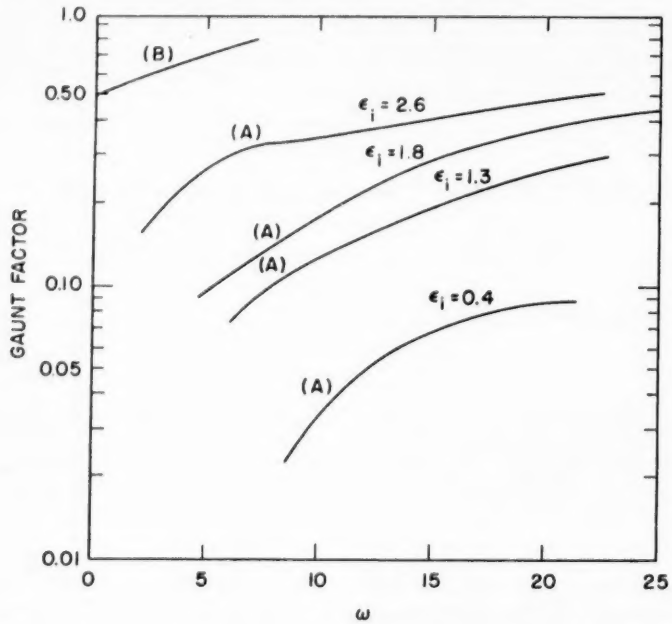

FIG. 4.—Gaunt factors for the free-free transitions. A, Gaunt factor for $a = 0.5a_0$. B, Gaunt factor for $a = a_0$.

the thermal dependence of the radiation intensity that makes opacity vary with temperature. Calculations do not cover the region for T_a greater than unity, since the assumption made on the degeneracy of the gas is no longer valid when the condition that $T_a/\epsilon_{F_0} \ll 1$ is not satisfied. The actual Fermi energy will be displaced, and there will be some unoccupied, as well as occupied, states below and above the Fermi energy. As the electrons near the top of the Fermi band give the major contribution to the absorption, change of ϵ_F will affect the value of the opacity. To get a better determination of opacity for such cases requires a recalculation of the self-consistent potential.

Equation (21) shows that the density does not appear explicitly in the determination of the absorption coefficient, which is characteristic of a strongly degenerate gas. The increase in electron concentration results in the addition of electrons with energies greater than the original Fermi band.

When temperature is such that the high-density atomic hydrogen gas is nondegenerate, the opacity varies approximately as $T_a^{-3.5}$. As temperature decreases, opacity in-

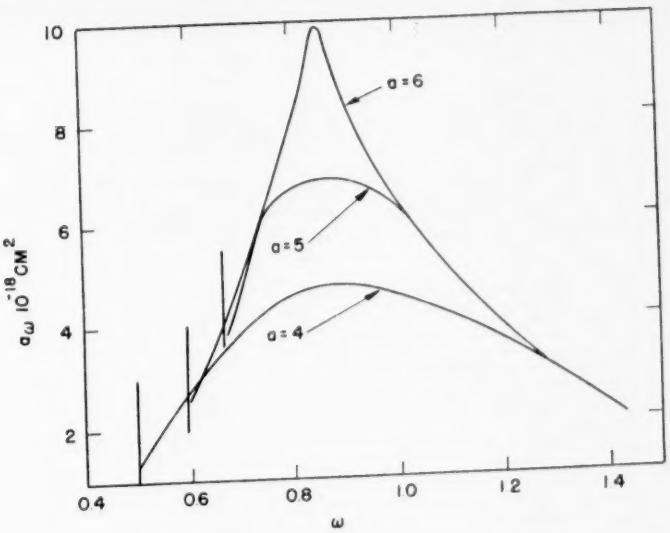

FIG. 5.—Absorption coefficients as functions of frequency

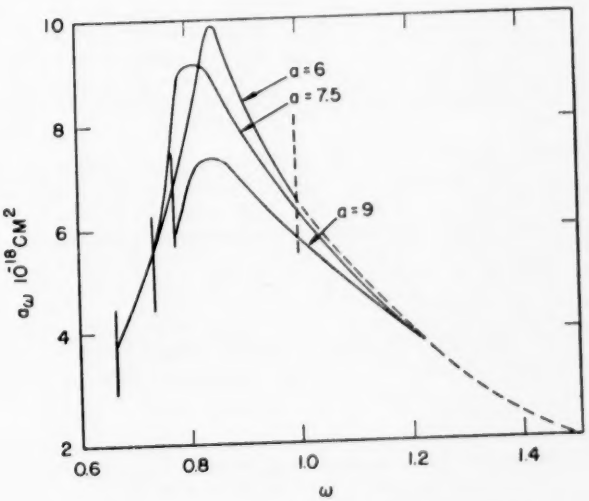

FIG. 6.—Absorption coefficients as functions of frequency

creases more slowly than that determined by $T_a^{-3.5}$; this is caused by the fact that it becomes less probable for the upper state to be vacant when the temperature is lowered.

From the form of the integral of the Rosseland mean, one can show that the absorption of frequencies below the absorption edges contributes the most to the value of the integral when the temperature is low; consequently, the free-free transition is more important. The opacity of a nondegenerate gas increases with density at a given temperature. In the lower-temperature ranges, the opacity first increases with density and then decreases, on account of the low value of the Gaunt factor for the high-density gas. This is usually considered a "saturation effect" and is shown at $T_a \backsim 0.1$ in Figure 7.

The opacity of a pure hydrogen gas is lower than that obtained previously for a gas mixture. For electrons in an ordinary Coulombian field of a nucleus of charge Ze, the

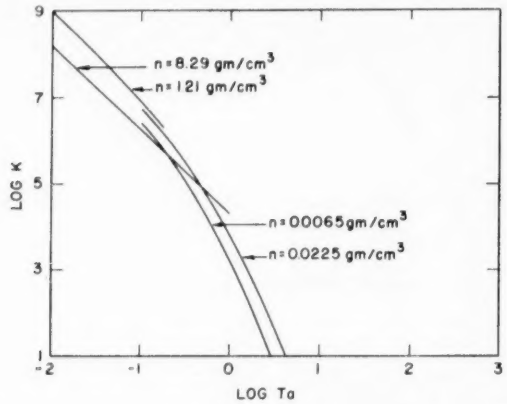

FIG. 7.—Coefficients of opacity as a function of temperature for the following densities: *a:* 8.29 gm/cm³; *b:* 1.21 gm/cm³; *c:* 2.25×10^{-2} gm/cm³; *d:* 6.50×10^{-3} gm/cm³.

energy of the K electron is $E = -Z^2/n^2$, if the shielding due to the presence of the other electrons in the atom is neglected. The ionization potential of the K electrons of heavier elements, though reduced by the presence of high pressure, is still considerably larger than that of a hydrogen gas. At a density when hydrogen is completely ionized, the K electrons of heavier elements still exist, and the absorption of those electrons favors an increase in opacity. Also, of course, conductive opacity,[16] which has been neglected here, will increase the over-all opacity somewhat.

Although hydrogen gas is one of the chief constituents of stellar matter, the study of opacity for stellar material cannot be considered complete without considering the heavier elements, and extensions of the present method to gases other than hydrogen must be made.

The author is indebted to Professors P. M. Morse and W. P. Allis for suggesting the problem and for valuable advice and encouragement. The writer is also indebted to the Physics Department and the Gaseous Electronics Group of M.I.T., who made the work possible.

[16] R. E. Marshak, *Ap. J.*, **92**, 321, 1940.

ON THE SOLUTION OF AN INTEGRAL EQUATION OF CHANDRASEKHAR AND MÜNCH

ALLADI RAMAKRISHNAN AND P. M. MATHEWS
Department of Physics, University of Madras, Madras, India
Received December 13, 1952; revised July 17, 1953

ABSTRACT

A technique is suggested to solve a class of difference equations where the difference relates to a continuous variable. To illustrate its use, the problem of the fluctuations in brightness of the Milky Way dealt with by Chandrasekhar and Münch is discussed, using this technique.

In a series of papers[1] on the "Fluctuations in Brightness of the Milky Way," Chandrasekhar and Münch discussed an integrodifferential equation and obtained the solutions in particular cases. One of us (A. R.), by the application of Mellin's transformation, reduced the problem to a difference-differential equation. As it was a difference equation with respect to a complex variable, it was supposed that the equation could not be solved directly by iteration. It is the purpose of this paper to suggest an operational technique by means of which such difference equations can be solved formally. To illustrate its use, we shall obtain some of the results of Chandrasekhar and Münch by its direct application. The technique consists in the formal identification of the moment sequence of a function with its Mellin transform. This procedure will lead to results with formal meaning only when the expression for the moment sequence is interpreted in a suitable form. In this paper we rewrite the expression for the integral moments of the function occurring in the problem of Chandrasekhar and Münch in a form convenient for the identification of the Mellin transform. By using the classical inversion formula, a tentative solution is derived; and, by substitution in the original equation and boundary conditions, it is verified that, in fact, it is the desired solution. Chandrasekhar and Münch arrived at the following equation:[2]

$$\frac{\partial g(u,\epsilon)}{\partial \epsilon} = -g(u,\epsilon) - \frac{\partial g(u,\epsilon)}{\partial u} + \int_q g\left(\frac{u}{q}\right)\psi(q)\frac{dq}{q}. \tag{1}$$

The physical conditions of the problem require that u should be nonnegative;

$$\int_u g(u,\epsilon)\,du = 1$$

for all ϵ; $g(u, 0) = \delta(u)$ where δ is the Dirac delta-function; and $0 \leqslant q \leqslant 1$.

Defining

$$f(u,\epsilon) = \int_u^\infty g(u',\epsilon)\,du',$$

we obtain

$$f(u,0) = 0 \text{ if } u > 0\,; \qquad f(u,0) = 1 \text{ if } u = 0\,. \tag{2}$$

It will be shown later that one of the consequences of this is that $g(u, \epsilon)$ has a delta-function singularity at $u = \epsilon$, i.e., $f(u, \epsilon) = 0$ when $u > \epsilon$, and $f(\epsilon, \epsilon) = e^{-\epsilon}$.

[1] S. Chandrasekhar and G. Münch, *Ap. J.*, **112**, 380, 393, 1950; **114**, 110, 1951; **115**, 94, 1952.

[2] In this paper, the symbol $\int_x$ denotes integration over the whole domain of the variable x.

Defining the Mellin transformations[3] of $g(u, \epsilon)$ and $\psi(q)$ in the form

$$p(s, \epsilon) = \int^{\infty} g(u, \epsilon)\, u^s du\,,$$

$$q_s = \int_0^{\infty} \psi(q)\, q^s dq = \int_0^1 \psi(q)\, q^s dq\,, \tag{3}$$

where s is a complex variable, one of us (A. R.) obtained the equation[4]

$$\frac{\partial p(s, \epsilon)}{\partial \epsilon} = -p(s, \epsilon) + q_s p(s, \epsilon) + s\, p(s-1, \epsilon)\,. \tag{4}$$

The corresponding initial conditions for $p(s, \epsilon)$ are

$$p(s, 0) = 0 \text{ if } s \neq 0\,, \qquad p(0, 0) = 1 \tag{5}$$

since at $\epsilon = 0$, $g(u, \epsilon) = \delta(u)$ and $p(0, \epsilon) = 1$ for all ϵ.

The inverse transformation corresponding to equation (3) is

$$g(u, \epsilon) = \frac{1}{2\pi i} \int_{\sigma - i\infty}^{\sigma + i\infty} p(s, \epsilon)\, u^{-s-1} ds\,. \tag{6}$$

Since s is complex, it is quite clear that equation (4) cannot be solved directly by iteration. When we put $s = n$, $n \geq 0$ being an integer, $p(n, \epsilon)$ represents the nth moment of u, and $p(n, \epsilon)$ satisfies equation (4) and the initial conditions (5). By iteration it is found that

$$p(n, \epsilon) = n! \sum_{k=0}^{n} \frac{e^{-(1-q_k)\epsilon}}{\prod_{j=0,\ j\neq k}^{j=n} (q_k - q_j)}\,. \tag{7}$$

The aim of this paper is to suggest a formal procedure by means of which it is possible to identify $p(s, \epsilon)$ from $p(n, \epsilon)$. If $p(s, \epsilon)$ is found to satisfy the differential equation and the initial conditions (5), it is the required solution.

The essential point in this technique is the expressing of $p(n, \epsilon)$ in a form such that the substitution of the continuous variable s for the integer n is meaningful. We observe with caution that $p(s, \epsilon)$ thus obtained will "normally" satisfy the difference-differential equation. But to find out whether $p(s, \epsilon)$ is actually the solution, we examine whether the initial conditions (5) and equation (4) are satisfied. It is suggested that $p(s, \epsilon)$ will be the solution, provided that $p(n, \epsilon)$ is expressed in such a form that it involves such functions of n as will satisfy the same difference relations as those obtained by substituting s for n.

To cast $p(n, \epsilon)$ in a suitable form, the following devices may be employed.

[3] Normally the Mellin transformation of a function $f(x)$ is defined as

$$\int_0^{\infty} f(x)\, x^{s-1} dx\,.$$

Here we define it according to eq. (3) for convenience of comparison with the integral moment,

$$\int_0^{\infty} f(x)\, x^n dx\,,$$

where n is an integer. We also use the notation q_s instead of η_s adopted in the previous paper of (A.R.) to conform to the notation of Chandrasekhar and Münch.

[4] Alladi Ramakrishnan, *Ap. J.*, **115**, 141, 1952.

a) Suppose $p(n, \epsilon)$ involves a function $f(n)$ which is expressed as

$$\sum_{i=1}^{n} a_i .$$

Obviously, there is no meaning in substituting s for n. But if we write

$$\sum_{i=1}^{n} a_i = \sum_{i=1}^{\infty} a_i - \sum_{i=1}^{\infty} a_{n+i} ,$$

we can substitute s for n and write $f(s)$ as

$$\sum_{i=1}^{\infty} a_i - \sum_{i=1}^{\infty} a_{s+i} .$$

Note that $f(s)$ and $f(n)$ satisfy the same difference relation, $f(s) - f(s-1) = a_s$ and $f(n) - f(n-1) = a_n$. This operational rule leads to a meaningful result only when

$$\sum_{i=1}^{\infty} a_i$$

is absolutely convergent.

b) If $p(n, \epsilon)$ involves a function

$$f(n) = \prod_{i=1}^{n} a_i ,$$

write $f(n)$ as

$$\frac{\prod_{i=1}^{\infty} a_i}{\prod_{i=1}^{\infty} a_{n+i}} \quad \text{and} \quad f(s) \text{ as } \frac{\prod_{i=1}^{\infty} a_i}{\prod_{i=1}^{\infty} a_{s+i}} .$$

This rule is meaningful only if the infinite product

$$\prod_{i=1}^{\infty} a_i$$

is absolutely convergent.

c) In cases where $p(n, \epsilon)$ involves functions like $n!$, rule *b* cannot be employed. We then substitute $s! = \Gamma(s+1)$ for $n!$.

To illustrate the use of the method, we shall obtain $p(s, \epsilon)$ from equation (7) in three particular cases of astrophysical interest.

CASE I

Consider the case

$$\psi(q') = \delta(q' - q) , \qquad \text{i.e.,} \qquad q_j = q^j .$$

Then

$$p(n, \epsilon) = n! \sum_{k=0}^{n} \frac{e^{-(1-q^k)\epsilon}}{\prod_{j=0,\ j\neq k}^{j=n} (q^k - q^j)} . \tag{8}$$

In order to express $p(n, \epsilon)$ in a form such that we can substitute s for n, we use identities proved by one of us (A. R.).[5]

We define

$$(-1)^n A_k^n = \frac{1}{\prod_{j=0,\ j\neq k}^{n} (q^k - q^j)}. \tag{9}$$

Then

$$\begin{aligned} p(n, \epsilon) &= (-1)^n n! e^{-\epsilon} \sum_{k=0}^{n} A_k^n e^{q^k \epsilon} \\ &= (-1)^n n! e^{-\epsilon} \sum_{m=0}^{\infty} \frac{\epsilon^m}{m!} \sum_{k=0}^{n} A_k^n q^{mk}. \end{aligned} \tag{10}$$

In Paper A it was proved that

$$\sum_{k=0}^{n} A_k^n q^{mk} = \frac{1 - q^m}{1 - q^{m-n}} \sum_{k=0}^{n} A_k^n q^{(m-1)k} \tag{11}$$

and also that

$$\sum_{k=0}^{n} A_k^n = 0.$$

Hence, from equation (11),

$$\sum_{k=0}^{n} A_k^n q^{mk} = 0 \qquad \text{if} \qquad m < n.$$

To evaluate

$$\sum_{k=0}^{n} A_k^n q^{mk}$$

for $m > n$, we must know

$$\sum_{k=0}^{n} A_k^n q^{nk},$$

which cannot be determined by equation (11), since it becomes indeterminate (of the form 0/0). To obtain it, we write

$$\sum_{k=0}^{n} A_k^n q^{(n-1)k} - \sum_{k=0}^{n} A_k^n q^{nk} = \sum_{k=1}^{n} A_k^n q^{(n-1)k} (1 - q^k) = \sum_{k=0}^{n-1} A_k^{n-1} q^{(n-1)k}. \tag{12}$$

Since

$$\sum_{k=0}^{n} A_k^n q^{(n-1)k} = 0,$$

we get the recurrence relation

$$\sum_{k=0}^{n} A_k^n q^{nk} = -\sum_{k=0}^{n-1} A_k^{n-1} q^{(n-1)k}; \tag{13}$$

[5] This astrophysical problem was discussed in detail in a paper on "A Class of Stochastic Processes" (*Proc. Cambridge Phil. Soc.*, **49**, 473, 1953). This paper will be referred hereafter as "Paper A."

and, since $A_0^0 = 1$,

$$\sum_{k=0}^{n} A_k^n q^{nk} = (-1)^n . \tag{14}$$

From equation (14) we can obtain the values of

$$\sum_{k=0}^{n} A_k^n q^{mk}$$

for $m > n$, using equation (11). We find

$$p(n, \epsilon) = e^{-\epsilon}\epsilon^n + n! e^{-\epsilon} \sum_{m=1}^{\infty} \frac{\epsilon^{n+m}}{(n+m)!} \prod_{j=1}^{m} \frac{1 - q^{n+j}}{1 - q^j} . \tag{15}$$

It can be shown that (see Appendix A)

$$\prod_{j=1}^{m} (1 - q^{n+j}) = 1 + \sum_{k=1}^{m} q^{nk} \prod_{j=1}^{k} \frac{q^{m+1} - q^j}{1 - q^j} ; \tag{16}$$

and hence we can write

$$p(n, \epsilon) = e^{-\epsilon}\epsilon^n + n! e^{-\epsilon} \sum_{m=1}^{\infty} \frac{\epsilon^{n+m}}{(n+m)!} \prod_{j=1}^{m} (1 - q^j)^{-1} \left\{ 1 + \sum_{k=1}^{m} q^{nk} \prod_{j=1}^{k} \frac{q^{m+1} - q^j}{1 - q^j} \right\} . \tag{17}$$

Noticing that

$$\prod_{j=1}^{m} (1 - q^j)^{-1} \prod_{j=1}^{k} \frac{q^{m+1} - q^j}{1 - q^j} = (-1)^m A_k^m q^{km} \tag{18}$$

and

$$\prod_{j=1}^{m} (1 - q^j)^{-1} = (-1)^m A_0^m , \tag{18a}$$

we have

$$p(n, \epsilon) = e^{-\epsilon}\epsilon^n + n! e^{-\epsilon} \sum_{m=1}^{\infty} \frac{\epsilon^{n+m}}{(n+m)!} \sum_{k=0}^{m} (-1)^m A_k^m q^{(n+m)k} . \tag{19}$$

We can now replace n by the complex variable s and write

$$p(s, \epsilon) = e^{-\epsilon}\epsilon^s + s! e^{-\epsilon} \sum_{m=1}^{\infty} \frac{\epsilon^{s+m}}{(s+m)!} \sum_{k=0}^{m} (-1)^m A_k^m q^{(s+m)k} . \tag{20}$$

This is the correct solution of equation (4) when $q_s' = q^s$, since it satisfies equation (4) and the initial conditions (5). It remains to find $g(u, \epsilon)$, the inverse of $p(s, \epsilon)$.

We notice that

$$\frac{s!}{(s+m)!} = \frac{1}{(m-1)!} \frac{(m-1)!}{(s+1)(s+2)\ldots(s+m)}$$

$$= \frac{1}{(m-1)!} \sum_{r=0}^{m-1} (-1)^r \binom{m-1}{r} \frac{1}{s+r+1} ; \tag{21}$$

and thus we can write

$$p(s,\epsilon) = e^{-\epsilon}\epsilon^s + \sum_{m=1}^{\infty}\sum_{k=0}^{m}\sum_{r=0}^{m-1} \times \frac{(-1)^m A_k^m (\epsilon q^k)^m e^{-\epsilon}}{(m-1)!}(-1)^r \binom{m-1}{r} \frac{(\epsilon q^k)^s}{s+r+1}. \tag{22}$$

Now the inverse of $e^{-\epsilon}\epsilon^s$ is the delta-function $e^{-\epsilon}\delta(u-\epsilon)$.

To evaluate the inverse of the remaining part of the expression on the right-hand side of equation (22), we have to calculate

$$\frac{1}{2\pi i}\int_{\sigma-i\infty}^{\sigma+i\infty} \frac{(\epsilon q^k)^s}{s+r+1} u^{-s-1} ds = \frac{1}{2\pi i u}\int_{\sigma-i\infty}^{\sigma+i\infty} \frac{v^s}{s+r+1} ds \quad \text{where} \quad v = \frac{\epsilon q^k}{u}. \tag{23}$$

This integral can be written as

$$\frac{v^{-(r+1)}}{2\pi i u}\int_{\sigma-i\infty}^{\sigma+i\infty} \frac{\exp\{(s+r+1)\log v\}}{s+r+1} d(s+r+1). \tag{24}$$

Remembering that

$$\frac{1}{2\pi i}\int_{\sigma-i\infty}^{\sigma+i\infty} \frac{e^{sz}}{s^n} ds = \frac{z^{n-1}}{(n-1)!} \quad (z \text{ real and greater than zero}) \tag{25}$$

and that the contour integral vanishes if $z < 0$, equation (24) reduces to

$$\frac{v^{-(r+1)}}{u} \quad \text{if} \quad \log v > 0, \quad \text{i.e.,} \quad v > 1, \quad \text{i.e.,} \quad u < \epsilon q^k, \tag{26}$$

and to zero if $u > \epsilon q^k$.

Hence, if $\epsilon q^l < u < \epsilon q^{l-1}$, the terms in the summation over k vanish for $k > l-1$; and, after performing the summation over r, we obtain

$$g(u,\epsilon) = e^{-\epsilon}\delta(u-\epsilon) - e^{-\epsilon}\sum_{m=1}^{l-1}\sum_{k=0}^{m} \frac{A_k^m (u-\epsilon q^k)^{m-1}}{(m-1)!} - e^{-\epsilon}\sum_{m=l}^{\infty}\sum_{k=0}^{l-1} \frac{A_k^m (u-\epsilon q^k)^{m-1}}{(m-1)!} \qquad (\epsilon q^l < u \leqslant \epsilon q^{l-1}). \tag{27}$$

We have, further,

$$\sum_{k=0}^{m} A_k^m (u-\epsilon q^k)^{m-1} = 0, \tag{28}$$

since, by expanding $(u-\epsilon q^k)^{m-1}$ binomially, we obtain

$$\sum_{k=0}^{m} A_k^m \sum_{r=0}^{m-1} (-1)^r (\epsilon q^k)^r u^{m-1-r} \binom{m-1}{r} = \sum_{r=0}^{m-1} (-1)^r \epsilon^r u^{m-1-r} \binom{m-1}{r} \sum_{k=0}^{m} A_k^m q^{kr},$$

an expression that vanishes because

$$\sum_{k=0}^{m} A_k^m q^{kr} = 0 \qquad \text{for} \qquad r < m .$$

Thus we finally have

$$g(u, \epsilon) = e^{-\epsilon}\delta(u-\epsilon) - \sum_{m=l}^{\infty}\sum_{k=0}^{l-1} \frac{A_k^m (u-\epsilon q^k)^{m-1}}{(m-1)!} \qquad (\epsilon q^l < u \leqslant \epsilon q^{l-1}) . \tag{29}$$

Notice that

$$g(u, \epsilon) = 0 \qquad \text{if} \qquad u > \epsilon . \tag{30}$$

This general solution is different in form from that of Chandrasekhar and Münch. In Appendix B the two solutions are proved to be equivalent. The peculiar features of the problem are as apparent from equation (29) as from the Chandrasekhar-Münch form—as, for example, the delta-function singularity of the function $g(u, \epsilon)$ at $u = \epsilon$ and the finite discontinuity at $u = \epsilon q$. The function $g(u, \epsilon)$ is continuous everywhere else, including the points $u = \epsilon q^l (l > 1)$.

The same general solution (29) was obtained by one of us (A. R.) in Paper A, using an entirely different technique, known in stochastic theory as the "method of regeneration points." However, in that paper the finite discontinuity at $u = \epsilon q$, apparent from a mere examination of equation (29), was not noticed.

CASE II

We take the case when ϵ tends to infinity and the stationary state is reached, i.e., $\partial p(n, \epsilon)/\partial \epsilon = 0$ for all n as $\epsilon \to \infty$. Then the solution of equation (4) with $\partial p(n, \epsilon)/\partial \epsilon = 0$ as $\epsilon \to \infty$ is obtained as

$$p(n, \infty) = p(n) = \frac{n!}{\prod_{j=1}^{n} (1 - q^j)} , \tag{31}$$

i.e., all terms in equation (7) vanish as $\epsilon \to \infty$, except the term obtained by putting $k = 0$.

In particular, we take $q_j = q^j$, i.e., in equation (1) $\psi(q') = \delta(q' - q)$, where δ is the Dirac delta-function. Thus

$$p(n) = \frac{n!}{\prod_{j=1}^{n} (1 - q^j)} . \tag{32}$$

We write

$$\frac{1}{\prod_{j=1}^{n} (1 - q^j)} \qquad \text{as} \qquad A_0 \prod_{j=1}^{\infty} (1 - q^{n+j}) , \qquad \text{where} \qquad \frac{1}{A_0} = \prod_{j=1}^{\infty} (1 - q^j) ,$$

which is convergent, since $q < 1$. If we now use the identity proved by Chandrasekhar and Münch,

$$\prod_{i=1}^{\infty} (1 - q^{i+n}) = 1 + \sum_{j=1}^{\infty} (-1)^j q^{nj} \prod_{i=1}^{j} \frac{q^i}{1 - q^i} , \tag{33}$$

it is possible to substitute s for n, and we obtain the required solution,

$$p(s, \infty) = p(s) = A_0 s! \left\{1 + \sum_{k=1}^{\infty} (-1)^k q^{sk} \prod_{j=1}^{k} \frac{q^j}{1-q^j}\right\}. \tag{34}$$

Hence

$$g(u, \infty) = g(u) = A_0 \left\{e^{-u} + \sum_{k=1}^{\infty} (-1)^k e^{-u/q^k} \prod_{j=1}^{k} \frac{q^j}{1-q^j}\right\}, \tag{35}$$

which is a result obtained by Chandrasekhar and Münch.

CASE III

Now consider the case when ϵ tends to infinity and[6]

$$\psi(q) = (m+1)\, q^m, \qquad \text{i.e.,} \qquad q_j = \frac{m+1}{m+j+1}, \qquad 1 - q_j = \frac{j}{m+j+1}. \tag{36}$$

Hence

$$p(n, \infty) = p(n) = \frac{(m+n+1)!}{(m+1)!}.$$

If $p(n)$ is written in this form, the substitution s for n is possible. Hence

$$p(s, \infty) = p(s) = \frac{(m+s+1)!}{(m+1)!}, \tag{37}$$

which yields

$$g(u, \infty) = g(u) = e^{-u} \frac{u^{m+1}}{(m+1)!}, \tag{38}$$

a result derived by Chandrasekhar and Münch.

We are thankful to the referee for his helpful criticisms and suggestions and to Mr. S. K. Srinivasan for his elegant proof of the equivalence of solution (29) and that of Chandrasekhar and Münch.

APPENDIX A

The proof of identity (16) follows on the same lines as equation (33), which was proved by Chandrasekhar and Münch. To prove

$$\prod_{j=1}^{m} (1 - q^{n+j}) = 1 + \sum_{k=1}^{m} q^{nk} \prod_{j=1}^{k} \frac{q^{m+1} - q^j}{1 - q^j}, \tag{A1}$$

consider the function

$$\phi(x) = \prod_{j=1}^{m} (1 - x q^{n+j}),$$

which satisfies the functional equation

$$(1 - x q^{n+m+1})\, \phi(x) = (1 - x q^{n+1})\, \phi(xq), \tag{A2}$$

[6] Chandrasekhar and Münch used the notation $\psi(q) = (n+1)q^n$. We use m to distinguish it from n in $p(n, \epsilon)$.

where $\phi(x)$ and $\phi(xq)$ can be expanded in a series of the form

$$\sum_{k=0}^{m} a_k x^k \qquad \text{and} \qquad \sum_{k=0}^{m} a_k (xq)^k,$$

respectively. Substituting these series in equation (A2) and equating coefficients of x^k, we obtain

$$\begin{aligned} a_k(1-q^k) &= a_{k-1}(q^{n+m+1}-q^{n+k}), \\ a_k = \frac{q^{n+m+1}-q^{n+k}}{1-q^k}\, a_{k-1} &= q^n \frac{q^{m+1}-q^k}{1-q^k}\, a_{k-1}. \end{aligned} \tag{A3}$$

Using the above recurrence relation and knowing that $a_0 = 1$, we find

$$a_k = q^{nk} \prod_{j=1}^{k} \frac{q^{m+1}-q^j}{1-q^j} \qquad (k = 1, 2, \ldots), \tag{A4}$$

and hence

$$\prod_{j=1}^{m} (1 - x q^{n+j}) = \phi(x) = 1 + \sum_{k=1}^{m} x^k q^{nk} \prod_{j=1}^{k} \frac{q^{m+1}-q^j}{1-q^j}. \tag{A5}$$

Putting $x = 1$ in this, we get the identity (A1). In particular, when m tends to infinity, we get equation (33).

APPENDIX B

Chandrasekhar and Münch obtained the solution of equation (1) in the form

$$g(u,\epsilon) = K e^{-\epsilon} \sum_{k=0}^{l-1} \frac{Q_k}{q^k} \sum_{r=0}^{\infty} \frac{Q_r}{q^{(k-1)r}} \exp\left[q^r \left(\epsilon - \frac{u}{q^k}\right)\right] + e^{-\epsilon}\delta(u-\epsilon) \tag{B1}$$
$$(\epsilon q^l < u \leqslant \epsilon q^{l-1}),$$

where

$$\frac{1}{K} = \prod_{j=1}^{\infty} (1-q^j) \qquad \text{and} \qquad Q_k = (-1)^k \prod_{j=1}^{k} \frac{q^j}{1-q^j},$$

$$g(u,\epsilon) = K e^{-\epsilon} \sum_{k=0}^{l-1} \frac{Q_k}{q^k} \sum_{r=0}^{\infty} \frac{Q_r}{q^{(k-1)r}} \sum_{m=1}^{\infty} \frac{q^{r(m-1)}(\epsilon - [u/q^k])^{m-1}}{(m-1)!} + e^{-\epsilon}\delta(u-\epsilon) \tag{B2}$$
$$(\epsilon q^l < u \leqslant \epsilon q^{l-1})$$

$$g(u,\epsilon) = K e^{-\epsilon} \sum_{k=0}^{l-1} \frac{Q_k}{q^k} \sum_{m=1}^{\infty} \frac{(\epsilon - [u/q^k])^{m-1}}{(m-1)!} \sum_{r=0}^{\infty} Q_r q^{(m-k)r} + e^{-\epsilon}\delta(u-\epsilon) \tag{B3}$$
$$(\epsilon q^l < u \leqslant \epsilon q^{l-1}).$$

Now

$$\begin{aligned} \sum_{r=0}^{\infty} Q_r q^{nr} &= \prod_{j=1}^{\infty} (1-q^{n+j}) && (n \geqslant 0), \\ &= 0 && (n < 0). \end{aligned} \tag{B4}$$

Hence we have

$$g(u,\epsilon) = Ke^{-\epsilon}\sum_{k=0}^{l-1}\frac{Q_k}{q^k}\sum_{m=k}^{\infty}\frac{(\epsilon-[u/q^k])^{m-1}}{(m-1)!}\prod_{j=1}^{\infty}(1-q^{m-k+j}) + e^{-\epsilon}\delta(u-\epsilon) \qquad (B5)$$
$$(\epsilon q^l < u \leqslant \epsilon q^{l-1})$$

$$= e^{-\epsilon}\sum_{k=0}^{l-1}\frac{(-1)^k}{q^k}\prod_{i=1}^{k}\frac{q^i}{1-q^i}\sum_{m=k}^{\infty}\frac{(\epsilon q^k-u)^{m-1}}{q^{k(m-1)}(m-1)!}\prod_{j=1}^{m-k} \qquad (B6)$$
$$\times(1-q^j)^{-1} + e^{-\epsilon}\delta(u-\epsilon)$$

$$= -e^{-\epsilon}\sum_{k=0}^{l-1}\sum_{m=k}^{\infty}\frac{(u-\epsilon q^k)^{m-1}}{(m-1)!}A_k^m + e^{-\epsilon}\delta(u-\epsilon) \qquad (B7)$$
$$(\epsilon q^l < u \leqslant \epsilon q^{l-1}).$$

On changing the order of summation in the above expression, we obtain

$$-e^{-\epsilon}\sum_{m=0}^{l-1}\sum_{k=0}^{m}\frac{(u-\epsilon q^k)^{m-1}}{(m-1)!}A_k^m - e^{-\epsilon}\sum_{m=l}^{\infty}\sum_{k=0}^{l-1}\frac{(u-\epsilon q^k)^{m-1}}{(m-1)!}A_k^m + e^{-\epsilon}\delta(u-\epsilon) \qquad (B8)$$
$$(\epsilon q^l < u \leqslant \epsilon q^{l-1}).$$

The first part of this vanishes (see eq. [28]), and hence we get

$$g(u,\epsilon) = -e^{-\epsilon}\sum_{m=l}^{\infty}\sum_{k=0}^{l-1}\frac{(u-\epsilon q^k)^{m-1}}{(m-1)!}A_k^m + e^{-\epsilon}\delta(u-\epsilon) \qquad (\epsilon q^l < u \leqslant \epsilon q^{l-1}), \qquad (B9)$$

which is equation (29).

COMPARISON OF THE SYNTHETIC AND ACTUAL DISTRIBUTION OF GALAXIES ON A PHOTOGRAPHIC PLATE*

E. L. SCOTT
Statistical Laboratory
C. D. SHANE
Lick Observatory
AND M. D. SWANSON
Statistical Laboratory, University of California
Received May 10, 1953

ABSTRACT

The present work was undertaken with the following two questions in mind: (i) If it is true that galaxies occur only in clusters, then why is there such difficulty in identifying these clusters so that only a few of them are sufficiently conspicuous to be studied per se? (ii) Would a visual comparison between the actual photographic plate and the implications of the recent theory, by Neyman, Scott, and Shane, of clustering of galaxies provide indications for modifying the probabilistic model underlying this theory? In order to answer these questions, the specificity of the probabilistic model was used to construct a "synthetic" photographic plate. Following the postulates of the model a series of random sampling experiments was performed leading to the determination of positions of galaxies in a $6^\circ \times 6^\circ$ square representing a photographic plate, without the images of stars. This synthetic plate is then compared with the chart of a real photographic plate with the images of stars removed. The general appearance of the two plates is very similar. In particular, the clusters of galaxies which compose the entire distribution on the synthetic plate appear superimposed and mixed together and are unidentifiable. This result answers question i. As to question ii, the galaxies on the actual plate appear somewhat more tightly clustered than on the synthetic plate, and this visual impression is confirmed by an examination of the counts in $10' \times 10'$ cells. If this difference is not due to chance variation, then it implies the necessity of a change in the specialization of the probabilistic model, presumably affecting the details of the hypothesis regarding the internal structure of clusters.

I. INTRODUCTION

In a recent paper[1] (hereafter referred to as "Paper I") a general model of the spatial distribution of galaxies was developed. In a subsequent paper[2] ("Paper II") this model was specialized so as to permit numerical characterization of the distribution of galaxies implied by the model. The specialized model depends on several constants; estimates of these constants were obtained by comparing the theoretical moments and serial quasi-correlations of counts of galaxies in $1^\circ \times 1^\circ$ squares with their empirical counterparts computed from actual counts made at the Lick Observatory.

The agreement between the theoretical and empirical quasi-correlations is very good, and this suggested that the specialized model of the distribution of galaxies may not be too far from the true distribution. It is clear, however, that the model must be subjected to a number of checks before it can be considered as more than a tentative working hypothesis. The serial quasi-correlations reflect but one aspect of the entire situation. Furthermore, being based on counts in 1° squares, these quasi-correlations leave out of consideration all the small-scale details of the distribution of galaxies that occur *within* 1° squares.

* All computations for this paper were performed at the Statistical Laboratory, University of California, with the partial support of the Office of Naval Research. Counts of galaxies were made at the Lick Observatory by C. D. Shane and C. A. Wirtanen. This paper is a joint publication of the Statistical Laboratory and the Lick Observatory, *Contributions from the Lick Observatory*, Ser. II, No. 47.

[1] J. Neyman and E. L. Scott, *Ap. J.*, **116**, 144, 1952.

[2] J. Neyman, E. L. Scott, and C. D. Shane, *Ap. J.*, **117**, 92, 1953.

The present paper was prepared as an attempt to determine some of the aspects in the model that may need modifying. As the principal means of achieving this end, we selected a visual comparison between actual photographs of galaxies and a plate prepared synthetically by means of a large-scale sampling experiment that follows the probabilistic model of Paper II in as many details as practicable. As a starting point for the investigation, we had in mind demonstrating the answer to the often asked question: If the total distribution of galaxies is, in fact, a conglomeration of clusters, then why have so few large clusters thus far been identified and isolated?[3] In other words: If one actually distributed the cluster centers in space and then placed the galaxies in the clusters exactly as prescribed by the model, would the resulting picture on the photographic plate look anything like that on an actual plate, and would it present similar difficulties in identifying individual clusters?

In order to answer these questions, a large sampling experiment was performed at the Statistical Laboratory. The resulting $6° \times 6°$ synthetic photograph of galaxies is shown in Figure 5. Figures 2–4 illustrate various stages of constructing the synthetic plate. This synthetic plate is then compared with an actual $6° \times 6°$ photographic plate from the collection at the Lick Observatory. Charts of the actual plate are reproduced in Figures 6 and 7.

In addition to the purely visual comparison of the distribution of galaxies, on the synthetic and the actual plates, an effort was made to obtain a numerical small-scale characterization of the distribution, with particular reference to the variation that one may expect from one plate to another. For this purpose the number of galaxies within $10' \times 10'$ cells was counted both on the synthetic plate and on sixteen actual plates. A comparison of the resulting frequency distributions of counts is given in Section VI.

II. SPECIFIC DISTRIBUTIONS AND NUMERICAL CONSTANTS USED

In order to build a $6° \times 6°$ synthetic "photograph" according to the model, we specialize the underlying distribution as in Paper II and assign numerical values to the constants involved. However, as emphasized in Paper II, none of the constants is well determined, largely because the distribution of the absolute magnitude of the galaxies is not well known. From the range of plausible values for the dispersion σ_M in absolute magnitude and for the difference $m_1 - M_0$ between the limiting apparent magnitude of the plate and the mean absolute magnitude of the galaxies, the convenient value $\sigma_M = 1$ and $m_1 - M_0 = 32.5$ were chosen for use in the present paper. These two constants fix the numerical values of the remaining parameters, as described in Paper II.

The specific postulates and distributions used are enumerated below.

a) The number γ of cluster centers.—The number of cluster centers in any volume element is a Poisson random variable with density estimated to be 1.6×10^{-19} cluster centers per cubic parsec.

b) The positions of the cluster centers.—Given any bounded region and given the number of cluster centers it contains, the model in Papers I and II implies that the positions of these cluster centers are uniformly and independently distributed throughout the region contemplated.

c) The number of galaxies belonging to a given cluster.—The model assumes that the number ν of galaxies belonging to a cluster is a random variable. The information obtained in Paper II regarding the distribution of ν is even less secure than that regarding other variables in the model. However, it was found that a negative binomial distribution provides a satisfactory fit to the available quantitative and some qualitative observations. According to this distribution, the probability that the number ν of galaxies

[3] On the other hand, observations with the Schmidt telescopes at Mount Palomar reveal a large number of clusters (see F. Zwicky, *Pub. A.S.P.*, **64**, 247, 1952).

belonging to any particular cluster is, say, k is

$$P\{\nu = k\} = (91.5)^{k-1}\,(92.5)^{-k} \text{ for } k = 1, 2, \ldots .$$

d) The position of a galaxy within a cluster.—The rectangular co-ordinates of each galaxy with respect to its cluster center are postulated to be independent of those of any other in the cluster and to depend only on the distance from the cluster center. The specialization adopted assumes that these co-ordinates follow a trivariate normal distribution with standard deviation equal to 5×10^5 psc, as determined by the serial quasi-correlations.

e) The apparent magnitude of a galaxy.—In Paper II the absolute magnitude M of a galaxy is assumed to be a normal random variable independent of that of any other galaxy. The mean M_0 and dispersion σ_M are not well known. The formula adopted for the apparent magnitude m of a galaxy at distance ξ from the observer is

$$m = M - 5 + 5 \log_{10} \xi + 5.15 \times 10^{-9}\, \xi\,, \tag{1}$$

where the last term represents the dimming due to red shift. In this paper the only purpose of considering the absolute magnitude M is to calculate the apparent magnitude m in order to compare m with the limiting magnitude m_1 of the plate. It is easy to see that the probability that $m < m_1$ (so that the galaxy will be "visible" on the plate) depends on the difference $m_1 - M_0$ rather than on the two quantities taken separately. It was found in Paper II that a wide range of possible combinations of values of σ_M and $m_1 - M_0$ is compatible with the observations. Out of these we select $\sigma_M = 1$ (for simplicity) and $m_1 - M_0 = 32.5$ mag., as mentioned earlier. Unfortunately, the value of m_1 is not known exactly. For purposes of "labeling" we write $m_1 = 18.3$ and $M_0 = -14.2$.

All the specific assumptions listed above relate to the distribution of characteristics of galaxies that are supposed to develop in space. By means of five series of random sampling experiments, the co-ordinates and the magnitudes of synthetic galaxies were determined in accordance with these five assumptions. Then all galaxies with apparent magnitude of 18.3 or less were "photographed." The resulting synthetic plate (see Fig. 3) represents what would be described in Papers I and II as an *idealized* synthetic plate, corresponding to the constant limiting magnitude 18.3, which is the presumed extreme limiting magnitude of the Lick Observatory survey. However, the idealized synthetic plate is not directly comparable to a real plate, because we have not taken into account the effects of variation in the limiting magnitude, of errors in counting, and of other factors arising in the observations. The postulates necessary to describe the effect of factors arising in the observations are given in Section V.

III. TECHNIQUE OF SAMPLING EXPERIMENTS

The production of the synthetic plate made repeated use of sampling experiments, each experiment designed to exhibit what might be the outcome of a particular machinery of chance variation out of those postulated in the model. In order to abbreviate the subsequent explanations, it seems appropriate to introduce this section describing, in general terms, the technique of sampling experiments.

Denote generally by X a random variable with a given distribution function, and consider the problem of finding what the outcome of n independent observations performed on X might be. There are two important cases to consider separately: (i) X is a discrete variable capable of assuming any one of a finite, or of an infinite, sequence of values $u_1 < u_2 < \ldots < u_m < \ldots$, with probabilities $p_1, p_2, \ldots, p_m, \ldots$. This implies that the probability that $X \leqq u_1$ is p_1; the probability that $X \leqq u_2$ is $p_1 + p_2$; and so forth. (ii) X is a continuous variable capable of assuming any value x out of a finite or infinite interval $a < x < b$.

In both cases the problem is solved by using an approximating discrete variable Y that may occasionally coincide with X. We select a substantial integer number N such that any errors not exceeding $1/N$ in the probabilities may be neglected. $N = 10{,}000$ is a frequent choice. Dealing first with case i, we replace each probability p_i by its rational approximation,

$$q_i = \frac{N_i}{N} \qquad i = 1, 2, \ldots, m, \ldots ,$$

where N_i is an integer selected so that $|p_i - q_i| < 1/N$ and also $\Sigma q_i = 1$. If all the p_i are rational numbers, it may happen that $q_i = p_i$ for all i. If this is so, then $Y \equiv X$. Whatever the situation, we define Y as the random variable capable of assuming the values $u_1, u_2, \ldots, u_m, \ldots$, in principle the same as those for X but with probabilities $q_1, q_2, \ldots, q_m, \ldots$, respectively. It may happen that some of the q_i equal zero. Then the corresponding values of X will not actually be possible values of Y.

Our next step is to refer to the published tables[4] of random sampling numbers. Each of these tables contains a sequence of "random digits," each digit obtained by a more or less perfect procedure imitating the process of selecting one of the numbers 0, 1, 2, 3, 4, 5, 6, 7, 8, 9, with the same probability 1/10 and so that each selection is independent of the outcomes of the preceding selections. The latter requirement is very difficult to achieve in practice. The words "random digits" are printed in quotation marks in order to emphasize the philosophical point that, once the numbers are printed or punched on cards, there is nothing random about them, just as there is nothing random about the sequence of digits representing the square root of 2. However, if due care is taken in preparing a set of "random digits," then their use appears to imitate satisfactorily the successive outcomes of random experiments.

Thus, in order to obtain successive outcomes of independent observations on the approximating variable Y, with $N = 10{,}000$, we open up a set of random digits at any page and treat the groups of four digits as integer numbers, $y = 0001, 0002$ up to 9999 and, finally, 0000, which we shall regard as 10,000. Also, we shall agree that the "observation" of a number y that is between the limits $0001 \leqq y \leqq N_1$ is equivalent to observing $Y = u_1$. Similarly, if we observe a value y between the limits $N_1 < y \leqq N_1 + N_2$, we shall consider it equivalent to observing $Y = u_2$, and so forth. Thus, if

$$\sum_{i=1}^{k} N_i < y \leqq \sum_{i=1}^{k+1} N_i ,$$

then this is interpreted as an observation of Y equal to u_{k+1}. Since, with a good table of random digits, the probability of "observing" any integer y between 0001 and 10,000 inclusive is equal to 1/10,000, it is obvious that, with the above agreement, we have $P\{Y = u_i\} = q_i$. Furthermore, if the table is satisfactory, then the successive observations of Y will be substantially independent.

In case ii we proceed in a similar manner. We begin by dividing the interval (a, b) of the variation of X into a substantial number of relatively small partial intervals. One possible way of doing this is to divide (a, b) into N subintervals (a_i, a_{i+1}) such that $P\{a_i < X \leqq a_{i+1}\} = 1/N$ for $i = 1, 2, \ldots, N$. In each subinterval we select arbitrarily a number u_i such that $a_i < u_i < a_{i+1}$; and we define Y to be the variable capable of assuming the values $u_1, u_2, \ldots, u_N$, each with the same probability $1/N$. Then we use the sets of random digits and carry out the "observations" of Y as in case ii.

It will be noticed that the intervals (a_i, a_{i+1}) as described above will ordinarily be of different lengths. According to the availability of tables, it is occasionally more convenient to use intervals (a_i, a_{i+1}) all of the same length. This, of course, would imply that the probabilities $P\{a_i < X \leqq a_{i+1}\}$ will have different values.

[4] L. H. C. Tippett, *Tracts for Computers*, No. 15 (1927); and M. G. Kendall and B. Babington Smith, *Tracts for Computers*, No. 24 (1939) (Cambridge: At the University Press).

IV. CONSTRUCTION OF THE IDEALIZED SYNTHETIC PLATE

In the present section we describe certain details regarding each particular step in the construction of the synthetic plate. Each step corresponds to a particular source of random variation involved in the probabilistic model as enumerated in Section II.

a) The number of clusters contributing galaxies to the 6° × 6° solid angle to be covered by the synthetic plate.—For brevity, we adopt the symbol ω to denote the $6^\circ \times 6^\circ$ solid angle that is to be covered by the synthetic photograph. According to the model, no matter where the center of a cluster may be, the cluster may still contribute galaxies to the solid angle ω. Since it is impossible to use sampling experiments to distribute cluster centers over the entire infinite space, it was necessary to limit the sampling to some bounded region. This is possible because of the obvious fact that the farther the cluster center is from ω, the smaller the probability that this cluster will contain galaxies falling within ω.

Considerations of this kind showed that, for purposes of constructing the synthetic plate, the process of distributing cluster centers by sampling experiments may be limited to a bounded region Ω^* defined as follows: For every number k of degrees we use the

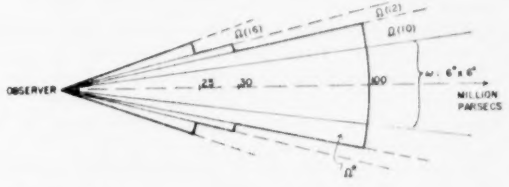

FIG. 1.—Schematic representation of regions $\Omega(k)$, Ω^*, and ω

symbol $\Omega(k)$ to denote the $k^\circ \times k^\circ$ solid angle with the same axis and orientation as ω. Then Ω^* is defined to contain (i) the part of $\Omega(16)$ extending to the distance of 25 million parsecs from the observer, plus (ii) the part of $\Omega(12)$ extending from 25 to 30 million parsecs from the observer, and (iii) the part of $\Omega(10)$ extending from 30 to 100 million parsecs. The situation is illustrated schematically in Figure 1.

The possibility that clusters centered outside Ω^* may contribute galaxies to the solid angle ω was not entirely ignored. Preliminary calculations indicated that the contribution to ω from the clusters outside Ω^* but at distances less than 100 million parsecs is negligible; and this contribution was consequently ignored. On the other hand, the calculations show that we can expect that about 80 clusters centered in $\Omega(10)$ but beyond Ω^* will contribute visible galaxies to $\Omega(10)$. However, a negligible number of these clusters will contribute more than one visible galaxy. Consequently, in order to allow for the contribution to ω of the clusters centered beyond Ω^*, a total of 80 single galaxies were randomly distributed on the projection of $\Omega(10)$ on the plane of the photographic plate. The determination of the apparent magnitudes of these single galaxies required a special method, explained below. As a result of these modifications, the galaxies on the synthetic photograph taken over ω belong either to clusters having their centers in Ω^* or to "distant" clusters with centers in $\Omega(10)$ but beyond Ω^*.

Strictly speaking, specialization *a* of Section II requires that the number, γ, of clusters centered in Ω^* be treated as a Poisson random variable, with expectation estimated to be 1.63043×10^{-19} clusters per cubic parsec *times* the volume of Ω^*. This would imply just one random selection of γ in accordance with the appropriate Poisson distribution. However, the effect of random machinery is significant only if this machinery is allowed to operate repeatedly. In the present circumstance, with only one value of γ required, it was decided to select this value in a nonrandom fashion to be exactly equal to its expectation, namely, 1702.

b) *The positions of the cluster centers in* Ω^*.—In accordance with specialization *b* of Section II, three series of sampling experiments were performed to determine the three co-ordinates of each of the $\gamma = 1702$ cluster centers assumed to be contained in Ω^*.

c) *The number of galaxies belonging to a given cluster.*—The next step is to determine the number, ν, of galaxies to be assigned to each of the clusters centered in Ω^*. This required that another series of 1702 random experiments be carried out in conformity with part *c* of Section II.

d) *The position of a galaxy within a cluster.*—After the number of galaxies for each of the clusters in Ω^* was determined, it was necessary to "observe" three sequences of random digits for each galaxy, in order to determine its three co-ordinates with respect to its cluster center. This sampling was facilitated by the availability of tables[5] of random normal deviates giving the co-ordinates directly in σ-units.

e) *The apparent magnitude of a galaxy.*—The next step in the construction of the synthetic plate is the determination of the apparent magnitude of each galaxy falling within the solid angle ω. Two procedures were used, one for galaxies belonging to clusters centered in Ω^* and another for the visible galaxies belonging to the "distant" clusters centered in $\Omega(10)$ but beyond Ω^*.

The results of steps *b* and *d* determine the distance ξ from the observer of any galaxy attached to a cluster centered in Ω^*. Thus, in order to determine the apparent magnitude of any such galaxy, it was sufficient to obtain a value of $M - M_0$ from a table of random normal deviates, add $M_0 = -14.2$, and then substitute the value of M in formula (1).

However, the distance from the observer to galaxies belonging to "distant" clusters was not determined. For this reason, the apparent magnitudes of those galaxies that happened to fall within ω (29 of the 80) was obtained by sampling from a special conditional distribution derived on the assumptions that (i) the cluster center is at a distance greater than 100 million parsecs and (ii) the apparent magnitude of the galaxy is less than or equal to 18.3.

Step *e* completes the sampling procedures that relate to the galaxies in space. Any galaxy with apparent magnitude exceeding 18.3, the presumed extreme limiting magnitude, was discarded as "invisible," and each of the remaining galaxies was plotted to produce the distribution of galaxies on the idealized synthetic plate. Because of the great number of galaxies, the plotting was cumbersome and had to be done in parts. First, and also in order to show the effect of chance variation, the original sample of clusters (obtained in step *a*) was divided at random into five equal parts to be plotted separately. Then in each part the cluster centers were arranged according to distance into six zones, and the galaxies from clusters with centers in each zone were plotted separately. For purposes of illustration, 6 out of the total of 30 plots are shown in Figure 2. Two (out of the 5) partial plots for the nearest distance zone, 0–25 million parsecs, are given in Figure 2, *a* and *b*. Similarly, Figure 2, *c* and *d*, gives two partial plots for the third zone, 30–35 million parsecs, while Figure 2, *e* and *f*, gives two of the plots for the fifth zone, 40–60 million parsecs. However, only those galaxies belonging to clusters with their centers within $\Omega(10)$ are plotted in Figure 2. Each symbol represents a galaxy. In order to facilitate the separation of the several clusters located at different distances within the same zone, a further division into five subzones was used in each zone with five symbols: the larger the symbol, the closer the cluster to which the galaxy belongs.

The $6° \times 6°$ idealized synthetic plate was obtained by superposition of the central parts of the 30 plots exemplified in Figure 2 plus the contributions from clusters centered outside Ω (10). Figure 3 reproduces the result. Here again each symbol represents a galaxy, and the size of the symbol characterizes the distance from the observer to the corresponding cluster center: 0–30, 30–40, and >40 million parsecs.

It is interesting to note that all the plots making up Figure 2, particularly the plots

[5] P. C. Mahalanobis, *Sankhyā*, **1**, 1, 1933; and H. Wold, *Tracts for Computers*, No. 25 (Cambridge: At the University Press, 1948).

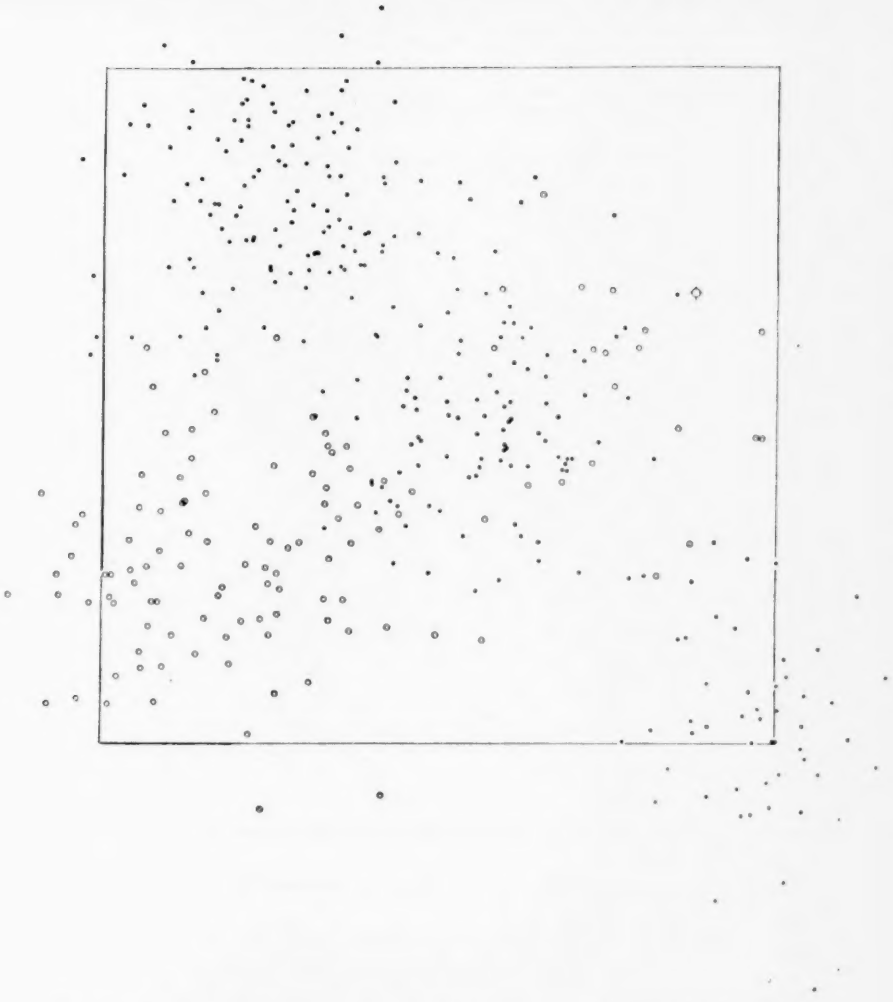

FIG. 2*a*.—Construction of the synthetic plate. Visible ($m \leqq 18.3$) galaxies belonging to clusters centered in a $10° \times 10°$ square. The plot is one of the five partial plots used in the construction for each distance zone. Size of symbol denotes a subdivision of distances to the cluster centers within each zone. The larger the symbol, the closer the cluster to which the designated galaxy belongs.

One of the five plots for distance zone 0–25 million parsecs.

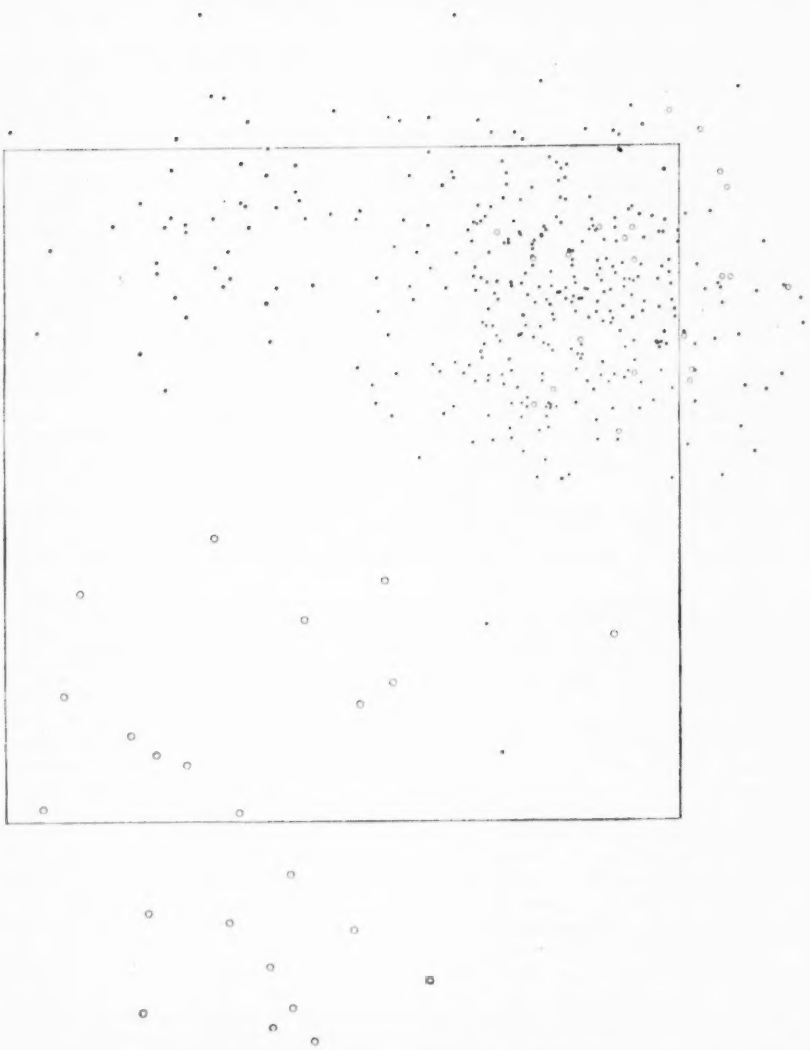

FIG. 2*b*.—Another of the five plots for distance zone 0–25 million parsecs

corresponding to medium distance zones, show clearly discernible groupings of galaxies. However, some of the groupings that may be interpreted as single clusters are, in reality, combinations of two or more separate clusters. Another interesting feature of Figure 2 is the change in the appearance of the clusters as they become more distant: they become more compact, owing to perspective, but also the number of *visible* members decreases, owing to the increase in apparent magnitude with distance. Thus, as the distance to the

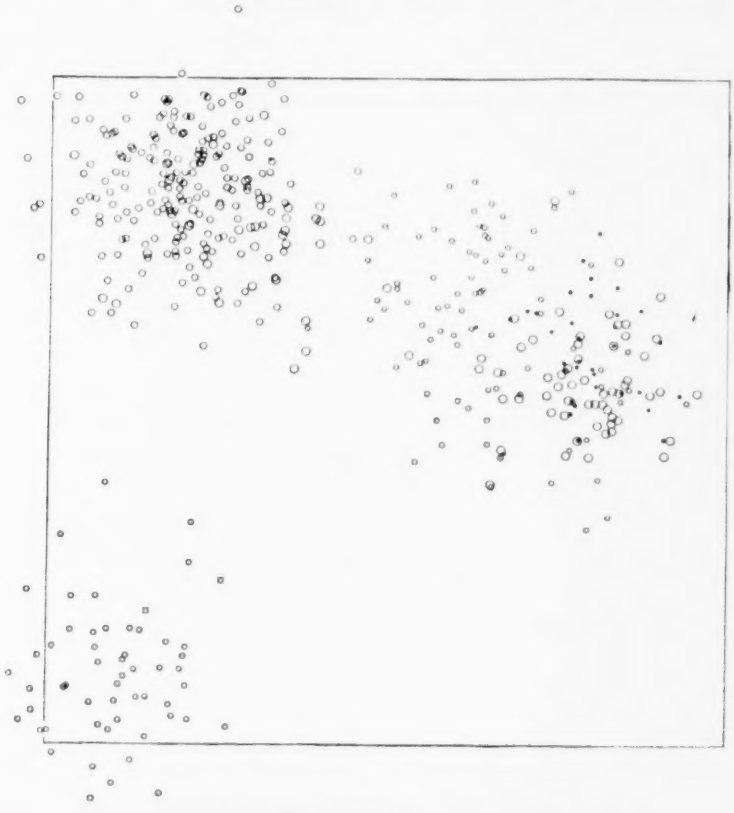

FIG. 2*c*.—One of the five plots for distance zone 30–35 million parsecs

center of the cluster increases, the observable clustering effect first increases, comes to a maximum, and eventually decreases.

Turning to Figure 3, we see that the detailed groupings that were more or less discernible in Figure 2 disappear and the single clusters of galaxies sink into an irregular background. At the same time, a contrary phenomenon is observable. In different sections of Figure 3 one distinguishes rather regular chains of galaxies, similar to the star chains observable on actual photographs. The regularity of these chains may suggest some physical connection among the component galaxies. In a number of instances the galaxies forming chains on the synthetic plate were traced back to their clusters, and al-

most invariably each galaxy was found to belong to a different cluster. Thus, in spite of their regularity, the evidence is that the chains on the synthetic plate result from purely random superposition of the images of more distant and of near-by clusters. It may be presumed that a similar conclusion applies to actual photographs.

A final remark relating to Figure 2 is concerned with the difference in appearance between the two parallel plots of galaxies referring to the same zone. We should emphasize

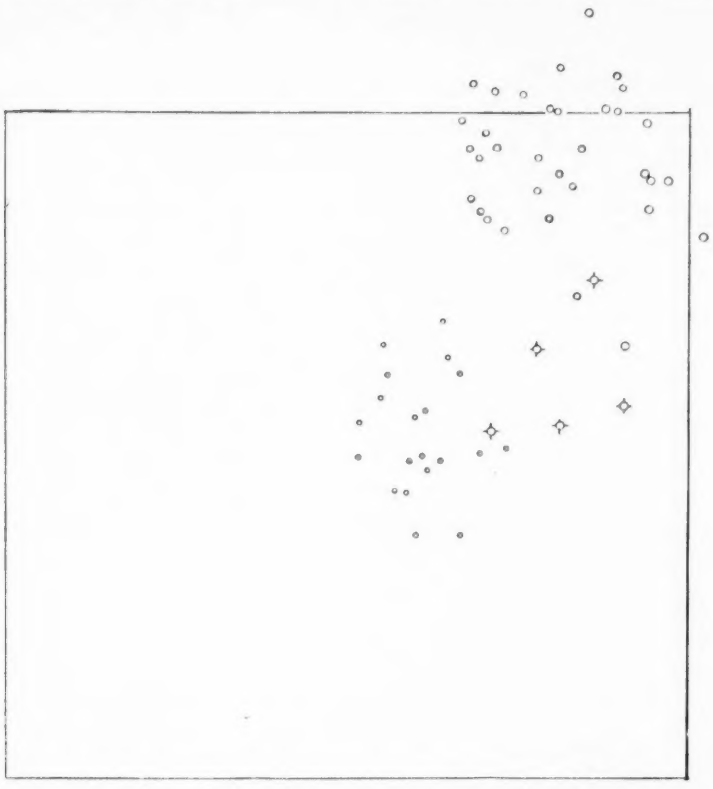

FIG. 2*d*.—Another of the five plots for distance zone 30–35 million parsecs

that each plot in a pair was constructed by exactly the same method, so that the differences between them are due to chance only. These differences combine to produce the variation in the density of galaxies over the final idealized plate of Figure 3. The conclusion is that if the model of the spatial distribution of galaxies is reasonably related to fact, then a substantial part of the variation observed from one actual plate to the next is due to random causes.

The image of the idealized synthetic plate exhibited in Figure 3 is not directly comparable to any possible reproduction of a real plate. One reason is, of course, that on a real plate there is no positive way to distinguish the galaxies from near-by and from more distant clusters. On the other hand, a real plate involves some differentiation of

galaxies according to their brightness. Another reason for the noncomparability of Figure 3 with a reproduction of a real plate from the collection at the Lick Observatory is that the limiting magnitude is not constant in the latter plates and, most frequently, is less than 18.3. Thus the idealized synthetic plate contains too many galaxies.

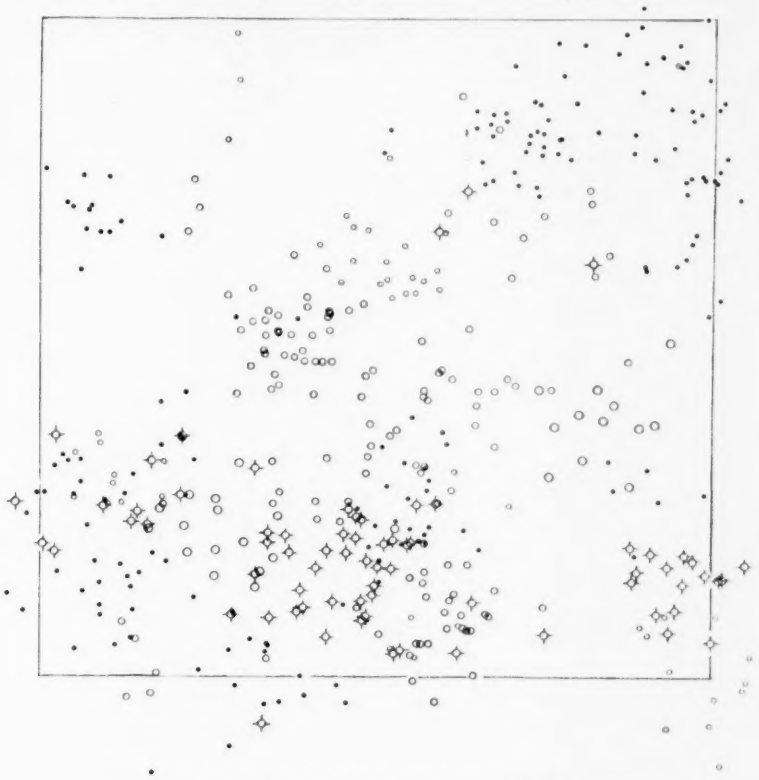

FIG. 2*e*.—One of the five plots for distance zone 40–60 million parsecs

V. OBSERVATIONAL FACTORS INFLUENCING THE DISTRIBUTION OF GALAXIES ON A PLATE

In the present section we deal with modifications to which the idealized plate must be subjected in connection with several factors arising in the observations and affecting the appearance of any actual photographic plate. The first factor to be considered is (*a*) the variation of the limiting magnitude from one part of the plate to another. This factor is not included in the probabilistic model of Papers I and II, and its treatment is entirely empirical in character. The other factors are lumped together into a single hypothetical factor (*b*) labeled "error in counting." On this point Paper II contains two alternative probabilistic models. Only the second of these models is used in the present paper.

a) Variation of the limiting magnitude over the plate.—A study by Shane[6] of the counts

[6] C. D. Shane and C. A. Wirtanen, in preparation.

of galaxies on the photographic plates taken for this survey indicated that the limiting magnitude at a given point on the plate may be approximated by a simple formula. Let the origin of co-ordinates be at the center of the plate with the Ox-axis directed east and the Oy-axis north. Let $m_1(x, y)$ denote the limiting magnitude of the plate at the point

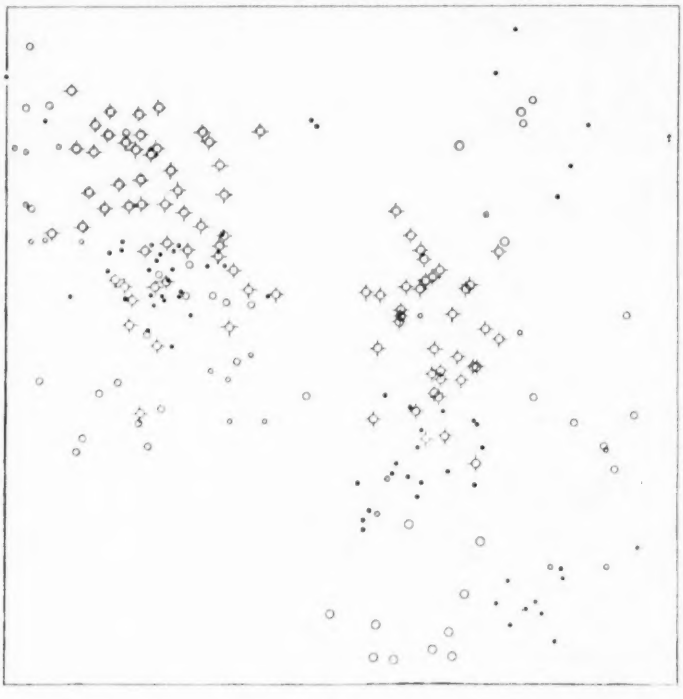

FIG. 2*f*.—Another of the five plots for distance zone 40–60 million parsecs

(x, y), $-3 \leqq x, y \leqq 3$. Then

$$m_1(x, y) = 18.2 - 0.00034 \exp 1.7 \sqrt{(x^2 + y^2)} + 0.031x, \tag{2}$$

where the constant 18.2 is the presumed extreme limiting magnitude of the center of the plate, the middle term represents the effect of increasing distance from the plate center, while the last term gives the little-understood but pronounced "east-west effect."

In order to bring the idealized plate of Figure 3 closer to the conditions of actual observations, it was necessary to subject it to modifications dictated by the variation in limiting magnitude recognized to be present in each actual plate. This was done in two steps. First, we used formula (2) to represent the nonrandom changes in the limiting magnitude over the plate. Next we assumed that the limiting magnitude of any plate—and this includes the synthetic plate—exhibits local random deficiencies below the level implied by formula (2). The effect of these local random deficiencies in the limiting magnitude is dealt with in subsection *b* below.

Figure 4 was obtained from Figure 3 by giving effect to the nonrandom variation over

FIG. 3.—$6^{\circ} \times 6^{\circ}$ idealized synthetic plate. Limiting magnitude $m_1 = 18.3$. Each symbol represents a visible galaxy. *Large circles:* cluster centers 0–30×10^6 parsecs distant; *small circles:* cluster centers 30–40×10^6 parsecs distant; *dots:* cluster centers $>40 \times 10^6$ parsecs distant.

the plate. The apparent magnitude of each galaxy was compared with the limiting magnitude $m_l(x, y)$ at its position (x, y) on the plate. All those galaxies in Figure 3 with apparent magnitudes greater than the limiting magnitude were omitted in plotting Figure 4. As usual, each symbol represents a visible galaxy, but now the size of the symbol indi-

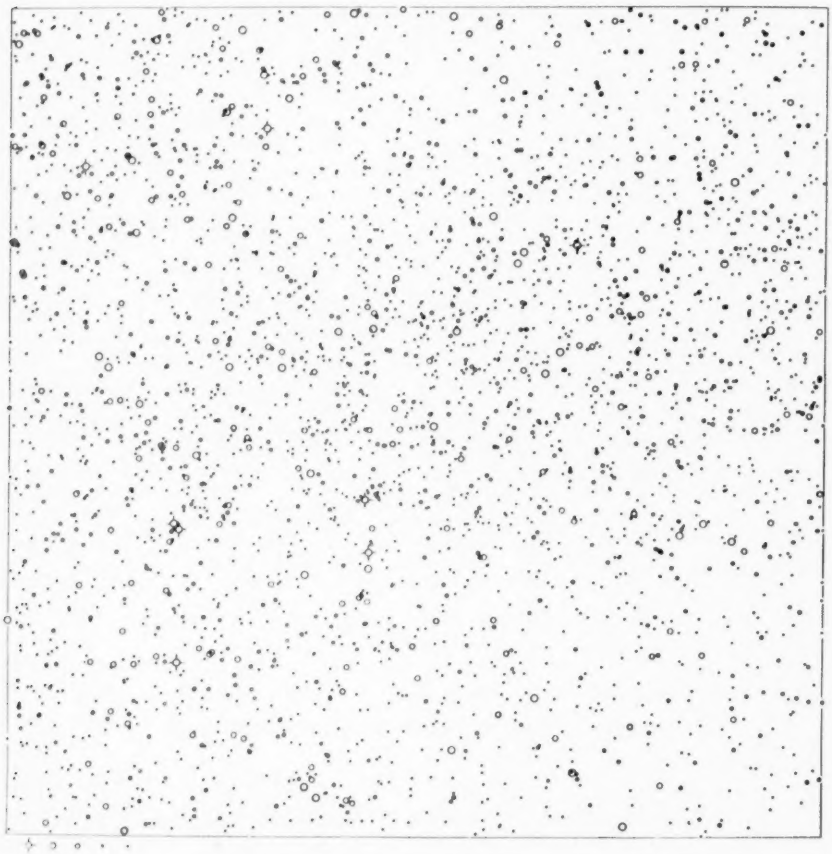

FIG. 4.—6° × 6° synthetic plate with varying limiting magnitude. Each symbol represents a galaxy, and symbol size denotes difference between apparent magnitude m and local limiting magnitude m_l. In decreasing symbol size: $m_l - 5 < m \leqq m_l - 4$; $m_l - 4 < m \leqq m_l - 3$; $m_l - 3 < m \leqq m_l - 2$; $m_l - 2 < m \leqq m_l - 1$; $m_l - 1 < m \leqq m_l$.

cates the difference between the apparent magnitude m of the galaxy and the limiting magnitude m_l appropriate for the position of this galaxy. The largest symbol indicates $m_l - 5 < m \leqq m_l - 4$; the next, $m_l - 4 < m \leqq m_l - 3$; and so forth.

b) *Random "errors of counting."*—The appendix to Paper II gives a probabilistic model of the complex variation in counts of galaxies made in the same 1° squares on two overlapping plates. The sources of this variation include variations in the emulsion (as mentioned in subsection *a* above), errors in distinguishing galaxies from stars, etc. The error

model postulates that to each 1° square there corresponds a probability, δ, that a galaxy will be counted. Also, the counting of one galaxy is independent of any other. The probability δ is itself a random variable, independent from one square to the next, whose probability density was approximated from counts on overlapping squares. The estimated density of the probability δ evaluated at any point d between 0 and 1 is

$$\frac{d^{\alpha-1}(1-d)^{\beta-1}}{B(\alpha, \beta)},$$

with $\alpha - 1 = 3.12256$, $\beta - 1 = -0.34479$, and $1/B(\alpha, \beta) = 1.7907$.

Using this density, a new sampling experiment was performed to obtain 36 values of δ for the $1^\circ \times 1^\circ$ squares on the synthetic plate. However, it seems unrealistic to assume that the same value of δ, obtained from the sampling experiment, applies to each of the $10' \times 10'$ cells within a 1° square and then changes to another value corresponding to the next $1^\circ \times 1^\circ$. For this reason, it was postulated that the probability that a galaxy in a $10' \times 10'$ cell will be counted changes gradually from one such cell to the next in such a way that the average of the δ's corresponding to the particular $10' \times 10'$ cells within a given 1° square approximately equals the corresponding sampled value of δ.

In conformity with this assumption, a smooth surface was fitted to the 36 sampled values of δ corresponding to the same number of 1° squares within the plate. Then the value of δ was read from this surface separately for each $10' \times 10'$ cell. The 1296 values of δ so obtained were used to perform the last sampling experiment leading from Figure 4 to the final synthetic plate exhibited in Figure 5.

Figure 5 contains only such galaxies in Figure 4 as were "counted" by a hypothetical astronomer inspecting Figure 4. In order to decide whether or not a given galaxy is "counted," reference was made to the value of δ for the $10' \times 10'$ cell containing the galaxy. This value of δ was used to perform a simple sampling experiment with only two possible outcomes: "counted," with probability δ, and "not counted," with probability $1 - \delta$. The symbols used in Figure 5 have the same meaning as in Figure 4, that is, the larger the symbol, the brighter (apparently) the galaxy with respect to the limiting magnitude of the plate.

Figure 5 represents, then, the final outcome of the sampling experiment and is ready to be compared with the reproduction of an actual plate. This is given in Figure 6, facing Figure 5, and also in Figure 7. Comments on Figures 6 and 7 are given in Section VI.

VI. COMPARISON OF SYNTHETIC AND ACTUAL PLATES

The visual appearance of the distribution of galaxies on an actual photographic plate is confounded by the presence of star images, so that, when comparing the actual plate with the synthetic plate, these star images should be removed. Furthermore, the appearance depends strongly on the total number of galaxies present. Since the number of galaxies counted on actual plates varies substantially from one plate to another, even if these plates are restricted to the region near the galactic pole, in order to obtain a fair comparison with the synthetic plate, it is advisable to choose the actual plate for which the total number of galaxies counted agrees approximately with 2725, the number of galaxies "counted" on the synthetic plate. However, the choice of the actual plate should be made without regard to any other characteristic that it may exhibit.

The best agreement on total count is provided by the photograph centered at $\alpha = 14^h40^m$, $\delta = +5^\circ$, for which the first count (April, 1950) was 2813 galaxies. In order to obtain a representation of the selected plate with the star images removed, the co-ordinates of each galaxy on the plate were measured and its position plotted as shown in Figures 6 and 7. In constructing Figure 6, care was taken as far as possible to place in each $10' \times 10'$ cell the same number of galaxies as were recorded in the original counts. This process necessitated omitting from the plot some galaxies that were apparently

missed on the first count and including some very doubtful objects in order to make up, whenever possible, the required number for each cell. The galaxies are represented on Figure 6 by three different symbols based on rough estimates of brightness on an arbitrary scale.

The plate was charted independently a second time without reference to the original counts. The resulting plot is shown in Figure 7. Comparison of Figures 6 and 7 indicates that the unavoidable errors in counting do not influence the general appearance of the plots.

Now the synthetic plate of Figure 5 can be compared with the chart of an actual plate, either in Figure 6 or in Figure 7. Naturally, because of random variation of various sources affecting all plates, no identity can be expected, and the comparison must be limited to the general appearance.

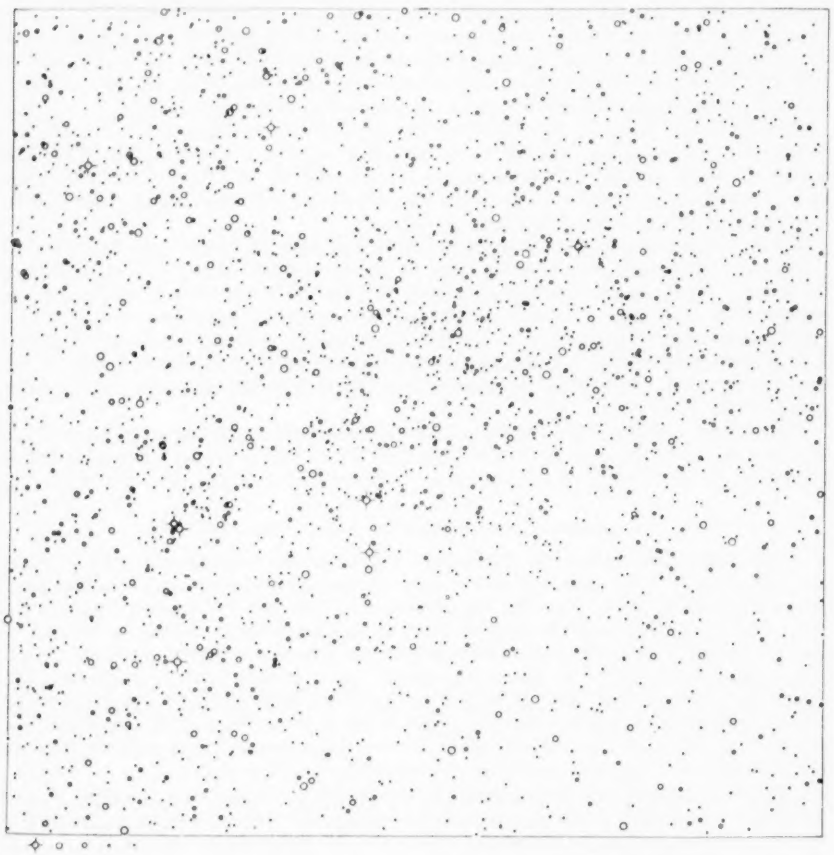

FIG. 5.—Final synthetic plate, including effects of varying limiting magnitude and errors in counting. Each symbol represents a galaxy, and symbol size denotes difference between apparent magnitude m and local limiting magnitude m_1. In decreasing symbol size: $m_1 - 5 < m \leqq m_1 - 4$; $m_1 - 4 < m \leqq m_1 - 3$; $m_1 - 3 < m \leqq m_1 - 2$; $m_1 - 2 < m \leqq m_1 - 1$; $m_1 - 1 < m \leqq m_1$.

The synthetic and actual plates do present many similar features; many of the chains, swirls, and other patterns appearing on the actual plates can also be found somewhere on the synthetic plate. But let us return to the original question asked: If the galaxies occur only in clusters as postulated in the model, then why do the actual plates exhibit so few clearly defined clusters? Examining both the synthetic and the actual plates with this question in mind, we find, perhaps unexpectedly, that even though the synthetic distribution was constructed from clusters, these clusters are not any more discernible on the synthetic plate than they are on the actual plate. In fact, while the general appearance of the plates is about the same, the actual plate suggests even greater clumpiness of the distribution of galaxies than does the synthetic plate. On the actual plate the gaps between the conglomerations of galaxies appear larger, and also some of the conglomerations seem denser.

This apparent excess of clustering in the actual plate over the synthetic plate raises

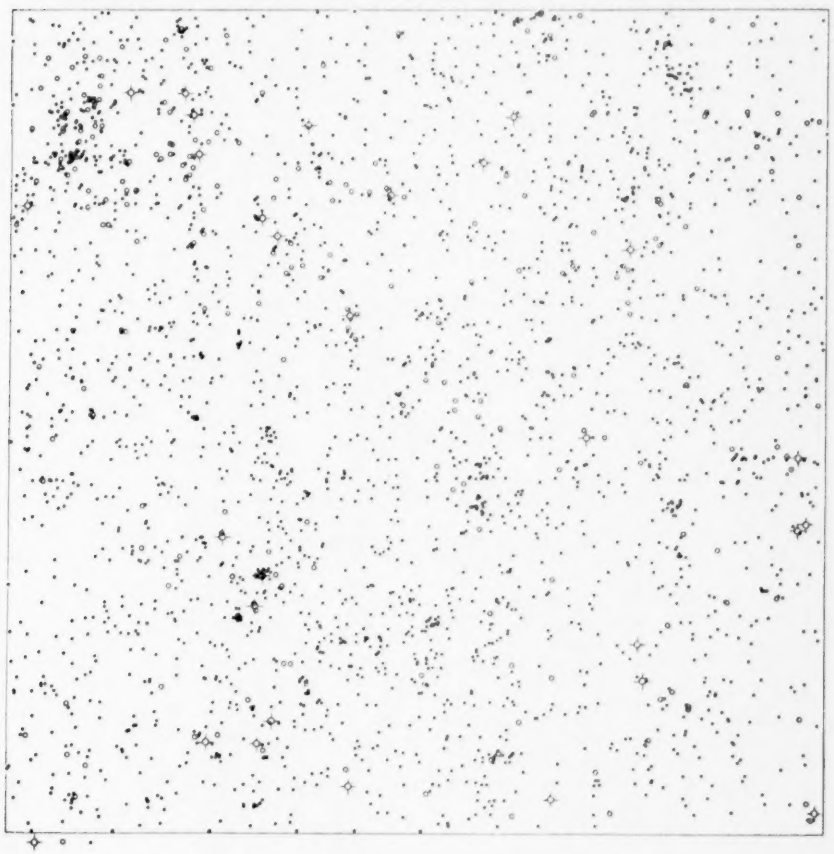

FIG. 6.—Reproduction of actual plate showing galaxies only and with reference to original counts. Plate centered at $\alpha = 14^h40^m$, $\delta = +5°$. Size of symbol indicates rough estimate of brightness on an arbitrary scale.

several questions. One is whether or not the difference may be ascribed to chance variation only. The other question, of a different nature, refers to the possibility that the apparently empty places on the actual plate may be the effect of small absorbing clouds in our galaxy. Efforts were made to investigate both these problems.

In order to study the seeming tendency for more apparent clustering of galaxies on the actual plate, the distribution of the number of galaxies per $10' \times 10'$ cell was obtained for the synthetic plate and for 16 actual plates. These 16 plates were selected out of the collection available because their apparent limiting magnitude was approximately equal to the average for the collection (as indicated by comparison with overlapping plates) and also because their total count of galaxies was not very different from 2725, the number "counted" on the synthetic plate.

The relative frequencies of cells containing 0, 1, 2, . . . , galaxies are exhibited in Table 1. Figure 8 gives a graph of this distribution for the synthetic plate (*dashed curve*) and of the average distribution on the 16 actual plates (*solid curve*). To each point on the

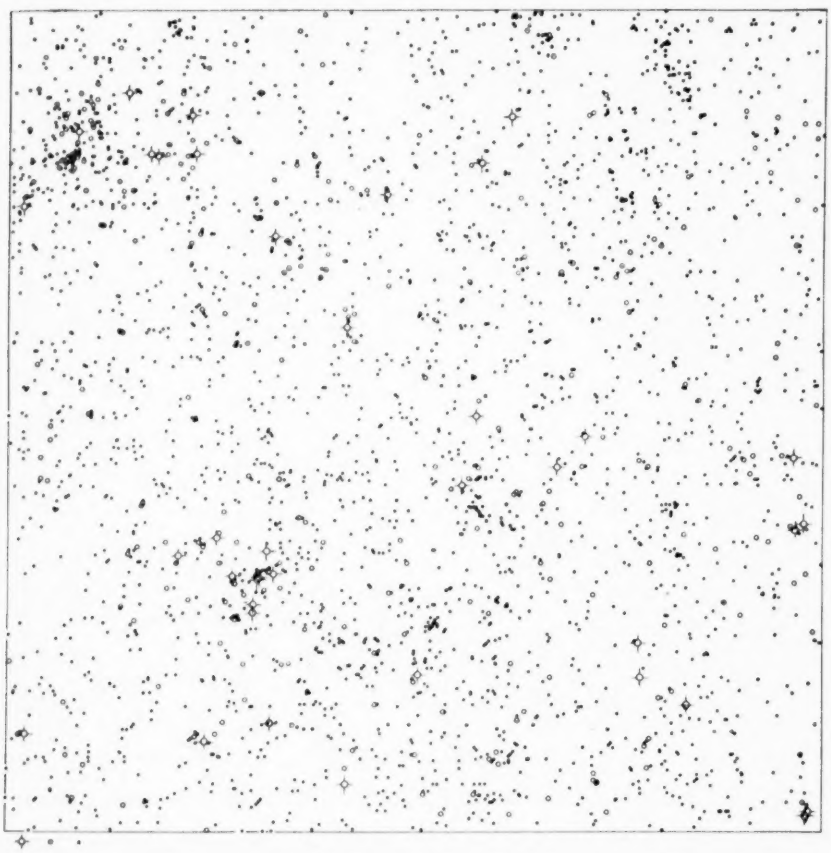

FIG. 7.—Reproduction of actual plate. Same plate as in Fig. 6 but recharted without referring to original counts.

TABLE 1

RELATIVE FREQUENCY OF 10′ × 10′ CELLS CONTAINING 0, 1, 2, . . . , GALAXIES

Plate:																		
α	$12^h\ 00^m$	$12^h\ 20^m$	$12^h\ 20^m$	$12^h\ 20^m$	$12^h\ 40^m$	$12^h\ 40^m$	$13^h\ 00^m$	$13^h\ 20^m$	$13^h\ 40^m$	$14^h\ 00^m$	$14^h\ 00^m$	$14^h\ 20^m$	$14^h\ 20^m$	$14^h\ 40^m$	$14^h\ 40^m$	$14^h\ 40^m$	AVERAGE OF 16 ACTUAL PLATES	SYNTHETIC PLATE
δ	$+20°$	$+15°$	$+10°$	$+5°$	$+10°$	$0°$	$+5°$	$+10°$	$+20°$	$+20°$	$+10°$	$+10°$	$0°$	$+20°$	$+15°$	$+10°$		
No. of galaxies:																		
0	0.231	0.160	0.118	0.196	0.248	0.231	0.179	0.234	0.248	0.194	0.208	0.234	0.220	0.132	0.180	0.220	0.202	0.146
1	.303	.265	.256	.316	.326	.312	.278	.330	.295	.323	.310	.334	.294	.282	.260	.300	.299	.273
2	.221	.216	.225	.222	.196	.180	.215	.191	.208	.218	.221	.201	.201	.231	.236	.222	.213	.245
3	.115	.143	.153	.120	.113	.129	.163	.108	.110	.117	.126	.095	.123	.147	.147	.110	.126	.149
4	.057	.086	.103	.065	.060	.060	.072	.057	.059	.070	.062	.054	.069	.093	.074	.076	.070	.108
5	.037	.049	.055	.035	.026	.033	.039	.040	.032	.031	.035	.034	.035	.042	.040	.028	.037	.042
6	.015	.037	.035	.022	.015	.017	.028	.012	.023	.022	.015	.014	.025	.029	.020	.016	.022	.023
7	.008	.019	.019	.010	.008	.020	.008	.012	.008	.015	.012	.015	.017	.016	.020	.009	.014	.008
8	.005	.012	.009	.004	.004	.005	.005	.006	.006	.004	.005	.009	.005	.008	.010	.006	.006	.003
9	.005	.005	.007	.005	.002	.006	.005	.002	.005	.001	.004	.002	.005	.008	.002	.005	.004	.001
10	.002	.002	.007	.002	.0	.003	.003	.001	.004	.003	.001	.002	.002	.004	.002	.003	.003	.002
>10	0.0	0.007	0.013	0.004	0.002	0.004	0.005	0.007	0.004	0.002	0.003	0.005	0.005	0.008	0.009	0.003	0.005	0.0

latter curve there is attached a vertical interval indicating the range of the 16 observed frequencies.

Table 1 shows that the synthetic plate differs from most of the actual plates in several respects. On the synthetic plate the densest cells have only 10 galaxies each, whereas on 15 of the 16 actual plates the maximum number of galaxies per cell is higher, reaching 30 on one plate. This difference is exhibited graphically by the tail of the frequency-curve in Figure 8. At the same time, the synthetic plate possesses fewer cells with zero galaxies. These facts indicate that the apparent difference in the degree of clustering may be real.

Looking at Figure 8, we notice another feature that may also suggest an essential difference between the model and the facts. The two distributions differ systematically, with the curve corresponding to the average actual distribution running below that corresponding to the synthetic distribution over a considerable range. If the two graphs corresponded to two sets of *independent* observations on some integer-valued random variables, then this systematic difference in frequencies would certainly indicate an essential difference in the two distributions. Also, this difference could be established beyond doubt by an appropriate statistical test. However, in the present case the number of galaxies in one $10' \times 10'$ cell is certainly *not* independent of the number in the next. This circumstance makes all the existing tests for identity of the distributions inapplicable. Also, because of this circumstance, the systematic difference between the two curves in Figure 8 may be due to random fluctuations. In order to illustrate this latter point, Figure 9 was constructed to picture the frequencies of $10' \times 10'$ cells, with 0, 1, 2, . . . , galaxies counted on two actual plates chosen at random, the third and the eighth, in Table 1. It is seen that the pair of curves in Figure 9 exhibits a systematic difference of nearly the same character as that in Figure 8 and over an even longer range. The conclusion is, then, that the systematic difference between the two curves in Figure 8 may easily be due to chance variation in the positions of the clusters (see Fig. 2) and does not indicate serious differences between the probabilistic model of Papers I and II and actual facts.

The question of whether the empty spaces between the conglomerations of galaxies, as noted on the actual plate in Figures 6 and 7, are due to small but dense galactic clouds is the subject of a separate study now in progress. At the present time it may be reported that a preliminary test indicates that this is not the case. This test is based on counts of stars made on two plates, one of which is the plate illustrated in Figures 6 and 7. The star counts were made in $4' \times 4'$ cells regularly spaced with $10'$ between centers. These counts were averaged separately for the entire $6^\circ \times 6^\circ$ plate and for each of the particular areas on the plate that contains "too few" galaxies. The averages exhibit only trivial nonsystematic differences. As another check, the distribution of $4' \times 4'$ cells containing 0, 1, 2, . . . , stars was compared with the Poisson distribution. The agreement was excellent, suggesting that the variation in the number of stars from cell to cell depends on no systematic cause.

VII. CONCLUSIONS

The general appearance of the synthetic plate gives a clear answer to whether or not the assumption that all galaxies occur in clusters is compatible with the rareness of clearly identified clusters that can be studied per se. A comparison of Figure 5 with Figure 2 indicates that the superposition of images of distant and near-by clusters tends to make these clusters unidentifiable.

A comparison of the synthetic and actual plates (Figs. 5 and 6 or 7) suggests that the clustering implied by the model may not be sufficiently intense to fit the observations in detail. This point may be brought out more clearly by a study of serial quasi-correlations of the number of galaxies counted in $10' \times 10'$ regularly spaced squares or by studying higher-order serial correlations. If confirmed, this circumstance will suggest the necessity for some change in the specialized model of Paper II reflected in the synthetic plate. One possibility is to reduce the numerical value of σ. A reduction to half the value used

here is not inconsistent with the results of Paper II. Another possibility, also consistent with Paper II, is to assume fewer clusters with more members in each. Still another possibility is to represent the internal structure of a cluster by a distribution more concentrated at the center than the trivariate normal distribution assumed here. A similar conclusion was reached by comparing the implications of the model with the observed structure of the Coma cluster. On the other hand, the Virgo cluster does not have this high central condensation, and similar clusters at any considerable distance could well escape detection. The assumed distribution may, therefore, represent an average that is

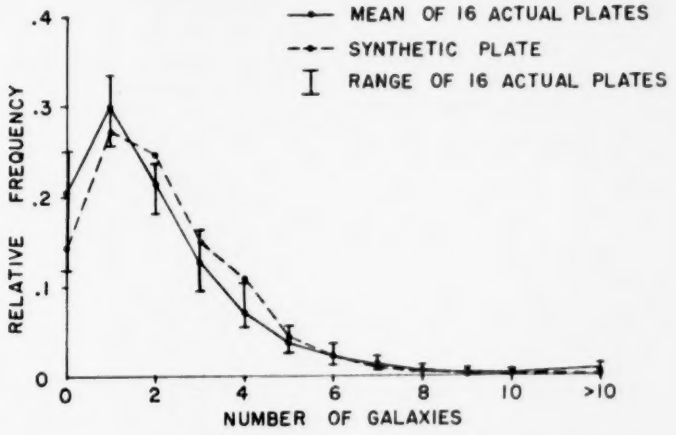

FIG. 8.—Relative frequency of 10′ × 10′ cells containing 0, 1, 2, . . . , galaxies. Comparison of synthetic plate with mean of 16 actual plates.

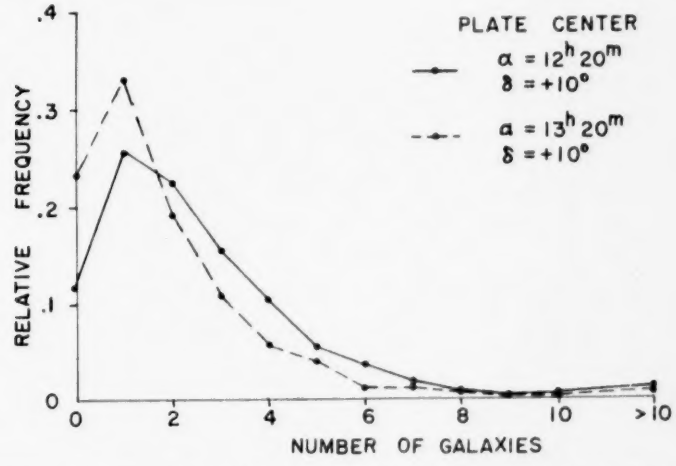

FIG. 9.—Relative frequency of 10′ × 10′ cells containing 0, 1, 2, . . . , galaxies. Comparison of two actual plates.

appropriate to a statistical discussion in the absence of more detailed information. In any case, a change in the form of the distribution of the co-ordinates of galaxies within a cluster would amount only to a change in an interpolation formula and would not affect the general model of Paper I.

In conclusion, we may say that the foregoing comparison of the synthetic and actual photographic plates does not provide any evidence against the general model of the spatial distribution of galaxies of Paper I. Even if the difference in local small-scale concentration on the synthetic and on the actual plate is real and not due to chance variation, the most that would be required to effect agreement is a change in an interpolation formula.

The authors are glad to acknowledge the valuable assistance of Mrs. Lorraine Keller, Mrs. Jeanne Lovasich, and Miss Lorraine Schwartz in carrying out the extensive sampling experiments and drawing the plots, which required a tremendous amount of care and attention. Also, they are indebted to Professor J. Neyman for his continued interest and for friendly discussions.

THE ABUNDANCE OF BERYLLIUM IN THE SUN

JESSE L. GREENSTEIN AND EINAR TANDBERG-HANSSEN*
MOUNT WILSON AND PALOMAR OBSERVATORIES
CARNEGIE INSTITUTION OF WASHINGTON
CALIFORNIA INSTITUTE OF TECHNOLOGY
Received August 10, 1953

ABSTRACT

The presence of lines of both neutral and ionized beryllium in the solar spectrum has been confirmed, and their intensities measured. Based on dependable f-values, the abundance ratios are found to be $Be/H = 10^{-10}$, $Be/Li = 8$, $Be/Ca = 6 \times 10^{-6}$. A striking excess of beryllium as compared with lithium is found in the sun. The *Be* abundance is about the same as on the earth or in meteorites. Thermonuclear disintegration of *Be* occurs rapidly at temperatures above 3.6×10^{6}° K. No processes are found that produce it. It is destroyed somewhat less rapidly than is *Li*. Convection or circulation mixing the atmosphere and the outer envelope would destroy *Li* and leave *Be* unaffected if it penetrated to layers at a temperature of 3.0 million degrees, but not above 3.6 million degrees.

THE PRESENCE OF BERYLLIUM IN THE SUN

Since beryllium is rapidly destroyed by thermonuclear reactions, its presence and abundance in the sun are of considerable interest. Lines of neutral and ionized beryllium have been previously identified in the sun, but their location in the crowded ultraviolet

TABLE 1

DATA ON BERYLLIUM LINES

No.	Element	λ_{lab}	Multiplet	E.P. (Volts)	f	$\lambda_{observed}$		W (mA)
						Rowland	G. and T.-H.	
1....	*Be* I	3321.013 (10) .086 (20)	$2^3P_0^\circ - 3^3S_1$ $2^3P_1^\circ - 3^3S_1$	2.71 2.71	0.034 .034	21.049 (−3*N*)	21.043 (−3)	6.6
2....	*Be* I	3321.347 (30)	$2^3P_2^\circ - 3^3S_1$	2.71	.034	21.366 (−3)	21.402 (21.352 (−3) 21.430 (−2))*	5.1
3....	*Be* II	3130.416 (50)	$2^2S_{1/2} - 2^2P_{3/2}^\circ$	0.00	.50	30.416 (1)	30.414 (3*d*)	79.9
4....	*Be* II	3131.064 (30)	$2^2S_{1/2} - 2^2P_{1/2}^\circ$	0.00	0.25	31.056 (1*N*)	31.058 (3*n*)	79.4

* This blending solar line seriously affects our measured wave length.

made remeasurement desirable. Spectrograms taken at the Hale Solar Laboratory were generously made available by Harold D. Babcock. High-contrast disk spectra at dispersions of 1.3 and 0.7 A/mm were used. The lines of *Be* II are strong, but those of *Be* I are only marginally visible. Three independent observers measured each of the three available plates without prior knowledge of the location of the *Be* I lines; the *Be* II lines were also measured. About ten near-by solar absorption lines were used as standards; the final wave lengths should be on a system close to that of the *Revision of Rowland's Table*. Table 1 gives the new measured solar wave lengths, together with the laboratory data, and our intensity measures.

A striking feature of our measures is that the *Be* II lines are found to be much stronger than the intensity estimates given in the *Revision of Rowland's Table*. H. D. Babcock has informed us that the older intensity scale in the far ultraviolet is somewhat erratic and generally low. The *Be* II lines, although λ 3130 is blended, are definitely present; λ 3131

* On leave from the Institute of Theoretical Astrophysics, Oslo, Norway, as Smith-Mundt-Fulbright scholar at the California Institute of Technology.

is essentially unblended and in a relatively clear portion of the spectrum. The two weaker *Be* I lines form an unresolvable blend, also in a relatively clear portion of the spectrum. The solar wave length agrees well with the mean of the two laboratory wave lengths, somewhat less well with a mean weighted by the expected intensities. On our best plate the Rowland line λ 3321.366 is resolved into two lines. The position of the shortward agrees well with the laboratory wave length of the strongest *Be* I line, λ 3321.347. We believe that *Be* I is definitely present in the solar spectrum.

In Table 1 we have numbered the lines for convenience. We will use line No. 1, a blend of two *Be* I lines, of fair quality and reliability, and line No. 4, of *Be* II, which is quite good. In our opinion the use, in addition, of the intensity measures of Nos. 2 and 3 would not increase the accuracy of the abundance determinations, because of the serious blending. The microphotometer tracings show this very clearly; line No. 3 is almost hopelessly blended with several strong lines. Lines Nos. 2 and 3 are important mainly as confirmation, by position and intensity, of the reality of the lines used.

INTENSITIES OF THE BERYLLIUM LINES

A number of H. D. Babcock's excellent plates of the ultraviolet solar spectrum are being analyzed by M. Minnaert and collaborators at the Utrecht Observatory. Their careful spectrophotometric work is based on the same type of material as was available to us here. We were fortunate in that Professor Minnaert kindly provided tracings, at a scale of 20 mm/A, of the two regions necessary for this study. While the entire ultraviolet apparent continuum of the sun is greatly depressed, the local depression near our lines is not particularly great. We have used the continuum as drawn by the Utrecht observers; it reaches 0.97 of the normal background, for example, near line No. 1; in contrast, for line No. 3 of *Be* II, which we did not use, it reaches only 0.50.

The *Be* II line used is slightly diffuse in appearance. Thermal Doppler broadening is the main source of line broadening, although there could be some Stark effect. The *Be* II line is on the flat part of the curve of growth; the *Be* I blend is unsaturated. Measured equivalent widths, W in milliangstroms, are given in Table 1 to one decimal place; but even our best lines have uncertainties of the order of 10 per cent. The measurements were made with respect to the near-by continuum and were corrected for the local depression of the latter from the "normal background" of the ultraviolet solar spectrum.

The oscillator strengths for the single-electron *Be* II system should be nearly hydrogenic; *Be* I is analogous to *He* I. Table 1 gives the f-values used. One of us (J. L. G.) estimated $f = 0.027$ for each of the *Be* I transitions, from the related *He* I lines. However, Dr. R. H. Garstang, of the Yerkes Observatory, very kindly computed $f = 0.034$, using the Coulomb approximation and the tables of Bates and Damgaard.[1] Garstang's value is preferable and has been used in our analysis. The uncertainty of the f-values should be small.

A few otherwise unidentified solar lines in the *Revision of Rowland's Table* are close to some *Be* I lines arising from a level at 5.2 volts. Some of these transitions are quite strong, $f \approx 0.3$. The population of that level is less by a factor of about 300, and the f-values are larger only by 10, so that the identification of these solar lines with highly excited *Be* I is doubtful.

ANALYSIS AND ABUNDANCE

The crowding of the solar ultraviolet spectrum is so great that normal methods of analysis cannot be applied. Blending of numerous weak lines and overlapping wings of strong lines establish a fictitious level of the continuous spectrum such that the effective opacity is much greater than that given by H^-; Dr. Guido Münch suggested that the rise toward the ultraviolet of his observed solar values of $k_\nu/\bar{k}$ justifies the use of $k_\nu = \bar{k}$

[1] *Phil. Trans. R. Soc., A*, **242**, 101, 1949.

FIG. 1.—Ultraviolet solar spectra by H. D. Babcock. Enlarged to scale 0.106A/mm, *Be* I; 0.068A/mm, *Be* II. Note the relatively favorable location of lines Nos. 1, *Be* I, and 4, *Be* II. The *Be* I line is only marginally visible.

in the 3100–3300 A region. Furthermore, since the observed solar $\bar{k}$ seems to be near 1.4 $\bar{k}$ (H^-), we will adopt $k_\nu = 1.4\ \bar{k}\ (H^-)$.

We cannot use the usual solar curve of growth, since the thermal motion for a light atom like *Be* is much larger than that of the metals used to define the empirical solar curve. The accepted value of the solar turbulence is also far below the thermal motion of *Be*. Consequently, we used a purely theoretical curve of growth,[2] based on the Milne-Eddington model, with a value $B^{(0)}/B^{(1)} = \frac{1}{3}$, which is close to the computed values (0.28 for *Be* II and 0.30 for *Be* I). We simultaneously reanalyzed in an identical fashion the material for the abundance of *Li*, based on earlier measures,[3] so that a direct comparison of *Be* and *Li* is possible; for *Li* I, $B^{(0)}/B^{(1)} = 0.60$. From the curve of growth we deduce the number of atoms in the particular lower level per gram of stellar material. From line No. 1 we obtain the sum of the populations of the excited levels $2^3\,P_1^o$ and $2^3\,P_0^o$ of *Be* I; line No. 4 gives essentially the total number of atoms of *Be* II, since $2^2\,S_{1/2}$ is the ground state, and excited states contribute very little. The excitation temperature, but not the kinetic temperature, is important for the determination of the amount of *Be* I, since the lines are on a straight-line curve of growth. The *Be* II line has $W/\Delta\lambda_D \approx 2.5$, and the concentration of *Be* II is therefore sensitive to the kinetic temperature.

We have analyzed the line intensities in two different ways. In the first we assume that the excitation, ionization, and thermal motion ($\Delta\lambda_D$) are dictated by the local temperature and that the lines of *Be* I and *Be* II and also the continuous spectrum are predicted by the conditions at some representative point in the solar atmosphere. We then determine the concentration at three different representative points, to see whether the results depend on the chosen optical depth. As before,[3] we chose to use B. Strömgren's solar model[4] to facilitate comparison with his abundances of other elements. A fourth analysis is carried through by using a low solar excitation temperature, $T = 4800°$ K, combined with the temperature, pressure and $\Delta\lambda_D$ from the model at $\tau_0 = 0.25$. The results are given in Table 2; $N(Be\ \text{I}^*)$ is the total number of *Be* I atoms per gram in levels $2\,^3P_1^o$ and $2\,^3P_0^o$; the ground state is $2\,^1S_0$; the Boltzmann correction to the ground state is the product of 0.25 $\exp(11{,}600 \times 2.71/T_{\text{excitation}})$ times $N(Be\ \text{I}^*)$. From a Milne-Eddington analysis we derive η_0 from observed equivalent widths. The number of atoms per gram of stellar material in the lower level, s, producing a line of ion r, N_{rs}, is obtained from

$$N_{rs} = \frac{m\,c}{\pi^{1/2}e^2}\,\frac{V\,\eta_0 k_\nu}{f\lambda}, \tag{1}$$

where V is the velocity dispersion. At each τ_0, η_0, V, and k differ. To obtain N, the total number of atoms per gram, in all stages of ionization, we correct for the excitation and ionization equilibria computed with Strömgren's value of the temperature and electron pressure at each τ_0. We use Chandrasekhar's value of the H^- opacity, but with $k_\nu = 1.4\ \bar{k}\ (H^-)$ for *Be* lines and $k_\nu = 1.4 \times 1.1 \times \bar{k}\ (H^-)$ for *Li* lines. If the determinations were perfect, we should get the same total beryllium concentration per gram, $N(Be)$, from $N(Be\ \text{I}^*)$ as from $N(Be\ \text{II})$ after ionization and excitation are taken into account. The two determinations, as shown in Table 2, differ by a factor of about 1.5 at $\tau_0 = 0.1$ and of about 3 at $\tau_0 = 0.25$ in the one case where a low excitation temperature is used.

Because of the weakness of the *Be* I line and its high excitation potential, we incline to weight the determination from *Be* II twice that from *Be* I*. We then derive the mean log $N(Be)$ given in the last line of Table 2. Weighting *Be* I equally with *Be* II would increase the abundance of *Be* about 15 per cent.

The reanalysis of the abundance of *Li* I is given in the fourth line; the essential difference from earlier work[3] is the use of $\bar{k} = 1.4\ k(H^-)$, which results in an increase of +0.15

[2] *Ap. J.*, **109**, 66, 1949.

[3] Greenstein and Richardson, *Ap. J.*, **113**, 536, 1951.

[4] *Pub. Copenhagen Obs.*, No. 127, 1940.

in $\log_{10} N(Li)$. This does not change our previous arguments based on the abundance ratio *Li/Ca*. Strömgren's analysis of the *Ca* abundance, if repeated with the increased k, would leave *Li/Ca* unchanged, i.e., leave *Li* with a low abundance in the sun as compared to the earth or meteorites.

A solar model might be used to obtain a decision as to which of the four cases in Table 2 is to be preferred. The largest discrepancy between the two determinations of *Be* abundance occurs when a low excitation temperature is used; we exclude the fourth case. The lines are fairly weak; if they were located in a spectral region where blanketing is small, the model $\tau_0 = 0.25$ would be satisfactory, and we will adopt it. At $\tau_0 = 0.25$, the *Be/Li* abundance ratio is 8.3; which, combined with the old *Li/Ca* ratio,[3] yields $Be/Ca = 5.8 \times 10^{-6}$. We find that there are 5×10^{13} *Be* atoms per gram, i.e., a ratio of $H/Be = 1.2 \times 10^{10}$, if we neglect helium.

TABLE 2

SOLAR CONCENTRATION OF BERYLLIUM AND LITHIUM ATOMS

(Logs to Base 10)

QUANTITY	REPRESENTATIVE POINT			$T_{exc} = 4800°$ K $\tau_0 = 0.25$
	$\tau_0 = 0.1$	$\tau_0 = 0.25$	$\tau_0 = 0.5$	
θ	1.005	0.963	0.905	0.963
$\log P_e$	0.64	0.87	1.15	0.87
$\log N(Li\ \text{I})$	9.85	10.01	10.18	10.01
$\log N(Li)$	12.56	12.77	13.03	12.77
$\log N(Be\ \text{I}^*)$	11.58	11.74	11.91	11.74
$\log N(Be\ \text{I})$	13.70	13.75	13.76	13.98
$\log N(Be\ \text{II})$	12.90	13.04	13.19	13.04
$\log N(Be)$ derived from *Be* I	13.80	13.89	14.01	14.12
$\log N(Be)$ derived from *Be* II	13.61	13.59	13.54	13.59
Mean $\log N(Be)$	13.67	13.69	13.70	13.77

The *Be/Li* ratio is in clear disagreement with that of H. N. Russell,[5] who gives $Be/Li = 1$. Our estimate seems preferable. At least part of the difference arises from the poor calibration of the Rowland scale in the ultraviolet, where intensities were systematically underestimated. H. C. Urey[6] gives $Li/Be = 6$ in the earth and meteorites, differing by a factor of 50 from our new value in the sun and indicating a great difference in the solar behavior of *Li* and *Be*.

Table 4 (below) contains the comparison of the solar abundances of *Li*, *Be*, and *Ca* with abundances in the earth and meteors. It is certain that *Li* is severely depleted in the sun, with respect both to *Be* (by a factor of 50) and to *Ca* (by a factor of 150). Further, it is clear that the *Be/Ca* ratio in the sun is relatively close to that in the earth. The original abundance determinations by Goldschmidt, Noddack, *et al.* in the earth and meteorites are not of high quality; the compilations by H. Brown and H. C. Urey are the best now available and differ somewhat from those used by Greenstein and Richardson.[3] It may be unsafe to assert that *Be* is depleted in the sun, as compared to the earth, since only a factor of 4 is involved. But it is quite certain that the *Li/Be* ratio in the sun is greatly reduced. Since thermonuclear processes will destroy *Li* and *Be* rapidly, the presence of *Be* in considerable abundance can be viewed as a further proof[3,7] that the mixing of the outer envelope of the sun is slow and does not carry material to very high temperatures.

[5] *Ap. J.*, **70**, 11, 1929; *Mt. W. Contr.*, No. 383.

[6] *Phys. Rev.*, **88**, 248, 1952.

[7] Greenstein, Richardson, and Schwarzschild, *Pub. A.S.P.*, **62**, 15, 1950.

NUCLEAR PROCESSES INVOLVING BERYLLIUM

Elements of low atomic number, like *Be*, have complex nuclear-level diagrams and enter into many reactions. All isotopes of *Be* represent difficult problems in theories of the origin of the elements. The isotope Be^7 decays by *K*-capture in 53.6 days and, even if ionized inside a star, will capture a free electron; Be^8 is extremely unstable; Be^{10} decays by electron emission with a half-life of 2.5×10^6 years. Only Be^9 is stable and, as a result of its relatively small binding energy, is difficult to produce. Absorption of a gamma ray above 1.5 mev energy results in the ejection of the least tightly bound neutron; the Be^8 residue then splits into two alpha particles. As a result, the formation of Be^9 by a three-body collision is difficult. Any excess of energy leaves the compound nucleus unstable with respect to loss of a neutron. Formation of Be^9 by spallation or fission is quite improbable, as compared to the formation of *Li* because of this limited range of stability (although both seem to occur in cosmic-ray stars). Be^{10} is produced by high-energy neutrons from C^{13} (n, α) Be^{10} or from B^{10} (n, p) Be^{10}; it would be difficult to imagine that solar *Be* is Be^{10}, in view of the improbably large density of neutrons required to maintain an isotope with a life of only a few million years.

Which isotope of *Be* exists hardly affects the thermonuclear reaction rate at low temperature. Experiments with Be^9 and protons of energies in the range 47 kev up to 400 kev are the most relevant in determining the cross-sections at solar energies. Two processes occur with about the same yield:

$$Be^9(p, \alpha)Li^6\,, \tag{2a}$$

$$Be^9(p, d)Be^8(2\alpha)\,. \tag{2b}$$

Laboratory measurements are rather old. J. S. Allen,[8] Williams *et al.*,[9] and G. T. Hatch[10] give thick-target yields. Thomas *et al.*[11] give cross-sections above 250 kev. Allen, who reached the lowest energies, gives results which must be multiplied by 4 to fit the measurements of the other investigators in the overlapping energy range. We fit the cross-sections by an expression of the form

$$\sigma = \frac{a}{E}\, e^{-b/E^{1/2}}\,, \tag{3}$$

where σ is in barns (10^{-24} cm^2) and E in mev. Recent work[11] showed that there is a strong resonance in both reactions at 0.33 mev; this is easily seen in the values of a which we deduced from the experimental data, using equation (3) in the range 150–400 kev. Near 135 kev, a reaches a minimum value of 52 mev-barns and then steadily rises to 95 mev-barns at 47 kev. It has been pointed out by W. A. Fowler, of the Kellogg Laboratory, that the behavior at low energies is consistent with the existence of a level in B^{10} at 6.58-mev excitation, which is very close to the mass-energy value of 6.585 mev for Be^9 plus a proton. An extrapolation to very low energies yields, in the laboratory system, a value for a_L of 115 mev-barns with a large uncertainty. One-level resonance formulae would not be applicable. If we convert to the center-of-mass system, and round off a_{CM}, we may adopt:

$$a_{CM} = 0.9\,a_L \approx 100 \text{ mev-barns}\,, \tag{4}$$

$$b_{CM} = 0.993 Z_{Be} Z_p \left(\frac{A_{Be}}{A_{Be} + A_p}\right)^{1/2} = 3.767 \text{ (mev)}^{1/2}\,. \tag{5}$$

After integrating the cross-section, given by equation (3), over the Maxwellian velocity distribution, we finally obtain the life of a given beryllium nucleus as

$$t_0 = \frac{(\frac{2}{3})^{5/2} A^{1/2} m_p^{3/2} e^{\tau} b_{CM}}{X \rho \tau^2 a_{CM}} \text{ sec}\,. \tag{6}$$

[8] *Phys. Rev.*, **51**, 182, 1936.
[9] *Phys. Rev.*, **52**, 1031, 1937.
[10] *Phys. Rev.*, **54**, 165, 1938.
[11] *Phys. Rev.*, **75**, 1612, 1949.

Here A is the reduced mass in units of the proton mass, X the abundance of hydrogen, and ρ the density. The parameter τ is

$$\tau = 3\left(\frac{b^2 c_M}{4kT}\right)^{1/3} \tag{7}$$

if the units are properly defined; for Be^9, $\tau = 104/T^{1/3}$ with T in millions of degrees K. Finally, we need the solar density and temperature. We adopted one of Mrs. Harrison's solar models, for which $X = 0.71$, $T_c = 14.5 \times 10^6$, and $\rho_c = 150$ gm/cm^3. Table 3 gives, as a function of $r/R\odot$, the temperature, density, and lifetime of Be^9. A computation for Li had already been made.[3] A revision is included in Table 3 now, using the

TABLE 3

LIFETIMES OF BERYLLIUM AND LITHIUM IN THE SOLAR INTERIOR

$r/R\odot$	$T\times10^{-6}$	ρ	Be $\log_{10} t_0$	Li $\log_{10} t_0$
0.00	14.47	150	3.10	3.15
.30	6.49	12	9.61	8.64
.38	4.86	3.9	12.46	11.02
.45	3.90	1.6	14.82	13.03
.48	3.56	1.1	15.83	13.83
.53	3.00	0.61	17.76	15.50
.55	2.76	0.46	18.74	16.25
0.60	2.29	0.25	21.00	18.20

older cross-sections for Li disintegration in the same solar model as is here used for Be. Note that the lifetimes of Be and Li are the same at the center of the sun, but that Be rapidly becomes more stable because of the larger barrier-penetration factor; the relatively long life of Li is due to its small cross-section after correction for barrier.

Reaction (2b) produces deuterons, but, because of the small barrier, these are almost instantaneously converted to He^3 in any region where reaction (2b) will occur. A temperature of even a million degrees will destroy D; thus, even if D, Li, and Be exist in cosmic rays and are captured in the solar atmosphere, mixing will rapidly destroy them.

CONCLUSIONS

We have shown that beryllium exists in the sun in a high abundance when compared to lithium. Our conclusion as to the relatively high abundance ratio Be/Li in the sun is fairly well grounded observationally and does not depend on the particular set of abundance data (terrestrial or meteoritic) with which we compare the solar value. If we take the abundance of H (on an arbitrary scale) as 10^{12}, we obtain, in logarithms to the base 10, the values given in the accompanying tabulation. Note that no simple readjustment and no reasonable estimate of the errors of the solar determinations can make the pattern of abundances agree. The beryllium abundance is nearly the same as on earth, while that of lithium is much reduced.

Our discussion of nuclear processes has revealed no easy way of producing beryllium and has shown that its rate of destruction is high. It is possible to find a point in the solar envelope, approximately halfway out from the center, where lithium is rapidly destroyed and beryllium is not. In the accepted age of the universe, 10^{17} seconds, at $r/R\odot = 0.53$, beryllium would be unaffected, and lithium would essentially vanish. Mixing which penetrates to just that depth could have resulted in a decrease of the Li/Be ratio from an initially high value, say, the terrestrial one of 6, down to the presently observed solar

value of $\frac{1}{8}$. Such a hypothesis is tenable but places a severe limitation on the solar mixing time and depth of penetration. From Table 3 we require that the material subject to deep convection or mixing in the outer envelope should not spend any appreciable time at a temperature greater than 3.6 million degrees but that (to destroy *Li*) it does reach 3.0 million degrees.

The presence of *Be* in the sun, in any case, can be taken as compatible with a deep solar convective zone reaching from the surface down to points at a temperature just below 3.6 million degrees. Rapid circulation to higher temperatures would require that all

TABLE 4

ABUNDANCES OF ELEMENTS

ELEMENT	SUN	EARTH AND METEORITES	
		H. Brown	Urey
Li	1.26	3.30	3.50
Be	2.18	2.67	2.70
Ca	6.42	6.33	6.25

the atmospheric *Li* and *Be* be of secondary origin, accreted from interplanetary or interstellar space or produced in the solar atmosphere or corona by spallation by cosmic rays. The terrestrial and meteoritic ratio of *Be*/*Li* is low, so that accretion from the solar system seems improbable. Spitzer[12] has shown that neither *Li* nor *Be* in interstellar space can be much more abundant than in the earth. We cannot suggest any process that produces more Be^9 than Li^6 or Li^7 because of the stability considerations in Be^9. Therefore, we must conclude either that the solar mixing is sharply limited or that some unknown processes manufacture *Li* and *Be* in the outer layers of the sun.

We are indebted to W. A. Fowler for discussion of the nuclear processes connected with beryllium; to H. Brown for abundance data; to H. D. Babcock for the solar spectra; and to M. Minnaert for the tracings of some of Babcock's spectra.

[12] *Ap. J.*, **109**, 548, 1949.

SOLAR FLARES AND THE YELLOW CORONAL LINE*

FREDERICK P. DOLDER, WALTER ORR ROBERTS, AND DONALD E. BILLINGS
High Altitude Observatory of Harvard University and University of Colorado
Received July 27, 1953

ABSTRACT

Emission of the unidentified yellow coronal line visible at Climax from 1946 through 1950 is shown to be highly correlated with flares at the sun's limb at the same position, indicating a close relationship between the two phenomena. The probability of a chance correlation as close as the observed is less than 2×10^{-5}.

INTRODUCTION

The yellow emission line of the solar corona, at λ 5694, can be detected occasionally at the solar limb with a coronagraph. It is a more rarely observed phenomenon than red (λ 6374) and green (λ 5303) coronal-line emission. On the occasions when it is observed, it extends over only a few degrees of the solar limb and is always associated with intense solar activity.

The line was discovered by Lyot[1] in 1937 and was tentatively identified by Edlén[2] in 1942 as arising from *Ca* XV. Using this identification, Edlén computed the required ionization potential to be 814 volts. Objections to Edlén's identification were raised by Shklovsky,[3] Naqvi,[4] and Garstang,[5] so that the line must today be regarded as the only important unidentified coronal emission line.

Waldmeier[6] and Roberts[7, 8] showed the close correspondence between yellow-line emission and sunspot-type prominences. Roberts[8] observed that in many cases of yellow-line emission intense flarelike prominences frequently form at or near the center of activity. These observations confirmed a suggestion made by Waldmeier[9] that the yellow line is intensified over solar flares and suggested the need of a more detailed analysis of the association of these two solar phenomena.

In this paper we list the occasions on which the yellow coronal line has been observed and describe the close correspondence between these instances and the outbreak of flares at the limb of the sun. Another paper, now in preparation, describes the character of the solar prominences found at the same time and place as the yellow coronal-line emission.

OBSERVATIONAL DATA

On every day with suitable observing conditions during the last ten years, the High Altitude Observatory has obtained spectrograms of the corona by use of the coronagraph at Climax, Colorado. In the course of routine operation, six spectrograms are made each day, each spectrogram having its center at a different point on the sun's limb. These spectrograms overlap to the extent that every point on the solar limb appears on at least two spectrograms.

For the analysis reported here, Dolder carefully examined all spectrograms taken at Climax during the years 1946–1950 inclusive, some forty-five hundred spectra, as well as

* This work was supported by the Office of Naval Research.

[1] *M.N.*, **99**, 580, 1939.
[2] *Zs. f. Ap.*, **22**, 30, 1942.
[3] *Ann. Crimean Ap. Obs.*, **5**, 86 and 109, 1950.
[4] *A.J.*, **56**, 135, 1951.
[5] *Ap. J.*, **115**, 549, 1952.
[6] *Zs. f. Ap.*, **20**, 172, 1940.
[7] *Ap. J.*, **108**, 523, 1948.
[8] *Ibid.*, **115**, 488, 1952.
[9] *Astr. Mitt. Eidgenöss. Sternw. Zürich*, No. 146, p. 6, 1945.

a number of plates from 1951, searching for the presence of yellow coronal-line emission. He also examined a substantial number of spectra from the coronagraph at the Upper Air Research Observatory at Sacramento Peak, New Mexico, made during the same period. In a number of instances he thereby confirmed Climax observations, and in others he added new examples of the phenomenon. The examination was carried out independently of previous measurements of these spectra and without reference to the appearance of other emission lines on the spectrograms. All cases were discarded when the presence of the yellow line was doubtful.

The statistical studies reported here include 43 instances of emission of the yellow coronal line observed during the 938 days of 1946 through 1950 for which suitable coronal spectrograms were obtained at Climax. These cases are given in Table 1, which also includes 7 additional instances in 1951 found on Climax and Sacramento Peak spectra. Some of the cases (indicated by asterisks in Table 1) have been previously reported,[8] though the angles of position here reported differ slightly, in some cases, from those previously given, since they are derived from independent measurements.

TABLE 1

REGIONS OF EMISSION OF THE YELLOW CORONAL LINE

1946 TO 1950 INCLUSIVE=CLIMAX

Case No.	Date	Position Angle (Heliographic)	Case No.	Date	Position Angle (Heliographic)
1	Feb. 27, 1946*	60°– 70°	23	June 24, 1948	80°– 85°
2	July 27, 1946*	120 –125	24	Oct. 10, 1948	70 – 85
3	Nov. 27, 1946*	255 –265	25	Oct. 24, 1948	280 –290
4	Nov. 30, 1946*	280 –285	26	Dec. 3, 1948	100 –110
5	Dec. 18, 1946	245 –265	27	Dec. 27, 1948	275 –300
6	Dec. 28, 1946	280 –290	28	Feb. 6, 1949	105 –110
7	Jan. 12, 1947	105 –115	29	Feb. 11, 1949	255 –260
8	Jan. 21, 1947	250 –265	30	July 24, 1949*	105 –115
9	Feb. 12, 1947*	250 –260	31	Aug. 7, 1949*	245 –260
10	Mar. 6, 1947	285 –305	32	Sept. 16, 1949*	255 –260
11	Mar. 19, 1947*	70 – 80	33	Nov. 6, 1949	85 – 95
12	Apr. 14, 1947*	235 –245	34	Nov. 7, 1949*	285 –295
13	June 14, 1947*	100 –115	35	Nov. 19, 1949*	265 –280
14	July 25, 1947*	275 –295	36	Nov. 21, 1949*	70 – 80
15	Aug. 7, 1947	75 – 90	37	Nov. 21, 1949	275 –285
16	Aug. 14, 1947*	260 –270	38	Dec. 12, 1949	80 – 85
17	Aug. 20, 1947*	275 –290	39	Feb. 2, 1950*	280 –300
18	Aug. 24, 1947*	65 – 80	40	Feb. 13, 1950*	70 – 85
19	Nov. 12, 1947	110 –125	41	Feb. 26, 1950	285 –290
20	Nov. 28, 1947	245 –260	42	Apr. 20, 1950	285 –290
21	Dec. 31, 1947	280 –290	43	May 6, 1950*	75 – 90
22	May 21, 1948	260			

1951—CLIMAX (Cx) AND SACRAMENTO PEAK (SP)

Case No.	Date	Position Angle (Heliographic)	Case No.	Date	Position Angle (Heliographic)
1 (SP)	Feb. 4, 1951*	275°–290°	5 (Cx)	June 24, 1951	250°–260°
2 (SP)	Apr. 11, 1951*	75 – 85	6 (Cx)	Sept. 30, 1951	280 –290
3 (Cx)	Apr. 25, 1951*	280 –290	7 (Cx)	Nov. 7, 1951	255 –265
4 (Cx, SP)	May 9, 1951	75 – 85			

* Previously reported (Roberts, *Ap. J.*, **115**, 488, 1952).

We next examined published flare observations, in order to find whether flares at the solar limb had been observed in association with the yellow-line cases. As "limb flares" we listed all solar flares tabulated from 1946 through 1950 in the *Quarterly Bulletin of the International Astronomical Union* that occurred within 5° of the sun's limb. Table 2 gives the essential statistics of the relationship of these limb flares to the yellow-line cases at Climax and summarized in Table 1.

It is entirely possible that unobserved flares did occur in association with the 12 yellow-line cases in the last item of Table 2. Eleven of the 12 cases occurred in the winter and early spring months, during which the number of observing hours of flare-observing stations in the Northern Hemisphere is severely restricted—sometimes to as low as 1 hour per day. Similarly, the 60 limb flares which were not associated with known yellow-line emission, may very well have been accompanied by unobserved emission. Flare observations by the various stations reporting to the *Quarterly Bulletin* cover a 24-hour period, whereas the yellow-line data are generally obtained from routine coronal plates taken once per day, and yellow-line emission is not a long-lived phenomenon. Furthermore, unless unusually strong, the yellow-line emission can be detected only when observing conditions are outstandingly favorable.

STATISTICAL ANALYSIS OF RESULTS

To compute the probability, P', of 13 or more chance coincidences between flares and yellow-line emission given in Table 2, we need to consider the random probability of the occurrence of a flare or yellow-line case in any given latitude range on any given day. Whence, in turn, we must consider the latitude distribution of yellow-line maxima and of flares. These distributions are given in Table 3.

TABLE 2

STATISTICS FOR LIMB FLARES ASSOCIATED WITH YELLOW CORONAL LINE OBSERVED AT CLIMAX

No. of Climax observing days in 1946–1950 incl., with satisfactory coronal spectra	938
No. of yellow-line cases observed (Table 1)	43
No. of days from these 938 on which *Quarterly Bulletin* lists limb flares	91
No of cases of yellow-line emission and a limb flare on same date, within 5° latitude	13
No. of cases of yellow-line emission and a limb flare the same day, the preceding day, or the following day and within 5° latitude	31
No. of cases of yellow-line emission with no known limb flares within 1 day and within 5° latitude	12

TABLE 3

LATITUDE DISTRIBUTION OF YELLOW-LINE EMISSION AND LIMB FLARES FOR 938 CLIMAX OBSERVING DAYS

Heliographic Latitude (North and South Combined)	No. of Yellow-Line Maxima at This Latitude	No. of Flare Days with Flares at This Latitude	Heliographic Latitude (North and South Combined)	No. of Yellow-Line Maxima at This Latitude	No. of Flare Days with Flares at This Latitude
0–5	3	5	20–25	2	8
5–10	5	28	25–30	2	4
10–15	17	28	30–35	2	0
15–20	12	18			

Rather than attempt to compute P' exactly, we make the simplifying assumption that limb flares and the yellow-line cases are equally probable over each part of the 60° latitude belt extending from 30° north latitude to 30° south latitude and that the probability is that of the most favored zone. We thus assume a frequency of 56 flare days per 938 days per 20° zone and 17 yellow-line maxima per 938 days per 10° zone. This clearly overestimates the chance probability of a flare or yellow-line case for any given latitude range for any given day. On these assumptions we compute P, the probability of 13 or more chance coincidences between flares and yellow-line emission under the assumed conditions, and note that P is certainly greater than P'.

Under our assumptions, the probability of the occurrence of a flare anywhere on the limb on a given day is

$$\frac{3 \times 56}{938} = \frac{168}{938}.$$

Similarly, the probability of the occurrence of yellow-line emission on a given day with a maximum within a specified 10° latitude range is 17/938. Hence the probability of the occurrence of yellow-line emission on the same day as the flare, within 5° of the flare, is

$$p = \frac{168}{938} \times \frac{17}{938} = 0.0032 .$$

The probability, P, of 13 or more such coincidences in 938 days is the same as the probability of 13 or more successes in 938 tries, when the probability of a success in a single try is 0.0032. Since $p \ll 1$ and $13 \ll 938$, we may apply the Poisson formula,

$$P = \sum_{r=13}^{r=938} \frac{(np)^r e^{-np}}{r!},$$

where r = number of successes, p = probability of a success in a single try = 0.0032, and n = number of trials = 938. From this we can determine that $P = 1.8 \times 10^{-5}$, whence we know that the actual probability of 13 or more coincidences of limb flares and yellow-line emission, considering the actual latitude distribution of the phenomena, is less than 2×10^{-5}.

DISCUSSION

This result provides strong evidence of the phenomenological connection between flares and yellow-line emission. The evidence appears even more powerful when we consider that P' is probably much less than P and that we have not made any use of the additional 18 cases in which flares and yellow-line emission are separated by 1 day. If we consider the effect of observing conditions on the data, we see that it is entirely possible that limb flares are always accompanied by yellow-line emission, and vice versa. Whether or not the two phenomena have a one-to-one correspondence, their association is so very close that any future comprehensive theory of flares must explain greatly intensified coronal emission in the yellow line. Likewise, any theory of the corona which explains yellow-line emission must provide for close identification with solar flares.

We acknowledge with thanks the opportunity afforded us to examine spectra from the Harvard College Observatory coronagraphic program at the Upper Air Research Observatory of the Air Force Cambridge Research Center on Sacramento Peak in connection with this work.

THE ABSORPTION SPECTRA OF NOVA HERCULIS

A NEW INTERPRETATION

DEAN B. MCLAUGHLIN
University of Michigan Observatory
Received August 19, 1953

ABSTRACT

Radial velocities of the diffuse enhanced absorption system of Nova Herculis, previously published by the author, are revised and reinterpreted in the light of extensive additional data obtained from Mount Wilson spectrograms. On certain dates the earlier Michigan measures were affected by blending of components. A gap in the series in January, 1935, led to misidentification of components. During the interruption, a component of small velocity disappeared and one of higher velocity emerged, producing the illusion of a shift of the pattern. The Mount Wilson data close the gap and show that actual shifts of components were relatively small and slow.

The velocities and lifetimes of the early diffuse enhanced lines yield distances traversed that agree well with the hypothesis that clouds or shells of high velocity emerged later and overtook and merged with the principal shell. Diffuse enhanced components in the later stages require additional continuous ejection. Extremely complex changes of relative strength of components probably require explanation in terms of variable excitation rather than actual destruction of shells and emergence of new ones.

INTRODUCTION

In 1937 I published a general study of the spectrum of Nova Herculis,[1] based upon measurements of Michigan spectrograms, supplemented by plates obtained at the Cook Observatory. During much of the period of observation, the "diffuse enhanced" absorption system was multiple. Usually the components were just separable on the Michigan plates, but on some they were blended and yielded discordant velocities. Gaps in the series, due to interruptions by bad weather, left the way open to errors of identification of components. It has since developed that misidentifications were made across a gap from January 18 to 22, 1935, and that some apparent shifts of lines in later stages were due in part to unresolved blends. The main purpose of this paper is to present the corrected factual record. No complete discussion of physical interpretations will be attempted at this time, though some tentative explanations will be suggested in the discussion section.

THE PROBLEM OF IDENTITY OF COMPONENTS

On January 18 there was a pattern of absorption components with certain relative intensities. On January 22 a very similar pattern was present, but it appeared to have shifted shortward by an amount corresponding to a velocity of 120 km/sec. Accelerations larger than this had been reported in other novae. An especially clear-cut case was soon furnished by Nova Lacertae 1936, in which rapid and long-continued acceleration undoubtedly did affect the principal spectrum.[2]

The first doubts as to the correctness of my earlier interpretation of Nova Herculis were raised by Baldwin's analysis of the spectrum of Nova Cygni 1920.[3] He showed that the apparent rapid acceleration was illusory and was due to a blend of components in which the changes of strength of the separate lines produced a shift of the center of the blend toward shorter wave lengths. However, this seemed to be an isolated case, for

[1] *Michigan Obs. Pub.*, **6**, 107, 1937.

[2] McLaughlin, *Pub. A.A.S.*, **8**, 246, 1937; *A.J.*, **52**, 126, 1947.

[3] *Michigan Obs. Pub.*, **8**, 61, 1940.

critical examination served only to confirm the large changes in Nova Aquilae 1918 and Nova Lacertae 1936.

More serious doubts arose in my mind when Bertaud[4] published a compilation of velocities of the absorption systems of Nova Herculis. Although Bertaud accepted my interpretation, the inclusion of velocities for dates in the gap January 18–22 made it appear as if absorptions III and IV had made a very sudden jump. The trend of velocities plainly suggested that absorption IV previous to January 18 was identical with what had been called III after January 22. Correspondence with Dr. F. J. M. Stratton served to increase my doubts. He indicated quite clearly that he believed it probable that III and IV had been misidentified across the gap. His statement,[5] in which Roman numerals refer to my interpretation in 1937, was as follows: "My view is that in the interval Jan. 18–22, absorption III dropped out, being covered by a strengthening emission, belonging to IV and possibly V. At a later date VII is in my view a reappearance of III. At the same time as III goes, a new absorption, V, appears on the violet edge of IV."

Finally, Nova Lacertae 1950[6] presented a remarkably clear illustration of precisely the sort of change that was suspected in the case of Nova Herculis. Components of least displacement faded, those with larger shifts intensified, and additional lines with still greater displacement emerged. The record was continuous for several days, and there was no doubt concerning identification of components. Yet, if only two days' observations had been missed, the changing pattern could have been very easily misinterpreted as due to a bodily shift of all the lines toward shorter wave lengths.

It was evident that a complete re-examination of the absorption systems of Nova Herculis was required. An opportunity to settle the question came during a visit to Mount Wilson and Palomar Observatories in 1951, when I was given access to a long series of spectrograms of Nova Herculis, some of which filled very important gaps in the Michigan series.

THE SPECTROGRAMS

The Michigan plates were obtained with the one-prism spectrograph, dispersion 40 A/mm at $H\gamma$. One plate was taken with the two-prism spectrograph, dispersion 20 A/mm. The majority of the Mount Wilson observations were obtained with the three-prism ultraviolet spectrograph on the 60-inch reflector. With cameras of 10 and 15 inches focal length, the dispersions at $H\gamma$ are 38 and 27 A/mm, respectively. A few plates were obtained with the coudé spectrograph, which at that time employed a prism. These plates have dispersion 11 A/mm at $H\gamma$. In addition, several plates taken with the grating spectrograph, dispersion 33 A/mm, were measured for features of special interest in the visual region.

Practically all the Mount Wilson plates taken after January 16 were measured. On earlier dates no ambiguity had arisen, since only the principal spectrum and one or two weak diffuse enhanced components were present. On an earlier visit to Mount Wilson, some measures had been made on plates covering a few days before and after light-maximum. The results of these are included here, but they introduce no changes of interpretation.

RADIAL VELOCITIES

Radial velocities for the Michigan plates were in part taken from Tables 11 and 22 of my earlier paper, when re-examination or remeasurement confirmed that they were not greatly affected by blends. Velocities of some components on a number of Michigan plates were revised as a result of remeasurements.

The lines measured on the Mount Wilson plates for the study of the diffuse enhanced system were a selected list that showed the multiple components best. On a number of

[4] *Ann. Obs. Paris* (*Meudon*), **9**, Part I, 121 ff., 1945.

[5] Personal letter, November 11, 1946.

[6] McLaughlin, *A.J.*, **55**, 174, 1950.

plates the region longward of $H\delta$ was overexposed and not usable. In general, the measures of the Michigan plates depend upon more lines; but, because of their lower dispersion and lower purity even for the same dispersion, they are not entitled to greater weight. At $H\beta$ and $H\gamma$ the lines of the principal spectrum due respectively to λ 4856 *Cr* II and λ 4338 *Ti* II interfered with the measurement of close-in components of the diffuse enhanced system. No such interference occurred at $H\delta$, where the higher dispersion gave an added advantage. The Mount Wilson velocities and the revised Michigan velocities depend on measures of the lines in the accompanying tabulation.

$H\gamma$	*Ca* II 3933	*Fe* II 4233
$H\delta$	*Ti* II 3900	4549
$H\zeta$	3913	4584
$H\eta$	4164	4924
$H\theta$	4444	5018
	4468	

Tables 1 and 2 contain means of velocities for each date. Where two or more plates from the same observatory were measured, these are combined into a single mean. The

TABLE 1*

VELOCITIES OF PREMAXIMUM AND PRINCIPAL ABSORPTION; EARLY PHASE

Date U.T.	Observatory†	I‡ (Km/Sec)	II (Km/Sec)	K§ (Km/Sec)	*Ha* (Km/Sec)
1934					
Dec. 14.3	C	421 (6)	.....	.....	.....
15.3	C	272 (16)	.....	.....	.....
15.6	W	253 (11)	.....	.....	.....
16.1	W	261 (8)	.....	.....	.....
16.8	C	200 (23)	.....	.....	.....
18.0	M	176 (82)	.....	.....	.....
18.8	C	173 (40)	.....	.....	.....
21.8	C	171 (69)	.....	.....	.....
23.0	W	172 (48)	.....	265	.....
23.3	E	173 (32)	.....	.....	.....
24.0	W	184 (5)	.....	.....	337
24.6	W	180 (13)	290 (7)	411	347
25.0	W	184 (18)	300 (13)	419	324
25.6	W	178 (24)	307 (26)	406	303
26.0	W	175 (17)	309 (16)	397	309
26.6	W	177 (11)	310 (17)	419	308
27.0	M	170 (8)	318 (60)	.....	.....
27.2	C	.....	335 (30)	.....	.....
27.7	C	.....	336 (83)	.....	.....
28.0	M	.....	314 (17)	.....	.....
28.5	M_2	.....	315 (41)	.....	.....
29.0	W	173 (5)	311 (18)	389	.....
29.6	W	221*a*	.....	.....	332
30.5	WM	202*a*	326 (20)	.....	321
31.0	M	193 K	321 (52)	.....	.....
31.5	M_2	226 (3)	319 (68)	.....	323
1935					
Jan. 2.0	M	203 K	322 (19)	.....	.....

* All velocities are negative.

† C = Cambridge; E = Edinburgh; M = Michigan; W = Mount Wilson. Subscripts denote number of plates.

‡ a = velocity due to *Ha*.

§ K = velocity due to K line.

TABLE 2

RADIAL VELOCITIES OF THE ABSORPTION SYSTEMS OF NOVA HERCULIS 1934

All velocities are negative

Date, U. T.		Obs.	II	II_2	III_1	III_2	III_3	III_4	III_5	Other
1934			km/sec	km/sec	km/sec	km/sec	km/sec	km/sec	km/sec	km/sec
Dec.	26.0	W	309 (16)		477 ave	654 ave				
	26.6	W	310 (17)		505 ave	635 ave				
	29.6	W			527 ave		749 ave			
	30.5	WM	326 (20)		462 ave		696 ave			
	31.0	M	321 (52)				761 (2)			
	31.5	M_2	319 (68)		553 d	689 (5)	771 (2)			
1935	2.0	M	322 (19)		521 d	678 (3)	758 (3)			
Jan.	2.5	M_2	325 (29)		542 d	710 (8)				
	3.0	M	324 (13)							
	3.5	M	323 (17)		517 (2)	732 (5)	bl			
	4.0	M	326 (18)		517 d	738 (7)	bl			
	4.5	M	316 (31)			748 (6)	bl			
	5.0	M	327 (19)		536 d	734 (7)	bl			
	11.4	M	312 (24)		527 (10)	667 (5)	800 (2)			
	12.4	M	300 (36)		554 (13)	669 (4)	805 (3)			
	15.5	Ck	321 (18)		600 (8)	671 (8)				
	16.5	M	327 (32)		553 (5)	692 (8)	820 (3)	934 (1)		
	16.6	W	325 (10)		568 (5)	677 (7)*	833 (2)			*742 (3)
	17.5	W	322 (11)		567 (9)	676 (10)*	830 (1)			
	17.9	M	313 (22)		549 (3)	676 (4)*	867 (2)			*758 K
	18.5	M	327 (43)		550 (3)	672 (6)*	832 (2)			*761 K
	18.5	W_2	321 (21)		567 (16)	670 (18)*	822 (8)			*763 (2)
	20.6	W_4	324 (36)		566 (15)	674 (35)	790 (40)	899 (5)	977 (2)	
	21.6	W_5	325 (40)		588 (7)	673 (37)	786 (38)	905 (4)	988 (4)	
	22.6	W_3	326 (26)		595 (6)	669 (25)	787 (28)	874 (6)	966 (3)	
	22.9	M	330 (37)		550 (3)	664 (3)	773 (4)	915 (2)		
	23.5	M	330 (33)		522 (3)	667 (13)	789 (11)	953 (5)	bl	
	24.4	M	330 (33)			669 (15)	792 (6)	944 (2)	bl	
	24.6	W_2	323 (24)	426 K	594 (4)	666 (22)	794 (21)	913 (7)	990 (3)	
	25.6	W_2	325 (16)	429 K	583 (3)	670 (14)	808 (8)	941 (7)	bl	
	26.5	W	326 (11)	431 K		672 (10)	794 (3)*	926 (5)	bl	*845 (6)
	27.5	M	326 (36)			657 (14)	802 (12)		1029 (2)	
	28.4	Ck_2	336 (11)			666 (6)	833 (21)	bl	1046 (2)	
	29.5	W	335 (8)	434 K		682 (5)	794 (5)	892 (8)	999 (1)	
	30.5	M	345 (28)			672 (5)	839 (12)	bl	1120 (5)	
	31.5	W_2	340 (13)	457 K		676 (7)	788 (10)	896 (12)	1064 (5)	
Feb.	1.5	Ck	354 (5)			710 (2)	839 (3)	bl	1113 (1)	
	2.5	W_2	341 (10)	455 (3)		660 (8)	770 (11)	886 (15)	1025 (9)	
	3.4	M_2	350 (34)			674 (13)	bl	841 (21)	1089	
	6.4	M_2	356 (24)	473 (1)		690 (4)	804 (6)	880 (8)		
	7.4	M	355 (33)		619 (2)	666 (4)	773 (3)	881 (3)	995 (2)	
	11.5	W_2	363 (13)			699 (7)	795 (1)	890 (9)	1016 (3)	1153 (2)
	12.5	Ck	373 (7)			666 (6)	bl	862 (5)		

Table 2 (continued)

Date		Obs.	II	II_2	III_1	III_2	III_3	III_4	III_5	Other
Feb.	13.4	M_2	365 (32)		611 (2)	689 (16)	792 (7)	892 (23)	986	
	15.4	M	385 (22)	484 (3)		696 (5)		887 (3)		
	15.5	W	371 (12)	467 (2)		702 (6)	779 (9)	913 (11)		
	16.5	W_3	375 (18)	485 (3)		735 (9)*	783 (13)	898 (13)		*703 (5)
	17.5	W_3	372 (18)	491 (4)		732 (16)	798 (12)	911 (13)		
	18.4	Ck_2	386 (14)				799 (12)			1179 (4)
	20.5	M	377 (21)	495 (2)		724 (4)	826 (4)	906 (1)		
	20.5	W	381 (6)	501 (2)		724 (4)	814 (6)	917 (4)		
	21.5	Ck	384 (7)		661 (2)	bl	780 (6)			1149 (2)
	22.5	W	378 (8)	513 (4)	593 (3)	737 (5)	794 (4)*	922 (5)		*835 (5)
	23.5	M	379 (29)	491 (3)		745 (3)	811 (3)	932 (2)	1064 (3)	1177 (3)
	25.4	Ck_2	372 (18)		571 (6)		811 (10)			1208 (6)
	27.4	M_2	380 (28)	453 (1)	580 (7)	751 (9)	814 (18)	890 (10)	995 (5)	1330 (3)
	28.5	W_2	377 (8)	483 K	579 (3)	753 (1)	797 (8)	879 (7)		1152 (3)
Mar.	1.4	Ck	395 (7)		573 (4)			871 (3)	1066 (2)	
	3.4	M	374 (23)	498 (3)	563 (5)		814 (8)	900 (4)		
	5.4	Ck	402 (5)		593 (4)		bl	852 (3)		
	5.5	W	382 (2)				793 (1)	866 (2)		
	6.4	M	392 (23)	458 K	600 (3)	658 (3)	788 (3)	877 (2)	961 (1)	
	9.4	M	390 (22)	499 (2)	585 K	662 (4)	778 (4)	865 (4)		
	12.3	M	398 (14)	520 (3)		710 (5)	bl	854 (5)		
	12.5	W	386 (5)	509 (3)		668 (2)	763 (4)	859 (5)		
	12.5	Wc	381 (6)	499 (3)	558 (3)	702 (2)	768 (5)	844 (6)		
	13.5	W_2	384 (12)	495 (1)	569 (7)	671 (8)	762 (10)	855 (10)		
	13.5	Wc	378 (7)	503 (3)	567 (2)		769 (2)	857 (4)		
	14.5	W_3	381 (15)	490 K	560 (9)	680 (6)	762 (10)	855 (11)		
	15.4	M	388 (17)	533 (2)	584 (4)	673 (4)	743 (2)	839 (5)	1033 (1)	
	15.5	W_2	386 (11)		566 (8)	674 (4)	760 (9)	856 (8)		
	16.4	W_3	393 (13)		566 (9)	675 (2)	763 (9)	854 (10)		
	17.5	W	385 (7)	448 (2)	574 (6)	694 (4)	761 (6)	851 (6)		
	18.3	M	391 (14)	475 (1)	599 (4)	bl	733 (2)	839 (5)		
	18.5	W	388 (8)	481 K	575 (5)		762 (6)	851 (6)		
	20.4	M	386 (4)					812 (2)		
	20.5	W	379 (7)	467 (4)			721 (4)	844 (6)		
	22.3	M_3	387 (28)	486 (4)	584 (10)	661 (6)	732 (2)	846 (14)	977 (4)	
	23.4	M	387 (17)	481 (4)	588 (7)	679 (2)		846 (8)	1015 (2)	
	23.5	W	384 (9)	481 (5)	589 (6)			851 (6)	1005 (4)	
	24.3	M_2	387 (28)	482 (5)	580 (5)	692 (2)		847 (12)	1020 (2)	
	25.5	W	390 (7)	490 (5)	590 (5)	704 (3)		851 (5)	968 (1)	
	26.3	M_3	394 (28)	493 (8)	584 (12)	718 (11)		856 (13)	1004 (12)	
	26.4	W	388 (6)	496 (6)	593 (5)	721 (3)		852 (5)	980 (4)	
	27.3	M_2	390 (30)	504 (7)	592 (7)	704 (10)		855 (13)	972 (2)	
	29.3	M_2	394 (44)	499 (6)	603 (17)	702 (8)		864 (13)	1001 (4)	
Apr.	3.3	M	433 (13)		582 (2)	724 (3)		839 (1)	932 (2)	

number of lines given in parentheses following each velocity is the sum of the numbers measured on all the exposures. In no case have the plates from two observatories been combined. A single apparent exception is the observation of December 30.5, when the *Hα* velocities only were measured on a Mount Wilson plate and all others were from a Michigan plate.

In Table 1 the data are given for the premaximum (absorption I) and principal (absorption II) systems up to January 2.0, the last date on which a line attributed to absorption I was observed. In order to make the record as complete as possible, velocities published by Stratton[7] have been entered in Table 1. These depend on Cambridge plates and one Edinburgh spectrogram. Together with the Mount Wilson plates, they give a very complete picture of the premaximum spectrum.

Table 2* contains the velocities for the principal and diffuse enhanced (absorption III) systems. Several plates in Table 1 showed no components of III and are not repeated in Table 2. The several components of the diffuse enhanced system are designated III_1 to III_5 in order of increasing displacement. The last column records components of greater displacement. On six dates additional components were measured with velocities between those of the numbered ones. These also are given in the last column, and attention is called to them by an asterisk, both in the last column and in the column corresponding to the component to which the extra line was most closely related. Velocities depending on blended lines are shown underlined in the column corresponding to one of the blending lines, and the abbreviation "bl" appears in the column of the other contributor.

Table 3 gives velocities of the Orion absorptions, called VI and VIII in my earlier paper and here designated IV_1 and IV_2. The last column contains velocities of "absorption V," which is the same as the system called XI in my earlier paper. It consisted of extremely diffuse hydrogen lines, strong at *Hα* and *Hβ* but quite weak at *Hδ*. The data in Table 3 are presented here simply for completeness of the record, but no new interpretations have been necessary in these cases, and these systems will not be discussed further at this time.

The radial velocities of all components of absorptions II and III are plotted in Figure 1. The continuity is sufficiently evident in most parts of the diagram, and the drawing of continuous curves would be superfluous. In a few places where doubt might arise, a dashed line has been drawn to indicate the relationship of points according to the interpretation now adopted.

COMPARISON OF OLD AND NEW INTERPRETATIONS

It would be tedious to compare extensively the old and new interpretations of the diffuse enhanced system for the entire period of observation. Therefore, we restrict discussion to the month of January, 1935. These results have been published in a brief abstract.[8] In Figure 2 the velocities available in 1937 are plotted in the upper half, and curves are drawn in accordance with the interpretation then adopted. In the lower half of the figure the same data are plotted, with the addition of the measures of Mount Wilson plates and some remeasures of Michigan plates. The bridging of the gap January 18–22 definitely rules out the interpretation implied by the upper half of the figure. There was no acceleration of components; instead, the velocities were nearly constant or even decreased slightly for each component. But great changes occurred in their relative intensities.

If one views Figure 2 with the quotation from Stratton's letter before him, it will be evident that the interpretation suggested by Stratton has been confirmed in full. This

[7] *Ann. Solar Phys. Obs., Cambridge*, Vol. **4**, Part IV, 1936.

* Symbols used in Table 2 are the same as in Table 1 (see notes to that table). Additional symbols: Ck = plate from Cook Observatory, d = velocity of *Hδ*, ve = velocity of violet emission edge.

[8] McLaughlin, *Pub. A.S.P.*, **63**, 181, 1951.

would not have been possible without the superior resolution of the Mount Wilson plates or without the observations that fill the gap in the Michigan series.

Over the entire interval from early January to the end of March the results are so definite that no question can now remain as to the identity of the major components. Some minor mysteries will perhaps never be cleared up, for the reason that plates of coudé dispersion were not obtained on crucial dates.

THE CHANGING PATTERN OF COMPONENTS

Eye-estimates were made of the intensity of each line that was measured. As *quantitative measures* of absorption, these admittedly have little or no value. As indicators of *relative* strength, they are considered reliable and of sufficient accuracy for the immediate

TABLE 3*

VELOCITIES OF ORION AND HIGH-VELOCITY HYDROGEN LINES

Date (U.T.) 1935	Observatory†	IV$_1$ (Km/Sec)	IV$_2$ (Km/Sec)	V (Km/Sec)
Jan. 23.5	M	540 (1)	1030 (1)	
24.0	M		1015 (2)	1350 (1)
24.4	M		1000: (3)	1310 (1)
30.4	M	523 (5)	1026 (1)	1320 (1)
Feb. 3.4	M		980 (2)	1320 (1)
6.4	M	587 (1)	1015 (1)	1280 (1)
7.4	M	570 (1)	1055 (4)	
12.4	Ck			1290 (2)
13.4	M	560 (2)	1040 (2)	
15.4	M	295 (7)	1100 (1)	1320 (3)
18.4	Ck$_2$			1375 (4)
20.4	M	410 (2)	1000: (2)	1350 (2)
21.4	Ck$_2$			1260 (2)
23.5	M	500: (2)	1000: (2)	
25.4	Ck			1550 (2)
27.4	M	540: (2)	1060 (5)	1360 (4)
28.4	Ck			1350 (2)
Mar. 1.4	Ck			1350 (2)
3.4	M	474 (17)		1400: (3)
5.4	Ck			1500: (1)
6.4	M	392 (10)	1100 (10)	1370 (4)
9.4	M	329 (17)	633 (6)	1440 (2)
12.4	M	388 (8)	996 (5)	1400 (2)
15.4	M	406 (11)	1022 (9)	1500: (1)
15.5	W	428 (4)		
16.4	W	432 (6)		
18.3	M	423 (20)	923 (6)	1480 (2)
18.5	W	384 (6)		
20.4	M	457 (20)	630 (4)	1500 (2)
20.5	W	422 (7)		
22.3	M$_3$	466 (35)		1640 (3)
23.4	M	451 (4)	1020 (23)	1820 (1)
23.5	W		1032 (8)	
24.3	M$_2$	412 (29)	618 (7)	1580 (3)
25.5	W	449 (2)		
26.3	M$_3$	442 (25)	980 (25)	1665 (4)
26.4	W	461 (2)		
27.3	M$_2$	512 (41)	1035 (4)	1700 (2)
29.3	M$_2$	416 (50)	943 (8)	1630 (3)
Apr. 3.3	M	439 (20)		1570 (2)

* All velocities are negative.

† Letters have same meaning as in Table 1; in addition, Ck = plate from Cook Observatory. Subscripts denote number of plates.

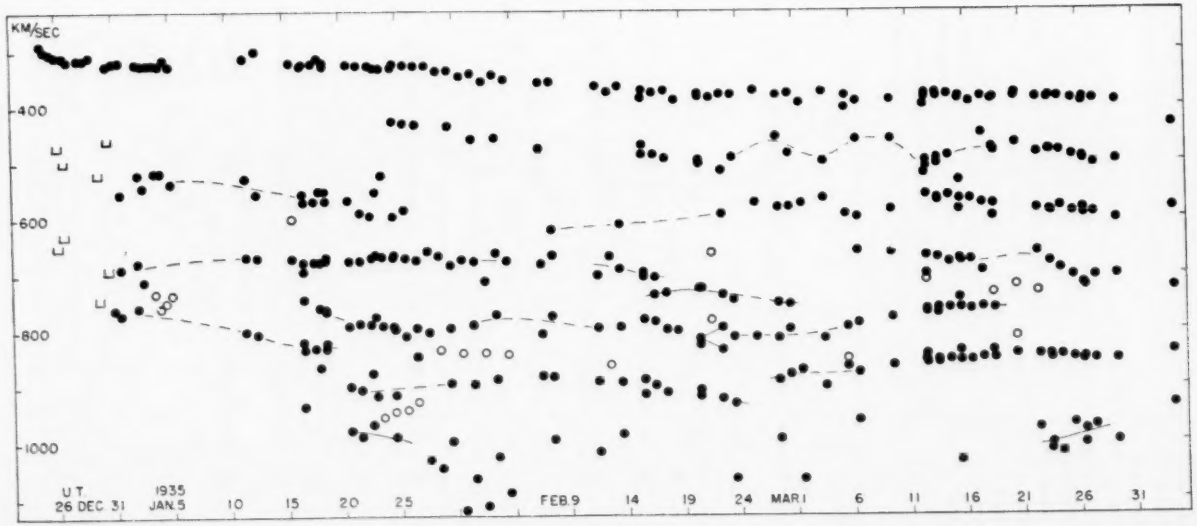

FIG. 1.—Radial velocities of Nova Herculis, absorption systems II (principal) and III (diffuse enhanced). Filled circles indicate separate components; open circles, blends; square U-shapes, violet edges of $H\alpha$ emission. The uppermost line of points is absorption II. For specific designations of other components see Fig. 3.

purpose of outlining the changes that occurred. They were obtained with the expenditure of a minute fraction of the labor that would have been involved in spectrophotometric measurements of the same lines.

It would serve no purpose to reproduce the individual data here. The results are shown diagrammatically in Figure 3. In each of the shaded bands the central line is the velocity-curve of an absorption component that would be obtained by drawing a smooth curve through the points in Figure 1. The vertical width of each band represents the strength of that component averaged over all the lines measured and with the small irregularities that are attributed to accidental errors of estimation smoothed out. *The widths do not represent line widths* and, in fact, have no well-defined relation to them.

Inspection of Figure 3 shows that the pattern of absorption components underwent a series of changes of extraordinary complexity and that some supposed shifts (based on measures of blended lines) were due to disappearance of one component and nearly si-

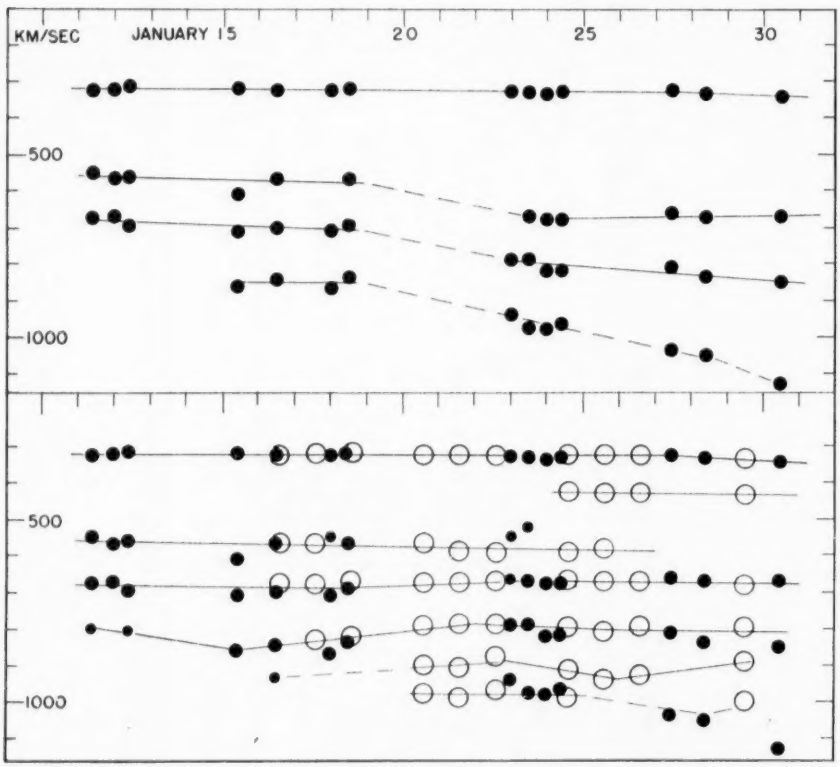

FIG. 2.—Comparison of former (1937) and present interpretations of absorption velocities of Nova Herculis, for the interval January 10–30, 1935. Upper half of figure contains only data based on velocities in *Michigan Obs. Pub.*, **6**, 150, Table 11, and 178, Table 22, 1937. Velocity-curves indicate the interpretation adopted in 1937.

Lower half contains the same data (*larger filled circles*), with the addition of new measures of Michigan plates (*smaller filled circles*) and Mount Wilson velocities (*open circles*). Velocity-curves indicate the new interpretation (1953).

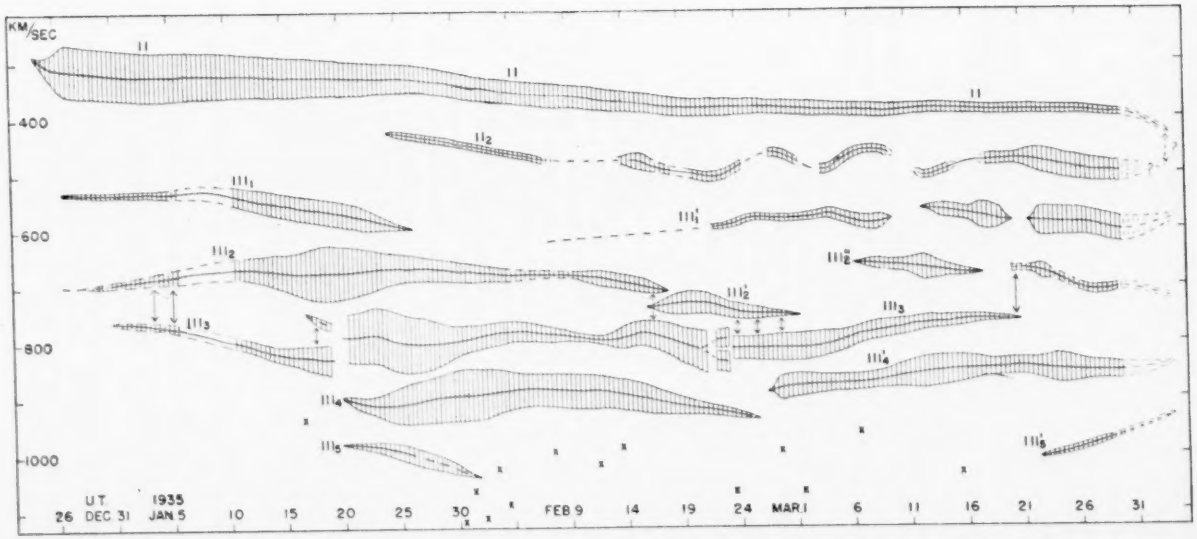

FIG. 3.—Velocity-intensity diagram for absorption systems II and III of Nova Herculis. Vertical width of each shaded band represents intensity (*not* line width) of component. Central line of each band is velocity-curve based on points in Fig. 1. Vertical arrows between bands indicate blending. Crosses represent velocities of isolated components of large displacement.

multaneous emergence of a new one. Especially noteworthy are some sudden disappearances followed by reappearance of what must undoubtedly be the same lines. Examples are seen particularly during March. These vanishings cannot be explained by any exposure effect. The components in question simply ceased to be visible, and continuum (or perhaps faint overlying emission?) appeared in their places. Several remaining interruptions of the record were filled in by close inspection of the spectra reproduced in Stratton and Manning's atlas of Nova Herculis.

A detailed account of the changes of strength is given in the appendix to this paper. It is not necessary to the continuity of the discussion and need be read only if one is interested in the behavior of various elements in the specific components.

DISCUSSION

The picture that emerges is in some ways simpler and in others more complex than that which was formerly entertained. On the one hand, the older interpretation involved accelerations that continued for a limited interval and then ceased, but the shells involved appeared to be discrete and to have a continued existence. The new interpretation is simple, so far as the velocities of components are concerned. No rapid accelerations remain, so that one complication that formerly required explanation has vanished. But another phenomenon, the systematic fading of one component and intensification of another, now poses a different problem of explanation.

As a working hypothesis, the diffuse enhanced system, absorption III, is assigned to a region inside the principal expanding shell. Observations that support this have been summarized elsewhere.[9] Briefly, they are of two kinds: (*a*) superposition effects, such as cutting of diffuse enhanced emission by principal absorption lines, and obliteration of diffuse enhanced absorption by principal emission of other elements and (*b*) secondary light-variations of the star, commonly accompanied by conspicuous changes in the diffuse enhanced absorption, while the principal spectrum shows relatively little response.

The higher velocity of the diffuse enhanced components would enable the atoms involved to overtake the principal shell. The great strength of the diffuse enhanced lines is attributed to a curve-of-growth effect of turbulent broadening. In spite of their strength, these lines probably are produced by a much smaller number of atoms than those in the principal shell. When the shells collided, the diffuse enhanced would simply merge with the principal, losing its identity and only slightly accelerating the principal shell.

The lifetimes of the earlier diffuse enhanced components in Nova Herculis agree rather well with this hypothesis. The rapid strengthening of the principal spectrum, absorption II, on December 26 may be taken as the date of "origin," that is, its emergence into view at some unspecified distance from the center of the star. Absorption III_1 was first fairly strong after January 5 but before January 11 and was weakening by January 23. We assume that January 8 was the date of emergence from a position close above the star's effective photosphere and that January 23 was the date when it overtook the principal shell. Then we have:

Absorption II: December 26–January 23; velocity 320 km/sec; distance traversed = 7.8×10^8 km.

Absorption III_1: January 8–23; velocity 550 km/sec; distance traversed = 7.1×10^8 km.

The already close agreement could be improved by assuming an earlier date for the emergence of III_1.

Table 4 contains the data and results of calculation for the preceding example and for each of the other components. In each case the choice of the date of first strong emergence is subject to a little leeway, and the date of fading is more uncertain, owing to its gradual character. But the interesting feature is that the largest discrepancy is less than 25 per cent.

[9] *Ibid.*, **59**, 247, 1947.

An objection can easily be raised to all these results except that for III_4. Thus each of the others was visible as a *faint* absorption for a number of days before it strengthened rapidly. If we counted the time interval from the first date on which it was detected, all the distances would be increased, and the agreement with distances traversed by the principal shell would be much poorer. However, these first faint trickles of atoms that preceded the development of the spectrum in strength are features of no consequence in the later history of the component. Certainly these first atoms would arrive at the principal shell long in advance of the main body, but their engulfment would be signalized by no observable event in the spectrum.

The gradual character of the disappearance of each component can be interpreted to mean that each shell or cloud had very great depth, so that the process of collision occupied an interval of several days. Each one, in turn, almost disappeared; and up to this point the hypothesis of successive ejection of clouds, successively overtaking the principal shell, appears to be in agreement with the facts.

TABLE 4

DISTANCES TRAVERSED BY ABSORBING SHELLS

Absorption Component	Dates of Emergence	Fading	Mean Velocity (Km/Sec)	Distance Traversed (Unit = 10^8 Km)
II	Dec. 26	.....	320	7.8
III_1	Jan. 8	Jan. 23	550	7.1
II	Dec. 26	.....	325	9.0
III_2	Jan. 10	Jan. 27	680	10.0
II	Dec. 26	.....	330	11.7
III_3	Jan. 19	Feb. 5	800	11.7
II	Dec. 26	.....	340	16
III_4	Jan. 24	Feb. 18	900	19.5

A really serious difficulty now develops in the apparent *revival* of each component. Thus III_2 strengthened slightly and lasted several days more, until February 16, then disappeared but was replaced by one of slightly greater velocity. Absorption III_3, or a successor with similar velocity, increased greatly after February 12, and, after some complicated behavior about February 22, an apparent lineal descendant persisted until March 19. Absorption III_4 disappeared February 25, but it was immediately replaced by a new line with velocity about 50 km/sec less. This component lasted until the end of March. If the disappearances in late January and early February were due to engulfment and destructon of identity, how can we explain these apparent continuations?

So far, the discussion has been based upon the probably naïve assumption that a nearly constant velocity implies the existence of a discrete cloud moving with the indicated speed. That this is not necessarily true will be obvious when we recall that P Cygni exhibits such an effect; yet over an interval of many years it has undergone no appreciable progressive evolution of the kind that would surely occur if the *region of absorption* moved outward with the *absorbing atoms*. Just as in the atmosphere of P Cygni, so in the diffuse enhanced atmosphere of Nova Herculis, we may have observed the velocities of atoms passing through a region within which they absorbed certain lines strongly and outside of which they were either too little or too highly ionized or excited to produce the lines in question.

Continuous ejection, then, is considered to hold the key to interpretation of the diffuse

enhanced system. As soon as one group of clouds has overtaken the principal shell and merged with it, losing its identity, a new set of clouds becomes visible. Until the first set disappeared, the lines of the second were covered by those of the first (which had similar velocities). When the first disappeared, the underlying ones were unveiled.

From about March 1 to the final disappearance of all absorptions early in April, the components of absorption III for the greater part lacked the diffuseness that had characterized them earlier. During this interval it is believed that no additional diffuse enhanced clouds were ejected from the star, and those that already existed simply continued outward as discrete shells, overtaking the principal shell and perhaps colliding with one another. The possibilities are so numerous that it may never be possible to work out the complete picture with any confidence in its specific details. But the complex strengthenings, fadings, and new formations during March do indeed suggest a chaos of interacting gas clouds.

We should not forget that ejection from the star was still continuing, even though not in the form of the diffuse enhanced spectrum. The Orion lines attained great strength in the latter part of March, and absorption V (called XI in my earlier paper) continued at the hydrogen lines. Both these systems are assigned an origin in the inner cloud about the star, well inside the expanding shells that the remaining diffuse enhanced components represented. This aspect of the problem will not be pursued further at this time.

A word should be said concerning the sudden vanishing and reappearance of components within a few days, as exhibited particularly by absorption III_1 about March 11 and 21. The first of these dates was at the end of a decline from a secondary maximum of light, and perhaps even at a slight minimum. The second date was midway in a very prominent light-minimum. Subordinate minima of light of a nova commonly coincide with increased excitation of the surrounding gases.[10]

The following hypothesis appears hopeful as an explanation of the changes about March 11 and 21. Granted that a number of expanding shells of gas exist about a nova, the *temporary* disappearance of a component represents a decreased number of atoms available for the production of the line in the particular cloud that has that velocity. It is suggested that this deficiency is produced by ionization of the gas in that shell. Thus a minimum of light, which represents a rise in temperature of the effective photosphere of the central star, might be accompanied by the temporary erasure of an absorption component arising in an innermost shell. This would mean that absorption III_1, *at the date under discussion*, was innermost. This, however, implies no contradiction of the suggestion that it was outermost in the January phase of the spectrum, since the original III_1 shell had long since disappeared and the the similar velocity of the newer component III_1 must be regarded as a coincidence.

Following the consequences of our hypothesis a little further, we note that the ionization would render the innermost shell transparent not only in its lines but in the Lyman continuum, so that radiation formerly screened from outer shells would reach them. Atoms of the outer shells would then be excited, and a corresponding intensification of their lines would occur. In this manner a succession of shells or clouds could be first excited and then ionized, so that the region in which a given type of spectrum was produced would progress outward in the surrounding material. It even seems possible that this hypothesis may prove to be a more acceptable explanation of the shifting of strength from absorption III_1 to III_2 to III_3, and finally to III_4, that occurred in January. According to this view, the shells were not ejected at later and later times with higher and higher speeds, but all may have been erupted almost simultaneously, so that the most rapidly moving was outermost.

The available data do not immediately suggest a way in which the decision could be made between these alternative interpretations. At the moment, however, I am inclined to give considerable weight to the agreement of traversed distances in Table 4 and to

[10] McLaughlin, *Michigan Obs. Pub.*, **8**, 180, 1943.

adopt the concept of successive ejection with increasing velocity for the components observed during January. For the later stages a totally new set of components, with velocities in the neighborhood of those of the vanished ones, is suggested. Of this new set of clouds or shells, the slowest may well have been the innermost. It must be emphasized, however, that all interpretations of this sort are tentative and that both of the suggested alternatives may be very far from correct.

It is a pleasure to acknowledge my indebtedness to Dr. I. S. Bowen, director of Mount Wilson and Palomar Observatories, for the privilege of using the Mount Wilson spectrograms of Nova Herculis. To Dr. F. J. M. Stratton is due the credit for specifically suggesting an interpretation that has proved to be correct. The expenses of travel to Pasadena, for the purpose of this study and others, were defrayed by a grant from Faculty Research Funds of the Horace H. Rackham School of Graduate Studies of the University of Michigan, which is gratefully acknowledged.

APPENDIX

DETAILED BEHAVIOR OF ABSORPTION COMPONENTS

DECEMBER 26–JANUARY 5

During this period the principal spectrum, absorption II, was at full strength, and the diffuse enhanced system, absorption III, began to develop. Component III_1 first appeared at *Hα* on Mount Wilson grating plates taken December 26.0. It was not seen unblended at *Hβ* and *Hγ*, but on December 31 it was present at *Hδ*. It was still weak on January 5. Component III_2 was probably present at *Hα* on December 26, for a definite violet emission edge at −650 km/sec was seen on Mount Wilson grating plates. Slowly strengthening absorption was seen from December 31 on at hydrogen lines and at λ 4924, λ 5018 *Fe* II. In the meantime, a more displaced violet emission edge appeared on December 29 at *Hα*, with velocity −750 km/sec. This probably indicates the emergence of absorption III_3. Weak absorption lines with velocity about −770 km/sec were measured at *Hγ* and *Hδ* on December 31. By January 3 the lines of hydrogen and *Fe* II were apparently inextricable blends of III_2 and III_3. The resulting diffuse line was becoming fairly conspicuous by January 5.

JANUARY 11–FEBRUARY 2

The next plate measured was taken January 11. On that date, III_1 was conspicuous at the lines of *Ti* II, where it was the strongest component. Already III_2 surpassed III_1 at the hydrogen lines and was strengthening at *Ti* II and *Fe* II. III_3 was again resolved from III_2 but was still weak. By January 16 a weak component of III_1 was present at K but was overshadowed by the great intensification of III_2. At the *Ti* II lines III_2 had by now become the stronger member. The greatest intensity of III_2 was attained on January 18, when it formed wide, diffuse components at hydrogen, the K line, and the strong *Fe* II lines.

The strengthening of III_3 was slower, and it was still quite subordinate on January 18. But by January 20 a marked change of both intensity and position had occurred. At the hydrogen and K lines, III_3 had risen to or even passed full equality with III_2, and it was strong at *Ti* II and *Fe* II lines. In the 2-day interval, III_3 had shifted position from a velocity of −840 km/sec to −800. This change has the appearance of a genuine discontinuity. In view of clear evidence in other cases, the hypothesis of a deceleration of a discrete shell is rejected. The shift is considered to be due to rapid intensification of a new unresolved component of smaller displacement. However, the same designation, III_3, is retained.

On January 21 and 22, III_3 was considerably stronger than III_2 at K and the hydrogen lines, but was already weakening again at the lines of *Ti* II. At the *Fe* II lines, III_2 and III_3 were approximately equal. The greatest strength of the diffuse enhanced spectrum,

January 22–24, was due in the greatest measure to component III_3 and only slightly less to III_2. The early fading of the *Ti* II lines of III_3 left III_2 as the strongest component of *Ti* II. Beginning January 20, component III_1 faded rapidly and soon disappeared. It remained longest at K, where it was last seen January 25. From January 24 on, III_2 weakened, and it had become rather minor by January 31.

Meanwhile, two new components of greater displacement had emerged. These were III_4 and III_5, first seen faintly at hydrogen lines on January 20. Of these, III_4 was always the stronger, but it was troubled by blending with III_5, which was imperfectly resolved for a few days, especially January 24 and 25, when the two formed a strong blend at the hydrogen lines and K. On January 27, III_4 and III_5 were resolved on a Michigan two-prism plate. The former was still strengthening, and, what with the simultaneous fading of III_3, by January 29, III_4 was much the strongest of the diffuse enhanced components at the hydrogen lines and K. At the *Fe* II lines, III_4 was approximately equal to III_3. The *Ti* II lines had not developed III_4 components. The lines of III_5 weakened after January 25 and were quite inconspicuous by February 2.

Summarizing the behavior of the diffuse enhanced components, during the period January 11 to February 2, there was a systematic transfer of the maximum strength from component III_2, through III_3, to III_4. On plates of lower dispersion this could and did produce the illusion of a single very diffuse line shifting rapidly to a position of greater displacement. The true situation was that only small changes of velocity affected any given component. The hydrogen and metallic lines of any one system had velocities that agreed satisfactorily. The ratios of intensity, however, were different. On plates of low dispersion this could result in rather conspicuous apparent systematic differences between hydrogen and metallic velocities.

During this interval the principal system, absorption II, was weakening. However, at the end of the time the hydrogen, *Ca* II, *Ti* II, and *Fe* II lines were still strong, and numerous other metallic lines, e.g., those of *Fe* I, were still present.

From January 24 on, a weak line was measured at K with a velocity of about −450 km/sec. No corresponding feature was found at the hydrogen lines. This is referred to as "absorption II_2." Much later in the history of the nova, components believed to belong to this system did finally appear at the hydrogen lines.

FEBRUARY 2–MARCH 1

Absorption III_4, wide and strong at the lines of hydrogen, *Ca* II, and *Fe* II, was the outstanding component at the beginning of this period, and it remained so until February 15. It was flanked by somewhat weaker III_3 and much weaker III_2 on the longward side and by very weak III_5 to the shortward. This last component practically disappeared immediately, though an occasional plate thereafter showed one or two lines that could be referred to it.

Absorption III_2 had almost disappeared at the hydrogen lines by February 6, but it persisted at *Ti* II, and probably weak III_4 components emerged at the *Ti* II lines. Absorption III_2 increased again slightly at the hydrogen lines on February 11.

Absorption III_3 remained measurable at the hydrogen lines until February 7, after which it was almost lost for a few days, though the velocities of the green *Fe* II lines seem to indicate that it persisted there. It then recovered slowly and was again strong by February 15, and inferior only to III_4. During the night of February 16.5 U.T., rapid change occurred. Apparently III_2 at −700 km/sec faded rapidly, while a new line at −730 km/sec strengthened. The change in *Ti* II seems to have preceded that in hydrogen. At any rate, a sudden shift toward the violet was evident; and on February 17 the new component, now called "III_2'," was conspicuous at a number of metallic lines as well as those of hydrogen, though at the latter it was subject to troublesome blending with III_3. A Mount Wilson coudé plate, February 20, showed the components resolved. Absorption III_3 had now become the strongest, III_4 was narrow and weaker, and III_2' was interme-

diate in strength at hydrogen and the K line. Another coudé plate on February 22 showed a further remarkable change. Absorption III_3 had split into two components, the shortward of which was slightly the stronger. Together they exceeded in strength the components III_2' and III_4. Their separation was too small to be resolved on the plates of lower dispersion on following dates. The trend of velocities of the blend before and after the clear doubling suggests that the shortward component was a new one that emerged briefly and then subsided. By February 27, III_3 was again near the position it had occupied before February 18 and was the strongest component. III_2' was still present but weak, and it was not seen after February 28.

Absorption III_4, which had been slowly drifting toward greater displacement, weakened gradually after February 15. As already noted, it was weaker than III_3 by February 20. It was still measurable with difficulty (velocity -940 km/sec) and was last seen on the spectrogram of February 24 reproduced in the Stratton and Manning atlas. It was definitely absent February 26. Then on February 27 a new component emerged at -900 km/sec. This is called "III_4'," simply because its position was not far from that of III_4, but the designation carries no implication of a genetic relationship.

The coudé plate of February 22 showed, for the first time, fine components at *Hζ*, K, and 4233 *Fe* II, with velocity about -590 km/sec. Several plates on following days showed weak lines of similar velocity at *Hζ*, K, *Hδ*, and occasionally a line of *Ti* II or *Fe* II. The position of this component suggests a remote possibility that it was a revival of absorption III_1 (though this is difficult to reconcile with the hypothetical model). It is designated "absorption III_1'."

In summary, fluctuations of intensity of the several components of the diffuse enhanced system presented a complexly changing pattern. The strongest and most displaced component weakened and disappeared, but almost immediately a new one of only slightly smaller displacement "stepped into the breach." A new component emerged faintly in a position near that of the least displaced line which had disappeared a month earlier. On plates of low dispersion these changes produced apparent oscillations of the blended lines, which plates of higher dispersion conclusively prove to have been illusory.

During the interval February 2 to March 1, the principal spectrum, absorption II, weakened steadily. At the end, only the lines of hydrogen, *Ca* II, *Ti* II, *Mg* I, and a few of the strongest of *Fe* II remained conspicuous. The component at K, designated "II_2," after a period of invisibility, became more conspicuous on February 15 and was measured sporadically thereafter not only at K, but at *Hζ*, *Hδ*, and 4233 *Fe* II as well.

MARCH 1–APRIL 3

The most striking change in the diffuse enhanced spectrum near the beginning of this interval was the rapid weakening of its components at the K line. By March 9 these were quite weak, but they were followed as fine lines until March 19. The hydrogen components were more persistent, though all of them had become narrow and well defined by March 20. At the beginning of the period, III_3 was the strongest. It was flanked on the shortward side by III_4', which had just appeared on February 27. To the longward, about halfway to absorption II, was a very weak and difficult line, III_1'.

Complex changes of strength of the several components followed. Absorption III_3 weakened slowly, with a gradual shift toward smaller displacement, while III_4' increased rapidly. By March 12, III_4' was the stronger of the two. Both were still moderately strong lines but had lost their diffuse wings. The weakening of III_3 continued, but on March 18 it was still seen at the higher Balmer lines. In the meantime, faint absorption appeared on March 6 at *Hγ*, *Hδ*, and 4233 *Fe* II, with velocity -660 km/sec. This will be designated "III_2''," since it fell in the vacancy left when III_2' disappeared. It remained weak, though measurable at a few hydrogen lines, until March 17, when it temporarily disappeared. The faint line called "III_1''" remained weak, disappeared on March 10, reappeared two days later, and strengthened until March 18, when it was conspicuous at

the higher Balmer lines and even exceeded III_4', which had become narrower. By March 20 another abrupt change had taken place. Absorptions III_2'' and III_3 had apparently both weakened and merged in a hazy blend, and the history of III_3 ended, since the later velocity trend indicates that III_2'' was dominant; III_1' had also completely vanished. This left a single sharp line, III_4', as the strongest remnant of the diffuse enhanced absorption, and it was appreciably weaker than the principal line, absorption II. By March 22 the pattern had again changed: III_1' had reappeared in considerable strength; III_2'' had apparently been freed of the blend with III_3 (which had vanished), and a fine weak absorption component had appeared with a velocity of about -1000 km/sec. This has the appearance of being a revival of the long-vanished component III_5.

During the period just described, absorption II_2 had been very weak but was measured on coudé plates on March 12 and 13. On March 22 it appeared suddenly stronger, almost equal to the principal component II. All the lines appeared decidedly stronger on March 23, save for III_2'', which was again difficult. From this date until March 29, all the components remained visible with little loss of intensity, except for III_4', which was weaker than III_1'. The latter was almost as strong as the principal line, absorption II. The last record of absorption lines was obtained on April 3, when the star was already beginning the steep decline. Absorption III_4' had vanished, II_2 was certainly weak but perhaps blended with II, while III_1' and III_2'' remained distinct, though weak. An extremely feeble line at $H\gamma$ and $H\delta$, with velocity -932 km/sec, was perhaps a remnant of III_5. Before the steep decline of light, the remaining lines in the principal absorption spectrum were chiefly those of hydrogen, *Ca* II, *Mg* I, a number of lines of *Ti* II, and a few of the strongest of *Fe* II.

ON THE SPECTRUM OF CHI CYGNI NEAR THE TIME OF LIGHT-MAXIMUM

YOSHIO FUJITA
Department of Astronomy, University of Tokyo
Received March 30, 1953; revised June 1, 1953

ABSTRACT

Spectrographic observations of χ Cyg were made before and after its light-maximum in the 1950 cycle. From microphotometric tracings we derived the central intensity of some absorption lines and the actual emission of some emission lines in units of the intensity of the neighboring continuous spectrum. In absorption, the features of the *Ca* 4227 line and the *TiO* band show interesting variations. In emission, Balmer lines are inclined to have M-type characteristics.

The variation of the spectra of the long-period variable stars following their light-cycles has been one of the interesting problems in stellar spectroscopy. It must be emphasized that this study offers us a key to the solution of the physical condition of these stars. Several investigators[1] have hitherto studied the spectra of the long-period variable stars of types M and S and obtained many interesting results. The main object of this paper is to add some observational data to the solution of the problem of the long-period variable stars.

Spectrographic observations[2] of χ Cyg were made before and after its light-maximum[3] in the 1950 cycle with the two-prism spectrograph attached to the 36-inch refractor of the Lick Observatory. The observational data are given in Table 1. The tracing of these

TABLE 1

OBSERVATIONAL DATA

Plate No.	Date	Spectrograph	Emulsion
188	October 8, 1950		
195	October 10		
211	November 6	Two-prism, 6-inch	Eastman IIa-O
219	November 23		
232	December 12		

spectrograms was carried out with the registering microphotometer of the Yerkes Observatory. As it was thought of no use to measure the equivalent width of each line shown in the low-dispersion spectra, the central intensity of each line was considered. That is, compared with the intensity marks of the standard lamp, in the case of the absorption line the central absorption of each line was expressed in units of the intensity of the neighboring continuous spectrum; and in the case of the emission line, the actual emission was derived in units of the neighboring continuous spectrum. The results of these measurements and their reduction are shown in Table 2. It must be noted that lines listed in the table are those of good definition. In the case of molecular lines, the central intensity of each band head which belongs to a vibrational transition was measured. Although the intensity of the continuum during the time interval of our observation is believed to

[1] P. W. Merrill and C. G. Burwell, *Ap. J.*, **71**, 285, 1930; P. W. Merrill, *Spectra of Long-Period Variable Stars* (Chicago: University of Chicago Press, 1940); and *Ap. J.*, **103**, 6, 1946; **106**, 274, 1947; **107**, 303, 1948; **116**, 18, 21, 337, 344, 1952; P. C. Keenan, *Ap. J.*, **106**, 295, 1947; L. H. Aller and P. C. Keenan, *Ap. J.*, **113**, 72, 1951; and J. G. Phillips, *Ap. J.*, **115**, 183, 1952.

[2] Y. Fujita, *Ap. J.*, **113**, 626, 1951.

[3] The date of the predicted light-maximum was November 3, 1950.

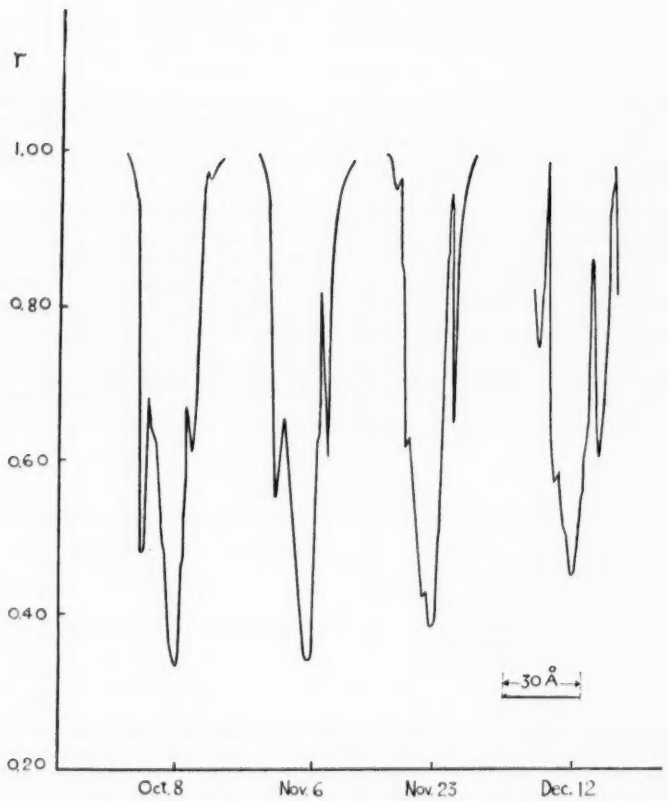

FIG. 1.—Standardized absorption profile of the *Ca* 4227 line

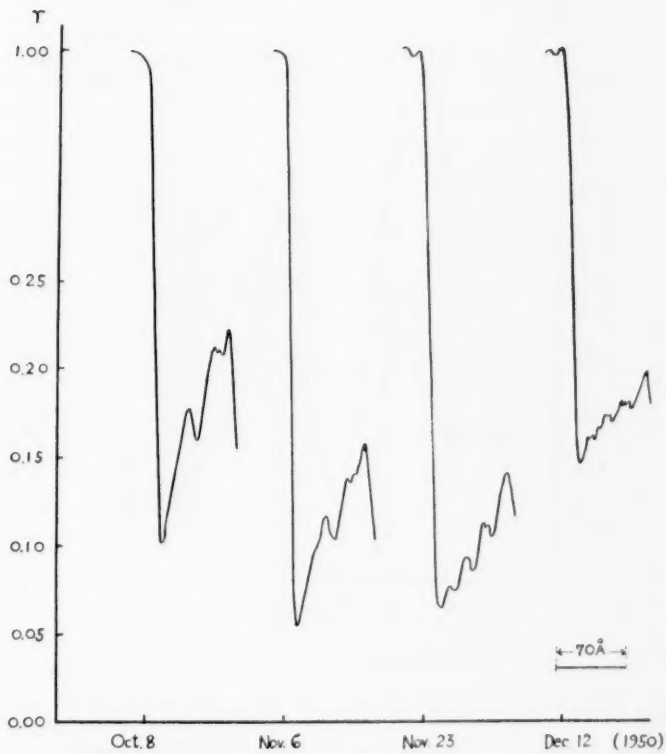

FIG. 2.—Standardized absorption profile of the (0, 0) sequence of the *TiO* band 5167

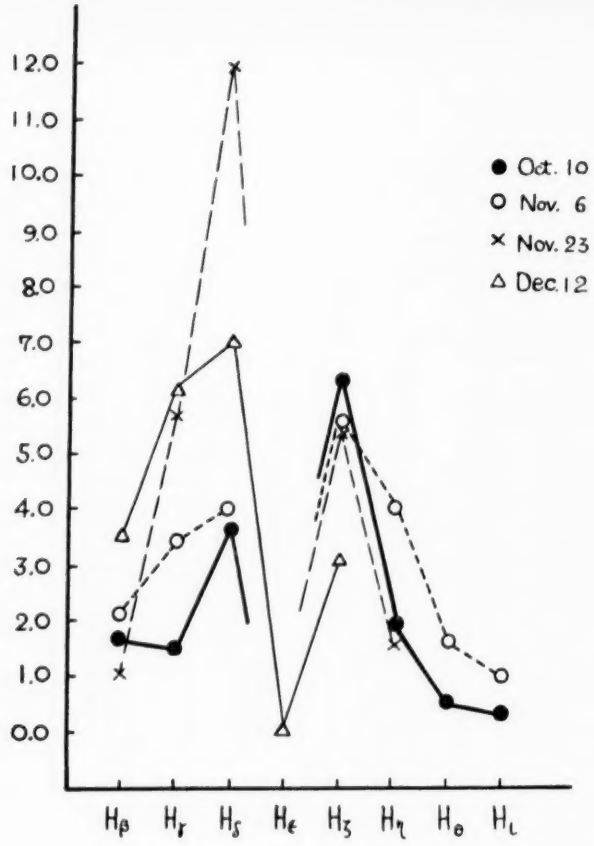

FIG. 3.—Intensity variation of Balmer lines

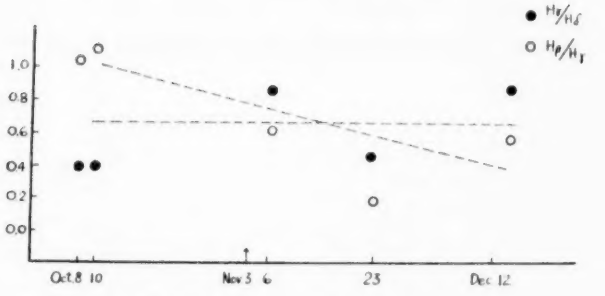

FIG. 4.—The relative intensity ratios $H\gamma:H\delta$ and $H\beta:H\gamma$

have changed, it will be interesting to compare the central intensity of the same spectral line corresponding to each different spectrogram.

The interesting change in the absorption profile through the time interval of our observation is indicated by the *Ca* 4227 line. Figure 1 shows the standardized profile of that line. Most of the absorption lines measured tend to show the low value of central intensity near the light-maximum. The behavior of the intensity variation, however, has a lack of symmetry with respect to the light-variation. The (0, 0) sequence of the *TiO* band 5167 also has a conspicuous variation in its behavior, which is shown in Figure 2. These

TABLE 2

CENTRAL INTENSITY OF SOME ABSORPTION LINES AND ACTUAL EMISSION OF SOME EMISSION LINES IN χ CYG

ELEMENT	DATE					ABSORPTION OR EMISSION
	Oct. 8	Oct. 10	Nov. 6	Nov. 23	Dec. 12	
TiO 5167	0.098	0.095	0.058	0.065	0.15	a
TiO 4955	0.36	0.38	0.23	0.22	0.15	a
Hβ	1.62	1.67	2.01	1.08	3.53	e
TiO 4761	0.39	0.40	0.26	0.25	0.15	a
TiO 4584	0.52	0.53	0.38	0.36	0.20	a
ZrO 4470	0.49	0.51	0.58	0.46	0.32	a
Hγ	1.55	1.50	3.32	5.66	6.14	e
Cr 4289.7	0.48	0.44	0.36	0.68	0.63	a
Cr 4274.8	0.49	0.47	0.36	0.47	0.53	a
Cr 4254.3	0.45	0.48	0.32	0.54	0.51	a
Ca 4226.7	0.33	0.32	0.35	0.38	0.45	a
Fe 4202.0	0.55	0.57	0.61	0.53	1.70	e
Hδ	3.79	3.76	3.97	12.05	7.00	e
Sr II 4077.7	0.76	0.76	0.47	0.65	0.69	a
K 4047.2	0.84	0.83	0.74	0.76	0.73	a
Ti 3998.6	0.93	0.89	0.62	0.71	0.89	a
Hε	*	Weak	Weak	Weak	0.12	e
Si 3905.5	*	2.17	2.88	1.86	1.08	e
Hζ	*	6.30	5.57	5.52	3.08	e
Hη	*	2.00	4.00	1.56	*	e
Hθ	*	0.54	1.66	*	*	e
Hτ	*	0.38	1.03	*	*	e

* No tracing.

changes may be explained mainly by the high temperature of the star at the time of light-maximum.

On the other hand, the appearance of some emission lines also shows interesting features. The intensity variation of Balmer lines indicates that χ Cyg has the characteristics of M-type stars, although some features of molecular lines clearly have a tendency toward S-type characteristics. In S-type stars Balmer lines show a gradual decrease toward the shorter-wave-length side. However, as is shown in Figure 3, it is seen that we have two maxima of intensity at *Hδ* and *Hζ*, and the weakness of *Hε* intensity is very pronounced. The relative intensity ratios $H\gamma/H\delta$ and $H\beta/H\gamma$ also show interesting features. The ratio $H\gamma/H\delta$ remains nearly constant, but $H\beta/H\gamma$ decreases with the advancing phase in the time interval of our observation. These appearances coincide well with the results obtained by Merrill[4] (Fig. 4).

In conclusion, I should like to express my appreciation to Dr. C. D. Shane, director of Lick Observatory, and Professor B. Strömgren, director of Yerkes Observatory, for having put at my disposal the observatory equipment.

[4] P. W. Merrill and C. G Burwell, *Ap. J.*, **71**, 285, 1930.

THE SPECTRA AND ROTATIONAL VELOCITIES OF THE BRIGHT STARS OF DRAPER TYPES B8–A2

ARNE SLETTEBAK
Perkins Observatory
Received June 25, 1953; revised July 28, 1953

ABSTRACT

Spectral types and rotational velocities of 179 stars of Draper types B8–A2 brighter than the fifth magnitude have been determined. Spectral types and luminosity classes were assigned to all normal stars on the Morgan-Keenan-Kellman system of classification. Equatorial rotational velocities multiplied by the sine of the inclination of the axis of rotation ($v \sin i$) were determined for all stars by comparing observed profiles of the *Mg* II 4481 line in each star with a set of profiles computed by the graphical method of Shajn and Struve.

The B8–A2 stars divide into a number of subgroups from the point of view of axial rotation: the supergiant, metallic-line, and peculiar A stars have small axial rotation; the normal stars of intermediate luminosity have moderate axial rotation ($\bar{v} = 93$ km/sec); and the normal main-sequence stars have the largest axial rotation ($\bar{v} = 177$ km/sec). The only comparison of the B8–A2 main-sequence stars with stars of other spectral types possible at this time is with the Be stars: the latter have about twice the average axial rotation of the B8–A2 main-sequence stars.

A number of emission-line stars and spectroscopic binaries included in this study are discussed. The variation of equivalent width of *Mg* II 4481 with spectral type is shown. Three stars were found to exhibit a general weakening of the spectral lines; it is suggested that these stars lie somewhat below the main sequence.

I. INTRODUCTION

The fact that some classes of stars are in rapid axial rotation while others are not is of great importance for the problem of stellar evolution. It is generally known through the researches of Struve, Elvey, Westgate, and others that axial rotation of single stars is limited to those of early type: stars of spectral type later than about F5 do not rotate with appreciable velocities. It is also generally known that among the early-type stars certain classes of stars are conspicuous for their very large or very small axial rotation: the B-emission stars are characterized by very large rotational velocities, while the supergiant stars and some groups of peculiar stars never show large rotations. Among the normal main-sequence and giant stars of early type, however, the dependence of axial rotation on spectral type and luminosity is not altogether clear. In order to obtain this information and further to provide a catalogue of rotational velocities for the brighter stars, the writer plans to investigate axial rotation in the brighter northern stars of early type. The Be stars and the more rapidly rotating B2–B5 stars have already been considered elsewhere.[1] In this paper the brighter stars of Draper types B8–A2 are considered.

II. THE OBSERVATIONS

The observational material was selected to include all stars brighter than magnitude 5.0 with Draper types between B8 and A2 and north of declination $-15°$. The total number of stars considered was 179. One or more spectrograms of each star were taken with the two-prism spectrograph attached to the 69-inch reflecting telescope of the Perkins Observatory, giving a dispersion of 28 A/mm at $H\gamma$ and 32 A/mm at λ 4481. All spectra were greatly widened, the ratio of spectrum width to the distance between $H\gamma$ and $H\delta$ being 4.5 to 1. This widening served the following purposes: (1) it permitted a more accurate spectral classification to be made, and (2) for those stars for which only one spectrogram was taken or for which only one spectrogram was of usable density, two

[1] *Ap. J.*, **110**, 498, 1949.

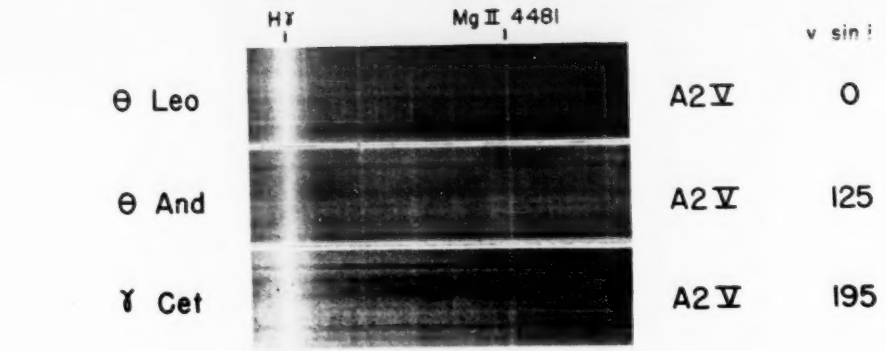

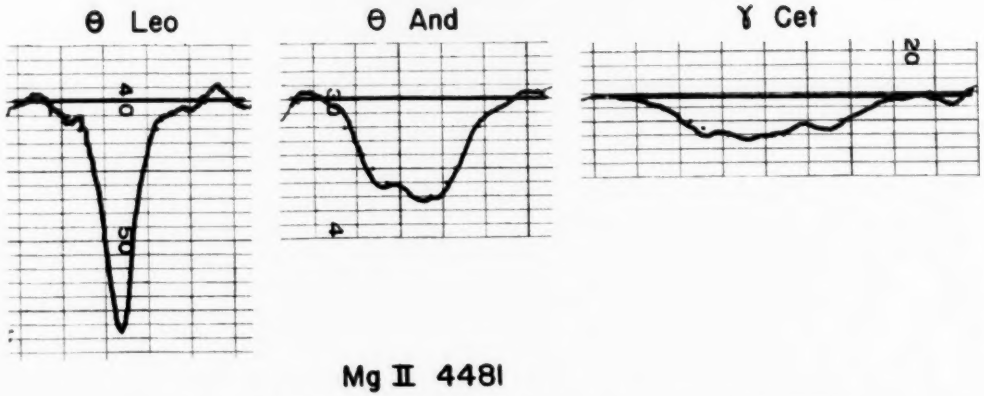

FIG. 1.—Line broadening by axial rotation in some representative A2 main-sequence stars

independent microphotometer tracings were still possible. Eastman 103-O plates treated with D19 developer were used for all stars, with the exception of the last eight stars to be observed, these being taken with Eastman IIa-O plates developed in promicrol. All plates were calibrated immediately after exposure with a spectral sensitometer located in the 69-inch dome. The sensitometer was calibrated photoelectrically with the very generous assistance of Dr. Robert Hardie. Line profiles were obtained from the plates with the aid of the Perkins microphotometer, a magnification of about 200 being employed. Figure 1, illustrating line broadening by axial rotation in some A2 V stars, shows the spectra employed in this paper and the resulting microphotometer tracings.

III. METHODS

1. THE ROTATIONAL VELOCITIES

The effect of axial rotation on a stellar spectrum is to broaden all spectral lines, the amount of the broadening depending upon the degree of axial rotation and the inclination of the axis of rotation. For single stars a study of line broadening interpreted as due to axial rotation will yield only values of $v \sin i$, where v is the equatorial rotational velocity and i is the angle of inclination between the axis of rotation and the line of sight. The latter quantity is usually unknown for single stars;[2] but for a large, homogeneous group of stars, assumptions can be made about the orientation of the rotational axes, and a mean value of the equatorial rotational velocity for the group can be obtained.

The method of obtaining the $v \sin i$'s is one suggested by Shajn and Struve[3] and was first employed by Elvey.[4] It is based on the assumption[5] that the contour of a line not influenced by rotation is similar to that actually observed in a sharp-line star of similar spectral type. The apparent disk of a star is divided into strips parallel to the axis of rotation, each of which produces the undisturbed contour, in an amount proportional to its relative area, for an undarkened star. An equatorial rotational velocity is then assigned to the star, and the contributions from the various strips, shifted by the necessary amount, are summed to give the rotationally broadened contour. By assigning various values of the equatorial rotational velocity, a series of computed contours is built up. Comparison with an observed contour of the same line in a star of unknown rotation will permit an estimate to be made of $v \sin i$ for the star.

The absorption line, *Mg* II 4481, was chosen for the determination of $v \sin i$ in all stars. It has the advantages of being free from Stark effect, unblended, and one of the strongest lines in the range of spectral types considered. The sharp-line stars, α Canis Majoris (A1 V) and α Lyrae (A0 V), were chosen as nonrotating standard stars, the former for comparison with strong lines and the latter with weaker lines. A set of rotationally broadened contours was then built up from each, using the mean of four independent profiles of *Mg* II 4481 for each standard. A limb-darkened stellar disk was assumed, divided into 40 strips. The value of the monochromatic darkening coefficient at λ 4481 employed was 0.73, obtained from the computations of Münch and Chandrasekhar.[6] This value refers to an A1 main-sequence star with continuous absorption by neutral hydrogen atoms and negative hydrogen ions. Figure 2 illustrates the observed contours of *Mg* II 4481 in α Canis Majoris and α Lyrae and the rotationally broadened line contours derived from them for values of the equatorial rotational velocity from 25 to 400 km/sec.

Two independent profiles were obtained for each of the stars considered. These were adjusted to have the same equivalent width as the appropriate standard profile by mul-

[2] Exceptions to this appear to exist among the Be stars, where inclination effects can be observed spectroscopically (see n 1).

[3] *M.N.*, **89**, 222, 1929.

[4] *Ap. J.*, **71**, 221, 1930.

[5] Justified by Carroll, *M.N.*, **93**, 478, 508, 680, 1933.

[6] *Harvard Circ.*, No. 453, 1949.

tiplying percentage absorptions in the line by the necessary scale factor. The comparisons were then made with the set of rotationally broadened profiles corresponding to the standard profile chosen. Finally, the two resulting values of $v \sin i$ were averaged, to give the rotational velocity of the star. These are listed in Table 1.

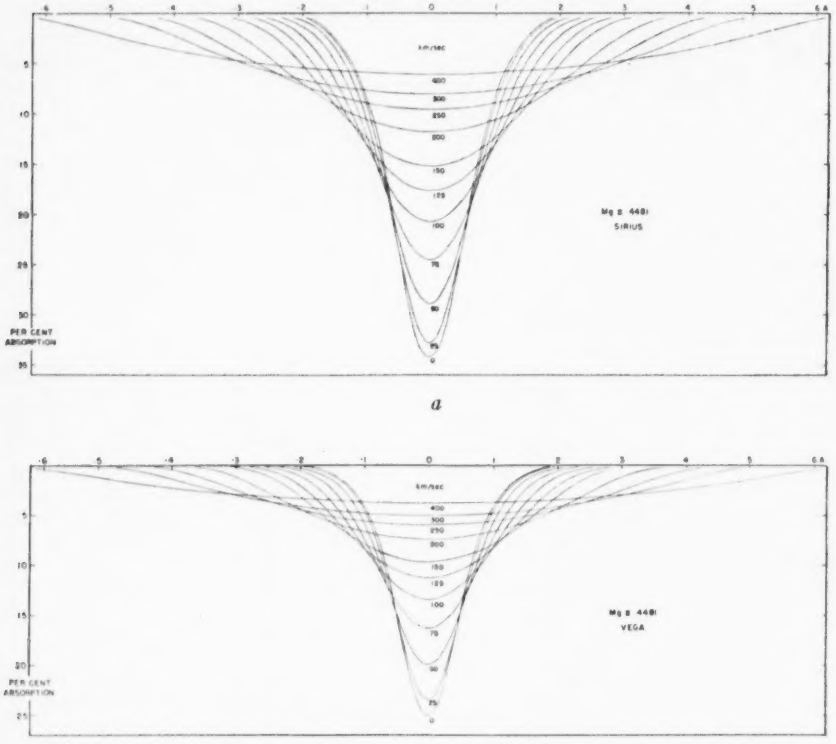

a

b

FIG. 2.—*a*, the observed profile of *Mg* II 4481 in α Canis Majoris (0 km/sec) and rotationally broadened line contours derived from it for ten values of the equatorial rotational velocity. *b*, the observed profile of *Mg* II 4481 in α Lyrae (0 km/sec) and rotationally broadened line contours derived from it for ten values of the equatorial rotational velocity.

2. THE SPECTRAL TYPES

The second observational datum which is required to be known accurately in this investigation is the spectral type. Further, for the normal stars a luminosity class must also be assigned, since axial rotation may depend upon luminosity as well as spectral class. A two-dimensional classification on the Morgan-Keenan-Kellman system[7] was attempted for each of the normal stars, using both Perkins and Yerkes plates. The procedure was the following: all stars were first classified as accurately as possible from the Perkins plates and were then classified independently from Yerkes spectrograms of dis-

[7] *An Atlas of Stellar Spectra* (Chicago: University of Chicago Press, 1943).

TABLE 1

SPECTRAL TYPES AND ROTATIONAL VELOCITIES OF THE B8-A2 STARS

Star	(1900)	(1900)	m_v	Sp(HD)	Sp(MKK)	v sin i (km/sec)	Δ/2 (km/sec)	Notes
α And	$0^h\ 3^m.2$	+28°32'	2.15	A0p	B9p	52	7.5	1
θ And	0 11.9	+38 8	4.44	A2	A2V*	125	0	
σ And	0 13.1	+36 14	4.51	A2	A2V	130	0	
μ And	0 51.2	+37 57	3.94	A2	A5V	80	0	
φ And	1 3.7	+46 43	4.28	B8	B7V	72	7.5	2
ν Psc	1 14.0	+26 44	4.67	A2	A2V	98	2.5	
τ And	1 34.7	+40 4	4.90	B8	B8IV	88	12.5	
γ' Ari	1 48.0	+18 48	4.75	A0p	B9V	182	17.5	
γ² Ari	1 48.0	+18 48	4.83		A1p	50	20	3
50 Cas	1 54.9	+71 56	4.05	A2	A1V	82	2.5	4
4 Per	1 55.6	+54 0	4.99	B8	B8V	81	1	
α Psc(br)	1 56.9	+ 2 17	4.33	A2p	A2p	92	7.5	5
58 And	2 2.5	+37 23	4.77	A2	A5V	155	15	6
γ Tri	2 11.4	+33 23	4.07	A0	A0V	230	10	
ρ Cet	2 21.1	-12 44	4.90	A0	B9V	230	40	
ψ² Cet	2 22.8	+ 8 1	4.34	A0	B9III*	62	7.5	
ζ Cet	2 38.1	+ 2 49	3.58	A2	A2V	195	15	7
π Per	2 52.4	+39 16	4.62	A2	A2V	168	17.5	
HR 932	3 1.1	+74 1	4.89	A2	A0V	270	5	
β Per	3 1.7	+40 34	2.2-3.5	B8	B8V*	65	0	8
ζ Ari	3 9.2	+20 40	4.95	A0	A0IV-V	142	7.5	
32 Per	3 14.7	+42 58	4.98	A2	A2V	155	5	
HR 1035	3 21.0	+59 36	4.42	B9p	B9Ia*	<18	7.5	
ψ Tau	3 21.8	+ 9 23	3.75	B8	B8p			9
HR 1040	3 21.9	+58 32	4.76	A0p	A0Ia*	0	0	
HR 1046	3 22.4	+55 6	4.99	A2	A1V*	178	2.5	
17 Eri	3 25.7	- 5 25	4.80	B9	B8V	72	17.5	
γ Cam	3 39.8	+71 1	4.67	A0	A3IV	205	15	
27 Tau	3 43.2	+23 45	3.80	B8	B8III*	160	10	
HR 1204	3 48.6	+62 47	4.87	B9	B9V	110	15	10
ν Tau	3 57.8	+ 5 43	3.94	A0	A1V	70	0	
λ Per	3 59.1	+50 5	4.33	A0	B9V	210	20	
68 Tau	4 19.7	+17 42	4.24	A2	A2IV	15	15	
π³ Ori	4 45.2	+ 8 44	4.35	A0	A0V	218	7.5	
7 Cam	4 49.3	+53 36	4.44	A2	A1V	42	12.5	11
π¹ Ori	4 49.4	+10 0	4.74	A0	A0p	108	17.5	12
4 Aur	4 52.5	+37 44	4.99	A0	A0V*	92	2.5	
ψ Eri	4 56.8	- 7 19	4.81	B8	B2V			13
11 Ori	4 58.9	+15 16	4.65	B9	A0p	90	5	14
ι Lep	5 7.6	-11 59	4.54	B8	B8V	195	35	
κ Lep	5 8.6	-13 4	4.46	B8	B8V	125	5	
β Ori	5 9.7	- 8 19	0.34	B8p	B8Ia*	<65	10	
β Tau	5 20.0	+28 31	1.78	B8	B7III*	82	12.5	
ζ Lep	5 42.4	-14 52	3.67	A2	A3V	245	5	
134 Tau	5 43.9	+12 37	4.92	B9	B9IV*	8	7.5	
ψ Aur	5 46.5	+55 41	4.92	A2	A2p?	68	17.5	15
136 Tau	5 47.1	+27 35	4.54	A0	A0III	30	10	16
β Aur	5 52.2	+44 56	2.1-2.2	A0p	A2IV*			17
θ Aur	5 52.9	+37 12	2.71	A0p	A0p	48	17.5	18
μ Ori	5 56.9	+ 9 39	4.19	A2	Am	20	15	19
3 Mon	5 57.1	-10 36	4.97	B8	B5IV	80	5	
θ Lep	6 1.6	-14 56	4.67	A0	A1V	215	20	
HR 2209	6 7.8	+69 21	4.73	A0	A0V	308	32.5	
2 Lyn	6 10.8	+59 3	4.42	A0	A2V	0	0	
HR 2244	6 11.2	-13 41	4.99	B9	B8V	235	10	

TABLE 1 (Continued)

SPECTRAL TYPES AND ROTATIONAL VELOCITIES OF THE B8-A2 STARS

Star	(1900)	(1900)	m_v	Sp(HD)	Sp(MKK)	v sin i (km/sec)	Δ/2 (km/sec)	Notes
13 Mon	$6^h27^m.5$	+ 7°24'	4.50	A0p	A0Ib*	<12	12.5	
γ Gem	6 31.9	+16 29	1.93	A0	A0IV*	48	12.5	
α CMa	6 40.8	-16 35	-1.6	A0	A1V*	0		20
θ Gem	6 46.2	+34 5	3.64	A2	A3III*	130	20	
16 Lyn	6 50.3	+45 13	4.80	A2	A2V	195	20	
δ Mon	7 6.8	- 0 20	4.09	A0	A0IV	155	15	
HR 2751	7 10.9	+49 39	4.80	A2	A3III-IV	210	10	
λ Gem	7 12.4	+16 43	3.65	A2	A3V*	150	5	
21 Lyn	7 19.2	+49 25	4.45	A0	A1IV	0	0	
β CMi	7 21.7	+ 8 29	3.09	B8	B8V*	260	50	21
α Gem A	7 28.2	+32 6	1.99	A0	A1V*	0	0	22
α Gem B	7 28.2	+32 6	2.85		Am	15	15	
24 Lyn	7 34.6	+58 57	4.96	A2	A3III	212	27.5	
ϕ Gem	7 47.4	+27 1	4.99	A2	A3V	165	5	23
27 Lyn	8 0.9	+51 48	4.87	A2	A2V	162	7.5	
HR 3314	8 20.7	- 3 35	3.95	A0	A0V*	120	0	
δ Hya	8 32.4	+ 6 3	4.18	A0	A0V	270	30	
ι Cnc	8 37.5	+21 50	4.73	A0	A1V	85	0	
ρ Hya	8 43.1	+ 6 12	4.42	A0	A0V	142	7.5	
θ Hya	9 9.2	+ 2 44	3.84	A0	A0V*	100	5	
38 Lyn	9 12.6	+37 14	3.82	A2	A3V*	160	10	24
26 UMa	9 28.0	+52 30	4.65	A0	A2V	180	5	
ν^3 Hya	10 0.3	-12 35	4.72	B8	B8V	70	10	
η Leo	10 1.9	+17 15	3.58	A0p	A0Ib*	<55	5	
α Sex	10 2.8	+ 0 7	4.50	A0	A0III	0	0	
α Leo	10 3.1	+12 27	1.34	B8	B7V*	352	7.5	
λ UMa	10 11.1	+43 25	3.52	A2	A2IV*	35	0	
HR 4072	10 16.9	+66 4	4.92	A0	A0p	8	7.5	25
ω UMa	10 48.2	+43 43	4.84	A0	A1V	15	15	26
54 Leo(br)	10 50.2	+25 17	4.51	A0	A1V	188	2.5	27
β UMa	10 55.8	+56 55	2.44	A0	A1V*	32	2.5	
60 Leo	10 57.0	+20 43	4.42	A0	Am	28	27.5	28
θ Leo	11 9.0	+15 59	3.41	A0	A2V*	0	0	
σ Leo	11 16.0	+ 6 35	4.13	A0	B9V	70	10	
θ Crt	11 31.6	- 9 15	4.81	B9	B9V	192	7.5	
β Leo	11 44.0	+15 8	2.23	A2	A3V*	110	12.5	
γ UMa	11 48.6	+54 15	2.54	A0	A0V*	165	5	29
δ UMa	12 10.5	+57 35	3.44	A2	A3V*	178	2.5	
η Vir	12 14.8	- 0 7	4.00	A0	A2V	0	0	30
23 Com	12 29.9	+23 11	4.78	A0	A0IV	65	0	31
ρ Vir	12 36.8	+10 47	4.95	A0	A0V	175	25	
4 UMa	12 49.6	+56 30	1.68	A0p	A0p	30	10	32
α^2 CVn	12 51.4	+38 51	2.90	A0p	A0p	42	17.5	33
θ Vir	13 4.8	- 5 0	4.44	A0	A1V	0	0	
ζ UMa(br)	13 19.9	+55 27	2.40	A2p	A2V*			34
ζ UMa(ft)	13 19.9	+55 27	3.96	A2	Am	75	0	35
78 Vir	13 29.1	+ 4 10	4.93	A2p	A2p	25	0	36
ζ Vir	13 29.6	- 0 5	3.44	A2	A3V*	178	7.5	
ψ Vir	13 56.8	+ 2 2	4.34	A2	A3III	165	15	
α Dra	14 1.7	+64 51	3.64	A0p	A0III*	0	0	37
HR 5313	14 7.2	+ 2 53	4.90	A0p	B9p	102	2.5	38
λ Boo	14 12.8	+46 33	4.26	A0	A0p	95		39
ψ Boo(br)	14 36.0	+16 51	4.94	A0	B9p	0	0	40
109 Vir	14 41.2	+ 2 19	3.76	A0	A0V*	335	35	
β Lib	15 11.8	- 9 1	2.74	B8	B8V*	230	30	

TABLE 1 (Continued)

SPECTRAL TYPES AND ROTATIONAL VELOCITIES OF THE B8-A2 STARS

Star	(1900)	(1900)	m_v	Sp(HD)	Sp(WKK)	v sin i (km/sec)	A/2 (km/sec)	Notes
γ UMi	15h20m.9	+72°11'	3.14	A2	A3II-III*	185	5	
α CrB	15 30.5	+27 3	2.3-2.4	A0	A0V*	132	7.5	41
γ CrB	15 38.6	+26 37	3.93	A0	A0III-IV	100	0	42
β Ser	15 41.6	+15 44	3.74	A2	A2IV*	202	27.5	
μ Ser	15 44.4	- 3 7	3.63	A0	A0V	80	2	
ε Ser	15 45.9	+ 4 47	3.75	A2	Am	35	0	43
ζ UMi	15 47.6	+78 6	4.34	A2	A3V	225	25	
ι CrB	15 57.4	+30 8	4.91	A0	A0p	0	0	44
π Ser	15 58.0	+23 5	4.82	A2	A3V	110	10	
ν Her	15 59.7	+46 19	4.64	B9	B9p	0	0	45
φ Her	16 5.6	+45 12	4.26	B9p	B9p	0	0	46
ψ Sco	16 6.5	- 9 48	4.91	A2	A2V	25	0	
ω Her	16 20.8	+14 16	4.53	A0p	A1p	0	0	47
ν Oph	16 22.4	- 8 9	4.68	A2	Am	65	5	48
λ Oph	16 25.9	+ 2 12	3.85	A0	A1V	142	7.5	49
15 Dra	16 28.2	+68 59	4.98	B8p	B9IV	150	0	50
σ Her	16 30.9	+42 39	4.25	A0	B9V	285	15	
52 Her	16 46.3	+46 9	4.85	A2p	A2p	52	2.5	51
ι Oph	16 49.3	+10 20	4.29	B8	B8V	102	22.5	52
ε Her	16 56.5	+31 4	3.92	A0	A0V	90	5	53
δ Her	17 10.9	+24 57	3.16	A2	A3IV*	305	15	
69 Her	17 14.2	+37 24	4.80	A2	A2V*	155	5	
ν Ser	17 15.2	-12 45	4.35	A0	A1V	125	10	
ρ Her(br)	17 20.2	+37 14	4.52	A0	A0p	90	5	54
μ Oph	17 32.4	- 8 3	4.65	B8	B8V	140	15	
ε Ser	17 35.8	-12 49	4.39	A2	A2V	135	15	55
γ Oph	17 42.9	+ 2 45	3.74	A0	A0V*	212	12.5	
68 Oph	17 56.7	+ 1 18	4.44	A2	A1V	232	7.5	
ο Her	18 3.6	+28 45	4.1-4.2	A0	B9V	138	27.5	
δ UMi	18 4.3	+86 37	4.44	A0	A1V	180	20	
φ Dra	18 22.2	+71 17	4.24	A0p	A0p	95	10	56
39 Dra	18 22.5	+58 45	4.9	A2	A1V*	180	10	
α Lyr	18 33.6	+38 41	0.14	A0	A0V*	0		57
γ Lyr	18 55.2	+32 33	3.30	A0p	B9III*	90	5	
ζ Aql	19 0.9	+13 43	3.02	A0	B9V	365	35	
λ Aql	18 1.0	- 5 2	3.55	B9	B8V	155	5	
π Dra	19 20.2	+65 31	4.63	A2	A2IV	30	0	
ι Cyg	18 27.2	+51 31	3.94	A2	A5V	210	15	
9 Vul	19 30.2	+19 33	4.88	B8	B7V	235	5	
δ Cyg	19 41.9	+44 53	2.97	A0	B9.5III*	128	7.5	
13 Vul	19 49.2	+23 49	4.50	A0	A0III	42	7.5	
ρ Aql	20 9.7	+14 54	4.96	A0	A2V	160	12.5	
30 Cyg	20 10.2	+46 31	4.96	A2	A3III	150	0	
29 Cyg	20 10.8	+36 30	4.98	A0	A2p	85	5	58
κ Cep	20 12.3	+77 25	4.40	B9	B9III	0	0	
ν Cap	20 15.1	-13 4	4.84	A0	B9V	0	0	
ζ Del	20 30.6	+14 20	4.69	A2	A3V	118	7.5	
29 Vul	20 34.1	+20 51	4.78	A0	A0V	48	7.5	
α Del	20 35.0	+15 34	3.86	B8	B9V*	160	10	
α Cyg	20 38.0	+44 55	1.33	A2p	A2Ia*	<18	17.5	
ι Aqr	20 42.3	- 9 52	3.83	A0	A1V*	105	5	
ν Cyg	20 53.5	+40 47	4.04	A0	A0V	245	5	
σ Cyg	21 13.5	+38 59	4.98	A0p	B9Ia*	<20	20	
ν Cep	21 42.6	+60 40	4.46	A2p	A2Ia*	<25	25	
ι Aqr	22 1.0	-14 21	4.35	B8	B8V	150	25	59

TABLE 1 (Continued)

SPECTRAL TYPES AND ROTATIONAL VELOCITIES OF THE B8-A2 STARS

Star	(1900)	(1900)	m_v	Sp(HD)	Sp(MKK)	v sin i (km/sec)	Δ/2 (km/sec)	Notes
θ Peg	$22^h\ 5^m.2$	+ 5°42'	3.70	A2	A2V	122	7.5	60
Y Aqr	22 16.5	- 1 53	3.97	A0	A0V	75	0	
32 Peg	22 16.7	+27 50	4.88	B8	B8V	68	17.5	
4 Lac	22 20.5	+48 58	4.64	B8p	B9Iab*	<25	25	
σ Aqr	22 25.4	-11 11	4.99	A0	A0IV	22	22.5	
∠ Lac	22 27.2	+49 46	3.85	A0	A2V	155	15	
η Aqr	22 30.2	- 0 38	4.13	B8	B8V	288	12.5	
ζ Peg	22 36.5	+10 19	3.61	B8	B8V*	210	10	
ο Peg	22 37.1	+28 47	4.85	A0	A1V	0	0	
ρ Peg	22 50.2	+ 8 17	4.95	A0	A1V	100	5	
∠ Peg	22 59.8	+14 40	2.57	A0	B9.5III*	155	5	
κ Psc	23 21.8	+ 0 42	4.94	A2p	A2p	42	7.5	61
ι And	23 33.2	+42 43	4.28	B8	B8V*	88	7.5	
κ And	23 35.5	+43 47	4.33	A0	B8V	195	0	

NOTES TO TABLE I

* These stars have been classified by Dr. W. W. Morgan and have been used as standards in this study.

1. Manganese star; spectrum variable. Also spectroscopic binary, P = 96.7 days.

2. A double star with $4^m.5$ and $6^m.0$ components separated by about $0''.3$. No trace of the fainter component is visible on either blue- or red-sensitive plates. Also, an emission-line star, MWC 420. See section VI, 2.

3. γ^2 Arietis is the fainter component of an 8" binary. It is a peculiar A star and spectrum variable. Peculiar features include chromium, europium and silicon.

4. Listed as having two spectra in the "Bright Star Catalogue". Only one spectrum is visible on the Perkins plate.

5. This star has a $5^m.23$ component 3" distant. The brighter component is a peculiar A star, with abnormally strong chromium and silicon.

6. Listed as having two spectra in the "Bright Star Catalogue". Only one spectrum is visible on the Perkins plate.

7. A double star with $3^m.7$ and $6^m.2$ components about 3" apart.

8. Algol. Morgan (Ap. J., 81, 348, 1935) and others have reported doubling of the Mg II 4481 line at and in the vicinity of primary light minimum. The Perkins spectrograms, taken out of primary light minimum, show Mg II 4481 as a single line.

9. ζ Tauri was observed to have variable radial velocity by Campbell in 1908 (L. O. B. 5, 62, 1908) and to show two spectra in 1928 (Lick Obs. Pub., 16, 43, 1928). A series of Perkins spectrograms taken in late 1951 confirms the aforementioned composite spectrum. Although not many lines are visible, the Ca II K-line and the Mg II 4481 line are clearly double on several plates. Two plates taken on October 12, 1951 appeared to show the widest splitting of the K-line recorded in the Perkins series: the separation was found to correspond to a radial velocity difference of 160 km/sec between the two components. A period of four days or less is indicated, although this is based on a very incomplete series of spectrograms. The components of the lines which appear double are about equal in strength and very sharp, indicating little or no rotational broadening. Both components are of spectral type B8. The spectrum appears to be peculiar, however, in the sense that the Helium lines are relatively broad and shallow, suggesting moderate axial rotation, at all phases, even when the K-line and Mg II 4481 line appear single and very sharp.

10. Emission-line star, MWC 77. See section VI, 2.

11. Spectroscopic binary, P = 3.9 days. See section VI, 3.

NOTES TO TABLE 1 (Continued)

12. Weak-line star. See section VI, 5.

13. No rotational velocity measured for this star. It will be considered in a forthcoming study of axial rotation in the B2-B5 stars.

14. Peculiar A star. Silicon is abnormally strong.

15. A possible weak-line star. See section VI, 5.

16. Spectroscopic binary, P = 6.0 days. Secondary spectrum visible but very faint, according to L. O. B. 199, 1911. Only one spectrum is visible on the Perkins plate. See section VI, 3.

17. Spectroscopic binary, P = 4.0 days, with two spectra visible. Both spectra are visible and of equal intensity on the Perkins plate. All lines are very narrow, indicating little or no component of axial rotation in the line of sight.

18. Peculiar A star and spectrum variable. Silicon is abnormally strong.

19. Metallic-line star: A3 K-line and A7 metallic spectrum. Also, spectroscopic binary, P = 4.4 days; visual binary with 4^m3 and 6^m6 components separated by 0".2.

20. Standard zero rotational velocity star.

21. Emission-line star, MWC 178. See section VI, 2.

22. α Gem B, the fainter of this 5" binary, is a metallic-line star: A1 K-line and A5 metallic spectrum. Both A and B are spectroscopic binaries, with periods of 9.2 and 2.9 days, respectively. See section VI, 3.

23. Two spectra, according to the "Bright Star Catalogue". Only one spectrum is visible on the Perkins plate.

24. Visual binary with 4^m0 and 5^m9 components 3" apart.

25. The spectrum is peculiar and most nearly resembles in its over-all features the spectrum of the manganese-star, ϕ Herculis. In particular, the unidentified line at λ3984 which is found in the manganese-stars is present in HR 4072. It is uncertain whether manganese is actually present in the spectrum of HR 4072. Mn II 4253 and possibly 4137 appear to be present but are on the threshold of visibility. If manganese is present, it is decidedly weaker than in the spectrum of ϕ Herculis. HR 4072 is also a spectroscopic binary with P = 11.6 days.

26. Spectroscopic binary with P = 15.8 days. See section VI, 3.

27. Visual binary, with 6^m30 companion at 6" distance.

28. Metallic-line star: A1 K-line and A5 metallic spectrum.

29. Reported to be emission-line star; MWC 583. See section VI, 2.

30. Spectroscopic binary with P = 71.9 days, and two spectra, as first pointed out by Frost and Adams (Ap. J., 17, 152, 1903). Only one spectrum appears on the Perkins plate.

31. Listed as having two spectra in the "Bright Star Catalogue". Only one spectrum is visible on the Perkins plate.

32. Peculiar A star and spectrum variable. Peculiar features include chromium and europium.

33. Peculiar A star and spectrum variable. Peculiar features include chromium, europium and silicon.

34. Mizar, visual binary with 14" separation. The brighter component is a spectroscopic binary, P = 20.5 days, with two spectra visible. The Perkins plate shows both spectra; the lines are about equal in strength and quite narrow, indicating little or no component of axial rotation in the line of sight.

NOTES TO TABLE 1 (Continued)

35. The fainter component of Mizar is a metallic-line star: A2 K-line and A7 metallic spectrum.

36. Peculiar A star and spectrum variable. Peculiar features include chromium and europium.

37. Spectroscopic binary, P = 51.4 days. See section VI, 3.

38. Peculiar A star of the silicon-type and spectrum variable.

39. Weak-line star; see section VI, 5. A v sin i determination from the contour of Mg II 4481 was impossible because of the weakness of that line. The value given was obtained from visual estimates of the broadening of the K-line.

40. Peculiar A star of the manganese-type and spectrum variable. The fainter component of this 6" binary is a metallic-line star.

41. Spectroscopic binary, P = 17.4 days. See section VI, 5.

42. A visual binary of less than 1" separation, with components of magnitude 4.0 and 7.0. Also, listed as having two spectra in the "Bright Star Catalogue". Only one spectrum is visible on the Perkins plate.

43. Metallic-line star: A3 K-line and F0 metallic spectrum.

44. The spectrum of ι Coronae Borealis is almost identical with that of HR 4072, described in note 24.

45. Peculiar A star of the manganese type.

46. Peculiar A star of the manganese type.

47. Peculiar A star: chromium is very strong.

48. Metallic-line star: A2 K-line and A7 metallic spectrum.

49. Visual binary: $4^m.0$ and $6^m.1$ components of about 1" separation.

50. Classified as B8p in the Henry Draper with the remark that the K-line is strong and the spectrum resembles that of β Orionis, although the lines are not as narrow. The Balmer lines appear relatively weak on the Perkins plate, suggesting that 15 Draconis does lie above the main sequence.

51. Peculiar A star: strontium and chromium are abnormally strong.

52. Listed as having two spectra in the "Bright Star Catalogue". Only one spectrum is visible on the Perkins plate.

53. Spectroscopic binary, P = 4.0 days. Also, composite spectrum (Adams, Ap. J., 18, 69, 1903), with lines of secondary reported rather weak. Only one spectrum is visible on the Perkins plate. See section VI, 3.

54. The brighter component of the visual binary ρ Herculis is a peculiar A star. The general level of excitation corresponds roughly to an A0 star, but the K-line is weak and silicon is strong. The fainter component, of magnitude 5.5 and 4" distance, is a B9V star in rather rapid rotation.

55. Listed as having two spectra in the "Bright Star Catalogue". Only one spectrum is visible on the Perkins plate.

56. Visual binary: $4^m.5$ and $6^m.2$ components, separated by less than 1". Reported to have two spectra, the Perkins plate shows only one: that of a peculiar A star of the silicon type.

57. Standard zero rotational velocity star.

58. Weak-line star. See section VI, 5.

59. Listed as having two spectra in the "Bright Star Catalogue". Only one spectrum is visible on the Perkins plate.

60. Listed as having two spectra in the "Bright Star Catalogue". Only one spectrum is visible on the Perkins plate.

61. Peculiar A star: chromium is abnormally strong.

persion 65 A/mm at $H\gamma$; any stars which then showed differing spectral types or luminosity classes were reclassified from the Perkins plates to give the final type. The writer owes a deep debt of gratitude to Dr. Morgan for making the Yerkes plates available, for providing standard stars, and for many stimulating conversations. The spectral types determined are listed in Table 1.

IV. THE ACCURACY OF THE OBSERVATIONS

1. THE ROTATIONAL VELOCITIES

As has been previously mentioned, two profiles for each star were measured, and the mean of the two values was taken as the $v \sin i$ of the star. In Table 1 the column $\Delta/2$ is a measure of the accidental errors involved in the $v \sin i$ determination of one star: $\Delta/2$ is the difference in rotational velocity between the mean and either of the two measured values. From an examination of Figure 2, one might expect the errors to increase as one goes to larger velocities, since the resolution decreases. A study of the $\Delta/2$'s bears this out, as Table 2, which tabulates the probable errors for different velocity ranges, shows.

TABLE 2

PROBABLE ERRORS OF MEASURED ROTATIONAL VELOCITIES

$v \sin i$ (Km/Sec)	No. of Stars	P.E. (Km/Sec)	$v \sin i$ (Km/Sec)	No. of Stars	P.E. (Km/Sec)
0–100	60	± 7	201–300	22	±14
101–200	58	± 9	>300	5	±19

The probable error listed in Table 2 is that of the mean $v \sin i$ for one star. It should be mentioned that a number of stars, primarily supergiant and peculiar stars, have been omitted from the foregoing discussion by virtue of having observed profiles which are narrower than the standard zero-velocity profiles. Inclusion of these would have led to a smaller probable error, which would have been spurious.

An examination of Figure 2 also shows that very little difference exists between the zero and the 25-km/sec contours. It follows that rotational velocities below 25 or 30 km/sec have little meaning other than indicating a very small axial rotation.

A number of stars had measured equivalent widths of *Mg* II 4481 roughly equidistant between those of the standard stars. For these, comparisons with both sets of computed contours were made and showed good agreement.

The presence of systematic errors will best be shown by comparisons with other $v \sin i$ determinations of common stars. Two such comparisons are possible for the stars in question. The first is with Elvey's values,[4] illustrated in Figure 3. Elvey was the first to apply the graphical method of Shajn and Struve, using it for a number of bright stars of representative type. He also used the *Mg* II 4481 line for his velocity determinations. Fourteen stars (excluding three supergiants) are in common, and these show scatter of about the expected amount, with no apparent systematic difference in our velocities. It should be pointed out that Elvey's computed contours were based on the assumption of an undarkened star and that his values might therefore be expected to run somewhat lower than those of the present paper. The effect of limb darkening on the line contour is quite small, however, and is probably masked by the various errors which go into a $v \sin i$ determination. The second comparison is with the values of Miss Westgate[5] and is shown in Figure 4. Miss Westgate's velocities were obtained by measuring *Mg* II 4481 line widths and converting these into rotational velocities by comparing with Elvey's values. Figure 4 shows considerable scatter, plus a systematic difference in the sense that the values here reported run higher than those of Miss Westgate.

[5] *Ap. J.*, **78**, 46, 1933.

2. THE SPECTRAL TYPES

Quoting W. W. Morgan: "Spectra of classes B9–A2 are most difficult of all to classify accurately. All lines with the exception of the Balmer series are weak, and the broad-line stars show few spectral features that can be used."[7] A luminosity classification for these stars is especially difficult, since the chief criterion is the appearance of the wings of the Balmer lines.

With regard to the spectral types, the maximum error for any given star is probably one-tenth of a spectral class on the MKK system. On the basis of the quality of the plates used, it is difficult for the writer to conceive of assigning, for example, a type of B8 or A2 to an A0 star, no matter how large the rotational broadening. Errors in the luminosity

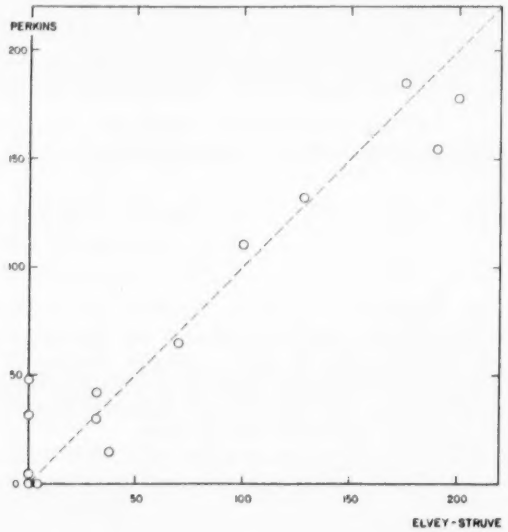

FIG. 3.—Comparison of rotational velocities measured at Perkins with those measured by Elvey and Struve.

classification are much more difficult to evaluate; the writer can only say that he did as careful a job as possible with the help of a set of excellent standards provided by Dr. Morgan. Nevertheless, the differences in the spectra of the stars of intermediate and lower luminosities (classes III–V) are exceedingly subtle, and it is possible that another investigator might make somewhat different luminosity classifications.

It will be shown (Sec. V, 4) that the B8–A2 stars of intermediate luminosity have less axial rotation than the corresponding main-sequence stars, while the reverse appears to be true for the stars of type F (see n. 14, below). Since this result may be of cosmogonical significance, the question as to whether the spectroscopic criteria of luminosity might depend to some extent upon axial rotation is a legitimate and important one. Because the grouping into luminosity classes among the F-type stars is more reliable than among the stars near A0, this question should be carefully considered for the B8–A2 stars. The negative absolute-magnitude effect shown by the Balmer lines is the chief luminosity criterion for the stars near A0. In the opinion of the writer, this effect is quite pronounced, regardless of the rotational broadening of the lines. The effects of axial rotation on the

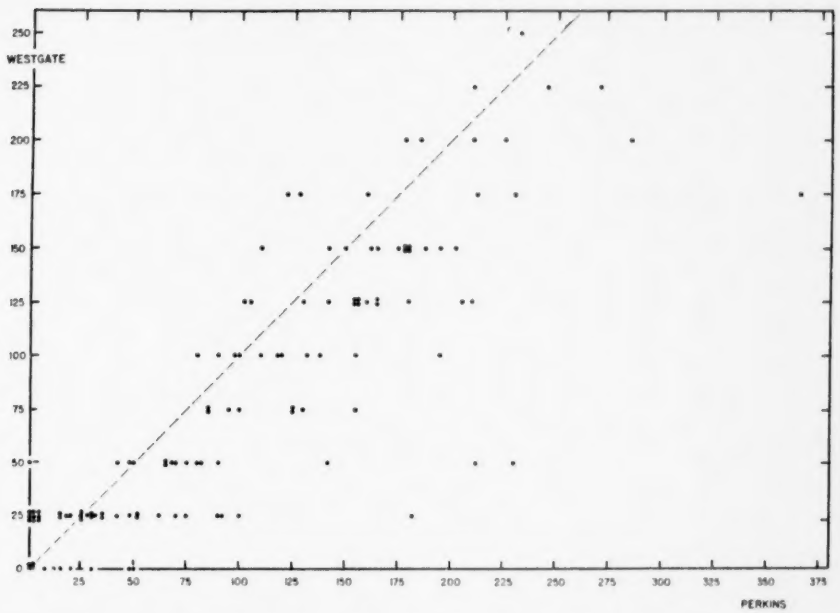

FIG. 4.—Comparison of rotational velocities measured at Perkins with those measured by Miss Westgate.

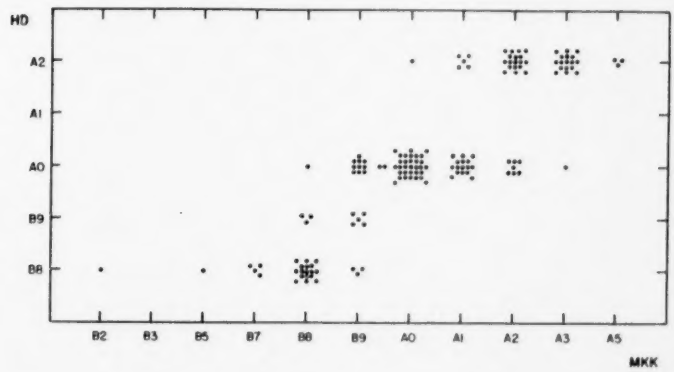

FIG. 5.—Comparison of spectral types assigned on the Morgan-Keenan-Kellman system with corresponding Henry Draper types, for the normal stars.

profiles of the Balmer lines were minimized in estimating luminosity classes by examining the spectrograms without magnification; it was felt that estimates of intensities of the Balmer lines could be made rather accurately in this way. The luminosity classification of these stars remains a very difficult and subtle problem, however, which should not be underestimated.

A comparison of the present MKK types for the normal stars with the corresponding Draper types is shown in Figure 5.

V. THE INTERPRETATION OF THE OBSERVATIONS

An inspection of Table 1 shows that the B8–A2 stars divide into a number of subgroups from the point of view of axial rotation. This is brought out more clearly in Table 3. Thirty-seven stars have been omitted from this table by virtue of being earlier in type

TABLE 3

AXIAL ROTATION OF SUBGROUPS COMPRISING THE B8–A2 STARS

Type	N	$\overline{v \sin i}$ (Km/Sec)	$\bar{v}$ (Km/Sec)	Type	N	$\overline{v \sin i}$ (Km/Sec)	$\bar{v}$ (Km/Sec)
B8 V	18	152	193	B8–A2 V	87	139	177
B9 V	11	177	225	B8–A2 III–IV	24	73	93
A0 V	20	165	210	Peculiar A	16	41	52
A1 V	20	99	126	Metallic-line	6	40	51
A2 V	18	120	153	Supergiant	9	<26	<34

than B8, later than A2, or having spectra which are peculiar in some manner. The third column gives the mean observed $v \sin i$, and the fourth column gives the mean true equatorial rotational velocity under the assumption that the axes of rotation are randomly distributed.[9] The latter quantity is probably not too meaningful for certain of the groups listed, in view of the small number of stars comprising the group. Again, the breakdown of the B8–A2 main-sequence stars into individual types is for the sake of completeness; it is not suggested, for example, that the apparent rapid drop in axial rotation at A1 is real, because of the small samples employed. A brief discussion of the subgroups follows.

1. THE PECULIAR A STARS[10]

Sixteen of the stars listed in Table 1 are well-known peculiar A stars, while three more [HR 4072, ι Coronae Borealis, and ρ Herculis (brighter)] have been found to be peculiar in this study. In the following discussion, only the aforementioned sixteen will be considered.

As a group, the peculiar A stars possess small axial rotation. The largest observed $v \sin i$ is 102 km/sec, measured in the "silicon star" HR 5313.[11] The stars, ϕ Draconis and α Piscium, have measured velocities of 95 and 92 km/sec, respectively. All the others have $v \sin i$'s of the order of 50 km/sec and lower. The "manganese stars" appear to be

[9] The relation between the moments of the true and observed frequency distributions, allowing the mean of the true rotational velocities to be determined directly from the mean of the observed distribution of $v \sin i$, is due to Chandrasekhar and Münch, *Ap. J.*, **111**, 142, 1950.

[10] A number of the peculiar A stars considered have been announced as spectrum variables. It should be pointed out that the use of the *Mg* II 4481 line as a measure of axial rotation in these stars is justified by the fact that this line has not been observed to be variable.

[11] This star has recently been announced as a spectrum variable by Deutsch, *Ap. J.*, **116**, 536, 1952. Assuming that the period of spectrum variation is equal to the rotation period and that the radius of HR 5313 is $1.9 R_\odot$, Deutsch finds that a $v \sin i$ of 170 km/sec gives satisfactory agreement with his observed profile of *Mg* II 4481.

among the sharpest-lined representatives of the peculiar A stars. The point to be stressed is that a comparison of the peculiar A stars with stars of similar temperature and absolute magnitude shows that the former are characterized by relatively small rotational velocities and should be considered separately from the point of view of axial rotation.

2. THE METALLIC-LINE STARS

Only six metallic-line stars are included in this study. Like the peculiar A stars, this group has small axial rotation, the observed $v \sin i$'s ranging from 75 to 15 km/sec. The sample is undeniably small, but the above conclusion has been verified by visual inspection of spectrograms of a larger number of metallic-line stars. It should be emphasized that the measured rotational velocities for these stars give only an order of magnitude; all have quite large *Mg* II 4481 equivalent widths, making necessary a large extrapolation to the computed line contours. These stars should perhaps be more properly included in a forthcoming investigation of axial rotation in the brighter *Henry Draper* A3–G0 stars. The conclusion that the metallic-line stars possess small axial rotation as a group remains valid, however.

3. THE SUPERGIANT STARS

Nine supergiant stars have been considered, and all have small rotational velocities. This is in agreement with the conclusion of Struve that "supergiants of early or late type never show conspicious rotations."[12] The $v \sin i$'s listed for the supergiants are to be regarded as upper limits; axial rotation, if any exists among the supergiants, must be extremely small. That turbulence is a more important broadening agent than axial rotation in these stars is evident from a visual inspection of the line contours on the spectrograms. All show the deep bell-shaped contours characteristic of small-scale turbulence, with the exception of the B8 I*a* star, β Orionis. This star exhibited the largest line broadening of the group, corresponding to a rotational velocity of 65 km/sec under the assumption that axial rotation is the sole broadening agent. Even here, however, it is possible that some sort of large-scale turbulence is contributing to the line broadening, as has been suggested by Struve for the O-type and early B-type supergiants.[13]

4. THE NORMAL B8–A2 STARS OF INTERMEDIATE LUMINOSITY

A total of 24 stars were judged to be of luminosity classes III and IV. The observed rotational velocities ranged from zero to 202 km/sec, the latter for the A2 IV standard, β Serpentis. As indicated in Table 3, the mean observed rotational velocity for the group was found to be 73 km/sec, corresponding to a mean true rotational velocity of 93 km/sec. This indicates that the normal B8–A2 stars of intermediate luminosity possess considerably less axial rotation than the corresponding main-sequence stars and that they, like the groups considered above, should be treated separately with respect to axial rotation.[14] This luminosity dependence of axial rotation is perhaps best seen by a com-

[12] *Pop. Astr.*, **53**, 211, 1945. However, Dr. Struve points out (private correspondence) that this earlier statement must probably be modified, since we now know a number of highly luminous early B-type stars which do possess appreciable, though never excessively large, rotational velocities (cf. Huang and Struve's paper on ρ Leonis, *Ap. J.*, **118**, 463, 1953).

[13] *Pub. A.S.P.*, **64**, 118, 1952.

[14] A totally different relation between axial rotation and luminosity appears to exist for the stars of later spectral type. At the time of writing (June, 1953), spectrograms have been taken of some thirty stars with spectral types between A7 and G0, as determined by Morgan (Johnson and Morgan, *Ap. J.*, **117**, 313, 1953). Of the eighteen main-sequence stars included, only four show some degree of rotational line broadening, the others having very sharp lines. On the other hand, ten of the thirteen stars of intermediate luminosity exhibit rotational line broadening as against only three sharp-line stars. The F5 V star, 45 Bootis, is the main-sequence star of latest spectral type in the sample considered which shows any degree of axial rotation. Among the stars of intermediate luminosity, however, axial rotation appears to exist to G0 at least, as evidenced by the broadened lines in the spectrum of the G0 III star, 31 Comae.

Note added October 10, 1953: The foregoing conclusions have been strengthened by the addition of a considerable amount of additional observational material and presented as a paper at the August, 1953,

parison of the histograms of observed rotational velocities for the stars of intermediate luminosity and the main-sequence stars, as shown in Figure 6. The frequency distributions of the two groups are seen to be quite different. It should be pointed out that the above conclusion rests upon two assumptions: (1) that the luminosity classifications are accurate, and (2) that the relatively small sample considered is representative of the B8–A2 stars of intermediate luminosity as a whole.

5. THE NORMAL B8–A2 MAIN-SEQUENCE STARS

After the various subgroups treated above were eliminated, an unfortunately small number of normal main-sequence stars remained—87. It was thus impossible to investigate the dependence of axial rotation upon spectral type in the B8–A2 range. The breakdown has been made in Table 3, but it is probably without physical significance. Considering the group as a whole, a mean observed rotational velocity of 139 km/sec was obtained, corresponding to a mean true rotational velocity of 177 km/sec. The largest rotational velocity measured for this group was 365 km/sec for the B9 V star, ζ Aquilae.

Figure 6 illustrates the observed distribution of rotational velocities for the B8–A2 main-sequence stars. Although Brown[15] has pointed out that it is hazardous to attempt to distinguish between different forms of the distribution of true rotational velocities unless large numbers of observations are available, the writer feels that the derivation of the distribution of true rotational velocities according to the method of Chandrasekhar and Münch[9] may be of some interest, if only for a comparison with the frequency distributions derived in the latter paper.

Assuming random orientation of the axes of rotation and a frequency function for the true rotational velocities of the form

$$f(v) = \frac{j}{\sqrt{\pi}} \left[e^{-j^2(v-v_1)^2} + e^{-j^2(v+v_1)^2} \right],$$

the predicted distribution of $v \sin i$ is compared with the observed distribution of $v \sin i$ in Figure 7. The parameters of $f(v)$ are listed in Table 4, following the notation of Chandrasekhar and Münch.

TABLE 4

PARAMETERS OF ROTATIONAL VELOCITY DISTRIBUTION OF B8–A2 MAIN-SEQUENCE STARS

$\overline{v \sin i}$ (km/sec)	139	$\bar{v}_j/(2[\bar{v}^2 - \bar{v}^2])^{1/2}$	1.37
$\overline{v^2 \sin^2 i}$ (km/sec)^2	26,480	j^{-1} (km/sec)	134
$\bar{v}$ (km/sec)	177	v_1 (km/sec)	174
$\bar{v}^2$ (km/sec)^2	39,720		

It is apparent that a discussion of axial rotation as a function of spectral type has little meaning if the various subgroups at any given spectral type, having intrinsically different axial rotations, are all combined and treated as a homogeneous group. This is illustrated in Figure 6, where the histogram labeled "All B8–A2" includes main-sequence, giant, supergiant, peculiar A, metallic-line, and peculiar stars. A comparison of this histogram with that for the main-sequence stars alone shows that the former is built up by

meeting of the American Astronomical Society at Boulder, Colorado. This paper was read by title, but an abstract will appear in a forthcoming issue of the *Astronomical Journal*. In July of this year Dr. Struve called my attention to the work of Dr. George Herbig, who had independently arrived at substantially the same conclusions. Dr. Herbig and Mr. J. F. Spalding, Jr., reported on their research at the June meeting of the Astronomical Society of the Pacific and published an abstract in the *Pub. A.S.P.*, **65**, 192, 1953. I am indebted to Dr. Herbig for sending me a copy of his paper in advance of publication.

[15] *Ap. J.*, **111**, 366, 1950.

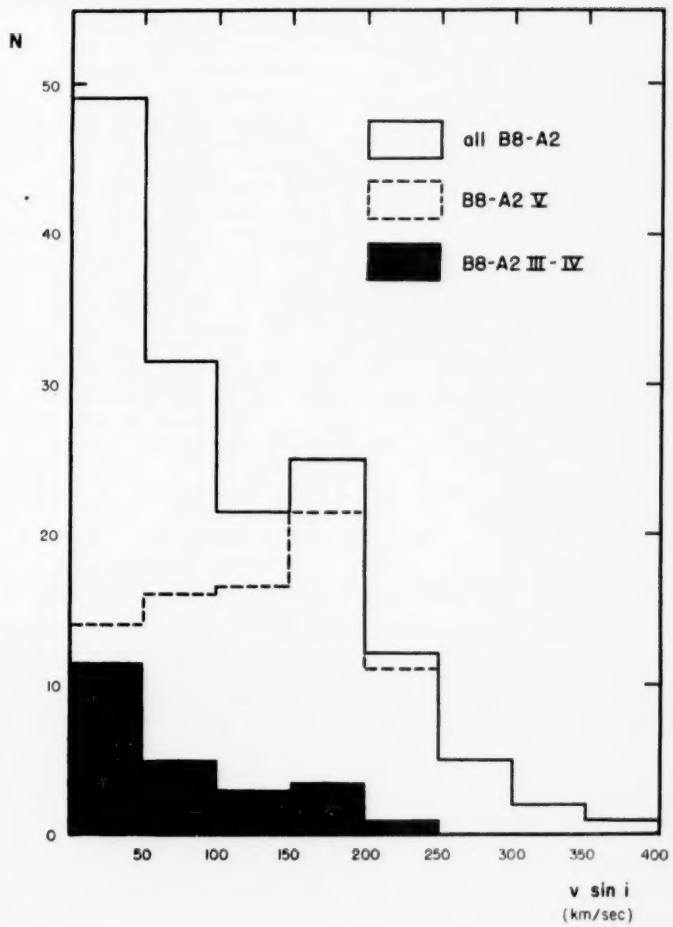

FIG. 6.—The distribution of observed rotational velocities for the B8–A2 stars. The histogram labeled "all B8–A2" includes supergiant, metallic-line, and peculiar A stars in this spectral range, as well as giant and main-sequence stars.

adding intrinsically slowly rotating subgroups to the more rapidly rotating main-sequence group.

Walter,[16] in a rediscussion of Miss Westgate's data,[8] finds that the distribution of rotational velocities for the A-type stars shows two maxima. He suggests that his group of slowly rotating stars be identified with Eggen's[17] "dwarfs" and "bright blue-dwarfs" and his rapidly rotating stars with Eggen's "blue-dwarfs" and possibly some "bright dwarfs." If Walter's double maximum frequency-curve is real, it would appear more likely to the

[16] *Zs. f. Ap.*, **29**, 9, 1951.

[17] *Ap. J.*, **111**, 65, 81, 1950.

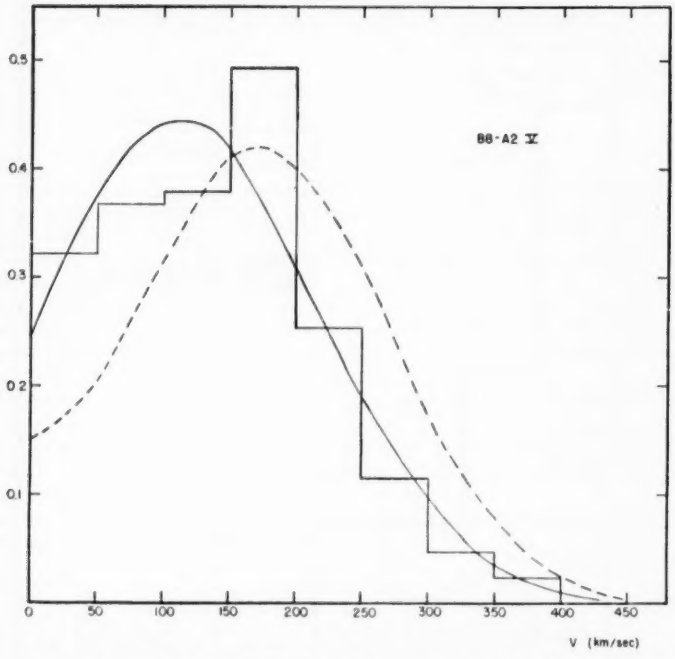

FIG. 7.—Comparison of the distribution of the observed rotational velocities of the B8–A2 main-sequence stars with those derived on the assumption of a true distribution of velocities of the form given in the text and for values of the parameters listed in Table 4. The observed distribution of $v \sin i$ is represented by the histogram, while the full-line curve represents the predicted distribution of $v \sin i$ for a true distribution of v given by the dashed curve.

writer that it is due to the addition of the slowly rotating subgroups listed above to the more rapidly rotating main-sequence group.

The only possible comparison of the B8–A2 main-sequence stars with early-type stars of other spectral types at this time is with the B2–B5 emission stars.[1] The latter, with a value of $\bar{v}$ equal to 348 km/sec,[9] have twice the average axial rotation of the B8–A2 main-sequence stars. The difference in the distribution-curves of true rotational velocities for the two groups is even more striking.

VI. MISCELLANEOUS REMARKS

1. DISTRIBUTION OF THE AXES OF ROTATION

The assumption that the axes of rotation are randomly distributed, supported by the work of Struve and others, is again supported in this investigation. A plot of $v \sin i$ versus galactic latitude and longitude for the main-sequence stars shows no conspicuous correlation. There is thus no reason to suspect that the rotational axes are not distributed in a random fashion.

2. EMISSION-LINE STARS

Four of the main-sequence stars considered are listed in the Mount Wilson catalogue of Be and Ae stars.[18] In view of the fact that axial rotation is undoubtedly associated

[18] Merrill and Burwell, *Ap. J.*, **78**, 87, 1933; **98**, 153, 1943; **110**, 387, 1949.

with the observed emission in these stars, it may be of some interest to consider them individually. Since there are only four, however, a comparison of axial rotation between the emission and the nonemission stars is not possible.

a) *HR 1204 = MWC 77.*—This star was reported to have a faint central *Hα* emission component in 1932. The only Perkins plate available for study was a 103-O plate taken in December, 1951, which shows a normal B9 V spectrum with no trace of emission. In view of the relatively low rotational velocity measured (110 km/sec), it appears that HR 1204 is being viewed nearly pole-on; assuming the critical velocity for rotational instability in a B9 V star to be of the order of 350–400 km/sec, the angle of inclination would be about 15°–20°. The weak dark cores in the higher members of the Balmer series reported by Miczaika on plates taken in 1948 are not visible on the Perkins 1951 plate.

b) *β Canis Minoris = MWC 178.*—This B8 V standard star was announced to have double *Hα* emission on Mount Wilson spectrograms taken in 1930 and 1932. Plates taken at Perkins in 1936, 1947, 1949, and 1950 show *Hα* in emission and *Hβ* in absorption. A 103-O plate taken in December, 1950, reveals *Hβ* and *Hγ* as broad absorption lines with weak central absorption cores. It is thus evident that the star is seen through at least a portion of its shell. Making the assumption that the critical rotational velocity of a B8 V star is of the order of 350–450 km/sec and employing the observed $v \sin i$ of 260 km/sec for β Canis Minoris, the inclination i would lie between 35° and 50°.

c) *φ Andromedae = MWC 420.*—Bright *Hα* was discovered in this B7 V star in 1940 and confirmed in 1943. A Mount Wilson spectrogram of December, 1944, revealed a very weak narrow emission line at *Hβ* centrally superposed on broad absorption, other lines being dark. Miczaika reported that *Hβ* was free of emission in September and October, 1948. A 1-N plate taken at the Perkins Observatory in September, 1949, shows *Hα* as an emission line, while *Hβ* appears to have a very weak narrow emission core on a 103-O plate taken in October, 1950. In view of the small measured rotational velocity of 72 km/sec, φ Andromedae is probably being viewed nearly pole-on. The spectrum appears perfectly normal, however, and shows none of the pole-on effects which have been observed in other sharp-line Be stars.

d) *γ Ursae Majoris = MWC 583.*—This A0 V standard star was announced to have variable *Hα* emission in 1938. A re-examination of old Perkins plates shows that if any emission is present at *Hα*, it is extremely faint and narrow. On a 1-N plate taken in April, 1950, *Hα* is a strong absorption line, while a 103-O plate taken in February, 1950, reveals a normal A0 main-sequence star with no trace of emission.

Five of the stars considered in this paper have measured rotational velocities in excess of 300 km/sec: ζ Aquilae (365 km/sec), α Leonis (352 km/sec), 109 Virginis (335 km/sec), HR 2209 (308 km/sec), and δ Herculis (305 km/sec). Since these stars must be rotating with a velocity near that required for rotational instability, it seemed relevant to examine all available Perkins spectrograms for possible traces of *Hα* emission. Red plates were available for three of the above stars, but the results were negative: ζ Aquilae has *Hα* as a pure absorption line in 1938, 1946, and 1947; *Hα* shows no trace of emission in α Leonis in 1936, 1938, 1943, 1944, 1946, and 1950; *Hα* appears without emission in δ Herculis in 1950.

3. SPECTROSCOPIC BINARIES

Fifteen of the stars listed in Table 1 are also listed in the Lick Observatory *Fifth Catalogue of the Orbital Elements of Spectroscopic Binary Stars.*[19] Of these, four have peculiar spectra, and two show two spectra on Perkins plates. The remaining nine are normal stars, in the sense that they can be placed uniquely on the H-R diagram and, further, show only one spectrum on Perkins plates. The latter are listed in Table 5, with the writer's spectral types and the corresponding visual absolute magnitudes and effective temperatures as determined by Keenan and Morgan in their recent calibration.[20]

[19] *Lick Obs. Bull.*, No. 521, 1948.

[20] *Astrophysics*, ed. J. A. Hynek (New York: McGraw-Hill Book Co., 1951), chap. i.

The fifth column of Table 5 lists the computed radii[21] of the nine stars, and the next column their measured rotational velocities. In the last two columns, the computed rotational period divided by the sine of the inclination is compared with the orbital period as listed in the Lick catalogue.[19] Of particular interest is the eclipsing system β Persei, for which sin i is known and which may be said to be synchronized, within the errors of observation. It is also possible that synchronism may occur in the 7 Camelopardi and 136 Tauri systems if the inclinations are not too great. On the other hand, the α Coronae Borealis and ϵ Herculis systems do not appear to be synchronized: even for sin $i \simeq 1$, the difference between orbital and rotational periods remains appreciable. Nothing can be said about synchronization for the remaining four stars, because of the indeterminancy of their rotational velocities.

TABLE 5

COMPARISON OF ORBITAL AND ROTATIONAL PERIODS FOR NINE SPECTROSCOPIC BINARIES

Star	Sp.	M_v	T_{eff}	$R/R_\odot$	$v \sin i$ (Km/Sec)	$P_{\text{rot}}/\sin i$ (Days)	P_{orb} (Days)
β Per	B8 V	−0.5	12,800	3.5	65	2.7	2.9
7 Cam	A1 V	+0.7	10,300	2.6	42	3.1	3.9
136 Tau	A0 III	−1.1	11,000	5.5	50	5.6	6.0
α Gem A	A1 V	+0.7	10,300	2.6	0	.....	9.2
ω UMa	A1 V	+0.7	10,300	2.6	15	8.7:	15.8
η Vir	A2 V	+1.2	9,700	2.3	0	.....	71.9
α Dra	A0 III	−1.1	11,000	5.5	0	.....	51.4
α CrB	A0 V	+0.3	11,000	2.9	132	1.1	17.4
ϵ Her	A0 V	+0.3	11,000	2.9	90	1.6	4.0

4. EQUIVALENT WIDTHS OF *Mg* II 4481

As has been pointed out earlier, equivalent widths of *Mg* II 4481 were measured on all plates, and these were reduced to the equivalent widths of one of the sharp-line standard stars, in order to derive the rotational velocities. The equivalent widths for individual stars are not included in the present paper, because the writer feels that the dispersion employed in this study is not sufficient to permit accurate individual values. Thus, among the B8–A3 main-sequence stars, the probable error of an equivalent-width determination for a single star is about 0.03 A. The uncertainty is particularly great for rotationally broadened lines, since it is difficult to ascertain the correct position of the continuous spectrum. Figure 8 illustrates the variation of equivalent width of *Mg* II 4481 with spectral type among the B7–A5 main-sequence stars included in this study. It will be seen that the scatter is enormous; this may be due largely to errors of measurement; but a visual comparison of spectrograms of stars of the same spectral type and rotational broadening shows that an intrinsic dispersion at a particular spectral type is also present. Figure 8 also shows a definite increase in equivalent width of *Mg* II 4481 with spectral type among the B7–A5 main-sequence stars. This is perhaps brought out more clearly in Table 6, in which the average equivalent width for each spectral type is listed. In so far as the small number of stars representing some of the spectral types permits drawing any conclusions, the equivalent width of *Mg* II 4481 appears to increase to A5 at least. This is in agreement with the earlier findings of Elvey.[4] A forthcoming study of rotational broadening among the bright *Henry Draper* A3–G0 stars should permit the establishment of the position of the maximum strength of the *Mg* II 4481 line on the HR diagram.

A number of other groups of stars of some interest have been included in Table 6. The supergiant and metallic-line stars have, of course, rather larger equivalent widths of

[21] Russell, Dugan, and Stewart, *Astronomy*, **2**, 738, 1938.

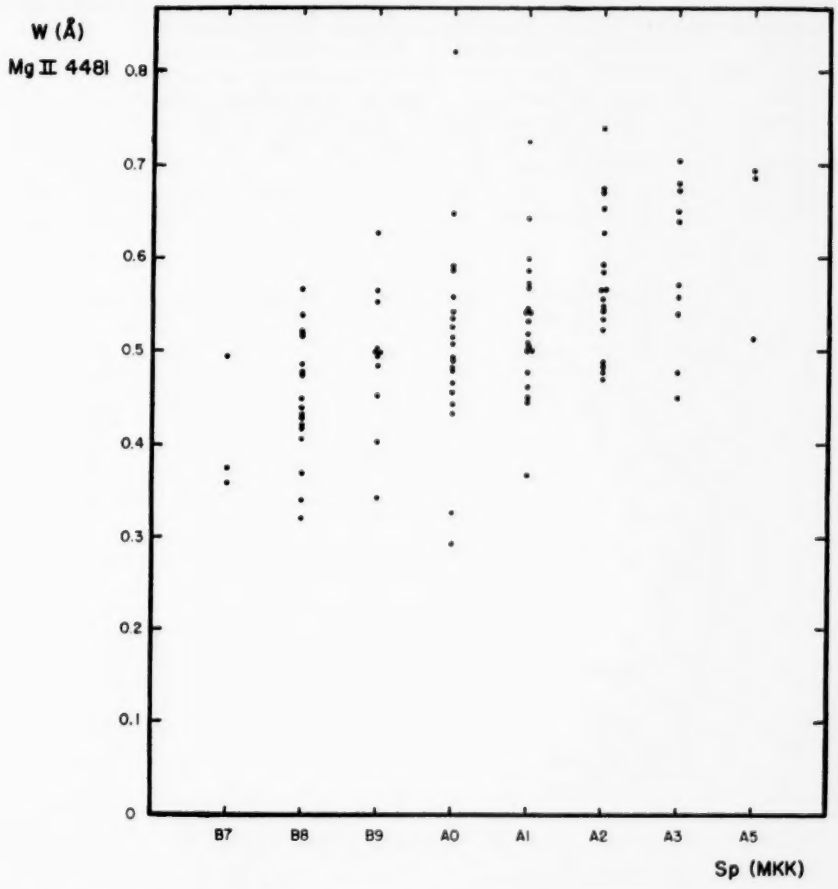

FIG. 8.—The variation of equivalent width of *Mg* II 4481 with spectral type for the B7–A5 main-sequence stars.

Mg II 4481 than the other stars included in this study. The peculiar A stars, on the other hand, have *Mg* II 4481 weaker than corresponding normal stars; and the manganese stars have particularly sharp and weak lines. The group with the weakest lines is the last group in Table 6, which is discussed in further detail in the next section.

5. THE WEAK-LINE STARS

Three of the stars included in this study are characterized by a general weakening of the spectral lines.[22] These stars are listed in Table 7. One of these, λ Bootis, was pre-

[22] A fourth star, ξ Aurigae, also appears to have weakened lines, but the effect is not nearly so pronounced as in the three stars considered above.

viously announced by Morgan, Keenan, and Kellman.[7] The spectrum of another, 29 Cygni, has been described elsewhere.[23] The spectral types listed in Table 7 are based essentially on the strength of *Ca* II K and the Balmer lines; the remaining metallic lines are then considerably weakened relative to a normal star of corresponding type. This weakening is not a result of rotational broadening, as the rotational velocities show; all three stars have only moderate axial rotation. Trigonometric parallaxes are available for two of the stars, λ Bootis and 29 Cygni; in both cases, they indicate that the stars are located somewhat below the main sequence. Further, the spectral peculiarities of the weak-line stars are similar to those exhibited by the subdwarfs of type A, although not so pronounced. It is tempting to regard the weak-line stars as located just below the main

TABLE 6

THE AVERAGE EQUIVALENT WIDTH OF *Mg* II 4481 FOR SOME GROUPS OF STARS

Type	No. of Stars	$\overline{W}$ (A)	Type	No. of Stars	$\overline{W}$ (A)
B7 V	3	0.41	A5 V	3	0.63
B8 V	18	.45	Supergiants	9	.71
B9 V	11	.49	Metallic-line	6	.71
A0 V	20	.51	Peculiar A (all)	16	.39
A1 V	20	.53	Peculiar A (Mn stars)	4	.31
A2 V	18	.57	Weak-line stars	3	0.20
A3 V	10	0.59			

TABLE 7

THE WEAK-LINE STARS

Star	Sp.	$v \sin i$ (Km/Sec)	W of *Mg* II 4481 (A)	Color Type
π^1 Ori	A0 p	108	0.22:	a2–3
λ Boo	A0 p	95	18:	a4
29 Cyg	A2 p	85	0.20:	a7

sequence on the H-R diagram, intermediate between the main-sequence stars and the true subdwarfs. In support of this is the fact that the colors of these stars are too red for their spectral types, as is indicated in Table 7. The color types of λ Bootis and 29 Cygni were obtained from the six-color photometry of Stebbins and Whitford.[24] The color type of π^1 Orionis was very kindly obtained for the writer by Dr. Robert Hardie, using the 69-inch reflector of the Perkins Observatory. These colors suggest that the weak-line stars have been classified systematically too early, a result predicted on theoretical grounds for the A-type subdwarfs by Chamberlain and Aller.[25] The space motions of these stars are not unusual, however: the largest is 18 km/sec, for λ Bootis, while the velocities of the other two are under 10 km/sec.

[23] *Ap. J.*, **115**, 575, 1952.

[24] "The Colors of 238 Stars of Different Spectral Types," *Ap. J.*, **102**, 318, 1945.

[25] *Ap. J.*, **114**, 52, 1951.

It is a pleasure to express my thanks to Dr. W. W. Morgan for his kind co-operation and advice on matters of spectral classification, and to Dr. R. H. Hardie for his generous assistance in several photometric problems. I am also indebted to Dr. Morgan and Dr. Otto Struve, and to my associates at the Perkins Observatory, for reading this paper in advance of publication and for valuable suggestions. Finally, I would like to thank Mrs. Mary Fenwick, Mr. Robert Howard, and my wife, for assistance in the reduction of the observations.

THE VELOCITY-CURVE OF BETA CANIS MAJORIS*

O. Struve, D. H. McNamara, S. M. Kung,
A. van Hoof, and R. Deurinck
Berkeley Astronomical Department, University of California,
and University of Louvain, Belgium
Received June 15, 1953

ABSTRACT

The two interfering oscillations of β CMa have retained, until 1953, their periods, as found previously from spectrograms taken in 1947–1948. But the amplitude of the smaller oscillation has slightly increased. The new material, consisting of 201 high-dispersion spectrograms, shows that the individual velocity-curves are frequently distorted by small, irregular variations. In this respect β CMa resembles ν Eridani and other stars of its class.

In a previous paper[1] the velocity-curve of β Canis Majoris was resolved into two components with closely similar periods, but with markedly different amplitudes:

$$P_1 = 0.25002246 \text{ day} \qquad K_1 = 5.8 \text{ km/sec}$$

$$P_2 = \begin{cases} 0.2513015 \text{ day for 1909–1931} \\ 0.2513003 \text{ day for 1931–1948} \end{cases} \qquad K_2 = \begin{cases} 4.2 \text{ km/sec for 1917–1934} \\ 2.0 \text{ km/sec for 1947–1948} \end{cases}$$

$$\text{Beat period} = \begin{cases} 49.1236 \text{ day for 1909–1931} \\ 49.1695 \text{ day for 1931–1948} \end{cases}$$

The second, variable, period was found to be associated with a change in the line profiles.

The purpose of our new investigation was to ascertain whether there has been a further change in P_2 and K_2 and whether there are additional variations in the velocity-curve, perhaps of an irregular character, such as are present in other stars of the same class, viz., 12 Lacertae,[2] 16 Lacertae,[3] ν Eridani,[4] σ Scorpii,[5] and β Cephei.[6]

Since December 10, 1950, 201 spectrograms of β Canis Majoris have been obtained at the Lick and Mount Wilson Observatories. Of these, 51 are Mount Wilson plates (dispersion 2.8 A/mm) taken on five nights: December 31, 1950; January 2, 3, and 27, 1951; and January 29, 1953. The remaining 150 spectra are all Lick plates (dispersion 11 A/mm at λ 4550) taken on eight nights: December 10, 17, 24, and 30, 1950; January 14 and 26, and February 4 and 9, 1951. The star lines employed to derive the radial velocity are listed in Table 1. Table 2 gives the radial velocity for each spectrogram. They are plotted in Figures 1 and 2; from the resulting curves the values of the time of maximum radial velocity, $2K$ and γ, have been estimated and listed in Table 3.

On those nights during which the observations show only a maximum of the velocity-curve or a minimum, but not both, an appropriate value of γ had to be adopted. Fortu-

* The Mount Wilson coudé spectrograms used in this work were obtained by Mr. Struve as guest investigator; those from the Lick Observatory were taken by Mr. McNamara.

[1] O. Struve, *Ap. J.*, **112**, 520, 1950.

[2] *Ibid.*, **113**, 589, 1951.

[3] O. Struve *et al.*, *Ap. J.*, **116**, 81, 1952. This was mentioned as a possibility in the original article. Subsequent observations make it appear almost certain that irregular changes are present.

[4] *Ibid.*, p. 398.

[5] R. D. Levee, *Ap. J.*, **115**, 402, 1952.

[6] O. Struve *et al.*, *Ap. J.*, **118**, 39, 1953.

nately, in the case of β Canis Majoris, the center of mass velocity changes very slowly, and +31 km/sec is a reasonable compromise, as found from three good nights, which give, respectively, γ = 30, 31, and 32 km/sec. The resulting amplitudes, $2K$, in Table 3, are inclosed in parentheses.

The slow variation in γ since 1931 is illustrated in Table 4, where the earlier values have been taken from Meyer's and from Struve's measurements.[1] We have, however, not investigated the possibility of small systematic differences arising from the adopted stellar wave lengths and from the choice of star lines made by the early measurers. It is

TABLE 1

LIST OF STAR LINES

λ	Element	Plate*	λ	Element	Plate*
3806.56	*Si* III	C	4340.47	*H*γ	C
3920.68	*C* II	C	4345.56	*O* II	C
3954.37	*O* II	C	4347.42	*O* II	C
3964.73	*He* I	C	4349.43	*O* II	C
3973.26	*O* II	C	4351.27	*O* II	L
3982.72	*O* II	C	4366.90	*O* II	C
4009.27	*He* I	C	4414.91	*O* II	C
4072.16	*O* II	C	4416.98	*O* II	C
4075.87	*O* II	C	4471.48	*He* I	L
4078.86	*O* II	C	4481.23	*Mg* II	C, L
4083.91	*O* II	C	4552.65	*Si* III	C, L
4085.12	*O* II	C	4567.87	*Si* III	C, L
4088.86	*Si* IV	C	4574.78	*Si* III	C, L
4092.94	*O* II	C	4590.97	*O* II	C, L
4101.74	*H*δ	C	4596.17	*O* II	C, L
4116.10	*Si* IV	C	4638.85	*O* II	C
4119.22	*O* II	C	4649.14	*O* II	C
4132.81	*O* II	C	4661.64	*O* II	C
4153.30	*O* II	C	4676.23	*O* II	C
4317.14	*O* II	C	4705.34	*O* II	C
4319.63	*O* II	C			

* C = Mount Wilson coudé spectrograph on the 100-inch telescope. L = Lick three-prism spectrograph on the 36-inch refractor.

therefore not certain that the decrease in γ from 35 km/sec in 1931 to 31 km/sec in 1951 has any physical significance.

Figure 3 shows the recent values of $2K$ plotted against the time and reduced to the same cycle in the beat period, with the help of Struve's 1931–1948 value, P_3 = 49.1695 days. We have omitted the observation on January 27, 1951, because the velocity-curve on that date was peculiar.

For comparison with the earlier observations we have also plotted the maximum and minimum values of $2K$ as observed in 1947–1948. It is probable that the 1950–1953 maximum lies higher, and the corresponding minimum lower, than in 1947–1948. The best tentative components are K_1 = 6.5 km/sec; K_2 = 3.0 km/sec. But we are not certain that K_1 has really changed since 1948. The beat period of 49.1695 days fits the observations reasonably well.

The scatter of the individual points is large and suggests that there are irregular changes in the velocity-curve. This conclusion is placed beyond doubt when we compare the two individual curves of December 24, 1950, and February 9, 1951. They are separated by 47 days and should therefore give closely similar values of $2K$. The measurements show conclusively that $2K$ was much larger on the earlier date than on the more recent date.

There are also unmistakable changes between successive cycles. This is brought out

TABLE 2

RADIAL VELOCITIES OF β CANIS MAJORIS

JD 2433000+	Radial Velocity (Km/Sec)	JD 2433000+	Radial Velocity (Km/Sec)	JD 2433000+	Radial Velocity (Km/Sec)
625.820	+33.1 L*	639.948	+33.8 L	672.659	+33.1 L
.833	+31.4 L	.956	+28.6 L	.668	+31.5 L
.845	+34.6 L	.964	+29.6 L	.682	+32.2 L
.856	+35.4 L	.971	+26.8 L	.692	+32.0 L
.864	+36.3 L	645.736	+25.4 L	.699	+29.8 L
.872	+36.1 L	.744	+25.6 L	.706	+26.8 L
.881	+36.0 L	.752	+23.1 L	.713	+28.3 L
.892	+34.7 L	.767	+23.6 L	.720	+28.0 L
.899	+35.5 L	.774	+22.8 L	.736	+25.3 L
.926	+34.4 L	.785	+22.4 L	.742	+24.9 L
.934	+32.0 L	.792	+21.4 L	.755	+26.8 L
.944	+31.4 L	.800	+26.8 L	.761	+25.3 L
.962	+31.1 L	.808	+24.9 L	.775	+27.1 L
.972	+28.4 L	.816	+27.8 L	.785	+28.8 L
.982	+30.8 L	.828	+27.7 L	.800	+29.3 L
.990	+30.4 L	.837	+30.1 L	.806	+31.9 L
626.001	+30.0 L	.862	+34.0 L	.820	+31.3 L
632.792	+23.9 L	.871	+39.3 L	.831	+33.3 L
.801	+27.0 L	.894	+39.6 L	.838	+31.3 L
.810	+26.6 L	646.769	+22.3 C	.844	+34.0 L
.825	+31.4 L	.792	+21.6 C	.857	+32.7 L
.835	+34.0 L	.815	+26.2 C	.864	+34.0 L
.844	+34.8 L	.841	+31.3 C	.875	+32.1 L
.853	+35.6 L	.876	+37.7 C	673.608	+36.1 C
.861	+37.4 L	.906	+39.6 C	.626	+33.7 C
.869	+38.7 L	648.678	+37.1 C	.645	+32.5 C
.894	+37.7 L	.706	+35.4 C	.664	+31.0 C
.915	+35.0 L	.734	+30.6 C	.675	+32.0 C
.922	+35.8 L	.768	+24.2 C	.689	+30.8 C
.933	+33.7 L	.796	+21.1 C	.706	+29.1 C
.940	+31.8 L	.823	+24.0 C	.717	+27.7 C
.950	+30.4 L	.848	+28.5 C	.733	+27.2 C
.958	+27.9 L	.874	+34.3 C	.744	+27.2 C
.966	+28.2 L	.899	+37.5 C	.756	+26.8 C
.973	+27.0 L	.926	+38.7 C	.769	+26.7 C
.982	+26.0 L	.951	+36.7 C	.784	+27.5 C
.991	+24.5 L	649.699	+35.3 C	.793	+29.1 C
639.784	+22.8 L	.724	+30.6 C	.806	+31.1 C
.792	+22.4 L	.750	+26.5 C	.825	+33.0 C
.801	+26.1 L	660.683	+35.4 L	.843	+35.1 C
.815	+24.3 L	.800	+26.9 L	.854	+36.3 C
.824	+29.0 L	.808	+29.3 L	681.603	+30.7 L
.833	+31.2 L	.824	+27.6 L	.610	+34.2 L
.840	+35.8 L	.831	+29.5 L	.618	+35.9 L
.848	+37.9 L	.850	+31.9 L	.634	+36.8 L
.856	+36.9 L	.859	+32.4 L	.643	+36.4 L
.862	+37.5 L	.867	+32.1 L	.649	+36.7 L
.869	+38.7 L	.879	+31.7 L	.658	+37.1 L
.878	+42.3 L	.888	+31.7 L	.681	+34.4 L
.892	+41.9 L	.896	+32.3 L	.688	+30.2 L
.899	+44.4 L	.903	+32.9 L	686.597	+33.0 L
.906	+43.7 L	.913	+35.1 L	.603	+35.5 L
.917	+41.1 L	672.616	+36.4 L	.611	+34.8 L
.927	+35.2 L	.624	+38.6 L	.621	+37.3 L
.934	+34.9 L	.631	+36.0 L	.634	+37.8 L
.941	+34.0 L	.641	+36.5 L	.641	+38.6 L

* "L" and "C" have significance indicated in note to Table 2.

TABLE 2—*Continued*

JD 2433000+	Radial Velocity (Km/Sec)	JD 2433000+	Radial Velocity (Km/Sec)	JD 2433000+	Radial Velocity (Km/Sec)
686.652	+37.2 L	686.774	+24.9 L	406.669	+35.9 C
.659	+37.3 L	.781	+24.0 L	.685	+35.3 C
.669	+35.7 L	.787	+24.4 L	.701	+34.6 C
.678	+37.7 L	.802	+24.5 L	.719	+35.8 C
.685	+37.0 L	.816	+25.7 L	.735	+35.6 C
.708	+33.3 L	.822	+26.9 L	.753	+35.3 C
.715	+32.1 L	.833	+29.0 L	.771	+30.8 C
.722	+28.9 L	.839	+28.8 L	.788	+30.7 C
.742	+27.6 L	.846	+33.1 L	.807	+29.4 C
.749	+23.9 L	406.636	+33.8 C	.826	+29.3 C
.762	+23.8 L	.653	+35.0 C	.847	+30.7 C

TABLE 3

OBSERVED TIMES OF MAXIMUM VELOCITY; VALUES OF $2K$, TWICE THE AMPLITUDES OF THE VELOCITY-CURVE, AND γ, THE CENTER OF MASS VELOCITY

(Computed Maximum = JD 2418367.78 + 0.25002246E)

Date	Observed Time of Maximum Velocity (JD)	E	O−C (Day)	$2K$ (Km/Sec)	γ (Km/Sec)
1950 Dec. 10	2433625.875	61027	−0.026	(8)	(+32)
17	632.880	61055	− .021	(16)	(+31)
24	639.895	61083	− .007	(22)	(+32)
30	(645.910)	61107	+ .008	(18)	(+31)
31	(646.912)	61111	+ .009	(19)	(31)
1951 Jan. 2	648.925	61119	+ .022	18	+30
14	660.9??	.....	.....	(8)	(+31)
26	(672.625)	61214	− .030	(10)	+31
27	673.???	.....	.....	(10)	(+31)
Feb. 4	681.648	61250	− .008	(12)	(31)
9	686.648	61270	− .008	14	+31
1953 Jan. 29	2434406.700	64150	−0.021	7	+32

strikingly by the coudé plates of January 26 and 27, 1951, and January 29, 1953. On the first, the height of the two maxima differs by an amount that is inconsistent with the internal precision of the measurements. On January 27, 1951, the separation between two successive maxima is greater than the normal 6-hour period. The critical spectrograms of this series have been remeasured, without any appreciable change in the curve. On the most recent date the curve is peculiar in shape. It is thus safe to conclude that the irregular variations which distort the velocity-curves of ν Eridani and 16 Lacertae are also present in β Canis Majoris.

We have listed in Table 3 the times of maximum radial velocity. The values for December 30 and 31, 1950, and for January 26, 1951, were not directly observed but were interpolated from the respective times of minimum velocity by applying a difference of one-half period, $\frac{1}{2}P_1 = 0.125$ day. To see whether this procedure is justified, we have examined all the radial velocity-curves of β Canis Majoris with well-defined maximum and minimum in a single cycle, as given by Struve, and we have estimated the time

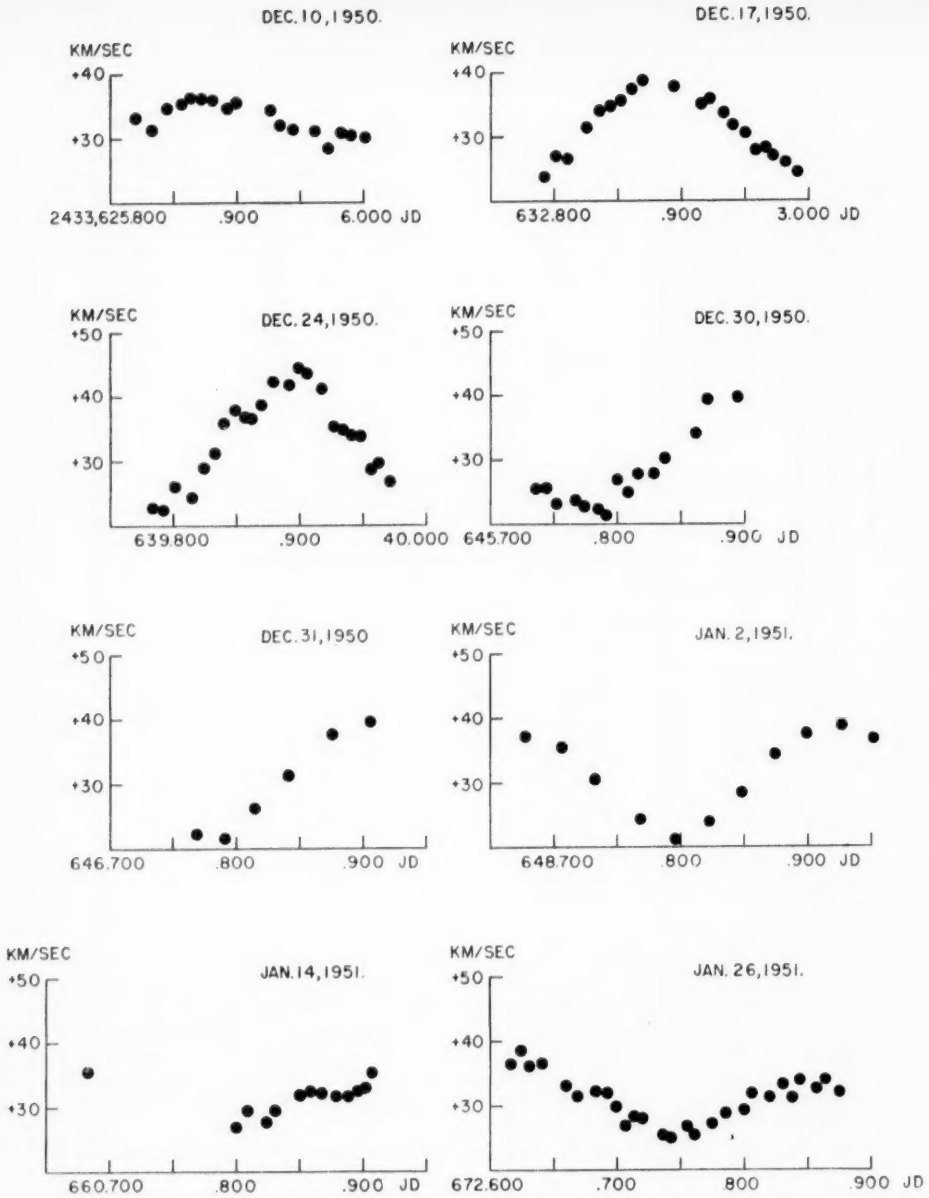

FIG. 1.—Radial velocities of β Canis Majoris

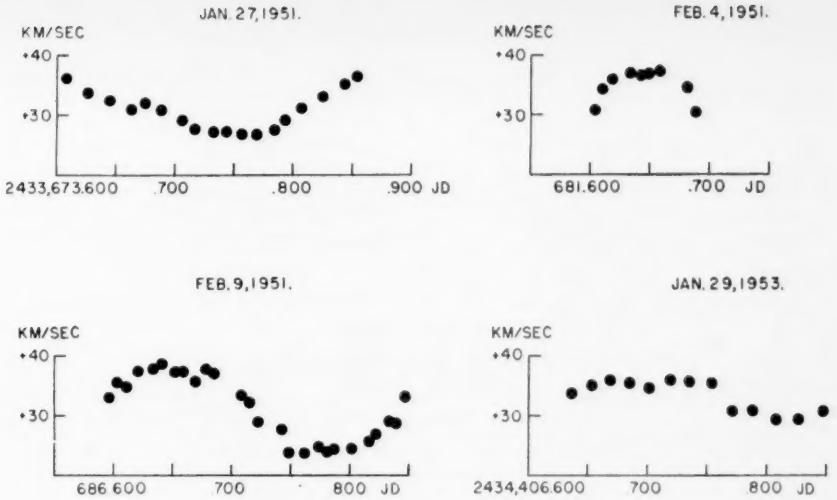

FIG. 2.—Radial velocities of β Canis Majoris

TABLE 4

TIME INTERVALS OF DESCENDING AND ASCENDING BRANCHES OF RADIAL VELOCITY-CURVES

Date	Descending Branch Maximum→ Minimum (Day)	Ascending Branch Minimum→ Maximum (Day)	γ (Km/Sec)
1931 Nov. 3	0.107	.....	+35
6	.107	.....	34
9	.....	0.120	33
12	.....	.123	35
19	.....	.111	33
24	.....	.123	34
30	.100	.148	34
Dec. 6	.084	.149	34
16	.....	.135	34
19	.....	.117	35
1932 Jan. 6	.121	.....	32.5
1947 Nov. 24	.....	.149	33
Dec. 13	.143	.....	33
24	.....	.111	33
30	.128	.....	33
1948 Jan. 18	.....	.108	32
25	.....	.118	33
Feb. 17	.....	.137	32
Mar. 1	.....	.111	32
1951 Jan. 2	.....	0.128	30
Feb. 9	.124	.....	31
1953 Jan. 29	0.117	.....	32
Average	0.115	0.126	.....
Corrected to give correct sum: 0.119+0.131=0.250	0.119	0.131	.....

intervals of descending and ascending branches. The results, together with three recent dates, are given in Table 4. The average time interval of the descending branch is 0.115 day, and that of the ascending branch is 0.126 day. The sum is 0.241 day, which is 0.009 day, or 2.8 per cent short of the true period, $P_1 = 0.25002246$ day. This departure is, of course, not real, because an error of a few per cent can be easily made in estimating the period from individual cycles. However, the ratio of the two intervals may have significance. It resembles the asymmetry of the velocity-curves of cepheid variables. Although the two branches are not exactly of the same duration, no serious error can result

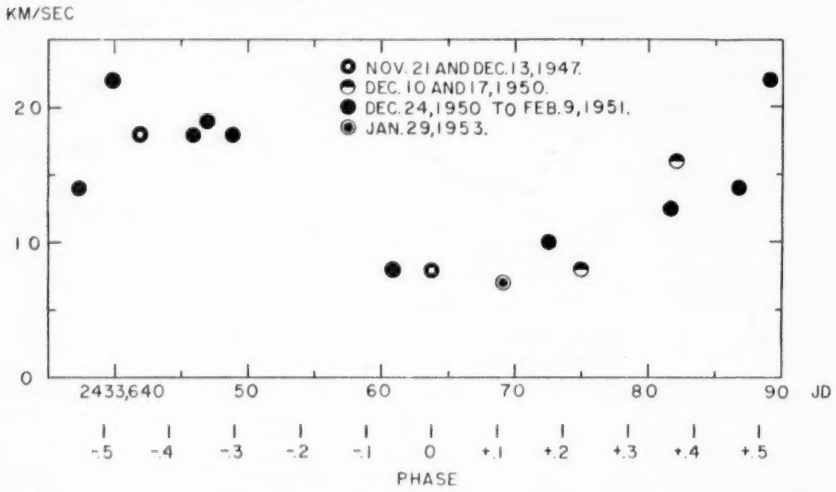

FIG. 3.—Variation of $2K$, twice the amplitudes of the radial velocity-curves, in β Canis Majoris based on a beat period, $P_3 = 49.1695$ days.

when we compute the time of maximum velocity by adding or subtracting $\frac{1}{2}P_1$ to the epoch of minimum velocity.

We have computed the times of maximum radial velocity by the following formula:[1]

$$T \max = 2418367.78 + 0.25002246E .$$

The differences between the observed and the computed times of maximum velocity, in the sense of observed *minus* computed, are given in Table 3. The largest difference is -0.030 day on January 26, 1951. The observed time was interpolated from the time of minimum on the descending branch of the velocity-curve. This departure would be reduced to -0.024 day if the average time interval of 0.119 day for the descending branch, instead of the half-period, had been taken.

The scatter of the values of (O−C) in Table 3 is so large that it would be futile to relate them to the phase in the beat period. But we conclude that the old value of P_1 still represents the observations correctly.

OBJECTIVE-PRISM SPECTRA OF LONG-PERIOD VARIABLES IN THE NEAR INFRARED

JASON J. NASSAU AND DONALD M. CAMERON
Warner and Swasey Observatory of the Case Institute of Technology
Received July 6, 1953

ABSTRACT

A study of low-dispersion spectra of late M-type stars in the near infrared ($\lambda\lambda$ 6800–8800) suggests the classification of these stars based on strengthening vanadium oxide absorption. It also shows that stars which show the vanadium oxide absorption are very likely to be variable. A list of 52 variables, 40 of which are new, is given in an area of about 20 square degrees centered at R.A. = 20^h00^m, dec. = 32.0° (1950). The spectra of these variables show large changes correlated with the light-variations. Two *TiO* bands at approximately λ 8210 and λ 8280 have been observed in a number of late M-type stars, which may assist in the identification of very late M-type stars.

I. INTRODUCTION

The spectra of long-period variable stars have been studied in considerable detail, particularly at maximum light, in the visible region of the spectrum; but relatively little work has been done in the infrared. With the advent of photographic emulsions of increased sensitivity in the near infrared, it appears that additional information of considerable value about these stars can be obtained. The present paper is a preliminary report of the work under way at the Warner and Swasey Observatory in this field.

In a brief note Nassau, van Albada, and Keenan[1] described two new bands which occur in the region around λ 7400 and λ 7900 and which appear usually in the spectra of long-period late M-type stars. Recently Keenan and Schroeder[2] identified these bands as due to vanadium oxide and called attention to the fact that irregular variables also show these bands. In the course of previous infrared investigations in Cygnus[3,4] the occurrence of these bands was frequently associated with light-variability. In very late M-type stars the *VO* bands strengthen to such an extent that almost the entire continuum on the short-wave-length side of λ 7900 seems to disappear, while on the long-wave-length side, where there is relatively little absorption, the continuum is very strong. This gives to the spectrum a unique appearance, definitely different from other types of spectra, especially on plates taken with the 2° objective prism. Stars having spectra of this type usually, if not always, show variability.

The present investigation is an outgrowth of such observations and has for its purpose the following: (*a*) the detection of variables of late M type from the appearance of the *VO* bands in their spectra and (*b*) the correlation of the changes in spectral appearance with the change in light. The estimation of the percentage of variables among the late M-type stars is left for future consideration.

II. OBSERVATIONAL MATERIAL

The observational material consisted of a series of direct and spectral plates taken with the Schmidt-type Burrell telescope. The spectral plates used were taken either with the 2° or the 4° objective prism. Kodak I-N emulsion with a Wratten No. 89 filter made

[1] *Ap. J.*, **109**, 333, 1949.

[2] *Ap. J.*, **115**, 82, 1952.

[3] Nassau and van Albada, *Ap. J.*, **109**, 391, 1949.

[4] Unpublished material by the present authors.

available for this investigation the spectral region from λ 6800 to λ 8800. The direct infrared plates were taken with the same combination of emulsion and filter, while the blue plates were taken either with Kodak 103*a*-O emulsion or IIa-O. Additional information with respect to the data may be obtained by referring to a previous paper by Nassau and van Albada.[3]

The choice of a field was governed by the material already available, since a period of several years would be required to secure the necessary data for an investigation of this type. The region chosen was a circular area of about 20 square degrees centered at R.A. = 20^h00^m, dec. = 38°.0 (1950). A list of all plates containing pertinent data is given in Tables 1 and 2.

TABLE 1

No.	R.A.	Dec.	Date	JD	Exposure (Min.)	Prism
1	20^h00^m	+38°.0	6-17-47	2432353	35	4°
2	20 15	38 .0	6-19-47	2432355	27	4°
3	20 00	38 .0	7-25-47	2432391	60	4°
4	20 00	38 .0	9-24-47	2432452	5	4°
5	20 00	38 .0	5- 4-48	2432675	10	2°
6	19 58	40 .5	8- 9-51	2433867	10	2°
7	20 16	38 .2	8- 9-51	2433867	14	2°
8	20 16	38 .2	8-11-51	2433869	30	2°
9	20 00	38 .0	6-29-52	2434192	30	2°
10	20 00	38 .0	10-17-52	2434272	30	2°
11	20 00	+38 .0	10-19-52	2434304	5	4°

TABLE 2

No.	R.A.	Dec.	Date	JD	Exposure (Min.)	Emulsion
1	20^h15^m	+38°.0	4-28-47	2432303	60	I-N
2*	20 00	38 .0	6-29-47	2432365	30	I-N
3*	20 00	38 .0	7-18-47	2432384	45	I-N
4*	20 00	38 .0	9- 8-47	2432436	15	I-N
5	20 00	38 .0	9-15-47	2432443	15	I-N
6*	20 00	38 .0	12-15-47	2432534	30	I-N
7*	20 00	38 .0	7- 8-48	2432740	45	I-N
8	20 00	38 .0	7-26-48	2432758	6	I-N
9	20 00	38 .0	7-27-48	2432759	10	I-N
10*	20 00	38 .0	8-25-49	2433153	30	I-N
11	20 15	38 .0	7-15-51	2433842	20	I-N
12*	20 00	38 .0	7-17-47	2432383	10	103*a*-O
13*	20 00	+38 .0	8-22-49	2433150	10	103*a*-O

* Indicates the plates used for magnitude determinations.

III. DETECTION OF VARIABLES

Two hypersensitized plates, one of 30-minute exposure with the 2° prism and the other with the same exposure and the 4° prism, were examined. All stars which were suspected to be variable from the appearance of their spectra, as previously described, were marked. The limiting infrared magnitude of the deeper of the two plates was about 13.5. Only stars well above the limiting magnitude were chosen. Since it is frequently difficult to determine the presence of the λ 7900 band when weak, a generous choice of stars was made by selecting all late M's, that is, M7 and later. However, since only two plates

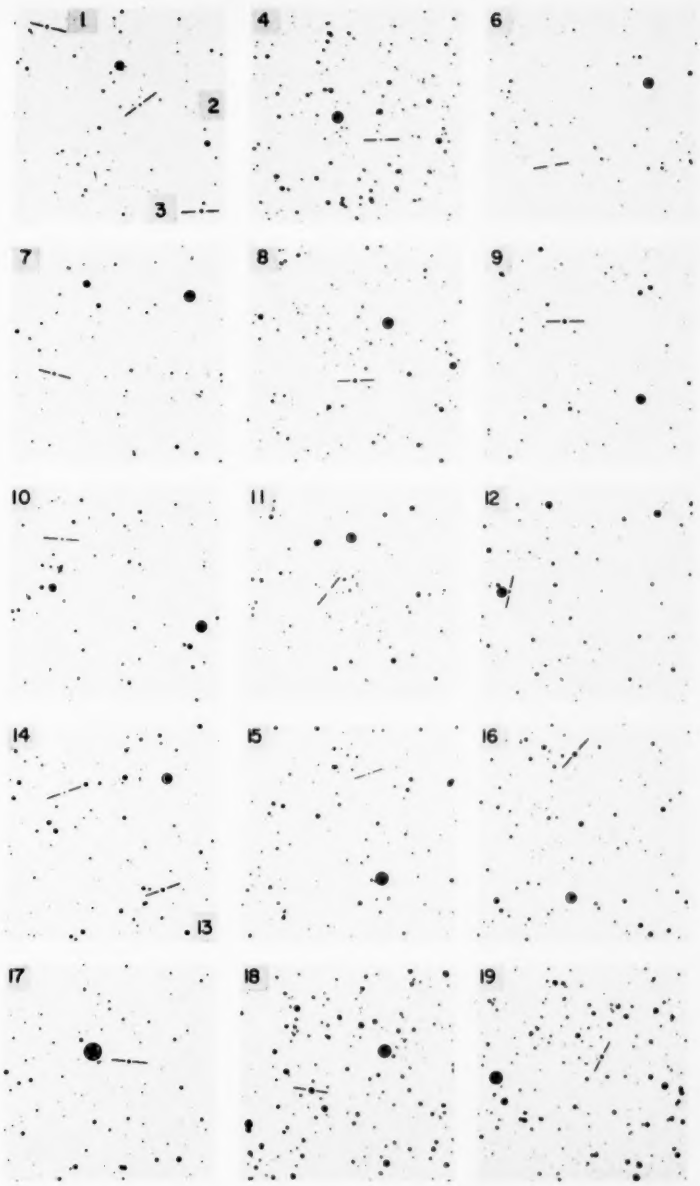

FIG. 1*a*.—The circle around a star image indicates a BD star. *1*, 35°3887; *2*, 35°3887; *3*, 35°3887; *4*, 35°3892; *6*, 35°3892; *7*, 35°3921; *8*, 35°3945; *9*, 36°3727; *10*, 36°3741; *11*, 36°3762; *12*, 36°3767; *13*, 36°3777; *14*, 36°3777; *15*, 36°3792; *16*, 36°3794; *17*, 36°3806; *18*, 36°3808; *19*, 36°3822.

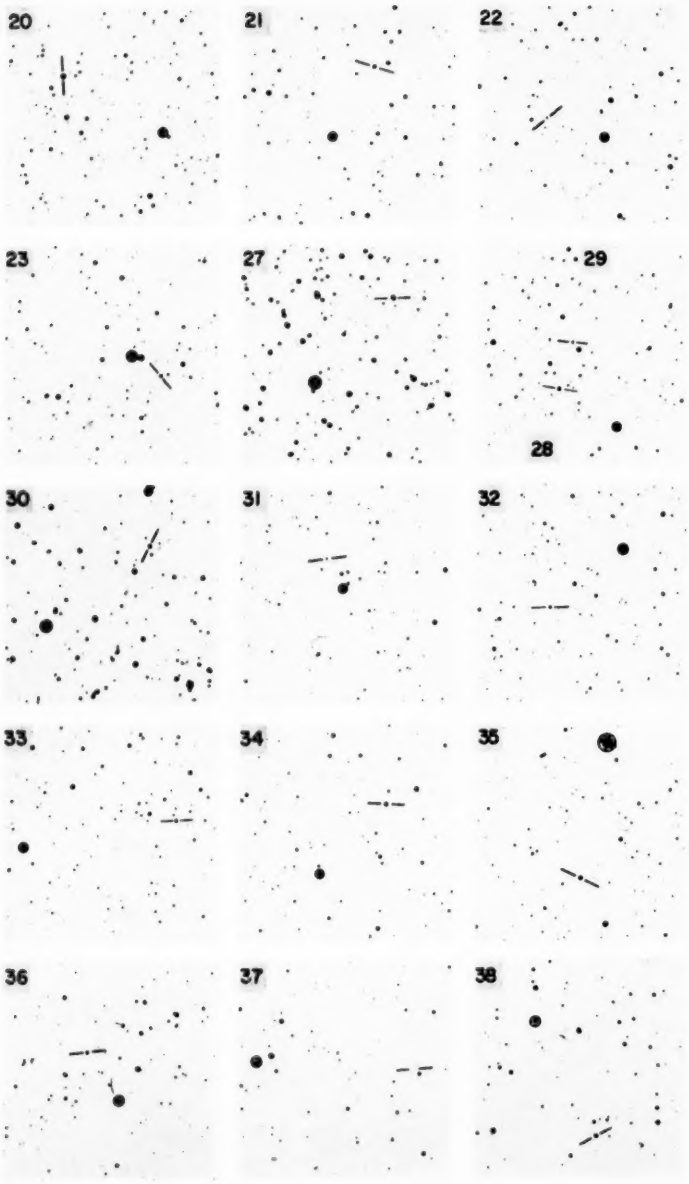

FIG. 1b.—*20*, 36°3823; *21*, 37°3633; *22*, 37°3654; *23*, 37°3724; *27*, 37°3757; *28*, 37°3773; *29*, 37°3773; *30*, 37°3819; *31*, 38°3812; *32*, 38°3860; *33*, 38°3868; *34*, 38°3874; *35*, 38°3896; *36*, 38°3928; *37*, 38°3941; *38*, 39°3964.

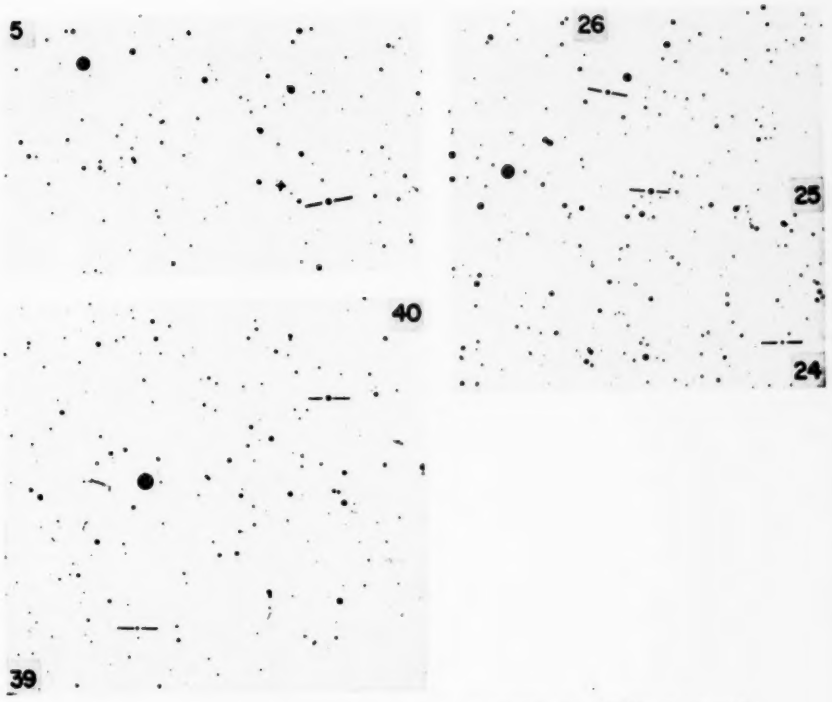

FIG. 1c.—*5*, 35°3892; *24*, 37°3732; *25*, 37°3732; *26*, 37°3732; *39*, 39°3965; *40*, 39°3965

taken at different dates were examined and in view of the existence of spectral variability, no effort was made to attain completeness.

In this manner 230 stars were chosen. They were examined in a blink comparator on at least three direct plates taken at different dates. No measurement of magnitude was involved here. Only stars whose range of variation was sufficiently great that visual examination in the blink showed *definite* variation were assigned as variables. In this manner 52 of the 230 stars examined were found to be definitely variable. Of the 52 stars, 12 were already known long-period variables as listed in the *General Catalogue of Variable Stars*.[5] The remaining 40 are presumably new long-period variables. Undoubtedly a further examination, involving photometry, of the suspected variables will result in the discovery of additional variables. The positions of the new variables are shown by charts (Fig. 1) which were made from an infrared plate. The identification is made possible by including in each field a BD, star which is circled.

TABLE 3

Name (Cygnus)	Period	1947		1949		m_{ip} (Max.)	Range (Mag.)
		I.I.	Phase	I.I.	Phase		
V 419	231*	5.6†	0.7	5.0	0.1	10.7	1.6
V 422	262	5.7†	.6	5.7†	.5	10.1	1.8
KK	268*	5.3:	.8	6.5	.7	9.2	2.4
AG	296.3	6.1	.7	5.5	.3	9.0	2.0
PX	309	5.8	.9	5.8†	.4	10.0	2.0
KS	312	6.0	.1			8.0	3.4
KM	334.7	6.9	.3	5.3	.6	8.6	2.1
V 341	351.3	6.6†	.9	4.5	.0	9.4	2.0
KO	353	5.8	.0	6.8	.2	8.8	3.2
NW	388	5.1†	.4	5.1†	.4	9.1	3.9
IZ	441	5.3	.1	6.0	.9	8.2	2.8
V 342	447	7.2	0.6	6.3	0.3	9.5	1.5

* Indicates that the period given in the *General Catalogue of Variable Stars* has been modified to agree better with our data.

† Indicates that the star's infrared color is greater than the value given.

IV. THE SPECTRUM AND LIGHT-VARIATIONS

Since the observational material available for the 52 variables is very limited, the study of the correlation between the spectral changes and the light-changes is based primarily on the 12 known variables of the region. The infrared magnitudes of these stars were measured on seven plates, which were taken on different nights. Using this material together with data secured from the *General Catalogue of Variable Stars*, mean light-curves were plotted. In addition, infrared color indices, as defined in the paper by Nassau and van Albada,[3] were obtained from two pairs of plates taken only a few nights apart. The results are shown in Table 3. The first column gives the name of the star. The second column gives the period according to the *General Catalogue of Variable Stars*. An asterisk following the period signifies that it has been modified to agree better with our data. In the third column the infrared color index obtained from plates taken on July 17, 1947 (103*a*-O), and July 18, 1947 (I-N), is given; and in the fourth column the corresponding phase in tenths of a period from maximum. The dagger indicates that the star's infrared color is greater than the value given. The fifth and sixth columns give the same data for plates taken on August 22, 1949 (103*a*-O), and August 25, 1949 (I-N). The seventh col-

[5] B. V. Kukarkin and P. P. Parengo, *General Catalogue of Variable Stars* (Academy of Sciences of the U.S.S.R., 1948).

umn gives the approximate infrared magnitude at maximum; and the eighth column gives the approximate range in magnitudes. Both have been estimated from the light-curves. Table 3 shows that, in general, the infrared index increases as the star varies from bright to faint and that the range in magnitude tends to increase with increasing period.

An average of six or seven plates was available for examination of the spectra of these stars. The spectral changes, which are due primarily to the change in strength of the *VO* bands at λ 7400 and λ 7900 relative to the *TiO* bands, were correlated with phase. The following four types describe these changes and provide means for their classification. Spectra illustrating these types are shown in Figure 2.

Type a.—This type shows the appearance of approximately a normal M6. In some cases weak *VO* at λ 7900 is visible.

Type b.—Both bands at λ 7400 and λ 7900 are well visible, and frequently the continuum is weakened in the region from λ 8432 to λ 8800.

Type c.—The λ 7400 and λ 7900 bands have increased in strength and broadness to such an extent as to appear as prominent as the *TiO* band at λ 7600. This gives to the region to the violet of λ 7900 the characteristic "fluted" appearance shown in Figure 2, *c*.

Type d.—Here the *VO* absorption has become so intense that practically all the continuum to the violet of λ 7900 has disappeared, producing the appearance of a sharp break at this wave length. In some cases the break is very great; in other cases the contrast is much less pronounced, showing a weak continuum on the short-wave-length side of λ 7900; in still other cases a faint trace of the "fluted" appearance is evident. In the region between λ 8432 and λ 8800 two different appearances may be distinguished. Some spectra show a narrow, rather weak λ 8432 band and very little, if any, weakening of the continuum between λ 8432 and λ 8800. Other spectra show a strong and broad λ 8432 *TiO* band and a general weakening of the continuum between this band and λ 8800.

In a broad sense the light-variations of a star from maximum to minimum follow the sequence of spectral types from *a* to *d*. However, some stars at maximum may be earlier or later than type *a*. One star was found to be as early as M4; and it is suspected that in a few cases it may be as late as type *d*.

Since the differences described above are based on the increasing strength of *VO* absorption, it is assumed that they represent a sequence of advancing spectral type and that type *d* represents the latest-type spectrum observed. The variation in the infrared color indices with respect to phase given in Table 3 strengthens this conclusion. This is consistent with Merrill's[6] statement based on observations in the visual region: "The *VO* bands appear to increase in intensity with advancing spectral type. Thus, at time of maximum light they are stronger in R Leonis than in *o* Ceti, and in a given variable become stronger as the light declines. The astrophysical data suggest that the dissociation energy of *VO* is less than that of *TiO*." This was also observed by Keenan and Schroeder.[2]

Some idea of the relation of our sequence of types to the Mount Wilson system of classification may be obtained by examination of a series of spectra of the long-period variable BB Scuti, taken at the Warner and Swasey Observatory between June 15 and August 24, 1951. Reproductions of these spectra are shown in Figure 3. In August, 1951, Dr. Morgan, at our request, obtained a slit spectrum of this variable at the Yerkes Observatory. He classed it as M9 because it appears later than RT Vir (M8), which is the latest-type spectrum given in the Mount Wilson list.[7] A 2° objective-prism spectrum of RT Vir shows very strong *TiO* bands and apparently no *VO*. Examination of our plates (Fig. 3) shows that the spectrum of BB Scuti was of type *b* during this period. In June, 1951, when the variable was faint, the spectrum was type *d*.

The results of the examination of all available spectral plates for the 12 known variables are given in Table 4. Enlargements of representative spectra secured with the 2°,

[6] P. W. Merrill, *Spectra of Long-Period Variable Stars* (Chicago: University of Chicago Press, 1940), p. 36.

[7] Adams, Joy, and Humason, *Ap. J.*, **64**, 225, 1926.

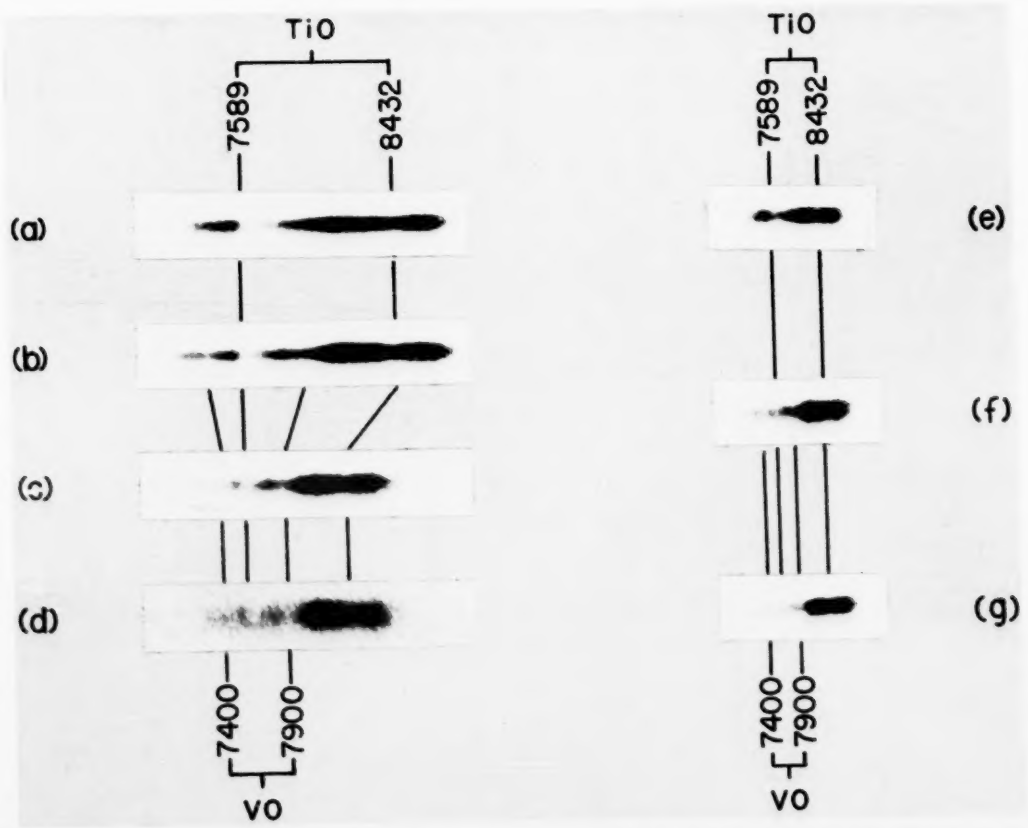

FIG. 2.—*a*, type *a*, 6°; *b*, type *b*, 6°; *c*, type *c*, 4°; *d*, type *d*, 4°; *e*, type *a*, 2°; *f*, type *c*, 2°; *g*, type *d*, 2°. The objective prism used is indicated in each case.

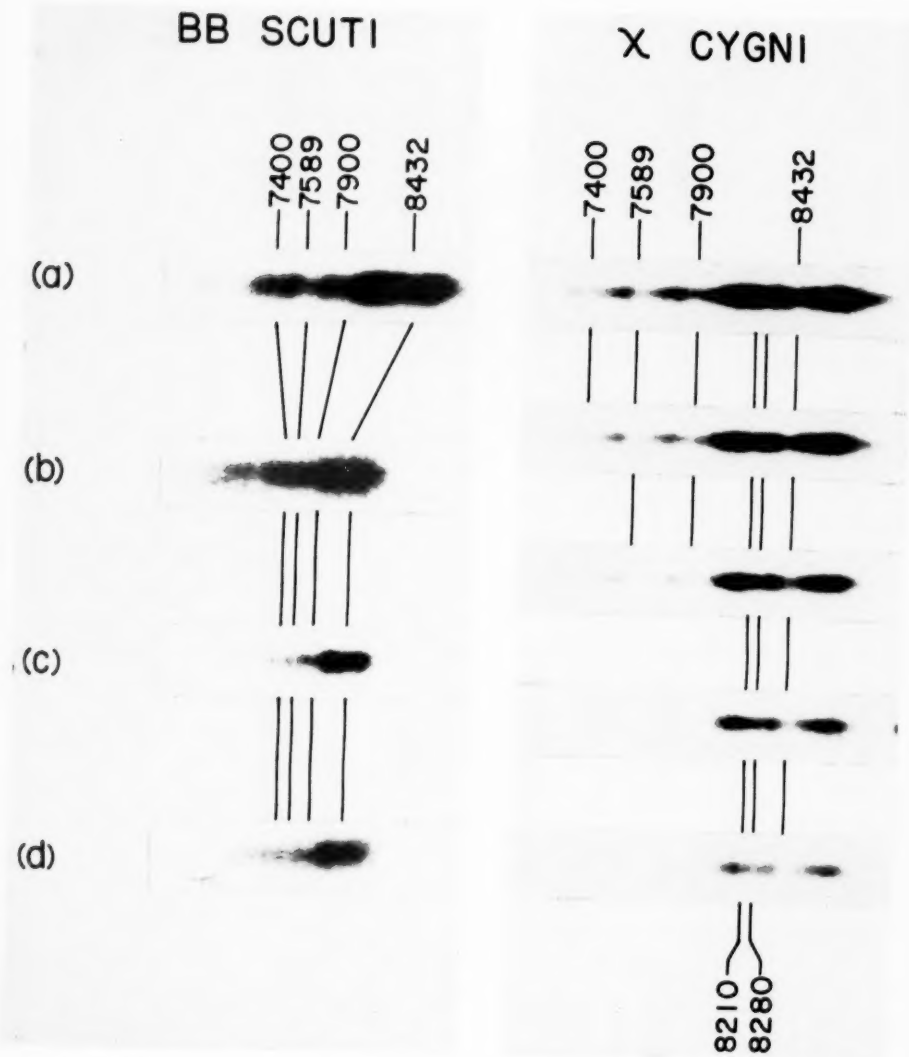

FIG. 3.—For BB Scuti: *a*, August 25, 1951—4^{m}; *b*, August 9, 1951—2^{m} (overexposed); *c*, July 7, 1951—2^{m}; *d*, June 15, 1951—2^{m}. The objective prism used is indicated in each case. The spectrum of χ Cygni is shown in five exposures made with the 6° objective prism.

4°, and 6° prisms are shown in Figure 2. The first column of Table 4 gives the name of the star. The second and third columns give the magnitudes at maximum and minimum. The fourth column gives the period, and the fifth column the spectral type. The data for the first five columns were taken from the *General Catalogue of Variable Stars*.[5] An asterisk after the magnitude at minimum indicates that it is greater than the value given. A dagger (†) after the period indicates that this value has been modified to agree better with our light-curves. A double dagger (‡) after the spectral type indicates that it has been estimated from our plates. The next ten columns exhibit the results of the examination of the spectral plates. A spectral type is given for each of the plates examined in the column corresponding to the phase of light-variation on the date when the spectral plate was taken. The letters *a*, *b*, *c*, and *d* are used to describe the spectrum as previously discussed.

TABLE 4

Name (Cygnus)	Magnitude		Period	Sp.	Phase (Tenths of Period) from Max.									
	Max.	Min.			0.0	0.1	0.2	0.3	0.4	0.5	0.6	0.7	0.8	0.9
V 419	13.0	16pg.*	231†	M5‡	*a* (M5) *b*	*b*	.....	.....	.....	*d:*	*d*	*d*	.....	*a*
V 422	14.1	15.5*	262	M6‡	.....	.....	.....	*d*	.....	*d*	*d*	*a*	*a:*	*a* (M5)
KK	14.5	15.5*	268†	M5‡	*a*	*a*	.....	.....	.....	.....	*d:*	*b*	.....	*b:*
AG	11.2	17.0	296.3	M6	*a* (M5)	.....	*a* (M6)	.....	.....	.....	*d*	*d*	.....	.....
PX	14.0	17.0*	309	M5e	*a:*	*d*	.....	.....	.....	.....	.....	*d*	*d*	*d*
KS	13.8	15.5	312	.....	*a:*	*a:* *b:*	*b:* *b:*	*d:*	*d:*	.....	.....	.....	.....	*b:* *a:*
KM	11.4	15.6*	334.7	M4‡	*a* (M4)	*a:*	*b*	*c*	.....	*d*	.....	.....	.....	*a:*
V 341	14.0	16.5*	351.3	M5e	*a* (M6) *a* (M5)	*a:*	*a:*	*d:*	.....	.....	.....	*d*	*d*	*d*
KO	13.4	15.5*	353	M6‡	*a:*	*a*	*d* *a*	.....	*d*	.....	.....	.....	*a:*	*a:* *b:*
NW	14.1	16.5*	388	.....	.....	.....	*d*	*d*	*d:*	.....	*d*	.....	.....	.....
IZ	11.0	15.0*	441	M7p	.....	*a:* *a:*	.....	*d*	*c*	*d*	.....	.....	*d:*	.....
V 342	14.0	16.0*	447	.....	.....	.....	.....	*d:*	.....	*d*	*d*	*d*	*d* *d*	*d*

* Indicates that the magnitude is greater than the value given.

† Indicates that the period given in the *General Catalogue of Variable Stars* has been modified to agree better with our data.

‡ Indicates that the spectral type has been estimated from our plates.

Here the colon indicates that the spectrum was too strong or too weak for positive classification. A progressive change in the spectrum of each star in the direction from type *a* to *d* is generally indicated as the light varies from maximum to minimum.

V. BANDS NEAR λ 8300

In addition to the spectra described above, which are fairly general, other features have been observed in a limited number of variables and only at certain phases. The most prominent such feature is an absorption band, or pair of bands, at about λ 8300, which appear in some long-period variables and in spectra of other stars which as yet have not been examined for variability. With the 2° and 4° dispersion, these new bands are separated from the λ 8432 *TiO* band by a short continuum, which is so narrow that it frequently appears like an "emission" feature. These bands are generally rather weak but in a few cases have appeared fairly strong. When the bands are weak, care must be taken not to confuse them with the atmospheric water-vapor band near the same region.

The two bands near λ 8300 were observed in the spectrum of χ Cygni taken with the 6° prism on July 2, 1952, when the variable was near minimum. An enlargement of the spectrum of this star in five exposures showing these bands is given in Figure 3. Approximate wave lengths of the bands are λ 8210 and λ 8280. They were derived by measuring 6° dispersion plates of χ Cygni, 555 Cygni, and another late M-type star near SV Draconis.

For the identification of these bands, which turned out to be blends of *TiO* bands, we are indebted to Dr. P. C. Keenan,[8] who has observed them in a number of slit spectra of late M-type stars and who has called our attention to the fact that there are other weak *TiO* and *VO* bands on the long-wave-length side of λ 8432 which probably contribute to the general weakening in this region, in very late M-type spectra. The average wave lengths of the blends are λ 8202 and λ 8287. Since these bands are very weak, they will appear only in very late M-type spectra and should be useful as a criterion for low temperature. Further work in this field is now in progress, as many very late M stars do not show these bands and in other cases they appear abnormally strong.

Bobrovnikoff[9] was the first to measure most of these bands in stellar spectra, and he identified them with *TiO*. Christy[10] predicted them but did not observe them in laboratory spectra. Wurm and Meister[11] and later Kiess[12] observed most of these bands in laboratory spectra of the *TiO* arc.

Note added October 10, 1953.—Spectra of χ Cygni taken during May and June, 1953, when the star was not near minimum light, show the bands near λ 8300.

[8] Private communication.

[9] *Ap. J.*, **78**, 211, 1933.

[10] *Ap. J.*, **70**, 1, 1929.

[11] *Zs. f. Ap.*, **13**, 199, 1936.

[12] Unpublished lists, National Bureau of Standards.

THE STANDARD REGION NEAR IC 4665

HAROLD L. JOHNSON
Lowell Observatory
Received July 18, 1953

ABSTRACT

Three-color photoelectric observations in the standard region near IC 4665, the third and last of these standard regions, are given. The observations are on the system defined by Johnson and Morgan for bright and near-by stars and should be considered to be part of the definition of that system. This third standard region has a declination of about +6° and is therefore accessible from both the Northern and the Southern Hemispheres.

Three-color photoelectric observations on the system defined by Johnson and Morgan[1] are given for the standard region near IC 4665. This region is the last of three standard regions[2] which, together with a number of representative near-by and bright stars, define a new photometric system of magnitudes and colors. For a complete description of the system the reader is referred to the paper by Johnson and Morgan.[1]

The observations in the standard region near IC 4665 are given in Table 1. The first column gives the BD numbers of the stars; the next three, the measured magnitudes and colors; and the last, the number of independent observations on each star. The observations were taken in the same manner as in all previous regional observations:[1,3] All stars in the region were compared directly with a regional standard star, BD + 5°3483, which was then tied in thoroughly on nine different nights with the fundamental system. The probable errors of the tie-in with the fundamental system and the relative probable errors within the standard region are given in Table 2.

Most of the observations were made at the Lowell Observatory during the month of June, 1953, but a few were made at the McDonald Observatory in June, 1951, and others at Mount Wilson Observatory during June, 1950, while the author was on the staff of the Washburn Observatory of the University of Wisconsin. The Lowell and the McDonald observations were made with the same filters that were used in the definition of the fundamental system,[1] but the Mount Wilson observations were made with filters that are known to give systematically different results.[1,4] All stars observed at Mount Wilson were observed at Lowell, and many were observed at McDonald as well. It is possible, therefore, to determine fairly accurately the transformation between the two color systems. Nevertheless, the Mount Wilson observations were given relatively low weight in forming the means; they do, however, permit a check on the variability over a three-year interval of some of the stars in the standard region. An asterisk following the BD number of the star in Table 1 indicates that the star was observed at Mount Wilson and has not been found to be significantly different, either in magnitude or in color, at Lowell.

The galactic cluster, IC 4665, which gives to this standard region its name, cannot be discussed adequately on the basis of the data given here. The cluster consists of a few stars in the range of spectral type B3–B5 and probably several fainter stars of later type. It is not possible, however, to separate photometrically the fainter cluster members, if they exist, from the field stars. The purely photometric method of determining the red-

[1] *Ap. J.*, **117**, 313, 1953.

[2] The other two are the regions of the clusters Praesepe and the Pleiades.

[3] H. L. Johnson, *Ap. J.*, **116**, 640, 1952; **117**, 353, 356, 1953.

[4] *Ibid.*, **116**, 272, 1952.

TABLE 1

PHOTOELECTRIC OBSERVATIONS IN THE STANDARD REGION NEAR IC 4665

BD Star	V	$B-V$	$U-B$	n
+5°3466*	8.05	+0.071	−0.17	5
+5°3469	7.83	+1.279	+1.10	2
+5°3471*	8.31	+0.056	−0.16	5
+5°3472	9.68	+1.270	+1.04	2
+5°3473*	9.39	+0.314	+0.17	4
+5°3474	10.21	+1.292	+1.27	2
+5°3476*	9.08	+0.186	+0.01	4
+5°3477*	10.10	+0.122	+0.01	4
+5°3478*	7.68	+0.031	−0.42	5
+5°3479*	9.10	+0.264	+0.10	3
+5°3480	9.87	+0.351	+0.18	2
+5°3481*	7.50	+0.128	+0.07	4
+5°3482*	7.59	+0.002	−0.49	5
+5°3483*	6.85	+0.011	−0.54	Std.
+5°3484*	7.34	+0.020	−0.46	5
+5°3485	10.61	+0.452	+0.15	2
+5°3487*	8.82	+0.237	+0.13	3
+5°3488*	7.94	+0.449	−0.01	13
+5°3489	10.28	+1.272	+1.07:	2
+5°3490*	7.12	+0.018	−0.48	4
+5°3491*	8.22	+0.113	−0.30	5
+5°3492	10.66	+0.563	+0.37	2
+5°3493*	8.89	+0.106	−0.27	5
+5°3494A*	8.01	+0.058	−0.44	4
+5°3494B	10.23	+0.31	+0.18	1
+5°3495	10.75	+0.368	+0.22	2
+5°3496*	9.81	+0.676	+0.23	3
+5°3497*	9.86	+0.238	+0.12	3
+5°3498	8.33	+1.728	+2.08	2
+5°3499	10.20	+0.272	+0.16	2
+5°3500*	8.40	+1.232	+1.04	3
+5°3502	10.67	+0.512	+0.25	2
+5°3503	8.96	+1.245	+1.07	2
+5°3504*	7.49	+0.016	−0.41	5
+6°3514*	7.43	+0.334	+0.15	4
+6°3520	9.80	+0.56	.....	2
+6°3523	11.33	+0.527	−0.05	2
+6°3524*	7.89	+1.028	+0.77	5
+6°3525*	7.74	−0.009	−0.55	5

* This star was observed at Mount Wilson in 1950; the results do not differ significantly either in magnitude or in color from the values obtained in 1953 at Lowell Observatory.

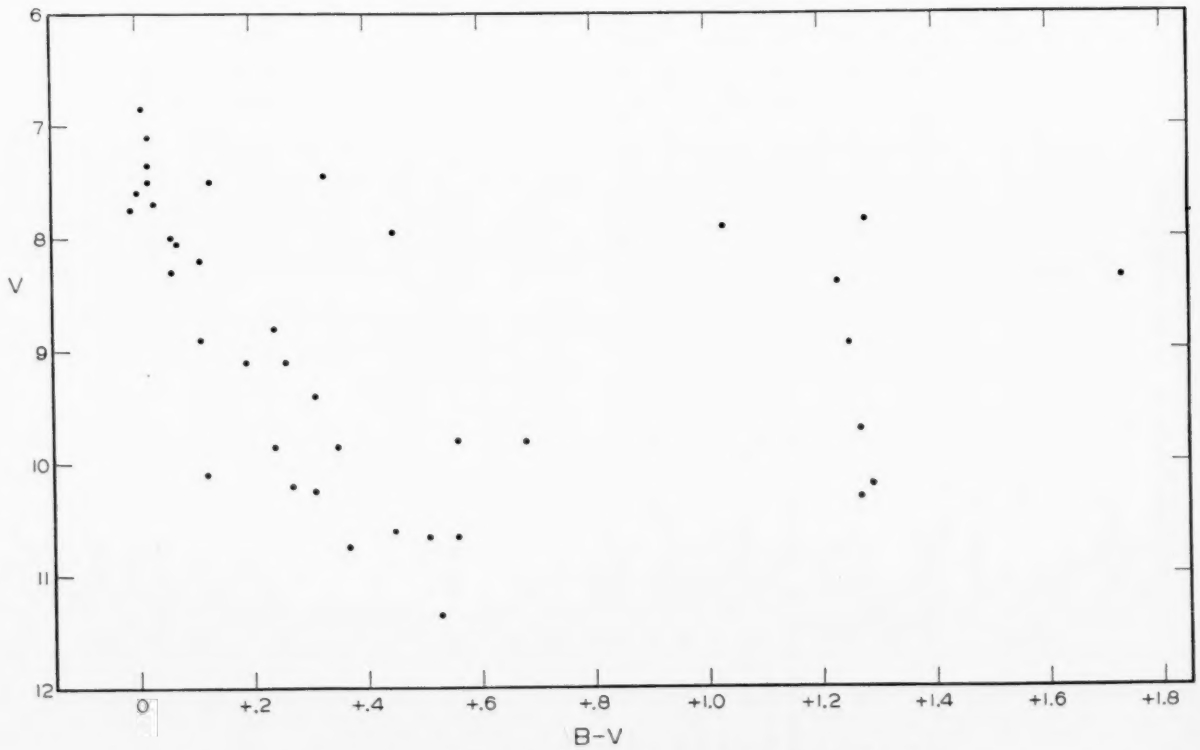

FIG. 1.—The color-magnitude diagram for the standard region near IC 4665

TABLE 2

PROBABLE ERRORS OF THE TIE-IN WITH THE FUNDAMENTAL SYSTEM

	V	$B-V$	$U-B$
p.e. (mag.)	±0.008	±0.004	±0.008

RELATIVE PROBABLE ERRORS WITHIN THE STANDARD REGION FOR ONE OBSERVATION

	V	$B-V$	$U-B$
p.e. (mag.)	±0.008	±0.008	±0.010

dening of galactic clusters containing B stars[1] gives +0.19 mag. for the cluster reddening. The true distance modulus of the cluster is about 8 mag.

The color-magnitude diagram for the standard region is shown in Figure 1. The magnitudes of the stars range from $V \cong 7$ to $V \cong 11$, and there are enough red stars of different magnitudes to permit determination of color equations that are independent of magnitude. It should be emphasized, however, that the stars in this standard region are not sufficient[1,4] for accurate transformations to the fundamental system, for which it is necessary to observe, in addition, a number of stars of the proper kinds selected from the list of near-by and bright stars.[1]

MAGNITUDES AND COLORS IN M34*

HAROLD L. JOHNSON†

Yerkes and McDonald Observatories

Received August 4, 1953

ABSTRACT

Three-color observations have been made on 42 members of the galactic cluster M34. At the same time, 15 nonmembers were also observed. The reddening of the cluster is +0.09 mag., and the true distance modulus is 8.6 mag., corresponding to a distance of 525 parsecs.

Three-color observations on the U, B, V system[1] have been made for 57 stars in the region of the galactic cluster M34. Of these 57 stars, 42 are classified by Brüggemann[2] from proper motions as members of the cluster. The observations were made in the same manner as that used for previous cluster observations.[1,3] The tie-in with the fundamental system was made on five different nights. The probable errors of this tie-in are given in Table 1*a;* the relative probable errors within the cluster, in Table 1*b*. The observations

TABLE 1*a*

PROBABLE ERRORS OF THE TIE-IN WITH THE FUNDAMENTAL SYSTEM

	V	$B-V$	$U-B$
p.e. (mag.)	±0.010	±0.005	±0.010

TABLE 1*b*

RELATIVE PROBABLE ERRORS WITHIN THE CLUSTER FOR ONE OBSERVATION

	V	$B-V$	$U-B$
p.e. (mag.)	±0.008	±0.005	±0.010

are listed in Table 2, in which the first column lists the numbers of the stars according to Brüggemann;[2] the second, third, and fourth, the observed magnitudes and colors; and the fifth, the number of independent observations on each star. The observations were made with the 82-inch telescope of the McDonald Observatory during the month of December, 1950.

Of the cluster stars that were observed, 15 are of spectral type earlier than A0. Table 3 lists these stars, with the values of Q, E_y, and S_Q.[4] The cluster is reddened by +0.09

* *Contributions from the McDonald Observatory, University of Texas*, No. 230.

† Now at Lowell Observatory, Flagstaff, Arizona.

[1] H. L. Johnson and W. W. Morgan, *Ap. J.*, **117**, 313, 1953.

[2] *Astr. Abh. der Hamburger-Bergedorf Sternwarte*, Vol. **4**, No. 7, 1935.

[3] H. L. Johnson, *Ap. J.*, **116**, 640, 1952.

[4] See Johnson and Morgan, *op. cit.*, for a definition of these three quantities.

TABLE 2

OBSERVATIONS

STAR	V	$B-V$	$U-B$	n	REMARKS
	Cluster Members				
37	9.64	+0.034	−0.18	2	BD+42°572
41	11.94	+ .47	+ .02	1	
42	10.93	+ .27	+ .10	1	BD+42°577
45+46	8.52	+ .03	− .06	1	BD+42°578 AB
51	10.51	+ .198	+ .11	2	BD+42°579
54	10.31	+ .134	+ .06	2	BD+42°580
58	10.16	+ .11	+ .07	1	BD+42°581
62	8.48	+ .051	− .04	3	BD+41°514
70	10.46	+ .164	+ .10	2	BD+42°583
74	10.46	+ .201	+ .10	3	BD+42°585
78	11.21	+ .350	+ .07	4	
80	12.20	+ .645	+ .08	3	
82	8.98	+ .001	− .19	3	BD+42°586
83	11.47	+ .36	+ .05	1	
90	8.52	+ .001	− .30	3	BD+42°588, ADS 2048 B
92	11.95	+ .469	+ .01	3	
93	8.46	+ .008	− .29	5	BD+42°589, ADS 2048 A
94	11.45	+ .351	+ .06	3	
96	9.72	+ .170	+ .08	4	BD+42°590
97	11.77	+ .278	+ .14	3	
99	9.89	+ .098	+ .05	3	BD+41°516
101	8.33	− .006	− .28	3	BD+42°591, ADS 2049 A
102	10.74	+ .276	+ .12	4	
105	11.18	+ .342	+ .08	3	BD+42°592
109	10.01	+ .115	+ .05	4	
111	9.93	+ .116	+ .06	4	BD+42°595
112	7.94	− .003	− .21	std	BD+42°598 AB, ADS 2052 AB
113	11.09	+ .398	+ .07	3	
114	8.80	+ .060	− .07	4	BD+42°596
116	10.45	+ .20	+ .18	1	BD+42°599
117	9.30	+ .053	− .08	3	BD+42°597
118	11.45	+ .38	+ .06	1	
123	8.85	+ .028	− .12	4	BD+42°601, ADS 2055
126	9.31	+ .049	− .06	4	BD+42°602
132	11.50	+ .360	+ .07	2	
137	11.45	+ .414	+ .11	2	
140	10.27	+ .136	+ .08	2	BD+42°605, ADS 2060 B
143	8.26	+ .010	− .25	4	BD+42°607, ADS 2060 A
150	10.28	+ .143	+ .07	2	BD+41°522
152	10.93	+ .156	+ .12	2	BD+42°609
165	9.56	+ .06	− .06	1	BD+42°612
171	8.89	−0.02	−0.22	1	BD+42°615
	Nonmembers				
39	9.45	+0.540	+0.06	2	BD+42°573
71	11.21	+1.088	+ .81	2	
89	11.13	+1.046	+ .75	4	
119	11.97	+0.677	+ .13	2	
124	10.96	+0.954	+ .53	3	
129	10.97	+1.012	+ .69	3	BD+41°519
134	7.33	+0.944	+ .63	std	BD+41°521
162	10.63	+0.531	+0.05	2	BD+42°611

mag. The apparent distance modulus, determined by fitting the cluster main sequence to the standard main sequence previously defined, is 8.9 mag. The true distance modulus, corrected for a ratio of total-to-selective absorption, $A_v/E_y = 3.0$, is 8.6 mag., corresponding to a distance of 525 parsecs. The color-absolute-magnitude diagram, corrected for interstellar reddening and absorption, is shown in Figure 1.

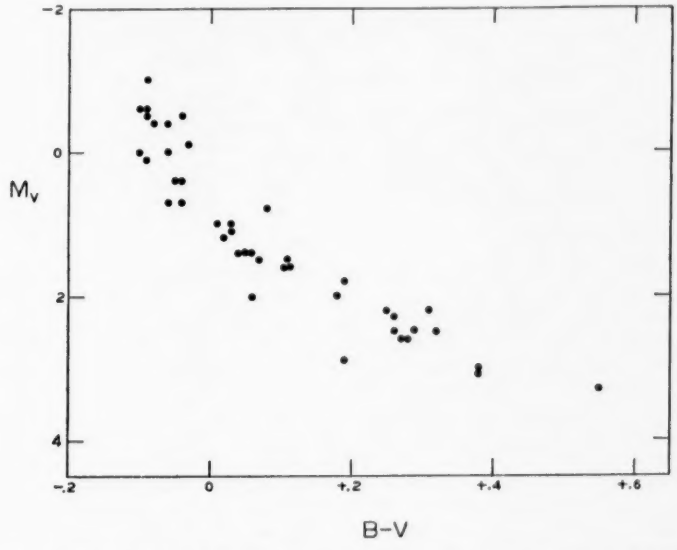

FIG. 1.—M_v versus $B - V$ for M34. The values have been corrected for interstellar absorption and reddening.

TABLE 3

DATA FOR STARS EARLIER THAN A0

Star	Q	E_y*	S_Q	Star	Q	E_y*	S_Q
37	−0.20	+0.11	B8	114	−0.11	+0.11	B9
45+46	− .08	+ .07	B9	117	− .12	+ .10	B9
62	− .08	+ .09	B9	123	− .14	+ .09	B9
82	− .19	+ .07	B8	126	− .10	+ .09	B9
90	− .30	+ .11	B7	143	− .26	+ .11	B8
93	− .30	+ .12	B7	165	− .10	+ .10	B9
101	− .29	+ .10	B8	171	−0.21	+0.06	B8
112	−0.21	+0.08	B8				

* $\overline{E_y} = +0.09$.

A STUDY OF THE GALACTIC CLUSTER NGC 2287*

ARTHUR N. COX
Goethe Link Observatory, Indiana University
Received June 22, 1953; revised July 27, 1953

ABSTRACT

Magnitudes and colors of 106 stars in the region of NGC 2287 (M41) have been observed with a photoelectric photometer mounted on the 24-inch Victoria telescope at the Royal Observatory, Cape of Good Hope. Spectral types and radial velocities for 22 cluster stars were found from low-dispersion spectra obtained at the McDonald Observatory. A proper-motion study was undertaken to eliminate some of the near-by field stars. The distance to the cluster based on the observed color-luminosity array and the interstellar reddening is 725 parsecs.

I. INTRODUCTION

This study was originally started to investigate fine structure in the color-luminosity array of the galactic cluster NGC 2287 (M41).[1] The existence of narrow sequences on the color-luminosity array which would have great interest in problems of stellar structure and evolution has already been investigated by Eggen[2] and by Johnson and Morgan[3] in the Pleiades cluster. Recent accurate photoelectric observations in the Coma Berenices cluster by Weaver[4] and in the Praesepe cluster by Johnson[5] have also been made to find fine structure in the main sequence of the color-luminosity array. The photoelectric results for NGC 2287 are supplemented with spectroscopic and proper-motion data.

Previous investigations of NGC 2287 are few. This cluster is listed by Raab,[6] Trumpler,[7] Shapley,[8] and Collinder,[9] and some data are given by all these authors. Star-position measures of a direct photograph are listed by Gould,[10] and a proper-motion study by Bhaskaran,[11] using the Gould and Hyderabad astrographic positions, is available.

The instrumentation used in the photometric aspects of this study has been previously described.[12] All the photometric data were obtained with a 1P21 photoelectric photometer mounted on the 24-inch Victoria refractor at the Royal Observatory, Cape of Good Hope. Spectra of twenty-two cluster stars were obtained by Dr. Frank K. Edmondson and Mr. Claude Knuckles, with the glass-prism Cassegrain spectrograph and the new Hiltner camera attached to the 82-inch McDonald reflector. This spectrograph gives a dispersion of about 110 A/mm at $H\gamma$.

Figure 1 shows a 20-minute 103*a*-O exposure of NGC 2287 taken with the Goethe Link 36-inch reflector diaphragmed to 24 inches. Figure 2 is a chart of the observed stars and their identifications. Only the stars that were observed are indicated; some close doubles could not be separated for photometric measures. The very close doubles, a, 1, 23, and 92, are shown single, and only the combined magnitude is known. No magnitudes or colors are available for stars 44 and 92.

* *Publications of the Goethe Link Observatory, Indiana University*, No. 12.

[1] $\alpha = 6^h44^m$; $\delta = -20°42'$ (1950.0); $l = 199°$; $b = -9°$.

[2] *Ap. J.*, **111**, 81, 1950.

[3] *Ap. J.*, **114**, 522, 1951.

[4] *Ap. J.*, **116**, 612, 1952.

[5] *Ap. J.*, **116**, 640, 1952.

[6] *Lund Medd.*, Ser. II, No. 28, 1922.

[7] *Lick Obs. Bull.*, **14**, 154, 1930 (No. 420).

[8] *Star Clusters* (New York: McGraw-Hill Book Co., 1930).

[9] *Lund Ann.*, Vol. **2**, 1931.

[10] *Córdoba Photographs* (Lynn, Mass.: Nichols Press, 1897).

[11] *M.N.*, **79**, 59, 1918.

[12] Cox, *Ap. J.*, **117**, 83, 1953.

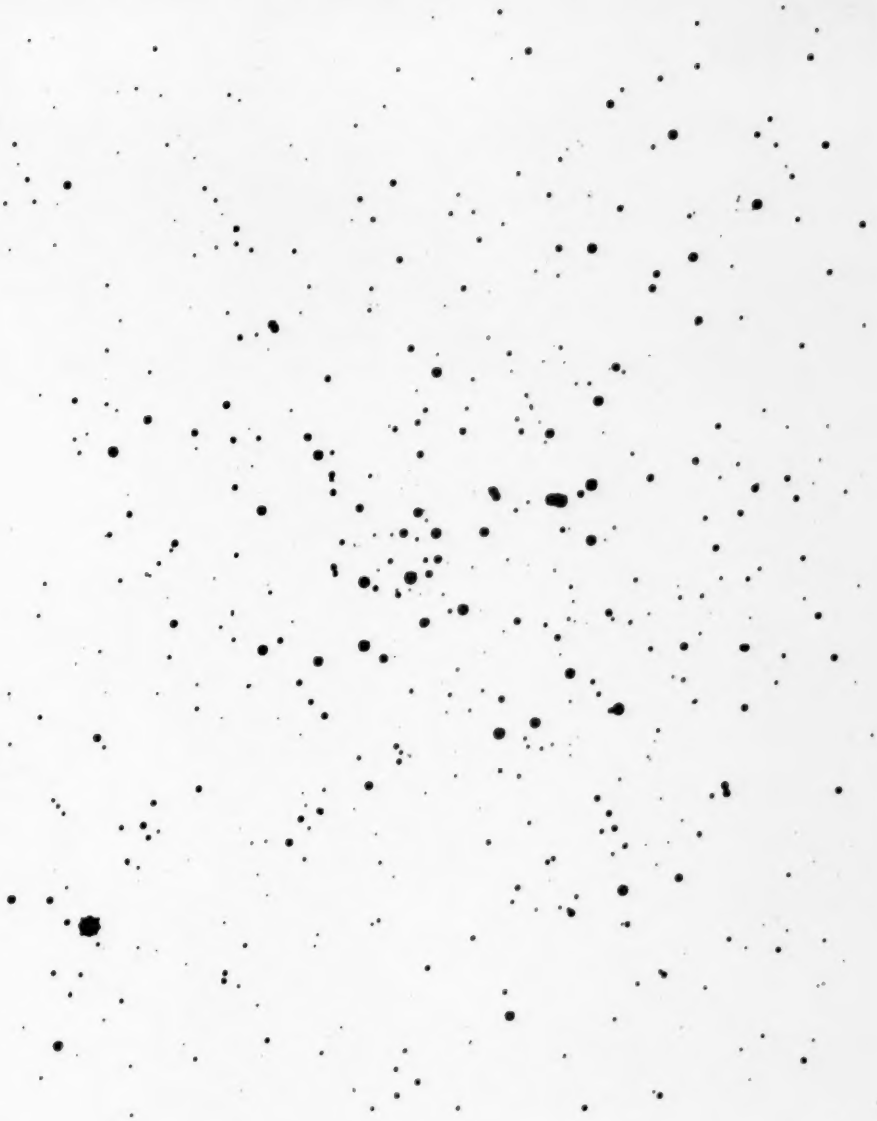

FIG. 1.—NGC 2287 photographed with 103*a*-O emulsion

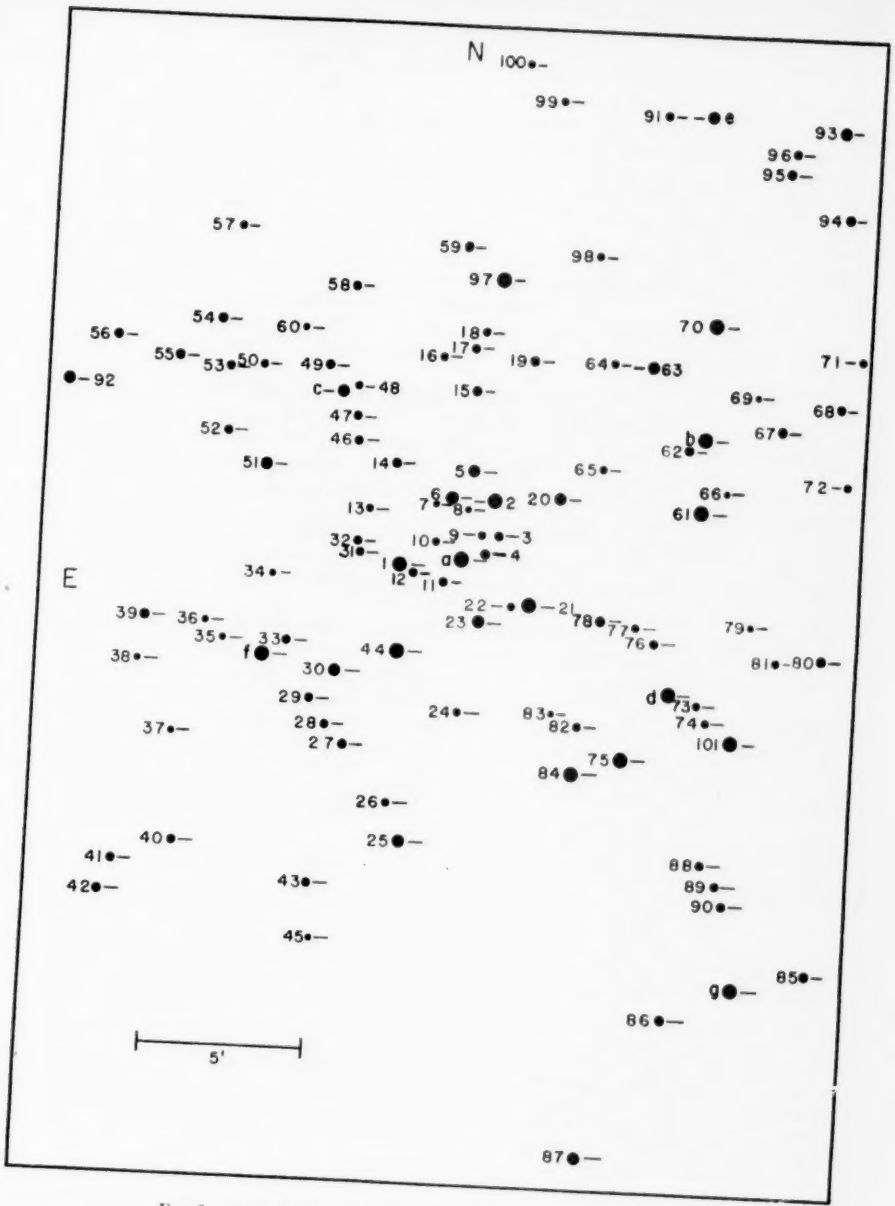

FIG. 2.—Identification chart for the stars observed in NGC 2287

II. PHOTOELECTRIC OBSERVATIONS

Two color photoelectric measurements were made of one hundred and six stars in the cluster and four standard stars in the neighboring Harvard Standard Region E3. All magnitudes were observed differentially with respect to the standards. The cluster stars with small letters for identification are standards within the cluster, and all the stars were compared to one or more of these standards. On four occasions the seven standards were repeatedly intercompared. Many other opportunities existed for comparison of some of these seven standards with one another. Star a is the primary standard in the cluster. Zero-point ties were made from stars a, b, c, d, and f to stars E3, E, H, L, and M. Each observation consisted of 2 measures with the yellow filter, 2 measures with the blue filter, and 1 measure of the near-by sky background in each color. One observation took less than 4 minutes to complete. A total of 501 observations were made within the cluster, and 45 more observations were made to compare the zero point with E3 on three different nights. Observations were made on eighteen nights from October, 1950, to January, 1951, inclusive.

Extinction corrections were applied differentially. The greatest zenith distance for all the observations was such that sec z equaled 1.39, and the average sec z was 1.09. If all the stars were the same color, then the differential extinction could be neglected, since it never amounted to more than 0.002 mag. However, a comparison of a blue star with a red star gives a relative blue magnitude which depends on the zenith distances of the two stars. With the wide-band blue filter a blue star is measured at a shorter effective wave length than the red star, and hence extinction is more effective for the blue star. The maximum value of this extinction due to a difference in color is 0.013 mag. for these observations. In only a few of the comparisons of a cluster star with a standard was it necessary to correct for the differential extinction.

Within the cluster the probable errors of a single observation for stars brighter than $\boldsymbol{V} = 11$ are ± 0.007 mag. for the $\boldsymbol{V}$ magnitudes and ± 0.005 mag. for the $(\boldsymbol{P} - \boldsymbol{V})$ color index. For stars fainter than $\boldsymbol{V} = 11$, the corresponding probable errors of a single observation are ± 0.013 and ± 0.012 mag. The three zero-point ties made to the four E3 stars show an internal probable error, as inferred from the residuals, of ± 0.010 mag. for both the yellow and the blue magnitudes. The three ties of the color zero point agreed exactly with one another; therefore, no probable error can be computed. A systematic error due to slight flexure of the optical system results in a correction of -0.01 mag. for all the cluster stars when directly compared to E3. The justification for this systematic flexure correction is given elsewhere.[12]

The raw blue and yellow magnitudes (B, Y) are related to the S' system as used by Cousins[12] as follows:

$$S'Pg = B + 0.05\,(B - Y), \qquad S'CI = 1.25\,(B - Y),$$

plus zero-point corrections. Using the previous tie of the S' system to the $(\boldsymbol{P}, \boldsymbol{V})$ system,[12] we find the direct conversion of the raw (B, Y) system to the $(\boldsymbol{P}, \boldsymbol{V})$ system to be

$$\boldsymbol{P} = B + 0.05\,(B - Y) + 4.18, \qquad (\boldsymbol{P} - \boldsymbol{V}) = 1.13\,(B - Y) - 0.14.$$

As in previous papers by the author, the (B, Y) magnitude system has its zero point set so that NPS 1 has zero magnitude and color. Table 1 lists $\boldsymbol{V}$, $(\boldsymbol{P} - \boldsymbol{V})$, and the number of observations of each star. Table 2 contains the magnitudes and colors of the E3 stars as determined and adopted previously.[12] A revision of these E3 standard magnitudes will imply the same revision of the cluster stars.

III. SPECTROSCOPIC OBSERVATIONS

At the McDonald Observatory Dr. Frank K. Edmondson and Mr. Claude Knuckles obtained 193 spectra of 22 cluster stars and thirty-three stars with known spectral types and radial velocities. The standard stars are listed in Table 3, and the spectral types

TABLE 1

MAGNITUDES AND COLORS OF STARS IN NGC 2287

Star	V	$P-V$	No. Obs.	Star	V	$P-V$	No. Obs.
a	7.30	+0.47	74	48	11.69	+1.08	3
b	8.42	−0.21	19	49	10.41	−0.04	3
c	9.19	−0.17	26	50	12.23	+0.16	3
d	9.10	−0.18	21	51	9.42	−0.21	3
e	9.36	−0.22	18	52	10.70	+0.98	3
f	7.79	+1.07	28	53	11.13	+0.41	3
g	8.83	−0.21	16	54	10.69	−0.14	3
1	8.50	−0.17	4	55	10.79	+0.04	3
2	8.96	−0.21	4	56	10.23	−0.21	3
3	10.31	−0.14	3	57	11.94	+0.12	3
4	10.79	−0.06	3	58	11.28	0.00	3
5	9.58	−0.16	3	59	11.04	+0.10	3
6	10.09	−0.18	3	60	12.86	+0.99	3
7	13.22	+0.49	3	61	9.00	−0.21	3
8	13.11	+0.31	3	62	11.01	−0.05	3
9	12.23	+0.27	3	63	9.64	−0.21	3
10	12.00	+0.19	3	64	11.52	+0.52	3
11	11.42	+0.18	3	65	12.67	+0.27	3
12	11.54	+0.13	3	66	12.41	+1.08	3
13	11.99	+0.21	3	67	10.78	−0.12	3
14	10.41	−0.11	3	68	11.11	+0.04	3
15	10.66	+0.14	3	69	12.53	+0.81	3
16	11.80	+0.19	3	70	9.17	−0.21	3
17	11.77	+0.06	3	71	12.01	+0.16	3
18	12.20	+0.28	3	72	12.49	+0.34	3
19	11.02	−0.06	3	73	10.83	+1.56	3
20	9.43	−0.17	3	74	12.44	+0.22	3
21	6.93	+1.46	3	75	7.46	+1.18	3
22	12.43	+0.19	2	76	11.22	−0.07	3
23	9.37	−0.16	2	77	11.80	+1.11	2
24	12.43	+0.31	3	78	10.67	+0.10	3
25	10.00	−0.17	4	79	12.61	+0.48	3
26	11.45	+1.35	4	80	10.29	−0.05	3
27	10.81	−0.05	3	81	12.43	+0.30	3
28	10.95	+0.97	3	82	11.06	−0.03	3
29	11.37	0.00	3	83	12.64	+0.79	3
30	9.31	−0.17	3	84	8.39	−0.21	3
31	11.70	+0.18	4	85	10.33	−0.15	3
32	11.61	+0.10	3	86	10.48	+0.05	3
33	11.55	+0.10	3	87	7.87	+1.30	3
34	12.91	+0.33	3	88	10.79	+0.64	3
35	12.84	+0.36	3	89	10.74	+0.82	3
36	12.42	+1.08	3	90	11.03	+0.42	3
37	12.78	+0.22	3	91	11.08	−0.04	3
38	12.88	+0.27	3	93	9.76	−0.18	3
39	10.42	−0.15	3	94	9.37	+1.08	3
40	11.09	+0.09	3	95	10.80	−0.08	3
41	11.80	+0.09	3	96	11.04	−0.03	3
42	10.86	+0.05	3	97	7.82	+1.08	3
43	11.20	−0.03	3	98	12.24	+0.22	3
45	12.01	+1.11	3	99	12.24	+0.21	3
46	10.01	+1.02	3	100	12.01	+0.81	3
47	11.32	−0.02	3	101	8.29	−0.16	3

listed are those of the revised Yerkes system.[13] All radial-velocity measures and reductions were made by the standard-table method described by R. H. Curtiss.[14] Moore's radial-velocity catalogue[15] was the source for the standard radial velocities.

The spectroscopic results are given in Table 4, together with the observed color index and the number of spectra for each cluster star. The spectral and luminosity classifications were made completely independent of the photoelectric results. For about half the cluster stars, only one spectrum was available, and the spectra were not always ideal

TABLE 2

ADOPTED MAGNITUDES AND COLORS OF E3 STARS

Star E3	V	$P-V$	Star E3	V	$P-V$
E	8.07	−0.26	L	9.02	+0.45
H	8.67	+0.13	M	8.60	+0.93

TABLE 3

STANDARD STARS FOR SPECTRAL TYPE AND RADIAL VELOCITY

Star	Spectral Type	Star	Spectral Type	Star	Spectral Type
16 Tau	B7 IV	β Leo	A3 V	δ Eri	K0 IV
α Leo	B7 V	λ Gem*	A3 V	σ Dra	K0 V
18 Tau	B8 V	ϵ Gem	G8 I*b*	HR 2334	K1 II
α Peg*	B9 V	56 Peg	G8 I*b*	56 Ori	K2 II
γ Gem*	A0 IV	56 UMa	G8 II	α Ari	K2 III
4 Aur*	A0 V	κ Gem	G8 III	ϵ Eri	K2 V
HR 3314	A0 V	ι Gem	G8 III	ι Aur	K3 II
HR 875	A1 V	o Tau*	G8 III	51 And	K3 III
HR 1046	A1 V	τ Cet	G8 V	δ And*	K3 III
θ And	A2 V	δ Aur	K0 III	β UMi	K4 III
θ Leo	A2 V	β Gem	K0 III	α Tau	K5 III

* Radial velocity variable. Not used for radial-velocity standard.

for accurate classification. Star 87, which is 18′ from the cluster center, may not be a cluster member because of its luminosity class. The radial velocities indicate that all twenty-two stars, except possibly stars d and e, are physical members of the cluster. For the K-type stars alone, the probable error of a single spectrum radial velocity is ± 4 km/sec, as inferred from the consistency of the radial velocities derived from each spectral line. The agreement from one spectrum to the next indicates a probable error of a single spectrum to be ± 7 km/sec. This latter probable error, which seems to be nearer to what one would expect at this dispersion, is used to compute the probable error of the final tabulated value. The B8- and B9-type stars show an internal consistency within each spectrum that gives the probable error of a single spectrum radial velocity as either ± 11 or ± 10 km/sec, depending on the number of spectral lines used in each spectrum. There are not enough duplicate spectra to determine the consistency of the radial veloci-

[13] Johnson and Morgan, *Ap. J.*, **117**, 313, 1953.

[14] *Ap. J.*, **20**, 149, 1904.

[15] *Pub. Lick Obs.*, Vol. **18**, 1932.

ties of the early-type star from plate to plate. For some of these early-type stars, only three lines in the spectrum could be measured, but the average number of lines measured in the K-star spectra was seven. Stars f and 75 show the 4150 anomaly which Miss Roman[16] has shown often appears in field stars of high velocity. Star 97 shows the effect more weakly, while all the other red giants seem about normal. The spectra of the early-type stars show that most of these stars have moderate rotation.

IV. PROPER-MOTION OBSERVATIONS

A 1-minute cluster exposure on 103*a*-D emulsion with a yellow filter was made with the Goethe Link 36-inch reflector diaphragmed to 24 inches. Measures of x and y on this plate were compared to the positions given by Gould[10] for sixty-two stars as faint as 11.4

TABLE 4

SPECTROSCOPIC DATA FOR NGC 2287

Star	Spectral Type	$P-V$	Radial Velocity (Km/Sec)	No. Spectra	Star	Spectral Type	$P-V$	Radial Velocity (Km/Sec)	No. Spectra
a	G–B9*	+0.47	(G)+36±6, (B9)−5±9	2	39	A0 V	−0.15	+37±9	2
					44	B8 V	.....	+26±10	1
b	B8 V	−0.21	+43±11:	1	51	B9 V	−0.21	+29±11	1
c	B9 V	−0.17	+34±11	1	56	Apec	−0.21	+55±10	1
d	B9 V	−0.18	+ 7±10	1	61	B8 V	−0.21	+35±10	1
e	B9 V	−0.22	+ 6± 9	2	75	K1 II–III	+1.18	+43±5	2
f	G8 II–III	+1.07	+26±5	2	84	B8 V	−0.21	+63±11	1
g	B8 V	−0.21	+58±11	1	87	K4 III	+1.30	+46±5	2
1	B9 V†	−0.17	+16±11	1	92	K0 II–III†	.....	+23±4	3
2	B8 V	−0.21	+22±9	2	97	K0 II–III	+1.08	+25±5	2
21	K3 II	+1.46	+45±3	5	101	B9 V	−0.16	+30±11	1
30	B9 V	−0.17	+54±10	1					

* Assumed spectroscopic binary.

† Combined light of visual double. The lines appear normal.

vis. mag. The two sets of measures are related by plate constants determined by least squares. Four stars were found to have improbably large residuals when the two series of measures were compared, and these four stars (53, 88, 92, and Hyderabad *Astrographic Catalogue* No. −20°15581) were assumed to be near-by proper-motion stars.

A second comparison was made with the *Astrographic Catalogue* positions in the Hyderabad zone. Seventy-five stars as faint as 12.7 vis. mag. were measured in common with this source. One more proper-motion star (64) was discovered in this comparison. Out of the total of five stars suspected to be near-by proper-motion stars, only three seem to be definitely established as such. One of the two stars discovered by Bhaskaran[11] and rediscovered in this work—Hyderabad *Astrographic Catalogue* No. −20°15581—shows different motions in the two determinations. Star 92 is a close double, and it is possible that only orbital motion is detected. The radial velocity of star 92 seems about right for cluster membership. The results of the proper-motion studies are given in Table 5. The centennial proper motions from the Gould comparison have a probable error of ±0".4, and the corresponding probable error for the *Astrographic Catalogue* comparison is ±0".7.

It is of interest to derive a proper motion of the cluster from published proper motions of cluster members. The *General Catalogue*[17] lists four stars (a, 21, 75, 97), and the Yale

[16] *Ap. J.*, **116**, 122, 1952.

[17] B. J. Boss, *General Catalogue of 33,342 Stars for the Epoch 1950* (Washington: Carnegie Institution of Washington, 1937).

Zone Catalogue[18] lists six (b, d, f, g, 97, 101). The centennial proper motion of the cluster stars from the *GC* data is $-2''.2 \pm 0''.4$ and $-1''.4 \pm 0''.4$ for right ascension and declination, respectively. The same values from the Yale proper motions are, respectively, $0''.0 \pm 0''.5$ and $+0''.7 \pm 0''.5$. To convert the Yale proper motions to the *GC* system, the Introduction to the Yale *Zone Catalogue* suggests corrections of $+0''.5$ and $0''.0$ to the above centennial proper motions in right ascension and declination, respectively. There seems to be a systematic difference between the proper motions as derived from these two sources; and it is not possible to say which is the more nearly correct result. The average of these centennial proper motions on the *GC* system is

$$100\ \mu_\alpha = -0''.8 \pm 0''.5; \qquad 100\ \mu_\delta = -0''.4 \pm 0''.5.$$

V. RESULTS

Standard normal colors as determined by Johnson and Morgan[13] are used to obtain a color excess for the stars in the cluster. For B8 V and B9 V stars the normal $(B - V)$ colors are, respectively, -0.09 and -0.06. Converting these normal colors to the $(P - V)$ system and comparing these normal colors with the colors of the cluster stars, we find

TABLE 5

CENTENNIAL PROPER MOTIONS OF STARS IN THE REGION OF NGC 2287

Star	Gould Comparison		Astrographic Comparison	
	$100\ \mu_\delta$	$100\ \mu_\delta$	$100\ \mu_\alpha$	$100\ \mu_\delta$
53	$+1''.5$	$-1''.5$	$+1''.1$	$-1''.1$
64	.....	.....	$+2.8$	-4.4
88	0.0	$+1.8$	$+0.3$	$+1.9$
92	$+0.7$	$+2.0$	$+0.6$	$+1.4$
$-20°15581$*	$+1.5$	-1.0	-1.4	-0.3

* Hyderabad *Astrographic Catalogue* number. This star is 17′ from the cluster center and for this reason may not be a cluster member.

the color excess of the cluster to be 0.06 mag. The color excess of the K giants is difficult to obtain, since unreddened colors are not available for stars in the Yerkes luminosity class II. Allowing for the fact that luminosity class II stars are intrinsically as much as 0.1 mag. redder than luminosity class III stars of the same spectral type, the color excess of the K giant stars is approximately 0.10 mag. The total absorption in visual light is then about 0.2 mag.

The distance modulus of the cluster is found by matching the main sequence of the color-luminosity array between the $(P - V)$ limits of -0.2 and $+0.3$ mag. to the standard main sequence according to Johnson and Morgan.[13] The distance modulus corrected for 0.2 mag. absorption is 9.3 ± 0.1, and the true distance is 725 parsecs. The corresponding linear diameter based on the angular diameter of 30′ is 6.3 parsecs. No stars more distant than 18′ from the cluster center were measured. Assuming that there are one hundred and fifty stars in the cluster, the mean star density is about 1.1 stars per cubic parsec.

The observed color-luminosity array is given in Figure 3. No definite fine structure is apparent. The scatter in the main sequence can be explained by double stars which are undiscovered and observed as single. The three crosses mark the positions of three double

[18] *Trans. Yale U. Obs.*, Vol. **13**, 1943.

stars (a, 1, 23) given in the Aitken double-star catalogue.[19] Star a at $(P - V) = +0.47$ can be explained by a combination of one of the late G giants with a B9 main-sequence star. The radial velocity derived from the G-star lines differs from the radial velocity from the hydrogen lines. This star is perhaps a spectroscopic binary; no light-variation has been detected. Seven small circles mark possible variable stars.

Within the area of the cluster, van Rhijn[20] predicts that there should be one field star brighter than $P = 10$ mag., four field stars brighter than $P = 11$, eleven stars brighter than $P = 12$, and twenty-nine stars brighter than $P = 13$. Thus all the twenty-two stars with $(P - V)$ greater than 0.4 and V greater than 9 could easily be field stars. These twenty-two stars include the three proper-motion stars which are not plotted in Figure 3.

The five red giants which are certainly cluster members have absolute magnitudes about -2. They are probably in the Yerkes luminosity class II, though the spectra do

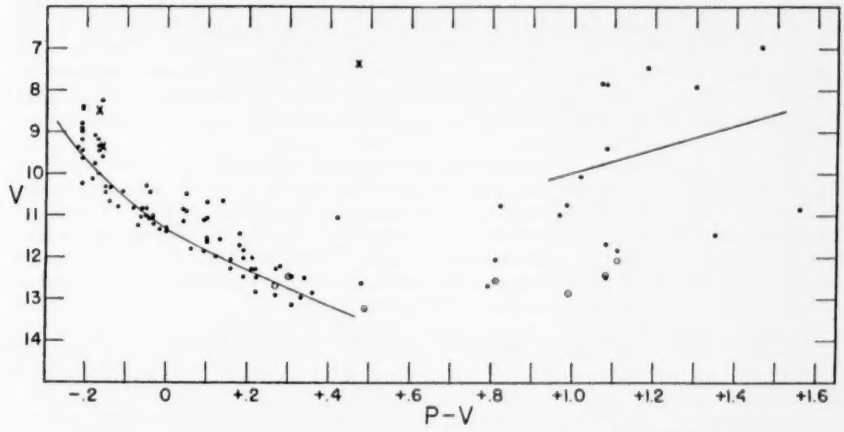

FIG. 3.—The color-luminosity array for NGC 2287 with the Johnson and Morgan main sequence and giant branch indicated. Known doubles are marked with crosses, and the open circles indicate possible variable stars. The standard Johnson and Morgan branches have been reddened by 0.06 mag. and adjusted for an apparent distance modulus of 9.5.

not definitely place four of them in this class. It is not possible to say whether the two red stars between apparent magnitudes 9 and 10 are members of the cluster or not. These two stars have the correct apparent visual magnitude to be classed as normal K giants if they are cluster members. Radial velocities and luminosity classifications of these two stars would decide their membership. There is a lack of blue main-sequence stars brighter than absolute magnitude -1. Star 56, with strong *Si* II and *Sr* II lines in its spectrum, has an absolute magnitude about $+0.7$, and the color is that of a B8 main-sequence star.

Figure 3 also shows the standard Johnson and Morgan branches. As is usually the case in galactic clusters, the earliest-type stars are too bright for their color and spectral type. The color excess of NGC 2287 is obtained, assuming that the B8 V and B9 V stars have normal intrinsic colors. A confirmation of the derived interstellar reddening, 0.06 mag., is found in the more poorly determined reddening of the K giants. The scatter about the Johnson and Morgan main sequence is about what is expected from observational errors, except for the possible double stars, which lie definitely above the main se-

[19] *New General Catalogue of Double Stars* (Washington: Carnegie Institution of Washington, 1932).

[20] *Gronigen Pub.*, Vol. **43**, 1929.

quence. Some of the stars near the fainter parts of the main sequence may possibly be field stars.

The average radial velocity of the cluster stars with respect to the sun is $+34 \pm 2$ km/sec. In this direction, almost at the solar antapex, the solar-motion component is $+20$ km/sec. Galactic rotation at a distance of 725 parsecs produces another component of $+14$ km/sec. The peculiar radial velocity of the cluster with respect to its local center of rest is then 0 ± 2 km/sec. Owing to the uncertainty of the proper-motion data, it is not possible to derive a reliable space motion of the cluster.

The individual radial-velocity determinations from each spectrum, the modern relative positions of the cluster stars, and the proper-motion data extracted from the *GC* and the Yale *Catalogue* are given in the author's Indiana University thesis.[21]

The results of this study show that the interstellar reddening of this cluster is 0.06 mag. and that the distance is 725 parsecs. The corresponding linear diameter is then about 6.3 parsecs. Attention should be called to the K giants in luminosity class II which usually do not occur in galactic clusters. A discussion of fine structure in the main sequence shows some evidence, but not confirmation, of the Eggen sequences drawn for the Pleiades cluster. The radial-velocity and proper-motion data indicate that only solar motion and galactic rotation contribute appreciably to the space motion of this cluster.

This work has been made possible by several grants from the Indiana University Graduate School. The hospitality of the Royal Observatory, Cape of Good Hope, and its director, Her Majesty's Astronomer at the Cape of Good Hope, Dr. R. H. Stoy, is gratefully acknowledged. Much of the discussion of the data was done while the author held a National Science Foundation Predoctoral Fellowship. Thanks are also due to Drs. John B. Irwin, James Cuffey, and Frank K. Edmondson for their help in some of the observations and in the discussion of the data.

[21] "A Study of the Galactic Cluster NGC 2287" (Ann Arbor: University Microfilms, 1953).

THE MASS OF THE GLOBULAR CLUSTER M92

O. C. Wilson and Mary F. Coffeen
Mount Wilson and Palomar Observatories
Carnegie Institution of Washington
California Institute of Technology
Received July 24, 1953

ABSTRACT

Radial-velocity measurements of 23 spectrograms of 15 red giant stars in M92 are discussed. A mass of 3.3×10^6 ⊙ is derived for the cluster, and the corresponding mass-to-luminosity ratio is 2.0 in solar units. It is probable that there are intrinsic velocity variations in some of the cluster stars.

The recent completion of the coudé spectrograph of the Hale telescope, particularly of the 8″.4-focus aplanatic-sphere camera,[1] offers the opportunity for a successful attack on observational problems hitherto beyond the range of existing equipment. One important problem of this type is that of the motions of stars within globular clusters. Is the radial-velocity distribution function the same all over a cluster, or are there systematic differences between the center and the outlying regions? The answer, if obtainable, has a direct bearing on the nature of the dynamical equilibrium of the system.[2]

With the intention of investigating the velocity distribution over the cluster, a number of spectrograms of red giants in M92 were obtained in 1952. Subsequently, exploratory work in other clusters has shown that M92 is the least suitable of the bright globular clusters for this purpose, because of the general weakness of the metallic lines in the spectra of its brighter members. It has been decided, therefore, to discontinue observing M92 and to pursue detailed studies in a more favorable system; and for this reason the material accumulated on M92 is presented here.

Measured radial velocities are in Table 1, where the symbol "B" indicates a star number from Barnard's list[3] and the other designations are co-ordinates measured from the axes used by Baum.[4] Columns headed V_w and V_c are radial-velocity measures by Wilson and Coffeen, respectively, which were obtained in the usual fashion by making settings on star and iron-arc lines with a standard measuring engine. After the measuring was completed, a careful study was made of the results, and a number of lines judged to be spurious were rejected. The wave lengths of a number of other lines were adjusted to remove systematic residuals, and the velocities given in Table 1 are the final values obtained with the adjusted wave lengths. Five of the spectrograms were taken by A. J. Deutsch and one by I. S. Bowen, and we are indebted to these colleagues for permission to utilize this material.

The velocity from a single plate depends in general upon measures of from 12 to 20 star lines; and the probable errors are satisfactorily small, considering the poor quality of the metallic lines and the narrowness of the spectra (about $\frac{1}{8}$ mm). The agreement between two measures of the same plate is also good in all but two or three instances; in fact, the average difference between the two measurers for 17 plates measured by both is only 3.5 km/sec. The situation is less favorable when the velocities from two plates of the same star are examined. Of the seven stars for which there are two plates well separated in time,[5] at least four—B 61, 74, 75, and 82—exhibit differences between the

[1] I. S. Bowen, *Ap. J.*, **116**, 1, 1952.
[2] See, e.g., G. L. Camm, *M.N.*, **112**, 155, 1952.
[3] *Pub. Yerkes Obs.*, Vol. 6.
[4] *A.J.*, **57**, 222, 1952.
[5] Plates 313–327 were taken in May, 1952; 406–414, in August.

two plates which are disconcertingly large. The reason for these differences cannot be exactly specified, but, for the present, one would be inclined to attribute them to intrinsic variations in the stars themselves. If this is so and if such variations prove to be a general characteristic of the red giants in globular clusters, it is clear that detailed studies of the internal motions in the clusters are going to be difficult and time-consuming.

The dependence of the mass of a cluster upon the internal motions can be found if the potential function is known. R. Kurth[6] has derived an approximate expression based upon a hypothetical division of the total mass between a point at the center and a surrounding sphere of uniform density. His equation, adequate for our purpose, is

$$M = 800\overline{(\Delta V)^2}r\ , \qquad (1)$$

where ΔV is the deviation of radial velocity of a star from the cluster velocity in kilometers per second and r is the cluster radius in parsecs. For M92, Shapley gives the radius as 21 psc.[7] The other quantity in equation (1), $\overline{(\Delta V)^2}$, is to be derived from the measured

TABLE 1

RADIAL VELOCITIES OF STARS IN M92

(Km/Sec)

Star	x	y	Plate (Pe)	V_w	V_c	Plate (Pe)	V_w	V_c
B 39	.....	.....	.....	.....	.....	421	−128.2±2.7	−121.0±2.1
43	.....	.....	.....	.....	.....	417	−123.4±2.5	−119.2±1.6
54	.....	.....	.....	.....	.....	420	−128.2±2.2	−128.9±2.6
61	.....	.....	322	−116.7±2.2	−115.6±1.3	410	−127.4±2.0	−123.0±1.6
62	.....	.....	327	−113.7±2.5	−118.3±1.7	413	−112.9±2.2	−121.5±1.8
74	.....	.....	319	−116.2±1.9	−117.6±1.7	409	−120.0±1.9	−123.8±2.0
75	.....	.....	325	−124.2±2.1	−126.9±2.1	414	−113.3±2.3	−115.4±1.9
82	.....	.....	315	−113.1±1.6	−112.6±2.1	408	−117.2±2.7	−118.9±2.4
85	.....	.....	314	−117.5±3.4	−114.3±2.4	407	−116.2±1.7	−118.9±2.6
88	.....	.....	313	−128.8±2.3	−129.7±2.0	406	−131.1±1.6	−141.5±2.2
III-13	+2′.65	+4′.61	914	−117.5±2.5	.....	929	−111.6±1.1	.....
III-65	+1′.27	+2′.54	.....	.....	.....	928	−124.3±2.0	.....
VII-18	−5′.35	−1′.91	.....	.....	.....	297	−122.7±0.9	.....
X-49	+1′.01	−2′.49	.....	.....	.....	927	−135.8±2.5	.....
XII-34	+2′.60	−0′.53	.....	.....	.....	917	−112.6±1.6	.....

radial velocities, with proper correction for scatter not due to real velocity differences between stars.

The data of Table 1 were treated as follows: For plates measured by both of us, the mean of the two measures was formed, and the values of ΔV were obtained by taking the differences of these means from the general mean of all the measures, −121.0 km/sec. Where only one measure was available, the corresponding ΔV followed directly, and no differences in weight were applied, whether a ΔV depended upon one or upon two measures. The measured mean-square deviation $\overline{(\Delta V)^2_m}$ obtained in this fashion is 45.7 (km/sec)^2.

A value, or rather estimate, of the deviation due to other causes than real differences in velocity between stars can be had only from those stars for which there are two plates. The differences between the mean velocities for the two plates have been taken for each star, and the mean of these quantities, without regard to sign, is considered to be a mean deviation (M.D.) between epochs. Table 1 yields M.D. = 5.8 km/sec. Multiplication of

[6] *Zs. f. Ap.*, **29**, 26, 1951.

[7] *Pop. Astr.*, **57**, 203, 1949.

the M.D. by 1.25 then gives $\sigma_e^2 = 52.5$ (km/sec)^2 for the standard deviation between epochs.

The true mean-square deviation $\overline{(\Delta V)^2_T}$ should be related to the other quantities mentioned above through the expression

$$\overline{(\Delta V)^2_T} = \overline{(\Delta V)^2_M} - \sigma^2 , \tag{2}$$

where the standard deviation σ is measured from the mean velocity for each star, which is, however, unknown.

Consider the two plates on a given star taken at two epochs, and let the measured velocities be V_1 and V_2 and the deviation from the true mean velocity for the star be ϵ_1 and ϵ_2. Then, if V_T is the true mean velocity for the star,

$$V_T = V_1 + \epsilon_1 = V_2 + \epsilon_2 .$$

Also

$$V_1 - V_2 = \Delta V = \epsilon_2 - \epsilon_1 .$$

Since there is no relationship between ϵ_1 and ϵ_2, it follows that

$$\overline{(\Delta V)^2_M} = \overline{\epsilon_2^2} + \overline{\epsilon_1^2} = 2\sigma^2 .$$

In other words, the value of σ^2 to be used in equation (2) should be half of σ_e^2, or 26.2 (km/sec)^2. Hence, from equation (2) one finds $\overline{(\Delta V)^2_T} = 19.5$ (km/sec)^2, and then, from equation (1),

$$M = 3.3 \times 10^5 \odot .$$

From Christie's[8] apparent photographic magnitude of the cluster and a modulus of 15.12, it follows that $M_{pg} = -7.82$. Taking the absolute photographic magnitude of the sun[9] to be $+5.26$, one finds, for M92, in solar units

$$\frac{M}{L} = 2.0 .$$

It does not appear feasible to estimate the order of accuracy of these results. Kurth's equation is an approximation which can be improved only by greater knowledge of the true potential function for the cluster. Also, our determination of σ is based on less extensive material than is desirable. Nevertheless, it is perhaps not unreasonable to expect that the foregoing values are not in error by more than factors of the order of 2 or 3.

We are greatly indebted to Dr. G. Strömberg for helpful discussion of the method of treating the data.

[8] *Ap. J.*, **91**, 8, 1940.

[9] G. P. Kuiper, *Ap. J.*, **88**, 429, 1938.

A STUDY OF THE ORION AGGREGATE OF EARLY-TYPE STARS. II*

STEWART SHARPLESS†
Yerkes and McDonald Observatories
Received June 30, 1953

ABSTRACT

Ultraviolet photoelectric colors of 184 members of the Orion aggregate are given, and spectral types are derived from the photometric data.

In Paper I photoelectric colors and magnitudes of a number of early-type stars in Orion were discussed.[1] These were obtained at the McDonald Observatory during November and December, 1951, with the 13 and 82-inch telescopes. Ultraviolet measures were obtained for these stars at the same time, and the results are given here.

The method of reducing the ultraviolet observations was similar to that described earlier,[1] with the exception that the ultraviolet color extinction coefficients were assumed to have no color dependence. A zero-point difference of 0.018 mag. in the color was found to exist between observations made with the two telescopes, and that correction was applied to the 82-inch observations. The observed color, C_u, was related to the $U-B$ system[2] by means of the transformation

$$U-B = E + FC_u .$$

From one to five observations of each of thirty-six of the standard stars of Johnson and Morgan[2] were obtained. From a least-squares solution it was found that $E = -0.683 \pm 0.003$ and $F = +0.964 \pm 0.003$.

The observed colors, C_u, and the values of $U-B$ computed from the above coefficients for the standard stars, as well as the values given by Johnson and Morgan, are listed in Table 1. A comparison of the two sets of values is shown in Figure 1. The internal probable error of C_u was computed on the basis of those Orion stars which were observed two or more times. The probable error of one observation of C_u was found to be ± 0.009 mag.

It has been shown by Johnson and Morgan[2] that a function, Q, of the colors $U-B$ and $B-V$ can be defined which is independent of interstellar reddening, where

$$Q = (U-B) - 0.72(B-V) .$$

They have shown that Q is related to spectral type for stars between B0 and A0 and that the color excesses of stars in this spectral range can be obtained from the expression

$$E_y(Q) = (B-V) - 0.337Q + 0.009 .$$

The coefficient, 0.72, in the first expression is confirmed, within the observational errors, by the colors of the Orion stars given here and in Paper I. This coefficient is the mean ratio of the ultraviolet and yellow color excesses. It is therefore evident that within the range of wave length covered by the two colors the curvature of the relation

* *Contributions from the McDonald Observatory, University of Texas*, No. 231.

† Now at the U.S. Naval Observatory.

[1] *Ap. J.*, **116**, 251, 1952.

[2] H. L. Johnson and W. W. Morgan, *Ap. J.*, **117**, 313, 1953.

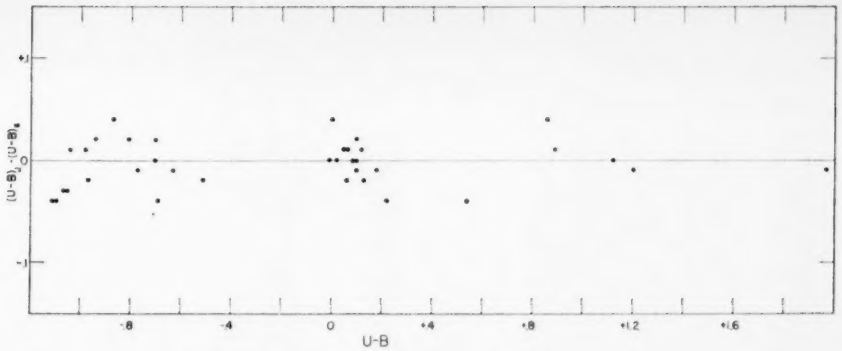

FIG. 1.—A comparison between the colors of standard stars obtained by Johnson and those obtained by the author.

TABLE 1

ULTRAVIOLET COLORS OF STANDARD STARS

STAR	SP.	$\overline{C_u}$	$U-B$		No.
			Johnson and Morgan	Sharpless	
β Cas	F2 IV	+0.798	+0.09	+0.09	2
50 And	F8 IV–V	+0.759	+0.06	+0.05	5
HR 483	G2 V	+0.823	+0.12	+0.11	5
β Ari	A5 V	+0.788	+0.10	+0.08	5
α Ari	K2 III	+1.865	+1.12	+1.12	18
δ Tri	G0 V	+0.729	+0.02	+0.02	3
16 Per	F2 III	+0.788	+0.06	+0.08	2
HR 875	A1 V	+0.745	+0.05	+0.04	18
ι Per	G0 V	+0.822	+0.10	+0.11	5
κ Cet	G5 V	+0.908	+0.18	+0.19	4
ϵ Eri	K2 V	+1.326	+0.54	+0.60	4
ζ Per	B1 Ib	−0.081	−0.77	−0.76	4
ϵ Per	B0.5 V	−0.319	−0.98	−0.99	4
π^3 Ori	F6 V	+0.670	0.00	−0.04	22
π^4 Ori	B2 III	−0.155	−0.81	−0.83	20
β Eri	A3 III	+0.800	+0.09	+0.09	2
β Ori	B8 Ia	+0.037	−0.69	−0.65	1
τ Ori	B5 III	+0.204	−0.51	−0.49	2
HD 35299	B1 V	−0.237	−0.87	−0.91	2
HD 35899	B5 V	+0.063	−0.63	−0.62	2
HD 36591	B1 V	−0.277	−0.97	−0.95	2
Cin 705	M1 V	+1.962	+1.20	+1.21	18
υ Ori	B0 V	−0.403	−1.11	−1.07	18
α Lep	F0 Ib	+0.975	+0.22	+0.26	1
ι Ori	O9 III	−0.406	−1.11	−1.07	2
ϵ Ori	B0 Ia	−0.361	−1.06	−1.03	1
κ Ori	B0.5 Ia	−0.358	−1.06	−1.03	1
δ Aur	K0 III	+1.564	+0.86	+0.82	2
χ^2 Ori	B2 Ia	−0.014	−0.70	−0.70	1
ι CMa	B3 II	−0.038	−0.70	−0.72	2
β Cnc	K4 III	+2.560	+1.77	+1.78	15
η Hya	B3 V	−0.082	−0.74	−0.76	13
10 Lac	O9 V	−0.382	−1.04	−1.05	20
HR 8832	K3 V	+1.620	+0.89	+0.88	20
υ Peg	F8 IV	+0.862	+0.13	+0.15	1
ι Psc	F8 V	+0.695	−0.01	−0.01	2

TABLE 2

OBSERVATIONS OF STARS IN THE ORION AGGREGATE

Star	$U-B$	ϵ	Q	Sp_Q	$E_{B-V}(Q)$	Star	$U-B$	ϵ	Q	Sp_Q	$E_{B-V}(Q)$
30836[a]	−0.83	2	−0.71	B2	+0.08	36487	−0.54	9	−0.46	B5	+0.05
31237[b]	−0.84	5	−0.70	B2	+0.05	36512[i]	−1.07	2	−0.88	O–B0	+0.04
−3°1013	+0.03	6	−0.14	B9	+0.30	36513	−0.11	9	−0.13	B9	+0.08
33647	−0.36	6	−0.32	B7	+0.07	36527	+0.10	9	0.00	A0	+0.15
34179	−0.47	6	−0.45	B5	+0.13	36540	−0.49	9	−0.52	B3	+0.23
34317	−0.01	6	+0.01	A0	−0.01	36541	−0.45	9	−0.39	B7	+0.06
34511	−0.69	6	−0.62	B3	+0.12	36559	−0.22	3	−0.19	B8	+0.02
34748	−0.78	6	−0.70	B2	+0.15	36560	−0.41	9	−0.34	B7	+0.03
34959	−0.53	6	−0.45	B5	+0.05	36591	−0.95	6	−0.81	B1	+0.09
34989	−0.90	6	−0.80	B1	+0.15	36607	−0.16	9	−0.13	B9	+0.01
35007	−0.67	6	−0.59	B3	+0.09	36627	−0.54	6	−0.47	B5	+0.06
35008	−0.32	9	−0.23	B8	−0.02	36629	−0.68	9	−0.69	B2	+0.26
35039[e]	−0.82	6	−0.71	B2	+0.09	36655	−0.27	3	−0.24	B8	+0.05
35079	−0.53	6	−0.51	B5	+0.15	36670	−0.05	9	−0.04	A0	+0.01
35203	−0.50	9	−0.43	B5	+0.06	36695[j]	−0.92	6	−0.80	B1	+0.11
35298	−0.59	6	−0.49	B5	+0.03	36697	−0.04	9	−0.08	B9	+0.10
35299	−0.91	6	−0.75	B1	+0.04	36741	−0.79	6	−0.65	B2	+0.03
35407	−0.64	6	−0.53	B3	+0.03	36779	−0.81	6	−0.68	B2	+0.05
35411[d]	−0.93	6	−0.79	B1	+0.09	36783	−0.11	9	−0.12	B9	+0.06
35439[e]	−0.92	6	−0.77	B1	+0.06	−3°1140	+0.11	9	−0.07	B9	+0.29
35501	−0.40	6	−0.36	B7	+0.07	36824	−0.72	6	−0.61	B3	+0.07
35502	−0.54	6	−0.52	B3	+0.15	36842	−0.51	9	−0.43	B5	+0.04
35575	−0.73	6	−0.61	B3	+0.05	36865	−0.43	9	−0.38	B7	+0.07
35588	−0.77	6	−0.64	B2	+0.05	36867	−0.16	9	−0.15	B9	+0.04
35640	−0.23	3	−0.20	B8	+0.03	36883	−0.47	9	−0.41	B5	+0.07
35673	−0.23	6	−0.23	B8	+0.09	36898	−0.43	6	−0.37	B7	+0.06
35715[f]	−0.94	6	−0.77	B1	+0.04	36899	−0.02	9	−0.06	B9	+0.08
35718	+0.01	6	−0.02	A0	+0.04	36916	−0.58	9	−0.50	B5	+0.08
35730	−0.69	6	−0.58	B3	+0.05	36917	+0.03	6	−0.09	B9	+0.20
35762	−0.73	6	−0.60	B3	+0.03	36936	−0.58	9	−0.50	B5	+0.07
35777	−0.75	6	−0.62	B3	+0.04	36938	−0.20	9	−0.25	B8	+0.16
35792	−0.64	6	−0.53	B3	+0.05	36939	−0.28	9	−0.29	B8	+0.12
35834	−0.37	6	−0.33	B7	+0.07	36954	−0.66	6	−0.60	B3	+0.12
35881	−0.50	6	−0.43	B5	+0.06	36957	−0.05	9	−0.08	B9	+0.09
35882	−0.48	9	−0.43	B5	+0.09	36958	−0.61	9	−0.56	B3	+0.13
35899	−0.62	6	−0.52	B3	+0.04	36959	−0.93	9	−0.77	B1	+0.05
35901	−0.14	9	−0.13	B9	+0.03	36960	−1.04	6	−0.86	B1	+0.05
35910	−0.55	6	−0.48	B5	+0.07	36981	−0.59	6	−0.52	B3	+0.08
35912	−0.75	6	−0.62	B3	+0.04	−3°1143	+0.04	9	−0.08	B9	+0.21
36012	−0.65	6	−0.58	B3	+0.10	36982	−0.62	9	−0.70	B2	+0.37
36013	−0.65	6	−0.56	B3	+0.07	36983	−0.20	9	−0.20	B8	+0.08
36120	−0.36	6	−0.34	B7	+0.09	36998	−0.21	9	−0.21	B8	+0.08
36133	−0.60	9	−0.54	B3	+0.10	36999	−0.45	6	−0.39	B7	+0.05
36151	−0.57	9	−0.48	B5	+0.04	37000	−0.67	6	−0.58	B3	+0.08
36166	−0.86	6	−0.71	B2	+0.05	37001	−0.27	9	−0.23	B8	+0.03
36219	−0.35	6	−0.31	B7	+0.05	37016	−0.69	9	−0.57	B3	+0.03
36234	−0.39	6	−0.34	B7	+0.05	37017	−0.79	9	−0.69	B2	+0.10
36285	−0.86	9	−0.74	B2	+0.09	37018[k]	−0.94	6	−0.80	B1	+0.08
36324	+0.05	9	−0.01	A0	+0.09	−4°1181	−0.43	9	−0.66	B2	+0.55
36351[g]	−0.84	6	−0.71	B2	+0.07	37019	−0.03	9	−0.06	A0	+0.07
−3°1119	+0.13	9	−0.02	A0	+0.23	37020[l]	−0.92	9	−0.96	O–B0	+0.39
36366	−0.02	9	−0.11	B9	+0.17	37021[m]	−0.49	9	−0.66	B2	+0.47
36392	−0.67	6	−0.57	B3	+0.06	37022[n]	−0.97	5	−1.01	O–B0	+0.41
36411	+0.05	9	−0.02	A0	+0.12	37023[o]	−0.64	5	−0.92	O–B0	+0.43
36429	−0.64	6	−0.54	B3	+0.06	37025	−0.63	6	−0.55	B3	+0.07
36430	−0.77	9	−0.66	B2	+0.08	37040	−0.71	9	−0.61	B3	+0.08
36486[h]	−1.07	6	−0.92	O–B0	+0.11	Bond 669	−0.35	9	−0.53	B3	+0.44

[a] π^4 Ori.
[b] π^5 Ori (var.).
[c] 22 Ori.
[d] η Ori.
[e] 25 Ori.
[f] ψ Ori.
[g] 33 Ori.
[h] δ Ori (var.).
[i] ν Ori.
[j] VV Ori (var.).
[k] 42 Ori.
[l] θ'(A) Ori = Bond 619.
[m] θ'(B) Ori = Bond 624.
[n] θ'(C) Ori = Bond 628.
[o] θ'(D) Ori = Bond 640.

TABLE 2—*Continued*

Star	$U-B$	ϵ	Q	S_Q	$E_y(Q)$	Star	$U-B$	ϵ	Q	S_Q	$E_y(Q)$
37041[p]	−0.94	9	−0.91	O–B0	+0.27	37397	−0.75	6	−0.64	B2	+0.08
37042	−0.93	9	−0.90	O–B0	+0.26	37411	+0.11	9	0.00	A0	+0.17
37043[q]	−1.07	6	−0.90	O–B0	+0.06	37428	−0.23	9	−0.34	B7	+0.27
37055	−0.63	9	−0.54	B3	+0.07	37468[s]	−1.05	9	−0.88	O–B0	+0.07
37056	−0.37	6	−0.32	B7	+0.06	−6°1273	−0.05	9	−0.27	B8	+0.41
37057	−0.14	9	−0.15	B9	+0.08	37469	0.00	9	−0.16	B9	+0.28
37058	−0.74	6	−0.62	B3	+0.06	37470	−0.27	9	−0.32	B7	+0.18
37059	−0.24	9	−0.22	B8	+0.06	37480	−0.06	9	−0.07	B9	+0.04
37060	−0.07	9	−0.09	B9	+0.06	37481	−0.92	3	−0.76	B1	+0.04
37061	−0.64	9	−0.85	B1	+0.59	37490	−0.84	6	−0.80	B1	+0.22
37062	−0.47	9	−0.51	B5	+0.23	37526	−0.56	3	−0.47	B5	+0.05
−5°1328	+0.02	9	−0.04	A0	+0.11	37547	−0.10	9	−0.10	B9	+0.04
37114	−0.12	9	−0.09	B9	0.00	37606	−0.34	6	−0.29	B8	+0.04
37115	−0.57	6	−0.52	B3	+0.12	37641	−0.39	9	−0.35	B7	+0.08
37128[r]	−1.03	9	−0.90	O–B0	+0.13	37663	−0.09	9	−0.08	B9	+0.02
37129	−0.73	9	−0.63	B3	+0.08	37700	−0.48	6	−0.41	B5	+0.06
37130	−0.11	9	−0.23	B8	+0.25	37742[t]	−1.05	6	−0.90	O–B0	+0.10
37150	−0.82	6	−0.69	B2	+0.05	37744	−0.91	6	−0.75	B1	+0.03
37151	−0.40	9	−0.34	B7	+0.04	37745	−0.07	9	−0.08	B9	+0.06
37174	−0.14	9	−0.11	B9	+0.02	37756	−0.85	6	−0.70	B2	+0.03
37187	−0.25	6	−0.24	B8	+0.08	37776	−0.86	6	−0.76	B1	+0.13
−3°1154	−0.09	9	−0.11	B9	+0.07	37807	−0.65	9	−0.58	B3	+0.11
37209	−0.93	9	−0.76	B1	+0.04	37887	−0.11	6	−0.10	B9	+0.03
37210	−0.41	9	−0.36	B7	+0.06	37888	−0.05	9	−0.08	B9	+0.09
37232	−0.85	6	−0.73	B2	+0.08	37903	−0.63	9	−0.70	B2	+0.34
37273	+0.04	9	−0.08	B9	+0.20	38051	−0.31	9	−0.58	B3	+0.58
37303	−0.96	9	−0.81	B1	+0.08	38088	+0.05	9	−0.07	B9	+0.19
37321	−0.55	6	−0.49	B5	+0.09	38120	−0.06	9	−0.09	B9	+0.08
37322	+0.01	9	−0.04	A0	+0.09	38239	+0.01	9	−0.03	A0	+0.08
37330	−0.56	6	−0.53	B3	+0.14	38563A[u]	−0.03	5	−0.48	B5	+0.79
37334	−0.77	9	−0.64	B2	+0.06	38563B[v]	+0.36	5	−0.53	B3	+1.42
37342	−0.55	5	−0.46	B5	+0.04	38755	−0.52	6	−0.44	B5	+0.05
37357	+0.01	9	−0.08	B9	+0.16	38771[w]	−1.03	9	−0.92	O–B0	+0.16
37373	−0.41	9	−0.35	B7	+0.04	39291[x]	−0.87	6	−0.73	B2	+0.07
37390	−0.09	9	−0.21	B8	+0.25	39777	−0.82	6	−0.68	B2	+0.05

[p] θ^2 Ori. [q] ϵ Ori. [r] ϵ Ori. [s] σ Ori.
[t] ζ Ori. [u] M78 (A). [v] M78 (B). [w] κ Ori.
[x] 55 Ori.

between interstellar absorption and wave length for the Orion stars does not differ appreciably from that for stars in general. It has been shown,[1] however, that the total amount of absorption in this spectral region is somewhat greater in the case of the Orion stars than for other stars of equal reddening.

Spectral types based on the colors alone can now be obtained by means of the values of $U-B$ given here, the values of $B-V$ in Paper I, and the calibration of Q with respect to spectral type given by Johnson and Morgan. The results are listed in Table 2, the columns of which contain (1) the star designation from the *Henry Draper* or *BD* catalogue; (2) the observed value of $U-B$; (3) a quantity ϵ such that the probable error of $U-B$ is $\pm 0^m001\epsilon$; (4) the value of Q computed from $U-B$ and $B-V$; (5) the spectral type, S_Q, corresponding to Q; and (6) the color excess, $E_y(Q)$, computed from the relation given above.

From a comparison of the spectral types in Paper I obtained from slit spectrograms and those obtained here from the colors, it is estimated that the probable error of either set of classifications is less than half a spectral subclass. The classifications in Paper I which were obtained from objective-prism spectra have been improved considerably by the new data.

An H-R diagram for the Orion stars based entirely on photoelectric observations can now be constructed. In Figure 2 Q is plotted against the corrected apparent visual magnitude, V_0, that is, V, corrected for interstellar absorption by $6E_y(Q)$[1]. This can be compared with Figures 5 and 6 of Paper I, where the H-R diagram is plotted from spectroscopic data. The essential features of the original H-R diagram are preserved here, and the resulting distance modulus of the Orion aggregate is the same in both cases, i.e., $m_0 - M = 8.5$. Two stars, θ^1(A) and θ^1(C) Orionis, have values of Q less than -0.92. These are omitted from Figure 2 because of the insensitivity of Q to intrinsic color in this range.

The main sequence later than B1 appears sharply limited on the lower side, with a scattering of somewhat higher luminosity stars (luminosity class IV) above it. Some of the latter may be field stars not physically associated with the aggregate. The spectral

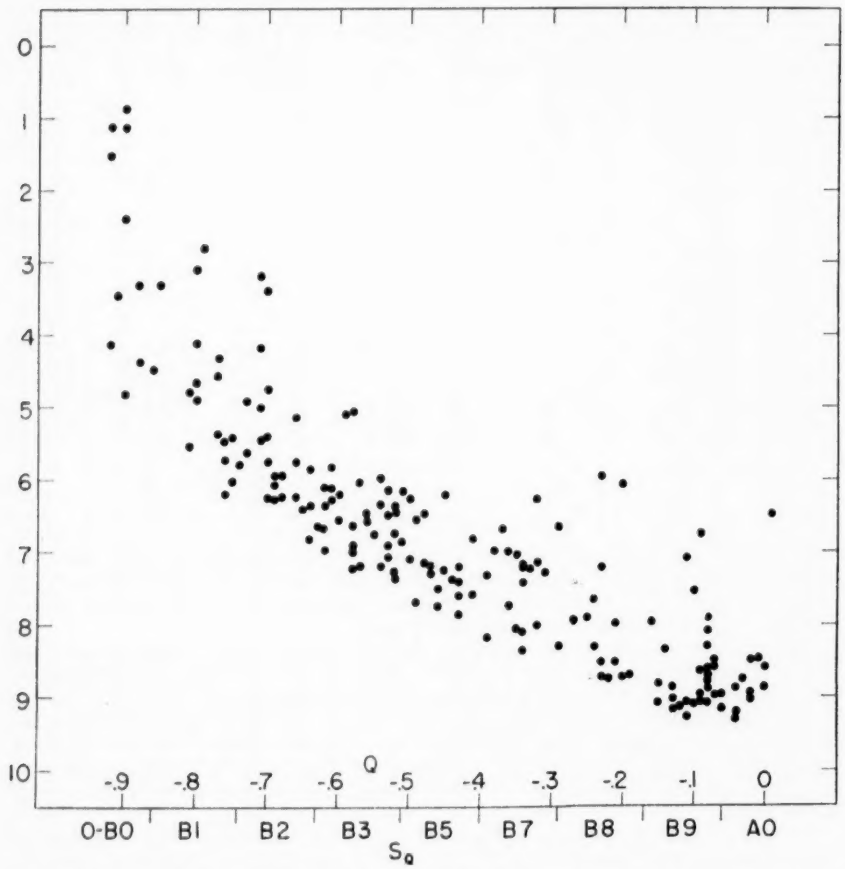

FIG. 2.—The H-R diagram for the Orion aggregate based on photoelectrically determined spectral types, magnitudes, and color excesses. Abscissas are values of Q and S_Q; ordinates are values of V_0 (visual magnitudes, V, corrected for absorption).

types predicted in Table 2 for the supergiants, δ, ϵ, ζ, and κ Orionis, are essentially correct. Their absolute magnitudes, as derived from Figure 2 are, within a tenth of a magnitude, the same as those obtained in Paper I. The width of the main sequence, after correction for observational errors and for the finite depth of the aggregate is approximately 1.2 mag.

The author is indebted to Drs. Johnson and Morgan for the use of some of their photometric results prior to publication.

IDENTIFICATION OF THE RADIO SOURCES IN CASSIOPEIA, CYGNUS A, AND PUPPIS A

W. Baade and R. Minkowski
Mount Wilson and Palomar Observatories
Carnegie Institution of Washington
California Institute of Technology
Received June 19, 1953

ABSTRACT

The radio sources in Cassiopeia and Puppis A are identified with a new type of galactic emission nebulosity. The outstanding features of these nebulosities are very large internal random velocities. The radio source Cygnus A is an extragalactic object, two galaxies in actual collision.

Only very few individual sources of cosmic radio emission have been identified with conspicuous astronomical objects.[1] Although the sources in Cassiopeia[2] and Cygnus A[3] are among the brightest and earliest-known radio sources of the sky, all attempts to identify them with astronomical objects in the visible range have failed so far. In the fall of 1951, F. G. Smith, of the Cavendish Laboratory, communicated to us in advance of publication new positions for both sources which were very much more accurate than any previous data. Using an interferometric method, Smith had reduced the uncertainties in the positions to $\pm 1^s$ in right ascension and $\pm 40''$ in declination. As it turned out, the new positions were accurate enough for an unambiguous identification of both radio sources on plates taken in September, 1951, at the 200-inch telescope. The Cassiopeia source coincides with a galactic-emission nebulosity of a new type, whereas Cygnus A is an extragalactic affair, two galaxies in collision. Quite similar to Cassiopeia is one of the fainter radio sources, Puppis A.

THE CASSIOPEIA SOURCE, RYLE 23.01[4]

On blue-sensitive plates, only an archlike nebulosity, $2'.8$ long, appears. Its detailed structure hardly leaves any doubt that we are dealing with an emission nebulosity (see Fig. 1). It is close to, but does not coincide with, the radio position which lies some $2'$ farther to the south.[5] Much more revealing are the red-sensitive plates (Fig. 2) which cover the *Hα* region (λλ 6400–6700). They show, besides the arc and mainly to the south of it, broken bits of nebulosity of a most remarkable kind. Some are elongated streaks up to $25''$ long, others have almost stellar appearance. In intensity they range from very bright objects to mere smudges just above the limit of the plates. Not a single one of these broken bits of nebulosity registers on the blue-sensitive plates. Although there are strong indications that interstellar reddening affects the field, there can be no doubt that the broken bits of nebulosity are intrinsically very red. A good illustration is the brightest of these, marked *2* on Figure 3. Not a trace of it appears on the blue-sensitive plate,

[1] For a general discussion see the following paper by the authors (p. 215).

[2] M. Ryle and G. Smith, *Nature*, **162**, 462, 1948.

[3] J. G. Bolton and G. J. Stanley, *Nature*, **161**, 312, 1948.

[4] Since no generally accepted system exists, the designation of the sources in the list of Ryle, Smith, and Elsmore (*M.N.*, **110**, 508, 1950) and in the list of B. Y. Mills (*Australian J. Sci. Res.*, *A*, **5**, 266, 1952) will be given.

[5] About an attempt by D. W. Dewhirst to identify the Cassiopeia source see *Observatory*, **71**, 212, 1951. The object noted as peculiar by Dewhirst is actually a blend of a star and some brighter spots of the northern arc of nebulosity.

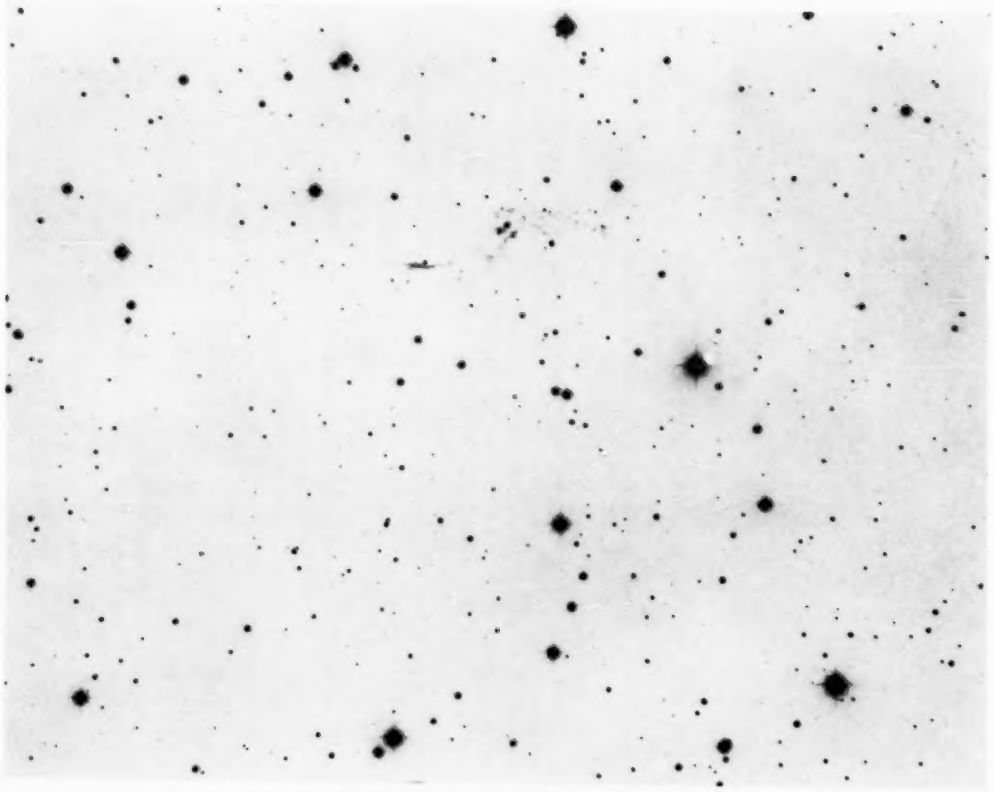

FIG. 1.—Nebulosity in Cassiopeia. λλ 3600–5000; 200-inch; 1 mm = 4.8

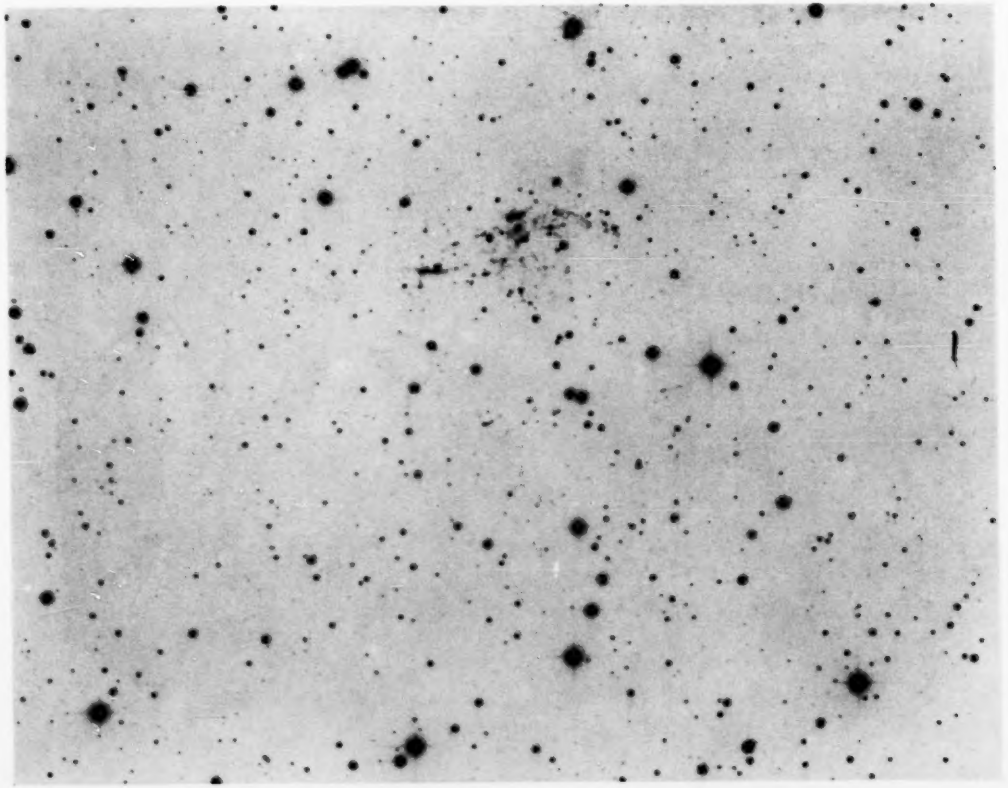

FIG. 2.—Nebulosity in Cassiopeia. λλ 6400–6700; 200-inch; 1 mm = 4".8

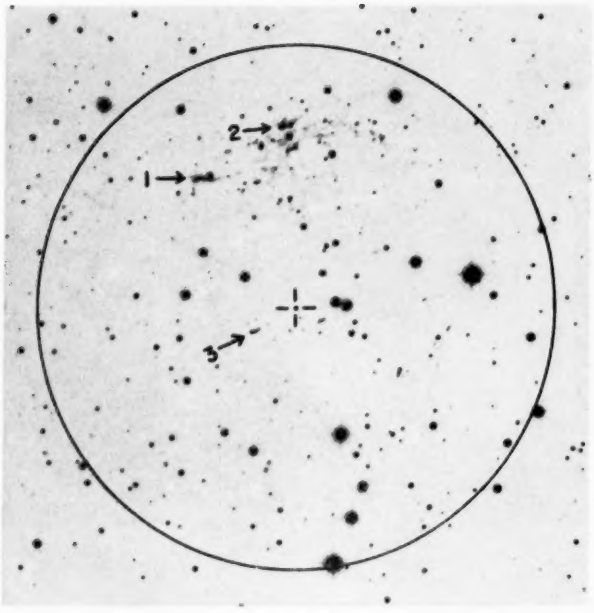

FIG. 3.—Nebulosity in Cassiopeia. λλ 6400–6700; 200-inch; 1 mm = 4".9

whereas the nebulosity of the arc in which it is imbedded appears almost equally bright on the blue and the red plates. There can be no doubt, therefore, that in these broken bits of nebulosity the emission in the blue is abnormally faint compared to that in the *IIα* region. So far as we know, it is for the first time that we encounter the type of nebulosity just described. The total area covered by these nebulosities is the circle of 6′.3 diameter in Figure 3. Its center, marked by a cross, has the position 1950.0, $23^h21^m11^s.38$, $+58°31'52''.9$, compared with F. G. Smith's radio position[6] of 1950.0, $23^h21^m12^s.0 \pm 1^s$, $+58°32'.1 \pm 0'.7$. Within the uncertainty of the present radio position, visible nebulosity and radio source coincide perfectly. All positions which have been obtained for the source are in Table 1.

TABLE 1

POSITION OF THE SOURCE IN CASSIOPEIA, RYLE 23.01

α (1950)	δ (1950)	Method	Observer
$23^h21^m12^s \pm 10^s$	$+58°32' \pm 4'$	Radio interferometer	Ryle, Smith, and Elsmore*
$23^h21^m12^s.0 \pm 1^s$	$+58°32'.1 \pm 0'.7$	Radio interferometer	Smith†
$23^h21^m36^s \pm 30^s$	$+58°38' \pm 10'$	Radio paraboloid	R. Hanbury Brown‡
$23^h21^m11^s.38$	$+58°31'52''.9$	Photographic	Baade

* *M.N.*, **110,** 508, 1950.
† *Nature*, **168,** 555, 1951.
‡ *M.N.*, **113,** 123, 1953.

Although the center of the visible nebulosity closely coincides with a star of photographic magnitude 18.9, there is no reason to identify this star with the exciting source of the nebulosity, since in no way does it stand out by its color. The same is true of the other stars near the center, so that there is no visible source of excitation for the nebulosity.

Obviously, the identification of the radio source with the nebulosity just described would be strengthened very much if it could be shown that the radio source has the same diameter as the visible nebulosity. At our request, F. G. Smith[7] measured the diameter of the Cassiopeia source interferometrically. It turned out that the radio source has indeed a measurable diameter. From his measures Smith derived $d = 5'.6 \pm 0'.2$ under the assumption of a uniformly radiating disk, or $d = 5'.0 \pm 0'.2$ if the shell is optically thin. Observations by Hanbury Brown, Jennison, and Das Gupta[8] indicate a slightly elliptical area of $3' \times 4'$, with the major axis approximately in position angle 25°. The values for the diameter of the radio source are in such good agreement with the diameter of the visible nebulosity that there can be no further doubt about the identification. Both in position and in diameter the two objects agree within the errors of measurements.

Exact agreement of the radio position with the center of the nebulosity and of the radio diameter with the diameter of the nebulosity can be expected only if all parts of the nebulosity contribute equally to the radio emission. The present evidence suggests strongly that this is true and that no direct relation exists between optical and radio emission. But the accuracy of the radio measures does not yet seem to be adequate to draw final conclusions. Of all sources identified until now, the Cassiopeia source seems to offer the best opportunity for studying this question.

[6] *Nature*, **168,** 555, 1951.

[7] *Ibid.*, **170,** 1064, 1952.

[8] *Nature*, **170,** 1060, 1952.

Added October, 1953: Interferometric measures by Jennison and Das Gupta, reported at the Symposium on Radio Astronomy at the Jodrell Bank Experimental Station in July, 1953, show that the source emits as a uniformly radiating disk with some limb darkening.

That in the Cassiopeia source we have for the first time come across a galactic nebulosity of extraordinary properties was strikingly shown by the spectroscopic investigation. Spectra of three filaments, marked on the chart in Figure 3 by arrows in the position angles of the slit, have been obtained with the nebular grating spectrograph at the prime focus of the 200-inch telescope.[9] A grating with 7500 lines/inch blazed for the third-order red was used with the 1.4-inch camera; for emission objects this grating can be used to observe the third-order red together with the overlapping fourth- and fifth-order green and violet, respectively, without serious interference by blending of lines from different parts of the spectrum. The dispersion is 220 A/mm in the third-order red, 165 A/mm in the fourth-order green, and 132 A/mm in the fifth-order blue.

The spectrum of filament *1* in Figure 4 is unique in regard to composition and to internal motions. The only lines recorded are λ 4959 and λ 5007 of [*O* III] and λ 6300 and λ 6364 of [*O* I]. The absence of *Hα* indicates a large intensity ratio [*O* III]/*Hα*, but not necessarily a larger one than that found in those planetary nebulae which show the highest value of this ratio. The [*O* I] lines, however, are abnormally strong relative to *Hα* as well as to [*O* III]. The unusual weakness of the hydrogen lines relative to the forbidden lines may be explained by the assumption that the excitation is by collisions rather than by radiation.[10] It should be noted that the situation is different from that in the Crab Nebula, where the relatively low intensity of the *H* lines compared to the permitted lines of both *He* I and *He* II suggests low hydrogen abundance.[11, 12]

Even more peculiar than the composition of the spectrum are the internal motions in the filament. Each line appears to have one strong component with three fainter components of greater wave lengths. Closer inspection suggests that these components are merely intensity maxima in a broad band. The velocities within this band range from −1000 to at least +2200 km/sec; faint extensions to about +3000 km/sec are suspected for λ 5007. Details of the intensity distribution are not the same in the [*O* I] lines as in the [*O* III] lines. This suggest differences of excitation in different parts of the filament.

A possible interpretation of the line structure is that the apparent filament is really a thin sheet of matter which is spreading out rapidly in the radial direction. The maxima in the lines would then correspond to regions of high intensity within this sheet. If this interpretation is correct, high tangential velocities comparable to the radial velocities should be expected, and, unless the object is at a distance larger than 500 psc, changes in the appearance of the filament should become noticeable after a few years. But other models for the motions in the filament are kinematically possible.

The spectrogram of filament *2* is in Figure 5. It shows *Hα* flanked by the [*N* II] lines λ 6548 and λ 6584. The relative intensities are 6548:*Hα*:6584 = 1.5:1:4.5. The [*O* I] line λ 6300, blended with the same line from the sky, is present. Spectra of this composition and with similar relative intensities are shown by some planetary nebulae. The radial velocity is −45 km/sec at the east end and +36 km/sec at the west end of the filament. The width of the lines corresponds to a velocity spread of about 400 km/sec.

Filament *3* shows a similar spectrum as filament *2*. Owing to the faintness of this filament, only the condensation of the southeast end is recorded in all three lines, and the rest shows only faintly in λ 6584 [*N* II]. The radial velocity is −170 km/sec at the southeast end. The values for the center and the northwest end, based on measures of one line and correspondingly uncertain, are −125 and −170 km/sec, respectively. The spectrogram is too faint to permit a reliable estimate of the width of the lines.

Filaments *1* and *2* are near the edge of the nebulosity; filament *3* is near the center. There are no indications that the nebulosity as a whole is expanding. Any possible veloci-

[9] J. S. Bowen, *Ap. J.*, **116**, 7, 1952.

[10] See the following paper by R. Minkowski and L. H. Aller, *Ap. J.*, **119**, 232, 1954.

[11] R. Minkowski, *Ap. J.*, **86**, 199, 1942; *Mt. W. Contr.*, No. 666.

[12] R. Minkowski and J. L. Greenstein, *Ap. J.*, **119**, 238, 1954.

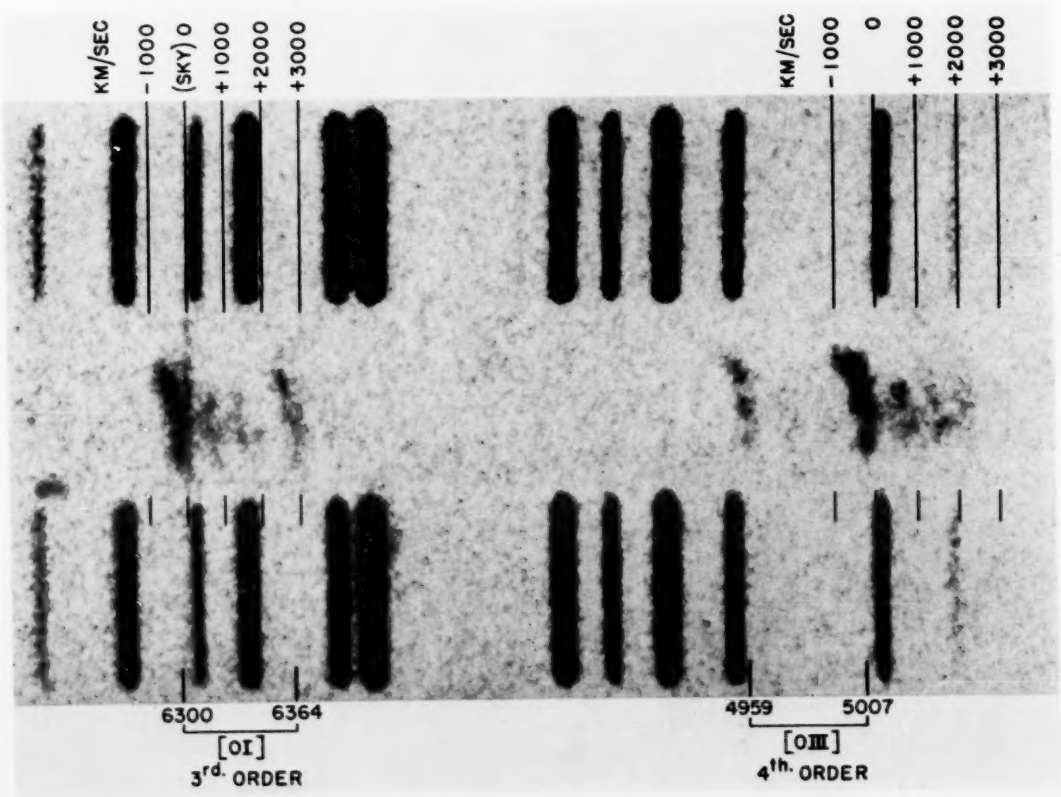

FIG. 4.—Spectrum of filament 1 of the nebulosity in Cassiopeia

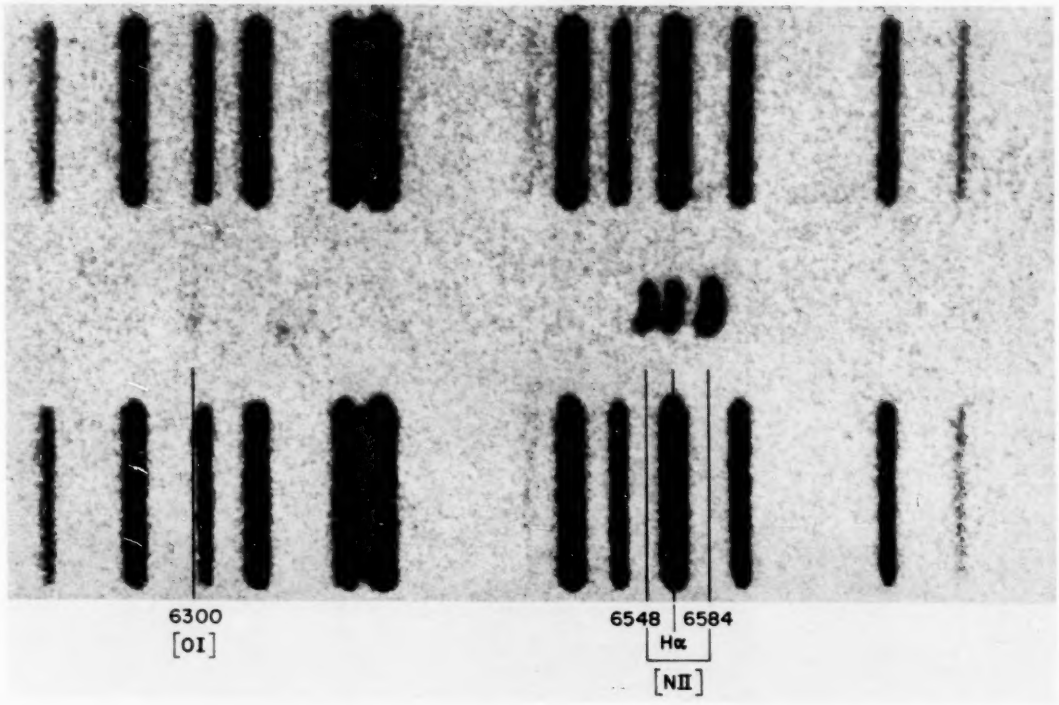

FIG. 5.—Spectrum of filament 2 of the nebulosity in Cassiopeia

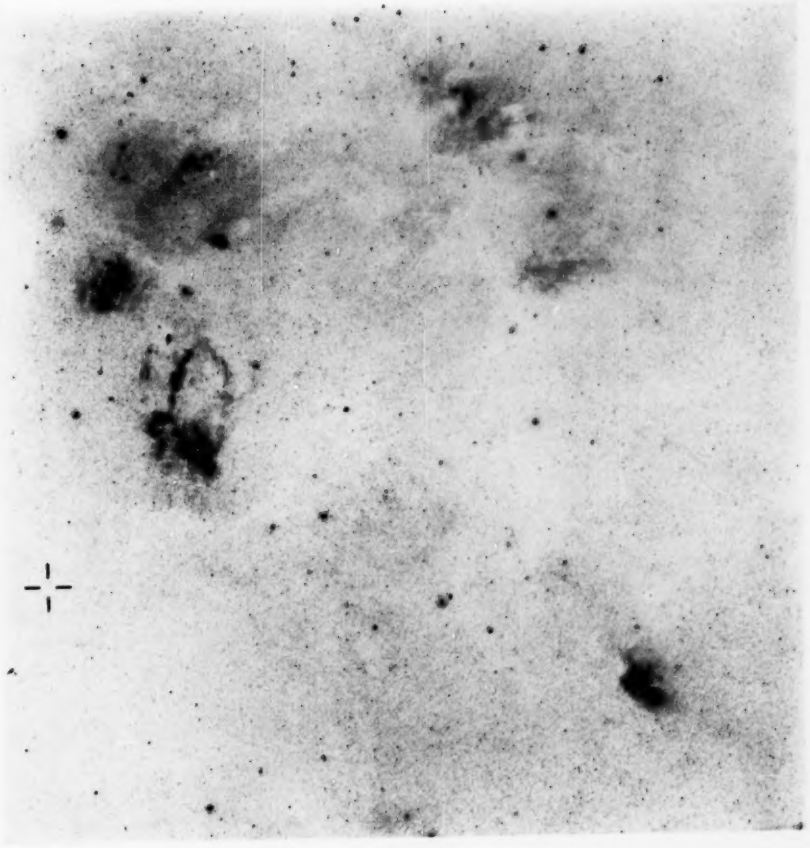

FIG. 6.—Field in Cassiopeia. Center (1950) 23^h40^m, $+61°24'$; λλ 6300–6700; 48-inch; 1 mm = 3'.1

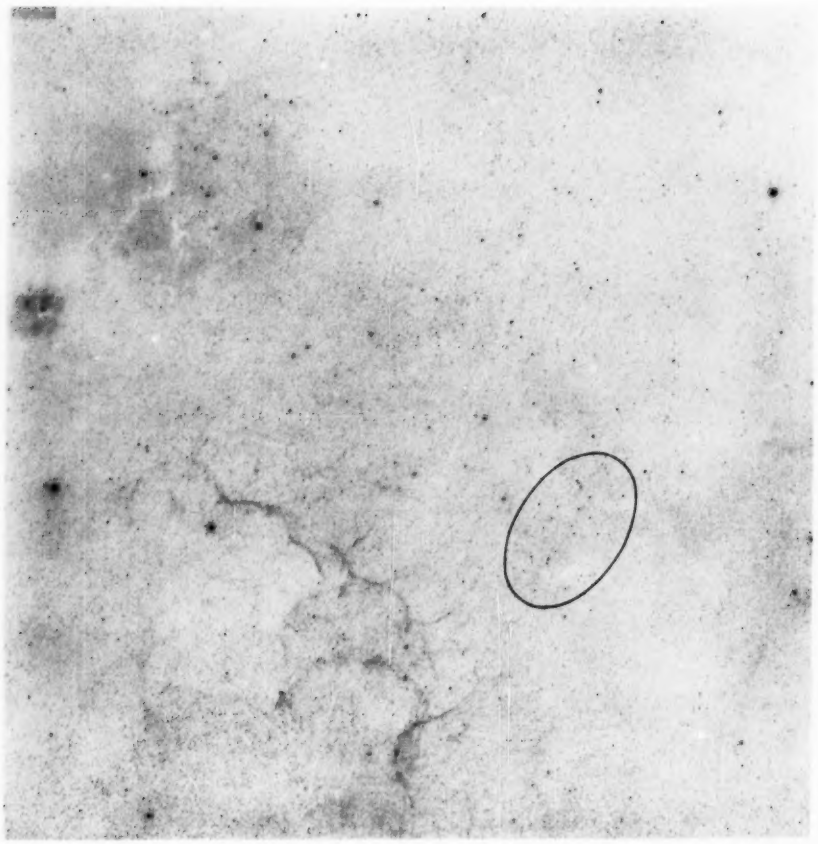

FIG. 7.—Field in Puppis. Center (1950) 8^h27^m, $-42°0'$; λλ 6300–6700; 48-inch; 1 mm = 3'.1

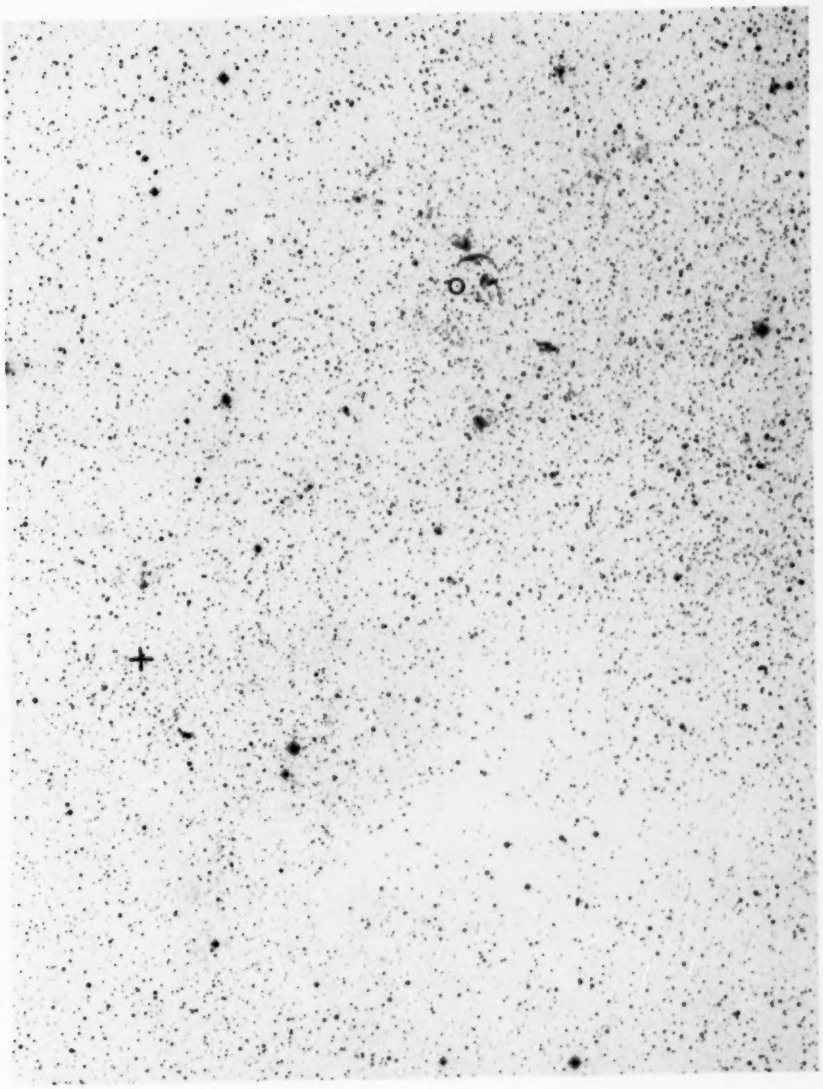

FIG. 8.—Filaments in Puppis. λλ 6200–6700; 48-inch; 1 mm = 29″

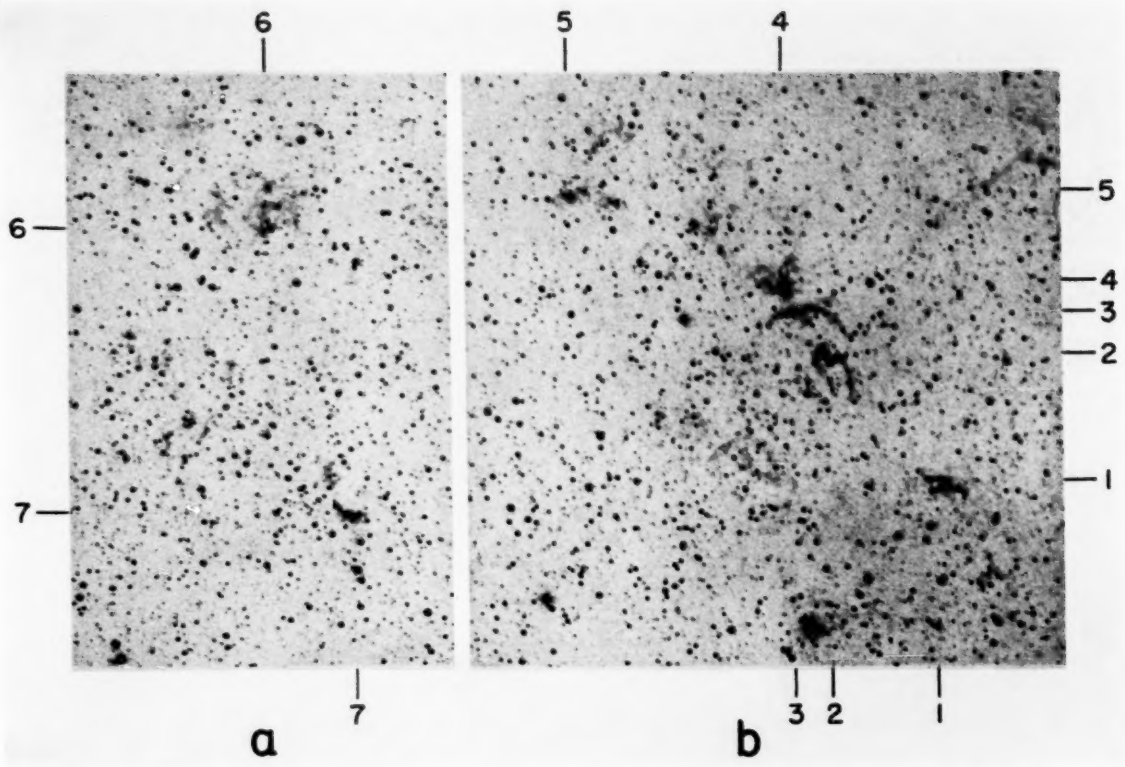

FIG. 9.—Filaments in Puppis. λλ 6200–6700; 48-inch; 1 mm = 15″

ty of expansion is obviously small compared to the random motions. This is quite different from the conditions found in shells of novae and supernovae and clearly shows that the nebulosity is not a shell of this type.[13]

The outstanding characteristic of the filaments is the large internal velocity dispersion. It seems plausible to assume that the unusually large internal motions in this nebulosity are directly connected with the strong radio emission. The present observations leave open the question of whether the filaments are being formed or dissolved. Unless the distance of the source is much larger than 500 psc, it should be possible after a few years to decide by observation between the alternatives.

The field containing the source is shown in Figure 6, reproducing a plate taken with the 48-inch Schmidt telescope. The position of the source is marked by the cross in the lower left corner; owing to the reduced scale, the faint nebulosity is not visible in Figure 6. The field is rich in large diffuse nebulosities and obscuring clouds, but none of these features coincides with the radio source, which is strikingly inconspicuous.

Added October, 1953: Intercomparison of plates taken in the fall of 1953 with the earlier plates of 1951 show marked motions and intensity changes in the filaments making up the northern arc of the nebulosity. In contrast, the red broken bits of nebulosity, such as filaments *2* and *3* in Figure 3, show neither perceptible motions nor intensity changes. Additional spectra have been obtained of seven more condensations. The diffuse filaments of the arc all have large radial motions of the order of 2000 km/sec, while the sharp red bits of nebulosity have small radial velocities around 50 km/sec.

PUPPIS A (MILLS 08−4)

When, in November, 1951, J. G. Bolton sent a list of certain sources with appreciable angular diameters, a search for these sources was made by Minkowski on 48-inch Schmidt plates. An extended visual object was found only in one of the positions, that of Puppis A.

A Schmidt plate containing the source is shown in Figure 7, reduced 2.8 times. The field is rich in large diffuse nebulosities. Not connected with these conspicuous nebulosities is a loose mass of filaments which greatly resemble the filaments of the Cassiopeia source. These filaments are within an approximately elliptical area of about $50' \times 80'$, with the major axis in position angle 145°; this area is marked in Figure 7. The filaments are not visible in Figure 7, owing to the reduced scale. The area containing the filaments is shown in Figure 8 on a larger scale. Parts of this area are still more enlarged in Figure 9, where those filaments are marked of which spectra have been observed. The centers of Figure 9, *a* and *b*, are marked in Figure 8 by a cross and a circle, respectively.

The two radio positions of the source in Table 2 agree in declination but not in right ascension. According to private communications from J. G. Bolton and B. Y. Mills, the position by Stanley and Slee may be more nearly correct. The position of the filamentary nebulosity, whose center cannot be determined with high accuracy, agrees with that by Stanley and Slee in right ascension, but the center of the nebulosity is 48′ south of the radio position. The northern border of the nebulosity at −42°13′ is, however, close to the radio position. Mills[14] found 33′ for the equivalent angular size of the source in right ascension. This is somewhat smaller than the extent of the nebulosity, but of the correct order. Radio source and nebulosity seem to overlap. In view of the faintness of this radio source and the low accuracy of its position, the agreement in regard to both position and size may be considered satisfactory. The possibility that the radio emission is stronger near the northern end of the nebulosity should not be disregarded. Exact agreement between optical and radio postion is therefore not to be expected.

[13] Since there is every reason to believe that the Cassiopeia source has nothing to do with supernovae, the attempt by I. S. Shklovsky (*Astr. J. U.S.S.R.*, **30**, 26, 1953) to identify the source with a new star of A.D. 369 is beside the point.

[14] *Australian J. Sci. Res.*, *A*, **5**, 266, 1952.

Spectra of seven filaments marked in Figure 9 have been obtained with a nebular spectrograph at the Newton focus of the 100-inch telescope. The spectrograph is similar to that used at the 200-inch telescope.[9] The same grating was used with a $F/0.67$ thick-mirror Schmidt camera; the dispersion at $H\alpha$ is 238 A/mm. Owing to the large zenith distance and the consequent high intensity of spectral features from city lights, only the strongest lines, $H\alpha$ and the [N II] lines λ 6548 and λ 6584, were observed; the presence of other lines is possible. The velocities and relative intensities are in Table 3. In several

TABLE 2

POSITION OF THE SOURCE IN PUPPIS, MILLS 08−4

α (1950)	δ (1950)	Method	Observer
$8^h18^m \pm 13^m$	$-42° \pm 40'$	Radio interferometry	Stanley and Slee*
$8^h35^m \pm 4^m$	$-42° \pm 20'$	Radio interferometry	B. Y. Mills†
8^h20^m3	$-42°48'$	Photographic	Minkowski

* *Australian J. Sci. Res.*, *A*, **3**, 234, 1950.
† *Australian J. Sci. Res.*, *A*, **5**, 266, 1952.

TABLE 3

VELOCITIES OF FILAMENTS IN PUPPIS

Filament	Km/Sec		6548/$H\alpha$	6584/$H\alpha$	Remarks
	$H\alpha$	[N II]			
1	+ 8	− 47	1.5	4.5	
2	− 12	− 18	3	9	Lines diffuse
3	+113	+124	0.5–1.5	1.5–4.5	Lines wavy
4	+ 57	+ 76	2	6	*
5	− 19	− 8	1.5	4.5	Lines diffuse
6*a*	+ 84	+ 70	1.5	5	Lines diffuse†
6*b*		+124			
7	+ 22	− 9	0.8	2.5	

* The tabulated velocity is for the strong condensation. Velocity at the east end of the filament is +42 km/sec; at the west end, +87 km/sec.

† Filament 6 contains a sharp filament approximately in position angle 20° superposed on fainter, more irregular, filaments. The velocity for 6*a* is for the sharp filament, that for 6*b* for the background. $H\alpha$ is present in 6*b* but is too faint to be measured.

filaments the lines are noticeably diffuse; the velocity dispersion indicated is of the order of 150–200 km/sec.

The conditions shown by the spectra resemble greatly those in the Cassiopeia source, but on a reduced scale in regard to the velocities. The velocity dispersion is large, and any possible velocity of expansion is smaller than the random velocities. If the radio emission is connected with large velocity dispersion in filaments, a smaller velocity spread in Puppis A than in the Cassiopeia source is to be expected, since the radio emission of Puppis A is substantially smaller than that of the Cassiopeia source. The general similarity of the conditions in the Puppis nebulosity to those in the Cassiopeia nebulosity in regard to appearance, spectrum, and motions strengthens the identification as the radio source.

CYGNUS A (RYLE 19.91; MILLS 19 + 4)

Except for the first positions by Bolton and Stanley,[15] all positions of the source given in Table 4 are within an area of 18′ in right ascension and 10′ in declination. This area

[15] *Nature*, **161**, 312, 1948.

is marked in Figure 10, which shows the field surrounding the source. No bright star or any other conspicuous object is near the position of the source. Faint outlying parts of the nebulosities near γ Cygni cover the field. But interstellar absorption is low, as shown by the fact that numerous faint galaxies appear in the field.

Previous observers[16] had already noted that the region around Cygnus A must be quite transparent in spite of its low galactic latitude ($b = -4°$), because extragalactic nebulae shine through in large numbers. The 200-inch exposures clearly show the reason why, aside from the general transparency of the field, extragalactic nebulae are so frequent. The radio source lies amid a rich cluster of galaxies, the brightest members of which are of about the seventeenth photographic magnitude. In conformity with the general rule, the dominating nebular types in the cluster are E- and So-systems. The radio source

TABLE 4

POSITION OF CYGNUS A (RYLE 19:01; MILLS 19+4)

α (1950)	δ (1950)	Method	Observer
$19^h58^m47^s \pm 10^s$	$+41°41' \pm 7'$	Radio interferometry	Bolton and Stanley*
$19^h58^m14^s \pm 60^s$	$+40°36' \pm 10'$	Radio interferometry	Stanley and Slee†
$19^h57^m46^s \pm 5^s$	$+40°30' \pm 7'$	Radio interferometry	Ryle, Smith, and Elsmore‡
$19^h57^m37^s \pm 6^s$	$+40°34' \pm 3'$	Radio interferometry	Mills and Thomas§
$19^h57^m44^s \pm 2^s5$	$+40°35' \pm 1'.5$	Radio interferometry	Mills‖
$19^h57^m22^s \pm 25^s$	$+40°22' \pm 16'$	Radio paraboloid	Hanbury Brown and Hazard#
$19^h57^m45^s.3 \pm 1^s$	$+40°35'.0 \pm 1'$	Radio interferometry	Smith**
$19^h57^m44^s.49$	$+40°35'46''.3$	Photographic	Baade

* *Nature*, **161**, 312, 1948. This position has been superseded by the value given by Stanley and Slee.
† *Australian J. Sci. Res.*, *A*, **3**, 234, 1950.
‡ *M.N.*, **110**, 508, 1950.
§ *Australian J. Sci. Res.*, *A*, **4**, 158, 1951.
‖ *Australian J. Sci. Res.*, *A*, **5**, 456, 1952.
M.N., **111**, 576, 1951.
** *Nature*, **168**, 555, 1951.

coincides in position with one of the brightest members of the cluster:[17] Cyg A (radio position by F. G. Smith[7]), 1950.0, $19^h57^m45^s.3 \pm 1^s$, $+40°35'.0 \pm 1'$; position of nebula, 1950.00, $19^h57^m44^s.49$, $+40°35'46''.3$.

In the center of this nebula (Fig. 11, *a*) are two bright condensations separated by about 2″ in position angle 115°. The bright central region of about 3″ × 5″ is surrounded by much fainter outer parts of elliptical outline, about 18″ × 30″, with the major axis in position angle 150°.

At first sight, this nebula is a very curious object which seems to defy classification. The clue to a proper interpretation lies in the fact that it has two nuclei which are tidally distorted and that hence we are dealing with the superimposed images of two galaxies. Both are late-type systems, judging by the low density gradients of the two disks. Spatially they are oriented face to face, they are slightly decentered, and we look upon them

[16] B. Y. Mills and A. B. Thomas, *Australian J. Sci. Res.*, *A*, **4**, 158–171, 1951.

[17] This coincidence was already noted in 1951 by Mills and Thomas (see n. 16), who had obtained for the radio position of Cyg A: 1950.0, $19^h57^m37^s \pm 6^s$, $+40°34' \pm 3'$; but it seemed unlikely at that time that a distant galaxy could be the radio emitter. Moreover, the coincidence established by them was not convincing, since, besides the nebula in question, three of the brighter members of the cluster fall into the area defined by the uncertainty of the position. Minkowski therefore wrote Mills that he did not think it was permissible to identify the source with one of the faint extragalactic nebulae in the area and emphasized that what was wanted was a more accurate radio position. The accuracy of Smith's position was needed to make the identification among the cluster members unambiguous. After Smith's position became known, the coincidence of the nebula with the radio source was also noted by D. W. Dewhirst (*Observatory*, **71**, 212, 1951). B. Y. Mills later gave the improved position: 1950.0, $19^h57^m44^s \pm 2\frac{1}{2}^s$, $+40°35' \pm 1\frac{1}{2}'$.

at an angle not far from 45°. Actually, the two systems must be in close contact because of the strong signs of tidal distortions which the nuclei show. This suggests that we are dealing with the exceedingly rare case of two galaxies which are in actual collision The main features of such a collision have been discussed by Spitzer and Baade.[18] On the cosmical time scale, collisions of galaxies are a rather frequent phenomenon in the rich clusters of galaxies. As far as the stars of the colliding systems are concerned, such a collision is an absolutely harmless affair. The average distance between two stars is so large that the two galaxies penetrate each other without any stellar collisions. The situation is very different for the gas and dust imbedded in the two systems. Because of the much shorter free paths of the gas and dust particles, the collision of the two galaxies means a real collision of the imbedded gas and dust, which are heated up to very high temperatures, since the collisional velocities range from hundreds to thousands of kilometers per second.

It is obvious that this behavior of the gas and dust provides a beautiful test of our hypothesis that the two galaxies which we identify with the radio source Cygnus A are actually colliding; for we should expect a very unusual spectrum for our nebula. Besides the continuous spectrum provided by the stars of the two systems, the emission spectrum of the colliding gases should be visible. In fact, this emission spectrum should be quite strong, since we are dealing with a face-on collision of the two galaxies, which makes it certain that maximum amounts of the gas are in collision simultaneously. Moreover, on account of the high velocities involved in the collision of two galaxies, the resulting emission spectrum should be one of unusually high excitation and the lines themselves should show broadening. Spectra taken at the 100-inch and 200-inch telescopes largely confirmed these predictions.

Spectra of the bright nuclear region have been obtained with the nebular spectrographs at the prime focus of the 200-inch telescope and at the Newtonian focus of the 100-inch telescope. The spectrum in Figure 12 was obtained with the grating mentioned earlier, which permits the simultaneous observation of the third-, fourth-, and fifth-order red, green, and violet, respectively. For the photographic region, a grating with 15,000 lines/inch blazed for violet has also been used with a dispersion of 435 A/mm.

The spectrograms show that the nebula is indeed a very peculiar, if not unique, object. Strong forbidden-line emission is recorded, while the continuous spectrum barely shows. Photoelectric measures by Dr. W. A. Baum indicate that more than 50 per cent of the total light of the condensations is in the emission lines. The emission lines and the nebular red shift derived from them are in Table 5. From the red shift, the distance of the nebula is 3.3×10^7 psc, with the value 540 km/sec per 10^6 psc for the red-shift constant.

The large red shift of 16,830 km/sec places all lines in regions of the spectrum where the plate sensitivity differs from its normal values for the lines; reliable estimates of relative line intensities, therefore, cannot be given at this time. It is obvious that *Hα* is relatively faint compared to the adjacent [*N* II] lines. The absence of *Hβ* from the observed lines indicates relatively low intensity compared to the neighboring [*O* III] lines. The lines are diffuse, but the dispersion is too low to determine reliable values of the width. Individual lines seem to differ in width, but at least part of this is caused by intensity differences. The velocity spread is of the order of 400 km/sec.[19] The [*O* II] line λ 3727 extends through the full length of the slit in Figure 12. The corresponding diameter of more than 30″ in position angle 90° is slightly larger than the visible size of the nebula.

[18] *Ap. J.*, **113**, 413, 18, 1951.

[19] The spectrum of the nebula resembles to a certain degree the spectra of those relatively rare nebulae whose nuclei show strong emission lines (C. J. Seyfert, *Ap. J.*, **97**, 28, 1943; *Mt. W. Contr.*, No. 671), but there are marked differences. In NGC 1068 and NGC 4151, the outstanding representatives of the emission nuclei, only 13 and 22 per cent of the light of the nucleus, respectively, is in the emission lines. The outstanding difference between Cygnus A and the nebulae with emission nuclei is that in Cygnus A the area of very strong emission has a diameter of 800 psc, whereas in the other nebulae the emission is restricted to diameters of the order of 25 psc.

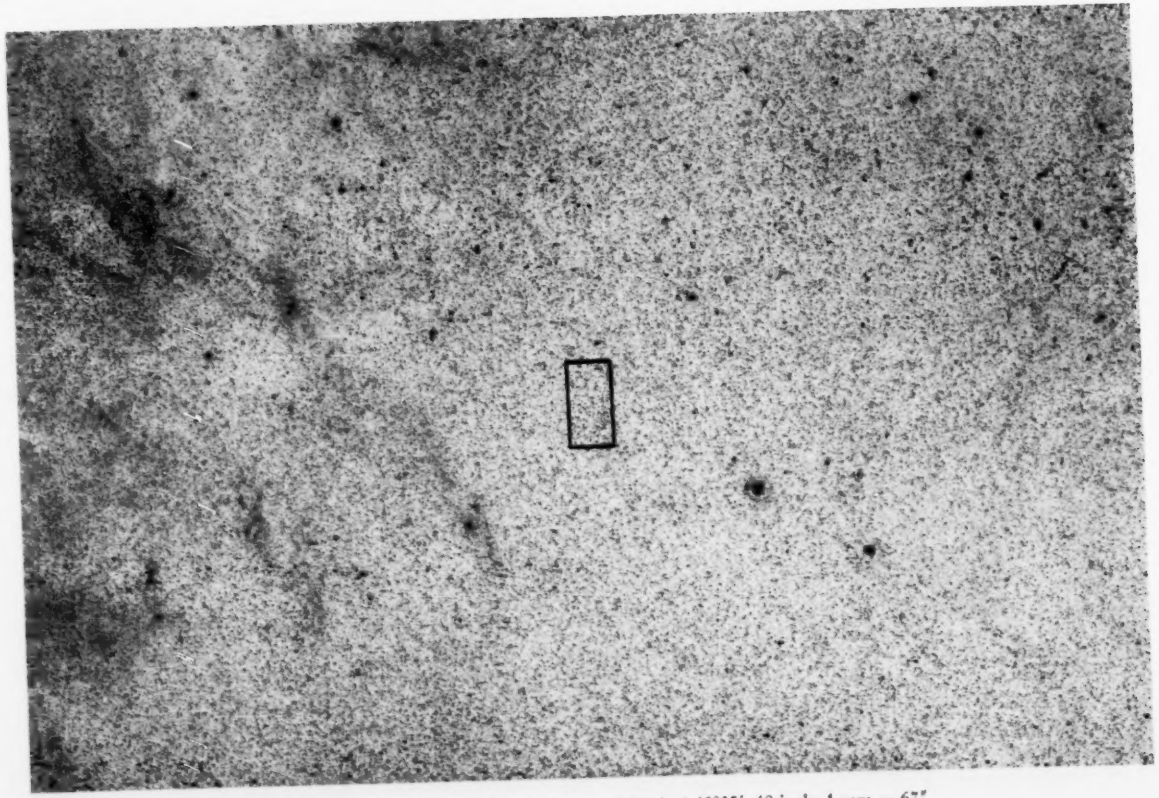

FIG. 10.—Field in Cygnus. Center (1950) 19^h57^m6, $+40°35'$; 48-inch; 1 mm = 67″

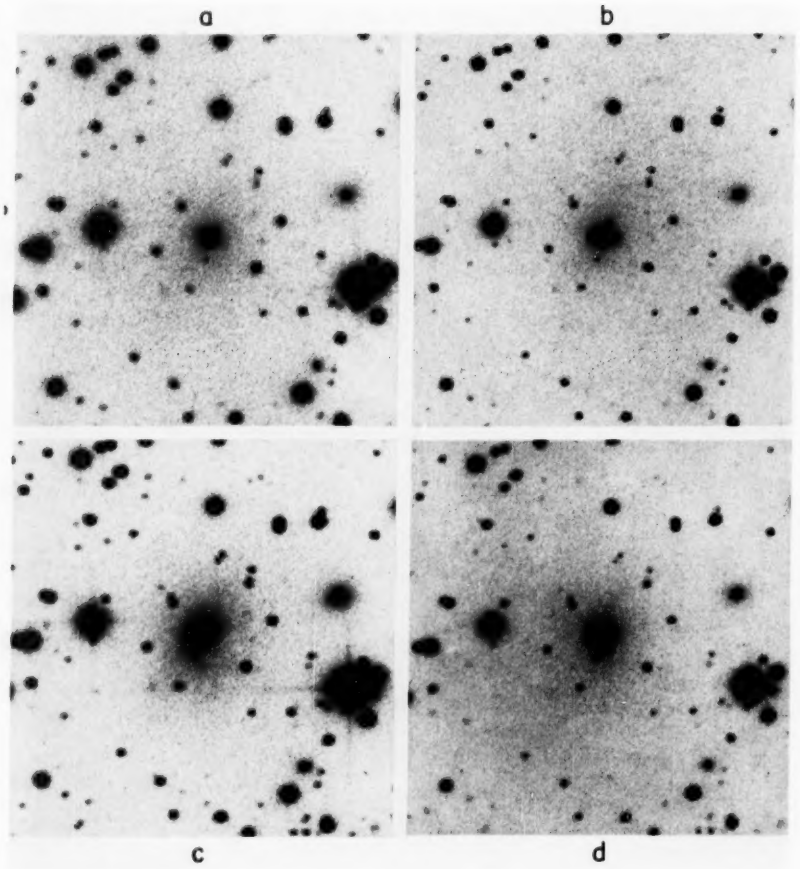

FIG. 11.—Extragalactic nebula in Cygnus. 200-inch; 1 mm = 1".2. *a*, λλ 3600–5000 [*Ne* V], [*O* II], [*Ne* III]; *b*, λλ 5000–5400 [*O* III]; *c*, λλ 5000–6200 [*O* III]; *d*, λλ 6700–7500 *Hα*, [*N* II].

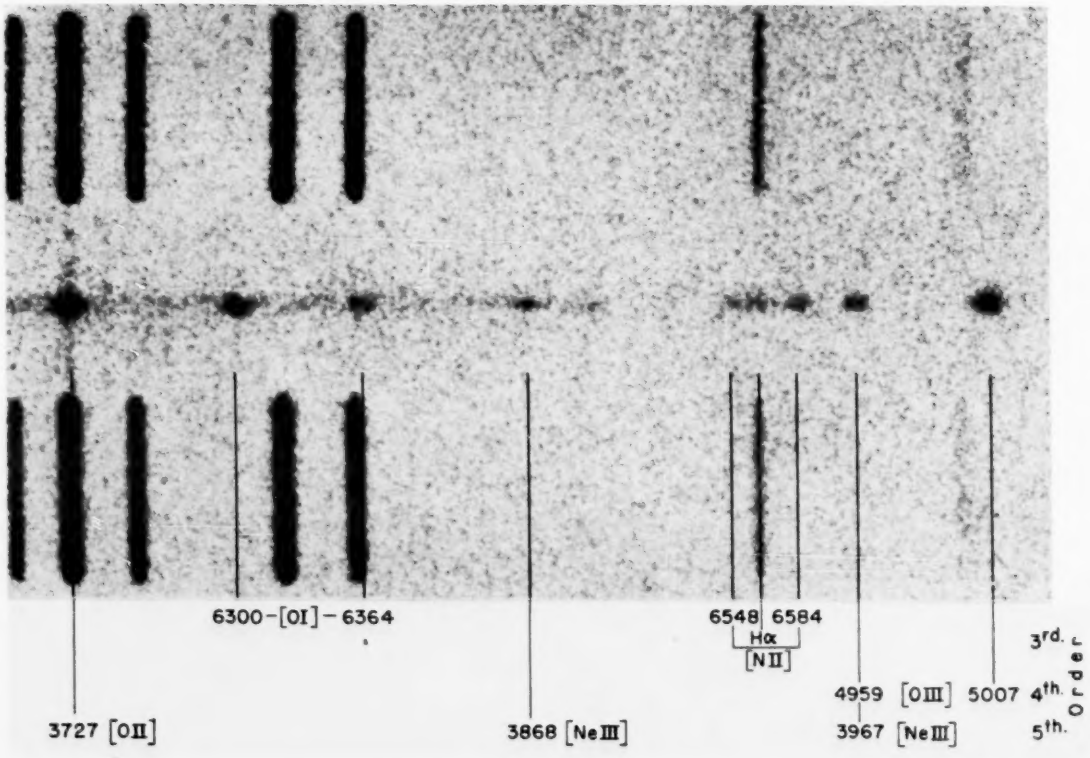

FIG. 12.—Spectrum of the extragalactic nebula in Cygnus

Inclination of the line indicates rotation of the nebula; the south-following side is receding relative to the center.

On account of the great intensity of some of the emission lines, it is possible, by selecting sufficiently narrow filter ranges, to photograph the emission regions. As Figure 11 shows, there are marked differences in the pictures, depending on the emission lines selected. Owing to the nebular red shift, the emission lines do not appear in their normal wave-length region; the main lines contained in each photograph are listed in the caption of Figure 11.

The determinations of the size of the radio source confirm that the source is not stellar, as had been assumed originally, but has a small diameter measurable with refined interferometric methods. Measures by Mills[20] give an effective size of 1′.1. Smith[21] finds a diameter of about 3′.5. Both values should apply to the east-west direction. Measures by Hanbury Brown, Jennison, and Das Gupta[22] suggest an elliptical outline of about

TABLE 5

EMISSION LINES IN CYGNUS A

λ Observed	Identification		$c\Delta\lambda/\lambda_0$ (Km/Sec)
3619.9	3425.86	[*Ne* V]	17,010
3937.2	3726.06/8.82	[*O* II]	16,930
4087.5	3868.77	[*Ne* III]	16,930
4189.6	3967.48	[*Ne* III]	16,820
5234.3	4958.91	[*O* III]	16,660
5284.6	5001.85	[*O* III]	16,955
6642.5	6300.27	[*O* I]	16,770
6718.6	6363.88	[*O* I]	16,720
6916.6	6548.06	[*N* II]	(16,870)*
6928.0	6562.66	*Hα*	(16,300)*
6949.2	6583.43	*N*II]	16,670
Mean			16,830

* λλ 6916.6 and 6928.0 are blended: the accuracy of the measured wave lengths therefore is low, and the values of the red shift for both lines have been excluded from the mean.

1′ × 2′.1, with the major axis in a position angle close to that of the major axis of the nebula. This is three to four times larger than the visible size, which, as is usual for faint nebulae, is only that of the main body of the nebula. The emission line λ 3727 [*O* II] extends beyond the main body, and it is quite possible that the fainter outer parts may have a diameter much larger than the main body. If, however, a large part of the disagreement has to be explained by an essential contribution of the outer parts to the radio emission, the radio and the optical emission cannot be related. It seems improbable that this assumption entirely suffices to explain the discordance. In view of the difficulty of the radio measures, however, the lack of agreement in regard to the precise extent seems less important than the agreement as to the order of magnitude of the size.

Photoelectric magnitude and color of Cygnus A have been measured by Dr. W. A.

[20] *Nature*, **170**, 1063, 1952.

[21] *Nature*, **170**, 1064, 1952.

[22] *Nature*, **170**, 1060, 1952.

Added October, 1953: Interferometric measures by Jennison and Das Gupta, reported at the Symposium on Radio Astronomy at the Jodrell Bank Experimental Station in July, 1953, show that the radio emission originates in two areas separated by 82″ and 43″ long in position angle 95° with a width of 30″. No object of this description can be seen on any of our plates which cover the wave-length range from the ultraviolet to the infrared.

Baum. With a diaphragm of 11″.5 diameter, the magnitudes and colors reduced to the international system are $m_{pg} = 17.90$; $m_{pv} = 16.22$; $CI = +1.68$. To determine the absolute magnitude, corrections have to be applied for interstellar absorption and for the size of the diaphragm. By comparison with nebulae of similar appearance, a conservative estimate is that the nebula is 0.75 mag. brighter than the part admitted by the diaphragm. The interstellar absorption cannot be determined from the color index of the nebula, since the color is affected by the emission lines. But, on the assumption that the elliptical nebula 25″ north-preceding is a member of the cluster to which Cygnus A belongs and therefore at the same distance, this apparently normal nebula may be used. Its magnitudes and colors are $m_{pg} = 18.95$; $m_{pv} = 17.42$; $CI = +1.53$. The color of an elliptical nebula with a red shift of 17,000 km/sec is[23] $CI = +1.08$. The color excess of +0.45 mag. between this value and the measured color index is due to interstellar reddening. The ratio of photographic absorption to international color excess is[24] somewhat less than 5. The photographic absorption, therefore, is 2.1 mag. Thus we have for Cygnus A the values in the accompanying tabulation.

	Mag.	
Apparent m_{pg}	17.90	
Correction for incompleteness	0.75	
Photographic absorption	2.1	
Corrected m_{pg}	15.05	
Distance modulus $m - M$	32.6	(from red shift)
M_{pg}	−17.5	

The system, therefore, is a giant system which may be expected to have a diameter of more than 10,000 psc. The major axis of 30″ of the visible main body of the nebula is only 5000 psc. The assumption is justified that the nebula has a larger diameter than this; but a diameter of 20,000 psc, which would correspond to the radio interferometer measures, would call for strong radio emission from the outermost parts of the nebula, where the average density is exceedingly low.

Since the distance of the nebula is known, the total energy emitted in the radio region may be computed. The flux received from the nebula is of the order of 1.3×10^{-22} watts m^{-2} $(c/sec)^{-1}$ in a band of an equivalent width of 500 Mc/sec. The total flux, therefore, is of the order of 6×10^{-14} watts m^{-2} or 6×10^{-11} ergs cm^{-2} sec^{-1}. With the source at the distance of 3.3×10^7 psc, the total energy emitted in the radio region is 8×10^{42} ergs/sec. This is larger than the total optical emission of 5.6×10^{42} ergs/sec and larger than the energy contained in the line emission. The source of energy for the radio emission may be the relative kinetic energy of the colliding nebulae, which is of the order of 10^{59} ergs for a relative velocity of 500 km/sec.

We want to express our sincere thanks to all members of the radio-groups in Sydney, Cambridge, and Manchester for their generous co-operation.

[23] J. Stebbins and A. E. Whitford, *Ap. J.*, **108**, 413, 1952.

[24] J. L. Greenstein, in *Astrophysics: A Topical Symposium*, ed. J. A. Hynek (New York: McGraw-Hill Book Co., 1951), chap. xiii, p. 538.

ON THE IDENTIFICATION OF RADIO SOURCES

W. Baade and R. Minkowski
Mount Wilson and Palomar Observatories
Carnegie Institution of Washington
California Institute of Technology
Received June 19, 1953

ABSTRACT

A discussion of the astronomical evidence concerning objects identified as discrete radio sources shows that the following four types of objects are now recognized: (I) remnants of supernovae; (II) galactic nebulosities of a new type; (III) peculiar extragalactic nebulae; (IV) normal extragalactic nebulae. A discussion of the distribution of the general galactic radiation favors the assumption that this radiation is emitted by objects in population II and therefore probably by stars.

The problem of identification of the discrete radio sources with visible objects has now reached a stage in which a full discussion of the astronomical evidence appears necessary. The low accuracy of the early positions of the sources made their identification a difficult problem. Only very few sources were close to known objects which could be considered seriously, but the two most intense sources were not among them. Only for 7 out of 67 sources known in 1950 [1, 2] were identifications suggested. The objects identified were the Crab Nebula—the remnant of the supernova of 1054—and certain extragalactic nebulae. A survey by Mills[3] increased the number of observed sources considerably but did not add any convincing identifications. Many objects in that part of the sky common to the surveys by Ryle, Smith, and Elsmore and by Mills are in only one of the two lists. This may indicate that neither of the two surveys is approximately complete. Unpublished results by Bolton, however, suggest that some of the positions listed actually refer to blends of objects rather than to individual sources. Since one temporary source is known[4] variability should not be entirely disregarded as a possible explanation of discrepancies. But the percentage of such cases obviously must be exceedingly low. This is shown directly by Ryle's observation[5] that, of about 100 sources, none showed variations greater than about 0.1 mag. over a period of 18 months.

Some of the first objects suggested as radio sources were known to be peculiar astronomically, but the low accuracy of the radio positions admitted considerable doubt as to the validity of the proposed identifications. It seemed definitely established, however, as a result of the surveys, that certain classes of objects were not among the discrete sources: stars brighter than magnitude 4, the nearest stars, stars having a large proper motion, stars with strong magnetic fields, old novae, planetary nebulae, diffuse nebulae, and star clusters. Negative evidence of this kind can be accepted only with reservations. It does not answer the question of whether some stars—other than the sun—are observable radio sources.

When the development of improved techniques led to precise positions and established the fact that many sources have a measurable angular extent, the way was open for an effective search with large telescopes for visible objects. As a result of these searches, the

[1] G. J. Stanley and O. B. Slee, *Australian J. Sci. Res.*, A, **3**, 234, 1950.

[2] M. Ryle, F. G. Smith, and B. Elsmore, *M.N.*, **110**, 508, 1950.

[3] B. Y. Mills, *Australian J. Sci. Res.*, *A*, **5**, 266, 1952.

[4] G. J. Stanley and O. B. Slee, *Australian J. Sci. Res.*, *A*, **3**, 234, 1950.

[5] M. Ryle, *Nature*, **168**, 555, 1951.

two strongest sources—Cygnus A and Cassiopeia—and one fainter source—Puppis A—were identified.[6] Certain more tentative identifications will be included in the present paper. It is now well established that a variety of objects can be strong radio emitters. They will be discussed in the following order: (I) remnants of supernovae, (II) galactic nebulosities of a new type, (III) peculiar extragalactic nebulae, and (IV) normal extragalactic nebulae.

A large part of the published positions of unidentified sources has been inspected by now on plates taken with the 48-inch Schmidt telescope. These attempts to identify more sources are being continued. But little further progress can be expected as long as radio positions have probable errors of the order of a degree or more and as long as marked discrepancies exist between the content of lists of different observers. Even the most precise determinations of positions, however, may not lead to identifications. No visible objects which might be considered as possible radio sources of the required intensity or extent have been found near Hydra A and Fornax A, for which Mills[7] has determined accurate positions. Actually, the identification of the strongest sources entails the conclusion that even relatively strong sources may be objects too faint to be seen or photographed. On the other hand, some objects not in the present lists of sources should be observable in the radio range if certain of the identifications are correct. Radio investigation of such objects is at least as important as attempts to determine more precise positions for all fainter sources.

The close agreement of the position of a radio source with that of an astronomical object is not sufficient for a definite identification. Data on the angular extent of the source are, in general, of equal importance, particularly if the position cannot be determined with high accuracy. Only for one type of source—normal extragalactic nebulae—is a correlation of radio intensity and optical brightness possibly to be expected. To compare intensity and brightness, it is convenient to express the intensity in magnitudes, as has already been done by Ryle, Smith, and Elsmore[2] and by Hanbury Brown and Hazard.[8] The magnitude system of Hanbury Brown and Hazard, which gives comparable radio and photographic magnitudes for normal extragalactic nebulae and almost entirely avoids negative magnitudes, seems more suitable and will be used here. The radio magnitude on this system is

$$m_R = -53.4 - 2.5 \log i ,$$

where i is the intensity in watts $m^{-2}(c/sec)^{-1}$. If the dependence of the intensity on the frequency f is f^{-n}, the color index between two frequencies f_1 and f_2 is

$$C = m_R(f_1) - m_R(f_2) = 2.5n \log \frac{f_1}{f_2}.$$

The measures of the intensity distribution indicate values of n between 1.3 and 2. Thus the color difference between 100 and 158.5 Mc/sec, for instance, is between 1.0 and 1.5 mag. The intensity of the radio spectrum integrated over all frequencies would be infinite and cannot be determined as long as the true distribution for very low frequencies is not known. But the total energy emitted in the radio region is a datum of some significance, and values will be given based on the assumption that the total energy is

[6] W. Baade and R. Minkowski, *Ap. J.*, **119**, 206, 1954.

[7] *Australian J. Sci. Res.*, *A*, **5**, 456, 1952. The accurate position of Fornax A (Mills 03 − 3)—(1950) $\alpha = 3^h19^m30^s \pm 6^s$, $\delta = -37°18' \pm 3'$—rules out the identification with NGC 1316, $\alpha = 3^h20^m8$, $\delta = 37°24'$, which has been proposed by I. S. Shklovski, *Astr. J. U.S.S.R.*, **30**, 30, 1953. Moreover, Shklovski's statement that NGC 1316 is similar to NGC 5128 is not correct. NGC 1316 is an SO or Sa nebula with a few faint absorption patches.

Added October, 1953: Mills now admits that Fornax A may be a blend of several sources. Attempts to identify Fornax A should therefore be postponed until the situation is cleared up.

[8] *Phil. Mag.*, **43**, 137, 1952.

equivalent to that contained in a band of 500 Mc/sec width with a constant intensity equal to that at 100 Mc/sec.[9]

The photographic magnitudes quoted for extragalactic nebulae are marked by letters denoting their source, as follows (H) Holmberg,[10] (SW) Stebbins and Whitford,[11] (P) Pettit,[12] (B) Bigay,[13] (SA) Shapley and Ames.[14] According to Holmberg,[10] magnitudes of the Shapley-Ames catalogue are systematically too faint for bright nebulae; where necessary, values corrected for this systematic error are also given.

I. REMNANTS OF SUPERNOVAE

1. THE CRAB NEBULA (RYLE 05.01; MILLS 05 + 2)

The Crab Nebula is the remnant of the supernova of 1054, a supernova of type I. The identification of the source discovered by Bolton[15] with the Crab Nebula was first suggested by Bolton, Stanley, and Slee.[16] Except for the discovery position, all positions given in Table 1 are in excellent agreement with the position of the Crab Nebula. The

TABLE 1

NGC 1952 (RYLE 05.01, MILLS 05 + 2)

α (1950)	δ (1950)	Frequency (Mc/sec)	m	Observer
5^h13^m	$+28°$	100	4.0	Bolton*
$5^h31^m20^s \pm 30^s$	$+22°02' \pm 8'$			Bolton, Stanley, and Slee; Bolton and Stanley†
$5^h31^m30^s$	$+22°01'$	100	3.3	Stanley and Slee‡
$5^h31^m37^s \pm 10^s$	$+22°10' \pm 20'$	81.5	+3.9	Ryle, Smith, and Elsmore§
$5^h31^m34^s5 \pm 3^s$	$+22°4' \pm 5'$			Smith‖
$5^h30^m \pm 2^m$	$+22° \pm 20'$	100	+3.4	Mills#
$5^h31^m20^s \pm 2^s5$	$+22°00 \pm 3'$			Mills**
$5^h31^m30^s$	$+21°59'.3$	*pg*	9.0††	NGC

* *Nature*, **162**, 141, 1948.

† J. G. Bolton, G. J. Stanley, and O. B. Slee, *Nature*, **164**, 101, 1949; J. G. Bolton and G. J. Stanley, *Australian J. Sci. Res.*, *A*, **2**, 139, 1949.

‡ *Australian J. Sci. Res.*, *A*, **3**, 234, 1950.

§ *M.N.*, **111**, 508, 1950.

‖ *Nature*, **168**, 555, 1951.

Australian J. Sci. Res., *A*, **5**, 266, 1952.

** *Ibid.*, p. 456.

†† W. Baade, *Ap. J.*, **96**, 188, 1942; *Mt. W. Contr.*, No. 665.

two most precise positions by Smith and by Mills have estimated probable errors which are not larger than the size of the nebula. An effective angular size of 4′ in the east-west direction has recently been determined by Mills.[17] This value agrees well with the size of the nebula. Recent unpublished measures by Mills give an elliptical brightness contour $3'.5 \times 5'$, with the major axis in position angle 143°, in excellent agreement with the size and orientation of the nebula which are given below. The identification thus is safely established.

The discussion of the structure and the spectrum of the Crab Nebula[18, 19] shows that

[9] See the following paper by Minkowski and Greenstein (pp. 238–242).

[10] *Lund Medd.*, ser. 2, No. 128, 1950.

[11] *Ap. J.*, **115**, 284, 1952.

[12] Personal communication.

[13] *Ann d'ap.*, **14**, 319, 1951.

[14] *Harvard Ann.*, Vol. **88**, No. 2, 1932.

[15] *Nature*, **162**, 141, 1948.

[16] *Nature*, **164**, 101, 1949.

[17] *Nature*, **170**, 1062, 1952.

[18] W. Baade, *Ap. J.*, **96**, 188, 1942; *Mt. W. Contr.*, No. 665.

[19] R. Minkowski, *Ap. J.*, **96**, 199, 1942; *Mt. W. Contr.*, No. 666.

the nebula consists of an envelope of filaments, about 4'.0 × 6'.0, which inclose an inner diffuse mass, about 3'.2 × 5'.9; the major axis is in position angle 130°. The spectrum of the filaments consists of emission lines, that of the central mass is continuous, but the radio emission cannot be considered as the extension of the visible continuous spectrum into the radio region.[20]

If the visible continuous spectrum is interpreted as thermal emission of the ionized gas, the radio emission must be of nonthermal origin. The observational data do not permit us to decide whether the filaments, the diffuse mass, or both are the seat of the radio emission. More detailed investigation of the size and shape of the source, possibly with the aid of an occultation by the moon, may help to settle this question.

The Crab Nebula is at a distance of 1000 psc. The total radio energy emitted by the nebula thus is 7×10^{32} ergs sec^{-1}.

2. B CASSIOPEIAE

The light-curve of B Cassiopeiae, Tycho Brahe's nova of 1572, shows that, like the Crab Nebula, it was a supernova of type I;[21] but no visible remnant of this supernova has been found.

Recently, Hanbury Brown and Hazard[22] have reported a radio source near the position of the supernova. The pertinent data are in Table 2. The positions of radio source and supernova are in satisfactory agreement, but, particularly in view of the uncertainty of the radio position, the identification can be considered as only tentative. An observation of the size of the source may give supporting evidence, since an angular diameter of the same order as that of the Crab Nebula is to be expected.

Data for a comparison of B Cassiopeiae with the supernova of 1054 are in Table 3.

TABLE 2

B CASSIOPEIAE

α (1950)	δ (1950)	Frequency (Mc/Sec)	m	Observer
$0^h21^m49^s \pm 2^m$	$+64°15' \pm 35'$	158.5	6.1	Hanbury Brown and Hazard*
0^h22^m0	$+64°52'.2$	*pg*	$>+15$	Tycho Brahe†

* *Nature*, **170**, 364, 1952.

† W. Baade, *Ap. J.*, **102**, 309, 1945; *Mt. W. Contr.*, No. 711.

TABLE 3

COMPARISON OF THE SUPERNOVAE OF 1054 AND 1572

	m_v at Maximum	m_{pg} of Remnant	m_v at 158.5 Mc/Sec
AD 1054	-6.5 to -7.0	$+9$	4.0*
AD 1572	-4.0	$>+15$	6.0

* From unpublished data of the Radiophysics Laboratory, Sydney, Australia, communicated by Bolton.

[20] J. L. Greenstein and R. Minkowski, *Ap. J.*, **118**, 1, 1953.

[21] W. Baade, *Ap. J.*, **102**, 309, 1945; *Mt. W. Contr.*, No. 711.

[22] *Nature*, **170**, 364, 1952.

In comparing these two objects, the differences in interstellar absorption cannot be disregarded, but no accurate values are available. It is certain that B Cassiopeiae is heavily obscured compared with the Crab Nebula.

The difference between the visual magnitudes at maximum corrected for interstellar absorption may therefore be quite small, almost certainly smaller than the radio differences between the remnants. But the photographic magnitudes of the remnants after correction for absorption would still differ by more than 4 mag. Since radio and optical emissions of the remnants do not seem to be related phenomena,[20] there is no reason why the differences between the radio and between the photographic magnitudes of the remnants should be identical.

3. UNIDENTIFIED AND UNOBSERVED SOURCES

Of the three known galactic supernovae, two have been observed as radio sources, but the third—Kepler's nova of 1604—is not yet observed, although its remnant has been discovered by Baade.[23] Since its position is close to that of the galactic center, high intensity of the general galactic radiation presents certain difficulties for the observation of this source. But, to make the evidence final that the remnants of supernovae of type I are radio sources, a search for a radio source in the position of Kepler's nova and an attempt to measure its size would be of great value.

In a giant stellar system like the Galaxy, supernovae of type I should appear with a frequency of several, perhaps five, supernovae per 1000 years.[24] Since the relatively high radio intensity of the Crab Nebula shows that the radio emission probably will persist for much more than 1000 years, a certain number of unknown supernova remnants must be observable as individual radio sources. This number could be estimated only if it were known how the radio emission decreases with time. But since the emission seems to be nonthermal,[20] its rate of decay cannot be computed. While it is thus impossible to predict how many unidentified sources might be supernova remnants, it is possible to conclude with some confidence that supernova remnants contribute, at most, an insignificant fraction of the general galactic radiation. It is certain that the radio emission of the Crab Nebula must decrease greatly during the next 20,000 years, when its density reaches that of interstellar space. If the radio emission should continue with undiminished intensity until that time, the 100 supernovae appearing within 20,000 years would emit a total radio energy of 5×10^{34} ergs sec^{-1}, not more than a few tenths of 1 per cent of the total emission of the Galaxy. The actual contribution obviously will be even less.

II. PECULIAR EMISSION NEBULOSITIES

The identification of the source in Cassiopeia and of Puppis A has led to the discovery of a new type of galactic nebulosity,[6] filamentary nebulae with large internal motions. Unusual filamentary structures have been found near the positions of one other source. These filaments do not have quite the same character as those in Cassiopeia and in Puppis A, and no data on their velocities are available. The suggestion that they are sources of radio emission is therefore entirely tentative.

Cygnus X, a region of high radio intensity, was initially considered as a feature of the general galactic emission. Measurements at 1210 Mc/sec by Piddington and Minnett[25] have shown, however, that the emission in this region is very probably due to a strong discrete source extending over many square degrees. The region containing this source is

[23] *Ap. J.*, **97**, 119, 1943; *Mt. W. Contr.*, No. 675; see also R. Minkowski, *Ap. J.*, **97**, 128, 1943; *Mt. W. Contr.*, No. 676.

[24] Actually, three supernovae appeared during the last 1000 years. That these are within 1000 psc of the sun, or in a volume of the order of 1 per cent of that of the Galaxy, must be due to a statistical fluctuation in the galactic distribution, since the resulting frequency of the order of one supernova per 3 years in the Galaxy as a whole is clearly contradicted by the evidence from other giant Sb nebulae.

[25] *Australian J. Sci. Res.*, *A*, **5**, 17, 1952.

shown in Figure 1. The position of the center, $20^h27^m \pm 3^m$, $+40°.5 \pm 1°$, is marked by a cross, and the full-drawn curves are contours of equal aerial beam temperature given by Piddington and Minnett. Recent observations by Hanbury Brown and Hazard[26] confirm these results. Their center, 20^h22^m, $+40°00'$, is marked by a circle, and their curves of equal intensity are drawn as broken curves.

The region near γ Cygni in which this source is located is one of the most complicated parts of the sky, presenting layers of emission nebulosity and heavily absorbing clouds. The following half of Cygnus X is in the most heavily obscured region; obviously, any object in this area would be expected to be hidden from sight. The preceding half is in a more transparent area, and the preceding end may be expected to be affected least by obscuration. Here appear some very unusual filaments. The areas containing these filaments are shown in Figures 2 and 3. The filaments are shown on a larger scale in Figures 4 and 5. Some of these filaments are sharp but longer than those which appear in the Cassiopeia source and in Puppis A; others look like an enlarged picture of the Cassiopeia filaments. Filaments of this type are very rare. Their appearance near that edge of Cygnus X where obscuration is smallest suggests that the radio emission originates in a system of such filaments which is almost entirely hidden by obscuration.[27]

Identification of Cygnus X with thermal radiation from the bright nebulosities surrounding γ Cygni has been suggested by Piddington and Minnett. One obvious objection to this assumption derives from the fact that the Orion Nebula has not been observed as a radio source. This exceptionally dense *H* II region should be barely detectable as a radio source.[20] Compared with it, the Cygnus nebulosities are so much fainter that their thermal radiation cannot be expected to be observable. It is possible, of course, that the heavy obscuration in the galactic plane hides the brightest part of the nebulosity from sight. The nebulosities near γ Cygni and the North America nebula could indeed be the fainter outer parts of an extremely dense *H* II region with observable thermal radio emission, or of several such regions distributed in depth. But, in this case, the radio source should extend in the direction of the galactic equator, not in the direction, inclined about 45°, of Cygnus X. The radio spectrum of Cygnus X can be explained as well by the assumption of nonthermal radio emission combined with the opacity of hydrogen in the low-frequency region[20] as by the assumption of thermal emission from an optically thick *H* II region.

Both the sources in Cassiopeia and Puppis A are near regions in which heavy absorption and diffuse nebulosities appear, and Cygnus X is actually within such a region. It is tempting to assume that they are connected with the interstellar gas, representing regions in which peculiar conditions lead to strong nonthermal emission.

The fact that the only two definitely identified sources of this type seem to have approximately spherical or elliptical outlines suggests some central origin for the peculiar condition, and one might suppose that the nebulosities were formed by an ejection process. But the observed random velocities are so large that they hide so far any expansion which may be present. The largest velocity of expansion admitted by the observations is certainly much smaller than that observed in the Crab Nebula. The conditions in the radio-source nebulosities are thus diametrically opposed to those in the filaments of supernova remnants, where a large velocity of expansion exceeds the relatively small internal random velocities. Moreover, the general appearance of the Cassiopeia nebulosity, with its two distinct kinds of filaments, is entirely different from that of the known remnants of supernovae. Altogether, no observed fact supports the view that the radio-source nebulosities are remnants of supernovae.

[26] *M.N.*, **113**, 109, 1953.

[27] *Added October, 1953:* A spectrogram of one of these filaments has recently been obtained. The composition of the spectrum, which shows *H*α, [N II], and [O II], is normal, and the velocity spread is small. There is therefore no evidence at present that the filamentary structures near Cygnus X are of the same type as the filaments in Cassiopeia source and in Puppis A. Hence the identification of Cygnus X remains an unsolved problem.

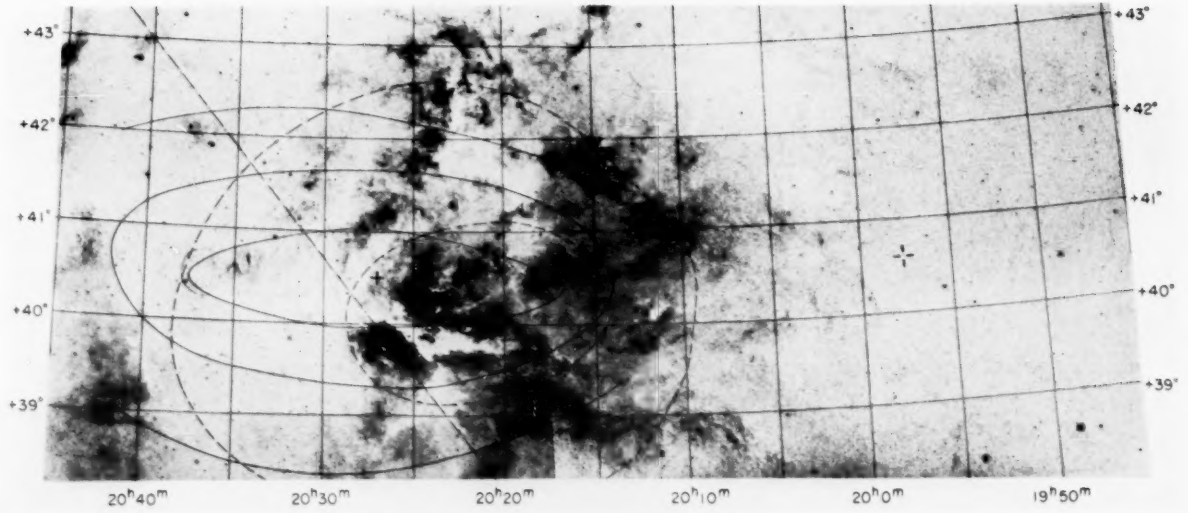

FIG. 1.—Region in Cygnus. Epoch 1950. Galactic equator marked by broken straight line. Cygnus X: Cross at 20^h27^m, $+40°5$ and solid curves from Piddington and Minnett; circle at 20^h22^m, $+40°$ and broken curves from Hanbury Brown and Hazard. Cygnus A is marked by an open cross at $19^h57^m45^s$, $+40°35'36''$.

Fig. 2.—Field in Cygnus. Center (1950) 20^h12^m, $+39°42'$; λλ 6300, 6700; 48-inch; 1 mm = 67″

FIG. 3.—Field in Cygnus. Center (1950) 20^h23^m5, $+39°47'$; λλ 6300–6700; 48-inch; 1 mm = 67″

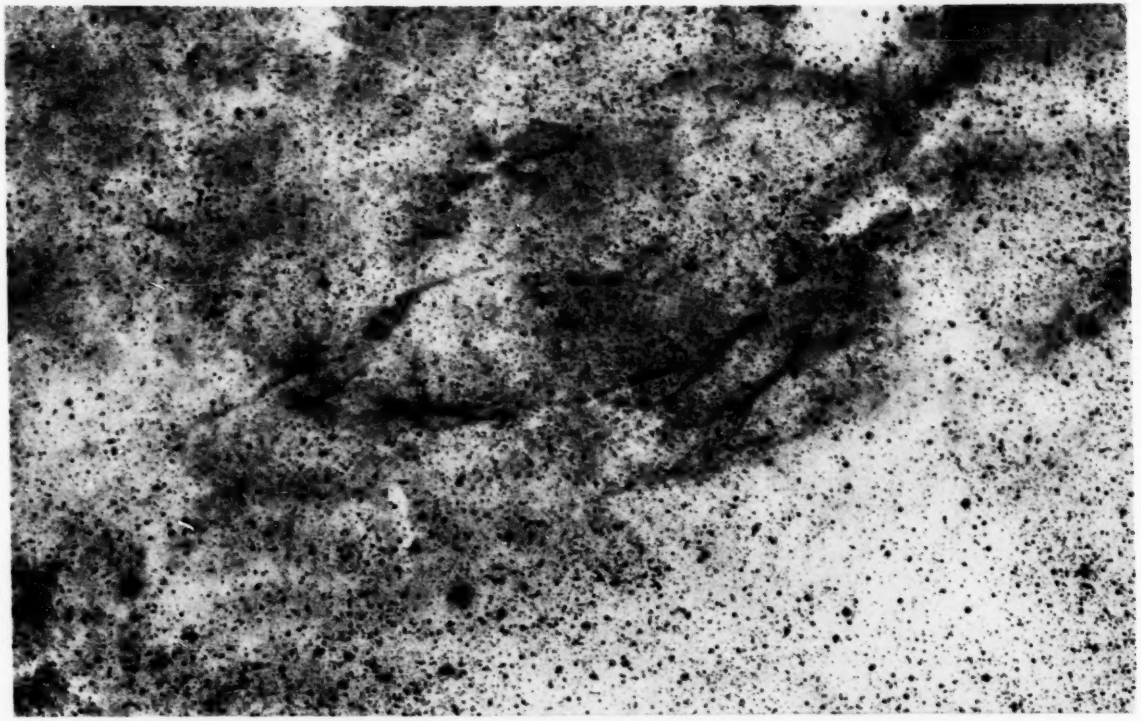

FIG. 4.—Filaments in Cygnus. Center (1950) $20^{h}13^{m}0$, $+39^{\circ}38'7$; λλ 6300–6700; 48-inch; 1 mm = 21″

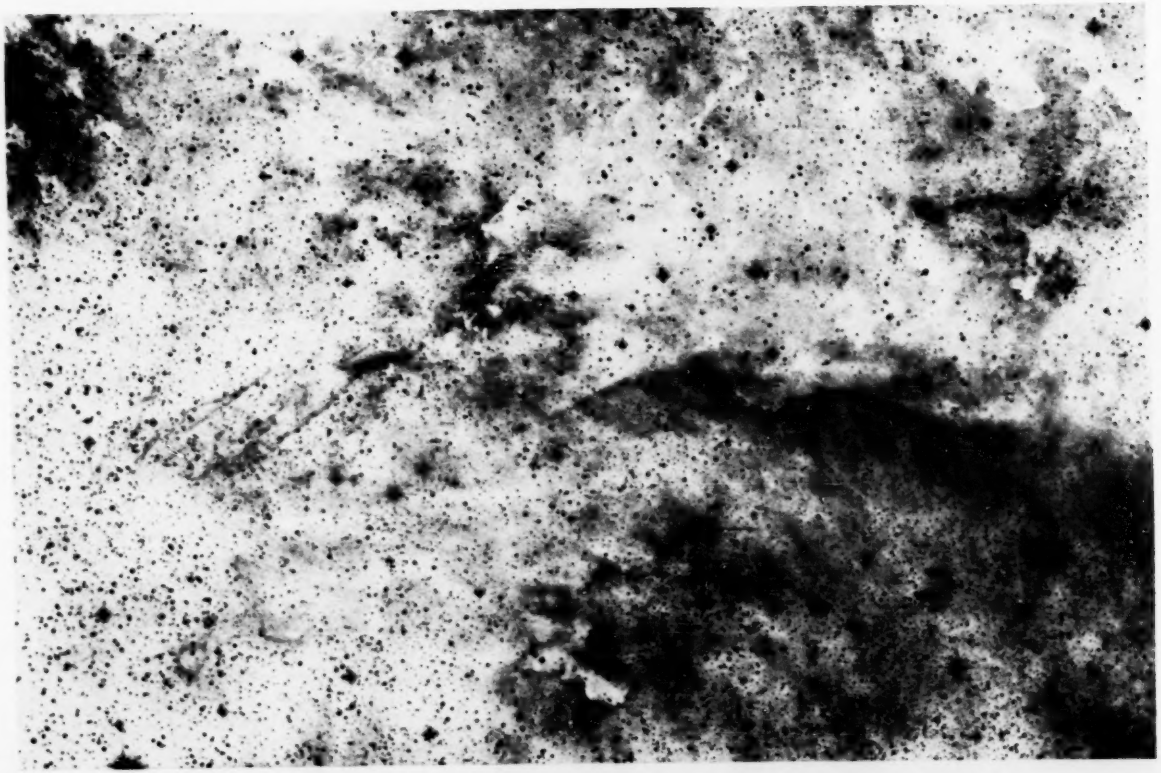

FIG. 5.—Filaments in Cygnus. Center (1950) $20^{h}19^{m}0$, $+39^{\circ}22'.6$; λλ 6300–6700; 48-inch; 1 mm = 21″

All three sources are close to the galactic equator, as is to be expected if they are connected with the interstellar gas and thus belong to population I. Sources of this type may not be the only ones which show strong concentration toward the galactic plane. They are certainly only a part of the group of stronger sources with concentration toward the galactic plane which Mills[3] has grouped in his class I of sources. This class does not represent a homogeneous group of objects but contains at least one extragalactic source, Cygnus A, the remnants of the supernovae of type I which are in population II, and the Cassiopeia type nebulosities which are probably in population I. Radio stars, if they exist, would also be in Mills's class I. The attempts to derive distances from statistical analysis of such an inhomogeneous group are, of course, hopeless. In particular, a high degree of galactic concentration is not necessarily an indication of large distances if sources belonging to population I exist.

A certain number of sources found by Mills and by Hanbury Brown are so close to the galactic plane that they might be population I objects. Most of the positions have by now been inspected on 48-inch Schmidt plates. Almost always the positions were found to be in heavily obscured areas, frequently in the neighborhood of large diffuse nebulosities. Near the galactic plane such a result is not surprising.

Since frequency and distances of the peculiar nebulosities are unknown, their absolute emission cannot be determined, and therefore their contribution to the radiation of the Galaxy cannot be estimated. If the distance of the Cassiopeia source is 300 psc, the total radio emission is 11×10^{32} ergs sec^{-1}, less than 10^{-4} of the total emission of the Galaxy. That the peculiar nebulosities contribute more than an insignificant fraction of the galactic emission is therefore very improbable.

III. PECULIAR EXTRAGALACTIC NEBULAE

The identification of two radio sources with the extragalactic nebulae NGC 4486 (M87) and NGC 5128, first suggested as a possibility by Bolton, Stanley, and Slee,[16] is now well established. Neither of the nebulae is of outstanding apparent brightness, but both show outstanding peculiarities. No explanation can be suggested of why and how the peculiarity in NGC 4486 leads to strong radio emission. Another type of peculiarity, in which the basic features of the physical processes seem obvious, is shown by the strong radio source Cygnus A, where the radio emission is due to a collision of two extragalactic nebulae. It is probable that NGC 1275 and NGC 5128 also belong in this class. Thus the group of peculiar extragalactic nebulae whose radio intensity is disproportionate to their luminosity comprises a variety of objects which cannot be assumed to be fully known at this stage.

1. NGC 4486 (RYLE 12.01; MILLS 12 + 1)

The identification of this source with NGC 4486 was first suggested by Bolton, Stanley, and Slee.[16] The agreement of the positions in Table 4 strongly supports the identification.

The field surrounding NGC 4486 is shown in Figure 6. NGC 4486, in the center of the field, is a member of the Virgo cluster of nebulae. At first sight, it is not obvious why this object should be a relatively strong radio source; it does not differ essentially in size or brightness from other bright members of the cluster. It is shown on a larger scale in Figure 7, clearly a nebula of type E0 with a rich envelope of globular clusters; this is not a rare type of nebula. However, NGC 4486 has a unique peculiarity which has been known for a long time.[28] In the center of the nebula, overexposed in Figure 7, is a straight jet, extending from the nucleus in position angle 290°. This feature, relatively much bluer than the nebula itself, is shown from a shorter exposure in the ultraviolet in Figure 8. Several strong condensations are in the outer parts of the jet, which extends

[28] H. D. Curtis, *Pub. Lick Obs.*, **13**, 31, 1918.

about 20″ from the nucleus and has an average width of about 2″. As a member of the Virgo cluster, NGC 4486 is at a distance[29] of 3×10^6 psc. The linear length of the jet therefore is 300 psc, its average width about 30 psc. The total radio emission of the source is 5×10^{39} ergs sec^{-1}.

Spectra obtained by Humason show that the jet has a continuous spectrum, indicating a rather blue color but showing neither absorption nor emission lines. The nebula has a normal spectrum of type G, but superposed on the nucleus appears a strong emission line of [*O* II] λ 3727, which is shifted relative to the nuclear G-type spectrum by -295 ± 100 km/sec. The interpretation which suggests itself is that the jet was formed by ejection from the nucleus and that the [*O* II] line is emitted by a part of the material which forms the jet and is still very close to, if not still inside, the nucleus. The angle between the jet and the line of sight is not known. If it is assumed that this angle is 45°, tangential and radial velocities are equal, and if the velocity of the ejection has remained constant, the formation of the jet has taken place during a time of 10^6 years.

No possibility exists at this time of forming any hypothesis on the formation of the jet, the physical state of its material, and the mechanism which connects the existence of the jet with the observed radio emission.

TABLE 4

NGC 4486 (RYLE 12.01; MILLS 12 + 1)

α	δ	Frequency (Mc/Sec)	m	Observer
$12^h28^m6^s \pm 37^s$	$+12°41' \pm 10'$	100	3.7	Bolton, Stanley, and Slee;* Stanley and Slee*
$12^h28^m25^s \pm 70^s$	$+12°55' \pm 20'$	81.5	4.0	Ryle, Smith, and Elsmore†
$12^h28^m18^s \pm 3^s$	$+12°37' \pm 10'$			Smith‡
$12^h30^m \pm 2^m$	$+12°30' \pm 20'$	100	3.8	Mills§
$12^h28^m15^s5 \pm 2^s5$	$+12°44' \pm 6'$	100		Mills‖
$12^h28^m18^s$	$+12°40'.1$	*pg*	9.9(SW)	NGC

* J. G. Bolton, G. J. Stanley, and O. B. Slee, *Nature*, **164**, 101, 1949; G. J. Stanley and O. B. Slee, *Australian J. Sci. Res.*, *A*, **3**, 234, 1950.

† *M.N.*, **111**, 508, 1950.

‡ *Australian J. Sci. Res.*, *A*, **5**, 266, 1952.

§ *Australian J. Sci. Res.*, *A*, **5**, 266, 1952.

‖ *Ibid.*, p. 456.

Recent measures by Mills[17] give 5′ as the effective size of the radio source in the east-west direction. Unpublished measures by Mills show an elliptical half-brightness contour of $2'.5 \times 6'.0$ with the major axis in position angle 45°, almost perpendicular to the direction of the jet. Since the diameters of other radio sources obtained in the same series of observations agree well with their visible sizes, there is no obvious reason to doubt the measure for NGC 4486. However, a diameter of 5′ is of the order of the diameter of the whole system, as can be seen from Figure 7. Therefore, if the measured effective size of the source is correct, the radio emission is not confined to the jet but is distributed through the whole nebula. The jet would then be only the visible sign of a peculiar condition extending over a volume 10^6 times larger than the jet.

2. NGC 1275 (MILLS 03 + 4)

A radio source possibly identical with Ryle 03.02 observed by Hanbury Brown and Hazard[8] and by Mills[3] coincides with the Perseus cluster of extragalactic nebulae shown

[29] All distances for extragalactic objects in this paper are still given on the old scale, and the recent correction to the zero point of the type I cepheids has been disregarded. This correction leads to an increase by a factor of about 2 for all extragalactic distances.

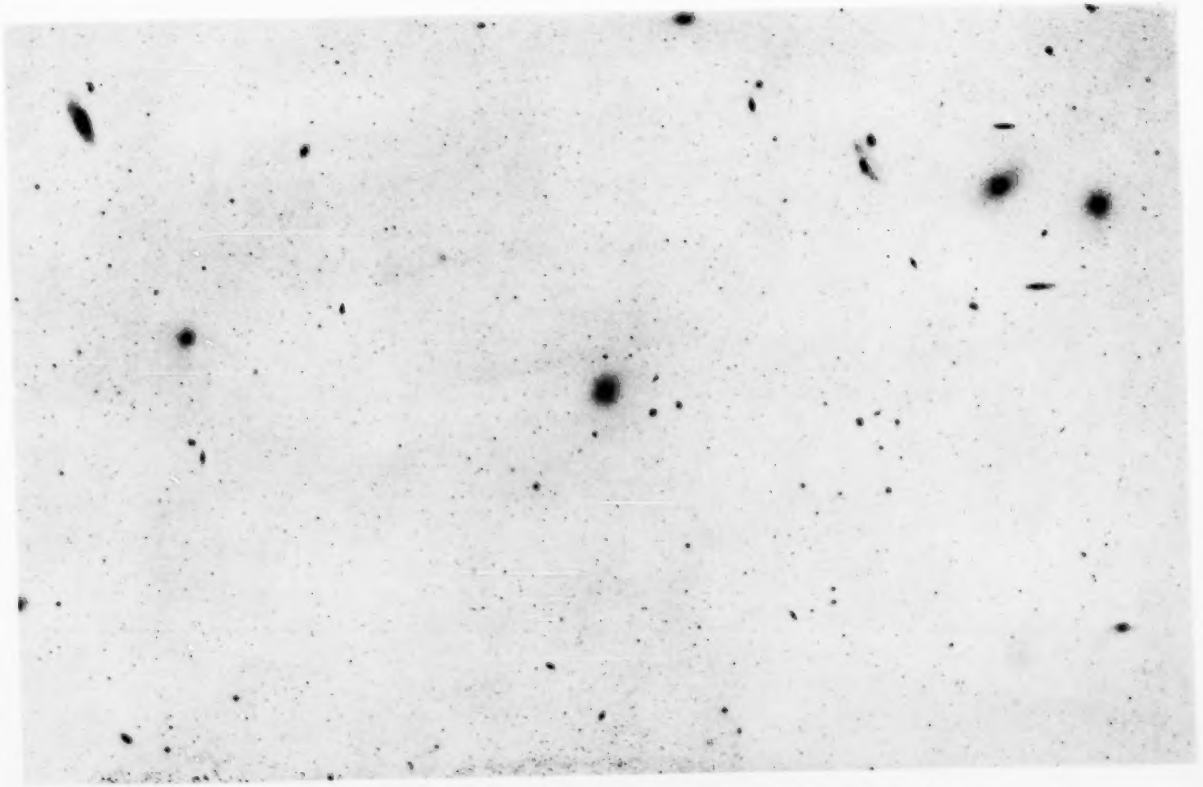

FIG. 6.—Field in Virgo. NGC 4486 in center. λλ 3600–5000; 48-inch; 1 mm = 67″

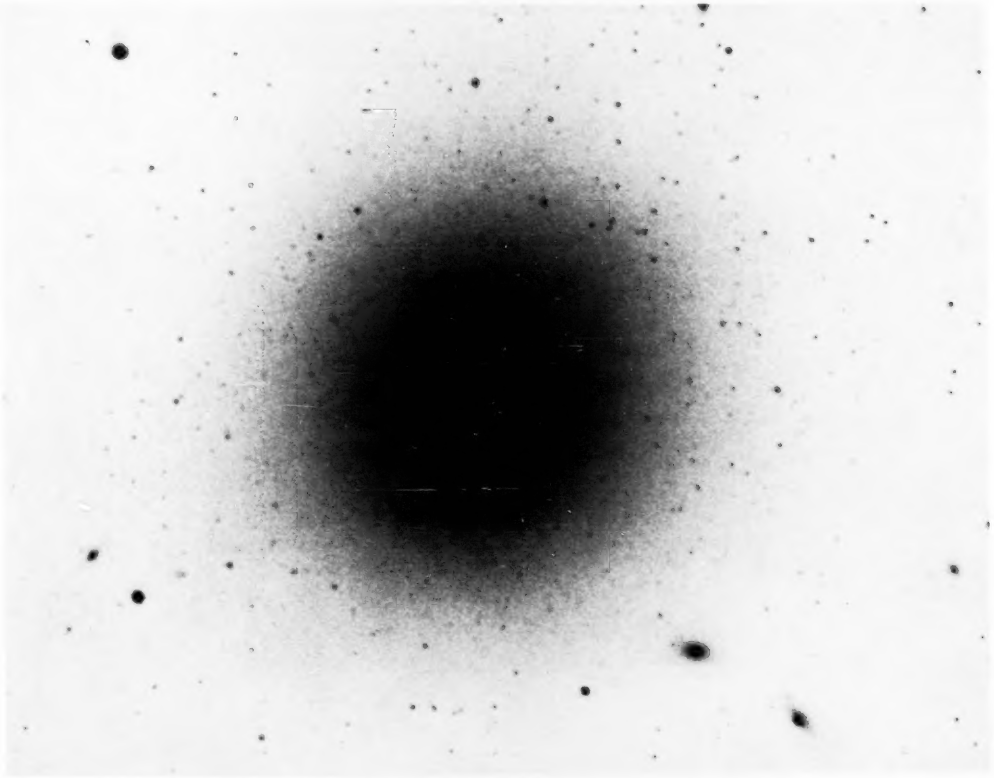

FIG. 7.—NGC 4486, λλ 3600–5000; 200-inch; 1 mm = 2".2

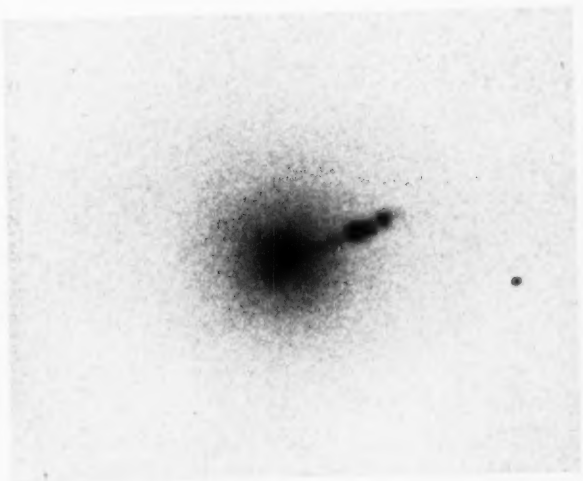

FIG. 8.—Center of NGC 4486. $\lambda < 4000$; 100 inch; 1 mm = 0".8

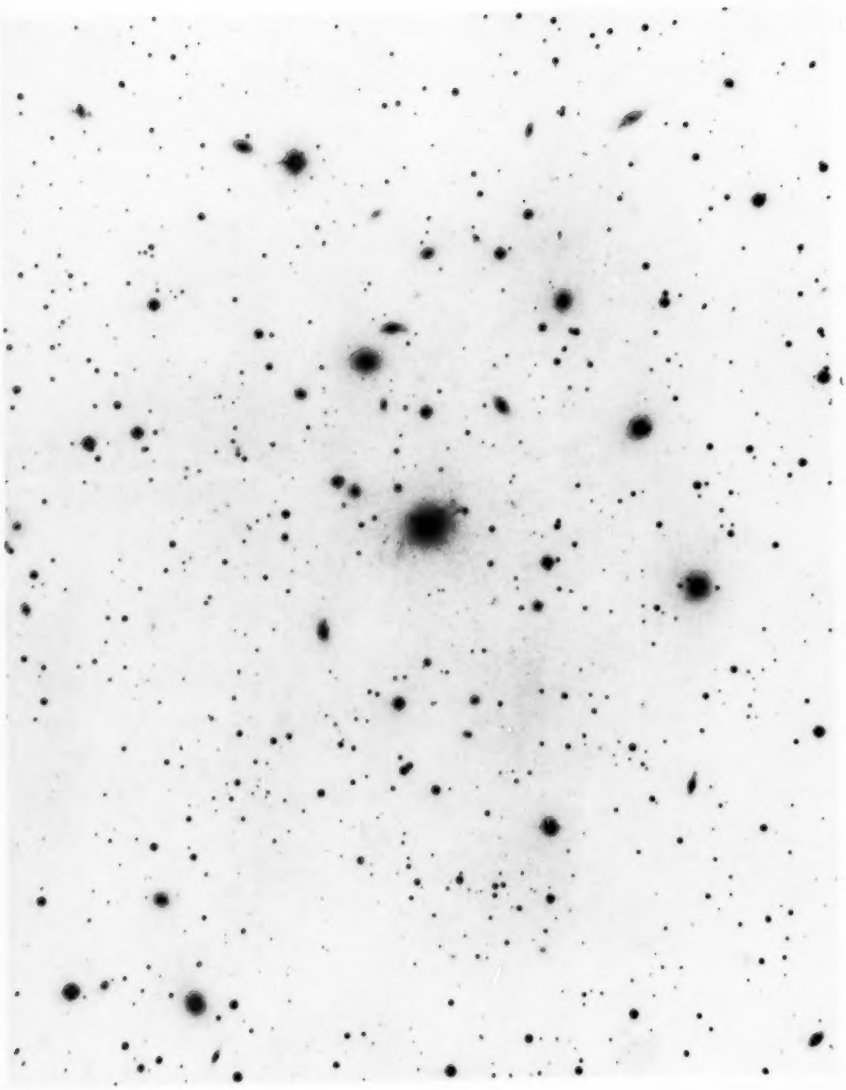

FIG. 9.—Cluster of nebulae in Perseus. λλ 3600–5000; 200-inch; 1 mm = 7".4

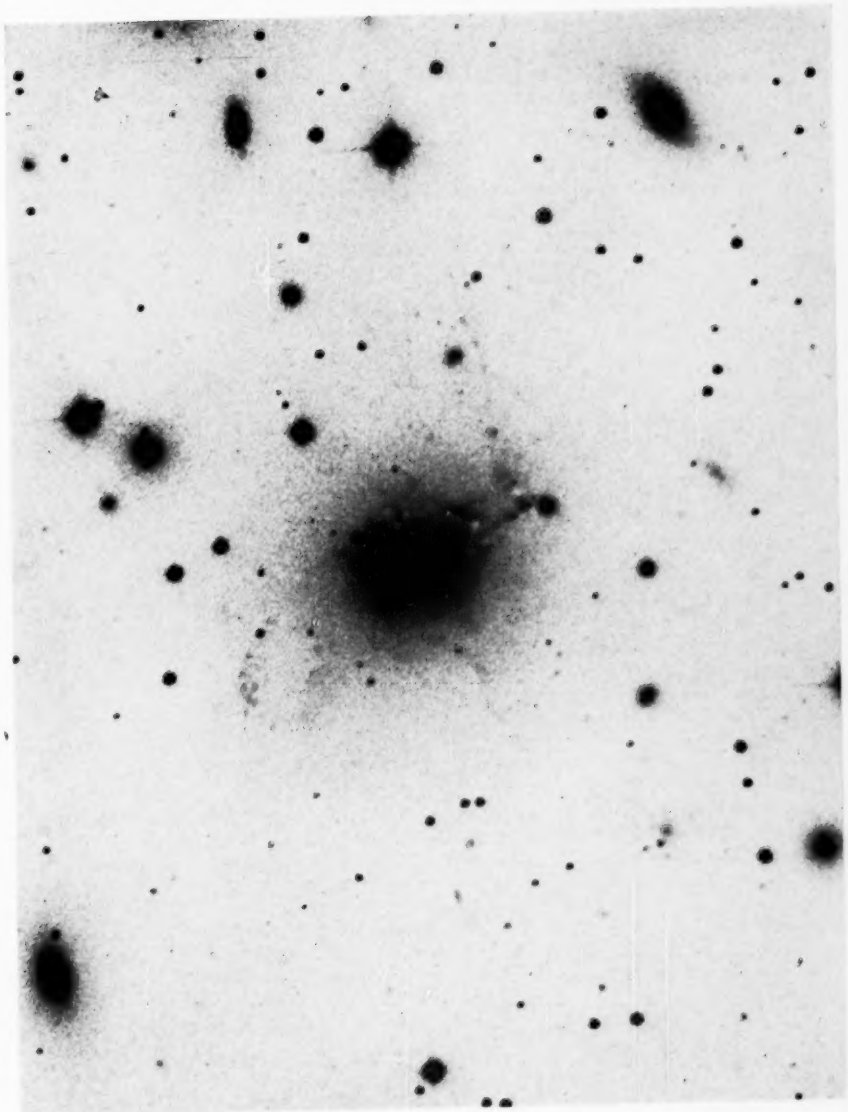

FIG. 10.—NGC 1275. λλ 3600–5000; 200-inch; 1 mm = 2″.0

in Figure 9. The identification of this source with the cluster as a whole is not convincing. Not only is the source more intense than one would infer from the integrated brightness of the cluster on the assumption that the cluster contains normal nebulae only, but other clusters which should be observable on the same basis have not yet been found to be radio sources. This suggests that actually not the cluster but a peculiar nebula in the cluster is the radio source. The Perseus cluster, indeed, contains as its brightest member a highly peculiar nebula, NGC 1275, shown enlarged in Figure 10. Since the position of this nebula is usually given for that of the cluster, the coincidence of the positions, in Table 5, remains unchanged.

The structure and the colors of NGC 1275 admit of only one interpretation—that this object shows an apparently tightly wound nebula of the spiral type penetrating from the south a late-type, very loose spiral whose arms are entirely distorted by strong

TABLE 5

POSITIONS OF NGC 1275 (MILLS 03 + 4)

α	δ	Frequency (Mc/Sec)	m	Observer
$3^h15^m15^s+90^s$	$+41°22'+30'$	158.5	7.2	Hanbury Brown and Hazard*
$3^h10^m+4^m$	$+42°+20'$	100	5.6	Mills†
$3^h16^m52^s$	$+40°50'$	.....	.....	Mills‡
$3^h16^m15^s$	$+41°19'$	*pg*	13.28 (P)	NGC

* *Phil. Mag.*, **43**, 137, 1952.

† *Australian J. Sci. Res.*, *A*, **5**, 266, 1952.

‡ Unpublished. This position has very little random error but considerable uncertainty caused by interfering sources.

tidal forces. Thus NGC 1275 may present a case of radio emission caused by a collision of two nebulae.

Like Cygnus A, NGC 1275 shows emission lines in its spectrum, but superposed on a strong continuous spectrum which contains most of the light.[30] It has been considered as belonging to the group of nebulae whose nuclei show emission lines,[31] but it deviates from the other nebulae of this type in some respects. Exposures with different plate-filter combinations suggest that the emission in NGC 1275 is not restricted to the nuclear region. The width of all emission lines in NGC 1275 seems to be of similar size, corresponding to approximately 4500 km/sec, while pronounced differences are observed in the nebulae with nuclear emission. The hydrogen lines in these objects are very much wider than the forbidden lines, which show individual differences. The forbidden lines in NGC 1275 are unusually wide, but the pronounced asymmetry observed on only one plate for one [*O* III] line cannot be considered as definitely established. The evidence suggests that NGC 1275 does not belong to the group of nebulae with nuclear emission, none of which has been observed as a radio source.

At a distance of 9×10^6 psc, NGC 1275 emits a total radio energy of 7.5×10^{39} ergs sec^{-1}, roughly 1000 times less than Cygnus A, but still about 300 times more than the Galaxy.

3. NGC 5128 (MILLS 13 − 4)

The identification of the source Centaurus A with NGC 5128, first suggested by Bolton, Stanley, and Slee,[16] appears well supported by the later, more precise positions given in Table 6. Recent measures of the effective size of the source by Mills[17] give a value of 6′, which agrees with the diameter of the bright central part of the nebula

[30] M. L. Humason, *Pub. A.S.P.*, **44**, 267, 1932.

[31] C. K. Seyfert, *Ap. J.*, **97**, 28, 1943; *Mt. W. Contr.*, No. 671.

shown in Figure 11. Unpublished measures by Mills show an elliptical half-brightness contour of $1.'3 \times 7'$ with the major axis in position angle 135°. This contour is shown in Figure 13 superimposed on the image of NGC 5128. There can be no doubt that the radio emission is associated with the absorption band extending across the nebula. Bolton [32] finds that the strong concentration near the center of the source is surrounded by an extended source nearly 2° in diameter. This is definitely larger than the visible size of the nebula, which does not exceed 30′ in any direction.

NGC 5128 is an unresolved E0 nebula with an unusually strong and wide central absorption band, a combination highly anomalous for a spherical nebula. On plates taken with the 48-inch Schmidt telescope (Fig. 12), however, faint outer parts of the nebula become visible, which extend in position angle 45°, a direction almost normal to that of the absorption band. This suggests a new interpretation, that the object actually consists of two nebulae—an elliptical nebula with the major axis in position angle 45°

TABLE 6

NGC 5128 (MILLS 13 − 4)

α	δ	Frequency (Mc/Sec)	m	Observer
$13^h22^m20^s \pm 60^s$	$-42°37' \pm 8'$	100	3.3	Bolton, Stanley, and Slee; Stanley and Slee*
$13^h20^m \pm 2^m$	$-43° \pm 10'$	100	3.6	Mills†
$13^h22^m30^s \pm 4^s$	$-42°46' \pm 2'$	100	2.8	Mills‡
$13^h22^m28^s$	$-42°45'.6$	*pg*	7.2 (SA) 6.1 (corrected)	NGC

* J. G. Bolton, G. J. Stanley, and O. B. Slee, *Nature*, **164**, 101, 1949; G. J. Stanley and O. B. Slee, *Australian J. Sci. Res.*, *A*, **3** 234, 1950.

† *Australian J. Sci. Res.*, *A*, **5**, 266, 1952.

‡ *Ibid.*, p. 456.

and a second nebula of much later type, seen practically edgewise in position angle 135°. This second system, probably a spiral, contains the heavy absorption lanes and lies in front of the E nebula. Near the outer parts of the absorption lanes, the structure typical for beginning resolution of spiral arms can be seen. The curvature of the outer parts of the spiral system and the irregular distribution of absorbing clouds outside the main absorption bands clearly indicate tidal distortion by the E nebula. The two nebulae thus are not merely optically superimposed but form a close pair in a state of strong gravitational interaction, perhaps actually in collision.

Since the E nebula presumably contains little interstellar gas, the strong radio emission may not be caused by the interaction of the gas of one system with that of the other. Differential velocities in the gas of the late-type system, produced by tidal forces, may lead to collisions of gas clouds within this system.

Spectrograms obtained with the nebular spectrographs at the 100-inch telescope by Minkowski and at the 200-inch telescope by Humason show a spectrum of type Gp with λ 3727 [OII] in emission in the brightest part of the spherical mass south of the absorption lane. The brightest patch near the north edge of the absorption lane shows, in addition, *Hβ* and *Hγ* as emission lines. The radial velocity is +450 km/sec. There are indications of velocity differences within the nebula. Both type of spectrum and radial velocity confirm the extragalactic nature of NGC 5128. Hubble's observation[33] of *H* lines in emission on objective-prism plates is verified; the *He* II line λ 4686 reported by Hubble has not

[32] J. G. Bolton, "Extended Sources of Galactic Noise," Union radio-scientifique internationale Report (1952).

[33] *Ap. J.*, **56**, 162, 1922; *Mt. W. Contr.*, No. 241.

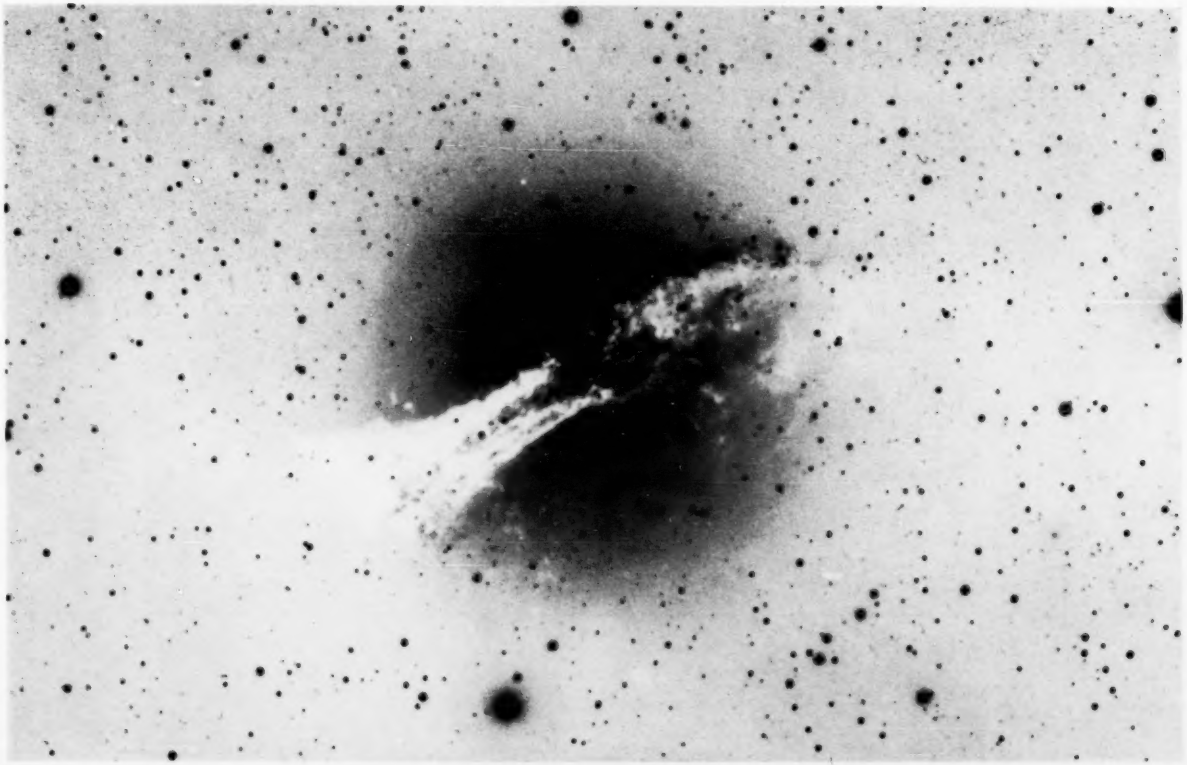

FIG. 11.—NGC 5128. λλ 5500–6300; 200-inch; 1 mm = 5".5

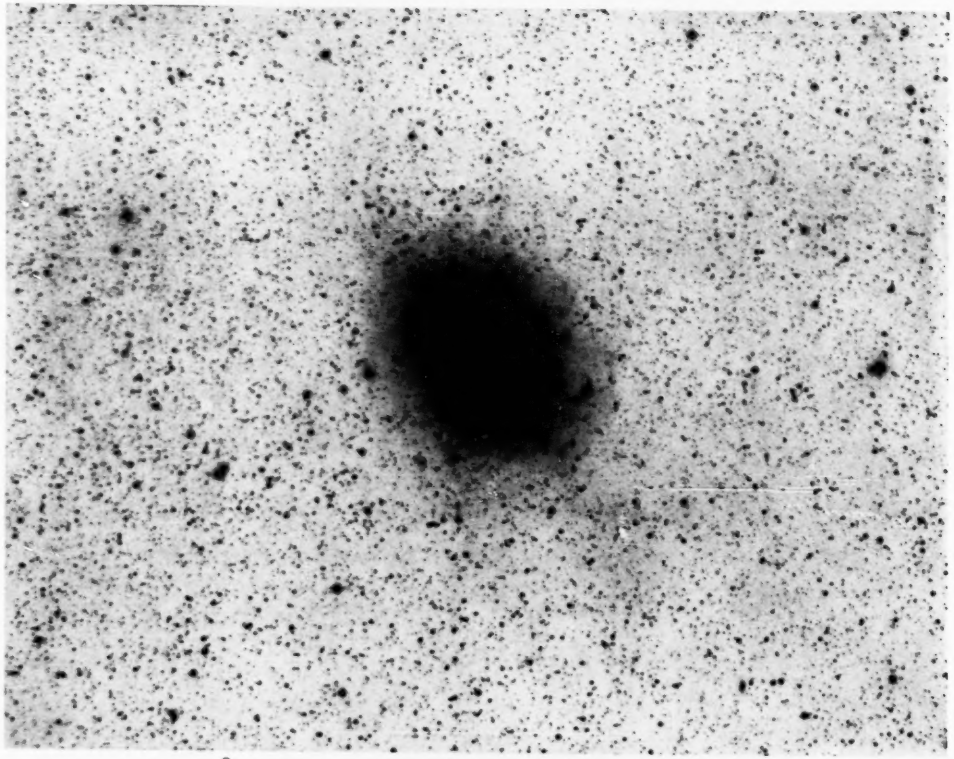

FIG. 12.—NGC 5128. λλ 6300–6700; 48-inch; 1 mm = 37″

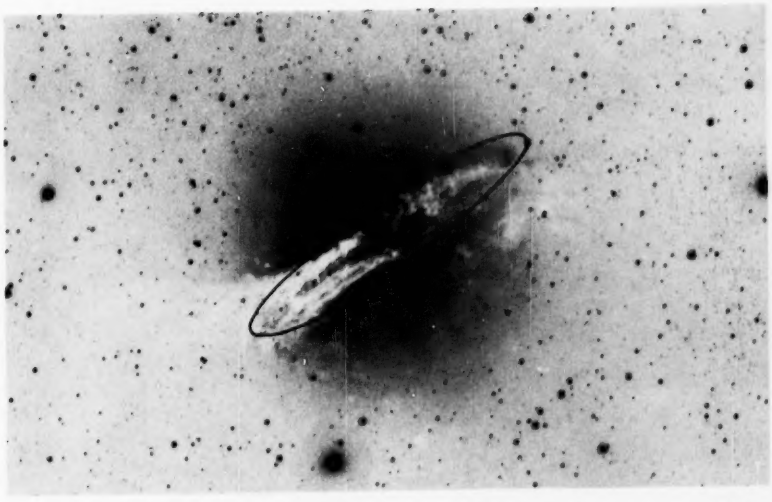

FIG. 13.—NGC 5128. The half-brightness contour by Mills is superimposed. 1 mm = 8".3

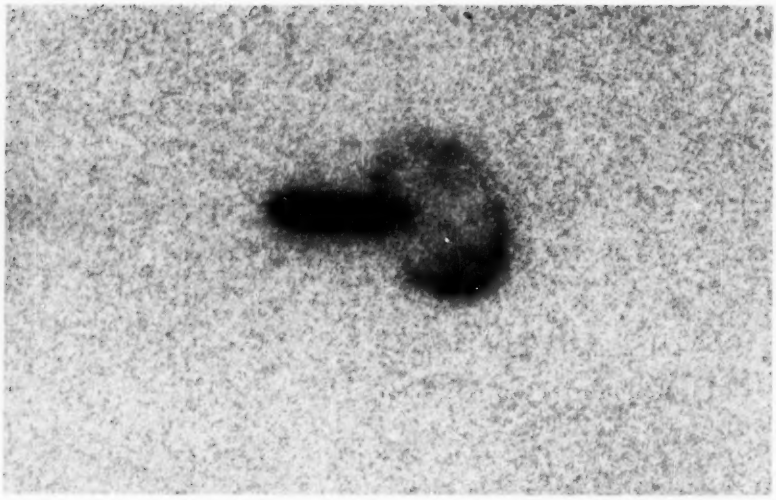

FIG. 14.—Mayall's object. (1950) 11^h1^m2, $+41°7'$; λλ 3500–5000; 1 mm = 0.8

been found on the slit spectrograms but could be present in other parts of the object. The system is too far south for extensive work on Mount Wilson or Palomar, but a more detailed spectroscopic investigation would be of great value.

The distance of NGC 5128 is not known but must be greater than that of NGC 224, since the spherical mass remains entirely unresolved with the 200-inch telescope and only beginning resolution can be seen in the spiral system near the outer parts of the absorption lanes. With a distance larger than 5×10^6 psc and $m_{pA} = 6.1$ (see Table 6), the system is brighter than $M_{pg} = -17.5$, without correction for the effects of the heavy absorption in the system and of galactic interstellar obscuration at the relatively low galactic latitude 20°. Most of the light belongs to the E nebula, which thus must be one of the most luminous spheroidal galaxies, near the upper end of the luminosity function. The total radio emission of the source at a distance of more than 5×10^6 psc is larger than 1.3×10^{38} ergs sec^{-1}, or at least about 10 times larger than that of NGC 224. The observed radio emission is probably too strong to consider NGC 5128 as a normal system, as far as radio emission is concerned.

4. UNIDENTIFIED SOURCES

Cygnus A is without doubt an object of exceedingly rare type. But its intensity is so high that at a 10 times larger distance it would still be an easily observable source. At such a distance it would cease to be an optically observable astronomical object; and even at a distance of only twice that of Cygnus A recognition as a peculiar nebula and observation of the spectrum would become very difficult. Thus a large volume of space is easily accessible to radio observations but is practically or entirely beyond the limit of astronomical work, even with the largest telescope. The number of observed or observable sources in this volume cannot be determined. It may be sizable, and it would be no contradiction to any known fact if the majority of the unidentified sources should turn out to be of this type. Whether this is so, only the future can decide.

Less effective collisions than in Cygnus A should be more numerous. But even collisions of the type producing the radio emission of NGC 1275 and NGC 5128 are relatively rare. Certainly, not every close approach or tidal distortion of two nebulae causes enhanced radio emission. We are not yet in a position to predict whether an object representing some kind of collision is likely to be a radio source of enhanced intensity, and some object of this kind can almost always be found in the large area admitted by positions of low accuracy. Occasionally a rather peculiar object can be found, as, for instance, the queer galaxy (Fig. 14) discovered by N. U. Mayall[34] at the Lick Observatory which is near the source 11.01 of Ryle, Smith, and Elsmore. Since other objects of similar character are not observed as radio sources, it does not seem justified to consider such objects even as tentative identifications on the basis of positions of low accuracy.

IV. NORMAL EXTRAGALACTIC NEBULAE

The identification of some faint radio sources with near-by extragalactic nebulae was first suggested by Ryle, Smith, and Elsmore.[2] Any doubt that normal extragalactic nebulae are observable radio sources was removed when Hanbury Brown and Hazard[35] were able to show that the size and shape of the radio source coinciding with the Andromeda Nebula (NGC 224) agree with those of the nebula and that the total intensity of the source is comparable to the integrated intensity of the Galaxy, a system closely similar to NGC 224. The total emission of NGC 224 is 9×10^{36} ergs sec^{-1}, that of the galaxy 24×10^{36} ergs sec^{-1}. The conclusion that normal extragalactic nebulae are radio sources is also supported by the way in which the record of the background radiation obtained by Hanbury Brown and Hazard[8] shows the Ursa Major cloud of nebulae. This

[34] R. T. Smith, *Pub. A.S.P.*, **53**, 187, 1941.

[35] *M.N.*, **111**, 357, 1951.

region, rich in nebulae from the tenth to the thirteenth magnitude, is quite correctly outlined as a broad maximum near right ascension 12^h at declinations 44°–51°.

Data on the radio sources for which identification with normal extragalactic nebulae has been suggested are in Table 7. With the exception of NGC 598, which is outside the region accessible to the Manchester paraboloid, the sources reported first by Ryle, Smith, and Elsmore have been reobserved by Hanbury Brown and Hazard, who have added three sources which may be identified with normal extragalactic nebulae. The radio intensities of the brighter nebulae at 81.5 Mc/sec are somewhat higher, compared to those at 158.5 Mc/sec, than the expected difference, which is between 1.0 and 1.5 mag.; but this obviously is not a significant discrepancy.

The data now available are not sufficient to decide whether there is a fixed ratio between optical and radio intensity for normal extragalactic nebulae. The conclusion by Hanbury Brown and Hazard that the ratio of radio intensity to brightness increases with decreasing apparent brightness was derived by including the source in Perseus, assumed to be the cluster of nebulae. Since it is much more probable that this source is NGC 1275—a peculiar nebula which should be excluded—the question of a possible dependence of observed radio emission on apparent brightness is actually quite open. The data are not inconsistent with the assumption of a fixed ratio between radio and optical intensity. For the following discussion it is adequate to consider the radio magnitudes both at 81.5 Mc/sec and at 158.5 Mc/sec as of the same order as the photographic magnitude.

All the extragalactic nebulae suggested as radio sources are spirals of types Sb and Sc. The general galactic radiation may be included in this statement. It represents the normal radiation of the Galaxy, an Sb spiral. The obvious question arises as to whether there is any significance in the fact that no elliptical nebula has been observed as radio source.

Elliptical nebulae in general are relatively faint. The apparently brightest nebulae of the type are

NGC 205, $m_{pg} = 8.89$ (H)
NGC 221, $m_{pg} = 9.06$ (H)
NGC 3115, $m_{pg} = 9.8$ (SA); corrected, 9

Fornax system, $m_{pg} = 9.1$[36]
Sculptor system, $m_{pg} = 8.8$[36]

These nebulae, all of almost equal apparent brightness, may be expected to be sources with an intensity of the order of 10^{-25} watts m^{-2} $(c/sec)^{-1}$. The companions of the Andromeda Nebula—NGC 205 and NGC 221—are within range and above the limit of detectability for the Manchester paraboloid but are so close to NGC 224, which is almost 5 mag. brighter, that they cannot be expected to be easily observable. The other three nebulae are well isolated, but their expected intensity is well below the limit reached in the survey by Mills.[3] That no elliptical nebula has been observed as a radio source is thus in agreement with expectation, if a fixed ratio between optical and radio intensity exists, and permits no conclusions concerning the contribution of interstellar gas to the galactic radio emission.

Much more serious questions are raised by the fact that no sources have been observed in the positions of certain objects which, on the basis of their brightness, should be observable. Since the discussion of the general galactic radiation suggests that it originates in objects belonging to population II, it is appropriate to discuss separately the unobserved nebulae according to their content of population I and II.

Systems which are rich in population I are nebulae of type Sc and irregular nebulae of the type of the Large Magellanic Cloud.[37] The Large Magellanic Cloud, $m_{pg} = 1.2$, should be a very strong source, with an expected intensity of 10^{-22} watts $m^{-2}(c/sec)^{-1}$, comparable to Cygnus A and Cygnus X but spread over an area in the sky almost 10

[36] W. Baade, *Ap. J.*, **100**, 147, 1944; *Mt. W. Contr.*, No. 697.

[37] S. C. B. Gascoigne and G. E. Kron, *Pub. A.S.P.*, **65**, 32, 1952.

TABLE 7

NORMAL EXTRAGALACTIC NEBULAE IDENTIFIED AS RADIO SOURCES

OBJECT	TYPE	M_{pg}	POSITION OF NEBULA (1950)		m_{pg}	POSITION OF SOURCE (1950)		FREQUENCY (MC/SEC)	m_R	OBSERVER
			α	δ		α	δ			
NGC 224	Sb	−18.1	0^h40^m0	+41° 0′	4.33 (H)	$0^h42^m \pm 6^m$	+38° ± 5°	81.5	5.6*	Ryle, Smith, and Elsmore, 00.01†
						$0^h40^m15^s \pm 30^s$	+40°50′ ± 20′	158.5	6.0	Hanbury Brown and Hazard‡
NGC 598§	Sc	−16.1	1 31.1	+30 24	6.19 (H)	$1^h25^m \pm 5^m$	+30° ± 3°	81.5	6.8	Ryle, Smith, and Elsmore, 01.01†
NGC 891‖	Sb		2 19.3	+42 7	10.85 (H)	$2^h16^m \pm 3^m$	+44°15′ ± 2°	81.5	7.2	Ryle, Smith, and Elsmore, 02.01†
						$2^h19^m \pm 3^m$	+42°10′ ± 30′	158.5	9.3	Hanbury Brown and Hazard#
NGC 3031	Sb	−16.2	9 51.5	+69 18	7.85 (H)	$9^h51^m20^s \pm 2^m$	+69° ± 1°	158.5	9.3	Hanbury Brown and Hazard**
NGC 4258	Sb	(−15.6)	12 16.5	+47 35	9.4 (SW)	$2^h15^m0 \pm 5^m$	+47°30′ ± 1°	158.5	9.8	Hanbury Brown and Hazard#
NGC 5194	Sc	−15.3	13 27.6	+47 27	8.88 (H)	$13^h26^m \pm 4^m$	+48° ± 3°	81.5	7.8	Ryle, Smith, and Elsmore†
+5195	Irr				10.47 (H)	$13^h27^m30^s \pm 2^m$	+46°45′ ± 45′	158.5	9.7	Hanbury Brown and Hazard#
NGC 5457	Sc	−15.8	14 1.4	+54 35	8.20 (H)	$14^h1^m \pm 2^m$ ††	+51° ± 2° ††	81.5 158.5	7.1 9.1	Ryle, Smith, and Elsmore† Hanbury Brown and Hazard#

* This value is based on Ryle's revised intensity of 2.5×10^{-24} watts m^{-2} $(c/sec)^{-1}$, quoted by G. Westerhout and J. Oort, *B.A.N.*, **11**, 332, n. 3, 1951.

† *M.N.*, **110**, 508, 1950.

‡ *M.N.*, **111**, 357, 1951. The value of M_R is corrected according to a recent letter.

§ Recent unpublished results by J. G. Bolton suggest that the source observed by Ryle is a blend of two sources, one at $1^h38^m \pm 2^m$, +32° ± 1°; the other at $1^h30^m \pm 2^m$, +28° ± 2°. The identification of NGC 598 therefore remains doubtful.

‖ Hanbury Brown and Hazard have suggested identification of this source with the cluster of nebulae centered on NGC 911 (2^h22^m7, +41°43′). Both position and intensity of the source agree better with NGC 891 than with that of the cluster. According to private communication by Hanbury Brown, a second source is 1° north. Possibly the observation by Ryle, Smith, and Elsmore may represent the blend of these two sources.

Phil. Mag., **43**, 137, 1952.

** *Nature*, **172**, 853, 1953.

†† The presence of a source separated from the position of NGC 5457 by about 2° made the measurements of the weak source at the position of the nebula unreliable.

times larger than Cygnus X and therefore probably difficult to observe. With $M_{pg} = -15.9$, it is almost as luminous as the most luminous spirals of type Sc. According to a private communication, attempts by the Australian observers recently have succeeded in detecting radio emission from the Large Magellanic Cloud, but the intensity of this radiation is still uncertain. Two unobserved nebulae of type Sc are NGC 253, $m_{pg} = 7.0$ (SA; corrected, 6.0), in the region and probably well above the limit of the survey by Mills; and NGC 2403, $m_{pg} = 8.79$ (H), within reach and presumably above the limit of the Manchester paraboloid. At variance with this negative evidence is the fact that three radio sources have been identified with Sc nebulae. However, the identification of NGC 598 is made doubtful by the new results by J. G. Bolton;[38] and some doubt arises also concerning the identification of NGC 5457, since Hanbury Brown and Hazard found that the presence of a near-by stronger source made the measurements of the weak source in the position of the nebula unreliable. The identification of NGC 5194/5195 seems valid. The fainter component of this double nebula—NGC 5195—is a somewhat irregular E nebula containing population II. Within the uncertainties of the intensities, it is quite possible that a large part of the observed radio emission is due to NGC 5195. Thus there is at present no undebatable evidence that any Sc nebula is observed as a radio source. Altogether, the present evidence seems to suggest that population I contributes little to the radio emission, except the weak contribution of the ionized gas and of individual sources of the Cassiopeia type. Continued attempts to observe the Large Magellanic Cloud and Sc nebulae are of obviously great importance.

No doubt exists that Sb nebulae are observable radio sources, since the identification of NGC 224 is absolutely certain. A search for unobserved nebulae therefore is necessary not to prove that Sb nebulae are observable radio sources but to find out how close the correlation is which seems to exist between apparent brightness and radio intensity. The brightest Sb nebula which is still unobserved is NGC 4736, $m_{pg} = 8.4$ (B), within reach and above the limit of the Manchester paraboloid. This nebula is not bright enough to consider it as significant that it has not yet been observed. More important is the question of whether the Small Magellanic Cloud is an observable source. It clearly contains population I, as indicated by the presence of emission nebulae,[39] but it seems to contain a much higher content of population II than does the Large Magellanic Cloud. The Small Magellanic Cloud, $m_{pg} = 2.8$, should be a strong source of intensity 3×10^{-23} watts $m^{-2}(c/sec)^{-1}$. Its area is roughly half, its surface brightness only little less than, that of the Large Magellanic Cloud. According to private communication, attempts by the Australian observers have not yet definitely established radio emission from the Small Magellanic Cloud. If the Small Magellanic Cloud is really not a radio emitter of the expected order of intensity, the most plausible conclusion would be that the correlation between radio emission and photographic brightness is very loose. It would be premature to draw such a conclusion now, but a more systematic investigation of the correlation between radio intensity and brightness would be of the greatest value for the interpretation of the galactic radiation.

V. RADIO STARS AND THE GENERAL GALACTIC RADIATION

No star, except the sun, has been observed as a radio source. To permit the identification of a stellar source, the accuracy of its position has to be substantially the same as that of good optically determined positions, unless radio stars are spectroscopically highly peculiar. Since radio stars have not been found among the large variety of known peculiar stars, the probability of finding spectroscopic support for an identification is not large. A slim chance may exist of obtaining positions of the required high accuracy from observations of the occultation of sources by the moon.

[38] See Table 7, note to NGC 598.

[39] See, e.g., K. G. Henize and Freeman D. Miller, *Pub. Obs. U. Michigan*, **10**, 75, 1951.

Under the impression of the result that all sources so far identified are extended or of extragalactic origin, the concept of stars as radio sources has dropped into the background. It seems necessary to emphasize that an interpretation of the distribution of the general galactic radiation meets great difficulties without the assumption that radio stars exist.

A comparison of the distribution of the general galactic radiation with the distribution of stars, gas, and dust meets obvious difficulties in the immediate neighborhood of the galactic plane. Within a latitude range of about $\pm 3°$, thermal radio emission from the ionized regions of the interstellar gas should be observable. Results by Ryle and Scheuer[40] show, indeed, a narrow peak in the intensity profile across the galactic equator at longitudes between 338° and 16°, which probably represents the gas emission. A similar contribution from the ionized gas to the intensity profile at the longitude of the galactic center is suggested by unpublished measures by Bolton. Since the radio spectrum of the thermal gas radiation differs from that of the general galactic radiation, it should be possible to separate the two components.[41] But even if the true distribution of the radiation along the galactic equator can thus be established, a valid comparison with astronomical data is made difficult by the effects of heavy obscuration, which permits no more than spotty and incomplete astronomical observations. A discussion of the relation between the distributions of general galactic radiation and astronomical objects must, therefore, be based either on general features of the galactic distribution or on more local information from unobscured regions.

That the galactic radiation cannot be interpreted as thermal radiation of the interstellar gas and is most likely connected with the population II was first pointed out by Unsöld.[42] It is indeed obvious that the general galactic radiation is concentrated much less toward the galactic plane and much more toward the galactic center than the B-type stars[43] and the diffuse nebulae.[44] This is a clear indication that the general galactic radiation does not originate in objects which are part of population I. This conclusion is also suggested by the dissimilarity between the distributions of the continuous galactic radiation and of the 21-cm emission from neutral hydrogen. Christiansen and Hindman[45] emphasize certain similarities between these distributions. These similarities, however, are not conclusive. They arise mainly from the appearance of weak maxima of the continuous radiation near certain positions where the line emission has very strong maxima. A certain similarity of this kind is to be expected as long as the distribution of the continuous radiation is not freed from the possible weak contributions of thermal radiation from the ionized gas and from the effects of unresolved discrete sources, which belong to population I.

A comparison of the intensity distribution of the general galactic radiation with a model of the galactic system by Westerhout and Oort[46] indicates satisfactory agreement of the distribution of the radiation at 100 Mc/sec as measured by Bolton and Westfold[47]

[40] *M.N.*, **113**, 3, 1953.

[41] An attempt to make this separation has been carried out by I. S. Shklovski (*Astr. J. U.S.S.R.*, **29**, 418, 1952). The use of a heterogeneous set of data found by various observers gives this attempt very little weight. The resulting galactic distribution of the nongaseous component has no similarity to the distribution of any known type of galactic object.

Added October, 1953: Hanbury, Brown, and Hazard (*Phil. Mag.*, **44**, 939, 1953) have recently shown that the galactic distribution of the nongaseous component is very similar to the general stellar distribution in the Galaxy. Their method avoids the objections which can be made to Shklovski's discussion.

[42] *Zs. f. Ap.*, **26**, 176, 1949.

[43] R. Minkowski, *Pub. Obs. U. Michigan*, **10**, 25, 1952.

[44] S. Cederblad, *Lund Medd.*, ser. 2, No. 119, Fig. 8, p. 59, 1946.

[45] *Australian J. Sci. Res.*, *A*, **5**, 437, 1952.

[46] *B.A.N.*, **11**, 323, 1951.

[47] *Australian J. Sci. Res.*, *A*, **3**, 19, 1950.

with the distribution of common stars. The excess of the radiation near the galactic poles and in the hemisphere opposite the galactic center was tentatively interpreted by Westerhout and Oort as due to a background of distant extragalactic nebulae. This interpretation is supported by the identification of extragalactic nebulae as strong radio sources. While the general radiation from normal extragalactic nebulae is too small to explain the excess, sources of the Cygnus A type, for example, may provide the required intensity. Since the bulk of the stars in an Sb spiral such as the Galaxy belong to population II, the agreement of the distribution of the galactic radiation with that of the common stars is proof that the radiation originates in objects which are part of population II.

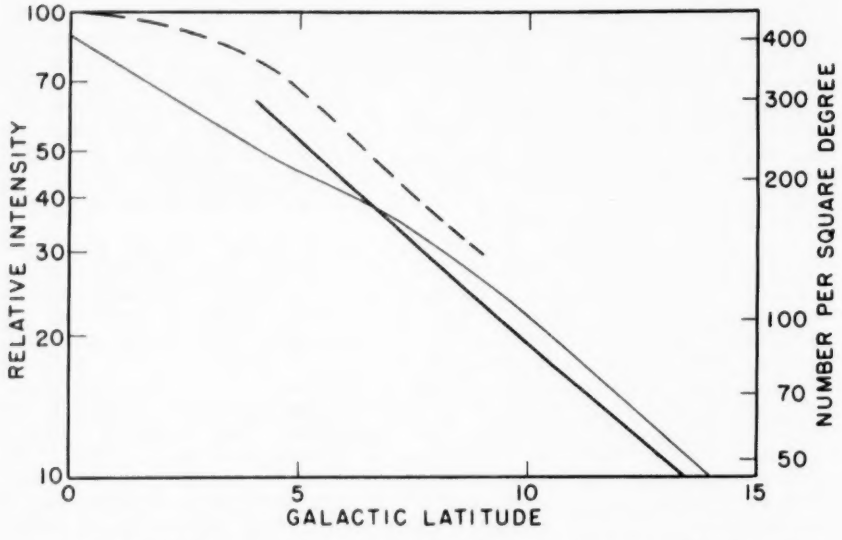

FIG. 15.—Relative radio intensity and number of cluster-type variables as function of galactic latitude at the galactic center. *Broken line:* radio intensity by Bolton and Westfold. *Thin solid line:* radio intensity by Bolton. *Heavy solid line:* number of cluster-type variables.

The same conclusion is reached if profiles of the galactic radiation in latitude across the galactic center are compared directly with the distribution of the cluster-type variables which represent the population II as one of its typical constituents. Owing to the obscuration in the galactic plane, the stellar distribution cannot be determined for the immediate neighborhood of the galactic center. Unpublished results by Baade show that the number of cluster-type variables per 10^6 cubic parsecs as a function of the distance r in kiloparsecs from the galactic center is

$$N = 20.4 \times 10^{-0.765r} \qquad \text{for } 0.6 < r < 3.5,$$

$$N = 0.813 \times 10^{-0.361r} \qquad \text{for } r < 3.5.$$

From these data, the number of cluster-type variables per square degree may be determined by numerical integration. This number is compared in Figure 15 with the intensity of the galactic radiation as a function of latitude at the galactic center. Starting at latitude 4°, which corresponds to the closest distance reached by the observations of

cluster-type variables, the comparison excludes that part of the distribution where radiation from *H* II regions may be observable. The agreement of the distribution of cluster-type variables with that of the galactic radiation is obvious. Similar agreement exists with the profile of Ryle and Scheuer at $l = 340°$.

If the general galactic radiation originates in objects which are part of population II, it is highly probable that these objects are stars. It is true that the presence of gas in population II is shown by the appearance of faint [*O* II] lines in the spectra of elliptical nebulae; but all evidence suggests that the mass of the gas in these systems is small. Consequently, its contribution to the radio emission should be even less important than that of the much larger mass of gas contained in population I.

While it is thus highly probable that radio stars exist, no estimate of their type or luminosity can be made. The attempts by several authors to estimate the number of radio stars on the basis of statistical analysis are completely invalidated by the fact that the strongest sources are now known not to be stellar and that it is completely unknown which, if any, of the known sources belong to the group of objects which emit the general galactic radiation.

We are greatly indebted to the members of the radio astronomy groups in Sydney, Cambridge, and Manchester for their generous communication of information in advance of publication.

THE SPECTRUM OF THE RADIO SOURCE IN CASSIOPEIA

R. MINKOWSKI AND LAWRENCE H. ALLER
Mount Wilson and Palomar Observatories
and
University of Michigan
Received April 27, 1953

ABSTRACT

The Cassiopeia radio source shows [*O* I] and [*O* III] lines which are of equal intensity but at least five times stronger than *Hα* or λ 3727 of [*O* II]. This unusual type of emission spectrum may be understood if we suppose that the electron density lies between 10^3 and 10^4/cm^3 and the electron temperature is less than 15,000° K. No high-temperature source of radiation appears to be involved. The emitted radiation appears to be derived from the kinetic energy of the free electrons. Dissipation of mechanical energy in the filaments may serve to maintain an electron temperature in the neighborhood of 10,000° K.

The filaments of the radio source in Cassiopeia[1] show, in addition to unusually large velocity displacements due to internal motions, optical spectra in which the bright hydrogen lines appear to be very weak relative to the forbidden lines. No obvious stellar source of excitation is visible.

The most outstanding example of this condition is shown by the filament 1, which also shows the extreme spread of velocities. Only the forbidden lines of [*O* I] and [*O* III] are recorded; *Hα* and the forbidden lines of [*O* II] are not visible. Approximate true relative line intensities have been estimated by comparison with planetary nebulae. The [*O* I] and [*O* III] lines are of equal intensity, but *Hα*, as well as the [*O* II] lines, is more than five times fainter. In gaseous nebulae the [*O* I] lines are always much fainter than either *Hα* or the [*O* III] lines.

Interstellar reddening may contribute to the weakness of the [*O* II] lines. The intensity ratios *Hα*/[*O* III] and [*O* I]/[*O* III], however, are affected by interstellar reddening in the same sense and degree as the ratio [*O* III]/[*O* II]. Thus, if interstellar reddening noticeably affects the relative intensities, the true relative intensities of [*O* I], [*O* II], and [*O* III] would be less abnormal, but the true relative intensity of *Hα* would be even smaller than it appears to be. Since the colors of stars in the area of the nebulosity do not suggest extreme conditions, the effect of interstellar reddening on the relative line intensities probably is not very large.

The unusually low intensity of the hydrogen lines relative to the forbidden lines cannot be considered as a sign of low hydrogen abundance. The situation is different from that in the Crab Nebula, where the low intensity of the hydrogen lines compared to the permitted lines of both *He* I and *He* II suggests anomalous chemical composition.

The spectral peculiarity of the Cassiopeia source may be interpreted as arising from the excitation mechanism. In an ordinary gaseous nebula the energy is supplied by a hot central star. Ultraviolet quanta detach electrons from atoms. These electrons collide with ions of oxygen, nitrogen, neon, and other heavy gases and excite them to metastable levels, whence they cascade to lower levels with the emission of characteristic forbidden lines. The recombination of protons and electrons results in the production of the Balmer lines. Consider, now, the situation in a gaseous mass where the energy is supplied not by a dilute high-temperature radiation field but by the dissipation of mechanical energy, as in the collision between two gas clouds or in the encounter of a gas cloud and a resisting medium. If the electron temperature is high enough, a bright-line spectrum, consisting largely of the permitted lines of hydrogen and other permanent gases, will be produced.

[1] See the preceding paper by W. Baade and R. Minkowski.

The radiation of energy will tend to cool the gas. Unless a large amount of kinetic energy is continuously supplied to the electrons, the electron temperature will fall, and if it falls too much below 15,000° K, *Hα* will become much weaker than the forbidden lines of oxygen. The spectrum ultimately has a considerably different appearance from that of a usual gaseous nebula, in that the permitted lines are wholly suppressed and only the forbidden lines appear.

Let us now estimate the rate of collisional excitation of the higher levels of hydrogen and of the low metastable levels of oxygen in various stages of ionization. In view of the unsatisfactory nature of the theory of collisional excitation, we can make only order-of-magnitude guesses at the rate of the various processes, but we can quickly identify the domains of temperature and density in which a pure collisional spectrum will mimic that observed in the Cassiopeia radio source.

Miyamoto[2] and, more recently, J. W. Chamberlain[3] have discussed the collisional excitation of hydrogen in a gaseous nebula. If Q_n is the target area for the collisional excitation of the nth level from the ground level, the number of collisional excitations of the nth level per cubic centimeter per second will be

$$\eth_{1n} = N_1 N_e \int_{v_n}^{\infty} Q_n(v)\, v \cdot f(v)\, dv \equiv N_1 N_e \alpha_n , \tag{1}$$

where $f(v)$ is the Maxwellian distribution function for velocities at a temperature T_e; N_e is the electron density; N_1 is the number of atoms in the ground level; and the integral α_n has been estimated by Chamberlain. We quote his results for the excitation of the third level in c.g.s. units (see accompanying table). The value of α diminishes rapidly as n increases.

	T (° K)		
	10,000	20,000	40,000
α_3	6.35×10^{-16}	6.7×10^{-12}	3.07×10^{-10}

The theory of the collisional excitiation of the metastable levels has been discussed by Menzel, Aller, and Hebb[4] for *O* III. The number of collisional excitations per cubic centimeter per second of a level B, of excitation potential χ_{AB}, will be

$$\eth_{AB} = 8.54 \times 10^{-6}\, \frac{N_A N_e \Omega_{AB}}{\varpi_A T_e^{1/2}}\, e^{-\chi_{AB}/kT_e} . \tag{2}$$

Here ϖ_A is the statistical weight of the ground level and Ω_{AB} is a parameter computed by quantum mechanics. Calculations of Ω for ions in the ground configurations of *O* I, *O* II, *O* III, and *N* II had been made by Yamanouchi and Amemiya,[5] by Aller,[6] by Hebb and Menzel,[7] and by Marvin White and Aller,[6] respectively. These earlier results were based on a somewhat inexact theory[8] and give target areas that were much too large. The status

[2] *Jap. Mem. Col. Sci.*, **21**, 173, 1938; *Contr. Inst. Ap., Kyoto Imp. U.*, No. 2.

[3] Thesis, University of Michigan, 1952; *Ap. J.*, **117**, 387, 1953.

[4] *Ap. J.*, **93**, 230, 1941.

[5] *Proc. Phys.-Math. Soc. Japan*, Ser. 3, **22**, 848, 1940.

[6] *Ap. J.*, **111**, 609, 1950.

[7] *Ap. J.*, **92**, 408, 1940.

[8] D. R. Bates, A. Fundaminsky, J. W. Leech, and H. S. W. Massey, *Phil. Trans. R. Soc. London*, **243**, 93, 1950.

of the target-area computations has been greatly improved by the recent work of Seaton,[9] who has obtained values of Ω for ions of astrophysical interest.

For the green nebular lines of [O III], Seaton gives $\Omega\,(^3P, {}^1D) = 1.73$; $\varpi = 9$. He finds that Ω for [O I] varies with the energy of the electron. For our present calculations we shall adopt $\Omega = 0.4$ for [O I] as an approximate mean value, and we may write

$$\mathfrak{F}_{PD}\,(O\,\text{III}) = 1.64 \times 10^{-6}\,\frac{N\,(O\,\text{III})\,N_e}{T_e^{1/2}}\,10^{-12,500/T_e} \tag{3a}$$

and

$$\mathfrak{F}_{PD}\,(O\,\text{I}) \sim 0.38 \times 10^{-6}\,\frac{N\,(O\,\text{I})\,N_e}{T_e^{1/2}}\,10^{-9900/T_e} \tag{3b}$$

for the number of collisional excitations from the ground ^3P term to the $^1D_2$ level in O III and O I, respectively.

The number of downward radiative transitions per cubic centimeter per second from the $^1D_2$ level will be

$$\eta = \mathfrak{F}_{PD}\,(1-\beta)\,, \tag{4}$$

where β is the fraction of ions that are collisionally de-excited. For [O III],

$$\beta = \frac{\mathfrak{F}_{DP}}{\mathfrak{F}_{DP}+F_{DP}} = \frac{1}{1+(9560\,\sqrt{T_e})\,/\,N_e)}\,. \tag{4a}$$

Here

$$F_{DP} = N_D A_{DP} = 0.028\,N_D \tag{4b}$$

is the number of radiative de-excitations of the $^1D_2$ level per second. Representative values of β are given in Table 1.

TABLE 1

REPRESENTATIVE VALUES OF β FOR O III

T_e (° K)	N_e				
	10^2	10^3	10^4	10^5	10^6
10,000.....	0.00	0.001	0.010	0.095	0.51
15,000.....	.00	.001	.008	.079	.46
20,000.....	0.00	0.001	0.008	0.072	0.44

The intensity of $H\alpha$ will be controlled primarily by the number of collisional excitations to the third level. Hence an estimate of the relative importance of $H\alpha$ and the green nebular lines of [O III] may be obtained by calculating the ratio

$$\frac{I\,(O\,\text{III})}{I\,(H\alpha)} \sim \frac{\mathfrak{F}_{PD}\,(O\,\text{III})\,\nu\,(O\,\text{III})}{\mathfrak{F}_{13}\,(H)\,\nu\,(H\alpha)} = \frac{1.6 \times 10^{-6} N\,(O\,\text{III})\,T_e^{-1/2}\,(1-\beta)\,\nu\,(O\,\text{III})\,10^{-12,500/T_e}}{N_1 a_{13} \nu\,(H\alpha)}\,. \tag{5}$$

Similarly, for the red nebular lines of [O I] we have

$$\frac{I\,(O\,\text{I})}{I\,(H\alpha)} \sim \frac{\mathfrak{F}_{PD}\,(O\,\text{I})\,\nu\,(O\,\text{I})}{\mathfrak{F}_{13}\,(H)\,\nu\,(H\alpha)} = \frac{0.4 \times 10^{-6} N\,(O\,\text{I})\,T_e^{-1/2}\,(1-\beta)\,\nu\,(O\,\text{I})\,10^{-9900/T_e}}{N_1 a_{13} \nu\,(H\alpha)}\,. \tag{6}$$

[9] *Phil. Trans. R. Soc. London*, **245**, 469, 1953; *Proc. R. Soc. London*, **218**, 400, 1953.

In Table 2 are given values of the ratios

$$\gamma\,(O\,\text{I}) = \frac{I\,(O\,\text{I})}{I\,(H\alpha)}\,\frac{N_1}{N\,(O\,\text{I})\,(1-\beta)} \tag{7}$$

and

$$\gamma\,(O\,\text{III}) = \frac{I\,(O\,\text{III})}{I\,(H\alpha)}\,\frac{N_1}{N\,(O\,\text{III})\,(1-\beta)}\,, \tag{8}$$

which determine the relative intensities for collisional excitation.

If, as in normal gaseous nebulae, hydrogen is excited by radiation, the intensity of $H\alpha$ is[10]

$$E_{H\alpha} = 4.83\times 10^{-19}\,\frac{N_1 N_e}{T_e^{3/2}}\,b_3 e^{17,450/T_e}\,. \tag{9}$$

TABLE 2

VALUES OF γ AND γ_r

T_e (° K)	$\gamma\,(O\,\text{I})$	$\gamma\,(O\,\text{III})$	$\gamma_r\,(O\,\text{III})$		
			A_2	B	C
10,000	1.9×10^{6}	6.3×10^{5}	3.4×10^{4}	1.4×10^{4}	830
15,000	1.1×10^{4}	3.5×10^{3}	9.2×10^{4}	4.3×10^{4}	5800
18,000	1.6×10^{3}	4.1×10^{2}	1.4×10^{5}	6.3×10^{4}	1.1×10^{4}

The intensity ratio of the [O III] lines to $H\alpha$ for radiative excitation is determined by

$$\gamma_r\,(O\,\text{III}) = 13.4\,b_3^{-1}T_e 10^{-20,100/T_e}\,, \tag{10}$$

where

$$\gamma_r\,(O\,\text{III}) = \frac{I\,(O\,\text{III})}{I\,(H\alpha)}\,\frac{N_1}{N\,(O\,\text{III})\,(1-\beta)}\,. \tag{11}$$

The value of b_3 depends on details of the conditions of excitation. Values of $\gamma_r\,(O\,\text{III})$ are given in Table 2 for Menzel and Baker's cases A_2 (nebula transparent to Lyman-line radiation), B (nebula opaque to Lyman-line radiation), and C (excitation by pure blackbody radiation).[11]

The ratio $\gamma\,(O\,\text{I})/\gamma(O\,\text{III})$ does not depend on the conditions of excitation of the hydrogen lines. The values in Table 2 shows that this ratio is almost independent of T_e and approximately equal to 3. With the same degree of approximation, we therefore have

$$\frac{I\,(O\,\text{I})}{I\,(O\,\text{III})} \backsim 3\,\frac{N\,(O\,\text{I})}{N\,(O\,\text{III})}\,. \tag{12}$$

The later discussion of the state of ionization shows that the filament cannot be in a state of equilibrium. The ratio $N\,(O\,\text{I})/N\,(O\,\text{III})$ therefore cannot be computed. The observed equality of the [O I] and [O III] lines requires that $N\,(O\,\text{I})$ approximately equal $N\,(O\,\text{III})$.

In normal stellar envelopes the abundance ratio of H to O is about 1000, and it seems not unreasonable to take $N\,(O\,\text{I})/N_1$—the ratio of neutral oxygen to neutral hydrogen—

[10] D. H. Menzel, *Ap. J.*, **85**, 330, 1937.

[11] D. H. Menzel and J. G. Baker, *Ap. J.*, **88**, 52, 1938; J. G. Baker, D. H. Menzel, and L. H. Aller, *Ap. J.*, **88**, 422, 1938.

and the equal ratio $N(O\text{ III})/N_1$ to be about 10^{-3} to 10^{-4}. Thus we see from Table 2 that $H\alpha$ will be weak compared with the red [O I] or the green [O III] lines either for collisional excitation at a low electron temperature or for radiative excitation at a high electron temperature. This is no longer true if the electron density exceeds about 10^6/cm^3. At higher densities, where β no longer is small, an appreciable fraction of the ions excited to the metastable levels would become collisionally de-excited, while essentially all hydrogen atoms excited to the level $n = 3$ are de-excited by radiation; thus the relative intensity of the hydrogen lines would increase.

The relative intensities of $H\alpha$ and the green [O III] lines obviously are not sufficient to decide between radiative and collisional excitation. In normal gaseous nebulae the Balmer decrement[12] suggests that the excitation of the hydrogen lines follows case B, with an electron temperature of the order of 20,000° K. If the filament is excited by radiation, case A_2 and a relatively high electron temperature would provide the best interpretation. Under these circumstances, however, it is hard to understand how a high electron temperature can be maintained against the very effective cooling suggested by the high intensity of the forbidden lines. The assumption of collisional excitation at an electron temperature well below 15,000° seems to provide a more satisfactory interpretation, which is favored also by the absence of an observed stellar source of excitation and the presence of very large internal motions.

A curious feature of the spectrum of the Cassiopeia radio source is that λ 3727 [O II] is five times or more weaker than the [O I] or [O III] lines. The near-equality of the intensities of the [O I] and [O III] lines indicates that comparable numbers of neutral and doubly ionized oxygen atoms exist. Hence we would expect similar numbers of singly ionized oxygen atoms. Why, then, are the radiations of [O II] not observed?

The equation of statistical equilibrium for the ^{2}D term of the $2p^2$ configuration of O II is

$$\tilde{\delta}_{SD} = \tilde{\delta}_{DS} + N_D A_D \,, \tag{13}$$

i.e., the number of collisional excitations from the ground ^{4}S level of O II to the ^{2}D term equals the number of collisional plus radiative de-excitations. Putting in the explicit expressions for these quantities, we find:

$$N(^2\text{D}) = N(^4\text{S}) \frac{(C_1 N_e/\varpi_s T_e^{1/2})\,\Omega_{SD}\, e^{-\chi_{SD}/kT_e}}{C_1 (N_e/\sqrt{T_e})\,(\Omega_{DS}/\varpi_D) + A_{DS}} , \tag{14}$$

where $C_1 = 8.54 \times 10^{-6}$. Then

$$\frac{I(3727)}{I(N_1 + N_2)} = \frac{N(^2\text{D})\, A_{3727}\nu_{3727}}{\tilde{\delta}(^3\text{P} - ^1\text{D})\,(1-\beta)\nu(N_1 + N_2)} . \tag{15}$$

Making use of equation (3*a*) and putting in the numerical values $\bar{A} = 8.87 \times 10^{-5}$, $\Omega(^4\text{S} - ^2\text{D}) = 1.44$, $\varpi_{4_S} = 4$, and $\varpi_{2_D} = 10$, we find

$$\frac{I(3727)}{I(N_1 + N_2)} = \frac{N(O\text{II})}{N(O\text{III})}\, 10^{-4200/T_e}\, \frac{181}{1-\beta}\, \frac{1}{[72 + N_e/\sqrt{T_e}]} , \tag{16}$$

since nearly all O II ions are in the ^{4}S level and nearly all O III ions are in the ^{3}P term in the respective ground configurations. Let us write

$$\delta = \frac{I(3727)}{I(N_1 + N_2)} \Big/ \frac{N(O\text{II})}{N(O\text{III})} . \tag{17}$$

Table 3 gives typical values of δ. If $N(O\text{ II}) \sim N(O\text{ I})$ or $N(O\text{ III})$, the observational re-

[12] L. H. Aller, *Ap. J.*, **113**, 125, 1951.

sults imply a density of the order of 10^4 electrons/cm^3 for the green and red forbidden oxygen lines to be an order of magnitude stronger than λ 3727. If it were much lower, λ 3727 should be comparable with the lines of [*O* I] and [*O* III]. At the higher densities, collisions of the second kind are much more important for the destruction of metastable states in *O* II than they are in *O* III or *O* I.

The physical state of the nebula cannot be an equilibrium one. The high velocities of the components of the individual lines would indicate a speedy dissipation of the fila-

TABLE 3

VALUES OF δ

T_e (° K)	N_e			
	10^2	10^3	10^4	10^5
10,000	0.94	0.8	0.4	0.07
15,000	1.3	1.2	.6	.12
18,000	1.4	1.3	0.7	0.14

ments. The state of ionization would appear to be a relic of the previous condition of the nebula. Clearly, if the electron temperature is as low ($\leq$ 15,000° K) as the absence of the *H* lines would imply, *O* II or even *O* I cannot be collisionally ionized, and the *O* III that is present must have been left over from a previous state of the gaseous mass. If the density is as high as 10^6 particles/cm^3, *O* III would recombine to *O* II in 2 or 3 days.[13] On the other hand, if N_e is as low as 10^3, the *O* III would require about 3000 years to disappear by recombination, and before such a time could elapse the filaments would have dissipated! If N_e is 10^4, the *O* III could last for about 30 years. It will be of interest to observe the spectrum of this filament a few years hence, to see if appreciable changes have occurred.

[13] L. H. Aller, "Spectrographic Studies of the Combination Variables Z Andromedae, BF Cygni, and CI Cygni," *Publ. Dom. Ap. Obs. Victoria* (in press).

THE POWER RADIATED BY SOME DISCRETE SOURCES OF RADIO NOISE

RUDOLPH MINKOWSKI AND JESSE L. GREENSTEIN
MOUNT WILSON AND PALOMAR OBSERVATORIES
CARNEGIE INSTITUTION OF WASHINGTON
CALIFORNIA INSTITUTE OF TECHNOLOGY
Received June 19, 1953

ABSTRACT

The identification by Baade and Minkowski of some of the strongest sources of radio noise permits us to estimate the energy emitted per unit volume. These strongest discrete sources radiate at a rate higher by many orders of magnitude than our Galaxy. Collisions of gas masses may provide sufficient energy.

INTRODUCTION

Some of the stronger radio sources have recently been identified by the radio astronomers and by Baade and Minkowski[1] with various interesting astronomical objects. Many other sources have also been tentatively identified with similar objects (gaseous or extragalactic nebulae). We wish to investigate the energy radiated by these sources, which are both apparently and intrinsically among the strongest known. If any one source had an improbably large intrinsic radio-frequency emission per unit volume (or mass), we might doubt its identification. In fact, we will show that they all radiate at about the same rate.

Let the emission per unit volume into 4π solid angle be J_ν; the volume of the source, V; the radius, R; and the distance, r. Then the power received is

$$P_\nu = \frac{VJ_\nu}{4\pi r^2} = \frac{rJ_\nu}{3}\left(\frac{R}{r}\right)^3 . \tag{1}$$

Let the source, assumed spherical, have an angular diameter of d minutes of arc; let the unit for r be parsecs, and for P_ν watts per square meter per cycle per second. Then

$$J_\nu = \frac{3.2 \times 10^{-4} P_\nu}{d^3 r} \text{ ergs cm}^{-3} \text{ sec}^{-1} \text{ (c/sec)}^{-1} , \tag{2}$$

or, alternatively, with V in cubic parsecs,

$$J_\nu = \frac{4.1 \times 10^{-15} P_\nu r^2}{V} \text{ ergs cm}^{-3} \text{ sec}^{-1} \text{ (c/sec)}^{-1} . \tag{3}$$

The radio luminosity is

$$L_\nu = J_\nu V = 1.2 \times 10^{41} P_\nu r^2 \text{ ergs sec}^{-1} \text{ (c/sec)}^{-1} . \tag{4}$$

Data for P_ν and d are given by various investigators, with mean values collected in Table 1; data for R and r, of astronomical origin, are discussed below. The velocity-distance relation, on the old scale of distances, is used for the extragalactic sources.

We wish to compare the total radio noise generated with that available from simple processes, for example, from the conversion by some type of gaseous plasma oscillation of

[1] Baade and Minkowski, *Ap. J.*, **119**, 206, 215, 1954.

kinetic into electromagnetic energy. For this purpose it is desirable to know the integrated emissivity,

$$J = \int_{\nu_1}^{\nu_2} J_\nu d\nu , \tag{5}$$

between the limits ν_1 and ν_2 in the radio-frequency range. Observations of P_ν are limited by the ionosphere, and the emission is presumably cut off by similar reflection and absorption effects in the source itself. Near 100 Mc/sec, where most observations are now made, we take an approximate interpolation formula for $P_\nu \approx \nu^{-(1+\epsilon)}$, where ϵ is positive

TABLE 1

EMISSIVITY OF IDENTIFIED RADIO SOURCES

Source	Energy Received P_ν (100 Mc) (Watts/M²[C/S])	r (Psc)	Diameter (d′ in Minutes or in Psc)	Total Radio Emission ($L = JV$ Ergs/Sec)	Total Volume Emissivity (J in Ergs/Cm³ Sec)	Remarks
Cas	2×10^{-22}	300	5′	1.1×10^{33}	8.5×10^{-22}	
Tau	1×10^{-23}	1000	5′	7.2×10^{32}	1.2×10^{-23}	Probably underestimated
Vir	1×10^{-23}	3×10^{6}	Jet 2″×20″ Neb. 5′	5.2×10^{30}	6.7×10^{-22} 4.2×10^{-27}	Upper limit Lower limit
Cyg	1.3×10^{-22}	3.4×10^{7}	Center 5″ 10,000×1500 psc	8.8×10^{42}	1.0×10^{-21} 2.5×10^{-24}	Upper limit Lower limit
Galaxy			20,000×1500 psc	2.4×10^{37}	1.4×10^{-30}	Integration by Westerhout and Oort
M31	2×10^{-24}:	2.3×10^{5}	16,000×1200 psc	9.0×10^{36}	1×10^{-30}:	

and ranges from 0 to 1. Integrals of such a formula diverge unless a cutoff exists at ν_1. Let the power at 100 Mc/sec be P_ν (100); then

$$P = P_\nu(100) \times \Delta\nu = \frac{P_\nu(100)\, 10^{8(1+\epsilon)}}{\epsilon \nu_1^{\epsilon}} . \tag{6}$$

The lowest possible frequency for ν_1 would be near that of the natural plasma oscillation, in which case $\nu_1 \approx 10^4$ c/sec if the electron density $n_e = 1/\text{cm}^3$; $\nu_1 \approx 10^6$ c/sec for $n_e = 10^4/\text{cm}^3$. If we adopt $\epsilon = 0.3$, the equivalent band width, $\Delta\nu$, varies as $n_e^{-0.15}$ and would be near 10^9 c/sec. On the other hand, we have recently shown[2] that free-free transitions within a radio source containing ionized gas produce appreciable self-absorption. Then there exists a maximum in the emitted radiation, near a frequency $0.77\, n_e r^{1/2}$ Mc/sec; with $n_e = 10^3/\text{cm}^3$ and a thickness $r = 0.1$ psc (a dense gas cloud or a nebular filament), $\nu_1 = 200$ Mc/sec, while in a thin cloud $\nu_1 = 2$ Mc/sec. The absorption cutoff at low frequencies should not be confused with the cutoff produced by total internal reflection (of the type that occurs in the ionosphere or solar corona). Interstellar gas has a refractive index very near unity at observable frequencies; the emitted power is unchanged by refraction of the ray. Even local condensations of density sufficient to produce reflection would not prevent the ultimate escape of radio noise unless its frequency is below that of the plasma oscillation at the average density of the medium.

An order-of-magnitude estimate of $\Delta\nu$ can be obtained if we take $\epsilon = 0.3$ and $\nu_1 = 20$ Mc/sec. The effective band width is then $\Delta\nu = 5 \times 10^8$ c/sec. In our estimates of

[2] Greenstein and Minkowski, *Ap. J.*, **118**, 1, 1953.

total power, P, and emissivity, J, we multiply the observed values at 100 Mc/sec by this $\Delta\nu$. It is quite possible that $\Delta\nu$ is somewhat overestimated because of the extrapolation of a power law[3] to low frequencies.

THE IDENTIFIED SOURCES

We will consider four exceptionally strong sources discussed by Baade and Minkowski. These are among the apparently and intrinsically strongest known.

1. *Cassiopeia A = (23.01).*—A gaseous emission nebula with many peculiar filamentary structures. The optical emission spectrum may be explained[4] by collisional excitation. The distance is unknown, but, if located in the spiral arm which contains most of the near-by gas and dust, it is probably about 300 psc.

2. *Taurus A = (05.01).*—The Crab Nebula, a supernova remnant. The radio spectrum is abnormal because of internal absorption.[2] The total power, P, is probably somewhat underestimated.

3. *Virgo A = (12.01).*—A spheroidal galaxy, NGC 4486, in the Virgo cluster. The most remarkable feature is a bright narrow jet of matter emanating in a nearly straight line from the nucleus. It is about 30 × 300 psc, broken up into several small knots, is bluer than the nebula, and shows no emission or absorption lines. This jet is the only one known, and no plausible interpretation has been advanced. If it is the radio source, the large observed radio diameter cannot be understood (see the discussion by Baade and Minkowski[1]). We derive J on these two hypotheses: (*a*) that the jet is the radio source and also (*b*) that whatever phenomenon causes the jet also results in radio emission over the whole optical diameter of the galaxy.

4. *Cygnus A = (19.01).*—A close collision of two apparently faint galaxies of high intrinsic luminosity. The spectrum shows emission lines of unusually high excitation. The radio diameter, an ellipse of 0′.5 by 2′.0, is larger than the optical one; if this is really a collision, the radiation may come either (*a*) from gas contained in a very small volume where the gas clouds of the two systems are crossing (for this extreme case we can adopt $d = 0'.08$, about 850 psc) or (*b*) from the entire volume of the gas in the nebula, which is about 10,000 psc in diameter and 1500 psc thick.

The last column of Table 1 gives the radio emission per unit volume, J. For comparison we determine the emissivity of two weak near-by radio sources, our own Galaxy and the Andromeda Nebula M31. For our own Galaxy, Oort and Westerhout[5] determined the average apparent temperature along a given line of sight near the sun; then from the known total mass of the Galaxy, they derived indirectly its total radio emission. The power received from M31 is observationally somewhat uncertain still; there is a difference of 2.5 between the results of Ryle and of Brown and Hazard. It will be noted that we have adopted a rather large emitting volume for both the Galaxy and M31. This was done partly for consistency with the other nebular sources and partly because the apparent galactic concentration of radio emission is somewhat like that of the population II stars. It should be emphasized that the average galaxy is a very weak radio emitter, and only peculiar galaxies should appear and be identified as strong discrete sources.[6] The

[3] If we fit an exponential rather than a power law to Bolton's unpublished results for Cygnus A, we find that $\Delta\nu$ is about 2×10^8 c/sec within the observable frequency range.

[4] Minkowski and Aller, *Ap. J.*, **119**, 232, 1954.

[5] *Bull. Astr. Inst. Netherlands*, **11**, 323, 1951.

[6] After this work was completed, the paper by I. S. Shklovski (*Astr. J. U.S.S.R.*, **30**, 15, 1953) was received here. He evaluates the total radio luminosity of several intrinsically weak extragalactic radio emitters. He recognizes that for Cygnus A the radio frequency radiation exceeds the optical radiation. Our Table 1 confirms this, since the radio emission 8.5×10^{42} ergs/sec corresponds to the absolute magnitude −18.5, which probably exceeds the visual luminosity of the colliding galaxies. Normal galaxies have very much smaller ratios of radio/optical energies. This result can be taken as further evidence that the

total emission of our Galaxy is equivalent only to 10^4 times that of such a strong source as the Cassiopeia emission nebula.

DISCUSSION

The observed values of J in Table 1 are sufficiently similar for the four strong radio sources to suggest that 10^{-22} ergs/cm^3 sec represents nearly the maximum emission level averaged over the source. (We have not discussed the degree to which the sources fill the observed volume; the filling may be small, so that in the actively emitting regions the emissivity must be greater.) None of the four strong sources differs sufficiently to cast any doubt on the identification.

One possible comparison, energetically, is with regions in the solar chromosphere or corona which generate nonthermal radio noise. The great storms or bursts are obviously too variable in emissivity to be useful, but the radiation associated with sunspots is much more regular. This radiation originates at a low level in the corona or chromosphere, so that it is observable only at high frequencies. But at 2800 megacycles it produces P_ν of about 10^{-20} watts m^{-2} (c/sec)$^{-1}$ at the earth, when the spotted area is about 0.4 per cent of the solar disk. (We can transform the latter into an equivalent volume.) The spectrum is severely altered by reflection in the chromosphere and corona, so that we observe only its high-frequency end. But we will assume that $P = P_\nu$ (2800 Mc/sec) $\times 3 \times 10^9$, i.e., an equivalent band width of 3000 Mc/sec. Then the derived $J = 1.8 \times 10^{-10}$ ergs/cm^3 sec. This is about 10^{11} times the maximum value found in the radio sources. Now the density of the layers from which the sunspot radio noise originates is about 10^{11} atoms/cm^3; in the uncompressed gas in a spiral arm of a galaxy, it is about 1 atom/cm^3. Thus the volume emissivities are about in the ratio of the densities, or the *radio emission per gram* is about the same. Magnetic fields are present near a sunspot radio source, but they may also be present in the interstellar gas and may rise to significant levels during collision.

ENERGY AVAILABLE IN COLLISIONS

Let two gas clouds of density ρ of size d, occupying volume $V = d^3$, collide with velocity v; let the fraction F of the kinetic energy appear as radio noise. The collision takes time measured by d/v; the rate of emission per unit time per unit volume, during the collision, is

$$J = \left(\frac{V \rho v^2 F}{2}\right)\left(\frac{v}{d}\right)\frac{1}{V} = \frac{F \rho v^3}{2d}. \tag{7}$$

Consider the collision of two gas clouds, where $\rho = 10^{-23}$ gm/cm^3, $v = 2 \times 10^8$ cm/sec, and $d = 10^{21}$ cm. This is typical of the initial densities, velocities, and dimensions that would occur during the collision of two small galaxies. The emission would be $J = 4 \times 10^{-20} F$, and the duration would be 1.6×10^9 years. Thus our colliding galaxies in Table 1 require $F = 0.01$, i.e., 1 per cent of the kinetic energy converted into radio noise. We have taken very modest values for our parameters; v should exceed the velocity of escape, and to this must be added the peculiar motions of the galaxies. The mass of gas used in the above example is about $10^7\ M\odot$; the probable mass is more nearly $10^9\ M\odot$. Ample energy is available, even if the conversion mechanism is inefficient.

Consider two small gas clouds with $\rho = 10^{-22}$ gm/cm^3, $v = 2 \times 10^8$, and $d = 10^{18}$ cm. In that case the duration of the collision is only 150 years, but $J = 4 \times 10^{-16} F$; so ample energy is available for a short period of activity. This is justified, since small colliding clouds with large internal motion must be very short-lived.

Finally, we may determine the maximum power in a collision between two galaxies

---

very intense radio sources tap another energy source than that of the stars. In fact, we show below that the translational energy of colliding gas masses is a possible source. A short lifetime for intense radio sources is then an inevitable consequence.

falling through each other normal to the galactic plane, with gas masses of the order of $10^9\ M\odot$ involved. The radio power emitted would be $3 \times 10^{45}\ F$ ergs; a detectable signal $P_\nu = 10^{-24}$ watts m^{-2} $(c/sec)^{-1}$ would be received at a distance of $10^{10}\ F^{1/2}$ psc, i.e., to the edge of the observable universe if $F = 0.01$. Thus radio methods may detect objects unobservable astronomically.

For much of the information used we are indebted to the radio astronomers at Manchester, Cambridge, and Sydney. Their generous communication of data on position. size, and power, in advance of publication, is gratefully acknowledged.

SPECTROPHOTOMETRY OF THE CENTRAL STARS OF FOUR PLANETARY NEBULAE

L. H. Aller and O. C. Wilson
University of Michigan Observatory and Mount Wilson and Palomar Observatories
Received August 31, 1953

ABSTRACT

An analysis of coudé spectrograms of the nuclei of four planetary nebulae with predominantly absorption spectra, viz., IC 418, IC 2149, NGC 2392, and IC 4593, yields spectral classes of O6–O7 on R. M. Petrie's system. The profiles of the hydrogen lines are compared with those of the O9 star 10 Lacertae. Electron densities somewhat lower than those previously obtained for other planetary nuclei with absorption-line spectra seem to be indicated. It is suggested that the *He/H* ratio can be greater in the planetary nuclei than in normal O stars and that the excitation temperatures can be systematically lower than those derived from Petrie's scale. A final decision will require a much more detailed analysis, involving the calculation of model atmospheres.

I. INTRODUCTION

Since all the energy emitted by a planetary nebula is ultimately derived from its central star, theoretical studies of the physical processes underlying the production of the nebular spectrum require a knowledge of the radiation emitted from this central star. Unfortunately, the radiation relevant to the excitation of the nebular spectrum all lies in the inaccessible ultraviolet. It is necessary to observe the spectrum of the central star in the accessible wave lengths and then try to infer the character of the radiation in the far ultraviolet. The problem is a difficult one, both observationally and theoretically. The central stars of the planetaries are invariably faint. Descriptions of the spectra have been published by a number of observers, but quantitative studies of the emission and absorption lines have been few.[1]

Some planetary nuclei, such as BD+30°3639, show Wolf-Rayet type spectra with relatively narrow lines, while others, such as the nucleus of NGC 6751, show broad emission Wolf-Rayet lines. We are concerned here, however, with objects that show a predominantly absorption spectrum with only a few, if any, relatively sharp emission lines. Some of these central stars show spectra similar to classical O and Of stars. Figure 1 compares the spectrum of the nucleus of NGC 2392 with two Of stars HD 14947 and HD 16691. Notice the prominent absorption lines of hydrogen and ionized helium and the strong emissions of λ 4686 *He* II and λ 4634, λ 4640 *N* III. Microphotometer tracings show that the emission lines in the nucleus of NGC 2392 are somewhat sharper than in Of stars (see Fig. 2, which compares the region from λ 4542 *He* II to λ 4686). The emission lines are somewhat weaker in IC 4593, stronger in IC 418, and missing in IC 2149.

Some years ago, one of us made a detailed study of the absorption-line spectra of the brighter central stars of the planetary nebulae.[2] The spectrograms were obtained with the quartz optics in the Cassegrain spectrograph at the McDonald Observatory and the highest available dispersions. Measures of the equivalent widths of the absorption lines yielded spectral classes by R. M. Petrie's method,[3] as well as estimates of the excitation temperatures and electron densities, and even permitted some speculations concerning the surface gravities and masses of these stars.

[1] See, e.g., the papers by Struve and Swings, *Proc. Nat. Acad. Sci.*, **26**, 454, 548, 1940; **27**, 225, 1941; *Ap. J.*, **92**, 289, 1940.

[2] *Ap. J.*, **108**, 462, 1948.

[3] *Pub. Dom. Ap. Obs. Victoria*, **7**, 321, 1947.

The fact most securely established by this investigation was that a satisfactory study of the central stars of the planetaries would require a much higher dispersion. For example, the profiles of the absorption hydrogen and helium lines should be obtained, so that the possible broadening agencies could be identified and inferences be drawn concerning the structure of the stellar atmosphere. The circumstance that makes observations of the planetary nuclei particularly difficult is that the star is involved in a nebula which is often rather bright. Not only does the presence of the bright nebula make guiding awkward, but the superposition of the strong nebular emissions on the stellar absorption lines makes it difficult to estimate the true profiles of the latter. With high dispersion at a large telescope, many of these difficulties can be overcome.

II. THE OBSERVATIONS

The present study was undertaken to provide improved data on the profiles and total intensities of the absorption and emission lines in four bright planetary nuclei. We employed the 100-inch coudé spectrograms taken by one of us (O. C. W.) in connection with a slit-spectrographic study of the internal motions in the planetaries.[4] The dispersion of

TABLE 1

OBSERVATIONS OF THE CENTRAL STARS OF PLANETARY NEBULAE

Planetary Nebula	α	δ	Photographic Magnitude (Berman)	Photovisual Magnitude (Liller)	Spectral Class	Plate No.
IC 418	5^h22^m8	$-12°45'$	10.8	.....	O7	Ce 5991, 6072
IC 2149	5 43.5	+46 07	.....	.....	O7.5	Ce 5402, 5547
NGC 2392	7 23.3	+21 07	10.5	10.6	O6	Ce 5093, 5094, 5546, 6071, 6975
IC 4593	16 7.0	+12 20	10.2	11.2	O7	Ce 4266, 5209, 5211, 5653

the 32-inch camera and grating combination is 10 A/mm. Owing to the extreme faintness of the central stars, it was possible to secure observations for only a small number of them. The spectrograms employed are listed in Table 1, which gives the planetary nebula, its position, the approximate magnitude and spectral class of the central star, and the plate number. Two columns of magnitudes are given. One set is from the compilation by Berman.[5] For NGC 2392 and IC 4593 we give the results obtained more recently by William Liller,[6] who employed photoelectric methods. Berman's value of 13.3 for the magnitude of the central star of IC 2149 is certainly too faint.

The usual strip-calibration system provided the photometric standards for the plates. We traced the spectrograms in the usual way and derived the profiles and total intensities of the absorption and emission lines. In many instances the central portions of the profiles of the hydrogen lines cannot be determined because of the overlapping of the strong nebular emissions. We indicate these portions of the profiles by dotted lines.

Figure 3 shows the measured profiles for $H\gamma$, $H\delta$, and $H\epsilon$. Some of the profiles show a suggestion of an asymmetry, in the sense that the wings are deeper on the violet side. This tendency is particularly marked on $H\gamma$ and $H\delta$ on plate Ce 5211 of IC 4593 but

[4] *Ap. J.*, **111**, 279, 1950.

[5] *Lick Obs. Bull.*, **18**, 57, 1937.

[6] Thesis, University of Michigan, 1953. We are indebted to Dr. Liller for allowing us to quote his results in advance of publication.

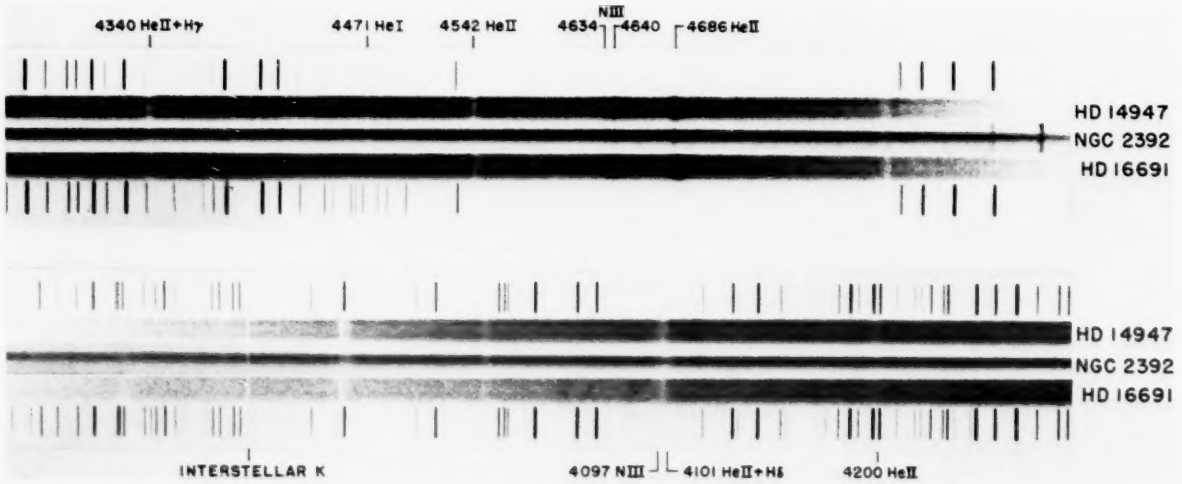

FIG. 1.—Comparison of the spectrum of the nucleus of NGC 2392 with those of the Of stars HD 14947 and HD 16691

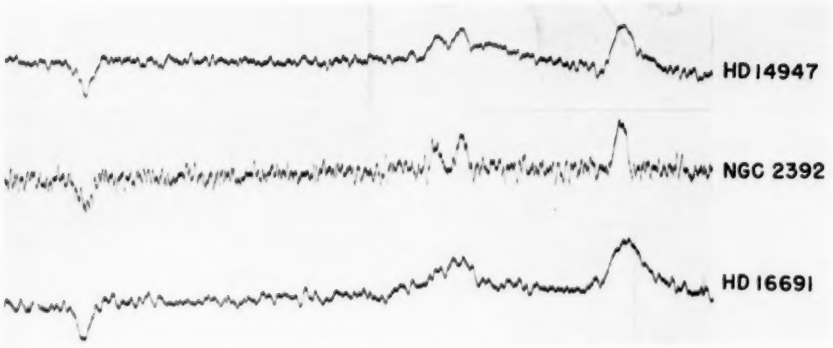

FIG. 2.—Comparison of tracings of HD 14947, NGC 2392, and HD 16691

may be shown by other plates as well. This asymmetry is probably due to blending with the *He* II lines, for it appears to be less marked, if present at all, in the higher members of the Balmer series. The strong, somewhat diffuse, nebular lines cannot be expected to exert much influence on the absorption-line profiles away from the line centers.

In Figure 4 we compare the profiles of the hydrogen lines in the central star of NGC 2392 with those observed in the spectrum of 10 Lacertae.[7] The planetary nuclei hydrogen lines are all weaker than the corresponding lines in 10 Lacertae, although the profile shapes are generally similar.

The equivalent widths, measured in the usual way and expressed in equivalent angstroms, are given in Table 2. The equivalent widths of the absorption lines are com-

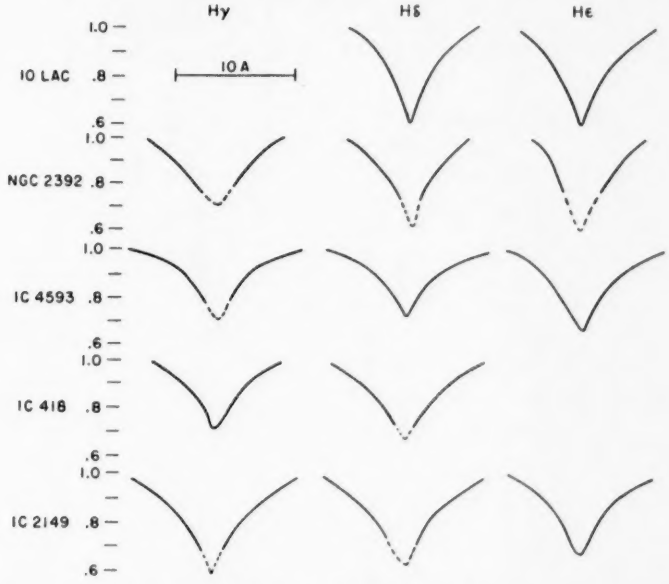

FIG. 3.—Comparison of the profiles of the Balmer lines in planetary nuclei with those in 10 Lacertae

parable with those measured in the classical Of stars. The intensities of the emission lines (denoted by "*E*") are expressed in equivalent angstroms in terms of the underlying continuum. These emission-line profiles are illustrated in Figure 5. They may show time variations such as those found by J. B. Oke for the classical Of stars.[8] Our data are not sufficient to establish the amplitude and period of such variations if they exist.

The accuracy of the tabulated equivalent widths depends strongly on the quality of the plate and the extent of blending with nebular emissions. On a well-exposed plate the average error of the intensity of an unblended line of moderate strength (e.g., $W_\lambda \sim 0.7$) is probably about 20 per cent. A comparison with previous intensity measures for three stars common to the two lists—the IC 418, IC 4593, and NGC 2392 nuclei—shows a number of discrepancies which are to be attributed to the inadequate dispersion em-

[7] L. H. Aller, *Ap. J.*, **104**, 347, 1946.

[8] Thesis, Princeton University, 1953.

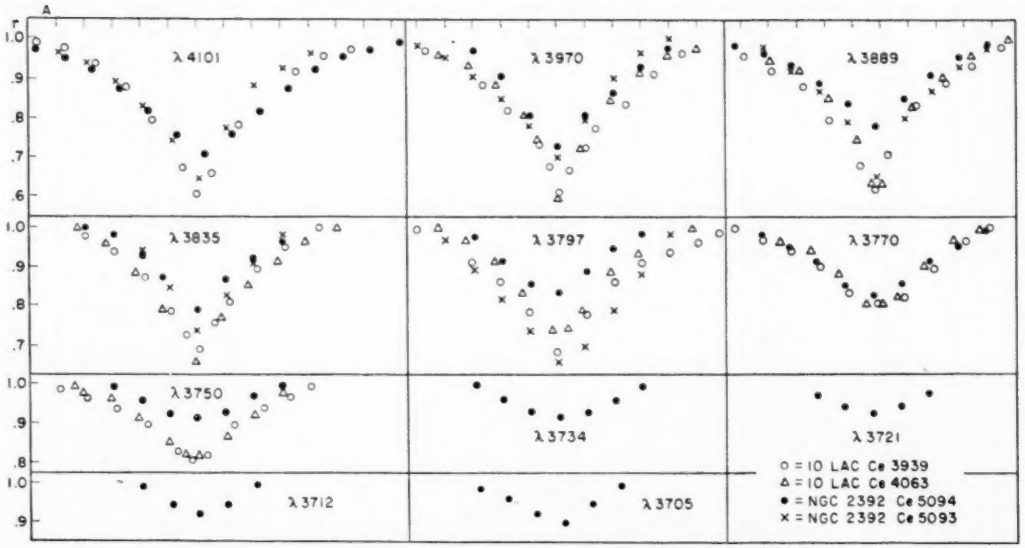

FIG. 4.—Detailed comparison of the hydrogen line profiles in 10 Lacertae with those in the nucleus of NGC 2392

ployed in the earlier work. In particular, it should now be possible to make improved estimates of such quantities as the spectral type, the excitation temperature, and the electron pressure.

III. TEMPERATURES AND SPECTRAL CLASSES OF PLANETARY NUCLEI

The photometrically measured line intensities permit a determination of the spectral classes by the method of R. M. Petrie,[3] who uses the *He* I/*He* II, *He* II/*H*, and *Si* IV/*He* II ratios. We have used the *He* I/*He* II ratio, i.e., I (λ 4471)/$\frac{1}{2}[I$ (4200) + I (4542)], and the *He* II/*H* ratio, i.e., $\frac{1}{2}[I$ (4200) + I (4592)]/$\frac{1}{4}[I_c$ (*Hγ*) + I_c (*Hδ*)], to fix the spectral classes. Here I_c (*Hγ*) and I_c (*Hδ*) denote the intensities corrected for blending with the helium lines. If the helium/hydrogen ratio in the planetary nuclei differs from that of normal O stars, the spectral class estimated from the *He* I/*He* II ratios will differ systematically from that estimated from the *He*/*H* ratio. In order to avoid the influence of abundance differences, we might prefer the *He* I/*He* II ratio; but in the low-excitation

TABLE 2

EQUIVALENT WIDTHS OF ABSORPTION AND EMISSION LINES IN THE SPECTRA OF PLANETARY NUCLEI

λ	Identification	IC 418	IC 2149	NGC 2392	IC 4593
4861	*Hβ*	2.06			2.46
4686 *E*	*He* II	0.81		1.35	0.78
4651.35 *E*	*C* III	0.38			0.40
4650.16 *E*	*C* III	0.70			
4647.40 *E*	*C* III	1.04			0.36
4640.64 *E*	*N* III	0.78		0.61	0.38
4634.16 *E*	*N* III	0.46		0.45	0.33
4541.59	*He* II	0.52	0.69	0.64	0.53
4771.50	*He* I	0.35	0.34	0.47	0.29
4340	*Hγ*+*He* II	1.20:	2.02	1.36	1.49
4325 *E*	*C* III	0.30			
4200	*He* II	0.46		0.60	0.52
4101.74	*Hδ*+*He* II	1.40	1.80	1.21	1.35
4097	*N* III			0.34	
4026	*He* I, *He* II	0.35	0.30	0.58	0.46
				0.24	
3969.5	*Hζ*, *He* II	1.45	1.42	1.00	1.26
3923.48	*He* II	0.11:		0.48	0.14
3889	*H*8, *He*, *He* II	0.90	1.30	1.23	1.36
3858.07	*He* II			0.30	
3835.3	*H*9+*He* II	0.86	1.27	0.92	1.02
3819.68	*He* I			0.28	
3797.9	*H*10+*He* II	0.80	1.01	0.92	1.14
3770.63	*H*11	0.60	0.73	0.86	0.72
3761:	*O* III, *Si* IV	0.28			0.14
3757.26	*O* III				0.14
3754.7	*N* III, *O* III				0.21
3750.15	*H*12	0.56	0.58	0.61	0.44
3734.37	*H*13	0.43	0.58	0.42	0.38
3721.94	*H*14	0.34	0.38	0.25	0.47
3711.97	*H*15	0.14	0.30	0.20	0.34
3705	*H*, *He* I	0.18	0.28	0.26	0.23
3697.15	*H*17		0.29		
3691.56	*H*18		0.21		
3686.83	*H*19		0.14		
3484.90	*N* IV			0.13	
3482.98	*N* IV			0.11	
3478.69	*N* IV			0.19	

planetaries IC 418, IC 2149, and IC 4593, the stellar λ 4471 line tends to be filled in by the nebular emission. Hence the spectral class tends to be estimated systematically too early for these stars. The second, third, and fourth columns of Table 3 give for each nucleus the basic intensity data: I (4471), I (*He* II) = $\frac{1}{2}[I\ (4200) + I\ (4542)]$, and $I\ (H) = \frac{1}{4}[I_e\,(H_\gamma) + I_e\,(H\delta)]$. The fifth, sixth, seventh, and eighth columns give the *He* I/*He* II and *He* II/*H* ratios with the corresponding spectral types. The ninth, tenth, and eleventh columns list the adopted spectral classes, the excitation temperature according to Petrie's calibration for normal O stars, and the previously estimated spectral classes. Notice that the *He* I/*He* II estimates tend to be earlier than those from the *He* II/*H* ratios because the intensity of 4471 tends to be estimated too low. A comparison of the temperatures with those estimated by Berman[5] from the Zanstra method is of interest (see accompanying tabulation). The excitation temperatures of IC 418 and

Nucleus	T (Sp. Class) (° K)	T (Zanstra) (° K)	Nucleus	T (Sp. Class) (° K)	T (Zanstra) (° K)
IC 418	33,200	25,000	NGC 2392	34,500	35,000
IC 2149	32,500	40,000	IC 4593	33,400	25,000

IC 4593 are definitely well in excess of the Zanstra temperatures. These are bright, presumably optically thick, nebulae, for which the Zanstra method should be valid. Deviations from a black-body energy distribution in the ultraviolet might account for some of

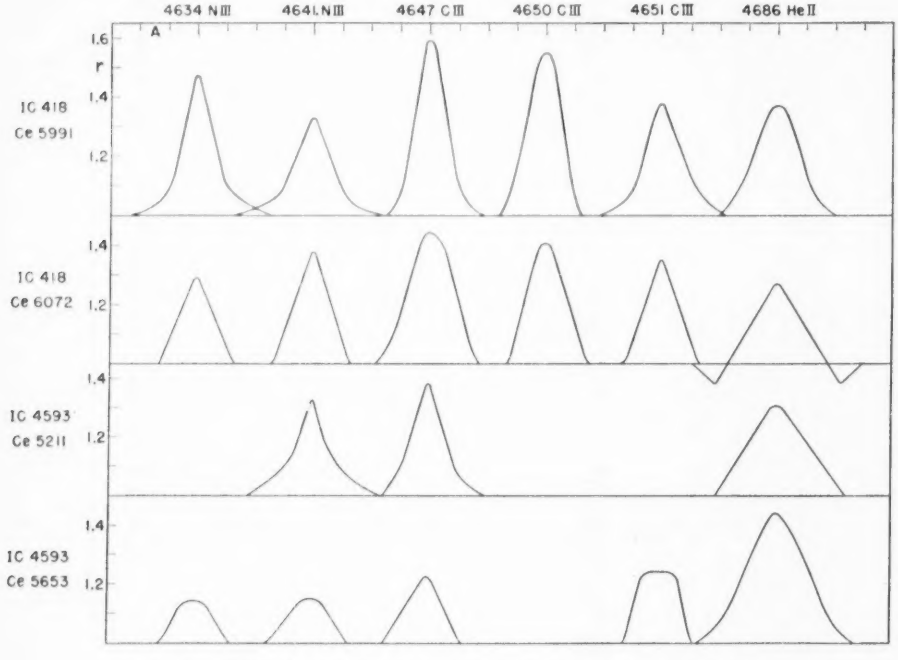

FIG. 5*a*.—Profiles of emission lines observed in the nuclei of planetary nebulae

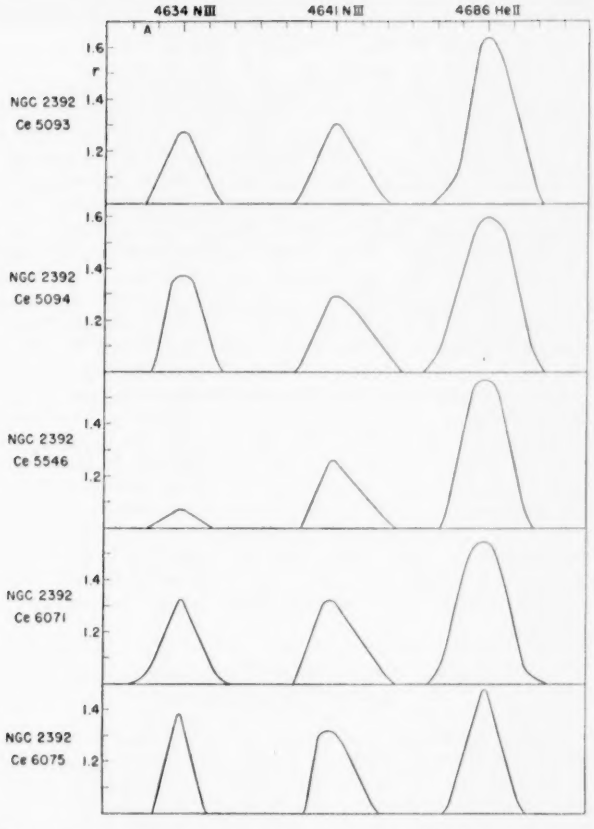

FIG. 5*b*.—Profiles of emission lines observed in the nuclei of planetary nebulae

TABLE 3

SPECTRAL CLASSES OF PLANETARY NUCLEI

Nucleus	*He* I	*He* II	*H*	*He* I/*He* II	Sp.	*He* II/*H*	Sp.	Adopted Spectrum	*T* (° K)	Previous Estimates
IC 418.....	0.35	0.49	0.44	0.71	O6	1.11	O7	O7	33,200	O5, +WC 7*
IC 2149....	.34	.65:	.72	.52	O5.5	0.90	O7.5	O7.5	32,500	O7*
NGC 2392...	.47	.62	.33	.76	O6.2	1.87	O5.9	O6	34,500	O5.5 †
IC 4593.....	0.29	0.53	0.50	0.55	O5.5	0.96	O7.3	O7	33,400	O6.5 †

* Verontsov-Velyaminov, *Russ. A.J.*, **24**, 88, 1947.

† L. H. Aller, *Ap. J.*, **108**, 462, 1948.

this discrepancy. Furthermore, the excitation temperatures are not necessarily the same as the effective temperatures. Finally, if the *He/H* ratio is not the same as in normal stars, there will be an error in the temperature scale. On the other hand, for no accountable reason, IC 2149 has an excitation temperature which is lower than the Zanstra temperature by about the same amount as the other two were higher. For NGC 2392 the agreement seems to be good, but, alas, even here there is trouble. The other three nebulae are all low-excitation objects with rather weak [*Ne* III] and rather prominent λ 3727 [*O* II] emissions. Ionized helium lines are not present in the nebula. On the other hand, NGC 2392 exhibits a very high level of excitation, with strong λ 4686 *He* II and [*Ne* V]. Comparison with other high-excitation nebulae and the Zanstra temperature from ionized helium would suggest a very high temperature[9]—in the neighborhood of 100,000° K! It is strange that nebulae showing such a difference of excitation as IC 418 and NGC 2392 should have nuclei differing in temperature by only a couple of thousand degrees. The nucleus of 2392 is also outstanding, in that it shows evidence of ejections of matter because of a systematic difference in velocity as a function of excitation of the absorption lines. We have estimated the systematic velocity differences between the nebular and stellar hydrogen lines from the microphotometer tracings. IC 2149 and IC 4593 give no conclusive evidence for such velocity differences, but there is some suggestion of a systematic velocity difference in the nebular and stellar hydrogen lines in IC 418, although the magnitude of the displacement fluctuates from line to line. We should expect the broad nuclear lines in IC 418 to be produced by ejected matter. It is possible that the nucleus of NGC 2392 has a somewhat different ultraviolet energy distribution than do other O-type nuclei of apparently the same effective excitation. Another way out of the difficulty is to suppose that the NGC 2392 nucleus is a double star,[10] the hot companion being invisible in the ordinary photographic range. Radial-velocity measurements might reveal such a component, but no observations have yet been made to test this hypothesis.

IV. ESTIMATES OF ELECTRON DENSITY AND NUMBERS OF ATOMS ABOVE PHOTOSPHERE

In order to compare our results with those previously obtained, we shall estimate the number of hydrogen and helium atoms above the photosphere by the method used by Unsöld.[11] It is necessary to correct the Balmer-line intensities for the ionized helium lines. The procedure is exactly the same as that described in the earlier papers. We give here only the results, which are compared with those previously obtained for IC 4593 and NGC 2392. The second and third columns of Table 4 give $\log N_{0,2}H$, the number of hydrogen atoms in the second quantum level above the photosphere. In our present series of observations, higher members of the Balmer series have been measured than in the earlier work, and the resultant $\log N_{0,2}H$ should be more reliable. Notice that the number of atoms above the photosphere is increased for both IC 4593 and NGC 2392. If we now make an extremely crude estimate of N_e from the intensities of $H\gamma$ and $H\delta$ (corrected for the ionized helium contribution) by the procedure suggested by Unsöld, we find the values of N_e entered in the fourth and fifth columns. This estimate is based on the assumption that the line is formed in an isothermal layer; the contribution of Doppler broadening is neglected. The two estimates of N_e are in poor agreement for IC 418 but are in reasonable accord for the other stars. The number of resolvable lines of the Balmer series gives an additional estimate of the electron density. If n_m is the principal quantum number of the last still-resolved line of the Balmer series, the concentra-

[9] See, e.g., the discussion by K. Wurm, *Die planetarischen Nebel* (Berlin: Academie-Verlag, 1951), p. 96.

[10] E.g., The nucleus of NGC 246 is a binary. The nucleus of NGC 1514 must be double, as an A0 star seems to be definitely too late in spectral class to excite a nebular spectrum.

[11] *Zs. f. Ap.*, **21**, 38, 1941.

tion of free electrons (or ions) per cubic centimeter is given by the Inglis-Teller formula[12]

$$\log N_e = \text{Const.} - 7.5 \log n_m.$$

Inglis and Teller give a numerical value of 23.26 for the constant. Experimental work by W. Lochte-Holtgreven and W. Nissen[13] at Kiel shows that the formula will give a rough determination of N_e unless the density is so high that n_m is smaller than 7. At the lower densities appropriate to the atmospheres of early-type stars, they find that the empirical value for the constant, 23.46, gives a better approximation to the electron density than that found by other methods.

Except for IC 2149, in which the Balmer lines can be followed to $n_m = 19$, we find $n_m = 16$. Hence we obtain the values for log N_e given under the heading "n_m" in Table 4.

TABLE 4

ELECTRON DENSITIES AND H/He RATIOS

CENTRAL STAR	LOG $N_{0,2}H$		LOG N_e				LOG $N_{1,4}H$ (He II)	LOG $[N(H^+)/N(He^{++})]$	H/He
	Present Series	McDonald Series (1945–1946)	$H\gamma$	$H\delta$	n_m	Adopted			
IC 418	15.37	.....	13.21	13.82	13.46	13.5	14.70	1.27	13
IC 2149	15.44	.....	13.96	14.07	12.86	13.3	14.60	1.44	20
IC 4593	15.50	15.35	13.48	13.64	13.46	13.5	14.65	1.45	20
NGC 2392	15.46	14.96	13.07	13.18	13.46	13.4	15.20	0.86	5

The adopted values of log N_e are given in the column headed "Adopted." Notice the striking discrepancy between the estimates from the higher series members and from $H\delta$ and $H\gamma$ for IC 2149; perhaps the higher members of the series are actually formed in a shell. The estimate of log N_e for IC 4593 is only slightly lower than that previously published, but the new value for NGC 2392 is lower by about a factor of 10! This result applies to the region of the atmosphere where the cores of the higher members of the Balmer series are formed.

If the method previously described for the estimation of effective surface gravities is employed,[2] somewhat smaller surface gravities than were earlier suggested are indicated. Our data are consistent with the suggestion that the masses of the planetary nuclei are not very much larger than that of the sun.

Finally, the same type of analysis as was applied to the Balmer lines to get the number of hydrogen atoms in the second-quantum level may be employed with the Pickering lines of ionized helium to get log $N_{1,4}H$, the number of ionized helium atoms in the fourth level. The determination is less certain; alternate lines of the Pickering series (those not blended with hydrogen) have to be used. The estimated values are given in the eighth column of Table 4. From a comparison of the second and eighth columns we obtain with the aid of the combined Boltzmann and Saha equations for hydrogen and ionized helium

$$\log \frac{N(H^+)}{N(He^{++})} = \log \frac{N_{0,2}H}{N_{1,4}H} + 0.60.$$

Now, employing the electron pressures and excitation temperatures previously derived, we get the hydrogen/helium ratios found in the last column. Except for NGC 2392, the abundance ratios are not very different from those found recently for normal stars, i.e., ~20.

[12] *Ap. J.*, **90**, 439, 1939.

[13] *Zs. f. Phys.*, **133**, 124, 1952.

It should, however, be obvious that this estimate is meaningless. The derived *He/H* ratio depends very critically upon the temperature. We assigned an excitation temperature on the basis essentially of the *H/He* II ratio and Petrie's calibration of the temperature scale for normal O stars, which assumes a normal *H/He* ratio. Hence it is inevitable that the same *H/He* ratio would be found as for normal stars.

Suppose that the *He/H* ratio is actually greater for the planetary nuclei than for the normal type I stars. At the higher temperatures the Pickering lines will be greatly strengthened, simulating the spectrum of a yet hotter star. Thus if the excitation temperatures are really a bit lower than we have supposed, the stars turn out to be helium-rich! In the earlier paper attention was called to the nucleus of NGC 246, whose spectrum corresponds to that of a high-temperature helium star and cannot be explained by a high-temperature atmosphere with a *He/H* ratio of $\sim\frac{1}{30}$.

At the moment, a clear-cut decision concerning the *He/H* ratio in the planetary nuclei cannot be given. A complete analysis of the spectrum by the method of model atmospheres appears to be the most promising approach, but the path is not an easy one. In the NGC 2392 nucleus, different lines have different radial velocities.[14] Under such circumstances the basis for the construction of a definite model is not clear. It is necessary to reproduce the observed Balmer-line profiles and the total intensities of other lines, with the temperature, surface gravity, and *He/H* ratio as free parameters. Furthermore, the lines may be broadened by rotation. We must defer this calculation to a second paper.

Since the Balmer-line profiles in NGC 2392 show a general similarity to those in 10 Lacertae, we might expect the excitation temperature to be lower than we had supposed. The dependence of the *H/He* ratio on the excitation temperature in this star is exhibited in the accompanying table, calculated for an isothermal atmosphere and log $P_e = 2.16$.

$\theta = 5040/T$	T (° K)	log $[N(He^{++})/N(He^{+})]$	*H/He*
0.145	34,800	+0.83	5.7
.150	33,600	+ .52	5.2
.155	32,400	+ .21	4.2
.160	31,500	− .10	3.0
.165	30,500	− .40	1.9
0.170	29,600	−0.71	1.1

The planetary nucleus observed in the globular cluster M15 falls about 1 mag. above the horizontal branch of blue stars in the color-magnitude array. If the nuclei represent fringe stars in such an array, they may show a fair spread in luminosity, diameter, and atmospheric chemical composition. It is possible that the *He/H* ratio varies from one such star to another, as Münch and Greenstein have found for the blue Humason-Zwicky stars.[15] The character of the spectra of the planetary nuclei is not such as to permit detailed abundance studies to be made.

If the upper part of the color-magnitude array of a globular cluster represents different evolutionary stages of stars that were once on the main sequence,[16] the great age of the type II population means that planetary nuclei—like other stars in the globular clusters—cannot have masses much greater than about 1.5 solar masses. The character of the spectra of the planetary nuclei tends to support this conclusion. The plan of the planetary nuclei in the scheme of stellar evolution cannot be assigned until the upper part of the color-magnitude array has been explained by theory.

[14] See the discussion by O. C. Wilson, *Ap. J.*, **108**, 201, 1948.

[15] J. L. Greenstein, private communication.

[16] See A. Sandage and M. Schwarzschild, *Ap. J.*, **116**, 463, 1952.

OBSERVATIONS OF THE ZODIACAL LIGHT

F. E. Roach, Helen B. Pettit, E. Tandberg-Hanssen,* and Dorothy N. Davis
U.S. Naval Ordnance Test Station, China Lake, California, and
Institute of Theoretical Astrophysics, Oslo, Norway
Received August 20, 1953

ABSTRACT

Observations of the zodiacal light for five nights between November, 1952, and April, 1953, are recorded. The variation of brightness in the plane of the ecliptic for elongations from the sun from 30° to 100° is given. A comparison with photometric measurements of the outer corona supports the hypothesis that the outer corona and the inner zodiacal light have a common physical origin. A study of the zodiacal light with filters centered on the upper-atmosphere emissions [*O* I] 5577, 6300, and *Na* I 5893 indicates (*a*) that the light has the spectral characteristics of the sun and (*b*) that there is no measurable enhancement of the nightglow in the zodiacal light.

I. INTRODUCTION

The study of the nightglow at Cactus Peak, California (latitude 36°05′ N.; longitude 117°49′ W.) is accomplished by systematic observations of the entire sky from the end of astronomical twilight to the beginning of astronomical dawn. The photometer, which has been used since January, 1951, includes four separate telescopes, each with an interference filter, three for the isolation of the nightglow radiations [*O* I] 5577, [*O* I] 6300, and *Na* D and one as a control centered at 5300 A. The sky is covered in a series of eight sweeps from the horizon through the zenith to the opposite horizon, with a shift of 22½° in azimuth between sweeps. The eight sweeps, which we call a "survey," require 32 minutes, and the sequence is repeated throughout the night. The zodiacal light is included in the observations in the evening and the morning. In this paper we shall report on a study of the zodiacal light for five nights in November and December, 1952, and in January and April, 1953.

It has been suggested by Grotrian[1] that the so-called "*F*-component" of the solar corona arises from the reflection of sunlight by solid particles in the line of sight near the sun's limb but not necessarily physically close to the sun. The zodiacal light is likewise thought to be largely due to the reflection (or diffraction) of sunlight by particles concentrated in the plane of the ecliptic. It is therefore reasonable to inquire whether the *F*-component of the corona observed within about 1°.5 from the sun during an eclipse and the zodiacal light, which is visible in the evening and morning skies at elongations greater than about 30° from the sun, are really two manifestations of the same physical phenomenon. This approach has been adopted by Allen[2] and by van de Hulst[3] following the original suggestion of Grotrian.[1] Van de Hulst noted that the slope of the straight line connecting the *F*-component of the corona and the zodiacal light was −2.4 when both the intensity and the elongation from the sun, ϵ, are on a logarithmic scale. Thus the relationship is

$$H = K\epsilon^{-2.4}. \tag{1}$$

This empirical result is especially striking, since Grotrian[1] and Baumbach[4] had found for the *F*-component of the solar corona a like variation with angular distance from the sun's

* Smith-Mundt fellow and Fulbright fellow at the California Institute of Technology, 1952–1953, on leave from the Institute of Theoretical Astrophysics, Oslo, Norway.

[1] *Zs. f. Ap.*, **8**, 124, 1934.
[2] *M.N.*, **106**, 137, 1946.
[3] *Ap. J.*, **105**, 471, 1947.
[4] *A.N.*, **263**, 121, 1937.

limb, the exponent in a relationship similar to equation (1) being −2.5. Thus a case can be made for the proposition that the two phenomena are physically related purely on the basis of the photometric measurements, with no recourse to any argument as to the physical nature or distribution of the particles scattering the light. Allen and, independently, van de Hulst did, however, examine the physical problem. Their analyses dealt with the diffraction of sunlight by small particles concentrated in the plane of the ecliptic.

A different approach to the problem of the physical origin of a portion at least of the

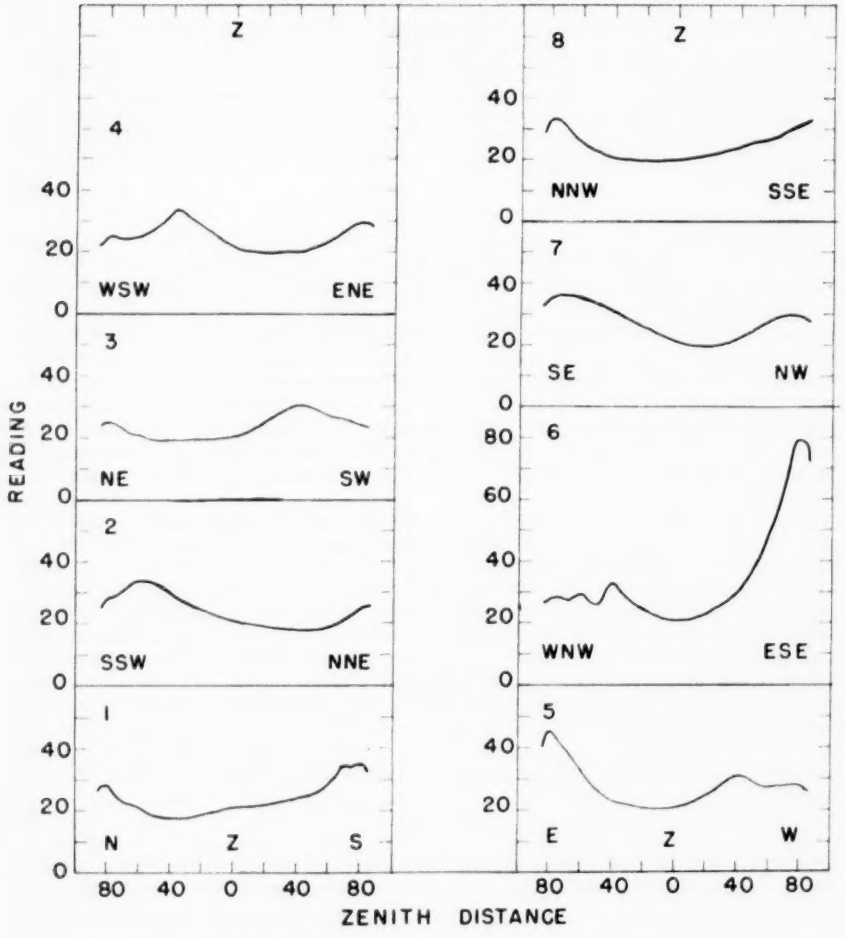

FIG. 1.—A complete survey of the sky, consisting of eight sweeps from horizon through the zenith to the opposite horizon, starting at 03^h48^m on the morning of November 19, 1952. The entire survey required 32 minutes. Filter: 5300 A. Ordinates are galvanometer deflections.

zodiacal light is indicated if, as reported by M. G. Karimov,[5] the radiations 5577, 6300, and 5893, which originate in the earth's upper atmosphere, are enhanced in the zodiacal light. This reported enhancement of the nightglow has been cited as evidence in support of the suggestion that the earth's atmosphere is stretched out in the plane of the ecliptic in a "gaseous tail" somewhat reminiscent of cometary tails.[6]

In this paper we propose to examine critically (*a*) the relationship between the intensity of the zodiacal light in the ecliptic and the elongation from the sun and (*b*) the absolute intensity of the zodiacal light in the three nightglow emissions and the control color, to detect, if possible, any enhancement of the former with respect to the latter.

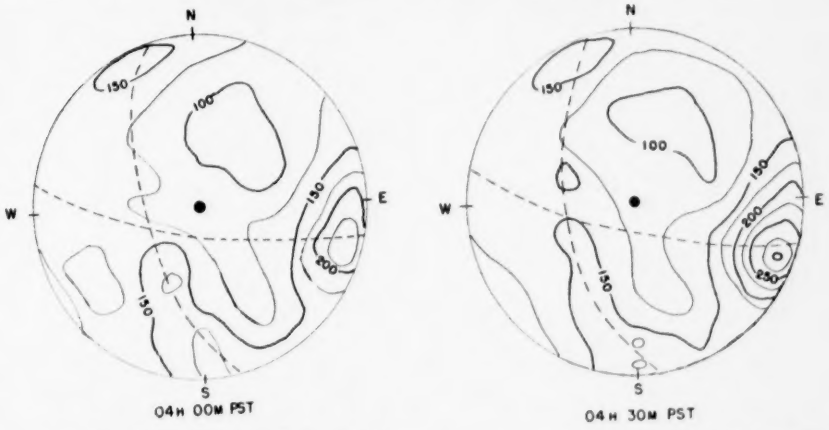

FIG. 2.—Isophote maps of the entire sky for 04^h00^m and 04^h30^m P.S.T. on the morning of November 19, 1952. 5300 Å. The ecliptic is represented by the dashed line running approximately from east to west; the galactic plane by a similar dashed line roughly from north to south. Note the concentration of the zodiacal light along the eastern part of the ecliptic, with a marked increase in intensity for the later time. Results are not corrected to outside the lower atmosphere.

II. THE OBSERVATIONS

Plots of the eight sweeps of a sky survey made with the 5300 A photometer before dawn on November 19, 1952, are shown in Figure 1. The zodiacal light is apparent in the east and east-southeast (sweeps *5* and *6*). It is more easily seen, however, on plots such as those of Figure 2, in which isophotes of the entire sky show the increase of brightness in the vicinity of the ecliptic in the eastern part of the sky. In this study we wish to restrict the problem to the measurement of the brightness of the zodiacal light along the ecliptic itself for elongations, ϵ, from the sun between 30° and 100°, leaving for later investigations (*a*) the region $100° < \epsilon < 180°$ along the ecliptic (which will include the Gegenschein) and (*b*) the region north and south to the poles of the ecliptic. For such a limited program, it is convenient to rearrange the data so as to plot the observations for a given altitude and time against azimuth, as we have done in Figure 3. The brightness of the zodiacal light (apparent as an intensification near the ecliptic) is seen to increase toward the horizon, that is, for ecliptic crossings successively closer to the sun.

In order to make a quantitative study of the variation of the intensity, H, of the zodiacal light with angular distance from the sun, it is necessary to select a convenient

[5] *Astr. J. U.S.S.R.*, **27**, 97, 1950.

[6] V. G. Fessenkov, *Astr. J. U.S.S.R.*, **27**, 89, 1950.

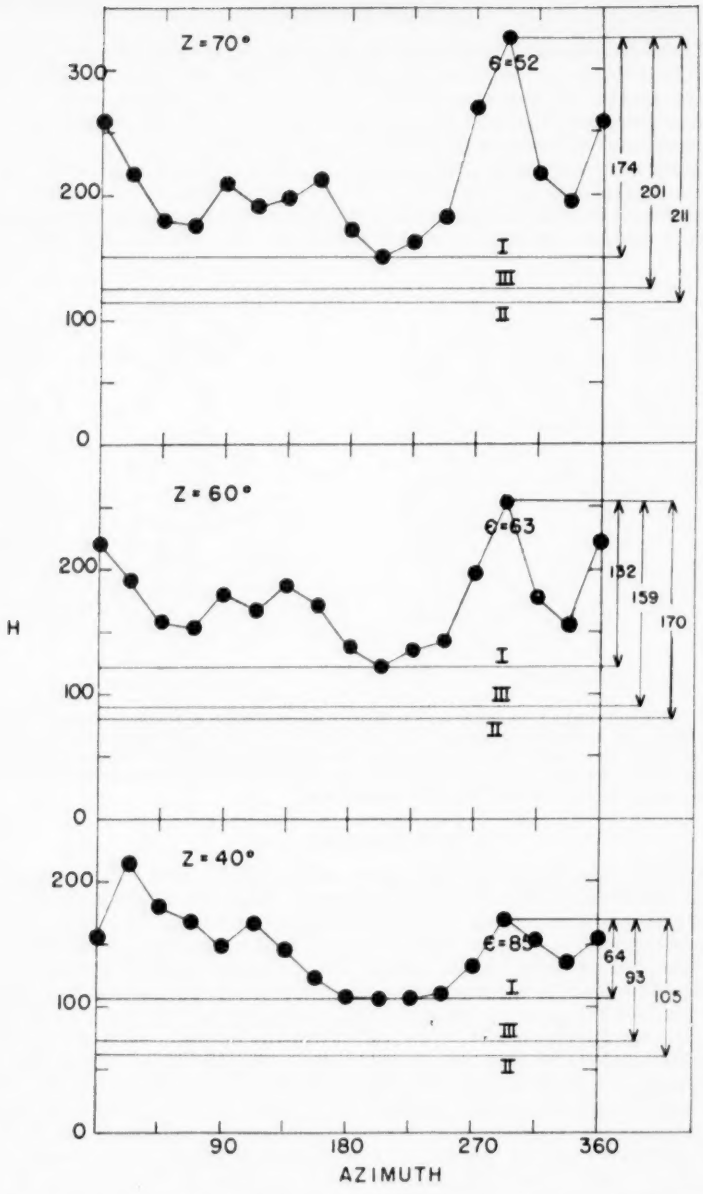

FIG. 3.—Brightness of sky in units of 10^{-18} the brightness of the center of the sun against the azimuth for $04^{h}00^{m}$ P.S.T. on November 19, 1952, for zenith distances of 70°, 60°, and 40°. Results are referred to outside the atmosphere. The zodiacal light-intensities corresponding to approximations I, II, and III (see Table 3) are indicated.

unit of brightness. We desire a unit which allows the use of three significant figures without a decimal point and which refers to the surface brightness of the sun. We choose 10^{-15} times the surface brightness of the *center* of the sun. It is convenient to calibrate the photometer by means of stellar deflections. The relationship between the surface brightness of the zodiacal light in the above unit and galvanometer deflection may be derived from a knowledge of the apparent visual magnitude of the sun (−26.72), the ratio of the surface brightness of the center of the sun to the integrated disk (1.37), the apparent area of the sun (0.20 square degrees), the area of the sky included by the photometer (19.6 square degrees), and the galvanometer deflection of a star of known visual apparent magnitude and spectral class. For convenience, we frequently use, as an intermediate unit, S, the number of tenth-magnitude (visual) G0 stars per square degree.

In Figure 3 we show plots of the brightness of the sky in units of H against the azimuth for 0400 P.S.T. on the morning of November 19, 1952. In order to obtain such a snapshot plot, it was necessary to make detailed time plots of the individual observations from which interpolated readings were made for the time desired. To estimate the intensity

TABLE 1

READINGS FOR 0400 P.S.T., NOVEMBER 19, 1952
(Zenith Distance = 70°)

Azimuth	H	Galactic Co-ordinates		Ecliptic Co-ordinates	
		b	l	β	$\lambda-\lambda_\odot$
0	441	0	220	−53	−102
22½	368	−17	205	−53	−138
45	304	−30	188	−43	−165
67½	300	−38	163	−25	−180
90	354	−37	137	− 5	−189
112½	325	−29	114	+14	−195
135	338	−14	97	+36	−197
157½	362	+ 3	85	+57	−198
180	294	+21	74	+77	−188
202½	257	+40	64	+79	− 61
225	276	+59	49	+59	− 45
247½	309	+76	9	+37	− 45
270	459	+74	285	+17	− 48
292½	555	+56	254	− 4	− 53
315	368	+37	241	−24	− 62
337½	332	+18	230	−41	− 76

of the zodiacal light from plots such as Figure 3, it is necessary to establish the level of zero intensity. In the present analysis we have approached the question of the zero by a series of successive approximations indicated by *I*, *II*, and *III* in Figure 3. In the first approximation we assumed that the lowest reading on the plot corresponds to zero zodiacal light; in the second, we assumed that the distribution of the zodiacal light over the entire sky corresponds to that determined by Elvey and Roach[7] (designated "LVR"); and in the third we made an empirical correction to the LVR distribution, to be described later. The procedure for approximation II is best illustrated by a specific example. In Table 1 we show the basic data, including the galactic and ecliptic co-ordinates corresponding to the individual points of the upper curve of Figure 2. The minimum reading occurred for an azimuth of 202½°, corresponding to galactic co-ordinates $b = 40°$ and $l = 64°$ and ecliptic co-ordinates $\beta = 79°$ and $\lambda - \lambda_\odot = \epsilon = -61°$. The maximum

[7] *Ap. J.*, **85**, 231, 1937.

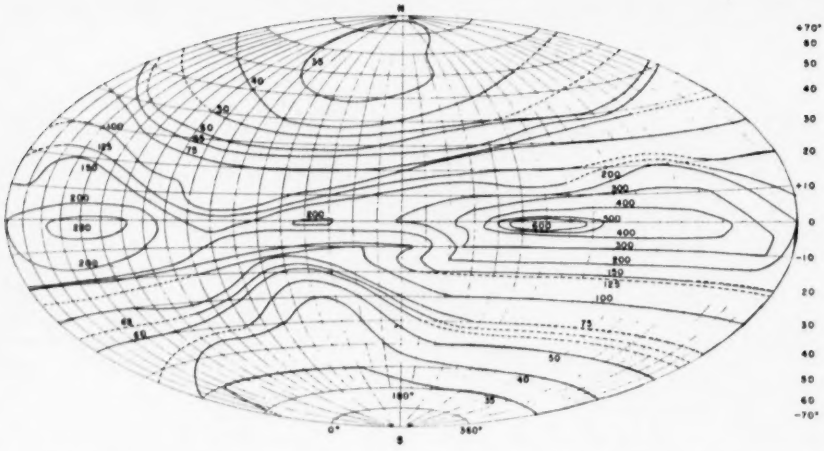

FIG. 4.—Distribution of brightness of sky due to integrated starlight in galactic co-ordinates (deduced from tables of van Rhijn, *Groningen Pub.*, No. 43). The resolution is not sufficient to show the details in the Milky Way. Unit is number of tenth-magnitude (visual) stars per square degree.

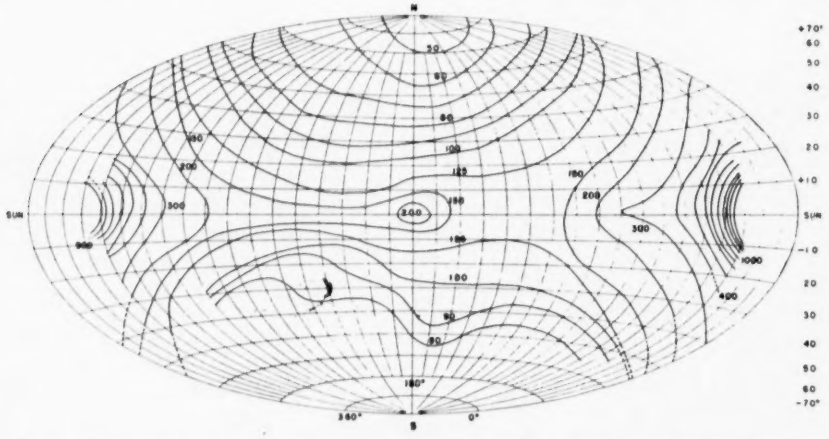

FIG. 5.—Composite curve of the distribution of the zodiacal light over the entire sky in ecliptic co-ordinates (from Elvey and Roach, *Ap. J.*, **85**, 231, 1937). Unit is number of tenth-magnitude (photographic) stars per square degree.

reading at an azimuth of $292\frac{1}{2}°$ corresponds to $b = 56°$, $l = 254°$; $\beta = -4°$, $\lambda - \lambda_\odot = -53°$.

We first make a correction for the difference between the contributions of direct starlight between the maximum and minimum readings by reference to a plot (Fig. 4) of the integrated intensity of starlight based on the extensive tables of van Rhijn.[8] Next we estimate the amount of zodiacal light at the minimum point by reference to Figure 5, based

[8] *Groningen Pub.*, No. 43, 1929.

on a composite of the several plots of the distribution of the zodiacal light over the sky given by Elvey and Roach.[7] The case under illustration is shown in Table 2. Note that Figure 4 is in the unit number of tenth-magnitude *visual* stars per square degree, and Figure 5, in number of tenth-magnitude *photographic* stars per square degree. In converting from number of tenth-mag. stars per square degree to units of H, the following were used:

$\log H = \log S$ (in unit of number of tenth-mag. photographic stars per square degree) $- 0.252$,

$\log H = \log S$ (in unit of number of tenth-mag. visual stars per square degree) $- 0.480$.

In Table 4 we show the results of such a systematic analysis (approximations I and II) for the morning observations of November 19, 1952, for the wave length 5300. The data are shown plotted as $\log H$ against $\log \epsilon$ ($= \lambda - \lambda_\odot$) in Figure 6. A smooth curve is drawn freehand through the observational points. On all the nights we obtained data for the 5300 A region. On the morning of November 19 we added results for 5577, 5890, and 6300; and on the morning of December 15, we included 5577.

Working plots similar to Figure 6 have been made for each half-night and for each color. From the smooth curves the values of the zodiacal light have been read for each 5° of ϵ from 30° to 100°. The results are summarized in Tables 5 and 6 for approximations I and II, respectively. The next step in the analysis was to compare the results of approximation II with the old data of Elvey and Roach. In Table 6 and Figure 7 the correspond-

TABLE 2

SAMPLE CALCULATION FOR APPROXIMATIONS I, II, AND III
(Z = 70°; 0400 P.S.T., November 19, 1952)

	Reading	S(vis) (Outside the Atmosphere)	S(ph) (Outside the Atmosphere)	H (Outside the Atmosphere)
Maximum reading	45.3	982	580	325
Minimum reading	21.0	455	269	151
Zodiacal light (approximation I)	24.3	527	311	174
Integrated starlight at maximum (from Fig. 4)	1.8	40	24	13
Integrated starlight at minimum (from Fig. 4)	2.5	54	32	18
Correction for starlight (minimum − maximum)	0.7	14	8	5
Zodiacal light at minimum (from Fig. 5)	4.4	96	57	32
Correction (approximations I–II)	5.1	110	65	37
Zodiacal light (approximation II)	29.4	638	376	211
Zodiacal light at minimum (Fig. 5×0.70)	3.06	66	39	22
Correction (approximations I–III)	3.76	82	48	27
Zodiacal light (approximation III)	28.0	608	359	201

TABLE 3

SUMMARY OF ZODIACAL LIGHT EVALUATION FOR THREE APPROXIMATIONS (SEE FIG. 3)

Z	70	60	40
ϵ	52	63	85
Approximations:			
I	174	132	64
II	211	170	105
III	201	159	93

ing data in the two studies are shown. It is seen that they are in substantial agreement for the lower intensities (large values of ϵ) but disagree significantly for the higher intensities (small values of ϵ). The reason is apparent on recollecting that, for large values of ϵ, the zero correction applied in approximation II is larger than the original reading and that the method of analysis thus forces case II to approximate equality with the LVR results. On the other hand, for small ϵ, the zero correction is small compared to the uncorrected reading, and the final deduced intensity is almost independent of the LVR solution. The difference between the two analyses for the higher intensities thus represents a systematic departure of one with respect to the other, due either to a real difference in the brightness of the zodiacal light between 1936–1937, when Elvey and Roach made

TABLE 4

MORNING ZODIACAL LIGHT, 5300 A, NOVEMBER 19, 1952

P.S.T.	Z	ϵ	log ϵ	log H	
				I	II
3.0	40	97	1.986	1.622	1.928
3.5		91	1.959	1.752	1.992
4.0		85	1.929	1.802	2.012
4.5		80	1.903	1.852	2.054
4.83		76	1.880	1.922	2.094
3.0	50	85	1.929	1.822	2.024
3.5		79	1.898	1.884	2.063
4.0		73	1.863	1.946	2.104
4.5		68	1.832	2.017	2.155
4.83		65	1.812	2.096	2.214
3.0	60	74	1.869	1.928	2.092
3.5		70	1.845	2.018	2.152
4.0		63	1.799	2.122	2.228
4.5		58	1.764	2.212	2.302
4.83		54	1.732	2.288	2.364
3.0	70	64	1.806	2.032	2.164
3.5		59	1.770	2.130	2.234
4.0		52	1.716	2.246	2.132
4.5		47	1.672	2.402	2.479
4.85		42	1.624	2.509	2.569
3.0	75	60	1.778	2.143	2.256
3.5		53	1.724	2.181	2.282
4.0		48	1.682	2.289	2.367
4.5		42	1.624	2.468	2.539
4.83		38	1.580	2.609	2.662
3.0	80	54	1.732	2.188	2.299
3.5		48.5	1.686	2.265	2.348
4.0		42	1.624	2.400	2.470
4.5		36	1.556	2.556	2.614
4.83		32	1.505	2.752	2.792
3.0	85	49	1.690	2.273	2.398
3.5		43	1.634	2.414	2.496
4.0		37	1.568	2.560	2.618
4.5		31	1.492	2.758	2.797
4.83		26.7	1.426	2.955	2.978

their observations, and 1952–1953 or to systematic errors in the calibration of one or both photometers.

In our third approximation we assumed that the LVR data could be reconciled with our present analysis by multiplying the zero correction from Figure 5 by 0.70, which corresponds to the difference between our approximation II at *small* values of ϵ and the old LVR analysis. The results of this approximation (III) are shown in Table 7. After completion of a detailed and independent study, now in progress, of the intensity of the zodiacal light over the entire sky, it is planned to make a fourth approximation; but it is probable that the present results will be modified only slightly by this further refinement.

III. THE VARIATION OF BRIGHTNESS WITH ϵ

In Figure 8 we have plotted log H versus log ϵ for approximations I, II, and III from the means of all the data as recorded in Tables 5, 6, and 7. Approximation I is very well

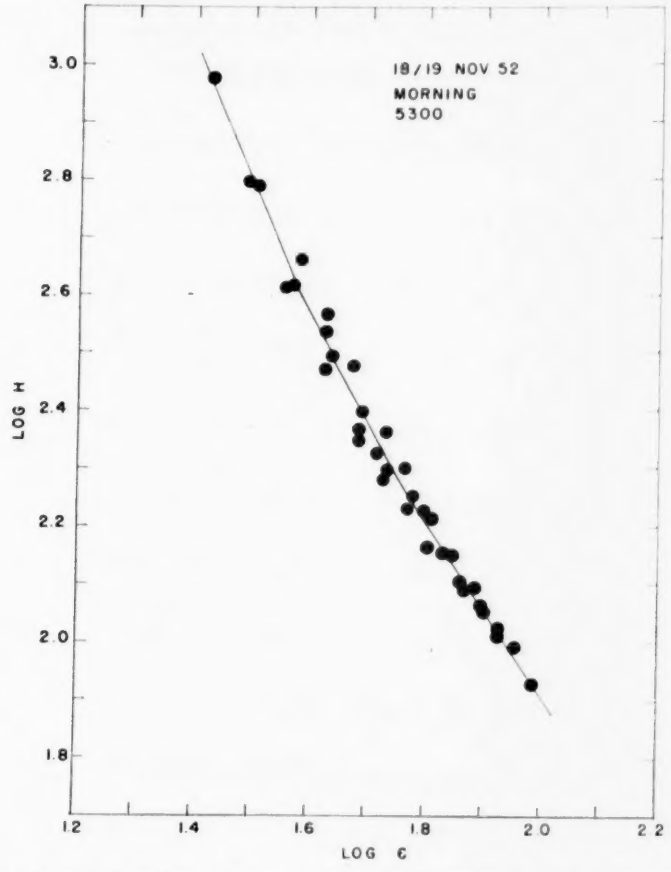

FIG. 6.—Plot of the logarithm of the morning intensities (November 19, 1952) of the zodiacal light against the logarithm of the elongation from the sun. Approximation II (see Table 4).

TABLE 5

APPROXIMATION I

ϵ	LOG ϵ	5300									5577		5893	6300	MEANS	
		Morning				Evening					Morning					
		Nov. 18/19	Nov. 19/20	Dec. 14/15	Jan. 14/15	Nov. 18/19	Nov. 19/20	Dec. 14/15	Jan. 14/15	Apr. 14/15	Nov. 18/19	Dec. 14/15	Nov. 18/19	Nov. 18/19	$\overline{H}$	log $\overline{H}$
30	1.477	660	740	976	.....	.....	.....	.....	.....	484	720	986	675	603	730	2.864
35	1.544	451	436	603	.....	.....	.....	.....	.....	376	597	493	436	406	475	2.677
40	1.602	331	302	398	.....	.....	.....	355	478	302	466	338	358	288	362	2.559
45	1.653	249	226	297	288	.....	416	263	331	248	364	254	284	214	286	2.457
50	1.699	195	166	229	204	.....	282	199	234	209	272	193	236	170	216	2.334
55	1.740	160	139	178	160	178	214	158	166	178	203	147	202	143	171	2.233
60	1.778	135	119	141	123	143	170	129	135	155	160	112	174	123	140	2.146
65	1.813	115	105	116	95.4	116	132	106	112	135	126	88.4	148	104	115	2.060
70	1.845	97.5	93.1	97.5	79.4	96.5	105	90.4	93.2	120	107	72.4	125	87.0	97.2	1.988
75	1.875	85.0	83.0	85.0	67.5	81.3	85.0	77.5	75.7	106	89.0	61.4	102	74.0	82.5	1.917
80	1.903	74.0	74.0	73.5	63.0	67.5	72.4	65.7	64.5	97.5	75.8	51.3	81.7	63.7	71.1	1.853
85	1.929	64.5	66.0	62.4	53.0	58.9	62.3	54.5	56.1	85.6	66.0	43.6	66.0	54.9	61.5	1.790
90	1.954	56.6	60.0	54.9	47.8	50.1	52.5	39.8	46.6	76.0	.....	37.8	50.0	46.6	51.6	1.713
95	1.978	46.3	55.0	49.5	44.6	41.6	43.6	29.5	37.2	70.7	.....	32.3	42.1	40.3	44.4	1.648
100	2.000	39.8	.....	43.6	40.6	34.6	34.6	22.4	.....	65.3	.....	26.9	36.2	36.3	38.0	1.580

TABLE 6

APPROXIMATION II

ϵ	LOG ϵ	5300									5577		5893	6300	MEANS		LVR SOLUTION	
		Morning				Evening					Morning							
		Nov. 18/19	Nov. 19/20	Dec. 14/15	Jan. 14/15	Nov. 18/19	Nov. 19/20	Dec. 14/15	Jan. 14/15	Apr. 14/15	Nov. 18/19	Dec. 14/15	Nov. 18/19	Nov. 18/19	$\overline{H}$	log $\overline{H}$	$\overline{H}$	log $\overline{H}$
30....	1.477	709	714	1050	.....	.....	.....	.....	.....	707	754	924	744	665	783	2.894	.....	.....
35....	1.544	492	481	645	.....	.....	.....	.....	.....	476	536	617	535	447	529	2.723	760	2.880
40....	1.602	370	355	450	.....	.....	.....	396	511	356	389	437	416	331	401	2.604	560	2.748
45....	1.653	288	268	343	330	.....	363	298	372	280	293	341	332	263	314	2.497	438	2.641
50....	1.699	244	208	272	263	.....	271	236	282	228	237	269	272	220	250	2.398	352	2.546
55....	1.740	200	177	219	213	240	210	197	209	195	200	218	230	190	208	2.318	286	2.457
60....	1.778	174	156	180	181	180	169	169	170	171	170	185	199	167	175	2.244	238	2.378
65....	1.813	154	142	154	155	147	138	148	151	152	148	157	173	147	151	2.180	206	2.313
70....	1.845	138	133	135	133	129	122	134	132	140	132	133	152	130	134	2.128	178	2.250
75....	1.875	125	123	119	116	117	112	121	123	128	117	117	137	117	121	2.084	155	2.190
80....	1.903	114	115	109	102	110	104	112	112	119	105	105	125	107	111	2.046	137	2.137
85....	1.929	104	109	100	93.4	102	98.2	103	104	112	95.8	95.8	115	98.6	102	2.009	123	2.092
90....	1.954	95.5	103	93.4	85.1	93.5	92.5	95.5	96.5	105	.....	87.0	107	91.2	96.3	1.984	109	2.036
95....	1.978	88.5	98.5	88.7	78.5	91.3	88.4	90.0	91.0	100	.....	80.5	98.7	84.8	89.9	1.953	98.3	1.992
100....	2.000	81.7	.....	83.6	73.3	87.0	83.6	85.0	85.4	95.0	.....	74.6	93.1	79.5	83.8	1.923	89.6	1.952

represented by a straight line of slope −2.41. The other approximations depart slightly, but significantly, from a straight line. For approximation III the slope is about −2.22 for the smaller values of ϵ. The curvature which is apparent for $\epsilon > 60°$ suggests that the Gegenschein brightening may be affecting the observations at angles much less than 180°. We plan to make an independent study of the Gegenschein for a test of this point. A comparison of our solutions I and III, the LVR solution, and a recent study by Behr and Siedentopf[9] is shown in Figure 9.

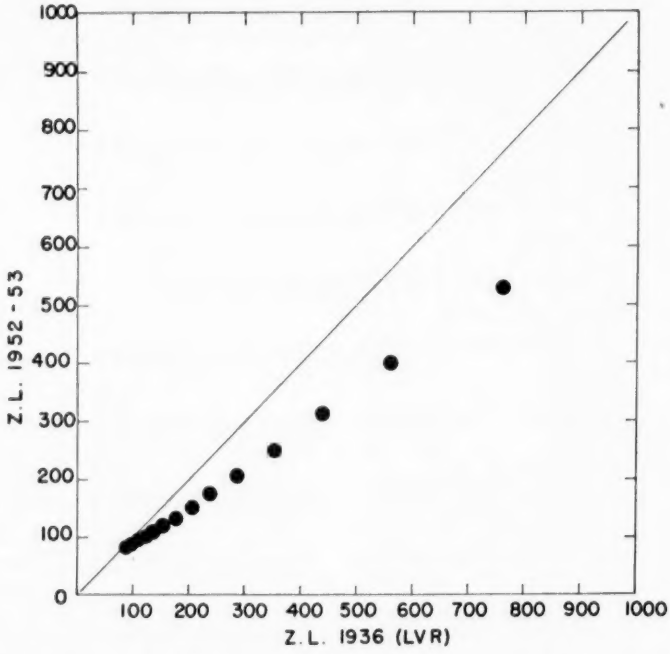

FIG. 7.—Comparison of the brightness of the zodiacal light from approximation II and the earlier results of Elvey and Roach (*op. cit.*). Unit of brightness is *H*.

A comparison of the brightness of the zodiacal light and the *F*-component of the solar corona is now in order. For the variation of corona-*F* with elongation from the sun, we use an approximation quoted by van de Hulst[3] based on a comparative study of the observational results of Baumbach[4] and of Grotrian:[1]

$$H_F(\rho) = \frac{0.053 \times 10^9}{\rho^{2.5}} + \frac{0.20 \times 10^9}{\rho^5}, \qquad (2)$$

where ρ is elongation from the center of the sun in *solar radii*. The formula is valid to $\rho = 5$ ($\epsilon = 1°.25$). Computed values of log H_F from equation (2) are given in Table 8. In Figure 10 we show a plot of log H versus log ϵ both for the *F*-corona from equation (2) and for the zodiacal light (our approximation III). The two sets of data can be joined

[9] *Zs. f. Ap.*, **32**, 19, 1953.

TABLE 7

APPROXIMATION III

ϵ	log ϵ	5300									5577	5893	6300	Means	
		Morning				Evening					Morning				
		Nov. 18/19	Nov. 19/20	Dec. 14/15	Jan. 14/15	Nov. 18/19	Nov. 19/20	Dec. 14/15	Jan. 14/15	Apr. 14/15	Nov. 18/19	Dec. 14/15	Nov. 18/19	Nov. 18/19	$\overline{H}$	log $\overline{H}$
30	1.477	664	740	1025	.....	.....	.....	.....	.....	676	811	890	706	660	772	2.888
35	1.544	484	490	684	.....	.....	.....	.....	.....	454	550	609	525	426	528	2.724
40	1.602	355	355	473	.....	.....	.....	350	501	331	406	441	406	302	392	2.594
45	1.653	282	263	354	354	.....	371	269	376	257	326	334	331	240	313	2.496
50	1.699	225	204	276	324	.....	272	214	295	214	262	251	269	199	250	2.398
55	1.740	188	170	221	202	204	204	181	218	183	218	196	228	172	199	2.299
60	1.778	162	150	172	165	162	162	155	172	160	186	155	199	150	165	2.218
65	1.813	145	135	141	138	133	136	134	141	143	157	123	170	133	141	2.149
70	1.845	126	123	123	120	112	114	120	121	130	135	104	148	118	123	2.090
75	1.875	113	112	110	104	97.5	98.6	107	107	118	120	90.0	130	105	109	2.038
80	1.903	102	104	98.7	92.3	89.6	89.6	97.6	96.5	108	110	79.4	115	95.4	98.3	1.993
85	1.929	94.2	97.5	91.0	83.2	84.0	83.6	89.0	89.0	99.4	98.6	70.6	102	87.0	89.9	1.954
90	1.954	85.2	91.0	83.7	75.5	78.4	78.5	81.0	81.6	92.0	.....	64.5	91.0	79.3	81.8	1.913
95	1.978	78.5	86.0	77.5	69.7	74.0	73.6	74.0	76.6	84.4	.....	58.5	83.0	73.5	75.8	1.880
100	2.000	73.3	.....	72.9	64.6	69.0	70.7	67.6	72.4	79.1	.....	55.7	75.7	68.5	70.0	1.846

by a straight line with a slope of -2.30, as compared with slopes of -2.5 for the outer part of corona-*F* and -2.22 for the inner zodiacal light (approximation III).

IV. ARE THE UPPER-ATMOSPHERE EMISSIONS ENHANCED IN THE ZODIACAL LIGHT?

We now wish to examine our data for any enhancement of the nightglow emissions in the zodiacal light. Numerous attempts have been made to evaluate the spectral character of the zodiacal light by conventional spectrographic methods. In order to obtain a spectrogram of suitable density, the exposure must be of such length that the stronger nightglow features appear as emission lines superimposed on the zodiacal light spectrum, which, under low dispersion, is a continuum of a color similar to that of the sun. Obtain-

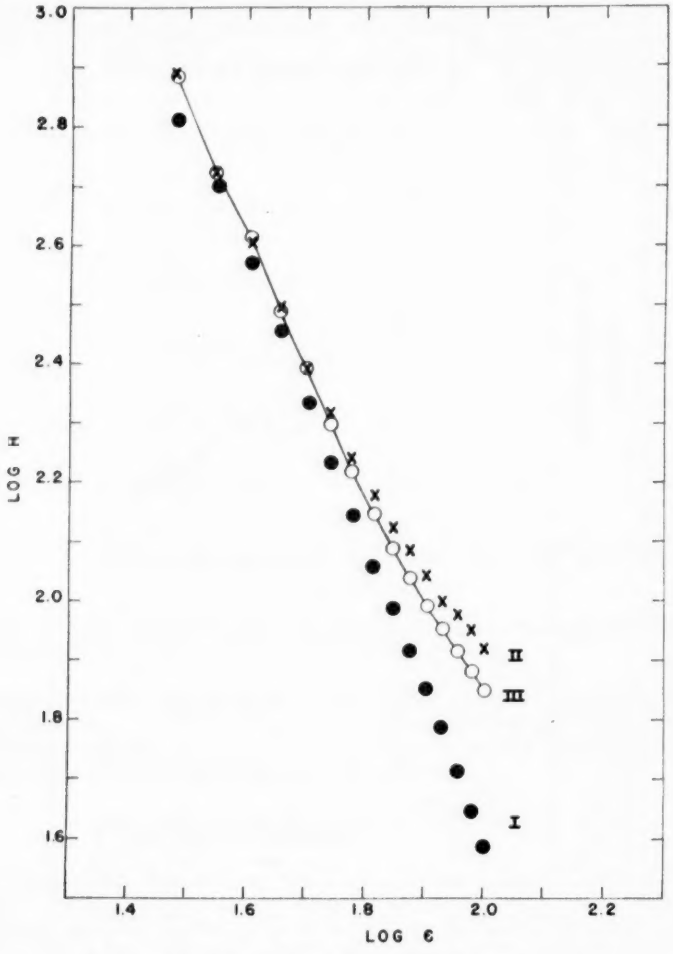

FIG. 8.—Log H versus log ϵ for approximations I, II, and III

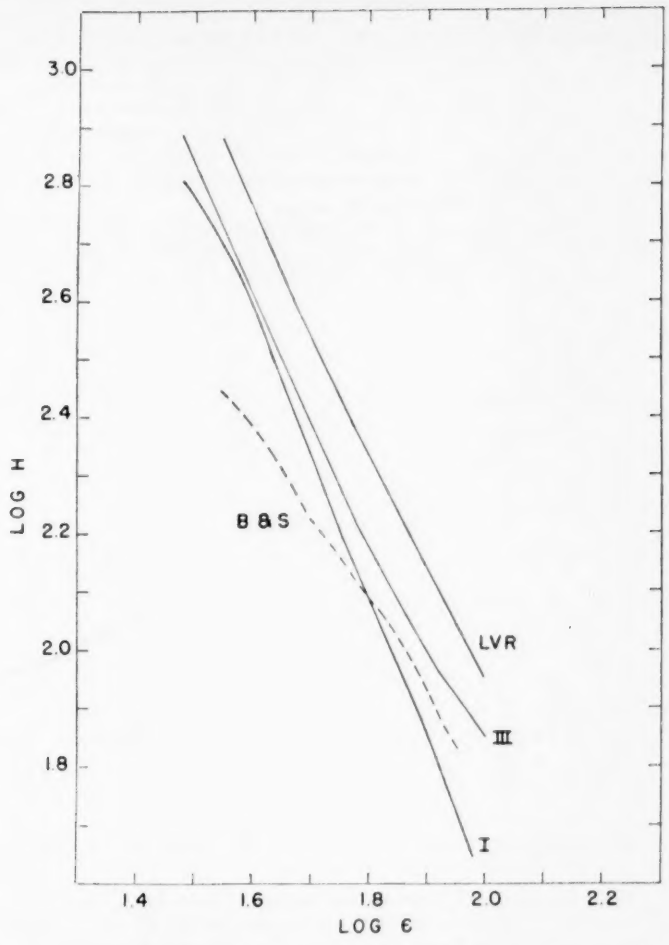

FIG. 9.—Log H versus log ϵ; approximations I and III, LVR solution, and recent results of Behr and Siedentopf (*Zs. f. Ap.*, **32**, 19, 1953).

TABLE 8

THE CORONA-F (FROM EQ. [2])

ρ	ϵ	log ϵ	log H_F	ρ	ϵ	log ϵ	log H_F
1.0	0°.250	−0.602	8.404	3.5	0°.875	−0.058	6.432
1.5	.375	− .426	7.653	4.0	1.000	.000	6.274
2.0	.500	− .301	7.220	4.5	1.125	+ .052	6.131
2.5	.625	− .204	6.868	5.0	1.250	+0.098	6.012
3.0	0.750	−0.125	6.622				

ing numerical estimates of the intensity of the emission lines involves the photometry of spectrograms of very low dispersion. The errors inherent in photographic spectrophotometry make the evaluation of *differences* in intensity of an emission line between the regions of strong zodiacal light and the sky in general a very difficult problem. A further complication is that the nightglow emissions are known to vary significantly with time and position in the sky, because of variations in the brightness of the upper-atmosphere emitting layers in the geographical sense, so that enhancements in the ecliptic are not necessarily associated with the zodiacal light.

A recent spectrophotometric study of the problem by Karimov[5] has indicated a significant enhancement of the three emissions 5577, 5893, and 6300 in the zodiacal light. He employed a spectrograph adapted to the simultaneous observation of three regions of

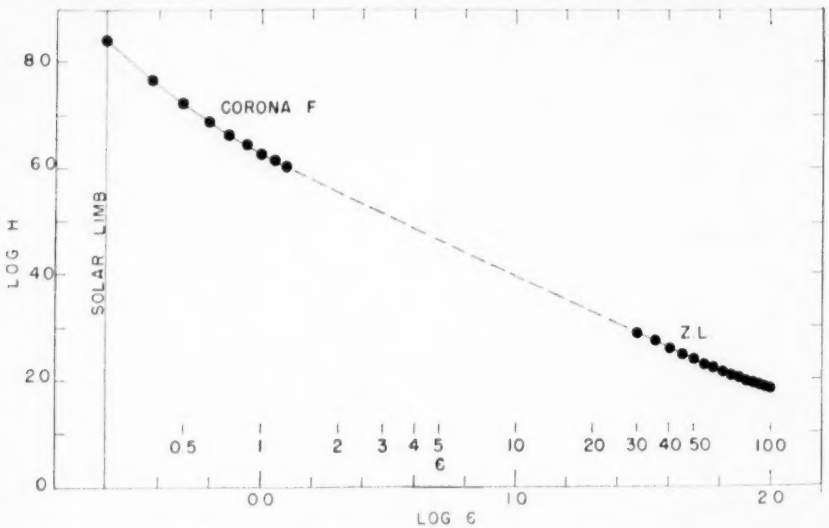

FIG. 10.—Log *H* versus log ϵ for the outer corona (eq. [2] of text) and the zodiacal light (approximation III).

the sky along an almucantar 15° above the horizon. Three totally reflecting prisms brought regions (*a*) on the ecliptic, (*b*) 20° to the south, and (*c*) 20° to the north to portions of the horizontal slit. The linear dispersion in the green was 300 A/mm, so that the separation of the three emission lines on the spectrogram was of the order of 1 mm. Karimov states that a wide slit was used, though the emission lines were still resolved. A summary of his results is given in Table 9 (his Table 2). The mean of six spectrograms (only four for sodium D) gives enhancements of 1.36 for 5577, 2.00 for 5893, and 1.44 for 6300, referred to the region 20° to the south as unity. We shall return to this study after discussing the results of our own work.

The basis for the initial discussion of our observations of the zodiacal light with filters centered on the nightglow radiations is found in Table 7. On two nights we made complete analyses of the variation of intensity with ϵ for the telescope transmitting 5577, and on one night for 5893 and 6300. Since in each case the intensities are referred to the sun's center, as is also done for the observations with the control filter, 5300, it becomes possible to compare the entries of Table 7 directly, to test for enhancement of the nightglow in the zodiacal light.

The transmission properties of the four filters are shown in Figure 11 and Table 10. We note that the integrated transmissions vary from 30 to 62 A, which is thus the effective "slit-width" of our photometers. Under these conditions the nightglow corresponds in general to about 50 per cent of the total deflection for the case of 5577 and slightly less for 5893 and 6300.

TABLE 9

ENHANCEMENT OF NIGHTGLOW IN ZODIACAL LIGHT
(According to Karimov)*

DATE	INTENSITY ON AXIS OF ZODIACAL LIGHT (UNITY FOR REGION 20° SOUTH)			INTENSITY (20° NORTH OF AXIS)		
	5577	5893	6300	5577	5893	6300
1947, Nov. 15–17	1.480	1.990	1.480	1.165	1.190	1.340
1948, Feb. 4–6	1.336	1.410	1.334	1.144	1.155	1.196
Mar. 5–9	1.280	3.360	2.010	1.080	1.105	1.120
Oct. 10–13	1.360	.....	1.430	1.160	.....	1.210
Nov. 2–8	1.430	1.240	1.160	1.152	1.180	1.290
Nov. 11–13	1.304	.....	1.250	1.080	.....	1.110
Mean	1.365	2.000	1.444	1.130	1.158	1.211

* *Astr. J. U.S.S.R.*, **27**, 89, 1950.

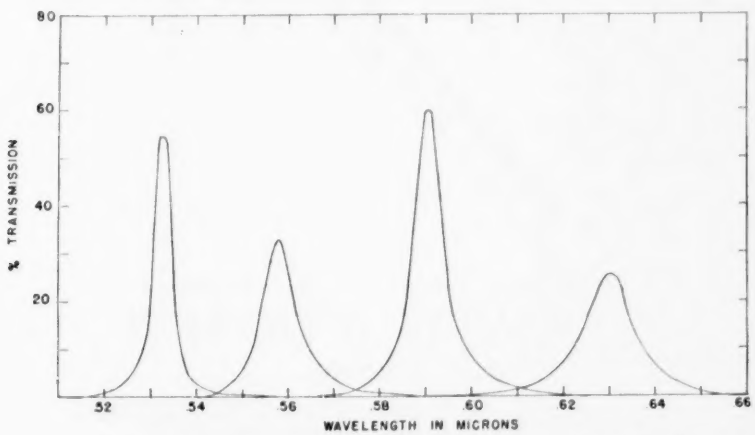

FIG. 11.—Transmission-curves of the interference filters used in this study

TABLE 10

CHARACTERISTICS OF FILTERS

	5300	5577	5893	6300
Total transmission (A)	30.6	37.8	62.2	38.0
Transmission at wave length of emission (per cent)	.....	32.0	55.0	23.0

We summarize a comparison of *H* (emission)/*H* (5300) from the entries of Table 7 in Table 11. In Figure 12 are plotted the individual observations as log *H* (emission) versus log *H* (5300) from the entries of Table 12. Although there are some departures from equality of intensity (emission versus control color), the enhancements of nightglow and control are about equally numerous and are probably included within the uncertainties of our method of analysis. Our observations thus indicate that the intensity of the zodiacal light is, within the precision of our analysis, the same in all four colors, and there is no evidence of any measurable enhancement due to the nightglow. This result is so contradictory to that of Karimov, quoted above, that it seems desirable to make a searching comparison of the two techniques employed.

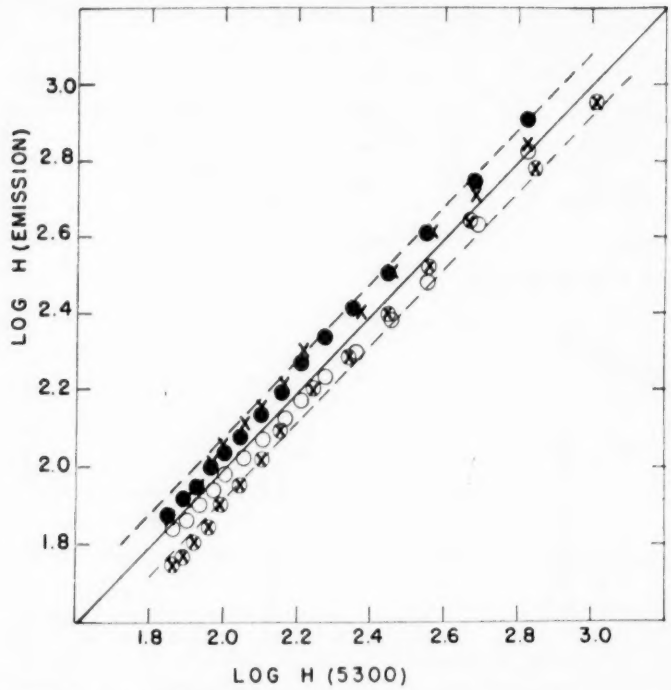

FIG. 12.—Log *H* (emission) versus log *H* (5300) from Table 12. The solid line corresponds to exact equality of brightness; the dashed lines to ±20 per cent enhancement.

TABLE 11

MEAN VALUES OF *H* EMISSION/*H* 5300

Date	Emission	H_{em}/H 5300	Date	Emission	H_{em}/H 5300
Nov. 19	5577	1.11	Nov. 19	6300	0.92
Dec. 15	5577	0.85			
Nov. 19	5893	1.13	Mean		1.00

In his paper Karimov gives one example of a detailed calculation. In his Table 1, here reproduced as our Table 13, he indicates the steps followed in obtaining the enhancement for the spectrogram of November 15–17, 1947. A study of the numerical results shows that the difference of intensity, line *plus* background *minus* background, was interpreted as the line intensity. The line intensities resulting from this differencing are in all cases small numerically, being about 21 per cent of the line *plus* background. The question arises as to what confidence can be placed in the *ratios* of the differences (row 8) used by Karimov to indicate enhancement of the nightglow in the zodiacal light.

The statistical theory of the uncertainty of the *ratio* of intrinsically small quantities is very complex, but an estimate of the significance of Karimov's results may be obtained

TABLE 12

LOG *H* FOR FOUR COLORS (FROM TABLE 7)

$-\epsilon$	Dec. 14/15, 1952		Nov. 18/19, 1952			
	5300	5577	5300	5577	5893	6300
30	3.020	2.965	2.845	2.877	2.871	2.823
35	2.810	2.790	2.692	2.729	2.728	2.650
40	2.653	2.640	2.568	2.590	2.619	2.520
45	2.536	2.533	2.460	2.467	2.522	2.420
50	2.435	2.430	2.387	2.375	2.436	2.344
55	2.341	2.340	2.303	2.302	2.361	2.280
60	2.256	2.268	2.241	2.232	2.300	2.222
65	2.189	2.197	2.187	2.170	2.238	2.169
70	2.130	2.125	2.140	2.122	2.182	2.113
75	2.077	2.070	2.096	2.070	2.137	2.070
80	2.038	2.020	2.056	2.020	2.098	2.030
85	2.000	1.981	2.018	1.981	2.063	1.994
90	1.970	1.939	1.980	.....	2.028	1.960
95	1.948	1.905	1.947	.....	1.994	1.928
100	1.922	1.873	1.912	.....	1.969	1.900

TABLE 13

EXAMPLE OF KARIMOV'S CALCULATIONS (HIS TABLE 1)*

	20° to the South	Axis of Zodiacal Light	20° to the North
1. Background reading	18.5	25	20.5
2. 5577 reading	22.5	31.5	25.5
3. log I (background)	0.410	0.550	0.460
4. log I (line+background)	0.510	0.653	0.565
5. I (background)	2.57	3.55	2.89
6. I (line+background)	3.23	4.52	3.67
7. I (line+background)$-I$ (background) $=6-5$	0.66	0.97	0.78
8. Enhancement†	1	1.480	1.165‡

* We have added the entries for rows 5 and 6 for clarification. They do not appear in Karimov's paper.

† Karimov made allowance for the differential absorption of the prisms, so that the entries in row 8 are not exactly the ratios of the entries in row 7.

‡ This entry in Karimov's Table 1 is 1.650, but a subsequent entry of 1.165 indicates the probability of a typographical error.

if we take for an index of the enhancement the *difference* in the line intensities on the axis and 20° to the south rather than the ratio. The probable error of the difference,

$$(4.52 - 3.55) - (3.23 - 2.57) = 0.97 - 0.66 = 0.31,$$

can be evaluated if the probable error of the individual entries is known. The uncertainty of the determination of relative intensities of emission features in low-dispersion spectrophotometry is probably of the order of 10 per cent. If we assign probable errors to the individual intensity measurements above of ± 5 and ± 10 per cent, we may evaluate the probable error of the double difference and find

$$\text{Enhancement} = 0.31 \pm 0.35 \text{ p.e. for the 5 per cent assumption,}$$

$$\text{Enhancement} = 0.31 \pm 0.71 \text{ p.e. for the 10 per cent assumption.}$$

In order that the enhancement may represent physical reality (i.e., be greater than zero) within 50 per cent confidence limits, it is necessary for the probable error of the individual intensity measurements to be *less than* 5 per cent. If the general level of intensity of the nightglow is lower than the above example, then an even lower probable error of measurement is necessary for the enhancements to be considered real. Since 5893 and 6300 are frequently appreciably fainter than 5577, it is expected that the estimation of their local enhancement by spectrophotometric measurements will call for precision of a very high order.

We note that there is a fundamental difference between the approaches of Karimov and ourselves. He poses the question: Are the upper-atmosphere emissions enhanced in the regions of strong zodiacal light with respect to the sky 20° to the south of the ecliptic? Our Table 12 and Figure 12 are based on the query: Is the zodiacal light enhanced in intensity when observed through filters transmitting a large fraction of upper-atmosphere emission? It is possible to treat our data in such a way that we ask essentially the same question as Karimov. In the nightglow research conducted at this laboratory for several years, it has proved useful to employ a two-color method, in which the 5300 filter is used as a control and readings with this filter are subtracted from simultaneous readings with the emission filters to give intensities of the emission. These differences in our two-color technique correspond to the differences in row 7 of Table 13 in the spectrophotometric procedure of Karimov.

In Figure 13 we show plots of the differences, 5577 emission *minus* 5300 control, for several nights and times. The shadings indicate relative intensities of the nightglow over the sky. The dashed lines show the position of the ecliptic. An examination of the region of the ecliptic in the western sky in the evening and the eastern sky in the morning indicates no significant raising of the intensity level or distortion of the isophote patterns that might be interpreted as an enhancement. In one case for which there is a suggestion of an enhancement (the morning of November 19, 1952), we note an even brighter region to the north. Furthermore, an examination of similar isophote maps for several hours before dawn shows clearly that the bright region to the east at 04^h30^m is the remnant of a patch which had been much brighter during the earlier hours and hence could not have been associated with the zodiacal light, which necessarily increases in intensity toward dawn.

The evidence from our photometric observations thus supports the proposition that the zodiacal light considered as a continuum has the same color as the sun over the spectral range 5300–6300 A, and that there is no significant enhancement of the nightglow in it.

V. CONCLUSIONS

The nature of the empirical relationship between the zodiacal light and the corona-*F* is strikingly illustrated by placing in juxtaposition the analytical expressions for the

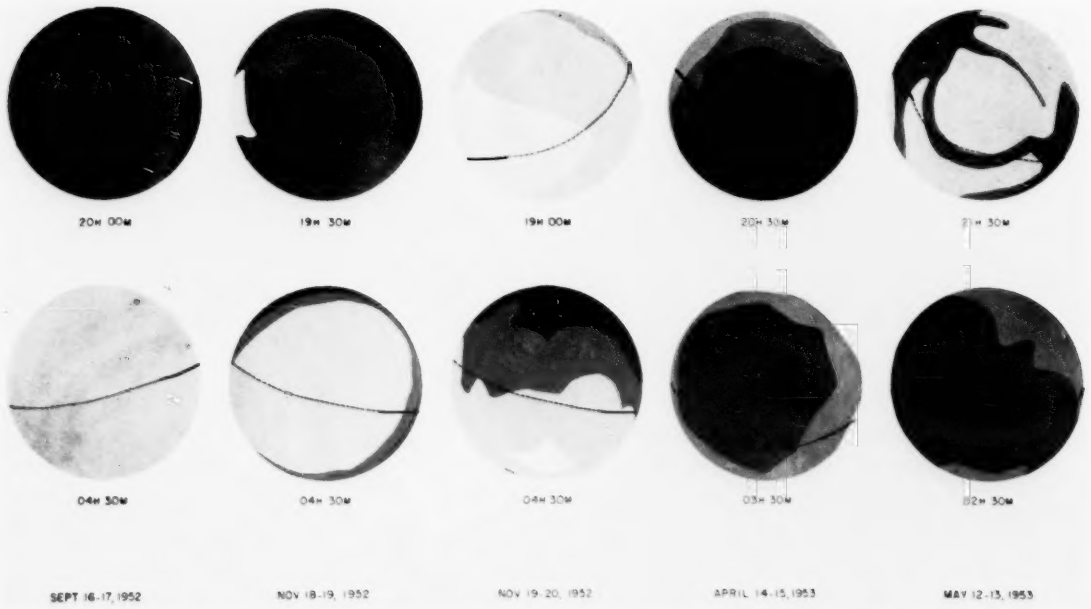

FIG. 13.—Isophote maps of the sky for a number of nights. The shadings represent the relative brightness of nightglow 5577 in steps of 25 units of H (darker shadings correspond to brighter regions). The ecliptic is indicated by a solid line in the region close to the sun, where enhancement of the nightglow in the stronger part of the zodiacal light was reported by Karimov (*op. cit.*), and by a dashed line over the rest of the sky.

variation of log H with log ϵ for (*a*) the F-component of the corona from the first term of equation (2); (*b*) the zodiacal light for $30° < \epsilon < 60°$ from our approximation III; and (*c*) the straight-line interpolation between the two sets of observations:

$$\log H = 6.22 - 2.5 \log \epsilon \qquad \text{(corona-}F\text{)}, \tag{3}$$

$$\log H = 6.17 - 2.22 \log \epsilon \qquad \text{(zodiacal light)}, \tag{4}$$

$$\log H = 6.26 - 2.30 \log \epsilon \qquad \text{(interpolation)}. \tag{5}$$

Only by an extremely unlikely coincidence could one expect to find such close agreement between equations (3), (4), and (5) if there were no physical relationship between the two phenomena. The evidence thus strongly supports the hypothesis that the outer corona and the zodiacal light have a common physical origin. The present argument, based purely on photometric observations, is strengthened by the work of Grotrian,[1] of van de Hulst,[3] and of Allen[2] based on fundamental physical analyses of the reflection (or diffraction) of sunlight by particles concentrated near the plane of the ecliptic.

We do not find any evidence for an enhancement of the atomic nightglow radiations 5577, 5893, and 6300 in the zodiacal light. The hypothesis that a significant fraction of the zodiacal light might be of atmospheric origin is thus not supported by our observations.

We are indebted to Mr. D. R. Williams for invaluable assistance with the observations at Cactus Peak on which this study is based, to Mr. E. L. Fortier for the drawing of Figure 13, and to Dr. Alexander Pogo for translations of the works referred to in footnotes 5 and 6.

THE LABORATORY DETERMINATION OF RELATIVE TRANSITION PROBABILITIES OF DIATOMIC MOLECULES

I. THE α-SYSTEM OF *TiO*

JOHN G. PHILLIPS
Berkeley Astronomical Department, University of California
Received August 10, 1953

ABSTRACT

An electric furnace and a photoelectric spectrum-scanning technique were used to produce the intensity distribution-curve in the spectrum of the α-system of *TiO* from 4500 to 6200 A. The relative intensities of individual bands of the system were determined by matching their observed profiles with profiles determined theoretically. The resulting relative transition probabilities are presented in Table 1.

A. INTRODUCTION

The relative transition probabilities of bands in the spectra of only a few diatomic molecules are known. Since such data are required before stellar atmospheric temperatures may be derived from studies of the intensities of molecular bands in stellar spectra, it is worth while to attempt a systematic study of the intensities of bands in the spectra of as many molecules of astrophysical interest as possible. This may be done most conveniently in the laboratory, using as a source of radiation an electric furnace of the carbon-resistance-tube type. Such furnaces, when operated under certain well-known conditions, approach closely to a condition of thermodynamic equilibrium. Furthermore, in view of the fact that the photographic plate introduces numerous uncertainties into the determination of the intensities of spectral features, greater photometric accuracy can be obtained if the spectra can be scanned photoelectrically. Using modern techniques, an electronic system, involving a photoelectric cell, an amplifier, and a strip-chart recorder, can be designed to be strictly linear over the entire useful range of incident intensities. The sensitivities of photoelectric cells are functions of the wave length of the incident light, but calibrations may be readily made, using a source of known spectral-intensity distribution.

Various features in a band may be used to obtain the relative intensities, $I_{v',v''}$, depending upon the particular situation and the degree of accuracy required. A few of these methods are listed below.

1. The total amount of radiation emitted in a band, integrating over all wave lengths, provides the most accurate measure of its strength, if it is completely unblended with any other spectral feature. In many cases the bands of a system fall into close sequences, with the "tails" of each band blended with following bands of the sequence. In these cases the method may still be used, provided that the rotational constants are known, since one can then readily compute the contour that each band would have exhibited if it had been unblended. In this way one may determine the contribution of each component band to the intensity of such a blend, unless, of course, bands overlap completely.

2. If the bands can be observed in absorption, with a resolution high enough completely to resolve the individual rotational lines, the relative transition probabilities of two bands can be readily determined by measuring the ratio of the combined absorptions of all lines in one band arising from a given initial state to the combined absorptions of those lines of the other band arising from the same lower state. This ratio will be independent of the number of molecules in the common lower state, provided that all lines are weak. Otherwise, curve-of-growth effects must be taken into account.

3. The peak intensities at the band heads may be used, if it can be shown that all the bands have the same structure, i.e., that the lines in each band contributing to its peak intensity lie within the same range of rotational quantum number, J, and, furthermore, the relative positions of these lines are the same for each band. The method is accurate if these conditions are fulfilled exactly and also if the individual bands are unblended, so that the true location of the background continuum at each head is known.

The first method has proved to be the most useful in the case of the α-system of *TiO*. The other methods have found application in the studies of the other molecules of interest.

Once the relative intensities of the bands of the system have been found, the relative transition probabilities may be computed immediately, since the ratio of the intensities of two bands is given by the equation

$$\frac{I_1}{I_2} = \left(\frac{\nu_1}{\nu_2}\right)^4 \left(\frac{|R_1|^2}{|R_2|^2}\right) \exp\left\{-\left[G_0(v_1) - G_0(v_2)\right]\frac{hc}{kT}\right\}. \tag{1}$$

In this equation, subscripts 1 and 2 refer to any two bands of a system; ν_1 and ν_2 are the frequencies of their respective band origins; $|R|^2$ is the transition probability; and $[G_0(v_1) - G_0(v_2)]$ is the difference in vibrational energy of the respective initial states. This equation is valid for an emission spectrum. In absorption the frequencies, ν, are taken to the first power. The Boltzmann exponential expression may be used to compute the relative populations in the various vibrational levels, since numerous investigators have found that conditions close to thermodynamic equilibrium are produced inside an electric furnace, if a partial pressure of an inert gas is introduced so that collisions between molecules are frequent.

It is proposed eventually to investigate the intensities of bands of as many molecules of astrophysical interest as possible. Exploratory studies have already been made of the spectra of C_2, *TiO*, *ZrO*, *CaH*, *YO*, *MgO*, and *MgH*. The present report presents the results of an extensive series of runs on the α-system of *TiO*.

B. EQUIPMENT

As mentioned in the introduction, the source of radiation was a carbon-resistance-tube electric furnace of the King type. The particular installation employed has been described elsewhere.[1] The spectrum was produced by a 3-meter concave-grating spectrograph with an Eagle-type mounting. The dispersion was 5 A/mm in the first order. The optical system was designed to admit to the spectrograph radiation only from the gas in the furnace and to exclude radiation from the walls of the heated graphite tube. This was accomplished by the use of a quartz lens between the furnace and the spectrograph, which threw an image of the rear of the heater tube onto the slit. In this way, one insured that the light from all parts of the inner wall of that hot tube would be out of focus on the plane of the slit and outside a circular zone defined by this image. A diaphragm at the slit then readily shielded it from this wall radiation. Scattered light was largely eliminated by limiting the aperture to $\frac{1}{4}$ inch, by means of a second diaphragm about 18 inches in front of the furnace. A field lens was employed at the slit to increase the size of the beam at the grating.

The receiver consisted of two parts: (*a*) a mechanical spectrum scanner and (*b*) an electronic amplifier and recorder. Each of these parts will be described in turn.

a) THE SPECTRUM SCANNER

The spectrum scanner is illustrated in Figure 1. It consists of a carriage traveling on a curved track, which is concentric with the Rowland circle of the spectrograph. The carriage is pulled by a rectangular block, which slides on the flattened top of the thread of

[1] L. Brewer, P. W. Gilles, and F. A. Jenkins, *J. Chem. Phys.*, **16**, 797, 1948.

the screw. A split nut fastened to the block engages the thread of the screw. The carriage is connected to the block by an arm, pivoted at the carriage. The arm slides between ways on the block, the direction of motion of the arm being perpendicular to the center line of the screw. The screw is turned by a synchronous motor through a reduction-gear train. Change gears make possible a series of scanning rates, from 0.67 to 84.66 A/min.

The scanner carriage, in turn, supports a box-shaped probe, which carries the adjustable scanning slit at one end and the photocell at the other. The probe is fastened to the carriage by means of a pivot concentric with the center line of the slit, which is held accurately on the focal line of the spectrograph. The plateholder, on which the scanner is mounted, permits travel of such a length that 2000 A of spectrum may be scanned at any particular spectrograph setting.

A complication is introduced into the design of the scanner by the requirement that the axis of the probe be centered on the grating for all wave lengths. This requires an appreciable change in the orientation of the probe, relative to the carriage, as it is driven along the spectrum. An obvious way in which this movement of the probe could be accomplished would be to let an arm on the probe move along an appropriately shaped cam. The method that was finally adopted, however, is quite a bit neater and is accurate enough for all practical purposes. It was made possible by the fact that it was planned to use the spectrograph primarily in the first order, in which case the grating is close to being diametrically opposite the scanner probe on the Rowland circle. Thus the change in direction of the probe's axis is close to being half the change in direction of the normal to the carriage as it moves along the spectrum. A simple linkage system was devised to move the probe, relative to the carriage, through the appropriate angle. It is illustrated schematically in Figure 2, which is not drawn to scale. In Figure 2, point A represents the center line of the perpendicular slit, in the focal plane of the spectrograph. The probe pivots about this point. B is the point at which the carriage is pivoted to the arm which connects it to the block. Now if a pin is fastened to the arm at point C, such that the distance C–B is equal to the distance A–B, then points A, B, and C form an isosceles triangle, and angle ψ will be half the angle θ for all positions of the carriage. Pin C slides in a slot in a sector plate, which is also pivoted at A. The probe is locked to the sector plate by a spring clip, so that angle ϕ is constant for a given spectrograph setting but may be changed if the spectral region to be scanned is changed. Thus, as the carriage moves down the spectrum, angle θ will change, and the direction of the center line of the probe will change by just half the angle θ.

b) AMPLIFIER AND RECORDER

The amplifier was built according to a design kindly furnished by Dr. Harold L. Johnson, now of the Lowell Observatory. While it was designed primarily for application to astronomical photometry, it has performed very satisfactorily as a laboratory instrument. It consists essentially of two parts: (1) a contact-modulated a.c. amplifier and (2) a d.c. power amplifier, which couples the a.c. amplifier to a Brown "Electronik" strip-chart recorder. While the amplifier was built to accept the output of various types of receiver (photomultipliers, photoelectric cells, photoconductive cells, and thermocouples), in the present application only 1P21 and 1P28 photomultiplier cells have been used. The voltages on the various stages of the photomultiplier were provided by a radio-frequency oscillator. The voltage drop per stage could be varied from 75 to 135 volts. All the records used in this study were made with 75 volts per stage.

No departure from linearity was observed over the useful amplification range of the amplifier. The linearity of the entire receiver (photocell plus amplifier plus recorder) was checked by observing the change, with temperature, of the intensity of the head of the (0–0) band of the Swan system of C_2, using the electric furnace as the source. The Swan system always appears whenever a carbon tube is heated above 2200° C. Theoretical considerations have shown[1] that one should obtain a straight line, if one plots $1/T$ against

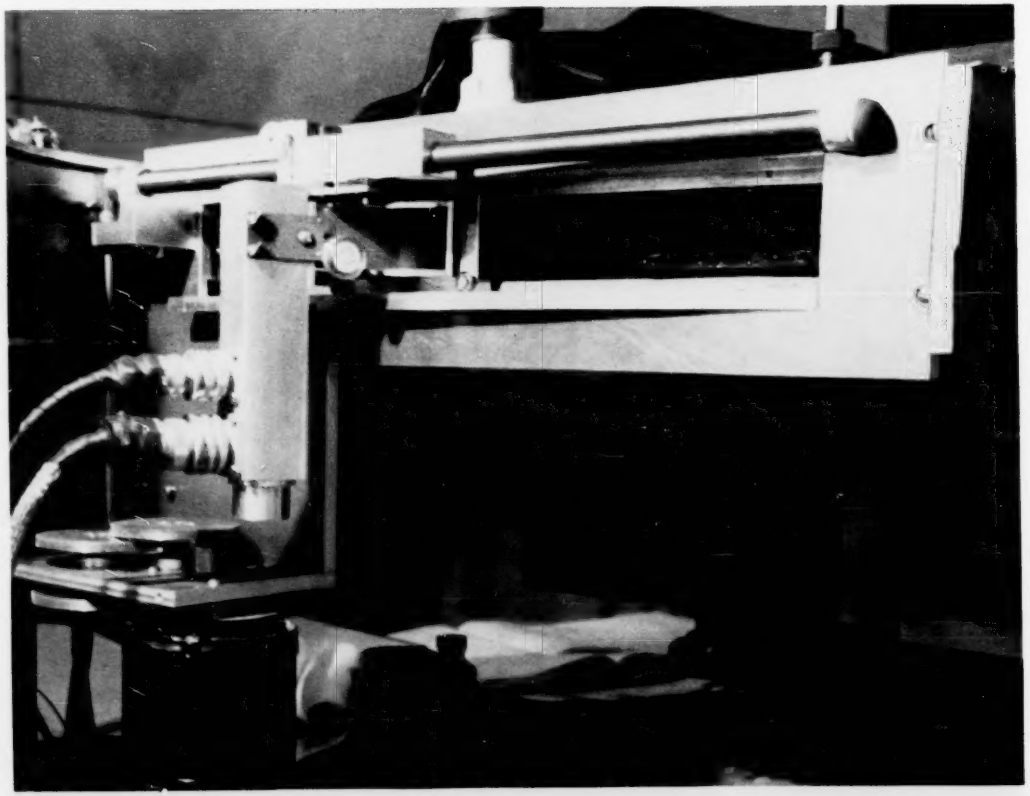

FIG. 1.—The spectrum scanner attached to the plateholder of a 3-meter concave-grating spectrograph

a complicated expression which includes, among other quantities, the logarithm of the band intensity. The observations with the photoelectric receiver did indeed result in such a straight line, over a range of 1:230 in the intensity of the head of the (0–0) band.

It was necessary to determine the relative sensitivity of the apparatus as a function of wave length. This was accomplished most conveniently by the use of the furnace itself. A solid graphite plug was inserted into the heater tube, midway down its length. About

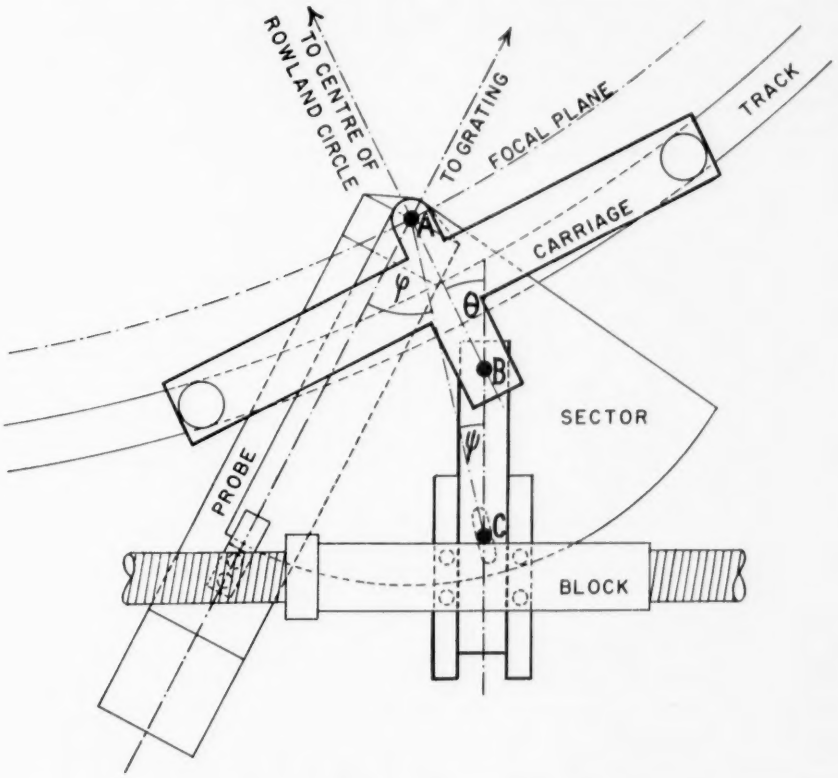

FIG. 2.—A diagram illustrating the way in which the correct orientation of the scanner probe is maintained. The diagram is not drawn to scale.

3 inches from the plug a baffle was introduced. Radiation from the cavity thus formed was allowed to pass through a small hole about $\frac{1}{8}$ inch in diameter in the baffle. The furnace thus became a good black body, and the radiation from the hole in the baffle could be considered to have an intensity distribution given by the Planck radiation law.

The advantage to be gained by using the furnace as its own calibrating device was that the effects of scattering and absorption of light in the optical system and spectrograph could be taken into account immediately. When the continuum produced by the black body was scanned, the spectrograph and optical system were placed in the same adjustment as was used later in scanning the molecular spectrum. A wave-length scale

was introduced into the continuum by interposing a mercury arc into the optical path at appropriate times. The response-curve of the photocell, as a function of wave length, could then be correlated with the emitted intensity, to give the over-all relative sensitivity-curve of the apparatus. As an example of the type of response-curve obtained, Figure 3 presents the results for a 1P21 multiplier tube.

C. THE OBSERVATIONS

The spectrum of *TiO* was produced by heating a mixture of equal amounts, by molecular weight, of TiO_2 and *Ti* in powder form. When the mixture was introduced directly into the carbon heater tube, the *TiO* bands appeared strongly when the tube was heated above 1800° C, but they soon faded, owing to the reaction with the hot carbon, which decomposed the oxide molecules, presumably producing *CO* and metallic titanium. A much longer life for the oxide bands was achieved by shielding the vapor from the hot carbon, through the use of an insert of tantalum foil, which completely covered the inside surface of the hot section of the tube. The mixture of powders was placed in a tungsten boat, which rested on the tantalum insert. The hot section of the tube was partially isolated from its cooler ends by the introduction of graphite baffles, with $\frac{1}{4}$-inch holes drilled concentrically through them. Commercial argon at a pressure of 10 cm was introduced into the furnace after evacuation. The baffles and the argon appreciably reduced the rate of diffusion of the *TiO* molecules from the ends of the heated section. With a fresh charge of powder in the furnace, a stable population of *TiO* molecules could be maintained for as long as 1 hour at the lower temperatures.

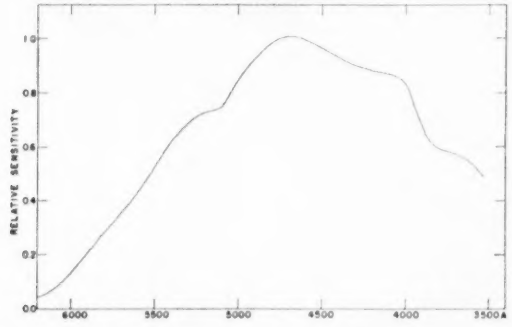

FIG. 3.—Spectral sensitivity-curve of the apparatus, when the 1P21 photomultiplier is used as receiver

Records were made, using the 1P21 phototube, with the furnace at three different temperatures—1850°, 2075°, and 2265° C. In addition, the records at 2265° C were repeated, using the 1P28 tube as receiver. The temperatures were measured with an optical pyrometer, which had been calibrated by the Bureau of Standards. A correction to the pyrometer reading was made for the absorption of radiation at the exit window; after correction, the above three temperatures became 2142°, 2375°, and 2567° K, respectively. The pyrometer actually measured the temperature of the heated walls of the tube; however, the presence of argon assured that there would be a sufficient number of collisions with the *TiO* molecules to establish thermal equilibrium with the walls.

After equilibrium conditions had been maintained at each temperature for several minutes, the spectrum was scanned several times in succession, from 4500 to 6200 A. The scanning rate was 84.66 A/min. The widths of both the entrance and the scanning slits

were 0.5 mm, so that each rotational line was instrumentally broadened into a triangular profile, with a base width of 5 A. Thus each rotational line was broadened enough to blend with its neighbors, resulting in band profiles that displayed no rotational structure. As an illustration, the profiles of two sequences obtained on two successive traversals are reproduced in Figure 4, in which one profile has been shifted vertically, relative to the other, to prevent overlapping. Even the finer details are reproduced quite well on successive traversals.

Two corrections must be applied to the observed intensity records before they can be used to derive band intensities. (1) They must be corrected for the changing sensitivity of the apparatus as a function of wave length, and (2) adjustments must be made for

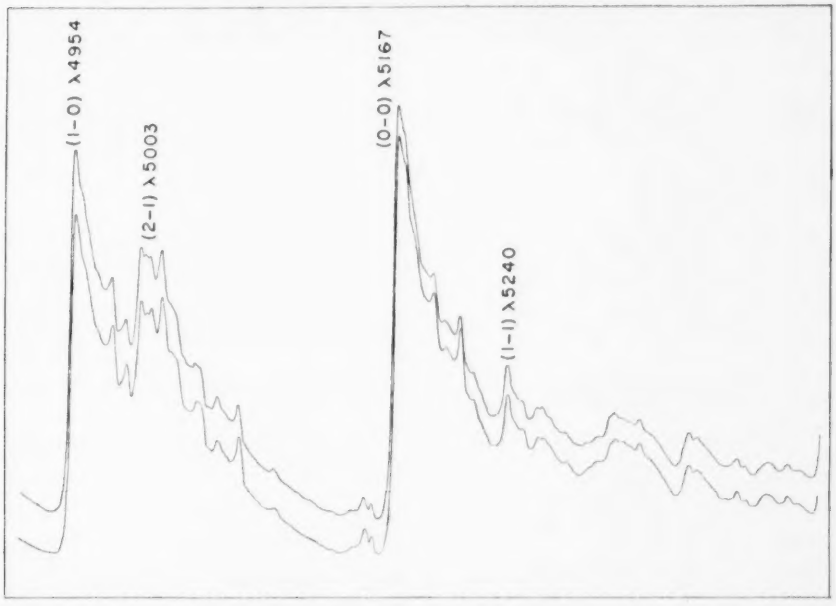

FIG. 4.—Direct tracings of sections of two successive traversals of the *TiO* spectrum. One tracing has been shifted vertically relative to the other, to prevent overlapping.

any changes, with time, of the number of molecules in the emitting column. One of the most serious limitations of the photoelectric technique is that the intensity can be measured at only one wave length at a time. Thus during a particular traversal of the spectral region of interest, both the temperature and the partial pressure of the molecules in the furnace must be kept constant. After equilibrium conditions have been reached, the temperature in the furnace, as measured by the optical pyrometer, is quite constant with time, but, nevertheless, slow changes are observed in the intensity of particular features on successive traversals. Such a change is illustrated in Figure 4; the vertical separation of the two profiles is not a constant. Such changes of intensity with time are produced by either (*a*) small changes in the vapor pressure of *TiO*, due to changes of temperature which are too small to be detected with the optical pyrometer, or (*b*) changes in the length of the emitting column. Corrections can be made for these changes by plotting, as a function of time, the intensities of various representative points on successive traversals

and then combining the resulting family of curves into a single curve by applying a constant multiplying factor to each curve. The resulting single curve may be called a "population"-curve. A typical population-curve is shown in Figure 5. Usually the population-curve is quite erratic for the first 10–15 minutes after the required temperature is reached. Then the curve becomes practically horizontal for sometimes as long as ½ hour, after which time it gradually drops as the solid material becomes exhausted. The population-curve may be used to correct the successive traversals, which may then be combined to form a single master-profile for that particular temperature. Only those traversals were combined for which the population-curve was well determined and exhibited no great vertical shifts. The corrected profiles, in general, fitted very well onto the single combined curve. A typical example is illustrated in Figure 6.

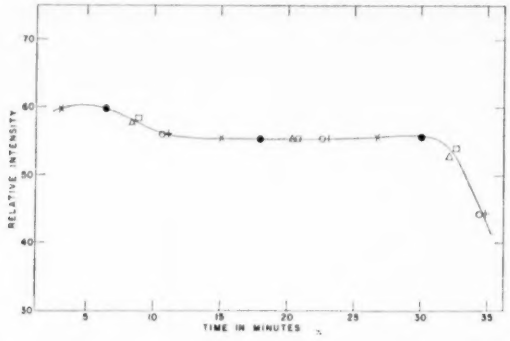

FIG. 5.—A typical population-curve. The various symbols identify the relative intensities of the same feature on successive traversals of the a-system.

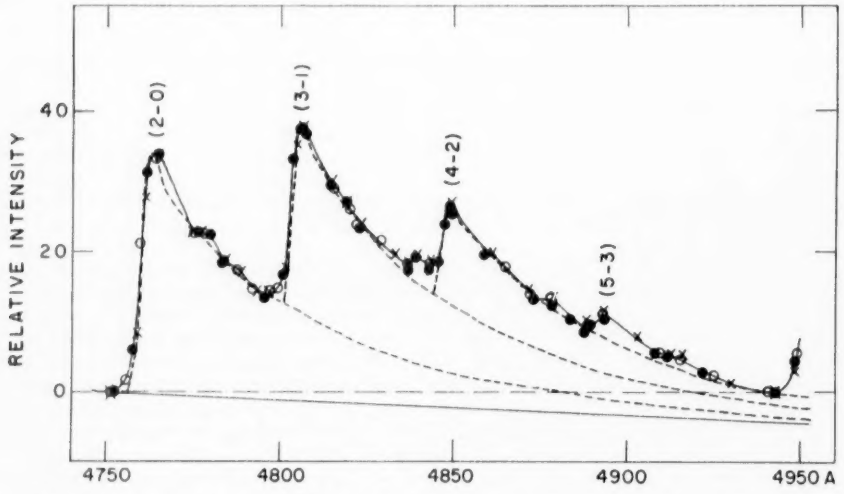

FIG. 6.—The relative intensity profile of the $\Delta v = +2$ sequence at 2567° K. The three symbols identify observed points on three successive traversals of the sequence. The dashed lines illustrate the way in which the computed band profiles may be fitted onto the observed profile.

D. THE BAND INTENSITIES

After the corrected band profiles had been obtained at each temperature, it was necessary to determine the integrated intensity of each band. This could have been done immediately if each band had been unblended with any other band over its entire profile. Unfortunately, the bands of the a-system fall into well-defined sequences, with the successive bands in each sequence superimposed on the tails of earlier bands of the sequence. Therefore, the following procedure was adopted. The relative intensity profile that each individual band would have had if it had been unblended with any other was computed from theoretical considerations, and then these theoretical profiles were fitted into the observed profile of the sequence, each band being given such a relative intensity that the observed intensity in the neighborhood of its head was reproduced. Each of these steps will be discussed in turn.

a) THE THEORETICAL PROFILES

The following equation gives the relative intensity in emission of a rotational line in branch X ($X = P$, Q, or R), resulting from a transition from an upper rotational level J':

$$I_J^X \propto \nu^4 i_J^X \exp\left\{-B_v' J'(J'+1)\frac{hc}{kT}\right\}, \tag{2}$$

where ν is the wave number, B_v' is the rotational constant of the upper vibrational state, T is the temperature, and i_J^X is the corresponding intensity factor, known from theory for various kinds of transition. The a-system is produced by a $^3\Pi - {}^3\Pi$ transition. Both the electronic states are good examples of case a type coupling. For such a transition, the following equations, derived theoretically by Hönl and London,[2] could be used for the intensity factors:

$$\begin{aligned} i_J^P &= \frac{2(J^2-\Omega^2)}{J}, \\ i_J^Q &= \frac{2(2J+1)\Omega^2}{J(J+1)}, \\ i_J^R &= \frac{2[(J+1)^2-\Omega^2]}{J+1}. \end{aligned} \tag{3}$$

The parameter Ω in these equations took the values 0, 1, and 2 for the $^3\Pi_0 - {}^3\Pi_0$, $^3\Pi_1 - {}^3\Pi_1$, and $^3\Pi_2 - {}^3\Pi_2$ subbands, respectively. It was obvious from the equations that, for all but the smallest values of J, the intensities of lines of the Q-branch would be very low relative to the intensities of lines of the R- and P-branches. Hence one could ignore the Q-branch in the computation of the intensity profile, without making any detectable error. The resultant band profile could be readily obtained by summing over the individual lines, since their relative locations within the bands were also known, either from previous analyses[3] or by computation from the rotational constants.[4] Such a procedure, however, while it was accurate, proved to be very time-consuming, so that a more rapid graphical method was adopted.

Since the slit widths were such that the individual lines of a particular branch were completely blended with their neighbors, the branch could, to a good approximation, be replaced by a continuous intensity distribution, derivable from equation (2). Examples

[2] See, e.g., W. Jevons, *Report on Band-Spectra of Diatomic Molecules* (Cambridge: At the University Press, 1932), p. 134.

[3] Andrew Christy, *Phys. Rev.*, **33**, 701, 1929.

[4] See, e.g., G. Herzberg, *Molecular Spectra and Molecular Structure*, Vol. 1: *Spectra of Diatomic Molecules* (2d ed.; New York: D. van Nostrand Co., Inc., 1950), p. 576.

of the resulting curves, when I_J^X was plotted against J, are presented as curves I_P and I_R in Figure 7. These intensity-curves would have corresponded to the profiles of the respective branches, if all lines in the branches had been equally spaced; but since they were not, the change in the line spacing had to be taken into account. This could be done by plotting on the same diagram those sections of the Fortrat parabola pertaining to the R- and P- branches, respectively. The resulting relative intensity, at any arbitrary point in the subband, could then be derived by using an appropriate weighting function and integrating over all parts of each branch which contributes to the intensity at that point. Each line was instrumentally broadened into a triangle with base width of 5 A,

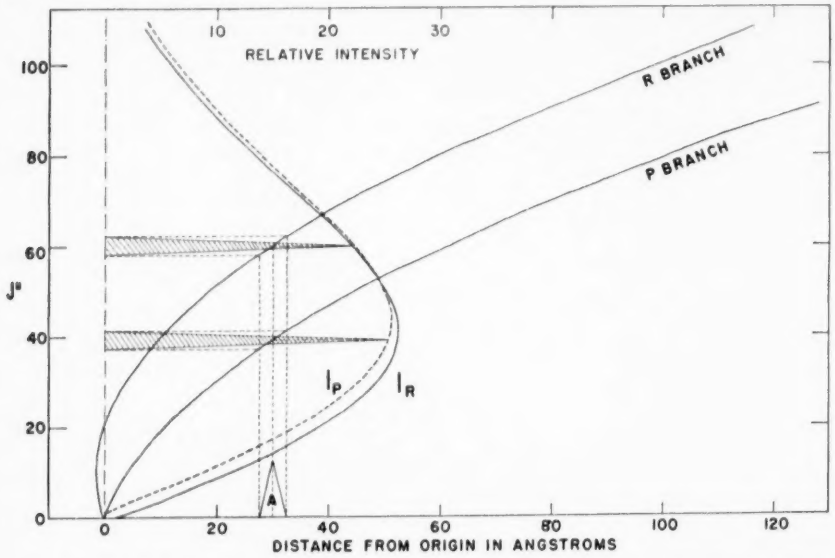

FIG. 7.—The derivation of the theoretical band profiles. Curves I_P and I_R give the relative intensities of lines of the P and R branches, respectively. The sections of a parabola give the corresponding distances of the lines from the origin in angstrom units. The triangle A is the weighting function which is applied, in the illustration, to the determination of the relative intensity at 30 A from the origin.

so that the weighting function would also be a triangle with the same base width. It is represented by the triangle A in Figure 7, which also illustrates the procedure that was followed in getting the integrated relative intensities; thus the relative intensity in the subband at a distance of 30 A from the band origin is represented by the sum of the crosshatched areas in the diagram.

Each band is composed of three subbands, so that a rigorous treatment should involve a study of each subband separately. However, it was found that the profiles of the different subbands were so much alike that no detectable error was made by assuming that they were identical. Thus the profile of only one subband needed to be treated, preferably that of the $^3\Pi_1 - {}^3\Pi_1$ transition. All that then remained, in order to obtain the final profile of a complete band, was to sum over the three component subbands, giving them relative positions corresponding to the observed separations of the subheads. This procedure was carried out for all bands of interest and for each of the three temperatures at which the furnace was operated. Figure 8 illustrates the way in which the profile of the (0–0) band, for example, changed as the temperature was changed.

b) THE OBSERVED PROFILES

In order to fit the theoretically derived relative intensity profiles onto the observed profiles of the sequences, it was necessary, first of all, to determine the location of the background underlying the observed sequences. If the integrated intensity in the tail of a sequence became zero before it reached the head of the next sequence to the red, then its background was, to a good approximation, a straight line connecting the intensity minima at the two heads. This proved to be the case for the main sequence, with head at 5167 A; its integrated intensity dropped to zero before its tail had reached the head of the following sequence at 5448 A. The theoretically derived profiles could then be

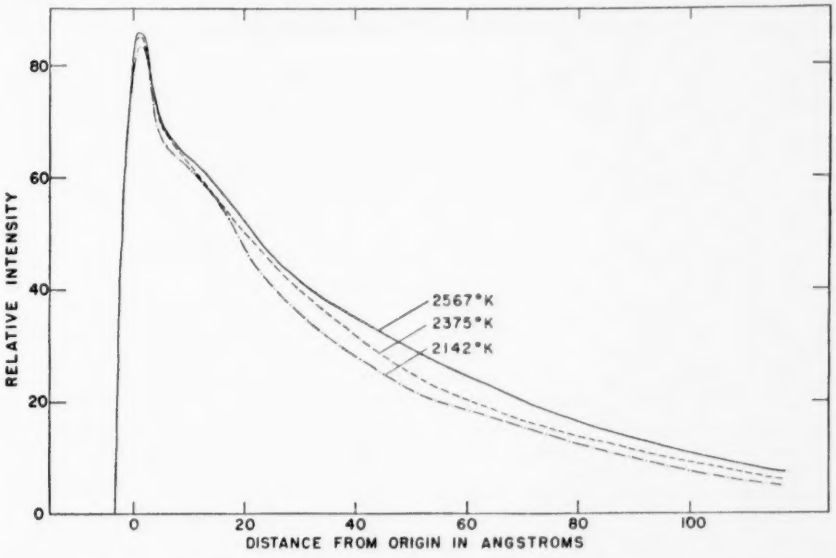

FIG. 8.—The theoretical intensity profile of the (0–0) band of the α-system of *TiO*

readily fitted into the observed profile, by first multiplying the relative intensities of the theoretical profile of the (0–0) band by an appropriate constant factor, so that the intensities between its head at 5167 A and the head of the (1–1) band at 5240 A were reproduced. The tail of the (0–0) band then became the background for the (1–1) band, and the same procedure could be repeated for that band.

Unfortunately, in the case of the $\Delta v = +1$ and the $\Delta v = +2$ sequences, with heads at 4954 and 4761 A, respectively, the respective tails did run through the following sequences. Since no prior information was available as to the actual intensity distribution in these tails, the initial assumption had to be made that the background could be drawn to the respective minima, just as in the case of the main sequence. This is illustrated by the horizontal dot-dash line in Figure 6. Successive improvements could then be made in the slope of the background, as attempts were made to reproduce the observations with an appropriate combination of theoretical profiles. This process converged rapidly; usually the third approximation proved entirely satisfactory.

The situation was even more complicated in the case of the $\Delta v = -1$ sequence, with head at 5448 A, which was badly blended with the β-system of *TiO* at 5597 A. However,

even in this case, it was still possible, again by successive approximations, to obtain the background fairly unambiguously.

The dashed lines in Figure 6 illustrate the way in which the theoretical profiles fitted into a typical sequence. In this way the integrated intensity of each seuqence could finally be divided up among the various contributing bands, and the various multiplying factors which led to the best fit could be regarded as being proportional to the respective relative intensities.

Once the relative intensities at each temperature were known, the relative transition probabilities could be derived immediately, since

$$\frac{|R_1|^2}{|R_2|^2} = \frac{I_1}{I_2}\frac{\nu_2^4}{\nu_1^4} \exp\left\{ [G_0(v_1) - G_0(v_2)] \frac{hc}{kT} \right\}. \quad (4)$$

All the quantities on the right-hand side of the equation were known. The final results are presented in Table 1, where the transition probabilities are expressed relative to the

TABLE 1

RELATIVE TRANSITION PROBABILITIES OF BANDS OF THE a-SYSTEM OF *TiO*

BAND	λ	1P21			1P28	WEIGHTED AV.
		1850° C	2075° C	2265° C	2265° C	
(0–1)	5448	0.876	0.786	0.940	1.020	0.877±0.026
(1–2)	5497	0.539	0.445	0.523	0.612	0.550± .018
(0–0)	5167	1.000	1.000	1.000	1.000	1.000
(1–1)	5240	0.157	0.103	0.219	0.195	0.162± .010
(1–0)	4954	0.940	0.924	0.968	1.020	0.962± .009
(2–1)	5003	0.686	0.635	0.807	0.750	0.740± .014
(2–0)	4761	0.636	0.615	0.645	0.688	0.652± .007
(3–1)	4804	0.739	0.705	0.858	0.881	0.829± .021
(4–2)	4848	0.621	0.769	0.820	0.780	0.757±0.018

transition probability of the (0–0) band. The table includes only those bands observed with sufficient intensity to provide significant results. Additional bands were observed, but they were too weak. An example is the (5–3) band of the $\Delta v = +2$ sequence, illustrated in Figure 6.

The results obtained at different temperatures show much more scatter than one would like. A check, in retrospect, as to the causes of this scatter showed that it was produced principally by a different decision being made each time as to how best to fit the theoretical profile to the observed profile. While the general fit was always quite good, there was always some inherent uncertainty due to scatter of the observational points. The probable errors that are quoted are the probabilities of accidental error, derived from the observed relative transition probabilities, after weighting the observations according to the closeness of the fit between theory and observation. There remains the possibility of fairly large systematic errors, which should be investigated. They are considered below.

a) One of the most serious sources of systematic error lies in the possibility of large self-absorptions in the emitting gas. It is believed that self-absorptions are small, if present at all, for the following reasons:

i) The peak intensity of the most intense feature of the spectrum, i.e., the head of the (0–0) band, is low, relative to the intensity of a black body at the same temperature and

wave length. At 2265° C its intensity ranged from 8.7 to 13.5 per cent of the intensity of the continuum. At the lower temperatures the ratio was much smaller.

ii) If self-absorption is appreciable, then one would expect departures from computed profiles for the strongest bands and little or no departure for weak bands. No such departures were found, i.e., the observed and computed profiles matched, in the case of the strongest bands, just as closely as they matched for the weakest bands of the system.

iii) The general intensity of the molecular spectrum at 2265° C was 26 times as great as at 1850° C. If self-absorptions were important, one might expect that the strongest bands at the higher temperature would be the ones most seriously affected. This would have the effect of increasing systematically the relative transition probabilities of weak bands at 2265° C, relative to their probabilities obtained at 1850° C. A comparison of the results obtained at these two temperatures does not reveal such a systematic effect.

b) Another source of systematic error might lie in the determination of the sensitivity-curve as a function of wave length. The observations at 2265° C with the 1P28 photocell provided a check on this possibility. The sensitivity-curve of this second cell was determined independently of that of the 1P21 cell, and the reductions were carried out completely independently. The final relative transition probabilities obtained with the 1P28 cell compared well with those obtained with the 1P21 cell; there was some scatter of results, but no systematic difference which could be attributed to the calibration-curves.

c) Another difficulty is inherent in the design of the electric furnace. In order to observe the emission from the *TiO* molecules, it is necessary that there be openings at the opposite ends of the heated section of the tube. Molecules will diffuse out of these openings and will find themselves in cooler surroundings, so that the distribution of the molecules among the various vibrational and rotational levels will be altered. Emission from these cooler regions will be superimposed on the emission from the hotter regions and will undoubtedly modify the relative intensities that are observed. There is no known way in which this difficulty can be eliminated. However, it is believed that it cannot be too serious; otherwise the agreement between the observed and the theoretical band profiles would not be as close as observed. The path length through the cooler gas must be much shorter than the path length through the heated section, which is approximately 6 inches, and, furthermore, the partial pressure of the *TiO* in the cooler zones must decrease rapidly with distance from the aperture, since the molecules will be rapidly removed by condensation on the cool walls.

d) A final source of error lies in the presence of temperature gradients within the hot section of the heater tube, the middle of the tube being somewhat hotter than the ends near the diaphragms. A systematic study at higher temperatures, around 2600° C, revealed a drop of 50° C from the tube center to the diaphragms. At the lower temperatures at which the *TiO* molecules were obtained, the gradients would be lower than this, and the gradient in the gas, as it diffuses toward the ends, will be even lower. In the extreme, if the pyrometer measured the temperature at the tube center, its reading would be, at most, 25° C higher than the mean temperature of the gas. This would have its effect principally on the distribution of molecules among the various initial vibrational levels. Computation shows that the corresponding extreme error in the population would amount to only 3 or 4 in the third decimal place at $v' = 4$, if the population of the $v' = 0$ level is taken as unity. Actually, for the reasons outlined above, the real error must be smaller than this. The corresponding effect on the relative transition probabilities of Table 1 would be negligible.

The electronic equipment used in this investigation was constructed under an Office of Naval Research contract. I am indebted to Dr. F. A. Jenkins, of the University of California, for making it possible to have the mechanical scanner built in the shops of the physics department, and also to Dr. Leo Brewer and Mr. Richard Porter, of the chemistry department, for many helpful suggestions and assistance in the observations.

VIBRATIONAL TRANSITION PROBABILITIES OF DIATOMIC MOLECULES; COLLECTED RESULTS II, N_2^+, CN, C_2, O_2, TiO*

P. A. Fraser, W. R. Jarmain, and R. W. Nicholls
Department of Physics, University of Western Ontario, London, Canada
Received July 7, 1953; revised July 27, 1953

ABSTRACT

Arrays of approximate vibrational transition probabilities, i.e., $p(v', v'')$ = (overlap integral)^2, are presented for the following molecular transitions of astrophysical interest:

N_2^+: $A\,^2\Pi_u \rightarrow X\,^2\Sigma_g^+$ (Meinel)	O_2: $b\,^1\Sigma_g^+ \rightarrow X\,^3\Sigma_g^-$ (atmospheric)
CN: $A\,^2\Pi \rightarrow X\,^2\Sigma^+$ (red)	$B\,^3\Sigma_u^- \rightarrow X\,^3\Sigma_g^-$ (Schumann-Runge)
$B\,^2\Sigma^+ \rightarrow X\,^2\Sigma^+$ (violet)	TiO: $A\,^3\Delta \rightarrow X\,^3\Pi$ (γ)
C_2: $A\,^3\Pi_g \rightarrow X\,^3\Pi_u$ (Swan)	

The methods employed in the computation of these values are indicated.

I. INTRODUCTION

A method of obtaining reliable values of the approximate vibrational transition probabilities,

$$p(v', v'') = (\int \psi_1^{(v')} \psi_2^{(v'')} d\tau)^2 = (v', v'')^2,$$

for molecular band systems was briefly discussed in a previous paper,[1] and results for a number of systems of astrophysical interest were presented. The method is approximate but avoids much of the extreme numerical tedium encountered in previous methods of evaluating $p(v', v'')$ arrays. Details of the method are published elsewhere.[2]

The basis of the approximation is replacement of the Morse potentials, $U_i(r) = D_i[1 - \exp - a_i(r - r_{ei})]^2$, where $i = 1, 2$, by two other Morse potentials in which a_1 and a_2 are both replaced by some mean value and a-dependent parameters are suitably adjusted. This approximation allows exact analytic evaluation of the overlap integral in $p(v', v'')$ and gives reliable results in most cases.

An improvement has been developed that allows treatment of band systems for which the approximation as above would be unsatisfactory. This technique is termed "r_e-shift," the name deriving from a systematic relative displacement of the wave functions to compensate for one of the distortions introduced by the approximation. The r_e-shift is described more fully elsewhere.[3]

II. RESULTS

Arrays of p-values for band systems of N_2^+, CN, C_2, O_2, and TiO, which are of astrophysical interest, are shown in Tables 1–7. Table 8 gives the basic molecular constants used in the calculations and their sources. In Table 3, for the CN violet system, some indication of the efficiency of the improvement effected by r_e-shift is seen. This system was used to establish the amount of relative shift needed to give results in good agreement with those of numerical integration.

* The research reported in this paper has been sponsored by the Geophysics Research Directorate, Air Force Cambridge Research Centre, Air Research and Development Command, under Contract AF 19(122)-470.

[1] W. R. Jarmain, P. A. Fraser, and R. W. Nicholls, *Ap. J.*, **118**, 228, 1953.

[2] P. A. Fraser and W. R. Jarmain, *Proc. Phys. Soc. A.*, **66**, 1145, 1953.

[3] W. R. Jarmain and P. A. Fraser, *Proc. Phys. Soc. A.*, **66**, 1153, 1953.

TABLE 1

N_2^+: $A\,^2\Pi_u \rightarrow X\,^2\Sigma_g^+$ (MEINEL)

$p(v', v'') = (v', v'')^2$

v'	v''						
	0	1	2	3	4	5	6
0	$.39_2$	$.40_0$	$.16_8$	$.03_8$	$.00_5$	$.00_0$	.000
1	$.33_1$	$.00_2$	$.26_8$	$.28_0$	$.10_2$	$.01_3$	
2	$.17_0$	$.15_3$	$.07_5$	$.08_6$	$.29_2$		
3	$.06_9$	$.19_6$	$.01_9$	$.15_5$			
4	$.02_5$	$.13_3$	$.12_1$				
5	$.00_8$	$.06_7$					
6	$.00_2$						

TABLE 2

C.V: $A\,^2\Pi \rightarrow X\,^2\Sigma^+$ (RED)

$p\,(v', v'') = (v', v'')^2$

v'	v''						
	0	1	2	3	4	5	6
0	$.49_9$	$.37_0$	$.11_1$	$.01_8$	$.00_2$	$.00_0$	.000
1	$.32_1$	$.04_6$	$.34_8$	$.22_2$	$.05_5$	$.00_7$	
2	$.12_8$	$.24_2$	$.01_2$	$.20_9$	$.28_8$		
3	$.04_0$	$.19_5$	$.10_7$	$.08_9$			
4	$.01_1$	$.09_4$	$.18_4$				
5	$.00_3$	$.03_6$					
6	$.00_0$						

TABLE 3*

C.V: $B\,^2\Sigma^+ \rightarrow X\,^2\Sigma^+$ (VIOLET)

$p\,(v', v'') = (v', v'')^2$

v'	v''			
	0	1	2	3
0	$.91_2$	$.08_1$	$.00_6$	$.00_1$
	$.91_7$	$.07_3$	$.00_5$	$.00_0$
	$(.92_6)$	$(.07_4)$	$(.00_5)$	$(.00_0)$
1	$.08_6$	$.75_2$	$.14_3$	$.01_7$
	$.07_7$	$.78_5$	$.12_1$	$.01_1$
	$(.07_9)$	$(.78_7)$	$(.12_1)$	$(.01_4)$
2	$.00_2$	$.16_2$	$.61_2$	$.18_8$
	$.00_3$	$.13_9$	$.69_2$	$.15_0$
	$(.00_3)$	$(.13_7)$	$(.69_1)$	$(.14_7)$
3	$.00_0$	$.00_2$	$.22_8$	$.49_0$
	$.00_0$	$.00_3$	$.17_4$	$.62_7$
	$(.00_0)$	$(.00_2)$	$(.18_0)$	$(.62_5)$

* The three lines in each group are identified in the following tabulation:

v''

v' ..... { p from approx. method, no r_e-shift (III)
p from approx. method, with r_e-shift (I)
(p) from numerical integration

TABLE 4

C_2: $A\ ^3\Pi_g \rightarrow X\ ^3\Pi_u$ (SWAN)

$p\ (v', v'') = (v', v'')^2$

v'	v''							
	0	1	2	3	4	5	6	7
0	$.73_1$	$.21_1$	$.04_2$	$.00_7$	$.00_1$	$.00_0$	.000	.000
1	$.23_7$	$.36_5$	$.28_0$	$.08_8$	$.02_0$	$.00_5$	$.00_0$	
2	$.02_4$	$.35_6$	$.16_2$	$.28_0$	$.12_4$	$.03_0$		
3	$.00_3$	$.06_0$	$.40_5$	$.05_7$	$.26_2$			
4	$.00_0$	$.00_5$	$.09_7$	$.42_7$				
5	.000	$.00_0$	$.00_6$					
6	.000	.000						
7	.000							

TABLE 5

O_2: $b\ ^1\Sigma_g^+ \rightarrow X\ ^3\Sigma_g^-$ (ATMOSPHERIC OXYGEN)

$p\ (v', v'') = (v', v'')^2$

v'	v''						
	0	1	2	3	4	5	6
0	$.93_3$	$.06_5$	$.00_2$	$.00_0$	.000	.000	.000
1	$.06_5$	$.80_2$	$.12_6$	$.00_7$	$.00_0$	.000	
2	$.00_2$	$.12_5$	$.67_5$	$.18_2$	$.01_6$		
3	$.00_0$	$.00_8$	$.17_9$	$.55_5$			
4	.000	$.00_0$	$.01_6$				
5	.000	.000					
6	.000						

TABLE 6

O_2: $B\ ^3\Sigma_u^- \rightarrow X\ ^3\Sigma_g^-$ (SCHUMANN-RUNGE)

$p\ (v', v'') = (v', v'')^2$

v'	v''															
	0	1	2	3	4	5	6	7	8	9	10	11	12	13	14	15
0	.000	.000	.000	.000	.000	$.00_0$	$.00_1$	$.00_2$	$.00_6$	$.01_5$	$.02_9$	$.05_0$	$.07_6$	$.10_2$	$.12_3$	$.13_2$
1	.000	.000	.000	.000	$.00_0$	$.00_1$	$.00_4$	$.01_2$	$.02_5$	$.04_6$	$.06_8$	$.08_4$	$.08_2$	$.06_0$	$.02_5$	$.00_4$
2	.000	.000	.000	$.00_0$	$.00_1$	$.00_5$	$.01_3$	$.02_8$	$.04_9$	$.06_7$	$.06_8$	$.04_9$	$.01_8$	$.00_3$	$.01_1$	$.04_1$
3	.000	.000	.000	$.00_1$	$.00_4$	$.01_1$	$.02_6$	$.04_6$	$.06_1$	$.05_7$	$.03_2$	$.00_5$	$.00_2$	$.02_8$	$.04_9$	$.04_0$
4	.000	.000	$.00_0$													
5	.000	.000	$.00_1$													
6	.000	.000	$.00_2$													
7	.000	$.00_0$	$.00_2$													
8	.000	$.00_1$	$.00_5$													
9	.000	$.00_1$	$.00_7$													
10	.000	$.00_2$	$.01_0$													
11	.000	$.00_3$	$.01_3$													
12	$.00_0$	$.00_4$	$.01_5$													
13	$.00_1$	$.00_5$	$.01_8$													
14	$.00_1$	$.00_6$	$.02_0$													
15	$.00_1$	$.00_8$	$.02_2$													

v'	v''									
	16	17	18	19	20	21	22	23	24	25
0	$.12_7$	$.10_9$	$.08_5$	$.05_9$	$.03_7$	$.02_1$	$.01_1$	$.00_6$	$.00_2$	$.00_1$
1	$.00_3$	$.02_8$	$.06_8$	$.09_6$	$.10_8$	$.09_9$	$.07_6$	$.05_1$	$.02_9$	$.01_5$
2	$.06_2$	$.05_3$	$.02_3$	$.00_1$	$.01_0$	$.04_4$	$.08_2$	$.10_2$	$.09_6$	$.07_4$
3	$.01_1$	$.00_1$	$.02_4$	$.05_3$	$.05_3$	$.02_4$	$.00_1$	$.01_1$	$.04_9$	$.08_7$

Table 6, the Schumann-Runge system, owes its extension to the use of formulae which are free of the large cancellation that limits the extent of such tables. Such general formulae have now been found for the v' or v'' equal to 0, 1, 2, or 3 progressions and are reported in detail elsewhere.[3] Other tables will also be thus extended.

III. DISCUSSION

The p-values have been calculated to three significant figures for all bands reported, but to preserve uniformity, tables have been set up to show three decimal places. This means that probabilities are often given as .000, .001, etc.; among these, some of low quantum number are of interest in absorption studies. Accordingly, such numbers to three significant figures will be published.

In the previous paper[1] a classification of results derived by the approximate method

TABLE 7

TiO: $A\,^3\Delta \rightarrow X\,^3\Pi\ (\gamma)$

$p\ (v', v'') = (v', v'')^2$

v'	v''						
	0	1	2	3	4	5	6
0	$.71_9$	$.23_6$	$.04_0$	$.00_4$	$.00_0$	.000	.000
1	$.23_6$	$.31_7$	$.33_1$	$.09_8$	$.01_5$	$.00_2$	
2	$.04_0$	$.33_0$	$.10_1$	$.33_2$	$.16_3$		
3	$.00_5$	$.09_9$	$.33_6$	$.01_3$			
4	$.00_0$	$.01_6$	$.16_2$				
5	.000	$.00_2$					
6	.000						

TABLE 8

MOLECULAR CONSTANTS*

Molecule	State	a (A^{-1})	$K=\omega_e/\omega_e x_e$	r_e (A)
N_2^+	$A\,^2\Pi_u$†	2.4886	127.62	1.182
	$X\,^2\Sigma_g^+$	2.5889	136.79	1.116
CN	$B\,^2\Sigma^+$	2.7863	106.87	1.1506
	$A\,^2\Pi$	2.2224	140.84	1.2327
	$X\,^2\Sigma^+$	2.2448	157.39	1.1718
C_2	$A\,^3\Pi_g$	2.4191	108.77	1.2660
	$X\,^3\Pi_u$	2.0382	140.65	1.3117
O_2	$b\,^1\Sigma_g^+$	2.5727	102.70	1.22675
	$B\,^3\Sigma_u^-$	1.9486	87.52	1.604
	$X\,^3\Sigma_g^-$	2.3934	130.90	1.20740
TiO	$A\,^3\Delta$‡	1.674	220.2	1.6641
	$X\,^3\Pi$‡	1.714	244.1	1.6200

* Except where otherwise indicated, the source is G. Herzberg, *Spectra of Diatomic Molecules* (2d ed.; New York: D. Van Nostrand Co., 1950).

† A. E. Douglas, *Ap. J.*, **117**, 380, 1953.

‡ J. G. Phillips, *Ap. J.*, **114**, 152, 1951.

was given. Three categories were mentioned: excellent (I), satisfactory (II), and indicative of trends (III). The r_e-shift improvement has all but eliminated classification III. For the transitions reported here the classification is given in the accompanying tabulation.

Molecule	Transition	Classification
N_2^+	$A\,^2\Pi_u \rightarrow X\,^2\Sigma_g^+$ (Meinel)	I
CN	$A\,^2\Pi \rightarrow X\,^2\Sigma^+$ (red)	I
CN	$B\,^2\Sigma^+ \rightarrow X\,^2\Sigma^+$ (violet)	I (r_e-shift)
C_2	$A\,^3\Pi_g \rightarrow X\,^3\Pi_u$ (Swan)	I (r_e-shift)
O_2	$b\,^1\Sigma_g^+ \rightarrow X\,^3\Sigma_g^-$ (atmospheric)	II
O_2	$B\,^3\Sigma_u^- \rightarrow X\,^3\Sigma_g^-$ (Schumann-Runge)	II
TiO	$A\,^3\Delta \rightarrow X\,^3\Pi$ (γ)	I

SOME REMARKS ON THE LIFE-HISTORY OF METEORITES*

S. F. SINGER†
Office of Naval Research, U.S. Embassy, London
Received February 20, 1953; revised August 3, 1953

ABSTRACT

Consideration of the production of helium 3 by cosmic rays in meteorites makes possible corrections to their "ages" by allowing the cosmic-ray-produced helium to be subtracted. A method is indicated here for placing some limits on the date of creation of a meteorite; it is based on the determination of the empirical rate of production of cosmic-ray helium, which is then compared with the theoretical value. This method is applied to the Bethany (Harvard) meteorite. Further applications are suggested for studying the physical history of the meteorite surface, particularly in its traversal of the earth's atmosphere.

THE PRODUCTION OF HELIUM 3 BY COSMIC RAYS

The production of helium in iron meteorites by cosmic rays, first indicated by Bauer,[1] has been treated quantitatively, taking into account the "transition effect" due to low-energy cosmic-ray secondaries and including the interactions of π-mesons.[2] In addition, a method was developed for separating the contributions from cosmic rays and from radioactivity (uranium and thorium) to the total helium content of the meteorite; namely, we deduced that the cosmic-ray-produced helium is composed of $\sim$30 per cent helium-3 isotope.[2] The helium 3 is produced mainly in evaporations of the iron nuclei, both directly and through beta decay of tritium.

The presence of helium 3 in iron meteorites has now been demonstrated experimentally by the measurements of Paneth, Reasbeck, and Mayne.[3] The values of $He^3:He^4$ ratios for five meteorites measured so far vary from 31.5 (Mount Ayliff) to 17.8 per cent (Bethany Harvard). They have used these results to correct the "ages" which had previously been computed under the assumption that all the helium is due to radioactive decay only.[4] Thus Bethany (Harvard), previously supposed to be $\sim 200 \times 10^6$ years old, is now found to be 75×10^6 years.[3]

It is of interest to note that, among the five meteorites measured, the sample from Mount Ayliff meteorite has the greatest percentage of cosmic-ray-produced helium (as judged by the closeness of the experimental $He^3:He^4$ ratio to the theoretical ratio); Mount Ayliff is therefore considerably younger than 7.6×10^9 years, the original estimated age.[4] This result indicates that the predominant contribution to the helium comes from cosmic rays rather than from radioactivity. Consequently, the radioactive age of the meteorite becomes very sensitive to the exactness of the calculated $He^3:He^4$ ratio. A more precise calculation of this ratio and, in particular, of its variation with depth in the meteorite is now in progress. It should lead to more precise ideas about the time of solidification of meteorites.

* Any views expressed in this article are those of the writer and are not to be construed as official or necessarily reflecting the views of the U.S. Navy Department.

† Now at the University of Maryland, College Park, Maryland.

[1] *Phys. Rev.*, **72**, 354, 1947; **74**, 225, 501, 1948.

[2] S. F. Singer, *Nature*, **170**, 728, 1952.

[3] *Geochim. cosmochim. acta*, **2**, 300, 1952.

[4] Arrol, Jacobi, and Paneth, *Nature*, **149**, 235, 1942.

A POSSIBLE METHOD FOR DATING THE CREATION OF METEORITES

We wish to point out here that another item of information, namely, the *rate* of helium production by cosmic rays, may be used to place limits on the time of creation of the meteorite. The rate of helium production by a flux of cosmic rays corresponding to the present-day value in the vicinity of the earth's orbit was calculated to be $[H\dot{e}_{CR}] = (5 \pm 1.5) \times 10^{-14}$ cc of helium at N.T.P per gram of meteorite material per year; this figure applies to a sample taken from a region 2–15 cm from the ("preatmospheric")[5] surface of a very large meteorite.[2]

It is necessary, first, to define carefully various dates in the life-history of a meteorite. The total amount of cosmic-ray helium accumulated by the meteorite can be expressed as

$$[H\, e_{CR}] = \int_{a \geq 0}^{b \leq T} [H\, \dot{e}_{CR}(x, t)]\, dt .$$

Here $[H\dot{e}_{CR}(x, t)]$ is the rate of helium production due to the cosmic-ray intensity experienced by the meteorite along its trajectory; $t = 0$ is the date of most recent solidification, i.e., the date when helium accumulation becomes possible; a is the time at which the meteorite becomes exposed to cosmic rays *and* begins accumulating cosmic-ray helium; b is the time at which the meteorite hits the earth's surface when the atmosphere essentially stops further helium production by cosmic rays; and T is the "age," i.e, time of chemical analysis.

As an example of the application of this method, one may consider the experimental figures for Bethany (Harvard):[3] total helium content $= 0.36 \times 10^{-6}$ cc/gm; $He^3:He^4 = 17.8$ per cent; $T = 75 \times 10^6$ years. Using the theoretical $He^3:He^4$ ratio for cosmic-ray-produced helium,[2] one finds $[He_{CR}] = 0.216 \times 10^{-6}$ cc/gm. Hence the average rate of production of cosmic-ray helium $[H\dot{e}_{CR}]_{av} = [He_{CR}]/T = 2.9 \times 10^{-15}$ cc/gm per year, roughly one-twentieth the calculated rate given above.

If one adopts the working hypothesis that the average cosmic-ray intensity has not varied appreciably[6] and takes $[H\dot{e}_{CR}(x,t)] =$ Constant, one finds that Bethany (Harvard) must have been exposed to cosmic rays for at least 4×10^6 years, i.e., that its parent-body broke up more than 4×10^6 years before Bethany fell on the earth. This simple calculation assumes that the sample came from the region of maximum cosmic-ray helium production, i.e., 2–15 cm from the surface; further measurements will undoubtedly ascertain the location of the sample more precisely, so that one may then be able to raise this lower limit for the time of breakup.

It is hoped that further measurements of helium isotopic ratios in meteorite samples can establish systematic groupings not only of meteorite ages but also of times of breakup. Such indications would be of the greatest importance for theories of the origin of meteorites.[7]

LOCATION OF METEORITE SURFACE BY HELIUM 3

It has been pointed out by Bauer[1] that the production of helium by cosmic rays can be considered as a surface effect. Because of the transition effect produced by cosmic-ray secondaries,[2] this statement applies only to large meteorites, i.e., with diameter greater than about 50 cm. For such meteorites, however, one may be able to use this effect to learn more about the physical processes undergone by the meteorite during and since its creation and in its travel through space.

[5] I.e., before any part of the surface is removed by ablation in the earth's atmosphere.

[6] The possible use of meteorites as cosmic-ray meters, to determine the intensity of cosmic rays both in prehistoric times and in different parts of the solar system, is discussed elsewhere (Singer, *Phys. Rev.*, **90**, 168, 1953).

[7] G. P. Kuiper, *Astrophysics—a Topical Symposium* (New York: McGraw-Hill Book Co., 1951), p. 399.

Thus it is already fairly evident from the preliminary measurements[8] that the five meteorites in question did not lose an overwhelming fraction of their mass in traversing the earth's atmosphere. This finding, in conjunction with the loss of mass as calculated from the theory of astroballistic heat transfer of a meteorite,[8] may enable us to make better estimates of the velocities with which meteorites approach the earth.[9]

This method may be capable of other applications, e.g., regions of high helium-3 content within complex meteorites could be identified as having once formed part of a surface exposed to cosmic rays. It might be possible also to apply this technique to test the suggestion[8] that the deep pits and cavities found on the surface of some meteorites[10] are produced in traversing the atmosphere.

[8] R. N. Thomas and F. L. Whipple, *Ap. J.*, **114**, 448, 1951.

[9] F. L. Whipple, private communication. *Note in proof:* For the measured meteorites they are well below the escape velocity from the solar system.

[10] E. P. Henderson, paper read at Yerkes Observatory Conference on the Abundances of the Elements, November, 1952.

NOTES

THE POSSIBLE ROLE OF ACCELERATED SECONDARY ELECTRONS IN THE AURORA

Laboratory experiments have recently been made at Yerkes Observatory on the interaction of high-energy ions with air. Protons and He^+ energies ranging in steps from 40 to 400 kev and air pressure of approximately 10^{-1} mm *Hg* were used. This range of energies was selected for the experiments, because an extra-terrestrial proton will penetrate the atmosphere vertically down to a height of 160–110 km above the earth's surface at 40–400 kev, respectively. It was found that the laboratory spectra thus obtained bore a close resemblance to the auroral spectrum,[1] except that in the infrared region the Meinel system[2] of N_2^+ was much too weak relative to the first positive system of N_2.

A new series of experiments has now been concluded, using electrons in steps ranging from 0.2 to 7 kev. The electrons were found to be the only particles which were able to excite the Meinel N_2^+ system efficiently. Electrons of energies less than 400 kev produced a ratio of intensities between the Meinel and the first positive systems of an order of magnitude similar to the auroral ratio. For energies of several kilovolts, the Meinel system becomes exceptionally intense compared to the first positive bands.

Three possible conclusions can be drawn from these experiments. First, if the electrons responsible for the Meinel bands in the aurora are primary electrons, then the velocity of the electrons must be many times higher than that of protons, since an extra-terrestrial electron would require approximately 10 kev to penetrate to the 120-km level. As a consequence, the auroral spectrum could be obtained only by assuming a stream of protons moving along with a stream of electrons of much higher velocities,[3] their motions being uninfluenced by the terrestrial magnetic field. This seems to be improbable.

A second possibility is that the auroral relative intensities could result from high-energy protons.[4] It is generally believed that in the high-energy range the behavior of all particles becomes alike.[5] This is evidenced by the accuracy with which Bethe and Bloch's formula represents the observed data for the stopping power of matter for energetic particles. Bethe and Bloch's region would not be attained until $Ze^2/\hbar v \ll 1$, where Z is the nuclear charge of the atom of the air, e is the electronic charge, $\hbar$ is the plank constant divided by 2π, and v is the velocity of the impinging particles. This requires an energy of incoming protons much greater than 1 mev. One-mev proton will penetrate the atmosphere down to 90 km. This is a rare case and thus is unlikely to provide an explanation of the intense Meinel bands.

The third possibility, and the one that we believe is the most likely, is that the electrons responsible for the excitation of the Meinel bands are of secondary origin. It is not possible for such energetic secondary electrons to be the result of ionizations, since only a few tens of volts can be transferred in such events. The only conclusion that can be drawn for this possibility is that the secondary electrons must subsequently have been

[1] Meinel and Fan, *Ap. J.*, **115**, 330, 1952.

[2] Meinel, *Ap. J.*, **112**, 562, 1950; **113**, 583, 1951.

[3] H. Alfvén, *Cosmical Electrodynamics* (London: Oxford University Press, 1950), p. 181.

[4] Our new experiment, using a 1.9-mev proton beam from the Van de Graaf generator of the University of Wisconsin, has ruled out this possibility. The author is indebted to Dr. R. G. Herb, Dr. H. T. Richards, and his group for their interest in this work and their help in performing the experiment.

[5] Massey and Burhop, *Electronic and Ionic Impact Phenomena* (London: Oxford University Press, 1952), p. 513.

accelerated to energies of several hundred volts. This mechanism therefore requires the presence of a potential gradient in the auroral regions.

It is interesting to consider how the conditions required by this third possibility could arise. If we assume that the primary particles penetrate the terrestrial magnetic barrier in some unknown manner and impinge on the atmosphere, then, regardless of whether the particles are of one sign or mixed at the particular point in their journey, the net result will be the creation of a potential gradient. If the particles are of one sign, the result of the accumulation of the charge will be the creation of a high potential. If the particles are ionized but grossly neutral and of approximately equal velocities, the protons will penetrate deeper than the electrons, and thus a potential gradient will still be produced.

The separation of the electrons from the protons by atmospheric resistance for an infinitely extended stream can be treated as the separation of one plate of a parallel plate condenser from the other, if the effect of the multiple scattering of the electrons by the atmospheric molecules and that of the terrestrial magnetic field can be neglected. For such a hypothetical model, one obtains a separation of the order of 30 km for an incoming flux of 10^6 particles /sec/cm^2 at a velocity of 10^9 cm/sec when the resistance is taken to be 2×10^{-14} ev/molecule/cm.[2] This is a small separation. A separation greater than several hundred kilometers seems to be necessary in order to explain some features of an auroral display. The required condition mught be obtained if a fraction of the electrons could be separated by the action of a terrestrial magnetic field from the protons before they enter the atmosphere. Then, allowing enough time for the accumulation of the charges, a high potential would be built up for the acceleration of high-energy electrons.

The hypothetical primary particles will then cause emission of radiation from the atmospheric constituents through three general mechanisms: (*a*) direct excitation of air by the primary particles; (*b*) excitation by low-energy ejected (secondary) electrons; (*c*) excitation by accelerated (secondary) electrons. Because of their high relative mobility, the electrons will be the only particles that can effectively accelerate to moderate energies per mean free path length. The direction of the accelerating potential gradient would, of course, depend on the nature of the primary particles.

It appears quite feasible to perform laboratory experiments to test this hypothesis. In the preceding laboratory experiments the absorbing chamber has always been grounded; consequently, no potential is created by the absorption of the protons by the air. In one instance, however, the ground connection was broken, and the chamber rapidly rose to a potential of several kilovolts. This insulated chamber should then reproduce the natural phenomenon by causing the secondary electrons to be accelerated by this potential gradient in the same direction as the incident protons. If the induced potential gradient and the mean free path were adjusted to allow the secondary particles to reach energies of 200–400 volts, then the physical situation with regard to electron energy should be a close counterpart of the actual aurora, if this is the correct interpretation. While if may be difficult to achieve this situation in the laboratory because of the tremendous scale reduction imposed by practical considerations, it should be interesting to see if evidence for this interpretation can be obtained by using an isolated absorption chamber.

The author wishes to express his sincere thanks to Dr. A. B. Meinel for his encouraging and kind guidance, and his appreciation to Dr. V. C. A. Ferraro for his valuable suggestions. This work is supported in part by the Geophysical Research Directorate of the Air Force Cambridge Research Center, under Contract AF 19(122)-480.

C. Y. Fan

Yerkes Observatory
July 30, 1953

ABUNDANCES OF METALS IN THE SOLAR CHROMOSPHERE

The size of the monochromatic crescents of the chromosphere, as obtained on a slitless photograph of the flash spectrum, indicates the height above the solar limb at which the monochromatic surface brightness of the chromosphere corresponds to the threshold sensitivity of the photographic plate. Using as a photometric device the "equality of height" for lines of several elements, R. Wildt developed a method for obtaining the relative abundance of metals in the chromosphere.[1] The ratio of the number of atoms of one element to the number of atoms of another is given by

$$\frac{Z_1}{Z_2} = \frac{1 + K_1/p_e}{1 + K_2/p_e} \frac{[gf\nu^3]_2}{[gf\nu^3]_1} \frac{u_1}{u_2},$$

where K denotes the ionization constant, p_e the electron pressure, and u the partition function of the atom. The spectroscopic characteristics (in brackets) refer to a pair of lines (of different elements) reaching the same height in the chromosphere.

The chromospheric temperature adopted was $T = 4830$. The electron pressure at the height of 500 km above the sun's limb, at which the comparison of line intensities was made, is $p_e = 0.11$ dynes/cm. The partition function for *Fe* I, *Ni* I, and *Cr* I at $T = 4830$ was found by an interpolation from Claas's tables.[2]

The ratio of nickel to iron was found by using the multiplets $a^3D - z^5F$, $a^3D - z^3P$, and $a^3D - z^3F$ of *Ni* I, and the multiplet $a^5D - z^5F$ of *Fe* I. The ratio of chromium to iron was obtained by using the multiplets $a^5S - y^5P$ and $a^5D - y^5P$ for *Cr* I, and the multiplet $a^5D - z^7F$ of *Fe* I.

The relative f-values for the iron lines were determined by R. B. King,[3] who later gave values for the corresponding absolute oscillator strengths.[4] It was on the basis of these values that R. Wildt computed the abundance of several metals. However, H. Kopfermann and G. Wessel[5] have shown that it is necessary to make a correction to the absolute f-values obtained by R. B. King in order to attain the correct absolute oscillator strengths. Thus Wildt's results must be revised.

The relative f-values of nickel were taken from R. B. King[6] and the absolute oscillator strengths from F. B. Estabrook.[7] The relative f-values of chromium were obtained by A. J. Hill,[8] and the absolute oscillator strengths by F. B. Estabrook.[9]

To correct for variations along the spectrum in atmospheric extinction, for transmission loss in the optical system, and for threshold sensitivity of the photographic emulsion, an empirical color correction as deduced by R. Wildt[1] was used.

The results are collected in Table 1, showing the logarithms of the relative abundances (by numbers of atoms). The first column contains the ratios obtained by Wildt (but including the Kopfermann correction) by using the above method, with the addition of the elements chromium and nickel. The second column contains the photospheric abundances determined by Claas.[2] The third column contains the abundances deduced by Menzel from emission lines.[10] The fourth column contains the difference between the

[1] *Ap. J.*, **105**, 36, 1947.
[2] *Rec. Astr. Obs. Utrecht*, Vol. **12**, Part I, 1951.
[3] R. B. King and A. S. King, *Ap. J.*, **87**, 24, 1938.
[4] R. B. King, *Ap. J.*, **95**, 78, 1944.
[5] *Zs. f. Phys.*, **130**, 100, 1951.
[6] *Ap. J.*, **108**, 87, 1948.
[7] *Ap. J.*, **113**, 684, 1951.
[8] A. J. Hill and R. B. King, *J. Opt. Soc. Amer.*, **41**, 315, 1951.
[9] *Ap. J.*, **113**, 684, 1951.
[10] *Pub. Lick Obs.*, **17**, 281, Table 19, col. T, 1931.

first and second columns; the fifth column gives the difference between the first and third columns.

Considering the accuracy obtainable by Menzel's and Wildt's methods, their chromospheric abundances are in fair agreement. But there are some indications of systematic

TABLE 1

RELATIVE ABUNDANCES OF METALS (BY NUMBERS OF ATOMS)

Metal	I $\log Z_1$ (Wildt-Schwartz)	II $\log Z_2$ (Claas)	III $\log Z_3$ (Menzel)	IV Δ(I−II)	V Δ(I−III)
Na	−0.3	−1.3	+0.2	+1.0	−0.5
Mg	+1.1	−0.1	+0.4	+1.2	+0.7
Al	−0.4	−0.5	−0.8	+0.1	+0.4
Ca	−0.2	−1.2	−0.4	+1.0	+0.2
Cr	−0.2	.....	−0.9	.....	+0.7
Fe	0.0	0.0	0.0	0.0	0.0
Ni	0.0	.....	−1.0	.....	+1.0
Cu	−3.0	−2.8	.....	−0.2	.....
Sr	−3.1	−4.7	−3.9	+1.6	+0.8

deviations from the photospheric abundances of Claas, especially for the elements *Mg*, *Al*, and *Ca*. Before the existence of such differences has been firmly established, it would be premature to speculate on their possible physical cause.

SANDRA SCHWARTZ

YALE UNIVERSITY OBSERVATORY
April 22, 1953

ON THE SPACE REDDENING OF ETA AQUILAE

The six-color observations of η Aquilae by Stebbins, Kron, and Smith[1] show excesses in U, V, and I when B, G, and R match the average colors of other c stars, though this effect is not present in the six-color observations of δ Cephei.[2] It is suggested that this is due to the interstellar reddening of η Aquilae.

The first two sections of Table 1 give the comparison of δ Cephei with α Persei, F5 I*b*, and with β Aquarii, G0 I*b*.[3] The next two sections show the comparison of η Aquilae with the mean color of 45 Draconis, F7 I*b*, and γ Cygni, F8 I*b*, and with the mean color of β Draconis, G2 II, α Aquarii, G2 I*b*, α^1 Capricorni, G3 I*b*, and 9 Pegasi, G5 I*b*, as given by the authors.[1]

The fifth section shows the comparison of η Aquilae with 14 Persei, G0 I*b*. It will be noted that the agreement in this case is much better than in the previous two comparisons. Comparison of 14 Persei with β Aquarii shows that the former is reddened by at least 0.23 mag. on the $V-I$ scale, so that it appears that η Aquilae would agree quite well with stars reddened by about 0.3 mag.

Assuming a color excess on the $V-I$ scale of 0.32 mag., corresponding to a total visual absorption of 0.3 mag., the color excesses in the six colors may be computed from the

[1] *Ap. J.*, **115**, 292, 1952.

[2] *Ap. J.*, **101**, 47, 1945.

[3] Color data are from Stebbins and Whitford, *Ap. J.*, **102**, 318, 1945; spectral data are by W. W. Morgan on the system of the Yerkes revised spectral atlas.

law of reddening obtained from a study of the O and B stars;[4] these are given in the sixth section of the table.

Adding these computed color excesses to the observed colors of α Persei and β Aquarii, we obtain "reddened" values, which are compared with the observed colors of η Aquilae in the last two sections of the table. The deviations so obtained are comparable to those given in the comparison with δ Cephei.

TABLE 1

	U	V	B	G	R	I	$V-I$	Remarks
α Persei	0.09	−0.28	−0.11	−0.02	0.13	0.21	−0.49	
δ Cephei	0.10	−0.28	−0.10	−0.02	0.12	0.21	−0.49	$0.05P$
	0.01	0.00	0.01	0.00	−0.01	0.00	0.00	
β Aquarii	0.56	0.18	0.07	−0.01	−0.05	−0.09	0.27	
δ Cephei	0.56	0.16	0.07	−0.01	−0.06	−0.10	0.26	$0.45P$
	0.00	−0.02	0.00	0.00	−0.01	−0.01	−0.01	
Mean cF7	0.34	−0.07	−0.03	−0.02	0.05	0.10	−0.17	
η Aquilae	0.28	−0.14	−0.03	−0.01	0.04	0.03	−0.17	$0.00P$
	−0.06	−0.07	0.00	0.01	−0.01	−0.07	0.00	
Mean cG3	1.02	0.46	0.19	−0.01	−0.18	−0.33	0.79	
η Aquilae	0.97	0.42	0.20	−0.02	−0.18	−0.37	0.79	Minimum
	−0.05	−0.04	0.01	−0.01	0.00	−0.04	0.00	
14 Persei	0.73	0.26	0.13	−0.01	−0.13	−0.24	0.50	
η Aquilae	0.71	0.245	0.13	−0.01	−0.12	−0.255	0.50	$0.40P$, $0.82P$
	−0.02	−0.015	0.00	0.00	0.01	−0.015	0.00	
Color excess	0.21	0.13	0.07	0.01	−0.08	−0.19	0.32	
α Persei	0.30	−0.15	−0.04	−0.01	0.05	0.02	0.17	"Reddened"
η Aquilae	0.28	−0.14	−0.03	−0.01	0.04	0.03	0.17	$0.00P$
	−0.02	0.01	0.01	0.00	−0.01	0.01	0.00	
β Aquarii	0.77	0.31	0.14	0.00	−0.13	−0.28	0.59	"Reddened"
η Aquilae	0.79	0.30	0.14	−0.01	−0.13	−0.29	0.59	$0.45P$
	0.02	−0.01	0.00	−0.01	0.00	−0.01	0.00	

It appears that the peculiar colors of η Aquilae may be explained by interstellar reddening; the exact amount is dependent on the amounts assumed for the comparison stars. Though the reddening is small, it revises the temperature on the T_1 scale[3] from 5770° to over 6300°. The necessity of evaluating the absorption, for even the brightest cepheids, before discussing the zero point of the period-luminosity relation is obvious. The six-color system or an equivalent provides a powerful method of analysis of the space reddening for these objects.

DANIEL L. HARRIS III

YERKES OBSERVATORY
September 8, 1953

[4] Unpublished investigation with W. W. Morgan, whose collaboration I gratefully acknowledge.

A NEW SPECTROGRAPHIC ORBIT OF 30 TAU CANIS MAJORIS*

Tau Canis Majoris is of particular interest because it is one of the O-type stars located within the galactic cluster NGC 2362 and was used by R. J. Trumpler[1] to demonstrate the existence of a systematic difference between the velocity of this star and the mean velocity derived from the fainter members of the cluster. An earlier orbit based upon Yerkes Observatory spectrograms was published in 1928.[2]

Table 1 gives the new radial velocities. Since the new observations confirmed the general character of the earlier velocity-curve, a new set of normal places was derived by combining the new observations with the older ones. After a small adjustment of the period had been made, the orbital elements listed in Table 2 were derived by a process of successive approximations.

TABLE 1

RADIAL VELOCITIES OF TAU CANIS MAJORIS

Date	Phase (Days)	Velocity (Km/Sec)	Date	Phase (Days)	Velocity (Km/Sec)
1951 Nov. 15.506	89.886	+65.3	1952 Nov. 10.499	141.079	+86.5
15.515	89.895	+59.9	11.502	142.082	+75.1
16.503	90.883	+59.8	Dec. 4.413	10.093	+ 2.8
16.514	90.894	+48.1	4.428	10.108	+12.8
1952 Jan. 19.324	154.704	+38.7	5.442	11.122	+ 0.2
19.335	154.715	+36.0	1953 Jan. 31.272	67.952	+42.5
20.326	0.806	+37.7	Feb. 2.299	69.979	+25.4
20.337	0.817	+35.4	22.165	89.845	+56.0
21.339	1.819	+38.2	Mar. 8.313	103.993	+70.7

TABLE 2

ORBITAL ELEMENTS OF TAU CANIS MAJORIS

P	154.90 days	e	0.30
T	JD 2425206.5	K	49.5 km/sec
ω	107°7	γ	+43 km/sec

The new value of the velocity of the system agrees closely with the value used by Trumpler,[1] which he had obtained from a combination of a preliminary orbit determined by himself at the Lick Observatory and the 1928 orbit obtained at the Yerkes Observatory. Hence the value of the Trumpler effect in the cluster NGC 2362 retains the value of +9 km/sec.

Although the Mount Wilson spectrograms used in this work have a somewhat better definition than the earlier Yerkes plates, no indication appears on them of the spectral lines of the second component. Nor is there any suggestion of an anomalous behavior of

* The first 16 spectrograms used in this work were obtained by Mr. Struve as guest investigator at the Mount Wilson Observatory; the last two plates were taken by Mr. Kraft at the Lick Observatory.

[1] *Pub. A.S.P.*, **47**, 249, 1935.

[2] *Ap. J.*, **68**, 335, 1928.

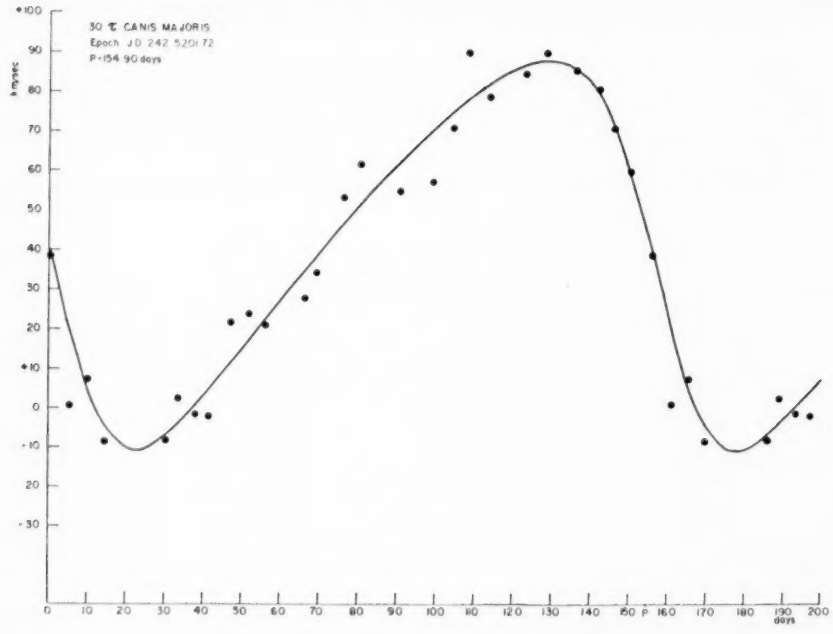

FIG. 1.—Velocity-curve of Tau Canis Majoris

the spectral lines that could account for the red shift. Figure 1 shows the velocity-curve, together with the normal points used in the determination of the orbital elements.

O. STRUVE
R. P. KRAFT

BERKELEY ASTRONOMICAL DEPARTMENT
UNIVERSITY OF CALIFORNIA
July 27, 1953

A WOLF-RAYET STAR OF TENTH MAGNITUDE
CORRECTION TO *HDC*

HD 197406 (20^h38^m4, $+52°14'$, 1900) appears on two McCormick prismatic camera plates as a WN5 star; it clearly shows the characteristic emission lines λ 4686 of *He* II and λλ 4605–4622 of *N*v. However, the *Henry Draper Catalogue* lists the spectrum as Ma. Mrs. Margaret W. Mayall has kindly checked the Harvard records and finds that Miss Cannon had crossed off Ma and inserted Oc in her copy of the catalogue. The correction had been subsequently overlooked; the original classification is believed to have been that of Mrs. Fleming.

A. N. VYSSOTSKY

LEANDER MCCORMICK OBSERVATORY
August 27, 1953

ABSTRACTS OF ASTROPHYSICAL JOURNAL
SUPPLEMENT SERIES

Supplement No. 1, Volume I, pages 1–38, March 1, 1954

CHROMOSPHERIC STRUCTURE OF THE K-TYPE COMPONENT OF ZETA AURIGAE

O. C. Wilson and Helmut A. Abt*

Mount Wilson and Palomar Observatories
Carnegie Institution of Washington
California Institute of Technology

Spectrograms of 10 A/mm dispersion taken during the 1947–1948 eclipse have been measured for line intensities and for radial velocities, and the results are compared with those obtained previously for the 1939–1940 eclipse. Egress of 1947–1948 is found to be quite similar to ingress and egress of 1939–1940; ingress at the more recent eclipse differs, however, from the other three transits in the direction of a considerably slower gradient, particularly at the greater chromospheric heights. This effect is found from lines of all types. However, ingress of 1947–1948 is not distinguishable from the other transits in the values of any of the derived parameters: excitation temperature, turbulent velocity, or degree of ionization.

It is shown that the apparent rise of $\Delta\lambda_D$ with height found in 1939–1940 is really due to a systematic difference in this quantity between the neutral and ionized lines. Ions indicate slightly higher turbulent velocities than do neutral atoms. The excitation temperature increases with height at about the same rate as indicated by the earlier results.

Ionization in the chromosphere is studied in some detail, and Strömgren's theory of the penetration of ionizing radiation from the B star into the chromosphere of the K star is applied to the problem. The outcome is that it appears impossible to account for the spectroscopic phenomena on the basis of a smooth distribution of the chromospheric material. In fact, it is necessary to assume that the matter occurs in condensations of rather small size (thickness of the order of 10^3 km) and high density ($\log n[H] = 13.8$) in order to keep the ionization at the required level and to avoid discordance with the solar abundance ratios. The model is in accord with all but one of the observed spectroscopic features, as well as with the recent interpretation of the photometric eclipse by Roach and Wood.

* Now at the Yerkes Observatory.

IMPORTANT COMPANION VOLUMES IN

ASTROPHYSICS

LAWRENCE H. ALLER

Associate Professor of Astronomy, University of Michigan

▶▶ NUCLEAR TRANSFORMATIONS, STELLAR INTERIORS, AND NEBULAE

Ready Spring 1954—This pioneering work offers a comprehensive study of thermal nuclear reactions, the interiors of stars, pulsating variable stars, and the interstellar medium. It covers not only the fundamentals necessary for an understanding of this specialized branch of astrophysics, but also the major modern developments in the field. Emphasis is placed on methods and procedures for obtaining results, rather than on a simple presentation of the current status of the science. The book treats of the properties of matter at high temperatures, stellar energy generation, internal constitution of stars, stellar evolution and the origin of the elements, novae and supernovae, gaseous nebulae, with particular attention given to discoveries achieved by the new technique of radio astronomy. The work is illustrated with numerous diagrams and photographs, many reproduced here for the first time. *52 illustrations, 10 tables, 344 pages.* $12

CONTENTS: STELLAR INTERIORS AND NUCLEAR TRANSFORMATIONS—MODEL STARS—THE CEPHEIDS AND LONG PERIOD VARIABLES—STARS WITH EXTENDED ENVELOPES, NOVAE, AND SUPERNOVAE—THE PLANETARY NEBULAE—THE INTERSTELLAR MEDIUM

▶▶ THE ATMOSPHERES OF THE SUN AND STARS

Now Available—Thorough coverage of present-day knowledge concerning the atmospheres of the sun and stars and solar-terrestrial relationships. Provides a short introduction to astronomy and a review of relevant physics. Treats all major astrophysical principles—atomic structure and spectra, gas laws and velocity distribution, ionization, excitation, etc.—and applies them to the radiation of the sun and stars, to their continuous and dark-line spectra, to solar phenomena, and to solar-terrestrial relationships. Each principle is applied to a definite numerical problem concerned with the interpretation of stars and nebulae. *116 illustrations, 44 tables, 412 pages.* $12

"Hard to overemphasize the importance of this book . . . presents the subject of stellar atmospheres as it is known and accepted today."—**Publications of the Astronomical Society of the Pacific**

CONTENTS: SURVEY OF BASIC DATA—ATOMIC AND MOLECULAR SPECTRA—GAS LAWS AND EQUATIONS OF STATE, TURBULENCE—EXCITATION, IONIZATION, AND DISSOCIATION—EMISSION AND ABSORPTION OF RADIATION—RADIATION OF STARS—CONTINUOUS SPECTRA OF SUN AND STARS—THE FRAUNHOFER SPECTRUM—SOLAR PHENOMENA

Order through your bookstore or from:

THE RONALD PRESS COMPANY • 15 E. 26th St., N.Y. 10

THE SUN

The Solar System

VOLUME I

***Edited by* GERARD P. KUIPER**

The Sun, the first of four volumes intended to collect and systematize all significant information on the sun, the planets, the satellites, the comets, and the smaller bodies of the solar system, is written by twenty-three solar physicists from six different countries. It is designed with a dual purpose. On the one hand, it is an invaluable reference handbook for the specialist. On the other hand, it is intelligible to anyone versed in the physical sciences.

The Sun covers the divisions of solar physics comprehensively: the solar interior and energy production, the photosphere and the Fraunhofer spectrum; the chromosphere and the solar electrodynamics; and the many modern techniques of solar observation. All are discussed in detail. The book contains, in addition, many new illustrations and over one thousand references to the literature.

New models are given for the solar interior, based on integrations using the latest information on nuclear cross-sections. The photosphere models are critically reviewed, and a new compromise solution is proposed. Similarly, a very recent model for sunspots is reviewed. For both the chromosphere and the corona the temperature and density data are critically examined. An extensive treatment of solar radio astronomy adds significantly to the optical studies of solar phenomena treated in other chapters.

A special feature of *The Sun* is its two tables of solar observatories and their equipment, accessories, and programs. Other features include the latest results on the magnetic field and the solar component of cosmic rays, recent additions to instrumental techniques, and a record, as complete as possible, of the far-ultraviolet solar spectrum photographed on rocket flights.

Many illustrations, 784 pages, $12.50

THE UNIVERSITY OF CHICAGO PRESS